NASA/TM—2003-212460

International Space Station Increment-4/5 Microgravity Environment Summary Report

Kenol Jules
Glenn Research Center, Cleveland, Ohio

Kenneth Hrovat and Eric Kelly
ZIN Technologies, Inc., Cleveland, Ohio

Kevin McPherson
Glenn Research Center, Cleveland, Ohio

Timothy Reckart
ZIN Technologies, Inc., Cleveland, Ohio

July 2003

The NASA STI Program Office . . . in Profile

Since its founding, NASA has been dedicated to the advancement of aeronautics and space science. The NASA Scientific and Technical Information (STI) Program Office plays a key part in helping NASA maintain this important role.

The NASA STI Program Office is operated by Langley Research Center, the Lead Center for NASA's scientific and technical information. The NASA STI Program Office provides access to the NASA STI Database, the largest collection of aeronautical and space science STI in the world. The Program Office is also NASA's institutional mechanism for disseminating the results of its research and development activities. These results are published by NASA in the NASA STI Report Series, which includes the following report types:

- TECHNICAL PUBLICATION. Reports of completed research or a major significant phase of research that present the results of NASA programs and include extensive data or theoretical analysis. Includes compilations of significant scientific and technical data and information deemed to be of continuing reference value. NASA's counterpart of peer-reviewed formal professional papers but has less stringent limitations on manuscript length and extent of graphic presentations.

- TECHNICAL MEMORANDUM. Scientific and technical findings that are preliminary or of specialized interest, e.g., quick release reports, working papers, and bibliographies that contain minimal annotation. Does not contain extensive analysis.

- CONTRACTOR REPORT. Scientific and technical findings by NASA-sponsored contractors and grantees.

- CONFERENCE PUBLICATION. Collected papers from scientific and technical conferences, symposia, seminars, or other meetings sponsored or cosponsored by NASA.

- SPECIAL PUBLICATION. Scientific, technical, or historical information from NASA programs, projects, and missions, often concerned with subjects having substantial public interest.

- TECHNICAL TRANSLATION. English-language translations of foreign scientific and technical material pertinent to NASA's mission.

Specialized services that complement the STI Program Office's diverse offerings include creating custom thesauri, building customized databases, organizing and publishing research results . . . even providing videos.

For more information about the NASA STI Program Office, see the following:

- Access the NASA STI Program Home Page at ***http://www.sti.nasa.gov***

- E-mail your question via the Internet to help@sti.nasa.gov

- Fax your question to the NASA Access Help Desk at 301–621–0134

- Telephone the NASA Access Help Desk at 301–621–0390

- Write to:
  NASA Access Help Desk
  NASA Center for AeroSpace Information
  7121 Standard Drive
  Hanover, MD 21076

NASA/TM—2003-212460

International Space Station Increment-4/5 Microgravity Environment Summary Report

Kenol Jules
Glenn Research Center, Cleveland, Ohio

Kenneth Hrovat and Eric Kelly
ZIN Technologies, Inc., Cleveland, Ohio

Kevin McPherson
Glenn Research Center, Cleveland, Ohio

Timothy Reckart
ZIN Technologies, Inc., Cleveland, Ohio

National Aeronautics and
Space Administration

Glenn Research Center

July 2003

Acknowledgments

The authors would like to acknowledge a number of people who contributed significantly to this report. Without their contribution, this report would have not been possible. Nissim Lugasy, Ted Wright, and Gene Liberman made significant contributions in the area of software development. The software enabled PIMS to process, analyze, troubleshoot, and display both MAMS and SAMS acceleration data acquired aboard the ISS. We would like also to acknowledge the development efforts of the SAMS-11 team and the MAMS project team at the Glenn Research Center and Canopus Systems, Inc.

Thanks to Jake Fox, Joel Falcon, and Clifton Amberboy (Lockheed Martin) who provided information regarding GASMAP equipment operations and characteristics.

Thanks to John Keller (JSC) and Ted Bartkowicz (Boeing, ISS Loads and Dynamics) for CEVIS and TVIS exercise and other timeline information that proved invaluable for correlation with acceleration measurements.

Thanks to Janelle Fine (University of California at San Diego, Department of Medicine Physiology/NASA Laboratory) for PuFF operations notes from her console logbook.

Thanks to S. Vaughn, B. McDonald, A. Powers, T. Days, M. Lammers, K. Flaherty, Attitude Determination and Control Officer (ADCO) (JSC) team members who provided information and explanations for various ISS attitude maneuvers and events.

Available from

NASA Center for Aerospace Information
7121 Standard Drive
Hanover, MD 21076

National Technical Information Service
5285 Port Royal Road
Springfield, VA 22100

Available electronically at http://gltrs.grc.nasa.gov

Table of Contents

List of Tables

List of Figures

PIMS ISS Increment-4/5 Microgravity Environment Summary Report:
December 2001 to December 2002

1 Introduction

The National Aeronautics and Space Administration (NASA) Office of Biological and Physical Research sponsors science experiments on various reduced-gravity carriers/platforms and facilities such as the Space Transportation System (STS), parabolic flight-path aircraft, sounding rockets, drop towers, and the International Space Station (ISS). To provide support for the science experiments which require acceleration data measurement on the ISS, the Physical Science Division sponsors two microgravity accelerometer systems, the Space Acceleration Measurement System (SAMS) and the Microgravity Acceleration Measurement System (MAMS). SAMS measures vibratory acceleration data in the range of 0.01 to 400 Hz for payloads requiring such measurement. SAMS has multiple, remotely located sensor heads. MAMS consists of two sensors, the Orbital Acceleration Research Experiment (OARE) Sensor Subsystem (OSS) and the High Resolution Accelerometer Package (HiRAP). The OSS is a low frequency range sensor used to characterize the quasi-steady environment for payloads and the ISS vehicle. The OSS measures up to 1 Hz, but is routinely trimmean filtered to yield much lower frequency acceleration data up to 0.01 Hz. The HiRAP is used to characterize the ISS vibratory environment from 0.01 Hz to 100 Hz. Both MAMS and SAMS were flown to the ISS on STS-100, which was launched April 19, 2001 from the Kennedy Space Center (KSC).

The residual acceleration environment of an orbiting spacecraft in a low earth orbit is a complex phenomenon [1]. Many factors, such as experiment operation, life-support systems, crew activities, aerodynamic drag, gravity gradient, rotational effects and the vehicle structural resonance frequencies (structural modes) contribute to form the overall reduced gravity environment. Zero gravity is an ideal state, which cannot be achieved in practice because of the various sources of acceleration present in an orbiting spacecraft. As a result, the environment in which experiments are conducted is *not zero* gravity. Most experiments can be adversely affected by the residual acceleration because of their dependency on acceleration magnitude, frequency, orientation and duration. Therefore, experimenters must know what the environment was when their experiments were performed in order to analyze and correctly interpret the result of their experimental data. In a terrestrial laboratory, where gravity is assumed a constant, researchers are expected to know and record certain parameters such as pressure, temperature, and humidity levels in their laboratory prior to and possibly throughout their experiment. The same holds true in space, where acceleration effects emerge as an important consideration.

The NASA Glenn Research Center (GRC) Principal Investigator Microgravity Services (PIMS) project has the responsibility for processing and archiving acceleration measurements, analyzing these measurements, characterizing the reduced gravity environment in which the measurements were taken, and providing expertise in reduced gravity environment assessment for a variety of carriers/platforms and facilities (such as the Space Shuttle, parabolic flight-path aircraft, sounding rockets, drop towers, and the ISS) in support of the NASA's Physical Science Division Principal Investigators (PIs). The PIMS project supports PIs from the microgravity science disciplines of biotechnology, combustion science, fluid physics, material science and fundamental physics. The PIMS project is funded by the NASA Headquarters and is part of the NASA GRC's Microgravity Environment Program (MEP), which integrates the analysis and interpretation component of

PIMS with the various NASA sponsored acceleration measurement systems. For the ISS, these acceleration measurement systems include SAMS and MAMS. The PIMS project is responsible for receiving, processing, analyzing, displaying, distributing, and archiving the acceleration data for SAMS and MAMS during ISS operations. This report presents to the microgravity scientific community the results of some of the analyses performed by PIMS using the acceleration data measured by the two-accelerometer systems during the period of December 2001 to December 2002 aboard the ISS.

2 International Space Station

2.1 Configuration at Assembly Complete

The ISS represents a global partnership of many nations. This project is an engineering, scientific and technological marvel ushering in a new era of human space exploration. Assembly of the ISS began in late 1998 [2] and is ongoing. During its assembly and over its nominal 10-year lifetime, the ISS will serve as an orbital platform for the United States and its International Partners to make advances in life science, microgravity science, space science, earth science, commercial product development, and engineering research and technology. The completed space station will have six fully equipped laboratories, nearly 40 payload racks [3] or experiment storage facilities in a pressurized environment, and more than 15 external payload locations for conducting experiments in the vacuum of space. The six main laboratories, which will house research facilities, are: the Destiny Module (US), the Centrifuge Accommodations Module (CAM-US), Columbus (European Space Agency (ESA)), Kibo (National Space Development Agency of Japan (NASDA)) and two Russian Research Modules (yet to be named). The pressurized living and working space aboard the completed ISS will be approximately 43,000 ft^3 [4] (Table 2-1). Its giant solar arrays will generate the electricity required to power the laboratories and their complement of experiments. An initial crew of three, possibly increasing to seven when assembly is complete (Figure 2-1), is living aboard the ISS. The space station represents a quantum leap in our ability to conduct research on orbit and explore basic questions in a variety of disciplines [4] such as biomedical, fundamental biology, biotechnology, fluid physics, advanced human support technology, material science, combustion science, fundamental physics, earth science, and space science.

TABLE 2-1 ISS SPECIFICATION AT ASSEMBLY COMPLETE

Wingspan Width	356 feet (108.5 m)
Length	290 feet (88.4 m)
Mass (weight)	About 1 million pounds (453,592 kg)
Operating Altitude	220 nautical miles average (407 km)
Inclination	51.6 degrees to the Equator
Atmosphere inside	14.7 psi (101.36 kilopascals)
Pressurized Volume	43,000 ft^3 (1,218 m^3) in 6 laboratories
Crew Size	3, increasing to 7

2.2 ISS Coordinate Systems

There are a multitude of coordinate frames in use on the station to coordinate activities such as robotics operations, payload operations, and the station's United States (U.S.) Guidance, Navigation, and Control (GNC) software processing. In addition, both U.S. and Russian GNC software use different frames. For the purpose of providing a common standard reference frame, PIMS archives and reports acceleration data to the microgravity scientific community using the ISS United States Orbital Segment (USOS) Analysis, USOS-ISS,

coordinate system (which PIMS refers to as SSA) beginning with the ISS Increment-3 report. This analysis coordinate system is the one used by crew/ground communications on attitudes and is based on the standard Euler angle sequence for station of yaw, then pitch, then roll from a 0,0,0 Local Vertical/Local Horizontal (LVLH) coordinate system.

2.2.1 Integrated Truss Segment S0 Coordinate System

This coordinate system defines the origin, orientation, and sense of the ISS analysis coordinate system. The YZ plane nominally contains the centerline of all four trunnion pins. The origin is defined as the intersection of two diagonal lines connecting the centers of the bases of opposite trunnion pins, running T1 to T3 and from T2 to T4 (Figure 2-3). The X-axis (X_{S0}) is parallel to the vector cross product of the Y-axis with the line from the center of the base trunnion pin T2 to the center of the base trunnion pin T3, and is positive forward. The Y-axis (Y_{S0}) is parallel with the line from the center of the base of trunnion pin T2 to the center of the base of trunnion pin T1. The positive Y-axis is toward starboard. The Z-axis (Z_{S0}) completes the right-handed Cartesian system (RHCS).

2.2.2 USOS Space Station Analysis Coordinate System

The USOS-ISS analysis system (SSA) [5] is derived using the LVLH flight orientation. When defining the relationship between this coordinate system and another, the Euler angle sequence to be used is a yaw, pitch, roll sequence around the Z_A, Y_A, and X_A axes, respectively (Figure 2-2). The Space Station Analysis (SSA) frame is aligned with the Integrated Truss Segment Zero (S0) Coordinate frame, and the origin (Figure 2-3) is located at the geometric center of the Integrated Truss Structure (ITS) S0. The X_A-axis is parallel to the longitudinal axis of the module cluster. The positive X_A-axis is in the forward (flight) direction. The Y_A-axis is identical to the S0 Y_A-axis. The positive Y_A-axis is in the starboard direction. The positive Z_A-axis is in the direction of Nadir (toward earth) and completes the RHCS. This analysis coordinate system is used by PIMS in its analysis and reporting of the acceleration data measured on ISS [5].

2.2.3 Russian Orbital Segment Analysis Coordinate System

The Russian Orbital Segment (ROS) ISS analysis coordinate system is shown in Figure 2-4 [6]. The origin is located at the aft end of the Service Module's widest section. The positive X-axis (X_R) points aft out of the "long" station axis, the positive Y-axis (Y_R) points out the top of the station (zenith), and the positive Z-axis (Z_R) points out of the port truss, as defined by completing the right-handed coordinate system [6]. The ROS Mission Control System (MCS) reports station attitude in this Space Station Analysis Coordinate System.

2.2.4 United States Laboratory Module (Destiny) Coordinate System

The US Laboratory module makes use of a RHCS [5], body-fixed to the pressurized module. The origin is located forward of the pressurized module such that the center of the bases of the aft trunnions have X_{LAB} components nominally equal to 1000 inches. The X_{LAB} -axis is perpendicular to the nominal aft Common Berthing Mechanism (CBM) interface plane and pierces the geometric center of the array of mating bolts at the aft end of the pressurized module. The positive X_{LAB} -axis is toward the pressurized module from the origin. The Y_{LAB} -axis completes the RHCS. The Z_{LAB} -axis is parallel to the perpendicular line from the X_{LAB} -axis to the center base of the keel pin base, and positive in the opposite direction as shown in Figure 2-5.

2.3 ISS Flight Attitude at Assembly Complete

When discussing the attitude of the Space Station, one usually refers to the vehicle as being in an "LVLH" attitude or an X-axis Perpendicular to Orbit Plane ("XPOP") attitude. This implies the Space Station's body axes are being controlled within an attitude envelope about the LVLH or XPOP reference frame. To visualize the station's orientation with respect to the reference frame, one must understand how the body axes are oriented on the Space Station. Body axes are a set of axes that remain fixed to the Space Station and therefore rotate with station rotation. Figure 2-4 shows how the U.S. and ROS GNC system define the station body axes.

The basic flight attitude [7] for ISS is called X body axis toward the Velocity Vector (XVV) Z Nadir Torque Equilibrium Attitude (TEA), or XVV TEA for short. XVV Z Nadir (XVV for short) stands for X body axis toward the velocity vector, Z body axis toward Nadir (earth), and TEA is for torque equilibrium attitude. The ISS vehicle design is optimized for the XVV attitude (Figure 2-6). The XVV attitude places the most modules in the microgravity volume; supports altitude reboosts, services vehicle dockings, and minimizes aerodynamic drag. The ISS is designed to tolerate deviations from perfect XVV Z Nadir of +/- 15 degrees in each axis. This envelope was expanded to -20 degrees in pitch.

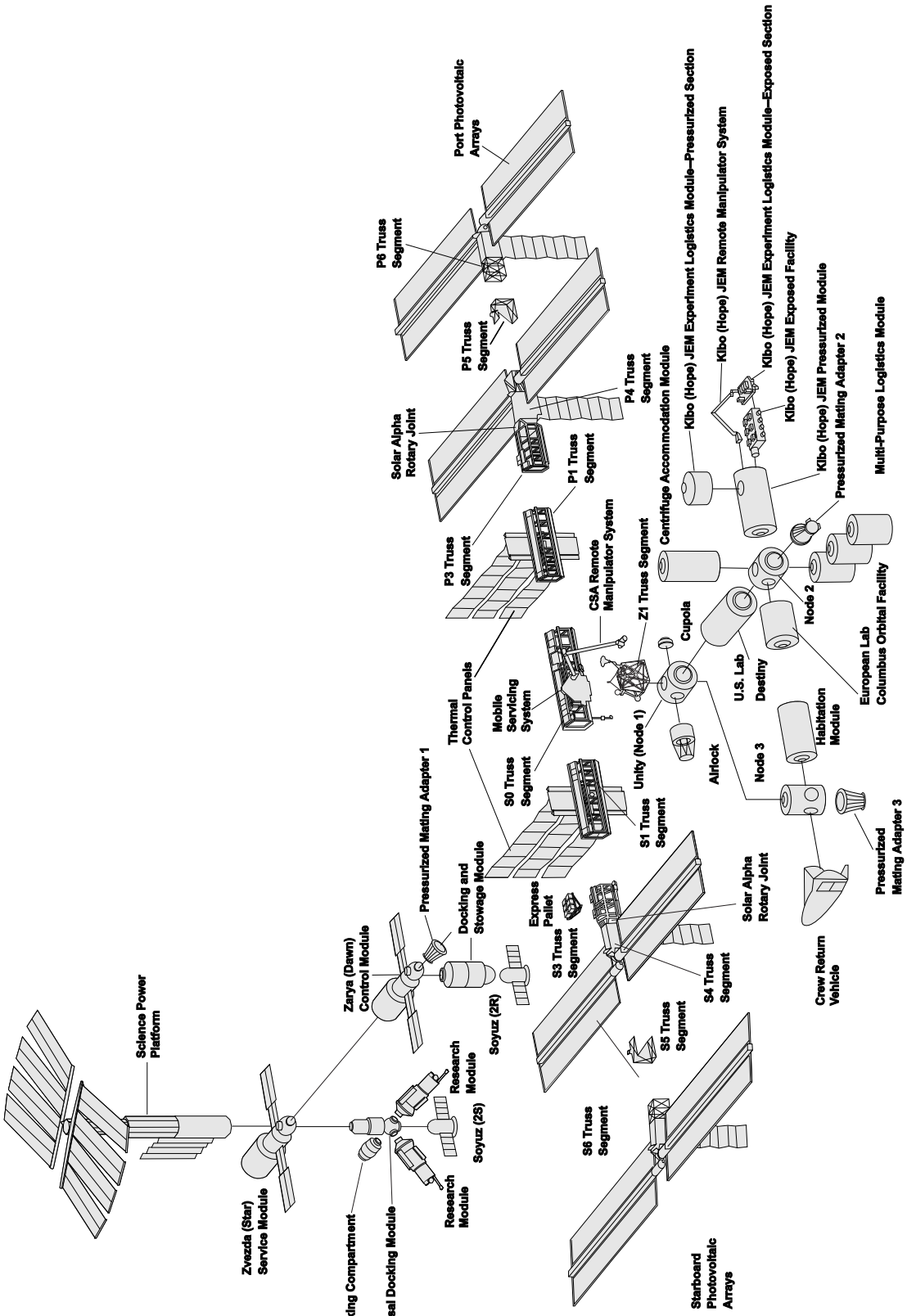

Figure 2-1 International Space Station at Assembly Complete

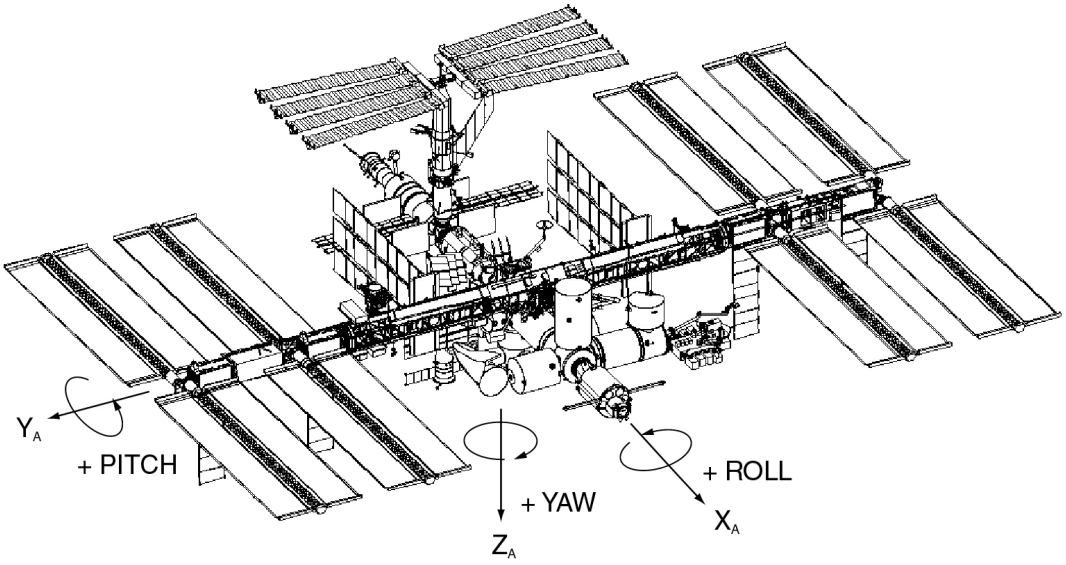

Figure 2-2 Space Station Analysis Coordinate System

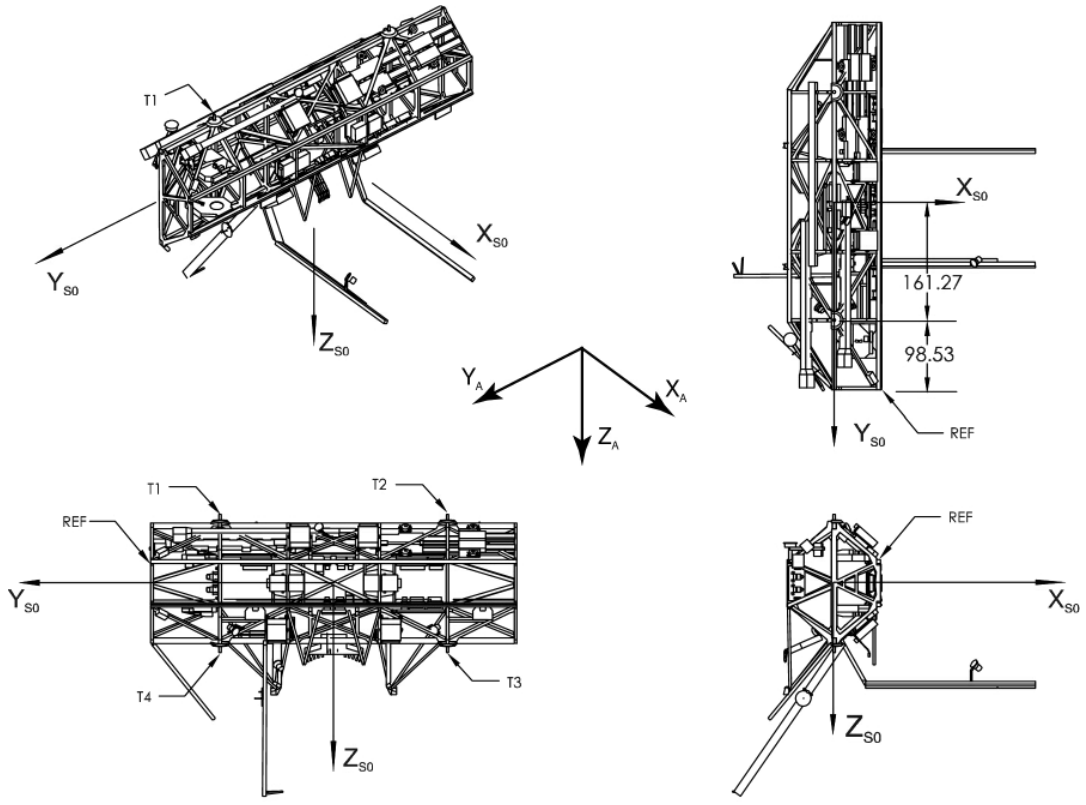

Figure 2-3 Integrated Truss Segment S0 Coordinate System

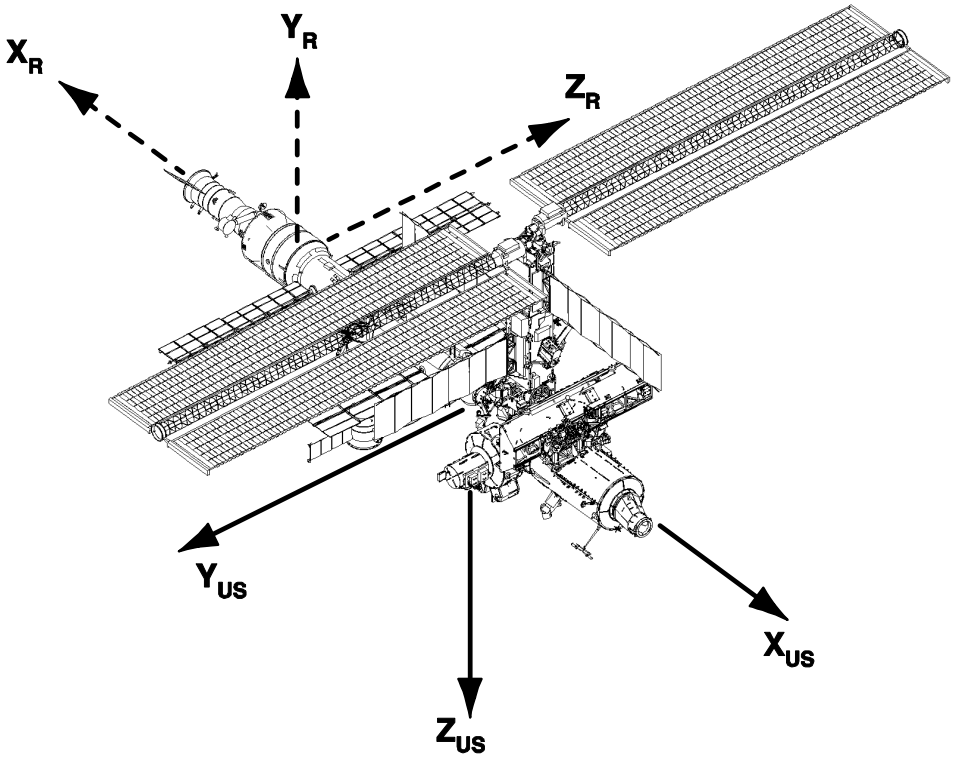

Figure 2-4 ISS-USOS / ROS Analysis Coordinate Systems

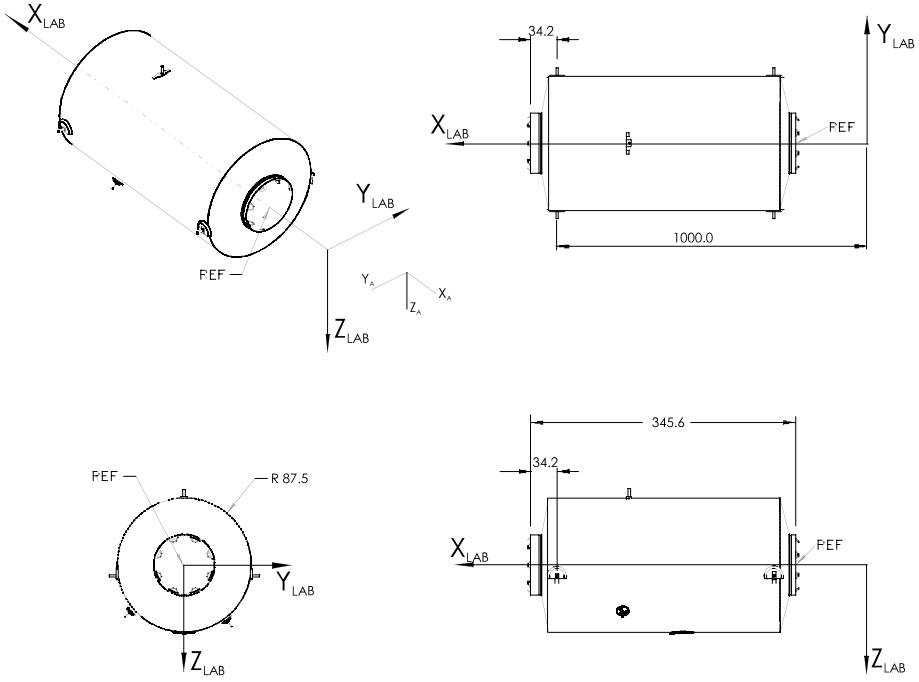

Figure 2-5 United States Laboratory Module (Destiny) Coordinate System

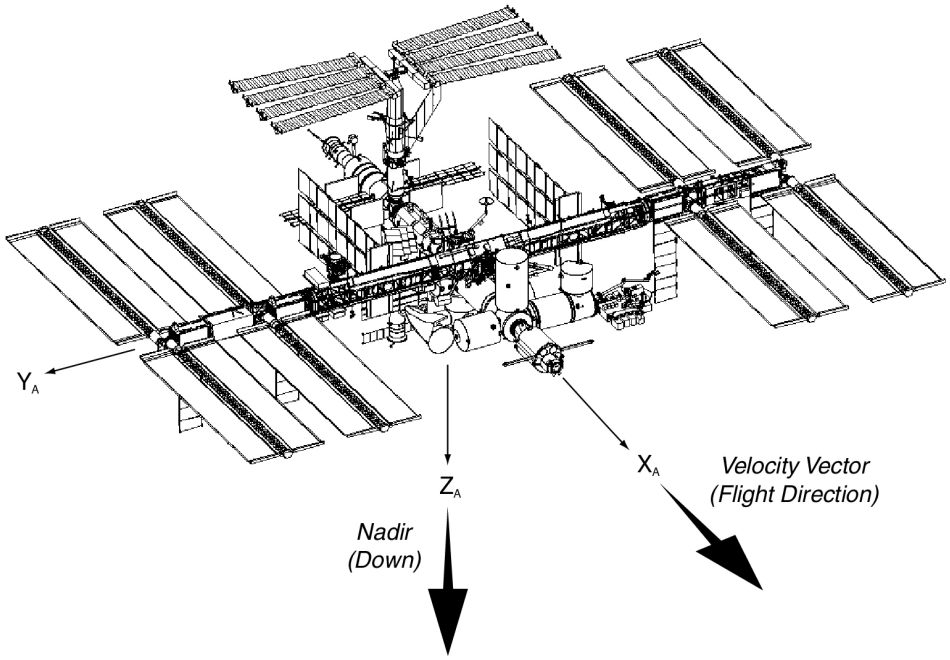

Figure 2-6 ISS XVV Flight Attitude

3 ISS Increment-4/5

An increment should average about 4 months (sometimes more--- Increment-4 lasted about 6 months) and is determined by crew rotations and flights to/from ISS. Each increment has a theme that focuses on the primary science or activities to be performed.

3.1 Increment-4 Configuration

This increment is called Increment-4 or Expedition Four and its theme is: Plants in Space [8]. The 3-member crew for Increment-4 was launched to ISS on December 5, 2001 on STS-108 from KSC and returned to earth on STS-111 on June 19, 2002 after a 196-day stay in space. During Increment-4, the Starboard Truss Segment 0 (S0) (13.2 meter-long, 4.6 meter-high, 1.83 meter-wide and weight of 12624 kg.) was delivered by STS-110 on April 10, 2002 to ISS. Two crewmembers of STS-110 performed four spacewalks and used the Shuttle and station robotic arms to install and outfit the S0 to the station. The S0 truss is the first of 11 such truss structures that will make up the station's external framework that will expand the ISS to 109 meters [9]. The S0 truss will support, among other things, four virtually identical solar wing assemblies [10]. The following modules are now on-orbit [11]: Unity (Node), Zarya (Functional Cargo Block), Zvezda (Service Module), Destiny, the Russian Docking Compartment (DC-1 (Pirs)) and the Joint Airlock (Quest) (Figure 3-1).

Table 3-1 is a list of missions to the ISS during Increment-4 [12]:

TABLE 3-1 INCREMENT-4 MISSIONS

Mission	Date	Mission Objective
UF-1 – STS-108	December 7-15, 2001	STS-108 docked with ISS and swapped crew: arrival of Expedition Four to ISS
6P – Progress	March 19, 2002	Undocking of Progress supply craft
7P – Progress	March 24, 2002	Docking of Progress supply craft
8A – STS-110	April 10-17, 2002	Space Shuttle Atlantis delivered the 43-foot-long S0 (S-zero) Truss to ISS
Soyuz 3S	April 20, 2002	"Old" Soyuz taxi vehicle at ISS is relocated
Soyuz 4S	April 27, 2002	"New" Soyuz taxi vehicle docked with ISS
Soyuz 3S	May 5, 2002	"Old" Soyuz taxi vehicle undocked
UF-2 – STS-111	June 7-15, 2002	STS-111 docked with ISS and swapped crew: arrival of Expedition Five to ISS

3.2 Increment-4 Science and Crew Members

During Increment-4 (Expedition Four), the crew worked with several experiments. The Increment-4 primary focus was the effects of plant growth during extended stays in space and how such phenomenon may relate to similar conditions on earth. Additional experiments during Expedition Four were intended to lead to new insights in the fields of embryo development, the long-term effects of spaceflight on humans, biotechnology, medicine, agriculture, electronics and pharmaceutical manufacturing. Several experiments begun on earlier expeditions were returned to earth, while several others continued operating during the Expedition Four's stay aboard ISS [10]. The three Expedition Four crewmembers

devoted nearly 500 hours to research during their stay aboard ISS [10]. The Increment-4 commander was cosmonaut Yury Ivanovich Onufrienko and the flight engineers were astronauts Daniel W. Bursch and Carl E. Walz.

3.3 Increment-5 Configuration

This Increment was called Increment-5 or Expedition Five and its theme was: From Molecules to Matter—Using Space To Prove The Forces That Structure Our World [8]. The 3-member crew for Increment-5 mission was launched to ISS on June 5, 2002 on STS-111 from KSC and returned to earth on STS-113 on December 7, 2002 after a 185-day stay in space. During STS-111 joint operations with the ISS, the Mobile Base System (MBS) was delivered and permanently installed onto the station. Also, the replacement of a wrist roll joint on the station's robotic arm was performed. The MBS measures about 5.7 by 4.5 by 2.9 meters. Its mass is about 1,500 kg. Its mass handling transportation capacity is about 20,900 kg [13]. During STS-112 joint operations (flight 9A — October 9 to October 16, 2002), the First right-side (starboard) Truss segment (Integrated Truss Structure (ITS) S1) with the additional cooling radiators and the Crew and Equipment Translation Aid (CETA) Cart A were delivered and installed to ISS (the cooling radiators were delivered, but will remain stowed until flight 12A.1). The CETA cart can be used by space walkers to move equipment along the truss. The S1 Truss was attached to the central truss segment, the S0 Truss (the starboard end of the S0). The S1 truss segment (13.7 meters long, 4.57 meters high, 1.83 meters wide and weight of 12598 kg.) is the second part of the station's ITS, joining the S0 Truss, which is the center of the ITS. It will support four virtually identical solar array assemblies, including the one now atop the P6 Truss of the ISS, along with radiators to cool the station. Finally, during STS-113 joint operations (flight 11A — November 25 to December 2, 2002), the First left-side (portside) Truss segment (ITS P1) and the CETA Cart B and cooling radiators were delivered and installed to ISS (the cooling radiators will be installed during flight 12A.1. The P1, which is primarily an aluminum structure, similar to the S0 and S1 truss structures, measures 13.7 meters long, 4.57 meters high, 1.83 meter wide and weighs 14, 032 kg. [13]. These two additional truss (S1 and P1) elements continue the build-up of the backbone of the ISS. They will support solar arrays, cooling radiators, a railroad capable of moving the station's Canadarm2 along its length, and other equipment.

Table 3-2 [13] shows the specifications for the three trusses installed during Increments 4 and 5 on ISS, while Table 3-3 lists the missions to the ISS during Increment-5 crew's stay aboard the station [14]:

TABLE 3-2 SPECIFICATION FOR S0, S1, AND P1 TRUSSES

Specifications	S0	S1	P1
Length: meter/ft.	13.2 / 43.3	13.7 / 45	13.7 / 45
Height: meter/ft.	4.57 / 15	4.57 / 15	4.57 / 15
Width: meter/ft.	1.83 / 6	1.83 / 6	1.83 / 6
Weight: kg/lb	12624 / 27,830	12598 / 27,717	14032 / 30,871
Flight Mission	STS-110	STS-112	STS-113

TABLE 3-3 INCREMENT-5 MISSIONS

Mission	Date	Mission Objective
UF-2 – STS-111	June 7-15, 2002	STS-111 docked with ISS and swapped crew: arrival of Expedition Five to ISS; delivery and installation of the Mobile Remote Servicer Base System (MBS); replacement of a wrist roll joint on the station's robotic arm
7P – Progress	June 25, 2002	Undocking of Progress supply craft
8P – Progress	June 29, 2002	Docking of Progress supply craft
8P – Progress	September 24, 2002	Undocking of Progress supply craft
9P – Progress	September 29, 2002	Docking of Progress supply craft
9A – STS-112	October 9-16, 2002	Delivery of the First right-side Truss segment (ITS S1) with radiators; Crew and Equipment Translation Aid (CETA) Cart A
Soyuz 5S	November 1, 2002	"New" Soyuz taxi vehicle docked with ISS
Soyuz 4S	November 9, 2002	"Old" Soyuz taxi vehicle undocked
11A – STS-113	Nov. 25-Dec. 2, 2002	STS-113 docked with ISS and swapped crew: arrival of Expedition Six to ISS; delivery of First left-side Truss segment (ITS P1) and cooling radiators; Crew and Equipment Translation Aid (CETA) Cart B

3.4 Increment-5 Science and Crew Members

During Increment-5 (Expedition Five), the crew worked with several experiments. The Increment-5 primary focus was on using space to prove the forces that structure our world. Additional experiments during Expedition Five were intended to contribute to human knowledge in the fields of materials, plant science, commercial biotechnology, and the long-term effects of spaceflight on humans. Several experiments begun on earlier expeditions were returned to earth, while several others continued operating during the Expedition Five's stay aboard ISS [15]. When Expedition Five arrived to the station, more than 70,000 hours of scientific experiments had been logged by research facilities aboard ISS [15]. The three Expedition Five crewmembers devoted approximately 420 hours to research during their stay aboard ISS. Those 420 or so hours brought the total of crew research time to about 1150 hours since continuous human presence began on the orbiting laboratory in November 2000 [15]. Increment-5 commander was cosmonaut Valery Korzun, assisted by flight engineers Astronaut Peggy Whitson and cosmonaut Sergei Treschev. The crew was launched to ISS on June 5, 2002 aboard the Space Shuttle Endeavour STS-111 and returned to KSC on December 7, 2002 aboard STS-113.

3.5 Increment-4/5 Coordinate Systems

The coordinate systems [16] shown in Figure 3-2 were used in performing the data analysis presented in this report. Figure 3-2 shows MAMS OSS and MAMS HiRAP positive acceleration axes alignment relative to the ISS analysis coordinate system (for SAMS, see section 4.4). However, the origin of the coordinate systems shown is not exactly at the location shown (except for the ISS analysis coordinate system). They are shown here for relative alignment only, not their origin. For their location relative to the ISS analysis coordinate system, the reader should refer to section 4.2. In Figure 3-2, XYZ_A refers to the ISS analysis coordinate system, XYZ_H refers to the MAMS HiRAP coordinate system,

XYZ_{OSS} refers to the MAMS OSS coordinate system. Figure 3-2 is provided only to illustrate the relative orientations between coordinate systems during Increment-4/5.

3.6 Increment-4/5 Overall Attitude

During the assembly stages (stages 2A through 12A.1), the ISS will not be capable of generating enough power to sustain the required electrical loads in the XVV flight attitude at mid-to-high solar beta angles because these vehicle configurations have only a single solar array gimbal axis, which is aligned so that it only perfectly tracks the Sun when the solar beta angle is near zero (see Figure 3-3). Therefore, the ISS is designed to accommodate a second basic flight orientation for these increments. This attitude is referred to as X Principal Axis Perpendicular to the Orbit Plane (XPOP) (see Figure 3-3), Z Nadir at orbital noon. The XPOP flight attitude [7] sets up geometry between the ISS and the Sun so that the Sun aligns with the ISS/XZ body axis plane. This allows all the solar arrays to track the Sun regardless of the solar beta angle. XPOP also places the dominant inertia axis in the local horizontal to minimize gravity gradient torques and allow Control Moment Gyro (CMG) non-propulsive attitude control.

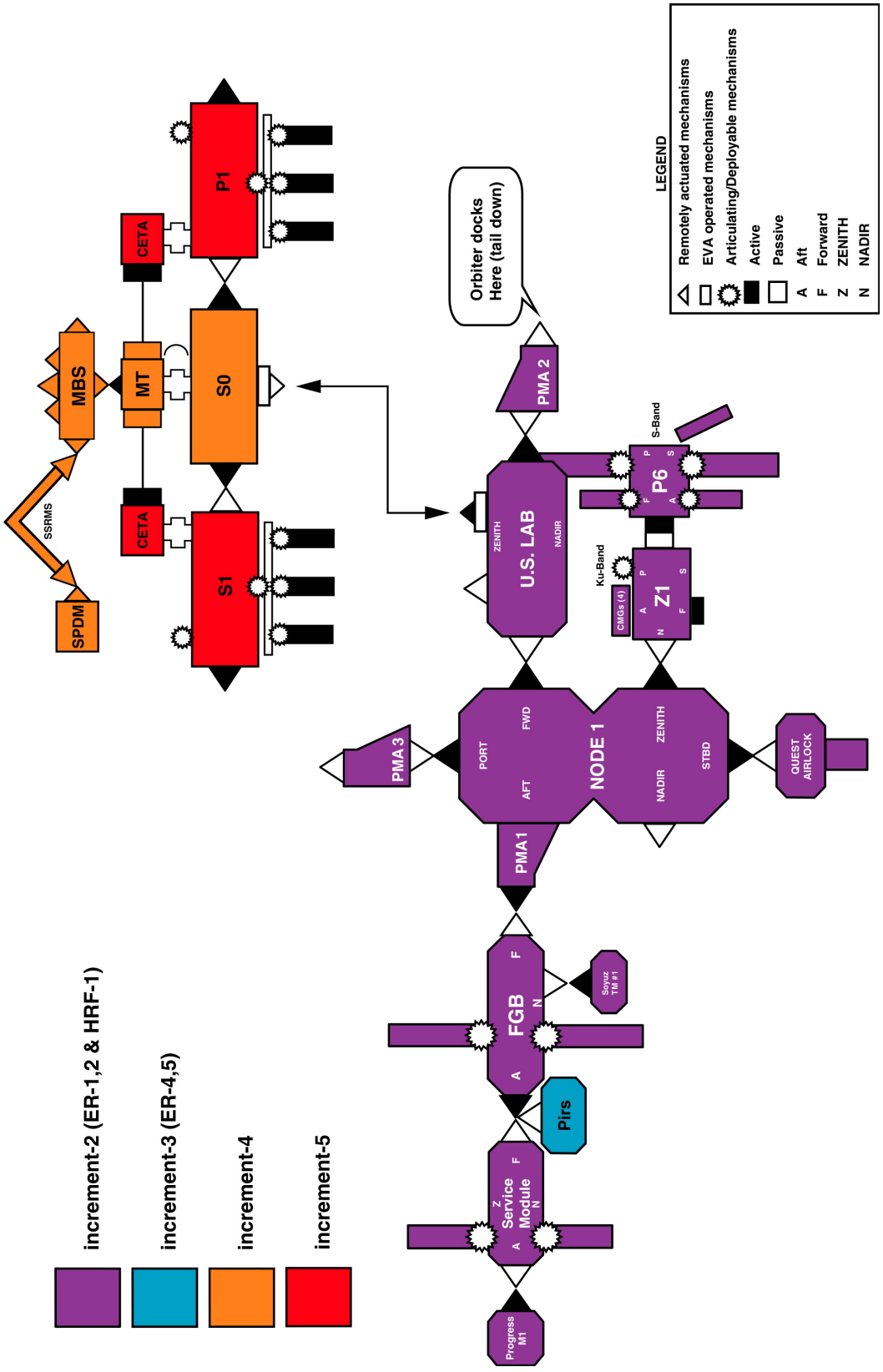

Figure 3-1 ISS Increment-4/5 Configuration

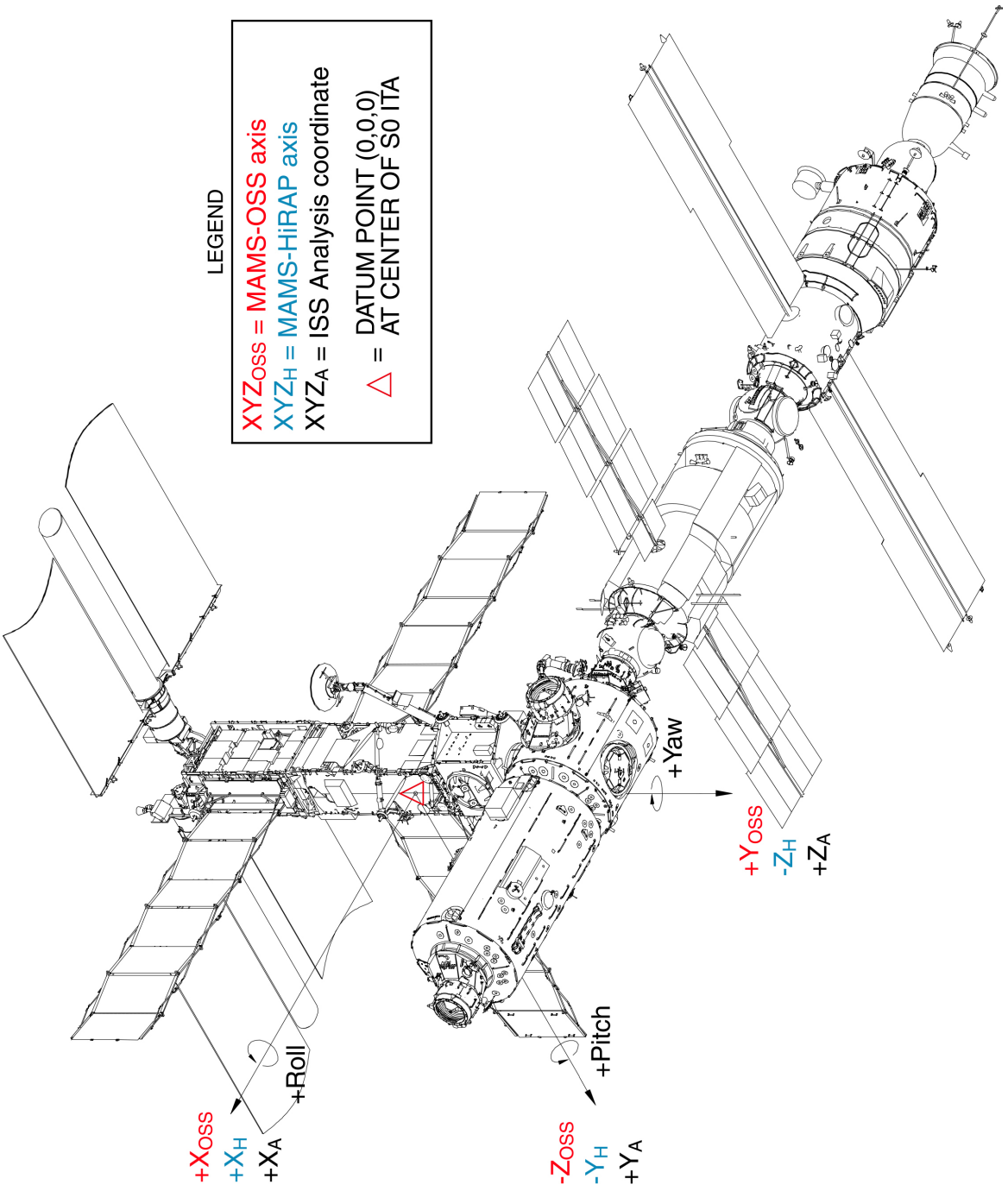

Figure 3-2 MAMS orientation relative to ISS-USOS Analysis Coordinate System.

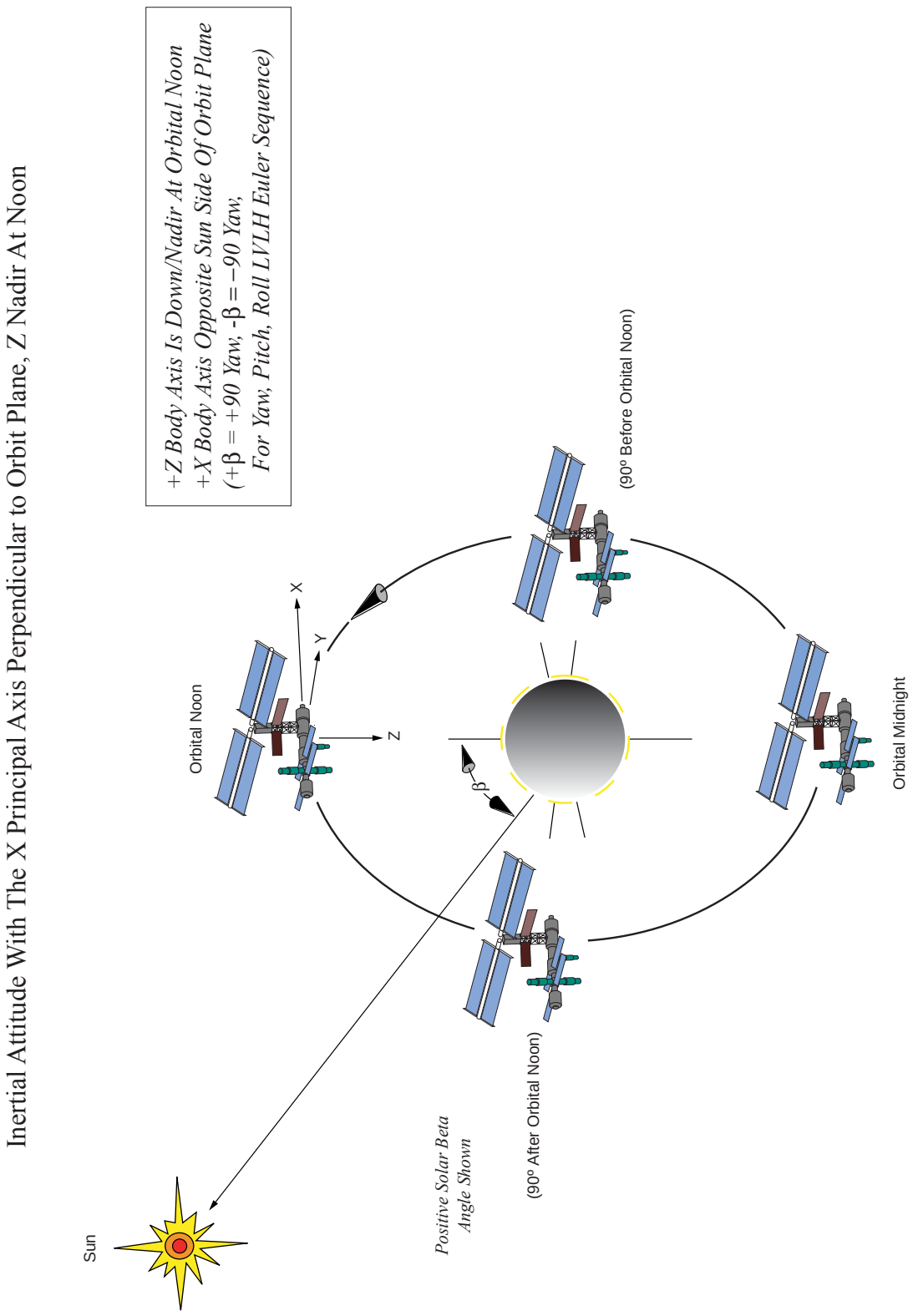

Figure 3-3 ISS in the XPOP Inertial Flight Attitude

4 Acceleration Measurement System Descriptions: Increment-4/5

One of the major goals of the ISS is to provide a quiescent reduced gravity environment to perform fundamental scientific research. However, small disturbances aboard the Space Station impact the overall environment in which experiments are being performed. Such small disturbances need to be measured in order to assess their potential impact on experiments. Two accelerometer systems, SAMS and MAMS, developed by NASA's GRC in Cleveland, Ohio, are being used aboard the station to acquire such measurements.

4.1 Microgravity Acceleration Measurement System (MAMS)

MAMS consists of two sensors. MAMS OSS, a low frequency sensor, is used to characterize the quasi-steady environment for payloads and the vehicle. MAMS OSS measures acceleration caused by aerodynamic drag, vehicle rotations, and vents of air and water. The raw MAMS OSS data are typically trimmean filtered to extract the quasi-steady acceleration data content. PIMS reports to the microgravity scientific community only the results of the MAMS-OSS trimmean filter data (0.01 Hz and below) for the quasi-steady regime. Details of the trimmean filter process and the exact implementation of it relative to MAMS OSS data are described in Appendix E.2. MAMS HiRAP [17] is used to characterize the ISS vibratory environment up to 100 Hz. For Increment-4/5, MAMS was located in a double middeck locker in the US Laboratory Module (Destiny) in the Expedite the Processing of Experiments to the Space Station (EXPRESS) Rack 1.

4.2 MAMS Coordinate Systems

MAMS was located in middeck lockers 3 and 4 of EXPRESS Rack 1, in overhead bay 2 of the US Laboratory Module (LAB1O2). The origin of the OSS coordinate system is located at the center of gravity of the OSS proof mass. Table 4-1 gives the orientation and location of the OSS and HiRAP coordinate systems with respect to USOS-ISS analysis coordinate system.

TABLE 4-1 MAMS SENSOR COORDINATE SYSTEM

MAMS Sensor	Location (inches)			Orientation (degrees)			Unit Vector in Analysis Coordinates			
	X_A	Y_A	Z_A	Roll	Pitch	Yaw	Axes	X_A	Y_A	Z_A
OSS	135.28	-10.68	132.12	90	0	0	X_{OSS}	1	0	0
							Y_{OSS}	0	0	1
							Z_{OSS}	0	-1	0
HiRAP	138.68	-16.18	142.35	180	0	0	X_H	1	0	0
							Y_H	0	-1	0
							Z_H	0	0	-1

4.3 Space Acceleration Measurement System (SAMS)

SAMS measures accelerations caused by vehicle, crew, and experiment disturbances. SAMS measures the vibratory/transient accelerations which occur in the frequency range of 0.01 to 400 Hz. For Increment-4, there were five SAMS sensor heads located in the EXPRESS Racks 1 and 2. However, prior to the visit of STS-110 to ISS, one head (121f06) was deactivated and stowed. For Increment-5, another head was deployed, 121f08, in support of the Microgravity Science Glovebox (MSG) rack. During Increment-5, 121f08 supported the Solidification Using a Baffle in Sealed Ampoules (SUBSA) experiment, the Pore Formation and Mobility During Controlled Directional Solidification in a Microgravity Environment Investigation (PFMI), as well as preliminary characterization of the MSG rack.

The sensors measure the accelerations electronically and transmit the data to the Interim Control Unit (ICU) located in the EXPRESS Rack drawer. Data is collected from all the sensors and downlinked to the Telescience Support Center (TSC) at GRC. Additional SAMS data flow details are provided in Appendix D. The PIMS project processes, and displays the data on the PIMS Web site for easy access by the microgravity scientific community at:

http://pims.grc.nasa.gov

4.4 SAMS Coordinate Systems

During Increment-4/5, SAMS Sensor Enclosure (SE) heads 121f02 through 121f06 and SE 121f08 were active (121f06 was deactivated and stowed prior to STS-110 visit to ISS during Increment-4 and 121f08 was activated during Increment-5 – see section 4.3). Each sensor head has a defined coordinate system whose location and orientation is with respect to USOS-ISS analysis coordinate system. The origin is defined as the triaxial center point of the three accelerometers that comprise the sensor head.

SAMS SE 121f02 was mounted in the SAMS ISIS drawer 1 in EXPRESS Rack 1. SAMS SE heads 121f03, 121f04 and 121f05 were installed in support of Active Rack Isolation System ISS Characterization Experiment (ARIS-ICE) activities. Head 121f03 was mounted on the lower Z Panel assembly below EXPRESS Rack 2, head 121f04 was mounted on the lower Z Panel assembly below EXPRESS Rack 1, and head 121f05 was mounted on a bracket around the upper Z Panel light assembly of EXPRESS Rack 2. SAMS SE 121f06 was mounted on the front panel of the EXPeriment of Physics of Colloids in Space (EXPPCS) test section on EXPRESS Rack 2 and SAMS SE 121f08 was mounted inside the MSG rack on the left back side of the ceiling plate. Table 4-2 summarizes the SAMS SE coordinate systems.

TABLE 4-2 SAMS SE COORDINATE SYSTEMS

Sensor	Location (inches)			Orientation (degrees)			Unit Vector in Analysis Coordinates			
	X_A	Y_A	Z_A	Roll	Pitch	Yaw	Axes	X_A	Y_A	Z_A
121f02	128.73	-23.53	144.15	-90	0	-90	X_{F02}	0	-1	0
							Y_{F02}	0	0	-1
							Z_{F02}	1	0	0
121f03	191.54	-40.54	135.25	0	30	-90	X_{F03}	0	-.866	-.500
							Y_{F03}	1	0	0
							Z_{F03}	0	-.5	.866
121f04	149.54	-40.54	135.25	0	30	-90	X_{F04}	0	-.866	-.500
							Y_{F04}	1	0	0
							Z_{F04}	0	-.5	.866
121f05	185.17	38.55	149.93	90	0	90	X_{F05}	0	1	0
							Y_{F05}	0	0	1
							Z_{F05}	1	0	0
121f06	179.90	-6.44	145.55	180	90	0	X_{F06}	0	0	-1
							Y_{F06}	0	-1	0
							Z_{F06}	-1	0	0
121f08	115.21	53.41	160.98	-90	-90	0	X_{F08}	0	0	-1
							Y_{F08}	-1	0	0
							Z_{F08}	0	1	0

5 ISS Facilities during Increment-4/5

5.1 Increment-4 Facilities

For Increment-4, one facility was added to the ISS: the Advanced Thermoelectric Refrigerator/Freezer (ARCTIC). ARCTIC-1 is the first permanent sample refrigerator/freezer installed on ISS and is the main cold storage facility until larger, more complex facilities, such as the Minus Eighty-degree-Celsius Freezer for ISS (MELFI) and the Refrigerator/Freezer Rack, become available. The unit provides cold storage for a range of perishable biomaterials and reagents [18]. ARCTIC-1 is installed in EXPRESS Rack 4. Research facilities that were launched to the ISS during prior increments, such as EXPRESS Racks 1, 2, 4 and 5, the Cellular Biotechnology Operations Support System (CBOSS), and Human Research Facility (HRF) continue to support existing and new experiments. Utilities provided to experiments by the four EXPRESS racks currently on the ISS include power, fluids, gasses, cooling, and data management support. Over the life of the Space Station, these facilities will support a wide range of experiments [19]. During Increment-4, the PIMS project supported EXPRESS Racks 1 and 2.

The EXPRESS Rack [20] is a standardized payload rack system that transports, stores, and supports experiments aboard ISS. The EXPRESS Rack system supports science payloads in several disciplines, including biology, chemistry, physics, ecology, and medicine. The EXPRESS Rack with its standardized interfaces enables quick, simple integration of multiple payloads aboard the station. Each EXPRESS Rack is housed in an International Standard Payload Rack – a refrigerator-size container that acts as the EXPRESS Rack's exterior shell—and can be divided into segments. The EXPRESS Racks [21] have eight middeck locker locations and two drawer locations each (Figure 5-1, Figure 5-2). Figure 5-3 illustrates the relative locations of each EXPRESS rack within the US laboratory volume.

5.2 Increment-5 Facilities

For Increment-5, three facilities were added to the growing list of facilities on ISS: ARCTIC-2, EXPRESS Rack 3, and MSG. With the arrival of ARCTIC-2 to the ISS, the two units (ARCTIC 1 and 2) provide a total of 38 liters of minus 20-degree cold aboard stowage [22]. Like EXPRESS Rack 2, EXPRESS Rack 3 is equipped with the Active Rack Isolation System (ARIS)--- a system that isolates the entire rack (and all the experiments being performed inside that specific rack) within a certain frequency band from vibrational disturbances present within the ISS microgravity environment. EXPRESS Rack 3 weighs 1,345 pounds. The empty weight of each EXPRESS rack is about 785 pounds [13]. The MSG—a sealed container with built-in gloves—provides an enclosed work space for investigations conducted in the unique, low-gravity environment created as ISS orbits earth [23]. MSG is designed to accommodate small and medium-sized investigations from many disciplines including biotechnology, combustion science, fluid physics, fundamental physics and materials science. The part of the unit that holds experiment equipment is called the work volume and has a usable volume of about 67 gallons (255 liters) [23]. An airlock under

the work volume can be accessed to bring objects safely into the work volume, while other activities are going on inside the glovebox. The glovebox has side ports, 16 inches (40 centimeters) in diameter, for setting up and manipulating equipment inside the box. The ports are equipped with rugged gloves that can be sealed tightly to prevent leaks. The glovebox provides vacuum, venting and gaseous nitrogen, and power and data interfaces to investigations. The MSG occupies an entire rack inside the Destiny lab and is more than twice as large as gloveboxes flown previously on the Space Shuttle. MSG is designed to support station investigations for the next 10 years [23]. During this increment, in addition to EXPRESS Racks 1 and 2, PIMS supported MSG and HRF. The Increment-5 facilities are listed in Table 5-1 [24].

TABLE 5-1 ISS INCREMENT-5 FACILITIES

Facility	Mission Information	Duration	Location on ISS	Research Area
EXPRESS Racks 1 and 2	Up on 6A	Permanent	Destiny lab module	Multi-disciplinary
EXPRESS Racks 4 and 5	Up on 7A.1	Permanent	Destiny lab module	Multi-disciplinary
Human Research Facility Rack 1	Up on 5A.1	Permanent	Destiny lab module	Human life sciences
EXPRESS Rack 3	Up on UF-2	Permanent	Destiny lab module	Multi-disciplinary
Microgravity Science Glovebox	Up on UF-2	Permanent	Destiny lab module	Multi-disciplinary
ARCTIC 1 and 2	1- Up on 8A 2- Up on UF-2	Permanent	EXPRESS Rack 4	Multi-disciplinary

5.3 Increment-4/5 Experiments Supported by PIMS

During Increment-4, new experiments and science facilities were ferried to ISS. The research complement grew from 18 to 26 NASA payloads, seven of them new to the ISS program. Of the 26, two were in fundamental biology, seven in human life sciences, six in microgravity science, six in space product development, and five were sponsored by the Office of Space Flight [10]. For Increment-4, the PIMS project actively supported the following experiments, which require acceleration data measurements to assess the impact of the ISS reduced gravity environment on the science: ARIS-ICE and EXPPCS.

During Increment-5, new experiments and three new facilities were ferried to ISS. The research complement included 24 new and continuing investigations—10 human life sciences studies, six in microgravity, five in space product development, and three sponsored by the Office of Space Flight [15]. For Increment-5, the PIMS project actively supported the PFMI and the SUBSA investigations. Both experiments were performed in the MSG facility. In addition to these two experiments, acceleration data measurement support was provided to the experiments conducted in EXPRESS Racks 1 and 2.

In addition to these experiments supported by PIMS, the PIMS project continues to characterize the reduced gravity environment of the ISS in an uninterrupted manner from increment to increment so that both current and future investigators can assess the impact of

the ISS reduced gravity environment on their experiments based on the analysis performed and distributed by PIMS using the two set of accelerometers aboard the ISS. It is hoped that future investigators will take such potential impact into account when designing their experiment scheduled to be performed aboard ISS. Table 5-2 shows the experiments that were performed by the Increment-4 crew [10] in the USOS-ISS, while Table 5-3 shows the ones performed in the ROS-ISS [10]. Table 5-4 shows the experiments performed by Increment-5 crew in the USOS-ISS [15], while Table 5-5 shows the ones performed in the ROS-ISS by the same crew [15].

TABLE 5-2 USOS ISS INCREMENT-4 PAYLOAD COMPLEMENT

Facility/Experiment	Mission information	Duration	Location on ISS	Research Area
Active Rack Isolation System	Mission 6A STS-100 and UF-2, STS-111	15 years	EXPRESS Racks 2 and 3; Destiny module	
EXPRESS Racks 1, 2, 3, 4, 5	Mission 6A STS-100; 7A.1 STS-105; UF-2, STS-111	15 years	Destiny module	Multidisciplinary
Human Research Facility	Mission 5A.1 STS-102	15 years	Destiny module	Human Life sciences
Payload Equipment Restraint System	Mission 5A.1 STS-102	15 years	Destiny module	
Bonner Ball Neutron Detector Radiation	Mission 5A.1 STS-102	8 months	Destiny module	Human Life Sciences —Radiation
Crew Earth Observation	Mission 4A STS-97	15 years	Destiny and Zvezda modules	Space Flight Utilization Earth observation
Earth Knowledge Acquired by Middle Schools (EarthKAM)	Mission 5A STS-98	15 years	Russian Service Module window	Space Flight Utilization—Earth observation and outreach
Hoffman-Reflex	Mission 5A.1 STS-102	Approx. 1 year (Expeditions 2-4)	Human Research Facility Rack Destiny module	Human Life Sciences--- Neurovestibular
Crew Interactions	Mission 7A.1 STS-105	28 months (Expeditions 2-6)	Human Research Facility Rack Destiny module	Human Life Sciences— Psychosocial
ARIS-ISS Characterization	Mission 6A STS-100	Approx. 10 months	Active Rack Isolation	Space Flight Utilization
Microgravity Acceleration Measurement System (MAMS)	Mission 6A STS-100	15 years	EXPRESS Rack 1 Destiny module	Physical Sciences— Environmental
Physics of Colloids in Space (EXPPCS)	Mission 6A STS-100	1 year (return on mission UF2 STS-111)	EXPRESS Rack 2 Destiny module	Physical Sciences— Fluids science
Space Acceleration Measurement System II (SAMS-II)	Mission 6A STS-100	15 years	Destiny module	Physical Sciences— Environmental
Sub-regional Assessment of Bone Loss in Axial Skeleton (Sub-regional Bone	Mission 5A.1 STS-102	2 years, 4 months (assigned to Exp. 2-6)	N/A—Preflight and post-flight data collection only	Human Life Sciences— Bone and muscle
Cellular Biotechnology Operations Support System	Mission 7A.1 STS-105	4 months (returns on STS-108, UF-1)	Mid-deck locker in EXPRESS Rack 4	Cell & tissue growth, cellular biotech research
Dynamically Controlled Protein Crystal Growth	Mission 7A.1 STS-105	4 months (return on STS-108, UF-1)	EXPRESS Rack 1 Destiny module	Physical Sciences— Protein crystallization
Renal Stone Investigation	Mission 7A.1 STS-105	40 months (Expeditions 3-12)	N/A—pre and post mission only	Human Life Sciences
Materials International Space Station Experiment	Mission 7A.1 STS-105	Approx. 1 year	Outside airlock between PMA1 and Destiny	Physical Sciences
Xenon 1	Mission 7A.1 STS-105	Approx. 16 months (Expeditions 3-6)	N/A pre-and post-flight	Human Life Sciences
Pulmonary Function in Flight	Mission 7A.1 STS-105	Approx. 1 year (Expeditions 3-6)	Human Rack Facility, Destiny module	Human Life Sciences

Table 5-2, Continued from previous page

Astronauts in EVA Radiation Study (EVARM)	Up on UF-1 Down on ULF-1	Expedition Four Through Six	U.S spacesuits during EVA operation	Human life sciences
Protein Crystal Growth-Enhanced Gaseous Nitrogen (PCG-EGN) Dewar	Up on 8A Down on UF-2	2 months	FGB	Microgravity biotechnology
Protein Crystal Growth-single Thermal Enclosure (PCG-STES) 007 Diffusion-controlled Crystallization Apparatus for Microgravity (DCAM) and PCG-STES 008 Protein Crystallization Apparatus for Microgravity (PCAM)	Up on UF-1 Down on 8A	4 months	EXPRESS Rack 4 / Destiny module	Microgravity biotechnology
Cellular Biotechnology Operations Support System	Up on 7A.1 & UF-1 Down on UF-1 & 8A	3 months	BTR1-EXPRESS Rack 4 / Destiny	Cell Science
Cell Biotechnology Operations Support Systems (CBOSS)			EXPRESS Rack 4 / Destiny	
Advanced Astroculture (ADVASC) 02	Up on UF-1 Down on UF-2	4 months	EXPRESS Rack 4 / Destiny module	Space product development
Commercial Generic Bioprocessing Apparatus (CGBA)	Up on 8A Down on UF-2	2 months	EXPRESS Rack 4 / Destiny module	Space product development
Commercial Biomedical Testing Module (CBTM)	Up and down on UF-1	No expedition ops	Shuttle middeck	Space product development
Commercial Protein Crystal Growth (CPCG)	Up on 8A Down on UF-2	2 months	EXPRESS Rack 4 / Destiny module	Space product development
Zeolite Crystal Growth Furnace (ZCG)	Up on UF-1	Permanent	EXPRESS Rack 2 / Destiny module	Space product development
Microencapsulation Electrostatic Processing System (MEPS)	Up on UF-1	Expedition four through Six	EXPRESS Rack 4 / Destiny module	Space product development

TABLE 5-3 ROS-ISS INCREMENT-4 PAYLOAD COMPLEMENT

Experiment Name	Research Objective	Hardware Used	Up/Down Flight or Vehicle	Research Area
KHT-1 “GTS”—Global Timing System	Verification of Global timing System	Electronic unit; Antenna unit with attachment mechanism	Existing on orbit	Commercial
KHT-2 “MPAC & SEED” (NASDA)	Recording meteoroid and man-made particle impact on ISS-RS SM	Micro particles collection device and material exposure array MPAC & SEED	Existing on orbit	Commercial
KHT-3 “HDTV” (NASDA)	Experiment in receiving HDTV images	Video camera HDTV & Interface unit	Existing on orbit	Commercial
KHT-4 “Vzgliad” (Glance)	Photo and video material acquisition inside & outside of ISS	Kodak photo camera, Digital video camcorder	Existing on orbit; Progress M 8	Commercial
ГФИ-1 “Relaksatsiya” (Relaxation	Study of the chemiluminescent chemical reactions and atmospheric light phenomena	“Fialka-MV Kosmos” spectral-zonal ultraviolet system	Existing on orbit	Geophysical
ГФИ-8 “Uragan”	Experimental testing and verification of the ground-space system for eliminating the impact of man-made catastrophes	Binocular telescopic device Rubinar; Photo camera Hasselblad; Video complex LIV	Existing on orbit	Geophysical
ГФИ-10 “Molnia-SM	Study of atmosphere, ionosphere and magnetosphere electromagnetic interaction related to storms & seismic activities	BFS-3M video-photometric system	Existing on-orbit; Progress M-8	Geophysical

Table 5-3, Continued from previous page

МБИ-2 “Diurez”	Study of fluid and electrolyte metabolism and volume hormonal regulation in microgravity	Urine collection kit; Kriogen-03/1 refrigerator; Plazma-03 kit; Gematokrit-03 kit; Reflotron-4 equipment	Progress M-8	Biomedical
МБИ-3 “Parodont”	Study of periodontal tissue condition under space flight conditions	Kriogem-03/1 refrigerator	Progress M-8	Biomedical
МБИ-4 “Farma”	Study of the specificities of pharmacological effects under long duration space flight	Reflotron-4 kit	Progress M-8	Biomedical
МБИ-5 “Kardio-ODNT”	Integrated study of the dynamics of the primary parameters of cardiac activity and blood circulation	“Gamma-1M” equipment, “Chibis” LBNP device	Existing on-orbit	Biomedical
МБИ-Biotest	Biochemical profile of human in spaceflight	Kriogen-03/1 refrigerator; Plazma-03 kit; Reflotron-4	Progress M-8	Biomedical
МБИ-8 Profilaktika (Countermeasure	Study of mechanisms and efficiency of countermeasures for preventing muscular skeletal apparatus degradation in microgravity	Reflotron-4 complex; TVIS treadmill; VB-3 bicycle ergometer; Bungee cords set; Gamma-1M equipment; Laptop; Kardiokasseta; power unit Tsentr	Existing on-orbit	Biomedical
РБО-1 “Prognoz”	Development of a method for real-time prediction of dose loads on the crews of manned space stations	Р-16 radiometer; ДБ-8 dosimeters (4 units)	Existing on-orbit (Progress М-4)	Biomedical
РБО-2 “Bradoz”.	Bioradiation dosimetry during spaceflight	“Bradoz” kit	Progress M-8	Biomedical
БТХ-1 “Glikoproteid”	Alpha virus glycoprotein E1-E2 isolation and investigation	Bio-crystallization equipment—CPCF	Progress M-8	Biotechnology
БТХ-2 “Mimetik-K”	Anti-idiotypical antibodies as mimetics of adjuvantly active glycoproteins	Bio-crystallization Equipment—CPCF	Progress M-8	Biotechnology
БТХ-3 “KAF”	Crystallization of CaflM protein and its structure	Bio-crystallization Equipment—CPCF	Progress M-8	Biotechnology
БТХ-4 “Vaktsina-k”	Structural study of candidate-proteins in vaccines against AIDS	Bio-crystallization equipment—CPCF	Progress M-8	Biotechnology
БТХ-11 “Biodegradatsia”	Evaluation of biodegradation initial stages and biodamage of structure materials surface	Biodegradatsia-G01 kit; GO2 kit	Progress M-8	Biotechnology
ТЕХ-3 “Akustika-M”	Acoustic study of ISS crew voice communication optimization	Akustika-M equipment	Progress M-8	Technical studies
ТЕХ-5 “Meteoroid” (SDT 16002-R)	Recording meteoroid and man-made particle impacts on the exterior of ISS RS SM	MMK-2 electronic unit; stationary capacitor sensors	Existing on-orbit	Technical studies
ТЕХ-13 “Tenzor” (SDTO 12001-R)	Determining ISS dynamic properties	ISS RS motion control system; sensors; star tracker; GPS GLONAS satellite system	Existing on-orbit	Technical studies
ТЕХ-14 “Vektor-T” (SDTO 12002-R)	Study of the ISS system for high-accuracy motion prediction using GPS	ISS RS sensors; ISS RS orbit radio tracking system; GPS	Existing on-orbit	Technical studies

Table 5-3, Continued from previous page

TEX-15 "izgib" (Bending-SDTO 13002-R)	Study of the effect of onboard system operating modes on ISS flight conditions by measuring vibration disturbances, sources, and vibration fields in the ISS modules	ISS RS accelerometers and rotational speed sensors	Existing on-orbit	Technical studies
TEX-16 "Privyazka" (Alignment-SDTO 12003-R)	Determination of science instruments orientation in space with allowance for deformation of the ISS hull	ISS RS sensors	Existing on-orbit	Technical studies
TEX-17 "Iskazhenie" (Distorsion-SDTO 16001-R)	Determine the factors affecting the accuracy of ISS attitude determination using a magnetometer	ISS RS SM attitude control sensors and control loop magnetometers	Existing on-orbit	Technical studies
TEX-22 "Identifikatsiya" (Identification) (SDTO 13001-R)	Identification of sources of perturbations in the ISS microgravity environment by measuring disturbances during vehicle dockings/undockings, cosmonaut exercises, and operations of onboard systems …	Linear optical accelerometer with cables; micro acceleration measurement device with cables.	Existing on-orbit	Technical Studies
TEX-3 "Skorpion"	Monitoring of environmental parameters inside the station compartments at various places	Skorpion equipment (CKP-1)	TBD	Technical studies
TEX-32 "Kolibri"	Educational project		Existing on-orbit	Technical studies
ИКЛ-1В "Platan"	Search for low energy heavy nuclei of solar and galactic origin	Platan-M equipment	Existing on-orbit	Technical studies
ПКЕ-1В "Kromba"	Study of the dynamics of contaminating particles from the control jets during pulse activations	Cassette with exposed samples with packing (passive hardware)	Existing on-orbit	Technical studies
Д33-2 "Diatomea"	Study of stability of geographic location and frontiers configuration of the biologically productive oceanic waters observed by the crew	Photo camera Nikon; Video camera; Dictaphone; Laptop # 3; "Diatomea" kit	Existing on-orbit	Study of Earth natural resources and ecological monitoring
КНТ-15 "Spika-S"	Investigation of spaceflight factors impact on electronic components tolerance to radiation	"Spika-S" equipment	Existing on-orbit	Technical studies
БИО-1 "Полиген"	Detection of genotype properties that determine individual differences in the tolerance of biological objects to long duration space flight factors.	"Drosophila" kit		Biomedical

TABLE 5-4 USOS-ISS INCREMENT-5 PAYLOAD COMPLEMENT

Experiment	Mission information	Duration	Location on ISS	Research Area
Advanced Astroculture-GC-03 (ADVASC)	Up on UF-2; Down on 9A	75 days	EXPRESS Rack 4	Commercial plant biotechnology
Commercial Generic Bioprocessing Apparatus (CGBA)	Up on 9A; Down on 11A	35 days	EXPRESS Rack 4	Commercial plant biotechnology

Table 5-4, Continued from previous page

Plant Growth Bioprocessing Apparatus (PGBA)	Up on 9A; Down on 11A	35 days	EXPRESS Rack 4	Commercial plant biotechnology
Protein Crystal Growth Single-locker Thermal Enclosure System housing the Diffusion-controlled Crystallization Apparatus for Microgravity (PCG-STES-DCAM)	Up on UF-2; Down on 9A	3 months	EXPRESS Rack 4	Biotechnology
Protein Crystal Growth Single-locker Thermal Enclosure System housing the Protein Crystallization Apparatus for Microgravity (PCG-STES-PCAM)	Up on 9A; Down on 11A	1 month	EXPRESS Rack 4	Biotechnology
Crew Earth Observations (CEO)	Expeditions 1-7	28 months	Destiny lab window or other ISS windows	Earth observations
Crewmember and Crew-Ground Interactions During ISS Missions (Interactions)	Expeditions 2-9	32 months	Human Research Facility	Human Life Sciences
Microgravity Acceleration Measurement System (MAMS)	Mission 6A STS-100	15 years	EXPRESS Rack 1 Destiny module	Microgravity
Space Acceleration Measurement System II (SAMS-II)	Mission 6A STS-100	15 years	Destiny module	Microgravity
Sub-regional Assessment of Bone Loss in Axial Skeleton (Sub-regional Bone	Expeditions 2-9	32 months	N/A—Preflight and post-flight data collection only	Human Life Sciences—Bone and muscle
Renal Stone Investigation	Expeditions 3-12	30 months	Human Research Facility	Human Life Sciences
Materials International Space Station Experiment (MISSE)	Up on 7A.1; Down on ULF-1	17 months	External attachment on Quest airlock	Material exposure
Effects of Microgravity on the Peripheral Subcutaneous Veno-Arteriolor Reflex in Humans (Xenon-1)	Expeditions 3-5	12 months	Human Research Facility	Human Life Sciences
Pulmonary Function in Flight (PuFF)	Expeditions 3-6	16 months	Human Rack Facility	Human Life Sciences
Astronauts in EVA Radiation Study (EVARM)	Expeditions 4-6	12 months	Human research facility	Human life sciences
Pore Formation and Mobility Investigation (PFMI)	Up on UF-2; Down on ULF-1	8 months	Microgravity Science Glovebox; Destiny module	Microgravity sciences
Solidification Using a Baffle in Sealed Ampoules (SUBSA)	Up on UF-2 Down on 11A	4 months	Microgravity Science Glovebox Facility; Destiny module	Materials science
Effect of Prolonged Spaceflight on Human Skeletal Muscle (Biopsy)	Expeditions 5-8	N/A	Pre-and post-flight	Human life sciences
Zeolite Crystal Growth Furnace (ZCG)	Furnace unit up on UF-1; samples up and down on most Shuttle flights	Expeditions 4-7	EXPRESS Rack 2	Space product development
Microencapsulation Electrostatic Processing System (MEPS)	Up on UF-2; Samples down on 9A	8 months	EXPRESS Rack 3	Space product development
Promoting Sensorimotor Response Generalizability (Mobility)	Expeditions 5-10	N/A	Pre-and post-flight	Human life sciences
Space Flight Induced Reactivation of Epstein-Barr Virus (Epstein-Barr)	Expeditions 5-10	N/A	Pre-and post-flight	Human life sciences
Test of Midodrine as a Countermeasure against Postflight Orthostatic Hypotension (Midodrine)	Expeditions 5-10	N/A	Pre-and post-flight	Human life sciences
Educational Payload Operations-5	Up on UF-2 Down on 11A	2 days	Stowed when not in use	Education
StelSys Liver Cell Research (StelSys)	Up on UF-2 Down on 9A	3 months	EXPRESS Racks 1 and 2	Commercial biotechnology

TABLE 5-5 ROS-ISS INCREMENT-5 PAYLOAD COMPLEMENT

Experiment Name	Research Objective	Hardware Used	Up/Down Flight or Vehicle	Research Area
МБИ-1 “Sprut-MBI”	Study of human bodily fluids under condition of long duration of flight	TSENTR power unit; Laptop	Existing on orbit	Biomedical
МБИ-9 “Pulse”	Study of the autonomic regulation of the human cardiorespiratory system in weightlessness	Computer	Existing on orbit	Biomedical
БИО-2 “Biorisk”	Study of space flight impact on micro-organisms-substrates systems	Biorisk-KM set; Biorisk-MSV containers; Biorisk-MSN set	Existing on orbit	Biomedical
БИО-5 “Rasteniya-2”	Study of the space flight effect on the growth and development of higher plants	BVP-70P video camera; computer	Existing on orbit	Biomedical
ГФИ-1 “Relaksatsiya” (Relaxation	Study of the chemiluminescent chemical reactions and atmospheric light phenomena	“Fialka-MV Kosmos” spectral-zonal ultraviolet system	Existing on orbit	Geophysical
ГФИ-8 “Uragan”	Experimental testing and verification of the ground-space system for eliminating the impact of man-made catastrophes	Binocular telescopic device Rubinar; Photo camera Hasselblad; Video complex LIV	Existing on orbit	Geophysical
ГФИ-10 “Molnia-SM	Study of atmosphere, ionosphere and magnetosphere electromagnetic interaction related to storms & seismic activities	BFS-3M video-photometric system	Existing on-orbit; Progress M-8	Geophysical
ТЕХ-20 “Plasma Kristall”	Study of the plasma crystals and fluids under microgravity condition	Plazmennyi kristall equipment; Telescience flight equipment	Existing on-orbit	Technical studies
МБИ-3 “Parodont”	Study of periodontal tissue condition under space flight conditions	Kriogem-03/1 refrigerator	Progress M-8	Biomedical
МБИ-4 “Farma”	Study of the specificities of pharmacological effects under long duration space flight	Reflotron-4 kit	Progress M-8	Biomedical
МБИ-5 “Kardio-ODNT”	Integrated study of the dynamics of the primary parameters of cardiac activity and blood circulation	“Gamma-1M” equipment, “Chibis” LBNP device	Existing on-orbit	Biomedical
ТЕХ-25 “Skorpion”	Development and testing multifunctional control equipment for conditions verification of scientific researches	Skorpion equipment	Progress M-8	Technical studies
МБИ-8 Profilaktika (Countermeasure	Study of mechanisms and efficiency of countermeasures for preventing muscular skeletal apparatus degradation in microgravity	Reflotron-4 complex; TVIS treadmill; VB-3 bicycle ergometer; Bungee cords set; Gamma-1M equipment; Laptop; Kardiokasseta; power unit Tsentr	Existing on-orbit	Biomedical

Table 5-5, Continued from previous page

РБО-1 “Prognoz”	Development of a method for real-time prediction of dose loads on the crews of manned space stations	Р-16 radiometer; ДБ-8 dosimeters (4 units)	Existing on-orbit (Progress М-4)	Biomedical
РБО-2 “Bradoz”.	Bioradiation dosimetry during spaceflight	“Bradoz” kit	Progress М-8	Biomedical
ПКЭ-1В “Kromka”	Study of the dynamics of extracting contaminating particles from the control jets during pulse activations	Cassette with exposed samples with packing (passive hardware)	Progress М-8	Space energy systems
КНТ-1 “GTS”	Verification of Global Timing System	Electronic unit; Antenna unit with attachment mechanism	Existing on-orbit	Commercial
КНТ-2 “MPAC & SEED”	Recording meteoroid and man-made particle impacts and exposure of material specimens on ISS RS SM	Microparticles collection device and materials exposure array MPAC & SEED	Progress М-8	Commercial
КНТ-3 “HDTV”	Experiment in receiving HDTV images	Video camera HDTV; interface units	Existing on-orbit	Commercial
КНТ-4 “Vzgliad”	Photo and video material acquisition inside and outside of ISS-RS	Kodak photo camera; Digital video camcorder	Existing on-orbit	Commercial
ТЕХ-5 “Meteoroid” (SDT 16002-R)	Recording meteoroid and man-made particle impacts on the exterior of ISS RS SM	ММК-2 electronic unit; stationary capacitor sensors	Existing on-orbit	Technical studies
ТЕХ-13 “Tenzor” (SDTO 12001-R)	Determining ISS dynamic properties	ISS RS motion control system; sensors; star tracker; GPS GLONAS satellite system	Existing on-orbit	Technical studies
ТЕХ-14 “Vektor-T” (SDTO 12002-R)	Study of the ISS system for high-accuracy motion prediction using GPS	ISS RS sensors; ISS RS orbit radio tracking system; GPS	Existing on-orbit	Technical studies
ТЕХ-15 “izgib” (Bending-SDTO 13002-R)	Study of the effect of onboard system operating modes on ISS flight conditions by measuring vibration disturbances, sources, and vibration fields in the ISS modules	ISS RS accelerometers and rotational speed sensors	Existing on-orbit	Technical studies
ТЕХ-16 “Privyazka” (Alignment-SDTO 12003-R)	Determination of science instruments orientation in space with allowance for deformation of the ISS hull	ISS RS sensors	Existing on-orbit	Technical studies
ТЕХ-17 “Iskazhenie” (Distorsion-SDTO 16001-R)	Determine the factors affecting the accuracy of ISS attitude determination using a magnetometer	ISS RS SM attitude control sensors and control loop magnetometers	Existing on-orbit	Technical studies
ТЕХ-22 “Identifikatsiya” (Identification) (SDTO 13001-R)	Identification of sources of perturbations in the ISS microgravity environment by measuring disturbances during vehicle dockings/undockings, cosmonaut exercises, and operations of onboard systems …	Linear optical accelerometer with cables; micro acceleration measurement device with cables.	Existing on-orbit	Technical Studies
ИКЛ-1В “Platan”	Search for low energy heavy nuclei of solar and galactic origin	Platan-M equipment	Existing on-orbit	Technical studies
Д33-2 “Diatomea”	Study of stability of geographic location and frontiers configuration of the biologically productive oceanic waters observed by the crew	Photo camera Nikon; Video camera; Dictaphone; Laptop # 3; “Diatomea” kit	Existing on-orbit	Study of Earth natural resources and ecological monitoring

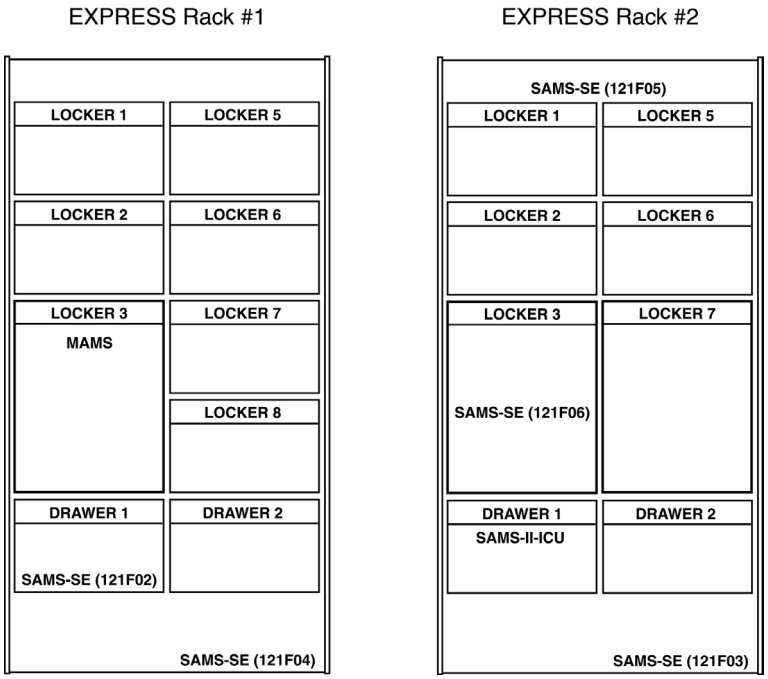

Figure 5-1 EXPRESS Rack Generic Configuration with SAMS/MAMS Locations

EXPRESS Rack / Flight	UF-1 (Inc 4)	8A (Inc 4)	UF-2 (Inc 5)	9A (Inc 5)
<EXP Rk #1>				
Locker1	BCSS-5	BCSS-5		
Locker2	BCSS-R	BCSS-R		
Locker3	MAMS	MAMS	MAMS	MAMS
Locker4	MAMS	MAMS	MAMS	MAMS
Locker5	MEPSII	MEPSII (Inactive)	MEPSII	MEPSII (Inactive)
Locker6		BSTC1 (stwd)		
Locker7		BTR1 (stwd)		
Locker8		GSM1 (stwd)		
Drawer1	SAMS-RTS1	SAMS-RTS1	SAMS-RTS1	SAMS-RTS1
Drawer2	SAMS-RTS2	SAMS-RTS2	SAMS-RTS2	SAMS-RTS2
<EXP Rk #2>				
Locker1	ARIS-ICE1	ARIS-ICE1		
Locker2	ARIS-ICE2	ARIS-ICE2		
Locker3	PCS-TS1	PCS-TS1		
Locker4	PCS-TS1	PCS-TS1		
Locker5	ZCG-FU1	ZCG-FU1	ZCG-FU1	ZCG-FU1
Locker6	ZCG-FU1	ZCG-FU1	ZCG-FU1	ZCG-FU1
Locker7	PCS-AS	PCS-AS	PCS-AS (Inactive)	PCS-AS (Inactive)
Locker8	PCS-AS	PCS-AS	PCS-AS (Inactive)	PCS-AS (Inactive)
Drawer1				
Drawer2				
<EXP Rk #4>				
Locker1	BSTC1	CPCG-H1	PCG-STES9	PCG-STES7
Locker2			PCG-STES10	
Locker3	ADVASC-GC2		ADVASC-GC3	
Locker4	ADVASC-SS1	ADVASC-SS1 (Inactive)	ADVASC-SS2	ADVASC-SS2 (Inactive)
Locker5	GSM1	CGBA3		CGBA2
Locker6	BTR1	ARCTIC	ARCTIC (Inactive)	ARCTIC (Inactive)
Locker7	PCG-STES7	BPS	DCPCG-C	PGBA1
Locker8	PCG-STES8	BPS	DCPCG-V	PGBA1
Drawer1	KU-REC	KU-REC	KU-REC	KU-REC
Drawer2	SAMS-II-ICU	SAMS-II-ICU	SAMS-II-ICU	SAMS-II-ICU
Continuously powered payload				

Figure 5-2 EXPRESS Rack Topologies for Increments 4 & 5

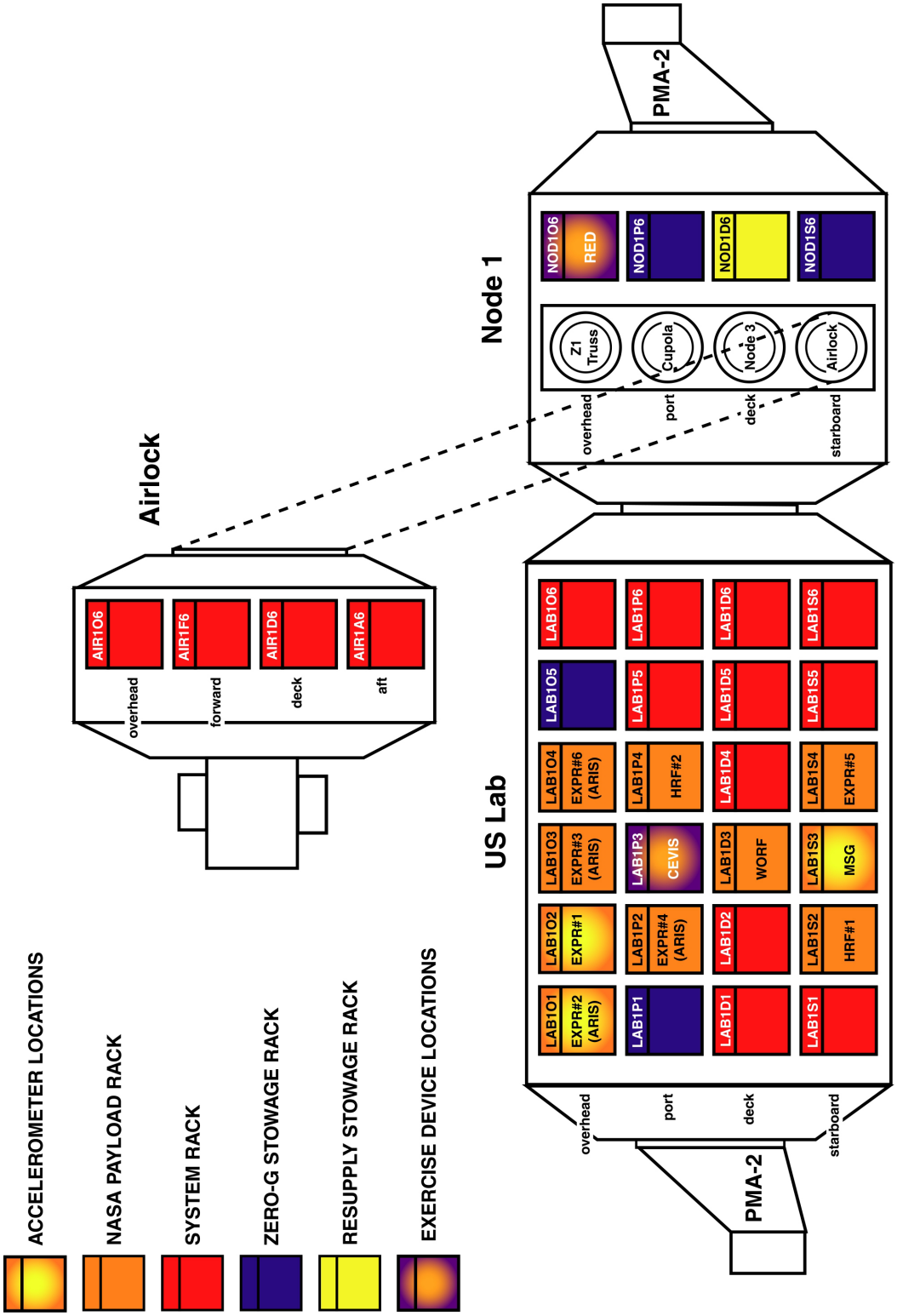

Figure 5-3 US Lab Rack Locations

6 ISS Increment-4/5 Reduced Gravity Environment Description

The reduced gravity environment for Increment-4/5 was measured by the SAMS accelerometer, the MAMS HiRAP accelerometer, and the MAMS OSS accelerometer. In order to readily observe the availability of acceleration data for a particular sensor for a particular time period**,** Figure 6-1 through Figure 6-13 were created. These figures show the available acceleration data for the active SAMS SEs, the MAMS OSS sensor, and the MAMS HiRAP sensor for the Increment-4/5 time span analyzed in this report. They can be accessed via the PIMS ftp site at:

ftp://pims.grc.nasa.gov/pad/

6.1 Quasi-steady Microgravity Environment

The quasi-steady regime is comprised of accelerations with frequency content below 0.01 Hz and magnitudes expected to be on the order of 2 μg or less. These low-frequency accelerations are associated with phenomena related to the orbital rate, primarily aerodynamic drag. However, gravity gradient and rotational effects may dominate in this regime, depending on various conditions and an experiment's location relative to the vehicle's center of mass (CM). Another source of acceleration to consider in this regime is venting of air or water from the spacecraft. This action results in a steady, low-level propulsive force. The different quasi-steady environment characteristics seen on the ISS for Increment-4/5 are primarily related to altitude and attitude of the station. Variation in atmospheric density with time and altitude contribute to the differences in the aerodynamic drag component. Different attitudes will affect the drag component due to the variation of the frontal cross-sectional area of the station with respect to the velocity vector.

6.1.1 Guidance, Navigation, and Control

The station's GNC system includes both the United States (US) GNC System and the functionally equivalent Russian Orbital Segment Motion Control System (ROS MCS) [6]. GNC performs six functions: guidance, state determination, attitude determination, pointing and support, translational control, and attitude control. Guidance tells the station which path to follow, say, from point A to point B. Navigation deals with state determination, attitude determination, and pointing and support. In brief, it provides answers to: where the station is, how it is oriented, and where everything else is. Control implements the path determined by guidance. Control of the station consists of translational control and attitude (or rotational) control. Translational maneuvers are used by the station to achieve a desired orbit and to perform orbital debris avoidance maneuvers, whereas attitude control is used to maintain the orientation of the station within a selected reference frame [6]. The US non-propulsive Attitude Control System (ACS) controls four CMGs located on the Z1 truss. The CMGs weigh about 300 kg. each [6] and are two degree-of freedom gyroscopes. The gimbals allow the US GNC software to reposition the direction of the rotor spin axis. By repositioning the axes of the four gyroscopes, the GNC software directs the CMGs to generate torques that counter some of the station's attitude disturbances. Each CMG can generate 256.9 Newton-meters (Nm) [6] of torque to counteract the disturbances due to gravity gradient forces, aerodynamic drag, and so on.

Since there is a limit to the amount of torque the CMGs can generate and the amount of momentum they can store, the disturbance torques in a particular direction can exceed the countering torque capability of the CMGs. This situation causes the CMG to saturate. If saturated, the CMGs are no longer effective in preventing undesirable station rotation. The system is designed to take corrective action by requesting the desaturation of the CMGs.

Once the CMG momentum reaches about 80 percent [6] of the way to saturation, the GNC system requests a Russian thruster firing. The thrusters are fired in a calculated manner such that they cancel the torques generated by the CMGs, which allows the GNC to reset the CMG gimbals to a more optimal position. Due to the limited torque available from the CMGs, the CMGs are used with thruster assist for desaturations to rotate the station when maneuvers are less than 10 degrees per axis [6]. During large maneuvers, the CMGs are likely to saturate often, prompting frequent use of thruster firings.

Handover of ISS attitude control from Russian to US systems and vice-versa is a common occurrence and is accompanied by the thruster firings to desaturate the CMGs. The effects of these events on the quasi-steady environment often vary in magnitude. These variations are most probably due to the degree of CMG saturation and attitude. Two examples are seen in Figure 6-14 and Figure 6-15. Figure 6-14 is an acceleration vs. time plot from GMT 04-July-2002, 185/04:00. Attitude control handover is seen at the 22.5 minute mark as a -2.5 μg peak in the Y_A-direction and a -1.8 μg in the Z_A-direction, measured as offsets from the mean. A 1.5 μg peaks follows in both the Y_A, and Z_A-directions approximately 1.45 minutes later. The momentum management event is seen at the 33.4 minute mark as 5.8 μg and 3.4 μg peak offsets in the Y_A, and Z_A-directions respectively. Figure 6-15 shows the quasi-steady vector during a Russian to US handover at GMT 06-September-2002, 249/13:00. In this plot no discernable effect is apparent during the handover event (called out in the ISS Attitude Timeline (ATL) at 14:00). The momentum management event is seen at the 70 minute mark with peaks measured from the mean of 2.4, -6.0 and -4.9 μg in the X_A, Y_A, and Z_A-directions respectively.

6.1.2 ISS Attitudes

As mentioned earlier, ISS currently uses two primary attitudes: TEA and XPOP. These two attitudes affect the reduced gravity environment provided by the station. The station is controlled about one of these attitudes, using the onboard CMGs. TEA is the best option when using the CMGs because the zero average torques over an orbit result in less frequent CMG system saturation and help minimize propellant usage. However, when flying TEA, the station is not flying an exact attitude. The GNC varies the attitude slowly over an orbit (± 2.5º at assembly complete and up to ± 11º during assembly buildup) [6] to use the CMGs' capabilities most effectively. XPOP attitude maintains the station attitude close to the quasi-inertial reference frame. This orientation allows the single solar array rotary joint along the station body Y-axis to track the sun at any solar beta angle.

6.1.2.1 +ZLV +XVV Torque Equilibrium Attitude (TEA)

TEA is an attitude that balances the vehicle's gravity gradient and aerodynamic drag torques. After ISS assembly is complete, this is the attitude that will be flown during microgravity mode to support research. However, TEA will vary with station configuration because of change in mass and aerodynamic properties. During Increment 4 new components, the S0 and S1 trusses, were installed to the ISS. The addition of the trusses shifted the center of mass of the station from $[X_A, Y_A, Z_A]$ = [-36.5, -1.09, 8.68] feet to $[X_A, Y_A, Z_A]$ = [-34.0, 4.36, 8.03] feet and the ISS increased in weight to 361,090 lbs. During Increments 4 and 5, prior to the addition the S0 and S1 trusses, the TEA was nominally Yaw, Pitch, Roll (YPR) = (350.0, 353.0, 0.0) relative to the LVLH coordinate system. After Flight 9A, nominal TEA was maintained near YPR = (347.0, 351.1, 0.0).

Figure 6-16 is a plot of MAMS OSS data measured during a crew sleep period of Increment 4 at GMT 06-February-2002, 037/23:00, while the ISS was in TEA. The black line in the plot represents the quasi-steady vector as measured by MAMS at the OSS location. The red line is an estimate of the quasi-steady vector at the Center of Mass (CM) and was calculated using telemetry data available through the Operational Data Request Center (ODRC) and the methods described in E.2.2. The OSS sensor was $[X_A, Y_A, Z_A]$ = [54.0, -1.46, 0.72] feet from the center of mass for this time period. Figure 6-17 is a plot of the acceleration magnitude at both the OSS and CM locations for the same time period as in Figure 6-16. Figure 6-18 and Figure 6-19 use data measured during Increment 5 at GMT 23-November-2002, 327/10:30, after the installation of the S1 truss. The added mass of the S0 and S1 trusses resulted in a change in the location of the CM. It is useful to compare these four plots to understand how the addition of a new ISS component may affect the quasi-steady profile seen at an experiment location, keeping in mind that the added mass not only changed the CM location, but also contributed to the drag profile and required a new attitude to achieve a balance of torques.

After the addition of the S1 truss, the distance of the OSS sensor to the new CM location was $[X_A, Y_A, Z_A]$ = [45.2, -5.25, 2.98] feet for the time period in Figure 6-18 and Figure 6-19, moving closer to the CM in the X_A-axis (+8.80 feet), but further away in the Y_A (3.79 feet) and Z_A-axes (2.26 feet). This resulted in an improvement of 0.17 µg in the X_A-axis average component, while there was a decrease in the Y_A-axis (-0.18 µg) and Z_A-axis (-0.36 µg) components. The overall magnitude of the quasi-steady vector at the OSS location was increased from 1.09 µg to 1.43 µg during TEA. Since the gravity gradient and the rotational component contributions are zero at the CM, comparison of the quasi-steady vector at the CM location give an estimate of the drag on the vehicle. The mean values obtained at the CM from Figure 6-17 and Figure 6-19 show that the magnitude of the drag component decreased from 0.40 µg to 0.23 µg, most likely resulting from the change in attitude profile. Similar effects were found for the addition of the P1 truss, which primarily moved the CM closer to the OSS location in the Y_A–axis and resulted in a drop of 0.27 µg in the magnitude of the Y_A–axis component (plot not shown). The CM changes due to the additions of the S1 and P1 trusses, and the resultant changes in the quasi-steady vector are summarized in Table 6-1.

6.1.2.2 X-Axis Perpendicular to Orbital Plane (XPOP) Inertial Flight Attitude

XPOP is a sun-tracking, quasi-inertial flight attitude used for power generation. In this attitude, the vehicle's X_A-axis is maintained perpendicular to the direction of flight. For the period shown in Figure 6-20 and Figure 6-21, starting at GMT 22-February-2002, 053/22:30, the nominal XPOP attitude was YPR = (359.4, 355.0, 0.0) relative to the J2000 inertial coordinate system. The time series plot for crew sleep during XPOP attitude at the OSS location in Figure 6-20 shows a nearly constant X_A-axis acceleration component of 1.90 µg. Because the rotational components are very small for this attitude, and the large distance from the CM in the X_A direction, the X_A component is nearly entirely due to gravity gradient effects. The in-plane axes, Y_A and Z_A, show more pronounced cyclical profiles, with means of 0.08 µg and -0.30 µg, respectively. The cyclical variations are larger in XPOP than in TEA because these axes are alternately subjected to the drag and gravity gradient vectors as the vehicle completes an orbit. When mapped to the CM, the X_A-axis acceleration component drops to -0.20 µg. The change in Y_A and Z_A-axis components are not as dramatic, since the distance to the CM in these directions are smaller.

Figure 6-22 and Figure 6-23 are plots of the quasi-steady vector during XPOP attitude from Increment 5 starting at 19-October-2002, 292/02:00, and are similar to Figure 6-20 and Figure 6-21, respectively. With the addition of the S1 truss, the ISS attitude was maintained at a nominal YPR = (355.0, 351.4, 0.0). In the new configuration, the magnitude of the X_A-axis component at the OSS location has dropped to 1.40 µg, the Y_A-axis component has increased to 0.65 µg and the Z_A-axis component has decreased to -0.58 µg. The mean quasi-steady vector magnitude at the OSS location has decreased by 0.21 µg to 1.83 µg. Along with the CM change, the 5 degrees change in yaw and pitch angles have contributed to these changes.

Table 6-1 summarizes the findings for TEA and XPOP attitudes during Increments 4, 5 and 6.

TABLE 6-1 QUASI-STEADY VECTOR FOR TEA AND XPOP ATTITUDES

Attitude	Location	Increment	Distance from CM (ft)			Mean X_A (µg)	Mean Y_A (µg)	Mean Z_A (µg)	Mag. (µg)
			X_A	Y_A	Z_A				
TEA	OSS	Inc 4, GMT 037	54.0	-1.46	0.72	-0.43	-0.36	-0.93	1.09
TEA	OSS	Inc 5, GMT 327	45.2	-5.25	2.98	-0.26	-0.54	-1.29	1.43
TEA	OSS	Inc 6, GMT 012	44.4	-0.96	3.21	-0.21	-0.27	-1.21	1.26
XPOP	OSS	Inc 4, GMT 053	54.0	-1.46	0.72	1.90	0.08	-0.30	2.04
XPOP	OSS	Inc 5, GMT 292	45.2	-5.25	2.98	1.40	0.65	-0.58	1.83
XPOP	OSS	Inc 6, GMT 349	44.4	-0.96	3.21	1.80	-0.49	-0.37	1.90
TEA	CM	Inc 4, GMT 037	0.00	0.00	0.00	-0.34	0.06	0.11	0.40
TEA	CM	Inc 5, GMT 327	0.00	0.00	0.00	-0.19	0.04	-0.04	0.23
TEA	CM	Inc 6, GMT 012	0.00	0.00	0.00	-0.06	0.06	0.03	0.13
XPOP	CM	Inc 4, GMT 053	0.00	0.00	0.00	-0.20	0.03	0.05	0.42
XPOP	CM	Inc 5, GMT 292	0.00	0.00	0.00	-0.27	0.28	-0.16	0.46
XPOP	CM	Inc 6, GMT 349	0.00	0.00	0.00	0.13	-0.44	0.09	0.51

6.1.3 Docking and Undocking Events

6.1.3.1 STS-112 Docking

At GMT 09-Oct-02, 282/15:16, the Space Shuttle Atlantis docked at the ISS Pressurized Mating Adapter (PMA2) port as part of the STS-112 mission. Figure 6-24 is a time series plot of MAMS OSS Best Trimmean Filter (OSSBTMF) data during the STS-112 docking operations. The docking softmate can be seen initially at the 1.27 hour of the plot, most notably as a 3-4 µg increase in Z_A-axis acceleration. Hardmate is approximately 10 minutes later, at around the 1.47 hour mark on the plot. The hardmate time was determined by the appearance in SAMS 121f02 data of the 17 Hz signal from the Ku-band antenna dither on the orbiter. The source of the three peaks in the X_A-axis of -77.1 µg, -75.4 µg, and -33.5 µg following hardmate are thruster firings from the Vernier Reaction Control System (VRCS) of the orbiter. Figure 6-25, Figure 6-26, and Figure 6-27 are 30 minute time series plots of raw MAMS OSS starting at GMT 09-Oct-02, 282/15:30 correlated with VRCS thruster firing data from ODRC. The X-axis plot, Figure 6-25, shows that the first two steps (beginning at the 6.47 and 14.7 minute marks) result from firings of the F5L and F5R, thrusters located in the nose of the orbiter. Figure 6-28 is a diagram detailing the position and orientation of orbiter thrusters. When fired in unison, these thrusters provide accelerations in the orbiter's Z_O-axis (Orbiter structural coordinates, Z-axis), which is aligned with the $-X_A$ axis when the orbiter is docked to the ISS, which is in agreement with the MAMS data. The last of the large peaks, beginning at the 25.5 minute mark of Figure 6-25, is a result of the combined firings of L5D and R5D thrusters, both of which are pointed in the Z_O-axis direction. The simultaneous firings of thrusters L5D and F5L at the 18.0 minute mark appear as peaks in both the $-X_A$ (-6.97 µg) and the Y_A (11.3 µg) directions. Note that many of the shorter duration thruster firings are not seen in Figure 6-24. These are often muted or erased by the trimmean filter processing of MAMS OSS data.

6.1.3.2 Progress 7P Docking

The docking of Progress 7P to the ISS at GMT 24-March-2002, 083/20:58 was preceded by an attitude change at GMT 24-March-2002, 083/18:31 from the –XPH +ZNN XPOP attitude ($-X_A$-axis pointing in the direction of the angular momentum vector, $+Z_A$-axis nadir at orbital noon), YPR = (179.1 354.1 1.3), to the inertial docking attitude, YPR = (245.4 336.4 283.7). After docking was completed, the ISS performed a maneuver to return to XPOP attitude, YPR = (179.2, 354.9, 0.0), at GMT 24-March-2002, 083/21:10. As seen in Figure 6-29 the largest effect on the quasi-steady environment was during the two attitude maneuvers. In fact, the actual physical mating of the two vehicles is not apparent in the trimmed mean filtered data. During the attitude maneuvers, quasi-steady accelerations as high as -16 µg were seen on the X_A-axis and -36 µg on the Z_A-axis. The mean acceleration values during the attitude maneuvers were [-6.55, 2.89, -1.20] µg. While in the inertial docking attitude the X_A-axis component has a mean of -1.02 µg.

6.1.3.3 Progress 8P Undocking

Progress 8P undocked from the ISS at GMT 24-Sep-2002, 267/13:59. Table 6-2 is a selection from the Increment 5A timeline for the undocking events. The maneuver from duty attitude to undock attitude, begins at the 2.47 hour mark in Figure 6-30, and is seen as a large -29.0 µg peak in the X_A-axis. The mean values for the time period during the maneuver was $[X_A, Y_A, Z_A]$ = [-20.3, -0.35, -0.17] µg. After undocking the ISS was maneuvered to "relaxation" attitude. This activity supported a Russian onboard experiment called "Relaksation". To calibrate the equipment associated with this experiment, the crew had to get specific stars or the moon in view in a specific ISS window. The mean acceleration values for this maneuver were $[X_A, Y_A, Z_A]$ = [-14.6, -0.43, -0.51] µg with a peak of -20.2 µg on the X_A-axis. The attitude placed the $-X_A$-axis in the local vertical vector and the $-Z_A$-axis in the velocity vector, YPR = (180.0 90.0 0). The mean values for the quasi-steady vector while in "relaxation" attitude were $[X_A, Y_A, Z_A]$ = [-5.18, -0.30, 0.73] µg. In Figure 6-30 "relaxation" attitude begins at the 5.79 hour mark and ends at the 6.12 hour mark.

TABLE 6-2 ATTITUDE TIMELINE SELECTION FOR PROGRESS 8P UNDOCKING

#	Start-Stop (GMT)	Beta Angle	Attitude Name	Ref Frame	[Yaw Pitch Roll]	Source (ACR)
156	267/11:35	+51	+ZLV +XVV Roll Bias	LVLH	[350.0 350.5 355.0]	US TO RS HANDOVER
157	267/12:00 267/12:02	+51	+ZLV +XVV	LVLH	[359.2 354.8 2.80]	MNVR TO LVLH DUTY ATTITUDE
158	267/13:20 267/13:40	+51	+ZLV -XVV	LVLH	[180.0 0.00 72.9]	MNVR TO UNDOCK ATTITUDE
159	267/13:55 267/14:04	+51	FREE DRIFT	FREE DRIFT	Free Drift for 8P Undock	UNDOCK @ 13:59
160	267/14:04 267/14:24	+51	+ZLV -XVV	LVLH	[179.1 353.4 3.4]	MNVR TO DUTY ATTITUDE
161	267/16:33 267/16:48	+51	-XLV -ZVV	LVLH	[180.0 90.0 0.0]	MNVR TO "RELAXATION" ATTITUDE
162	267/17:06 267/17:31	+51	+ZLV +XVV Roll Bias	LVLH	[350.0 350.5 355.0]	MANEUVER TO DUTY ATTITUDE
163	267/17:50	+51	+ZLV +XVV Roll Bias	LVLH	[350.0 350.5 355.0]	RS TO US HANDOVER
164	267/18:00	+51	+ZLV +XVV Roll Bias	LVLH	[350.0 350.5 355.0]	MOMENTUM MANAGEMENT

There were many docking and undocking events during Increments 4 and 5, but only a few interesting examples were picked to examine in detail. Table 6-3 is a summary of the major effects on the quasi-steady vector at the OSS location of docking and undocking events.

TABLE 6-3 QUASI-STEADY EFFECTS OF DOCKING AND UNDOCKING ACTIVITIES

Event	Event Time GMT	Major Quasi-steady Effect
STS-108 Docking	07-December-2001, 341/20:03	-87.3 μg peak in X_A-axis
6P Progress Undocking	19-March-2002, 078/17:43	17.0 μg peak in Y_A-axis
7P Progress Docking	24-March-2002, 083/20:58	-36.0 μg peak in Z_A-axis
STS-110 Docking	10-April-2002, 100/16:05	-83.1 μg peak in X_A-axis
Soyuz 3S Relocation	20-April-2002, 110/07:00	24-25 μg peaks in Y_A, Z_A -axes
Soyuz 4S Docking	27-April-2002, 117/07:57	40.1 μg peak in Z_A-axis
Soyuz 3S Undocking	05-May-2002, 125/00:28	-24.8 μg peak in X_A-axis
STS-111 Docking	07-June-2002, 158/16:25	-82.9 μg peak in X_A-axis
STS-111 Undocking	15- June -2002, 166/14:32	-83.4 μg peak in X_A-axis
7P Progress Undocking	25-Jun-2002, 176/08:23	-24.5 μg peak in X_A-axis
8P Progress Docking	29-Jun-2002, 180/06:25	-44.1 μg peak in Z_A-axis
8P Progress Undocking	24-September-2002, 267/11:00:03.418	-29.0 μg peak in X_A-axis
9P Progress	29-September-2002, 272/17:05	-23.7 μg peak in X_A-axis
STS-112 Docking	09-October-02, 282/15:16	-77.1 μg peak in X_A-axis
Soyuz 4S Undocking	09-November-2002, 313/20:44	-22.9 μg peak in X_A-axis
Soyuz 5S Docking	01-November-2002, 305/04:56	-10.7 μg peak in X_A-axis
STS-113 Docking	25-November-2002, 329/21:59	-71.7 μg peak in X_A-axis

6.1.4 Venting

6.1.4.1 US Lab Water Dump

Figure 6-31 shows the quasi-steady effects of a condensate water dump that occurred during Increment 4, beginning at GMT 012/15:30 and ending at GMT 012/16:50. Prior to venting, the ISS was maneuvered to an attitude, YPR= (273.3, 356.7, 307.0), that placed the vent in retrograde (opposite the direction of travel) to minimize contamination. The effects of the attitude maneuvers are out of the time range of this plot. The procedure for this water dump uses a Collapsible Water Container (CWC) that is used for storing waste water. During the dump it appeared to the crew that the venting had stalled as recorded in PIMS console log at GMT 012/ 15:41. At this point, a crew member put a "bear hug" on the CWC to increase pressure and the venting was observed to continue. The major disturbance occurs roughly about this time in the Z_A-axis, peaking in magnitude at approximately -6.4 μg at the 0.8 hour mark in the plot or GMT 012/ 15:52. Table 6-4 is an excerpt from the PIMS console log book. (Source: pimslog_2002_01_07_13_17_22.xls).

TABLE 6-4 PIMS CONSOLE LOG DURING US LAB WATER DUMP

12-Jan-2002 14:55:22	In dump attitude	EK
12-Jan-2002 15:07:42	Higher dump rate than anticipated (higher than last time)	EK
12-Jan-2002 15:08:12	Good flow out the PORT vent.	EK
12-Jan-2002 15:10:45	ECLSS says dump rate within spec	EK
12-Jan-2002 15:19:52	Rate 3 times faster than what they expected	EK
12-Jan-2002 15:40:56	One of the crew (Dan?), is doing a "bear hug" on the CWC(?) to help venting. Sounds like he basically squeezes the water bottle.	EK
12-Jan-2002 15:52:10	At one point it looked as though the tank was not venting (volume holding steady). Thought to be because of backflow into the tank. They now see the tank quantity decreasing.	EK
12-Jan-2002 16:00:17	CWC is almost empty	EK
12-Jan-2002 16:08:40	Dump is being stopped	EK

6.1.4.2 DC-1 Depressurization

Beginning at GMT 16-August-2002, 228/07:20, the Pirs docking compartment (DC-1) was depressurized in preparation for Russian Extravehicular Activity-7 (EVA-7). An event occurred that allowed for definitive identification of the effects of the DC-1 depressurization on the quasi-steady environment. The following excerpt is from the "ISS On-Orbit Status" for August 16, 2002 found on the Microgravity Research Program Office's website (times changed to GMT):

> After Valery Korzun and Peggy Whitson (on her first EVA), on the original schedule, had donned their Orlans (at 6:00 am GMT), started DC-1 airlock depressurization, completed the 30-min. O2 prebreathe for denitrogenation (to prevent "bends"), and disconnected umbilicals, going to internal power (at 07:41 GMT) and Orlan-stored oxygen, Caution & Warning (C&W) alarms in both suits indicated that the crucial flow control valves of the primary O2 tanks in both Orlan backpacks were inadvertently misconfigured. DC-1 had to be repressed (partially, to 550 mmHg; nominal being 760 mmHg), to allow Korzun to egress his Orlan, configure the O2 bottle valves in both suit backpacks, and then repeat the process of suit ingress, depress, prebreathe, etc.

The effects of the dual-depressurization can be seen in Figure 6-32 and Figure 6-33, predominantly on the X_A-axis. A final correlation is achieved in Figure 6-33 by overlaying the X_A-axis accelerations with the compartment pressure data obtained from ODRC. The first venting from 760 mmHg to approximately 570 mmHg is seen at the 0.45 hour mark in Figure 6-33 as a –3.59 μg spike. Another peak of -4.04 μg is apparent at the 0.95 hour mark. The compartment pressure data here is missing, but a slight drop can be seen, suggesting that a repressurization had taken place during the data outage. The first large drop in pressure from 570 mmHg to 28 mmHg occurs 1.4 hours into the plot and is accompanied by a -4.48 μg peak. The second large depressurization occurs at 1 hour and 36 minutes later at the 2.0 hour mark on the plot as a –5.2 μg peak on the X_A-axis. The Y_A and Z_A-axes show peaks during the two depressurizations varying between –4 μg and 2 μg. One item of interest is that the DC-1 valve (RSA-10) is T-shaped, which is a designed to eliminate propulsive effects. The quasi-steady data shows that some propulsive effect is seen.

6.1.5 SUBSA and PFMI

Both the SUBSA and PFMI experiments operated in the MSG during the time frame covered by this report. More details about the PFMI and SUBSA investigations are provided in sections 6.2.3.3.1 and 6.2.3.3.2. This section is a general characterization of the quasi-steady environment for times when these experiments were operating. The figures listed in Table 6-5 summarize the quasi-steady vector during time periods indicated by the SUBSA and PFMI project teams.

TABLE 6-5 PLOTS FOR SUBSA AND PFMI RUNS

Sample	Start	Stop	Reference
SUBSA-06	192:08:49	193:01:16	Figure 6-34, Figure 6-35
SUBSA-10	204:10:16	205:08:21	Figure 6-36, Figure 6-37
SUBSA-02	213:17:33	214:08:04	Figure 6-38, Figure 6-39, Figure 6-40
SUBSA-04	219:17:24	220:07:39	Figure 6-41, Figure 6-42
SUBSA-07	222:08:36	223:00:04	Figure 6-43,Figure 6-44 ,Figure 6-45
SUBSA-08	247:08:45	248:08:32	Figure 6-46, Figure 6-47
SUBSA-09	250:08:30	251:07:54	Figure 6-48, Figure 6-49
SUBSA-01	253:10:30	254:02:30	Figure 6-50, Figure 6-51
PFMI-12	262:14:02	263:10:59	Figure 6-52, Figure 6-53
PFMI-01	266:09:00	267:00:46	Figure 6-54, Figure 6-55
PFMI-07	273:11:50	273:23:22	Figure 6-56, Figure 6-57
PFMI-08	274:17:20	275:05:28	Figure 6-58, Figure 6-59
PFMI-05	279:12:11	280:00:03	Figure 6-60, Figure 6-61
PFMI-02	280:11:15	280:22:38	Figure 6-62, Figure 6-63
PFMI-10	300:11:55	301:00:12	Figure 6-64, Figure 6-65
PFMI-11	324:22:28	325:03:39	Figure 6-66, Figure 6-67

The run of SUBSA-02, seen in Figure 6-38, is of particular note. The run began at GMT 01-August-2002, 213/17:33, which was in the middle of a station reboost, which began at GMT 01-August-2002, 213/17:24. Figure 6-40 shows a close up of the entire reboost, with peaks as large as 583 µg on the X_A-axis and -44.8 µg on the Z_A-axis. Note that the bounds of the Quasi-Steady Three-dimensional Histogram (QTH) plot for this run (Figure 6-40.) are -4 µg to 4 µg, therefore the effects of the reboost do not appear in the plot.

The QTH plot for SUBSA-07, Figure 6-45, also is of interest. The X-Y panel shows that the quasi-steady vector was concentrated in two spots, $[X_A, Y_A]$ = [-0.22, -0.24] µg and $[X_A, Y_A]$ = [-0.22, -0.62] µg, as indicated by the red arrows. This 0.38 µg difference in the Y_A-axis is due to the unknown source described in 6.1.6.2. Figure 6-44 is a time series plot of the last few hours of the run. The stepping on the Y_A-axis is very apparent in this plot.

Table 6-6 and Table 6-7 contain mean values and magnitudes of the quasi-steady vector obtained from QTH plots and significant effects seen from acceleration vs. time plots. In analysis of the quasi-steady data, MAMS OSS data was mathematically mapped to the SUBSA

sample location, [X_A, Y_A, Z_A] = [106.65, 56.48, 181.12] inches, using the methods found in Appendix E.2.2.2.

TABLE 6-6 QUASI-STEADY SUMMARY DURING SUBSA SAMPLE RUNS AT SUBSA LOCATION

Sample	Start	Stop	Mean (μg)			Magnitude (μg)	Notes	Attitude
			X_A	Y_A	Z_A			
SUBSA-06	192:08:49	193:01:16	-0.22	-0.27	-1.30	1.34	13.1 μg spike Z_A-axis	LVLH
SUBSA-10	204:10:16	205:08:21	1.63	0.04	-0.21	1.64	8.2 μg spikes on Z_A-axis	XPOP
SUBSA-02	213:17:33	214:08:04	1.54	0.06	-0.44	1.54	583 μg on X_A-axis (Reboost)*	XPOP
SUBSA-04	219:17:24	220:07:39	1.62	-0.09	-0.46	1.69	6.2 μg peak on Z_A-axis	XPOP
SUBSA-07	222:08:36	223:00:04	-0.20	-0.42	-1.42	1.50	-9.5,12.6 μg peaks on Z_A-axis	LVLH
SUBSA-08	247:08:45	248:08:32	1.66	-0.15	-0.48	1.74	12.2 μg spike on Z_A-axis	XPOP
SUBSA-09	250:08:30	251:07:54	-0.28	-0.29	-1.46	1.52	-10.5 μg spikes Y_A-axis**	LVLH
SUBSA-01	253:10:30	254:02:30	-0.36	-0.28	-1.48	1.55	-8.76 μg spike on Z_A-axis	LVLH

* Values are without reboost. Mean with reboost [X_A, Y_A, Z_A] = [6.63, 0.10, -0.67].
** Missing ODRC Data for last 9 hours of this time period. Quasi-steady mapping was not calculated for that time span.

TABLE 6-7 QUASI-STEADY SUMMARY DURING PFMI SAMPLE RUNS AT SUBSA LOCATION

Sample	Start	Stop	Mean (μg)			Magnitude (μg)	Notes	Attitude
			X_A	Y_A	Z_A			
PFMI-12	262:14:02	263:10:59	-0.30	-0.17	-1.36	1.40	7.78 μg spike on Z_A-axis	LVLH
PFMI-01	266:09:00	267:00:46	-0.28	-0.08	-1.35	1.38	-15.9 μg spike on Z_A-axis	LVLH
PFMI-07	273:11:50	273:23:22	-0.37	-0.27	-1.48	1.55	6.61 μg spike on Z_A-axis	LVLH
PFMI-08	274:17:20	275:05:28*	-0.42	-0.31	-1.50	1.59	4.13 μg spike on Y_A-axis	LVLH
PFMI-05	279:12:11	280:00:03	-0.42	-0.38	-1.48	1.58	-9.67 μg spike on the Y_A-axis	LVLH
PFMI-02	280:11:15	280:22:38	-0.44	-0.37	-1.49	1.60	-12.3 μg spike on the Y_A-axis	LVLH
PFMI-10	300:11:55	301:00:12	1.57	0.16	-0.58	1.68	-24.8 μg spike on the Y_A-axis	XPOP
PFMI-11	324:22:28	325:03:39	-0.53	-0.31	-1.58	1.70	-4.66 μg spike on the Y_A-axis	LVLH

* MAMS Powered off at GMT 274/23:35 due to hurricane Lili at JSC.

6.1.6 Miscellaneous

6.1.6.1 Loss of GNC MDM

Figure 6-68 shows quasi-steady data for a failure of the primary GNC MDM (guidance, navigation and control computer) on GMT 31-March-2002, 090/10:37. In response there was an automatic handover to Russian GNC and an attitude snap and hold. This is seen as peaks up to -8.3 μg on the Z-axis. Figure 6-69 shows quasi-steady data for another GNC MDM failure event on GMT 11-February-2002, 042/08:00. The failure occurred at GMT 042/00:08, for which there is a data gap (probably as a result of the failure). Attitude control was handed over to the Russian segment. The US regained control at GMT 042/04:30 at which point some maneuvering was performed to return to nominal attitude. The red box highlights the impact on the quasi-steady environment, with the peak disturbance near -3.6 μg on the Y_A and Z_A-axes.

6.1.6.2 Unknown Disturbance

During Increments 4 and 5, an unidentified source caused disturbances in both the vibratory and quasi-steady regime. The focus of this section is on the effects in the quasi-steady regime. A brief vibratory background will be given to correlate with quasi-steady data, but a more detailed analysis on the vibratory component may appear in a future report as more information on the source is determined.

The nature of the signal in the vibratory regime can be seen in Figure 6-70, a spectrogram of SAMS 121F04 data starting at GMT 16-September-2002, 259/16:00. It is manifested as a broadband "fuzzy" signal centered on 120-130 Hz, a narrower 100 Hz signal, or a thin 158 Hz signal. In the spectrogram, the signal is at 120 Hz until the 17:20 mark, at which point it disappears and the 100 Hz signal is seen. This signal continues until approximately 20:30, where it again changes, this time to the narrow 158 Hz signal. It is the time that the 100 Hz signal is seen in SAMS data that the effects on the quasi-steady environment are seen. Figure 6-71 is a Y_A-axis time series plot of MAMS OSSBTMF data for the same time period of Figure 6-70. At the point at which the 100 Hz signal appears the Y_A-axis acceleration component in the quasi-steady data drops down approximately 0.50 μg. The mean Y_A-axis for the time period when the 100 Hz component was active is -0.41 μg. For time period when the 100 Hz was not active the mean was -0.91 μg.

A repeated switch from 100 Hz to 120 Hz and back gives the appearance of a "square wave" in the Y_A-axis of MAMS data. A good example of this type of behavior is shown in Figure 6-72, a time series plot of MAMS OSS data from GMT 15-August-2002, 227/22:00. The Y_A-axis of the plot shows the "square wave" phenomenon, especially in the early part of the plot when the crew was asleep. Figure 6-73 is a 1.5 hour spectrogram beginning at GMT 15-August-2002, 227/22:00 with the MAMS OSS Y_A-axis acceleration overlaid for correlation with the appearance of the 100 Hz signal. (Note: The MAMS OSS data was adjusted by -1.96 minutes due to a known discrepancy between SAMS and MAMS timing.)

6.1.6.3 Reboosts

The primary method for conducting a reboost is using the main engine of a docked cargo vehicle, typically a Progress M1. Progress' main engine is limited to burning only the amount of fuel contained within the Progress propulsion system propellant tanks. If necessary, the Service Module (SM) and the Functional Cargo Block (FGB) can transfer fuel to the docked Progress during a reboost. In that case, the Progress' rendezvous and docking thrusters are used, instead of the main engine, due to fuel flow limitations [6]. If a reboost is needed and there is no docked Progress, the SM engines can also be used to conduct such reboost.

Station reboosts are open loop burns, where the firing is initiated at a prescribed time and place in orbit. The basic sequence of events requires that the station maneuver to the reboost attitude. Then, at the appropriate time, commands are issued for the jets to fire for a specific length of time. A reboost usually requires two burns [6]. At the end of the second burn, the station is maneuvered to its nominal attitude.

MAMS OSSBTMF data for several reboost events during Increments 4 and 5 (and one from Increment 3) were analyzed to compare average acceleration with the expected results. The mean of the X_A-axis acceleration component was calculated for the burn and compared to the expected result obtained from information given to PIMS by the Boeing Company. Figure 6-74 is an example of a reboost burn starting at GMT 06-March-2002, 065/04:29. Two types of burns were studied. In the "4 Progress +X Thrusters" in which four thrusters are pointed in the $-X_A$ direction and four other YZ thrusters are used for attitude control. For "8 Progress +X Thrusters, Off-Pulsing", all thrusters are in the $-X_A$–axis direction; four on continuously, other four pulse on/off. The blue lines in the plot represent the start and stop times of the burn, and the red dots are the points included in calculation of the mean.

Table 6-8 and Table 6-9 summarize the comparison of 12 different reboost events. All the calculated results using MAMS measurements for the "4 Progress +X Thrusters" reboosts fall within ± 0.02 mg (compare last column of Table 6-8 to 2nd column of Table 6-9). However, the results for the "8 Progress +X Thrusters, Off-Pulsing" are low with respect to the expected values, with the exception of the burn at 13-March-2002, 072/00:52, which falls within 0.02 mg. The probable cause of this is in the nature of the MAMS OSS instrument. The MAMS sensor can be in one of three ranges: A, B or C, with A used to measure the highest acceleration and C used for the lowest. The MAMS instrument will not switch to a higher range unless an out-of-range acceleration is experienced for a specific time. During the non-microgravity like accelerations of reboosts, the MAMS sensor will saturate for a brief time until the sensor is switched to the higher range, which may result in a measured value lower than the actual. In addition, the A-range does not undergo periodic calibration and MAMS OSSBTMF data would be inaccurate. In a normal microgravity environment, A-range data is rarely seen and would be tossed out in the trimmean filter process. All data sets used were scanned for A-range data and results are included in Table 6-8 and Table 6-9.

TABLE 6-8 REBOOST DETAILS

Info from Donald.H.Sargent@Boeing.com, ISS Propulsion, via Rex Delventhal				
GMT Time of Ignition	**Duration (sec)**	**Δ V (m/sec)**	**Comments**	**ΔV/T (mg)**
11-October-2001, 284/10:31	1560	4.7	4 Progress +X Thrusters	0.31
11-October-2001, 284/15:54	1560	4.5	4 Progress +X Thrusters	0.29
10-January-2002, 010/01:35:15	1877	5.4	4 Progress +X Thrusters	0.29
10-January-2002, 010/03:43:26	1654	4.8	4 Progress +X Thrusters	0.30
21-February-2002, 052/08:27	239	1.35	8 Progress +X Thrusters, Off-Pulsing	0.58
21-February-2002, 052/09:59	243	1.35	8 Progress +X Thrusters, Off-Pulsing	0.57
06-March-2002, 065/03:37:12	158.2	1	8 Progress +X Thrusters, Off-Pulsing	0.65
06-March-2002,065/04:29:07	395.1	2.5	8 Progress +X Thrusters, Off-Pulsing	0.65
13-March-2002,072/00:04:10	319	2.2	8 Progress +X Thrusters, Off-Pulsing	0.70
13-March-2002,072/00:52:49	636.1	4	8 Progress +X Thrusters, Off-Pulsing	0.64
19-April-2002, 109/07:59	118	0.73	8 Progress +X Thrusters, Off-Pulsing	0.63
01-August-2002, 213/17:24:23	760	4.3	8 Progress +X Thrusters, Off-Pulsing	0.58

TABLE 6-9 MAMS MEASUREMENTS DURING REBOOSTS

Calculations from MAMS OSS Data				
GMT Time of Ignition	**X-Axis Mean (mg)**	**Duration (sec)**	**MAMS GMT Start**	**OSS Calibration**
11-October-2001, 284/10:31	0.29	1,629.30	10/11/01 10:32:39	OK
11-October-2001, 284/15:54	0.28	1,623.78	10/11/01 15:55:48	OK
10-January-2002, 010/01:35:15	0.29	1,863.90	01/10/02 01:36:20	OK
10-January-2002, 010/03:43:26	0.29	1,643.00	01/10/02 03:44:30	OK
21-February-2002, 052/08:27	0.52	237.40	02/21/02 08:27:55	OK
21-February-2002, 052/09:59	0.53	238.50	02/21/02 09:59:57	OK
06-March-2002, 065/03:37:12	0.60	157.70	03/06/02 03:38:38	X-axis A-Range*
06-March-2002,065/04:29:07	0.64	398.80	03/06/02 04:30:22	X-axis A-Range*
13-March-2002,072/00:04:10	0.61	300.30	03/13/02 00:05:55	X-axis A-Range*
13-March-2002,072/00:52:49	0.66	609.70	03/13/02 00:54:19	X-axis A-Range*
19-April-2002, 109/07:59	0.43	142.70	04/19/02 07:59:56	OK
01-August-2002, 213/17:24:23	0.56	761.10	08/01/02 17:26:13	OK

NOTE: *X-axis A-range Calibrations Warning. For a portion of the time period in these thruster firings, the X-axis went to A-range. MAMS does not actively calibrate A range data for bias. Therefore, the X-axis may be off as much as 14 μg.

6.2 Vibratory Microgravity Environment

In the vibratory regime, directionality of the acceleration measurement is typically not of key importance. However, the following should be considered for those concerned with the directionality of the Space Acceleration Measurement System (SAMS) data: (1) the SAMS data are opposite in polarity to the MAMS OSS data, and (2) positive direction accelerations appear as negative direction accelerations for SAMS data (and appear as positive direction accelerations for MAMS OSS data). To help explain this further, consider the inertial reference frame shown in the left side graphic below.

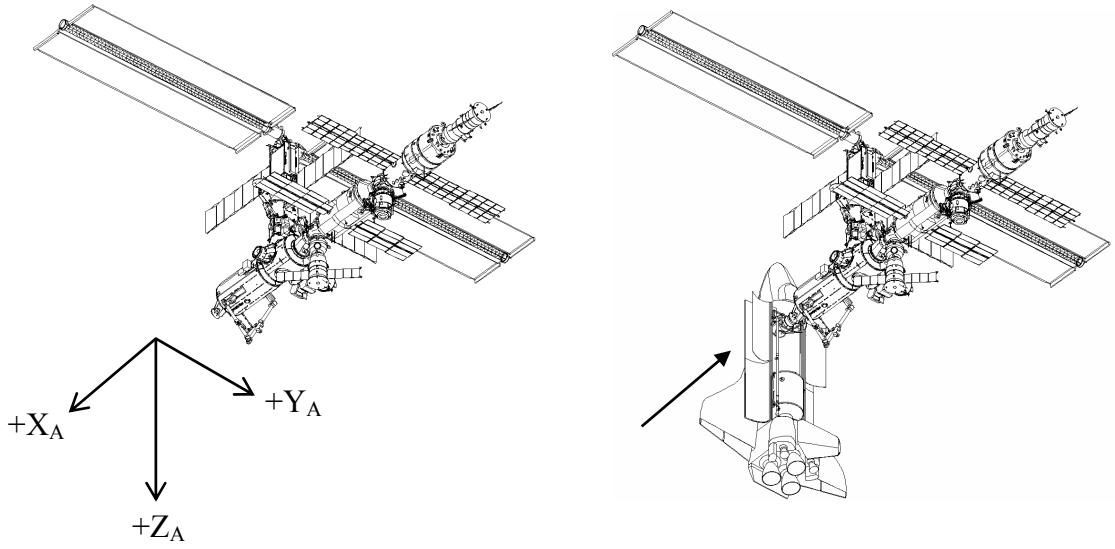

This shows the ISS before impact of a Shuttle for a docking event. At Shuttle impact during docking, the ISS rigid body accelerates in the $-X_A$ direction. This is depicted in the right side graphic above. MAMS OSS data show this as a brief $-X_A$-axis acceleration, while SAMS data show this as a $+X_A$-axis acceleration event. Another telltale acceleration event that bears this fact is that of a Progress vehicle reboost. Orbital dynamics dictate that in order to boost the altitude of the ISS, its velocity must be increased (it must be accelerated) in the direction of flight. The Progress vehicle shown in the graphics above is at the far right side of the stack. Its thrusters are pointed primarily in the $-X_A$ direction, so that by Newton's third law of action/reaction, when these are fired, the ISS accelerates in the $+X_A$ (flight) direction. For this event, the MAMS OSS would report primarily a $+X_A$-axis acceleration, while SAMS would report a $-X_A$-axis acceleration. Since there is sometimes confusion when referencing acceleration data collected on Earth, another point to consider is this scenario: Let's say there is an accelerometer at rest on a table on Earth. This is nice because we can unambiguously reference the sensor's top (farthest from center of Earth) and its bottom (slightly closer to the Earth's center). Aligned this way, we should expect the accelerometer to sense acceleration in the direction from its bottom toward its top, or upward, while it's sitting there at rest in Earth's 1g gravitational field. This is Einstein's equivalence principle. It helps to imagine this same setup as being sufficiently far from a large mass like Earth so as to be able to neglect gravity. Take this same configuration, a table with the accelerometer snug down flush on its top and sufficiently far away from any massive body so as to neglect gravity. Now put thrusters pointing "down" out the bottom of each table leg and fire them (all at same time with same force and direction). If the thrusters' force is such that the acceleration magnitude is 1g and the table is now pushing (accelerating) the accelerometer in the direction from the "bottom" of the sensor toward its "top" (as suggested by thrust out bottom of table legs), then the accelerometer reading should be the same as while it was sitting there at rest in Earth's 1g gravitational field.

The vibratory acceleration regime consists of the acceleration spectrum from 0.01 to 400 Hz, with magnitudes expected to vary greatly depending on the nature of the disturbance and on the transmissibility path from the source to locations of interest. The relatively high frequency accelerations that shape the vibratory environment of the ISS are usually associated with vehicle operations, vehicle systems, experiment-related equipment, and crew activity.

Section 6.2.1 of this report discusses the impact of vehicle operations such as Progress vehicle reboost, Shuttle docking and undocking. In section 6.2.2, we examine vehicle subsystems including the ARIS, Russian segment air conditioners, and control moment gyroscopes. Equipment used for Gas Analysis System for Metabolic Analysis of Physiology (GASMAP) and Microencapsulation Electrostatic Processing System (MEPS) are the focus of section 6.2.3. The last major category of vibratory disturbances considered for this report is crew activity. Activity such as exercise, Temporary Sleep Station (TeSS) entry/exit, EVA, and Public Affairs Office (PAO) events are the subject of section 6.2.4. Finally, section 8.2 serves to summarize the vibratory analysis results for Increment-4/5.

6.2.1 Vehicle Operations

All the Progress dockings are automated with little or no crew action required [6], but the station crew can fly the vehicle remotely from the SM, if needed. The sequence of events mandates that the Photovoltaic Arrays (PVAs) be "feathered" (oriented parallel to the velocity vector of the docking vehicle) to prevent the impingement of jet plumes of the approaching vehicle. Because the ISS arrays are feathered, they no longer track the sun, therefore, are no longer able to generate sufficient power outputs. As a result, all non-essential operations are suspended (i.e., payloads operations). The station is subsequently maneuvered to docking attitude. After docking, the station is maneuvered to its nominal attitude and the arrays resume sun tracking. The Progress vehicle undocks just before the arrival of the next one.

Shuttle docking is not that different from a Progress docking. For a Shuttle docking, the Shuttle crew has insight into ISS status and can command the ISS because of the data interface between the Shuttle and station. About 300 feet directly in front of the station, the Shuttle slowly moves toward the station's Shuttle docking port—moving at a speed of about a tenth of a mile per hour. Using a view from a camera mounted in the center of the Shuttle's docking mechanism as a key alignment aid, the docking ports of the two spacecraft are precisely aligned. For the actual docking, the Shuttle's relative speed to the station is maintained at about one-tenth of a foot per second (when the two spacecraft are about 30 feet apart), and the docking mechanism is aligned to within three inches of one another. When Shuttle makes contact with the station (soft mate), preliminary latches automatically attach the two spacecraft together. Immediately after the Shuttle docks, the Shuttle's steering jets are deactivated to reduce the forces acting at the docking interface. Shock absorber-type springs in the docking mechanism dampen any relative motion between the two spacecrafts. Once relative motion between the two spacecraft stops, the docking mechanism is secured and the Shuttle's mechanism retracts and closes a final set of latches between the Shuttle and station (hard mate) [13]. Typical mated operations involve 6-9 days docked.

Once the Shuttle is ready to undock, the docking mechanism is commanded for release. The initial separation of the spacecraft is performed by springs in the docking mechanism that gently pushes the Shuttle away from the station. The Shuttle's steering jets are shut off to avoid any inadvertent firings during initial separation. Once the docking mechanism's springs pushed the Shuttle away to a distance of about two feet, when the docking devices are clear of one another, the steering jets are turned back on and fire to begin very slowly moving away [13].

6.2.1.1 Progress Reboost

To assess the impact of burns for a couple of Progress reboost events (UF-1 stage reboost 3 and UF-1 stage reboost 4), consider an hour period around the times shown in the first 2 rows of Table 6-10. This table is an excerpt of the ATL using Greenwich Mean Time (GMT) found at:

http://mod.jsc.nasa.gov/df/df64/ADCO-Flight-Info/As Flown Info/Increment 4/As Flown ISS ATL Inc 4A.doc

TABLE 6-10 EXCERPT OF "INC 4A AS-FLOWN ISS ATTITUDE TIMELINE (ATL)"

#	MANEUVER START-STOP GMT	BETA ANGLE	ATTITUDE NAME	REF FRAME	YAW PITCH ROLL	EVENT	REMARKS
194	065/01:34 - 01:36	-38	+ZLV +XVV	LVLH	359.5 357.9 0.0	Mnvr to UF1 Stage Reboost 3 Attitude	Burn Start 03:37:12.00 Burn Stop 03:39:50.20
195	065/03:42 - 03:43	-37	+ZLV +XVV	LVLH	359.5 357.9 0.0	Mnvr to UF1 Stage Reboost 4 Attitude	Burn Start 04:29:07.00 Burn Stop 04:35:42.10
201	071/22:04 - 22:06	-5	+ZLV +XVV	LVLH	359.5 357.9 0.0	Mnvr to UF1 Stage Reboost 5 Attitude	Burn start: 00:04:10.00 Burn stop: 00:09:29.00
202	072/00:12 - 00:13	-4	+ZLV +XVV	LVLH	359.5 357.9 0.0	Mnvr to UF1 Stage Reboost 6 Attitude	Burn start: 00:52:49.00 Burn stop: 01:03:25.10

Considering the 1-hour period starting at GMT 06-March-2002, 065/03:08:30 for reboost 3, we see a noticeable upward step of the acceleration vector magnitude in Figure 6-75 around the 30-minute mark. The timestamps affiliated with the acceleration measurements indicate the reboost 3 burn went from GMT 06-March-2002, 065/03:37:23 to 03:40:03. This lags the ATL time by about 21 seconds. A full accounting of this timing discrepancy is not presently known. Likewise, around the 30-minute mark of Figure 6-76, the step up in acceleration magnitude for reboost 4 is apparent. The SAMS timestamps for this event show it lasted from GMT 06-March-2002, 065/04:29:36 to 04:36:22. This time the start lags the ATL by 29 seconds and the duration is nearly 9 seconds longer according to SAMS data. The previous 2 figures show the 1-hour span under consideration for SAMS sensor 121f03. If we consider the same span for SAMS sensor 121f02 and 121f04, then we can compare the median acceleration vector magnitudes for times before/after the burn to those during the burn and get the results shown in Table 6-11.

TABLE 6-11 PROGRESS REBOOST MEDIAN ACCELERATION MAGNITUDE COMPARISON

Sensor	Cutoff Frequency (Hz)	Location	State	Median Acceleration Vector Magnitude (µg)	Delta Vector Magnitude (µg)
121f02	25	LAB1O2, ER1, Drawer 1	Not During Burn 3	284	-----
			During Burn 3	745	461
121f03	25	LAB1O1, ER2, Lower Z Panel	Not During Burn 3	155	-----
			During Burn 3	769	614
121f04	25	LAB1O2, ER1, Lower Z Panel	Not During Burn 3	181	-----
			During Burn 3	747	566
121f02	25	LAB1O2, ER1, Drawer 1	Not During Burn 4	313	-----
			During Burn 4	770	457
121f03	25	LAB1O1, ER2, Lower Z Panel	Not During Burn 4	159	-----
			During Burn 4	758	599
121f04	25	LAB1O2, ER1, Lower Z Panel	Not During Burn 4	179	-----
			During Burn 4	737	558

Note that in each case, the median acceleration vector magnitudes were over 700 μg during the Progress reboost burn and the largest difference was seen in the 121f03 data for reboost 3.

Another set of Progress reboost burns took place on GMT 15-May-2002. The time series measured by SAMS 121f02 for this event are shown in Figure 6-77. From this figure, it is not obvious that the primary effect is quasi-steady and registered on the X_A-axis. The interval average plots of Figure 6-78, Figure 6-79, Figure 6-80, Figure 6-81, and Figure 6-82 for SAMS 121f02, 121f03, 121f04, 121f05, and 121f06, respectively, show the effect more clearly. These interval average plots are not intended to quantify this event in an absolute way, but they are intended to show the low amplitude DC shift on the X_A-axis. Note, as discussed earlier, that the polarity of SAMS (opposite of MAMS) is such that it gives counterintuitive directionality for this acceleration. Acceleration in the $+X_A$ direction (the flight direction) is registered as $-X_A$ acceleration. According to SAMS timing, the reboost plotted in the interval average figures started at GMT 15-May-2002, 135/22:29:51 and lasted approximately 188 seconds. Table 6-12 details the maximum acceleration magnitude in each SSA orthogonal axis and vector magnitude during the reboost.

TABLE 6-12 PROGRESS REBOOST PEAKS (START AT GMT 15-MAY-2002, 135/22:29:51)

Sensor	Cutoff (Hz)	Location	Maximum Magnitude (mg)			
			X_A-axis	Y_A-axis	Z_A-axis	Vector
121f02	200	LAB1O2 ER1 Drawer 1	13.62	5.65	7.61	14.77
121f03	200	LAB1O1 ER2 Lower Z Panel	3.06	7.13	9.25	9.84
121f04	100	LAB1O2 ER1 Lower Z Panel	2.02	6.58	6.91	8.99
121f05	25	LAB1O1 ER2 Upper Light Tray	3.53	7.03	6.74	9.93
121f06	25	LAB1O1 ER2 PCS Test Section	5.65	25.64	4.24	25.83

Table 6-13 details the median acceleration magnitude for each axis and for the vector magnitude.

TABLE 6-13 PROGRESS REBOOST MEDIANS (START AT GMT 15-MAY-2002, 135/22:29:51)

Sensor	Cutoff (Hz)	Location	Median Magnitude (mg)			
			X_A-axis	Y_A-axis	Z_A-axis	Vector
121f02	200	LAB1O2 ER1 Drawer 1	0.80	0.56	0.71	1.44
121f03	200	LAB1O1 ER2 Lower Z Panel	0.53	0.48	0.60	1.21
121f04	100	LAB1O2 ER1 Lower Z Panel	0.24	0.46	0.61	0.97
121f05	25	LAB1O1 ER2 Upper Light Tray	0.21	0.13	0.15	0.39
121f06	25	LAB1O1 ER2 PCS Test Section	0.18	0.11	0.10	0.31

A final set of Progress reboost burns was similarly analyzed. These took place on GMT 01-August-2002. The time series measured by SAMS 121f08 are shown in Figure 6-83. From this figure, it is again not obvious that the primary effect is registered on the X_A-axis. The interval average plots of Figure 6-84, Figure 6-85, and Figure 6-86 for SAMS 121f08, 121f02, and 121f03, respectively, show the effect more clearly. The nomenclature assigned to this reboost was "8 Progress +X Thrusters, Off-Pulsing", which implies all thrusters are primarily aligned

with X_A-direction and 4 are on continuously, while the other 4 pulse on and off. This results in the 2 plateaus seen in the DC shift during the reboost period. Again, these interval average plots are not intended to quantify this event in an absolute way, but to show the low amplitude DC shift on the X_A-axis, and in this case, the 2 plateaus that result from off pulsing. According to SAMS timing, the reboost plotted in the interval average figures started at GMT 01-August-2002, 213/17:24:12 and lasted approximately 764 seconds. Table 6-14 details the maximum acceleration magnitude in each SSA orthogonal axis and vector magnitude during the reboost.

TABLE 6-14 REBOOST PEAK ACCELERATIONS (START AT GMT 01-AUGUST-2002, 213/17:24:12)

Sensor	Cutoff (Hz)	Location	Maximum Magnitude (mg)			
			X_A-axis	Y_A-axis	Z_A-axis	Vector
121f02	100	LAB1O2 ER1 Drawer 1	27.22	15.11	8.69	29.32
121f03	200	LAB1O1 ER2 Lower Z Panel	6.05	5.41	6.55	7.53
121f04	200	LAB1O2 ER1 Lower Z Panel	5.69	7.06	8.76	10.12
121f05	100	LAB1O1 ER2 Upper Light Tray	12.76	64.79	57.11	86.51
121f08	25	LAB1S3, MSG, Ceiling Plate A2 A3	16.36	18.10	8.61	18.46

Table 6-15 details the median acceleration magnitude for each axis and for the vector magnitude.

TABLE 6-15 REBOOST MEDIAN ACCELERATIONS (START AT GMT 01-AUGUST-2002, 213/17:24:12)

Sensor	Cutoff (Hz)	Location	Median Magnitude (mg)			
			X_A-axis	Y_A-axis	Z_A-axis	Vector
121f02	100	LAB1O2 ER1 Drawer 1	0.57	0.21	0.24	0.75
121f03	200	LAB1O1 ER2 Lower Z Panel	0.91	0.66	0.90	1.83
121f04	200	LAB1O2 ER1 Lower Z Panel	1.40	0.58	0.79	2.04
121f05	100	LAB1O1 ER2 Upper Light Tray	0.56	0.44	0.89	1.25
121f08	25	LAB1S3, MSG, Ceiling Plate A2 A3	0.55	0.18	0.14	0.67

To provide some context for the values shown in the 2 tables above, consider the 95th percentiles computed for 4 hours (GMT 12:00 – 16:00) before the reboost event in the following table:

TABLE 6-16 95TH PERCENTILE BASELINE ACCELERATION MAGNITUDE BEFORE REBOOST

Sensor	Cutoff (Hz)	Location	95th Percentile Magnitude (mg)
			Vector
121f02	100	LAB1O2 ER1 Drawer 1	0.78
121f03	200	LAB1O1 ER2 Lower Z Panel	3.45
121f04	200	LAB1O2 ER1 Lower Z Panel	3.05
121f05	100	LAB1O1 ER2 Upper Light Tray	2.00

6.2.1.2 Space Shuttle Atlantis (STS-112), Flight 9A Docking/Undocking

According to the Shuttle archives at http://spaceflight.nasa.gov, the Shuttle docked with the ISS at Central Daylight Time (CDT) 09-October-2002, 10:17 (GMT 09-October-2002,

282/15:17:00). The data recorded by SAMS around this time show softmate occurred at about GMT 09-October-2002, 282/15:16:23 and hardmate at about GMT 09-October-2002, 282/15:27:27. The MAMS HiRAP data showed these events about 15 seconds later than the SAMS times. Telemetry data relayed to Principal Investigator Microgravity Services (PIMS) by Boeing engineers indicated that the closing contact velocity was approximately 0.2 ft/sec, which was about twice the nominal contact velocity.

For STS-112 Shuttle softmate, the maximum acceleration magnitudes recorded by SAMS and MAMS were as shown in Table 6-17.

TABLE 6-17 PEAK ACCELERATIONS FOR STS-112 DOCKING SOFTMATE

Sensor	Location	Cutoff (Hz)	Peak (mg)	Plot
121f03	LAB1O1, ER2, Lower Z Panel	200	68.3	Figure 6-87
121f04	LAB1O2, ER1, Lower Z Panel	200	60.6	Figure 6-88
121f05	LAB1O1, ER2, Upper Light Tray	100	26.0	Figure 6-89
121f02	LAB1O2, ER1, Drawer 1	100	13.8	Figure 6-90
HiRAP	LAB1O2, ER1, Lockers 3,4	100	12.4	Figure 6-91

For comparison, two other docking softmates on record (MAMS HiRAP at 100 Hz) imparted peak accelerations of 10 mg and 29 mg for the STS-104 and STS-105 dockings, respectively.

Also, according to the Shuttle archives at http://spaceflight.nasa.gov, Atlantis undocked from the ISS at CDT 16-October-2002, 08:13 (GMT 16-October-2002, 289/15:13). The spectrogram in Figure 6-92 shows a red vertical streak indicating an impulsive event at about GMT 16-October-2002, 289/15:13:32. For this Shuttle undocking event, the maximum acceleration magnitudes recorded by SAMS were as shown in Table 6-18.

TABLE 6-18 PEAK ACCELERATIONS FOR STS-112 UNDOCKING

Sensor	Location	Cutoff (Hz)	Peak (mg)	Plot
121f02	LAB1O2, ER1, Drawer 1	100	27.4	Figure 6-93
121f04	LAB1O2, ER1, Lower Z Panel	200	23.7	Figure 6-94
121f03	LAB1O1, ER2, Lower Z Panel	200	17.5	Figure 6-95
121f05	LAB1O1, ER2, Upper Light Tray	100	2.6	Figure 6-96

For comparison, two other undocking events on record (MAMS HiRAP at 100 Hz) imparted peak accelerations of about 7.5 mg and 9.5 mg for the STS-104 and STS-105 undockings, respectively.

6.2.2 Vehicle Systems

An example of a vehicle system is the Environmental Control and Life Support System (ECLSS) which provides a pressurized and habitable environment within the space station by supplying correct amounts of oxygen and nitrogen, controlling the temperature and humidity, removing

carbon dioxide and other atmospheric contaminants, and monitoring the atmosphere for the presence of combustion products, and major constituent proportions. Additionally, the ECLSS collects, processes, and stores water and waste used and produced by the crewmembers, and provides fire detection, suppression, and crew safety equipment.

This section includes analysis of vibratory disturbance sources such as ARIS, Russian segment air conditioners (part of ECLSS), and control moment gyroscopes.

6.2.2.1 Active Rack Isolation System (ARIS)

The following information was obtained from the ARIS-ICE team:

no SAMS data

```
Nov 14th in SLOW HOLD
GMT 318:17:14 thru 318:18:52, with a small rack command at 17:56

Nov 20th
GMT 324:21:13 Transition to HOLD.....see
GMT 324:21:21 Transition to ACTIVE.....see
GMT 324:22:49 Transition to REST.....see
GMT 324:23:02 Transition to IDLE.....see
```

While the spectrograms of Figure 6-99 and Figure 6-100 show no discernible effects at the transition times cited, the spectrograms of Figure 6-97 and Figure 6-98 show an 8-hour period around these transitions for SAMS sensors 121f03 and 121f04, respectively. The SAMS 121f03 sensor was located on the Z-panel of the ARIS rack (ER2) for the transition times cited above, while the SAMS 121f04 sensor was attached to the Z-panel of the adjacent rack (ER1).

To quantify the effect of ARIS in various modes from locations on the Z-panel of the ARIS rack and from the Z-panel of an adjacent rack, SAMS sensor 121f03 and 121f04 data were analyzed for the times shown above. The results are presented in the form of one-third octave (OTO) root-mean-square (RMS) values and are overlaid by the vibratory requirements curve. Figure 6-101 and Figure 6-102 show results for ARIS in hold mode. Figure 6-103 and Figure 6-104 show results for ARIS in active mode. Figure 6-105 and Figure 6-106 show results for ARIS in rest mode. Figure 6-107 and Figure 6-108 show results for ARIS in idle mode.

TABLE 6-19 ARIS MODE TRANSITION TIMES

ARIS Mode Transition	GMT	Reference Figure
HOLD to ACTIVE	28-Oct-2002, 301/14:38	Figure 6-109, Figure 6-112
ACTIVE to HOLD	28-Oct-2002, 301/18:55	Figure 6-110, Figure 6-113
HOLD to IDLE	29-Oct-2002, 302/09:53	Figure 6-111, Figure 6-114

Spectrograms for SAMS 121f03 sensor located on the Z-panel of the ARIS rack (ER2) for the transition times cited above are shown in Figure 6-109, Figure 6-110, and Figure 6-111; while Figure 6-112, Figure 6-113, and Figure 6-114 are spectrograms of the corresponding time frames for the SAMS 121f04 sensor attached to the Z-panel of the adjacent rack (ER1). Table 6-19 provides the GMT references for these ARIS mode transitions. The relatively strong broadband

disturbance above 80 Hz and two strong narrowband signals at about 94.8 and about 178.3 Hz that accompany the HOLD mode draw particular attention. This can be seen most clearly when comparing the Power Spectral Density (PSD) traces shown in Figure 6-115. These PSD traces highlight key differences between the modes in a relative way, but to quantify the comparison in an absolute sense, OTO quartile plots are more suitable. Table 6-20 lists references to the plots where the five markers in each OTO band are quartile statistics as follows:

1. top triangle: maximum value ("100th" percentile)
2. top of vertical line: 75th percentile
3. circle: 50th percentile (median)
4. bottom of vertical line: 25th percentile
5. bottom triangle: minimum value ("0th" percentile)

TABLE 6-20 OTO QUARTILE PLOTS OF ARIS MODES

Sensor	ARIS Mode	See
121f03	HOLD	Figure 6-116
121f04	HOLD	Figure 6-117
121f03	ACTIVE	Figure 6-118
121f04	ACTIVE	Figure 6-119
121f03	HOLD	Figure 6-120
121f04	HOLD	Figure 6-121
121f03	IDLE	Figure 6-122
121f04	IDLE	Figure 6-123

As another means of quantifying the effects of the ARIS mode transitions cited earlier in this section, the peak acceleration, or maximum acceleration vector magnitude, was extracted from the measurements made by SAMS sensors 121f03 and 121f04 for each of 3 transitions. The results are shown in Table 6-21.

TABLE 6-21 ARIS TRANSIENTS DURING MODE SWITCHES

Sensor	Mode Transition	Peak Acceleration (mg)	See
121f03	HOLD to ACTIVE	37.7	Figure 6-124
121f04	HOLD to ACTIVE	25.5	Figure 6-125
121f03	ACTIVE to HOLD	48.5	Figure 6-126
121f04	ACTIVE to HOLD	30.1	Figure 6-127
121f03	HOLD to IDLE	40.8	Figure 6-128
121f04	HOLD to IDLE	17.1	Figure 6-129

Since the SAMS 121f03 sensor was mounted on the Z-panel of the ARIS rack (ER2) it was expected to register larger acceleration magnitudes compared to the 121f04 sensor mounted on the adjacent ER1 during ARIS mode transitions.

6.2.2.2 Russian Segment Air Conditioners (SKV-1 and SKV-2)

The Russian segment air conditioning system is designed to circulate, cool, and dry the air in the Russian segment. It comprises two air conditioners (SKV-1 and SKV-2), which are installed in the Service Module (SM). Nominally, only SKV-1 is to operate with SKV-2 operating as a backup. However, it is possible for both to operate simultaneously and SAMS data has shown both SKV units operating coincidentally.

The on-orbit status report for GMT 04-September-2002 had this entry:

Thermal Control Systems:
Air conditioner SKV-1 is Off; SKV-2 is On.

while the report for GMT 23-September-2002 showed this:

Thermal Control Systems:
Air conditioner SKV-1 is On; SKV-2 is Off.

Based on this information, averaged spectra for these 2 days were computed in the form of the PSD of Figure 6-130 with the traces labeled accordingly. The red trace shows the spectral signature of the SKV-2 air conditioner, while the green trace is for the SKV-1 signature. These averaged spectra show: (1) the 2 air conditioners operated at slightly different frequencies – the SKV-2 at about 23.2 Hz and SKV-1 at about 23.4 Hz, and (2) the SKV-2 was registered as significantly stronger in the US Lab sensor locations. Another note regarding the spectra for these 2 days is that a broadband "swoosh" disturbance below 25 Hz was present on GMT 23-September-2002, which raised the spectra across all frequencies for that day.

To further quantify the disparity between the 2 air conditioners, approximately 16 hours of operation was considered for the interval Root-Mean-Square (RMS) plot of Figure 6-131. The red trace for SKV-2 is cyclic with an orbital period and RMS levels between about 20 μg_{RMS} and 50 μg_{RMS} for the frequency range from 23 to 24 Hz. Periodicity is not obvious in the green trace for SKV-1 and the measured RMS levels were nominally below about 10 μg_{RMS}.

Comparing spectrograms of SKV-1 operation shown in Figure 6-132 and Figure 6-133 for SAMS sensors 121f02 and 121f05, respectively, note the stop of the Russian SKV air conditioner signature at just over 23 Hz at about 10:00 and start again not long after 13:00. The interval RMS values for the span of these spectrograms was computed and clearly shows start/stop transitions at these times (see Figure 6-134 and Figure 6-135). For 121f05 (mounted to light tray on top of ER2), there is an obvious, strong second harmonic at about 46 Hz, but 121f02 (mounted in Remote Triaxial Sensor (RTS) drawer in ER1) does not register this harmonic (see Figure 6-136 and Figure 6-137 for interval RMS). The second harmonic at 46 Hz also was present in 121f03 (Z-panel of ER2) and 121f04 (Z-panel of ER1) data. It is presumed that the transfer function for that particular structural path to the 121f02 sensor location in the RTS drawer attenuates at this second harmonic frequency.

6.2.2.3 Control Moment Gyroscopes (CMGs)

A description of CMG operations was provided previously in section 6.1.1. While the small tolerance on the rotational rate of the CMGs simplifies identification of its spectral signature, it also confounds the identification of individual CMG signatures among the three (or four) that are operating simultaneously. As a possible lead for an investigation into a CMG failure, high-resolution frequency domain analyses were performed. The high-resolution spectrogram of Figure 6-138 was computed with a frequency resolution of 0.0076 Hz. With this setting and the frequency scale as shown, there only appeared one distinct signal at 110 Hz (6600 RPM). A closer look with Figure 6-139 shows more detail. With this frequency scale zoom, at least 3 distinct, narrowband traces are observed around the expected rotational rate of the CMGs. These 3 signals reside in consecutive frequency bins between 110 and 110.016 Hz. This does not preclude simultaneous operation of 4 CMGs, but does reflect insufficient frequency resolution. That is, multiple signals at nearly identical frequency could not be resolved. It is also possible that small changes in rotational rate over time could have happened during this span to have one disturbance source occupy multiple frequency bins over the time considered.

To enumerate the impact of CMG operation on the vibratory environment, the interval RMS trace of Figure 6-140 was computed. For this 48-hour span, a cyclic behavior for the acceleration RMS level was observed. The RMS level in the extremely narrow frequency band around the CMG rotational rate ($109.983 < f < 110.017$ Hz) varied between about 20 μg_{RMS} and about 100 μg_{RMS}. CMG-1 failed on GMT 08-June-2002, the day after these measurements were recorded. According to information at:

http://www.aviationnow.com/content/publication/awst/20020617/aw36b.htm

> One of the station's four 800-lb. control moment gyros (CMGs) failed on June 8, the day after Endeavour docked. The 6,600-rpm CMGs exert torque to change attitude without the use of Russian propellant. The CMGs were being used to maneuver the 700,000-lb. station/orbiter stack, when CMG-1 began to fly apart in its housing in the Z-1 truss above the Node 1.
>
> Astronaut Carl Walz, who was in the adjacent Destiny Module at the time, reported a "pretty loud noise, a kind of a growling sound" from inside the Node. Ground controllers saw the malfunction and quickly disconnected power to the unit. Since they run at such high RPMs, the big gyros normally take up to 20 hours to spin down. But with debris in its bearings, this one ground to a halt in only 1 hour, sending a grinding sound through the station structure until the spinning stopped.

The station attitude for the GMT June 6 - June 7, 2002 time frame considered above was the XPOP reference frame, -XPH +ZNN TEA, momentum management. For comparison a similar attitude (XPOP reference frame, +XPH +ZNN TEA, momentum management) was considered for a follow-up analysis starting with GMT 26-August-2002. The interval RMS plot of Figure 6-141 was computed for comparison to the pre-failure plot of Figure 6-140 for CMG-1. The later plot with only 3 operational CMGs does not exhibit the cyclic behavior discussed earlier and the mean RMS value for the 48-hour span starting on GMT 26-August-2002, 238/00:00:00 was approximately 48 μg_{RMS}.

6.2.3 Experiment Equipment

This section assesses the impact on the microgravity environment of different equipment used by the experiments. The help received from the science teams in charge of these experiments enabled characterization of these experiments on the overall microgravity environment during their operations.

Equipment used for the Pulmonary Function in Flight (PuFF) investigation in the HRF is the focus of section 6.2.3.1. In particular, the GASMAP device, which is used to monitor and analyze inhaled and exhaled breath streams to determine their gas concentrations. The Process Chamber Module (PCM) installation and operation of the MEPS hardware are analyzed as well.

6.2.3.1 GASMAP Sample Catheter Pump and Fan

Little is known about how human lungs are affected by long-term exposure to the reduced pressure in spacesuits during spacewalks (EVA) or long-term exposure to microgravity. Changes in respiratory muscle strength may result. The PuFF experiment focuses on the lung functions of astronauts both while they are aboard the ISS and following spacewalks [10]. PuFF is performed on the crew two weeks into their mission, then once monthly thereafter. Crewmembers also perform a PuFF session at least one week before each spacewalk. Following each spacewalk, the crewmembers perform another PuFF session, either on the day of the spacewalk or on the following day [10]. PuFF uses the GASMAP instrument located in the HRF rack, along with a variety of other equipment. Data is stored in a personal computer located in the HRF rack and then transmitted to the ground.

The GASMAP device is used to monitor and analyze inhaled and exhaled breath streams to determine their gas concentrations. The primary gases of interest are nitrogen (N_2), oxygen (O_2), carbon dioxide (CO_2), argon (Ar), acetylene (C_2H_2), sulfur hexafluoride (SF_6), helium (He), and carbon monoxide ($C_{18}O$).

The GASMAP flight hardware consists of two components: an analyzer module and a calibration module, both of which are housed in drawers inside the US Lab. The analyzer module contains all the sensor and electronic hardware of the GASMAP. The major sub-assemblies of the analyzer module are the Random Access Mass Spectrometer (RAMS), the Roughing system, the Gas Delivery system, the Interface Shell (IS) computer and the power connection. The module is controlled via the keypad and liquid crystal display (LCD) of the front panel, or via a laptop computer [25].

In an effort to correlate accelerations measured in the US Lab to nearby operating equipment, correspondence with HRF and GASMAP teams was pursued to track down timeline information as well as equipment operational characteristics. The correspondence that ensued along with some data analysis resulted in the identification of two narrowband signatures near 60 Hz that were positively attributed to GASMAP equipment. This equipment was located in the HRF rack #1 (US LAB Starboard 2 (LAB1S2)). The first and stronger of the two signatures identified was that of a sample catheter pump. The nominal operating range of this pump is 52-60 Hz. The second, weaker signature belonged to the GASMAP fan, which typically operates at 58.3 Hz or 3500 RPM. Timeline information from HRF activities such as rack (de)activation, ultrasound,

and PC data downlink did not yield discernible acceleration signatures in the SAMS measurements. However, an e-mail sent by Janelle Fine from the Department of Medicine Physiology at the University of California San Diego did lead to some conclusive results. Below is an excerpt of that e-mail:

> Here are selections from my console log of the PuFF session (with relevant GASMAP activities and modes noted), for the day 1/26/2002. The times might be off by a couple of minutes on either side, due to Loss of Signal (LOS) periods and things, but I think they'll be close enough to make correlations. Unless otherwise noted, the GASMAP is in operate mode.
>
> 16:20 Rack is on, laptop is on (not sure if GASMAP was powered at this point)
>
> **16:30 GASMAP put into operate mode**
>
> 16:35 PuFF software started on HRF PC
>
> **17:45 GASMAP calibration started, it lasts 6 minutes. GASMAP is put into calibration mode for these 6 minutes, then returned to operate mode at the end.**
>
> 17:51 Volume calibration started. GASMAP is put into standby mode for one to two minutes, the returned to operate mode.
>
> **18:10 [Crew's] PuFF run starts**
>
> **18:40 [Crew's] PuFF run complete**
>
> 18:40 [Crew's] PuFF run starts
>
> **19:00 [Crew's] PuFF [2nd] run complete**
>
> **19:55 Volume calibration, 1-2 minutes (see notes above)**
>
> 19:58 GASMAP calibration, 6 minutes (see notes above)
>
> **20:25 GASMAP and laptop are powered off**
>
> 20:30 Shutting down the rack
>
> 20:40 Rack is off

The spectrograms of Figure 6-142, Figure 6-143, and Figure 6-144 show the acceleration spectra for SAMS Sensor Enclosure (SE) 121f02 in RTS drawer 1 of LAB1O2, 121f03 on Z-panel of ER2 in LAB1O1, and 121f04 on Z-panel of ER1 in LABO2, respectively. For comparison with the highlighted entries in the timeline from the e-mail excerpt above, an annotated zoom of Figure 6-142 is shown in Figure 6-145. The white vertical dashed lines correspond to each of the 7 highlighted timeline entries. From these annotations, we note about a 4.6-minute lag of acceleration measurement times behind the e-mail times from early in the record and diminishing difference toward the end of the record. A caveat that may explain much of the time discrepancy prefaces the timeline in the excerpt above. As discussed with GASMAP payload developers, the frequency changes away from nominal operation are likely a function of varying loads on the sample pump. The pump frequency ranges from 54 Hz (for brief calibrations) up to 62 Hz after the second PuFF run. The fan is tightly controlled in frequency but also transitions from baseline of about 57.4 Hz up to 58.1 Hz noted during calibrations.

To assess the impact of the sample pump, 8-second interval RMS accelerations that span 8 hours around run time were computed and shown in Figure 6-146 for sensor 121f02 and in Figure 6-147 for sensors 121f03 (red trace) and 121f04 (green trace). Comparing these 2 figures, notice that sensor 121f02 registers the largest impact of the 3 sensors analyzed. Considering purely Euclidean distance from these 3 sensors to the geometric center of the HRF rack as shown in Table 6-22, we might make a case that closer sensor should register largest impact. No attempt is made here to assess transfer functions from vibrating source to measurement location, just a simple observation of linear distance.

TABLE 6-22 DISTANCE FROM SENSORS TO HRF RACK

Sensor	Location	SSA COORDINATES (IN.)			Δ FROM HRF GEOMETRIC CENTER (IN.)			EUCLIDEAN DISTANCE (IN.)
		X	Y	Z	X	Y	Z	
121f02	LAB1O2, ER1, Drawer 1	128.731	-23.53	144.146	-14.969	-80.541	-46.804	94.348
121f03	LAB1O1, ER2, Lower Z Panel	191.539	-40.545	135.252	47.839	-97.556	-55.6977	122.098
121f04	LAB1O2, ER1, Lower Z Panel	149.539	-40.545	135.252	5.839	-97.556	-55.6977	112.487

Two more notes regarding the interval RMS accelerations in Figure 6-146 and Figure 6-147: (1) at just before 18:00, the pump frequency dropped below the frequency band considered, so the RMS value drops back to baseline for this short time, and (2) between 19:00 and around 20:00, the pump frequency goes above the frequency band considered, so the RMS value drops back to baseline again. If we consider times when the pump frequency stayed in a relatively narrow band around nominal operation, we can tabulate more detail regarding the impact comparing times when the pump was off versus on as done in Table 6-23.

TABLE 6-23 GASMAP EQUIPMENT RMS ACCELERATIONS

Sensor	Location	Equipment	Frequency Range (Hz)	State	RMS Acceleration (μg_{RMS})
121f02	LAB1O2, ER1, Drawer 1	SAMPLE PUMP	58.2 – 61.2	OFF	24
				ON	>200
121f03	LAB1O1, ER2, Lower Z Panel			OFF	91
				ON	>115
121f04	LAB1O2, ER1, Lower Z Panel			OFF	70
				ON	>115
121f02	LAB1O2, ER1, Drawer 1	FAN	57.2 – 57.6	OFF	8
				ON	19

The bottom entry in Table 6-23 for the GASMAP fan resulted from analysis similar to that done for the sample pump except that sensors 121f03 and 121f04 were not considered because the narrow frequency band around the fan signature from the table is dominated by a broadband signal above 55 Hz and no transition to fan on/off is discernible. However, the fan off/on/off transition is quite clear for sensor 121f02 as seen in Figure 6-148.

Microgravity investigations in the US Lab that are sensitive to vibrations around 60 Hz should take GASMAP operations into consideration when planning sensitive run times.

6.2.3.2 MEPS PCM Insertion and Runs

Enclosing a drug in a tiny liquid-filled microballoon, a process called microencapsulation, has been shown [15] to provide better drug delivery and new medical treatments for solid tumors and resistant infections. During Increment-5, investigators encapsulated two different complementary drugs in the same microcapsule. The experiment included encapsulation of drugs and magnetic trigger particles that will enable physicians to break open the microcapsules with diagnostic levels of magnetic fields. These are applied externally to deliver a burst of drug into the tissues in which the microcapsules are deposited [15]. Hardware for the MEPS experiment consisted of a chamber housing that held self-contained process chamber modules, a video monitor/ recorder, an internal process control computer, which controls the opening and closing of valves, fluid pumping, and a front control panel. Up to 10 experiments—each in a separate Process Chamber Module—is flown on each mission. The built-in video microscope monitors and records the critical stages of the process.

John Cassanto of Instrumentation Technology Associates (ITA) relayed background information on the MEPS and PCM on December 11, 2002. An excerpt of the memo he sent follows:

> The MEPS hardware performs electrical, mechanical, and pneumatic functions. The potential MEPS sources of vibration are: insertion of the PCM into the PCM housing, insertion of the Personal Computer Memory Card International Association (PCMCIA) card into the computer, opening the door to the PCM housing, operation of the intake and exhaust fans, activation of solenoid valves that control the flow of samples into the processing chamber, operation of stepper motors, initiation of the stepper motors that are geared to push pistons that provide a pressure differential to transport fluid samples, intake and exhaust fans to cool the payload, initiation of a video camera to record the manufacture of the microcapsules.
>
> **Hardware description**
> The MEPS hardware consists of two separate elements: the base chassis unit, and the PCMs, which actually perform the microencapsulation of drugs. The base chassis unit resides on the ISS and the PCMs are transported up to ISS to bring specific samples in eight PCMs to be activated in the microgravity environment of space and are then transported back to Earth for harvesting the samples. The PCMs are then loaded again with new samples and transported to ISS to process a new batch of experiments. Figure 6-149 shows the base line chassis configuration in an EXPRESS rack locker with the door closed. Figure 6-150 shows a PCM outside of its housing.
>
> **Baseline Chassis Unit**
> The baseline chassis unit contains high and low voltage power supplies, a PC-104 computer to provide commands for the various operations which accepts PCMCIA cards to run the specific experiments for specific PCMs, a video camera to observe the microcapsules being made, and a commercial video tape recorder for recording the

video data, an intake and an exhaust fans at the rear of the hardware to cool the payload, and a process control module housing. A photograph of the front of the Baseline Chassis unit with the EXPRESS rack locker door open is shown in Figure 6-151. Note the door on the left hand side of the unit. The door is the opening through which a PCM is inserted for a particular experiment to be conducted. A close up of the door is shown in Figure 6-152. Note that there are two latches that require opening for the door to unlatch, but these should not provide any significant vibrations when they are unlatched. A photograph of the interior of the PCM housing is shown in Figure 6-153 and a 50-pin connector can be observed at the rear of the housing. This connector mates with a connector at the end of the PCM (see Figure 6-154), which supplies power and commands for the PCM to conduct experiments. The mating of this connector in some cases is a tight fit, particularly for new connectors. This is a potential source of an acceleration pulse.

The right of the front panel of the chassis unit contains a slot for a PCMCIA card (see Figure 6-155), which is inserted to run a specific program for a specific experiment. I don't believe insertion of the card would produce a measurable acceleration. There is a video camera contained in the baseline chassis that is wired to a commercial tape recorder (see the front view of the hardware in Figure 6-151) that records the microcapsules being made. In addition, the hardware has three fans to circulate air from the EXPRESS Rack and to provide cooling air. Figure 6-156 shows the rear of the hardware. The exhaust fans are shown on the left side of the hardware. It should be noted that only one of the exhaust fans is operating on ISS at the present time, the second exhaust fan is a back up. Any and/or all of the above elements represent possible vibration sources that the SAMS could possibly have picked up during the UF-2 mission.

Process Control Module

A photograph of the PCM hardware inside of the Aluminum outer shell is shown in Figure 6-150. A top-level assembly of the PCM is shown in Figure 6-157. The possible vibration sources within the PCM are two solenoid valves, which control the flow of fluids to make the microcapsule samples, and two stepper motors, which are geared to two plungers that move to complete the process of pumping the samples and making the microcapsules. Figure 6-158 shows a photograph of the inside hardware showing the plungers and one of the solenoid valves. Figure 6-159 shows a blow up of the plunger area.

The MEPS located in locker #8 of ER1 (LAB1O2) is in close proximity to the SAMS 121f02 sensor in RTS drawer 1. On GMT 18-July-2002 (day 199), the MEPS processed 5 samples and on GMT 19-July-2002 (day 200), another 3 samples were processed. The interval maximum plot of Figure 6-160 shows transients including one that extends above 103 mg from a baseline of about 3 mg for PCM insertion. The SAMS 121f02 timestamps show this large pulse occurred at GMT 18-July-2002, 199/15:12:29. For a broader perspective, a 24-hour spectrogram that readily shows these impulsive disturbances from PCM insertion was computed and displayed in Figure 6-161. This figure shows clear indication of the 5 runs with the start/stop delimited by 2

narrowband signals. The weaker of these was centered at 47.1 Hz and the stronger at 52.8 Hz. Note that each of the 5 runs is preceded by the impulsive events of PCM insertion.

The interval RMS versus time plot of Figure 6-162 corresponds to the same time frame as that of Figure 6-161. This RMS plot shows the contribution of the 2 narrowband signals that accompany the MEPS runs. The red trace gives the RMS acceleration for the fainter, low-frequency signal centered at 47.1 Hz. This signal steps from about 14 to 24 μg_{RMS} in the frequency range from 45.85 to 47.39 Hz. Likewise, the blue trace for the stronger signal centered at 52.8 Hz steps from about 9 to 54 μg_{RMS} in the frequency range from 52.63 to 53.07 Hz.

6.2.3.3 Microgravity Science Glovebox (MSG) Environment

Both the SUBSA and PFMI experiments operated in the MSG during the time frame covered by this report. This section is a general characterization of the vibratory environment for times when these experiments were operating.

6.2.3.3.1 Solidification Using a Baffle in Sealed Ampoules (SUBSA)

Material scientists want to make better semiconductor crystals to be able to further reduce the size of high-tech devices. To control the opto-electronic properties of the crystals, a small amount of an impurity—named a dopant—has to be added to the pure semiconductor. Uniform distribution of the dopant in the semiconductor crystal is essential for production of opto-electronic devices [15]. For this experiment, tellurium and zinc are added to molten indium antimonide specimens that are then cooled to form a solid single crystal by a process called directional solidification.

The goals of this experiment are to identify what causes the motion in melts processed inside space laboratories and to reduce the magnitude of the melt motion so that it does not interfere with semiconductor production [15]. SUBSA processed 10 samples with two spares available. Ten growth runs were conducted during Increment-4. SUBSA tested the performance of the automatically moving baffle in microgravity in order to show that the expansion of the melt is keeping the baffle at a constant distance from the interface; demonstrated the behavior and possible advantages of liquid encapsulation in microgravity conditions; demonstrated that the baffle reduces sensitivity to residual micro-acceleration in two systems with different segregation coefficients and achieve reproducible growth.

SUBSA was located in the MSG, which has fans for recirculating the air through the glovebox. The SUBSA experiment itself also has moving parts, which induce some disturbance. The PCM contains two small fans and there is a Cohu 3812 video camera, which has an integrated zoom and focus lens.

The dates and times in Table 6-24 indicate when the software program controlling the SUBSA hardware and acquiring the data was started and stopped. Actual sample processing (i.e., melting and resolidification) is enveloped by these times. SUBSA activities outside these times include sample installation and removal, hardware setup and takedown, and data transfers.

TABLE 6-24 SUBSA PROCESSING TIMELINE IN 2002

Sample	GMT Start	GMT Stop	Baffle	Dopant	Encapsulant	Orientation
SUBSA-06	192:08:49	193:01:16	No	Tellurium	No	<211>
SUBSA-10	204:10:16	205:08:21	No	Zinc	No	<211>
SUBSA-02	213:17:33	214:08:04	Yes	Tellurium	No	<211>
SUBSA-04	219:17:24	220:07:39	No	Tellurium	No	<111B>
SUBSA-07	222:08:36	223:00:04	No	Tellurium	Yes	<211>
SUBSA-08	247:08:45	248:08:32	Yes	Zinc	No	<211>
SUBSA-09	250:08:30	251:07:54	Yes	Zinc	No	<211>
SUBSA-01	253:10:30	254:02:30	Yes	Tellurium	No	<111B>

TABLE 6-25 SUBSA SPECTRAL CHARACTERIZATION

Sample	GMT Start	GMT Stop	See
SUBSA-06	11-Jul-02 08:49	12-Jul-02 01:16	no SAMS data
SUBSA-10	23-Jul-02 10:16	24-Jul-02 08:21	Figure 6-163 through Figure 6-166
SUBSA-02	01-Aug-02 17:33	02-Aug-02 08:04	Figure 6-167 through Figure 6-169
SUBSA-04	07-Aug-02 17:24	08-Aug-02 07:39	Figure 6-170 through Figure 6-171
SUBSA-07	10-Aug-02 08:36	11-Aug-02 00:04	Figure 6-172 through Figure 6-174
SUBSA-08	04-Sep-02 08:45	05-Sep-02 08:32	Figure 6-175 through Figure 6-178
SUBSA-09	07-Sep-02 08:30	08-Sep-02 07:54	Figure 6-179 through Figure 6-181
SUBSA-01	10-Sep-02 10:30	11-Sep-02 02:30	Figure 6-182 through Figure 6-184

Figure 6-185 shows cumulative percentage of occurrence for acceleration magnitudes on days that SUBSA was operating (for which there was SAMS data). From this figure, note that the median acceleration vector magnitude was about 0.14 mg, while over 95% of the recorded acceleration magnitudes were below 0.56 mg.

6.2.3.3.2 Pore Formation and Mobility Investigation (PFMI)

On Earth when scientists melt metals, bubbles that form in the molten material can rise to the surface, pop and disappear. In microgravity — the near-weightless environment created as the International Space Station orbits Earth, the lighter bubbles do not rise and disappear. Prior space experiments have shown that bubbles often become trapped in the final metal or crystal sample. In the solid, these bubbles, or porosity, are defects that diminish both the material's strength and usefulness. The Pore Formation and Mobility Investigation melted samples of a transparent modeling material, succinonitrile and succinonitrile water mixtures. Investigators were able to observe how bubbles form in the samples and study their movements and interactions.

This investigation was one of the first materials science investigations on the space station. This investigation gives scientists an opportunity to observe bubble dynamics in a sample being processed in a way similar to industrial methods. The intent is to gain insights that will improve solidification processing in a microgravity environment [15].

The dates and times in Table 6-26 indicate when the software program controlling the PFMI hardware and acquiring the data was started and stopped. Actual sample processing (i.e., melting and resolidification) is enveloped by these times with the exception of PFMI-11. For that experiment the MSG power failed during the run, and so the sample solidified after the stop time listed for that experiment. PFMI activities outside these times include sample installation and removal, hardware setup and takedown, and data transfers. The times below are for those PFMI samples processed during Increment 5. Other samples onboard are planned for processing during either Increment 6 or 7.

TABLE 6-26 PFMI PROCESSING TIMELINE IN 2002

Sample	GMT Start	GMT Stop	Water Dopant	Nitrogen Bubbles
PFMI-12	262:14:02	263:10:59	No	No
PFMI-01	266:09:00	267:00:46	No	Yes
PFMI-07	273:11:50	273:23:22	Yes	No
PFMI-08	274:17:20	275:05:28	Yes	Yes
PFMI-05	279:12:11	280:00:03	Yes	No
PFMI-02	280:11:15	280:22:38	No	Yes
PFMI-10	300:11:55	301:00:12	Yes	No
PFMI-11	324:22:28	325:03:39	Yes	No

TABLE 6-27 PFMI SPECTRAL CHARACTERIZATION

Sample	GMT Start	GMT Stop	See
PFMI-12	19-Sep-02 14:02	20-Sep-02 10:59	Figure 6-186 through Figure 6-189
PFMI-01	23-Sep-02 09:00	24-Sep-02 00:46	Figure 6-190 through Figure 6-192
PFMI-07	30-Sep-02 11:50	30-Sep-02 23:22	Figure 6-193 through Figure 6-194
PFMI-08	01-Oct-02 17:20	02-Oct-02 05:28[1]	Figure 6-195
PFMI-05	06-Oct-02 12:11	07-Oct-02 00:03	Figure 6-196 through Figure 6-198
PFMI-02	07-Oct-02 11:15	07-Oct-02 22:38	Figure 6-199 through Figure 6-200
PFMI-10	27-Oct-02 11:55	28-Oct-02 00:12	Figure 6-201 through Figure 6-203
PFMI-11	20-Nov-02 22:28	21-Nov-02 03:39	Figure 6-204 through Figure 6-205

Figure 6-206 shows cumulative percentage of occurrence for acceleration magnitudes on days that PFMI was operating (for which there was SAMS data). From this figure, note that the median acceleration vector magnitude was about 0.19 mg, while over 95% of the recorded acceleration magnitudes were below 0.64 mg.

[1] no SAMS data on GMT 02-Oct-02

6.2.4 Crew Activity

Experiment setups, equipment transfer or stowage, exercise, and locomotive push offs and landings all contribute to a category of disturbance called crew activity. These actions give rise to reactive forces, which are manifested as acceleration disturbances transferred through the vehicle's structure. In-depth analyses in this section include exercise, Temporary Sleep Station (TeSS) entry/exit, EVA, and PAO events.

6.2.4.1 Crew Exercise

The Countermeasures System (CMS), which is part of ISS Crew Health Care System (CHeCS), prevents crew's cardiovascular and musculoskeletal deconditioning that occurs as a result of exposure to spaceflight [6]. Prescribed exercise is performed daily by all ISS crewmembers to maintain muscle and bone mass and strength, in preparation for re-adaptation to the 1-g environment after landing. The CMS, among other hardware, includes a treadmill, resistive exercise device and cycle ergometer.

The four types of exercise equipment that are analyzed in this section are the Treadmill Vibration Isolation System (TVIS), the Resistive Exercise Device (RED), the Cycle Ergometer with Vibration Isolation System (CEVIS), and the Russian velosiped (VELO) – the Russian abbreviation VELO is to velosiped like bike is to bicycle.

6.2.4.1.1 Treadmill Vibration Isolation System (TVIS)

The TVIS is used to simulate 1-g walking and running. TVIS is used mainly for postural and locomotor musculoskeletal maintenance, with cardiopulmonary benefits [6]. TVIS minimizes vibration that might affect other ISS systems or payloads by isolating x, y, and z translation, roll, pitch, and yaw. TVIS allows a maximum translation of ± 0.5 inches and ± 2.5º rotation in any axis and should not pass a load greater than 5 pounds to surrounding connections or structures [6]. The restraints, or Subject Load Devices (SLDs), are located to the side of the crewmember. TVIS is located in the SM, and the running surface of the treadmill is flush with the floor of the module.

While the treadmill employs vibration isolation, it is not expected that total attenuation is achieved. Some remnant of this energetic endeavor may rise above the ambient environment and therefore be detectable. The intent of the analysis in this section was to identify the TVIS signature from measurements made in the US Lab and characterize its impact there.

Perhaps the largest challenge in front of this characterization effort is gathering GMTs for known exercise periods. It is not uncommon for daily plans to change, so instead of planned TVIS exercise times, we considered the following spans relayed from Ted Bartkowicz of the Loads and Dynamics team at Boeing:

> At 09:34 AM 6/5/2002 -0500, Ted Bartkowicz wrote:
> Kenol,
>
> Russians collected SM & FGB accelerometer data on **May 23 and May 24 during two separate TVIS exercise sessions.** Since their measurement system only works when

they are over a Russian ground station range, they were limited to about 20 minutes. **The actual GMTs for their data recording are provided below:**

(May 23) 143/17:26-17:48 (plan was 17:00-18:00) .....see Figure 6-207
(May 24) 144/11:45-12:03 (plan was 11:45-12:45) .....see Figure 6-208

From Figure 6-207, stop and start of the Russian air conditioner (SKV) signature above 23 Hz is easily seen at just after GMT 16:00 and 19:00 on that day, respectively. However, close examination of the first time frame cited above shows no trace suggestive of the start or stop of exercise signatures in the acceleration spectrum below 5 Hz. Heightened excitation is noted in this regime before about GMT 16:45, but this time excitation ends more than a half hour before the start of the time of interest.

From Figure 6-208, stop of the Russian air conditioner (SKV) signature above 23 Hz is obvious at GMT 11:00 on that day. Close examination of the second time frame cited above again shows no trace suggestive of the start or stop of exercise signatures. Heightened excitation again is noted, particularly in the structural mode regime below 5 Hz, but this excitation ends before the time of interest.

Additional times relayed through John Keller (JSC) for TVIS exercise times on GMT 24-December-2001, 31-December-2001, 4-January-2002, and 20-January-2002 were also analyzed and showed no obvious transitions at start/stop of exercise.

6.2.4.1.2 Resistive Exercise Device (RED)

The RED prevents muscle atrophy of the major muscle groups by maintaining strength, power, and endurance. RED provides resistance training for the major muscle group of the legs, hips, trunk, shoulders, arms, and wrists [6]. RED is mounted to TVIS for isolation. Up to 430 pounds [6] of resistance is available in increments of 5 pounds.

The RED acronym is generically used for the exercise device located in the Z1 alcove of Node 1. To be more explicit, the hardware currently on-orbit is the hardmounted interim Resistive Exercise Device (iRED). The iRED is suspended with 8 rods and 4 bumpers. The Advanced Resistive Exercise Device (ARED) will eventually replace the interim device. Table 6-28 shows a timeline of a RED exercise period.

TABLE 6-28 RED EXERCISE TIMELINE

VIDEO TIME	ACTIVITY	REPS
9/2/2002 08:57:35	attach harness	
9/2/2002 08:58:05	stand up/adjust	
9/2/2002 08:58:09	squats[2]	12
9/2/2002 08:58:26	heel raises[3]	21
9/2/2002 08:58:42	squats	11
9/2/2002 08:59:00	heel raises	20

Table 6-28, Continued from previous column

VIDEO TIME	ACTIVITY	REPS
9/2/2002 08:59:15	Squats	10
9/2/2002 08:59:30	heel raises	20
9/2/2002 08:59:46	squats	12
9/2/2002 09:00:04	heel raises	21
9/2/2002 09:00:22	squats	11
9/2/2002 09:00:39	heel raises	20
9/2/2002 09:00:58	squats	12
9/2/2002 09:01:17	heel raises	21
9/2/2002 09:01:37	reconfigure	

[2] about 0.75 Hz
[3] about 1.5 & 3 Hz

Table 6-28, Cont. from previous column, previous page

VIDEO TIME	ACTIVITY	REPS
9/2/2002 09:02:00	crank right canister	
9/2/2002 09:02:05	done with left	
9/2/2002 09:02:13	again crank right canister	
9/2/2002 09:02:22	done with left	
9/2/2002 09:02:37	quick jerk on harness	
9/2/2002 09:02:41	stand on toe bar	
9/2/2002 09:02:42	deep heel raises[4]	22
9/2/2002 09:03:13	deep heel raises	12
9/2/2002 09:03:23	pause	
9/2/2002 09:03:40	deep heel raises	13
9/2/2002 09:03:51	pause	
9/2/2002 09:04:06	deep heel raises	13
9/2/2002 09:04:13	pause	
9/2/2002 09:04:28	deep heel raises	12
9/2/2002 09:04:40	pause	
9/2/2002 09:04:52	deep heel raises	11
9/2/2002 09:05:02	reconfigure	
9/2/2002 09:05:20	crank right canister	
9/2/2002 09:05:27	done with left	
9/2/2002 09:05:33	crank left canister	
9/2/2002 09:05:39	done with right	
9/2/2002 09:05:57	stand up quickly	
9/2/2002 09:05:59	left leg squats[5]	11
9/2/2002 09:06:16	right leg squats	12
9/2/2002 09:06:34	left leg squats	12
9/2/2002 09:06:53	right leg squats	11
9/2/2002 09:07:11	left leg squats	13
9/2/2002 09:07:33	right leg squats	12
9/2/2002 09:07:54	left leg squats	12
9/2/2002 09:08:16	right leg squats	11
9/2/2002 09:08:36	left leg squats	11
9/2/2002 09:08:57	right leg squats	10
9/2/2002 09:09:15	remove/stow harness	
9/2/2002 09:10:05	install bar	
9/2/2002 09:10:13	crank right canister	
9/2/2002 09:10:16	done with right	
9/2/2002 09:10:21	crank left canister	
9/2/2002 09:10:24	done with left	
9/2/2002 09:10:46	deadlifts	14
9/2/2002 09:11:09	pause	
9/2/2002 09:11:16	deadlifts	12
9/2/2002 09:11:36	pause	
9/2/2002 09:11:48	deadlifts	11

Table 6-28, Cont. from previous column

VIDEO TIME	ACTIVITY	REPS
9/2/2002 09:12:07	pause	
9/2/2002 09:12:19	deadlifts	10
9/2/2002 09:12:36	pause	
9/2/2002 09:13:07	deadlifts	8
9/2/2002 09:13:21	pause	
9/2/2002 09:13:40	deadlifts	9
9/2/2002 09:13:57	crank right canister	
9/2/2002 09:14:04	done with right	
9/2/2002 09:14:08	crank left canister	
9/2/2002 09:14:12	done with left	
9/2/2002 09:14:28	shoulder shrugs	12
9/2/2002 09:14:39	reposition for situps	
9/2/2002 09:14:57	situps	26
9/2/2002 09:15:41	reposition for shrugs	
9/2/2002 09:15:58	shoulder shrugs	13
9/2/2002 09:16:10	reposition for situps	
9/2/2002 09:16:43	situps	24
9/2/2002 09:17:23	reposition for shrugs	
9/2/2002 09:17:43	shoulder shrugs	13
9/2/2002 09:17:53	pause	
9/2/2002 09:17:59	crank right canister	
9/2/2002 09:18:04	done with right	
9/2/2002 09:18:08	crank left canister	
9/2/2002 09:18:12	done with left	
9/2/2002 09:18:13	reposition for situps	
9/2/2002 09:18:15	situps	26
9/2/2002 09:18:27	reposition for bent rows	
9/2/2002 09:20:21	bent rows	8
9/2/2002 09:20:33	pause	
9/2/2002 09:20:44	forearm pulls	12
9/2/2002 09:20:56	reposition for bench press	
9/2/2002 09:21:08	bench press	8
9/2/2002 09:21:20	reposition for bent rows	
9/2/2002 09:21:52	bent rows	10
9/2/2002 09:22:08	reposition for forearm pulls	
9/2/2002 09:22:15	forearm pulls	11
9/2/2002 09:22:26	reposition for bench press	
9/2/2002 09:22:53	bench press	8
9/2/2002 09:23:05	pause	
9/2/2002 09:23:44	bent rows	11
9/2/2002 09:24:02	pause	
9/2/2002 09:24:36	forearm pulls	12
9/2/2002 09:24:50	reposition for bench press	
9/2/2002 09:25:06	bench press	8
9/2/2002 09:25:18	move	
9/2/2002 09:25:24	crank right canister	
9/2/2002 09:25:30	done with right	

[4] fundamental excitation at about 1.1 Hz with 2nd through 4th harmonics
[5] about 0.75 Hz with harmonics around 3 Hz

Table 6-28, Cont. from previous column, previous page

VIDEO TIME	ACTIVITY	REPS
9/2/2002 09:25:32	crank left canister	
9/2/2002 09:25:37	done with left	
9/2/2002 09:25:38	reposition for forearm pulls	
9/2/2002 09:26:02	forearm pulls	20
9/2/2002 09:26:19	LOS?	
9/2/2002 09:26:46	military press	10
9/2/2002 09:27:04	pause	
9/2/2002 09:27:52	forearm pulls	20
9/2/2002 09:28:10	pause	
9/2/2002 09:28:37	military press	9
9/2/2002 09:28:54	pause	
9/2/2002 09:29:38	forearm pulls	20
9/2/2002 09:29:56	pause	
9/2/2002 09:30:23	military press	9
9/2/2002 09:30:38	pause	
9/2/2002 09:30:42	crank right canister	
9/2/2002 09:30:50	done with right	
9/2/2002 09:30:53	crank left canister	
9/2/2002 09:30:57	done with left	
9/2/2002 09:31:32	lateral raises	10
9/2/2002 09:31:48	pause	
9/2/2002 09:31:55	jerk right crank	
9/2/2002 09:31:56	pause	
9/2/2002 09:32:29	curls	9
9/2/2002 09:32:51	pause	
9/2/2002 09:33:12	quick locomotion out of node	
9/2/2002 09:34:07	return sticks landing on RED	
9/2/2002 09:34:21	lateral raises	9
9/2/2002 09:34:34	pause	
9/2/2002 09:34:48	curls	8
9/2/2002 09:35:06	pause	
9/2/2002 09:35:35	lateral raises	8
9/2/2002 09:35:48	pause	
9/2/2002 09:36:17	curls	10
9/2/2002 09:36:41	reconfigure	
9/2/2002 09:37:25	cross-pulley rows	8
9/2/2002 09:37:39	pause	
9/2/2002 09:37:57	right wrist tweaks on left can	12
9/2/2002 09:38:11	reposition	
9/2/2002 09:38:21	left wrist tweaks on right can	12
9/2/2002 09:38:36	pause	
9/2/2002 09:38:55	cross-pulley rows	8
9/2/2002 09:39:10	reposition	
9/2/2002 09:39:15	right wrist tweaks on left can	11
9/2/2002 09:39:27	reposition	
9/2/2002 09:39:31	end of footage	

This timeline was constructed based on video footage. Note that the exercise regimen calls for several different types of movement: squats, heel raises, deadlifts, and so on. The signature for these various movements is annotated in the spectrogram of Figure 6-209, which shows effects below 30 Hz. To quantify the acceleration impact of these motions below 30 Hz, the interval RMS plot of Figure 6-210 was computed. Interval RMS computations similar to these for the same period, but now below 10 Hz (for comparison to historic acceleration data) for SAMS 121f02 data yield the results shown in Table 6-29.

TABLE 6-29 RMS ACCELERATIONS BELOW 10 HZ PRODUCED BY VARIOUS RED EXERCISES

Exercise Type	Maximum RMS Acceleration (μg_{RMS})	Dominant Spectral Peaks (Hz)
none (baseline)	60	
squats	301	0.75
heel raises	691	3
deep heel raises	336	1.2
one-leg squats	255	0.75
deadlifts	206	0.75
shoulder shrugs & situps	168	0.6, 1.2
bench press & bent rows	222	0.6, 1.2

Note that the heel raise motion, by far, transmits the largest accelerations from the Node 1 RED location to the SAMS 121f02 location in ER1 of the US Lab (LAB1O2). In reviewing the video, it was noted that there was a brief interruption in the exercise period. At about GMT 02-September-2002, 245/09:33:12, FE-1 quickly soared out of Node 1 through the hatch toward the US Lab. Correlation with SAMS 121f02 measurements showed that this produced a peak acceleration magnitude of 9.67 mg. When FE-1 returned and landed on the RED base plate, this produced an acceleration of 3.75 mg primarily aligned with the Z_A-axis.

Figure 6-211 shows the measurements made by SAMS 121f02 over a span of about 230 seconds early in the RED exercise period. The large excursions from baseline that occurred about every 45 seconds (the first starting at about the 30-second mark) were caused by heel raises. Figure 6-212 shows this same period, but lowpass filtered at 5 Hz. The black, vertical dashed lines shown on the Z-axis bound a set of squats and heel raises. Note the lower magnitude, lower frequency impact of squats relative to the higher frequency heel raises. To show this more clearly, Figure 6-213 was produced for a zoom in around the times indicated by the black dash lines of Figure 6-212.

6.2.4.1.3 Cycle Ergometer with Vibration Isolation System (CEVIS)

The CEVIS is used for systemic aerobic conditioning and can be used to perform independent upper and lower limb cycle activity. CEVIS is located in the US Lab. Similar to TVIS, CEVIS isolates x, y, and z translation, roll, pitch, and yaw [6].

Based on a large volume of acceleration data from various Shuttle microgravity missions, experience has shown that individual crew vigor was a fundamental factor on the impact of ergometer exercise. Naturally, the more vigorous the individual exercised, the more pronounced

was the impact. The intent is not to track just how energetic various crew were during CEVIS exercise, but consideration of this factor may prove useful at some point in the future. Proximity of the CEVIS (US LAB Port 3 (LAB1P3)) to ER1 (LAB1O2) and ER2 (LAB1O1) make it a candidate for propagating oscillatory disturbances from its mounting location to the vibratory sensors in the nearby EXPRESS racks (see Figure 6-214). Two time spans that include CEVIS exercise were analyzed to characterize the measured effects at various accelerometer locations. These particular periods were considered for two reasons, they both: (1) exhibit ergometer acceleration signature based on experience from Shuttle ergometer exercise, and (2) correlate well with exercise data collected independently of the accelerometers. The correlating data came in the form of spreadsheet files recorded on PCMCIA cards for TVIS and CEVIS with all personal or sensitive information having been filtered out on the ground at the JSC.

For the first exercise period analyzed, the spectrogram in Figure 6-215 clearly shows an ergometer signature (as marked near bottom right), starting just before GMT 01-January-2002, 001/11:13:34. The spreadsheet, on the other hand, shows a start time of GMT 01-January-2002, 001/11:13:11. Part of this roughly 20-second lag is attributable to the temporal resolution used to compute the spectrogram, which was 4.096 seconds. The spectrogram's end time truncates the exercise period because this time marks the beginning of a PIMS Acceleration Data (PAD) gap. Meanwhile, the spreadsheet indicates that the exercise was completed at about 11:23, and therefore lasted about 10 minutes. The narrowband peak at about 2.5 Hz marked on the lower right of the spectrogram is the pedaling frequency. For Shuttle ergometer exercise, the pedaling signature was accompanied by that of shoulder sway with frequency around half the pedal rate. On the ISS for this CEVIS exercise period, the shoulder sway signature is obscured by structural modes that fall in the same frequency range. Figure 6-215 qualifies the exercise regime from the 121f05 sensor location atop ER2. To quantify the impact of this exercise period from this and other sensor locations, the cumulative RMS acceleration versus frequency curves of Figure 6-216 were computed. The legend at the upper left shows which trace was computed for each of 4 different sensors. The curves in this figure all step up about 70 μg_{RMS} at the pedaling frequency, but vary to some degree across the rest of the acceleration spectrum below 10 Hz. The variability is expected as the SAMS sensors used for the analysis were distributed throughout ER1 and ER2 as indicated by the legend.

The second CEVIS exercise period analyzed is depicted in the spectrogram of Figure 6-217. Note the frequency scale is zoomed below 15 Hz and the color scale is zoomed beyond nominal settings. Close examination with these zoom settings, gives clear indication of ergometer pedal signatures in the dashed boxes. Again shoulder sway is hard to detect in the midst of structural modes around 1 Hz. The spreadsheet file for this time frame shows a CEVIS exercise from GMT 03-January-2002, 003/10:24:41 to 10:30:26 and therefore lasting slightly less than 6 minutes. These times corresponds closely with the later of the 2 pedal signatures in the right dashed box. An earlier exercise period (the left dashed box) was likely that from a different crew member. To quantify the impact of the earlier CEVIS period from this and other sensor locations, the cumulative RMS acceleration versus frequency curves of Figure 6-218 were computed. The legend at the upper left shows which trace was computed for each of 5 different sensors. The curves in this figure show this exercise period to be much quieter than the one quantified above for GMT 01-January-2002. Each curve steps less than about 2 μg_{RMS} at the pedaling frequency of nearly 2.8 Hz. Similar analysis for the later CEVIS period marked in

Figure 6-217 produced the curves in Figure 6-219. Again only minimal impact was registered at the pedaling frequency near 2.8 Hz. Also, note for the cyan curves of Figure 6-218 and Figure 6-219, the 121f06 sensor was mounted inside the ARIS ER2.

6.2.4.1.4 Russian Velosiped (VELO)

Perusal of roadmap spectrograms for GMT 25-July-2002 to 31-July-2002 shows what is most certainly the signature of daily VELO exercise for a couple of hours around noon and again around 18:00 (see below 5 Hz on and Figure 6-220 and Figure 6-221 and compare with highlighted times in excerpts of the short-term plan for that day shown in Figure 6-222 and Figure 6-223, respectively).

To quantify the impact of VELO exercise, consider the 10-minute span starting at GMT 31-July-2002, 212/12:50:00. A cumulative RMS acceleration versus frequency curve for 4 different SAMS sensors were computed and the results shown in Figure 6-224. A sharp step up at the pedal rate of about 2.2 Hz is evident in these curves along with smaller step at shoulder sway frequency. This marks a difference for VELO from CEVIS. The shoulder sway frequency is pronounced for VELO exercise. A more complete quantification for this pedal rate frequency can be seen in the 8-second interval RMS acceleration plot of Figure 6-225. The RMS acceleration was computed for the frequency range from 2.1 to 2.3 Hz. To the right of the 12:00 time tick, just before 13:00, there is the 10-minute period referenced above. This shows a step up from a baseline of about 2 μg_{RMS} without VELO to between 50 and 100 μg_{RMS} when VELO is being used. This step up from baseline occurs again around the 18:00 mark, which is when we see the VELO signature again below 5 Hz in Figure 6-221.

Short-term plans and roadmap spectrograms agree that more VELO exercise occurred around GMT 06-August-2002, 218/17:00:00 and lasted until about 18:45 (see Figure 6-226 for example). To measure the impact of this VELO exercise, Figure 6-227, Figure 6-228, Figure 6-229, and Figure 6-230 were generated to show the 8-second interval RMS accelerations below 5 Hz. For all these SAMS sensor locations, the sub 5 Hz RMS level was well below 100 μg_{RMS} when no VELO exercise took place, but often was in excess of 150 μg_{RMS} during the exercise.

A final VELO exercise period for analysis took place at around GMT 07-August-2002, 219/11:00. For comparison to the results for CEVIS exercise in Section 6.2.4.1.3, consider a 1-minute snapshot of the VELO period starting at GMT 07-August-2002, 219/11:12:45. Computation of cumulative RMS acceleration versus frequency curves for SAMS sensors in ER1 and ER2 yields the plot in Figure 6-231. From this figure, first note that the RMS scale for these curves is an order of magnitude greater than similar plots discussed earlier for CEVIS exercise. Also, note the pedal spectral peak for this snapshot was at about 2.3 Hz and produced a step of nearly 200 μg_{RMS}. Meanwhile, at the shoulder sway spectral peak (about 1.15 Hz), there was a step of over 50 μg_{RMS}. The data for the 121f02 SAMS sensor was considered for inclusion in this analysis, but rejected because of a transient during the 1-minute span of interest. CEVIS and VELO are similar devices, with exception of the vibration isolation afforded by the CEVIS. It is seen from this final comparison between CEVIS (located in the US Lab, relatively close to SAMS sensors) and VELO (located in the Service Module) exercise that the isolation provided by CEVIS results in far less of a vibratory acceleration impact.

For a spectral comparison to quantify the differences between exercise types in the previous 3 sections, the cumulative RMS acceleration versus frequency plot of Figure 6-232 was constructed.

6.2.4.2 Temporary Sleep Station (TeSS) Impact Test

Not having enough beds on the ISS was not a planning error; rather, it was the most efficient way to build the station. When the Space Station was redesigned in 1993, and Russia was added into the international partnership, a condition of the redesign was to use as much of the already-performed work from Russia's Mir 2 space station as possible. That would save money and time. The Zvezda habitation module was originally planned to be part of Mir 2, a station that would have a crew of two. With that plan in mind, Zvezda had only two crew quarters in the original design. Managers considered shuffling space to add another sleeping area to Zvezda, but such an addition would have meant an extensive redesign of the module.

The Temporary Sleep Station (TeSS) is not in the Zvezda module with the other crew facilities; it's housed in the Destiny science laboratory. TeSS is an entire portable bedroom. It has privacy, room for sleeping and changing clothes, communication, and space for recreational activities such as reading. TeSS has acoustic blankets to muffle outside noise, a caution and warning system to head off malfunctions, and an air ventilation system. Astronauts using TeSS can take advantage of lights, work surfaces, handholds, sleep and foot restraints, and personal storage areas.

During Increment 4, the Temporary Sleep Station (TeSS) was located in US LAB Starboard 1 (LAB1S1) and secured with a strap buckle. This buckle was in close proximity to the sensor connector for SAMS 121f05 (LAB1O1). See Figure 6-233, which shows a close up of TeSS strap buckle below SAMS 121f05 and a front view of the TeSS vent, strap buckle, and the SAMS 121f05 sensor. The 121f05 sensor was located near the top of LAB1O1 (on the light tray on top of ER2). Since the buckle was so close to the sensor, a TeSS impact test was conducted on GMT 01-April-2002, 091 to determine if this mounting configuration caused significant interference, especially during entry/exit by the crew. Below is an excerpt from an e-mail relayed by Helen Brown of the SAMS team:

> On GMT 091 (Monday, 4/1/02) Dan/FE2 called down at GMT 08:21 with the 4 entry/exit times for the TeSS Impact Test. Below is a transcription of the S/G communication on the test:
>
> **Dan:** Huntsville, Alpha, S/G 1.
> **Paycom:** Alpha, Huntsville, Go ahead Dan.
> Dan: Yes, Karen. I did the TeSS entrance and exit. I have the times when you are ready to copy.
> **Paycom:** I'm ready, Dan.
> **Dan:** I have 4 pairs of times. The first time in each pair is the entry time and the exit time will be the second. The hour for each is GMT 08. I will just give you the minutes and the seconds for each entry/exit pair.
> The first is 11:05 / 11:30.
> The second is 11:50 / 12:08
> The third is 12:27 / 12:45
> The fourth is 13:05 / 13:30

The position of the buckle at the beginning of the test looked to be 1/16" to 1/8" away. Right now, it looks like it's just resting on the electrical connector of the sensor head.
Paycom: OK, Dan, we copy that and we'd like to leave it "as is" at the moment.
Dan: OK. Copy. Leave it as is.
Paycom: We appreciate your help, Dan. Thanks a bunch!
Dan: As always, it is my pleasure.

The spectrogram of Figure 6-234 qualifies the nature of the impulsive interference caused by entry/exit. Note the series of 8 closely-spaced vertical streaks centered at around GMT 08:12:12. These correspond to the 4 pairs of entry/exit times of the test cited in the e-mail excerpt above.

In order to quantify the impact of the TeSS entry/exit test, the 0.5-second XYZ interval min/max plot shown in Figure 6-235 was produced. It shows that the Y_{F05}-axis (Z_A-axis) registered the largest accelerations overall. The largest acceleration for this axis was over 37 mg, but this occurred at about GMT 091/08:08, which is about 3 minutes before first documented entry/exit event. The largest acceleration magnitude during the test span was the second exit at over 32 mg (see the 0.5-second interval acceleration vector magnitudes in Figure 6-236). According to the SAMS 121f05 data, this second exit took place at a little after GMT 091/08:12:30 and this lags the time called down by about 22 seconds.

To more fully quantify the impact of TeSS entry/exit, a cumulative percentage of occurrences for acceleration vector magnitudes was computed and shown in Figure 6-237. Computational intensity was such that only hours 02, 08, and 10 on the day of test were selected for consideration – one-third sleep, two-thirds wake including test hour to put the TeSS impact into some statistical context. This analysis shows that of the over 5.5 million measurements (per axis) made in these 3 non-contiguous hours, the 95th percentile was at about 2.4 mg. That is, the red crosshair indicates that 95% of the data that were considered fell at or below 2.4 mg. Meanwhile the TeSS impact magnitudes were at least 6 times larger than this ranging somewhere between 15-35 mg.

6.2.4.3 Extravehicular Activity (EVA)

As explained at http://www.pbs.org/spacestation/station/walks.htm, about 160 spacewalks totaling 960 clock-hours, or 1,920 man-hours, will be performed during assembly of the ISS. Extravehicular Mobility Units (EMUs) based EVAs are normally planned for 7 hours, including 15 minutes to egress the airlock, 6 hours of useful tasks, 15 minutes to ingress the airlock, and 30 minutes of reserved unplanned time. The Crew Lock (C/L) is the portion of the airlock that is depressed to vacuum for the crew to go EVA. It provides the egress point to vacuum via the EVA hatch. As the C/L is depressed down to 3 psi, the depress pump in the airlock is used to reclaim 70-80 percent of the cabin atmosphere. The rest of the atmosphere (3 psi down to vacuum) is vented to space through the Manual Pressure Equalization Valve (MPEV) on the EVA hatch [6].

There are many operations that must be done before and after an EVA to ensure a successful EVA. The basic sequence is described here. Airlock preparation is performed usually the day before EVA to configure and activate the airlock. EMU checkout is performed to check suits integrity. Campout (to prevent decompression sickness) is performed the night before an EVA

and includes depress of joint airlock (A/L) to 10.2 psi overnight, repress to 14.7 for personal hygiene during post sleep, and depress of A/L back to 10.2 psi after personal hygiene break. EVA Prep includes preparation activities such as suit donning, N2 purge. Depress EV crew depresses C/L to 3 psi via the depress pump, stopping at 5 psi for a leak check of the EMU. The final depress to vacuum is accomplished by venting the remaining atmosphere through the EVA hatch MPEV. After the EVA, the same steps are followed in the reverse order.

Locomotion outside the station is more difficult and labored than inside and assembly tasks are expected to have substantive impact, particularly on the transient microgravity environment. The on-orbit status for GMT 16-August-2002, describes the 42nd station spacewalk (the 17th based from the orbital station) stated:

> **EVA-7:** [This] spacewalk did not go quite as planned but accomplished its main objective. [The crew's] egress from the DC-1 "Pirs" was delayed by 1 h 43 min from 3:40 am EDT to 5:23 am [GMT 16-August-2002, 228/09:23], and as a consequence Russian flight controllers deleted two of the three planned tasks from the EVA-7 timeline, (1) replacement of the Kromka payload, and (2) inspection/swabbing of the thruster effluent residues on the SM surface (both tasks are being rescheduled). Spacewalk duration, constrained by the Orlan LiOH (lithium hydroxide) CO_2 filters, could not be extended. The planned installation of six orbital debris protection panels on the SM's conical section circumference was completed without problems (17 more panels are to be installed over the next few years). The EVA ended with hatch closure at 9:48 am [GMT 16-August-2002, 228/13:48], after a total duration of 4 h 25 min.

Figure 6-238 shows a 24-hour spectrogram for this day. Note the vertical red streaks that, during the EVA time frame, demarcate impulsive events along with marked structural mode excitation.

To put the transient nature of these impulsive events into some context, the interval RMS plot of Figure 6-239 was computed. The red, dashed box in that figure shows the impact of the EVA on the RMS acceleration below 100 Hz, while the interval maximum vector magnitude plot of Figure 6-240 is a 20-minute excerpt near the beginning of the EVA. Furthermore, acceleration magnitude histograms were computed for each of 2 hours during the EVA and 2 hours before/after the EVA. Figure 6-241 shows the cumulative percentage of occurrence computed from these histograms. From this figure, we see approximately 95% of acceleration magnitudes were below 1.43 mg during EVA-7 (GMT hours 09 and 10), while approximately 95% of acceleration magnitudes were below 1.35 mg in GMT hours 08 and 14, which were the hours before and after the spacewalk. These impulsive accelerations were not happening all throughout hours 09 and 10, so consider this fact for the statistical context presented.

The 43rd station spacewalk is discussed in the on-orbit status for GMT 26-August-2002:

> **EVA-8:** [The crew's spacewalk] from the DC-1 module was completed successfully, throughout smoothly and in less time than expected. Hatch opening, at 1:27am (all times Eastern daylight) [GMT 26-August-2002, 238/05:27], was 25 minutes late because of a temporary air leak between DC-1 and SM Transfer Compartment (PkhO). After repressurization and hatch closure repeat, the spacewalk proceeded nominally, concluding with hatch close at 6:48 am [GMT 26-August-2002, 238/10:48], after a total duration of 5 h 21 min. All five scheduled tasks were completed OK: (1) installation of a platform frame (PF) for temporary Orbital Replacement Unit (ORU) (on-orbit replaceable unit) stowage outside the FGB, (2) installation of "fairleads" along the FGB (fixtures for

```
routing and attaching tethers used as translation guides/aids in future EVAs),
(3) retrieval of panel #1 of Japanese payloads MPAC (debris particle collector)
and SEED (materials exposure experiment), (4) changeout of the Russian Kromka
experiment "witness" (collector) plate, designed to collect thruster plume
residue to check out the efficacy of plume deflectors installed last year on
the SM, and (5) installation of two more ham radio antennas, WA3 and WA4, at
the SM aft end, with routing and installation of their cabling.
```

Figure 6-242 shows a 24-hour spectrogram for this day. Note the vertical read streaks that, during the EVA time frame, demarcate impulsive events along with marked structural mode excitation.

Now, to put the transient nature of these impulsive events into some context, the interval RMS plot of Figure 6-243 was computed. The red, dashed box in that figure shows the impact of the EVA on the RMS acceleration below 100 Hz, while the interval maximum vector magnitude plot of Figure 6-244 is a 20-minute excerpt near the beginning of the EVA. Again, acceleration magnitude histograms were computed for each of 2 hours during the EVA and 2 hours before/after the EVA. Figure 6-245 shows the cumulative percentage of occurrence computed from these histograms. From this figure, we see approximately 95% of acceleration magnitudes were below 1.98 mg during EVA-8 (GMT hours 06 and 07), while approximately 95% of acceleration magnitudes were below 1.93 mg in GMT hours 04 and 11, which were the hours before and after the spacewalk. These impulsive accelerations were not happening all throughout the EVA.

6.2.4.4 Public Affairs Office (PAO) Events

For a microgravity environment that mimics crew sleep, one can consider PAO events that occupy the entire crew (note that some PAO events occupy only part of the crew). These events typically last at least 10 minutes or so with the crew gathered in front of a video camera participating in an interview. During this time, the crew is usually quite still, but there are times when they demonstrate various things that require them to push-off or otherwise apply a force to vehicle structure. In the vibratory regime, since crew motion and activity has most of its impact below 5 Hz, a series of PAO events indicated in the short-term plans for Increment 5 were analyzed. These were events that showed all crew members participating. Table 6-30 shows the results of this analysis in the form of mean RMS acceleration levels below 5 Hz for one of three conditions: (1) sleep, (2) PAO, (3) wake, non-PAO.

TABLE 6-30 RMS ACCELERATION COMPARISON BELOW 5 HZ FOR SLEEP/PAO EVENT/WAKE PERIODS

GMT Date	SAMS		Crew Activity Mean RMS Acceleration (µg) / Duration (minutes)		
	Sensor	Location	Sleep	PAO Event	Wake
08-Jul-02	121f02	LAB1O2, ER1, Drawer 1	9.0 / 230	17.8 / 18	42.2 / 951
08-Jul-02	121f04	LAB1O2, ER1, Lower Z Panel	4.6 / 230	16.4 / 18	34.9 / 951
09-Jul-02	121f02	LAB1O2, ER1, Drawer 1	6.3 / 335	19.0 / 13	39.0 / 1060
09-Jul-02	121f04	LAB1O2, ER1, Lower Z Panel	5.2 / 335	16.1 / 13	30.2 / 1060
16-Jul-02	121f02	LAB1O2, ER1, Drawer 1	5.3 / 359	25.0 / 10	40.7 / 941
16-Jul-02	121f04	LAB1O2, ER1, Lower Z Panel	5.0 / 359	23.2 / 10	34.5 / 941
08-Sep-02	121f02	LAB1O2, ER1, Drawer 1	6.9 / 280	17.7 / 12	38.2 / 1006
08-Sep-02	121f04	LAB1O2, ER1, Lower Z Panel	5.0 / 280	14.4 / 12	32.0 / 1006
10-Sep-02	121f02	LAB1O2, ER1, Drawer 1	6.8 / 315	17.6 / 20	44.5 / 850
10-Sep-02	121f04	LAB1O2, ER1, Lower Z Panel	5.3 / 315	15.9 / 20	37.1 / 850
07-Oct-02	121f02	LAB1O2, ER1, Drawer 1	8.7 / 357	21.3 / 10	60.0 / 902
07-Oct-02	121f04	LAB1O2, ER1, Lower Z Panel	6.4 / 357	20.3 / 10	37.3 / 902

This table shows that the mean RMS acceleration values during PAO events are roughly midway between the crew sleep and crew wake categories. Note the PAO durations may be enough time for investigators to be opportunistic about scheduling certain autonomous or ground-commanded aspects of their experiment to be performed during this time, particularly for those sensitive below 5 Hz.

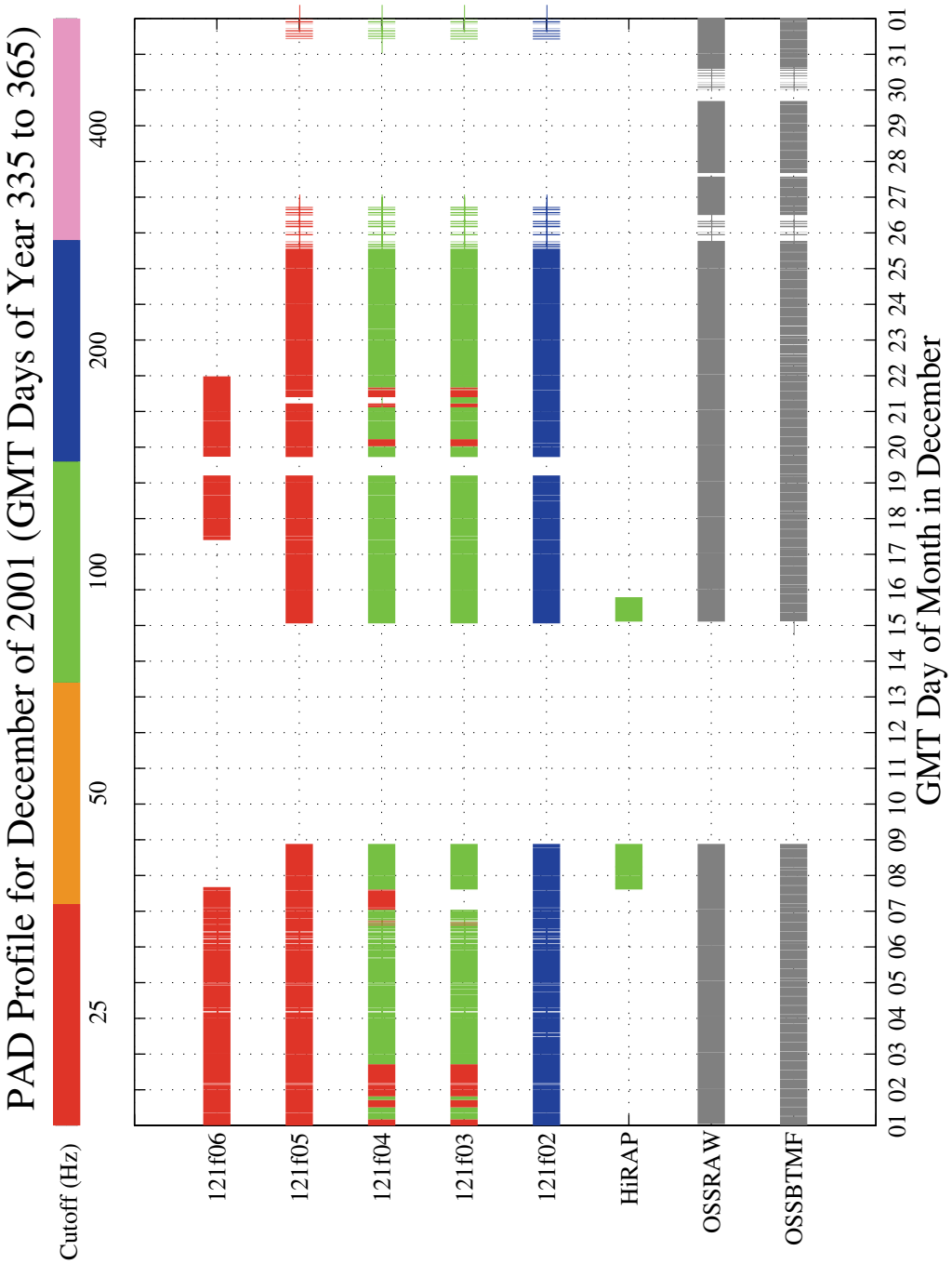

Figure 6-1 PAD Profile for December 2001

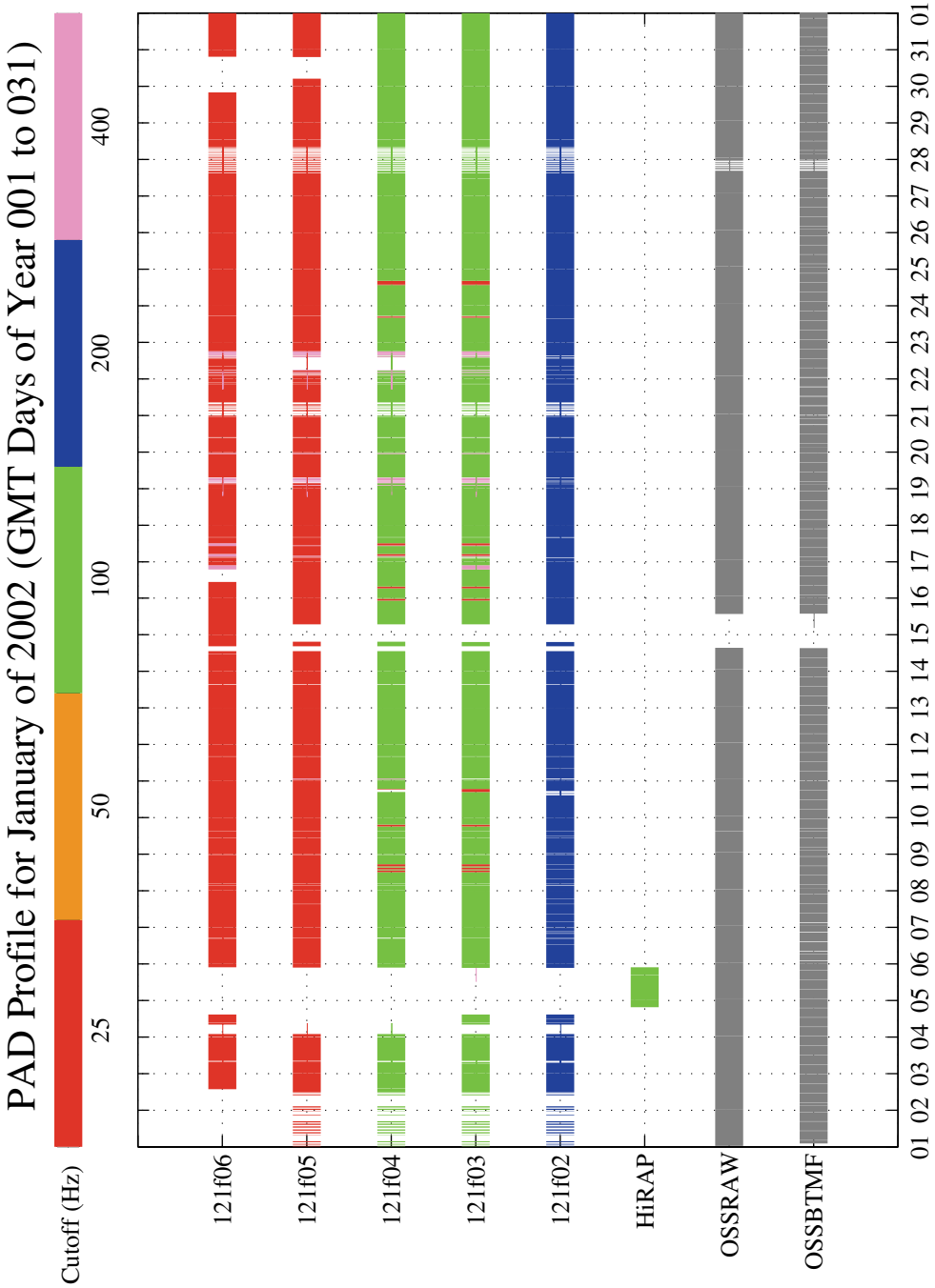

Figure 6-2 PAD Profile for January 2002

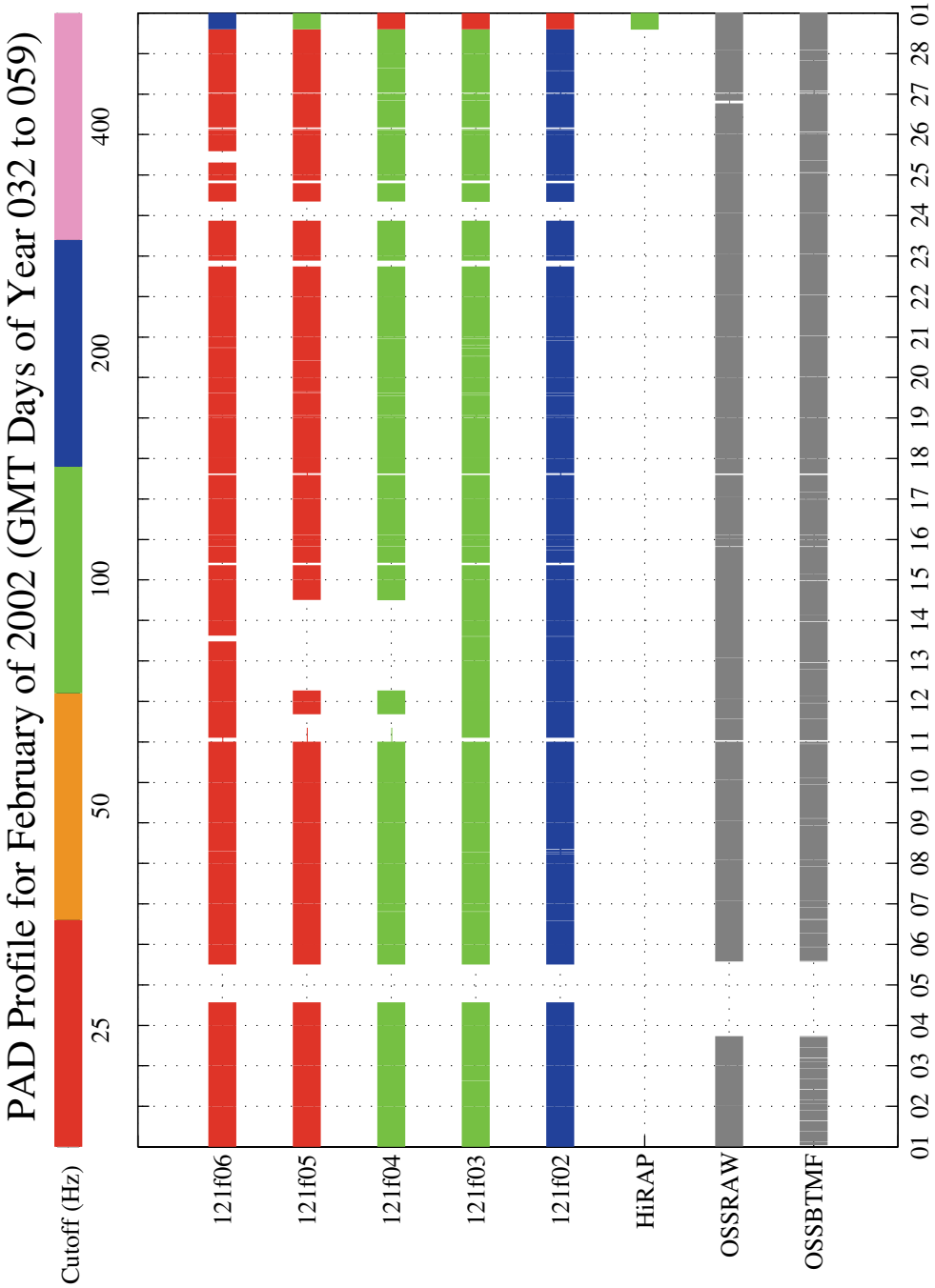

Figure 6-3 PAD Profile for February 2002

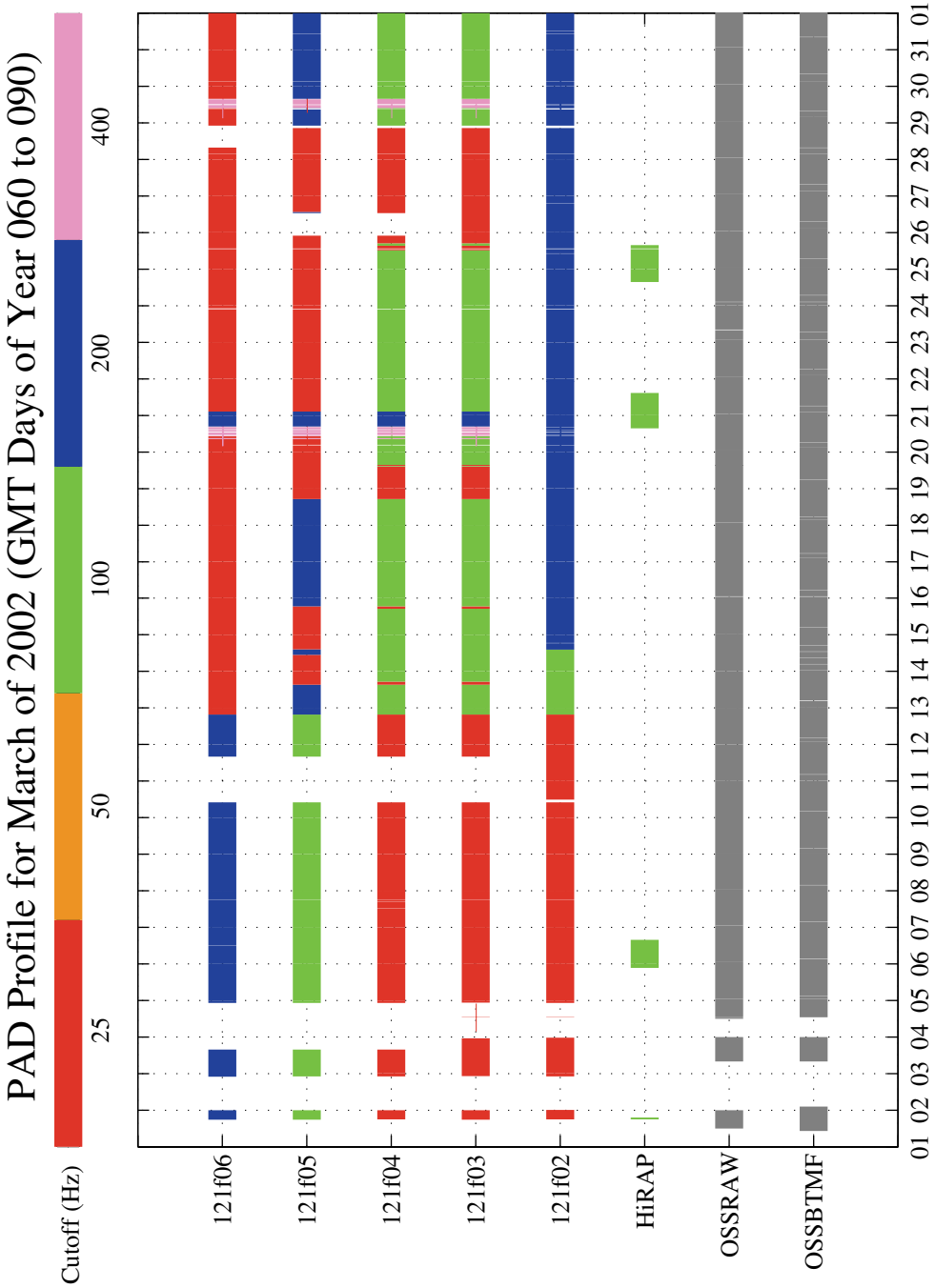

Figure 6-4 PAD Profile for March 2002

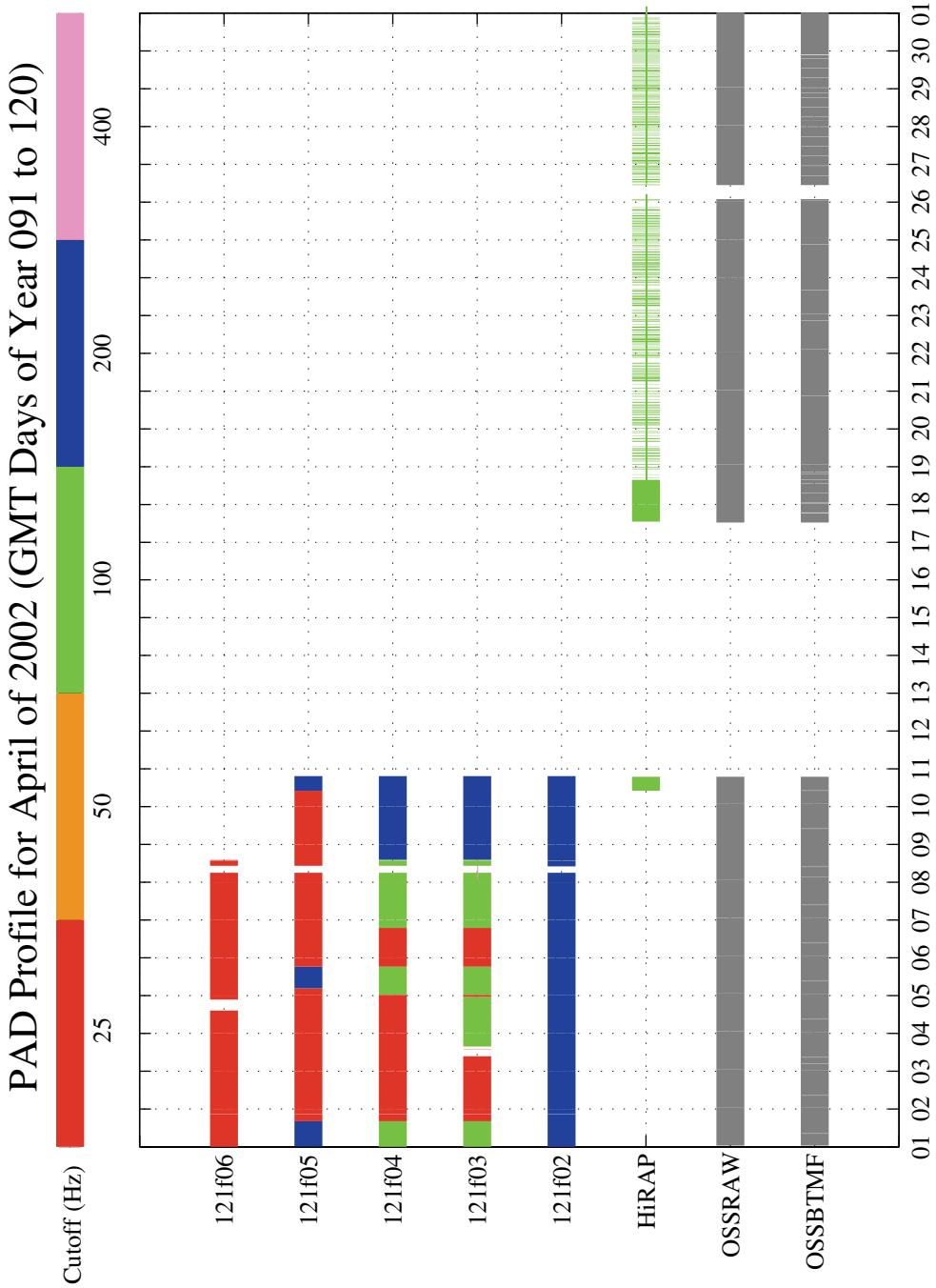

Figure 6-5 PAD Profile for April 2002

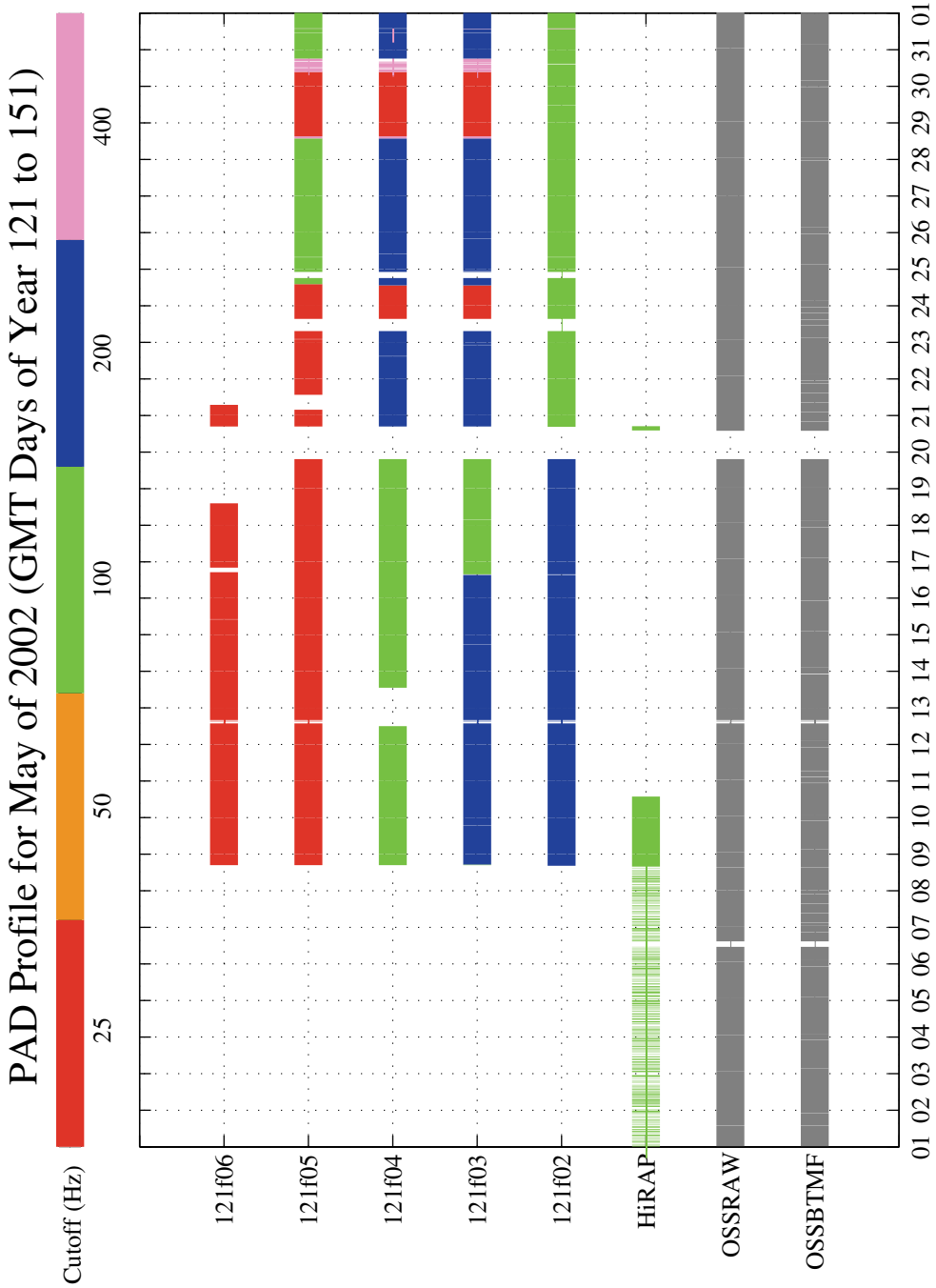

Figure 6-6 PAD Profile for May 2002

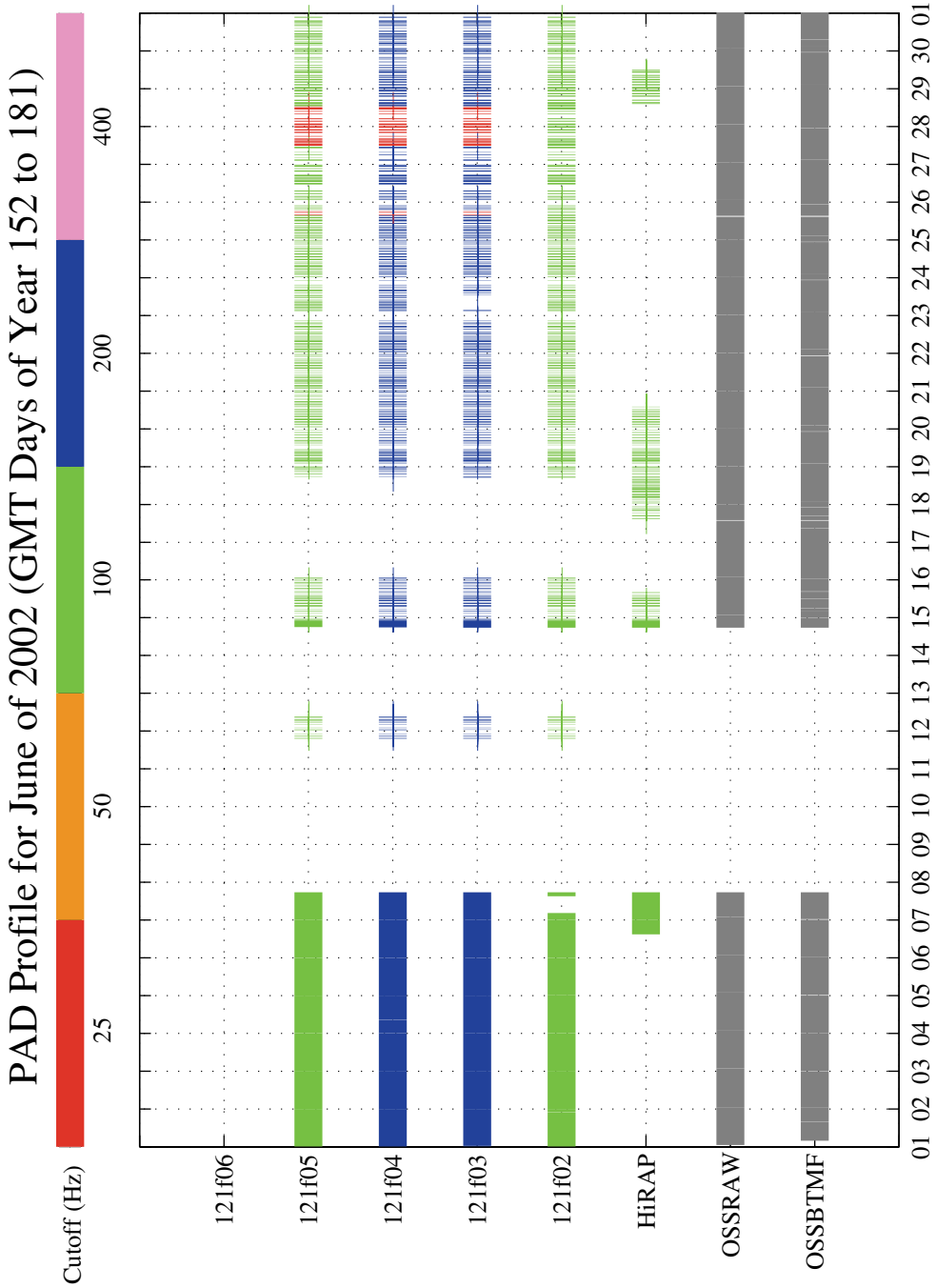

Figure 6-7 PAD Profile for June 2002

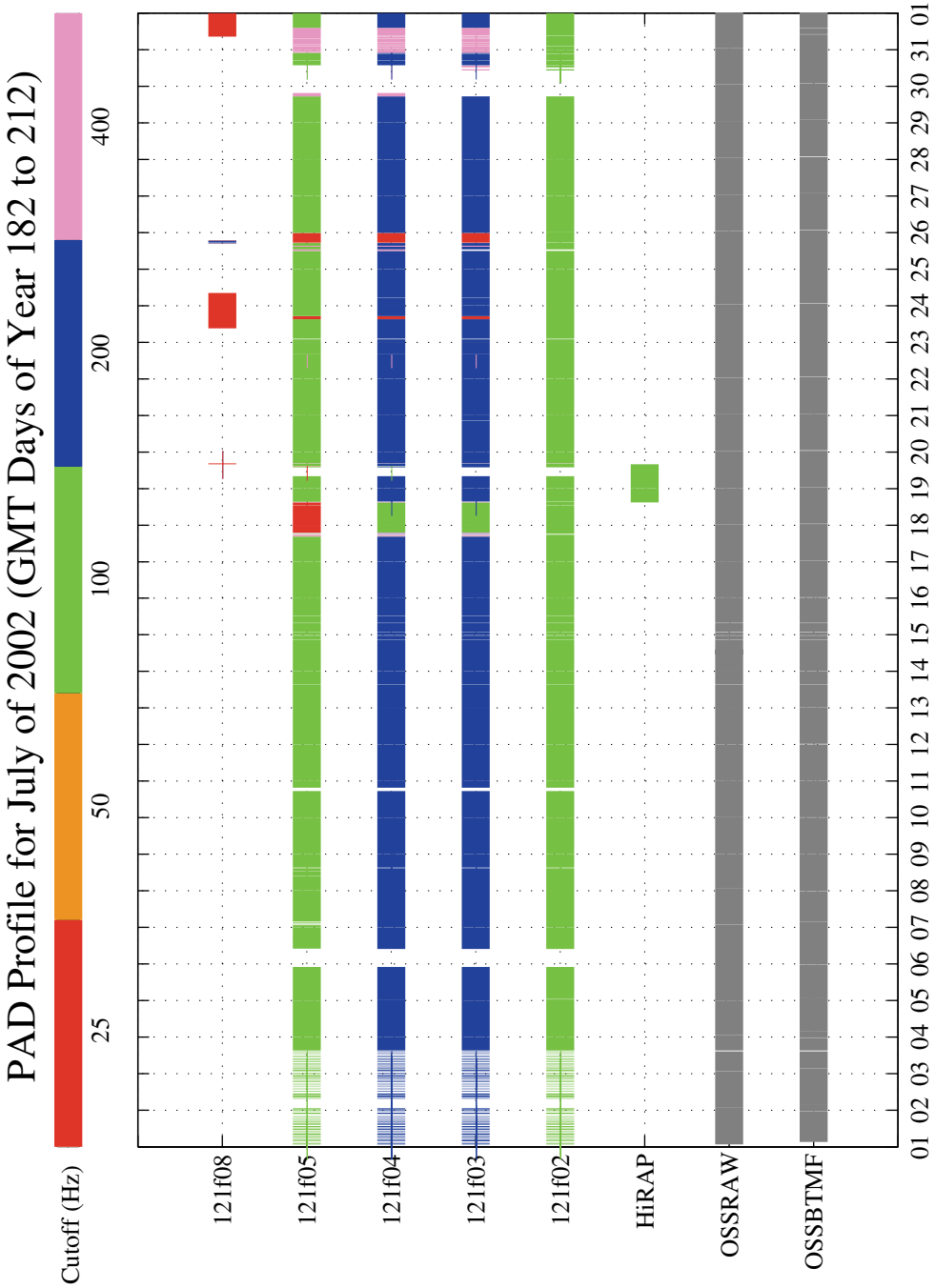

Figure 6-8 PAD Profile for July 2002

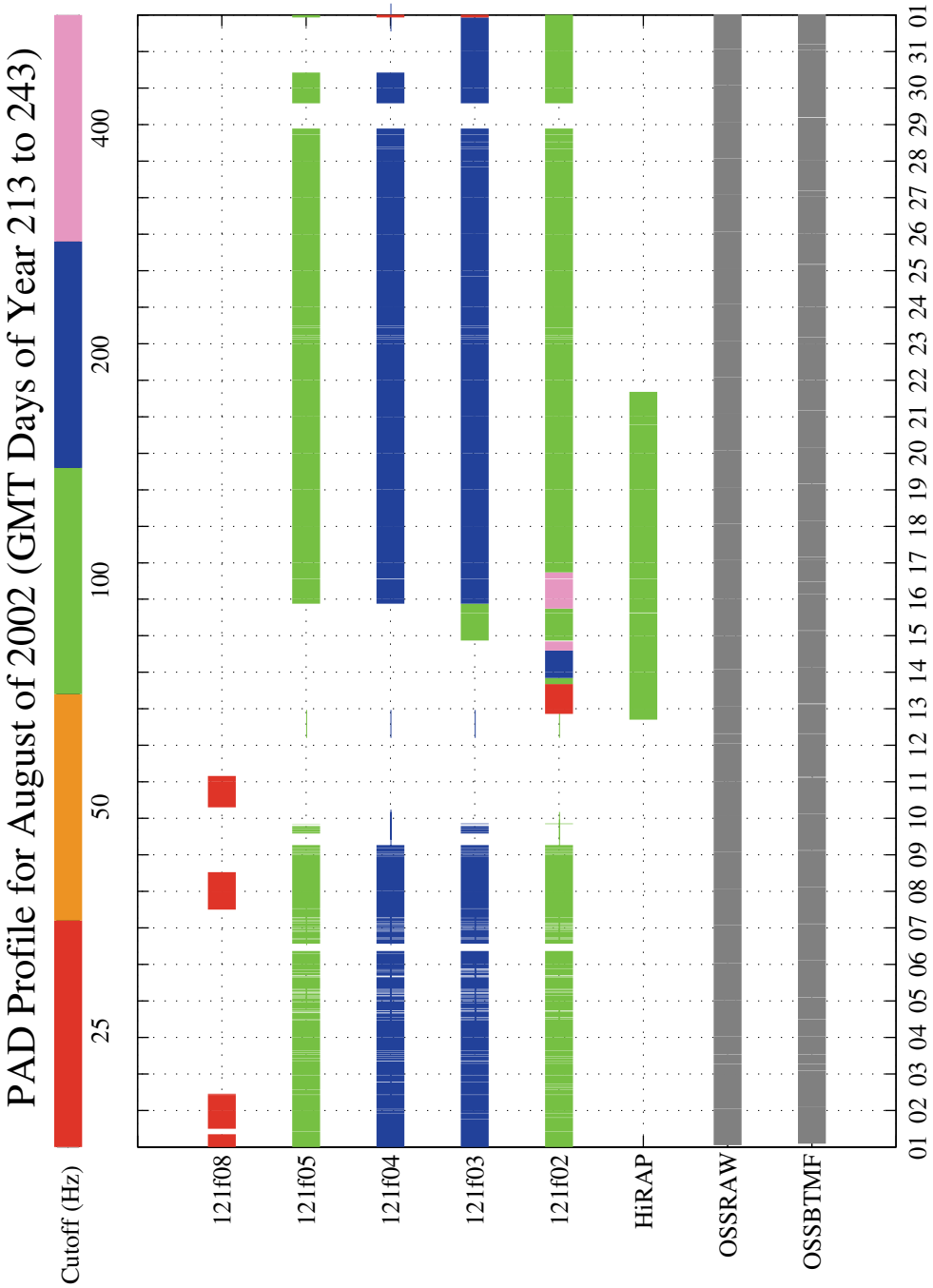

Figure 6-9 PAD Profile for August 2002

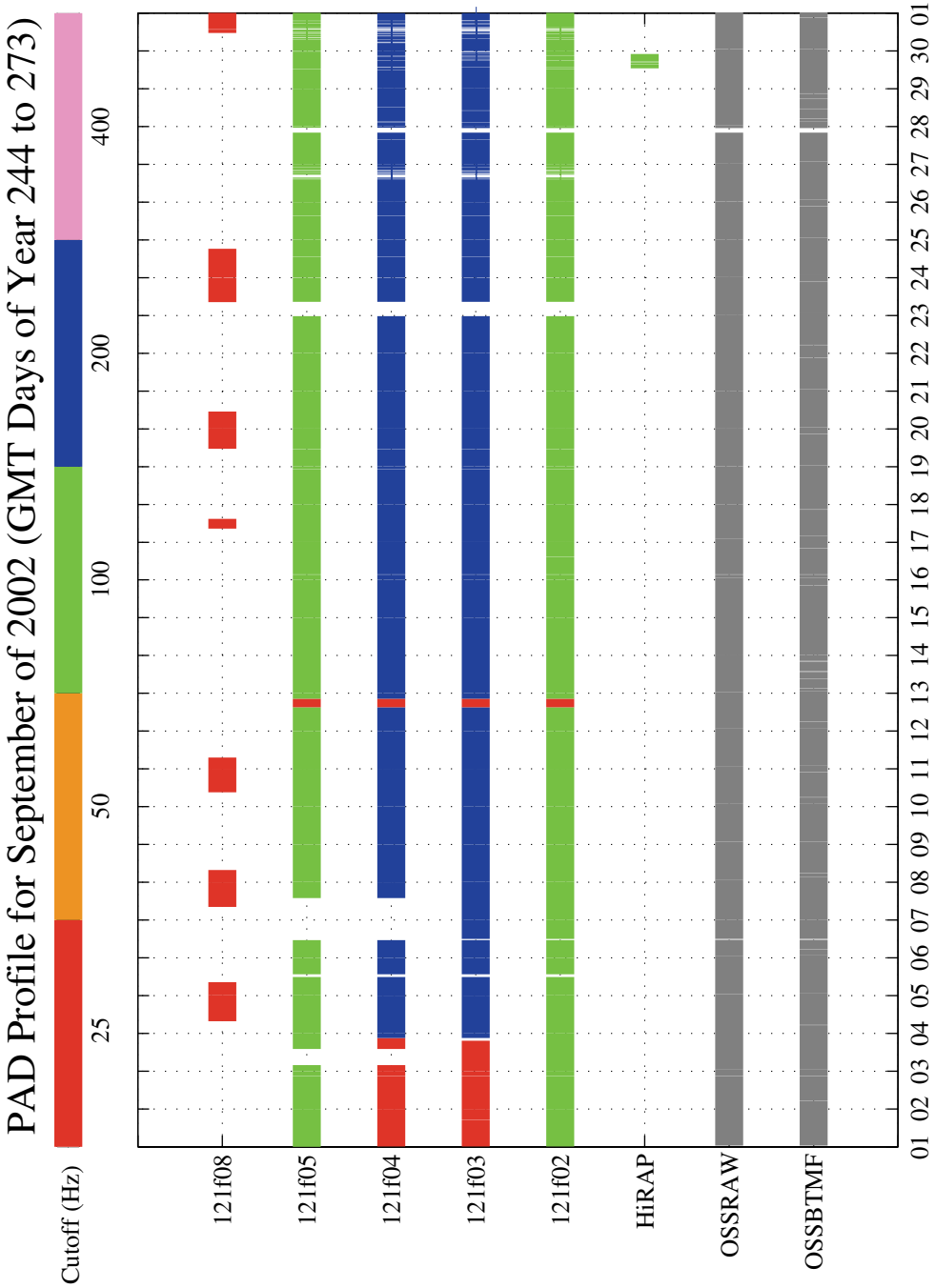

Figure 6-10 PAD Profile for September 2002

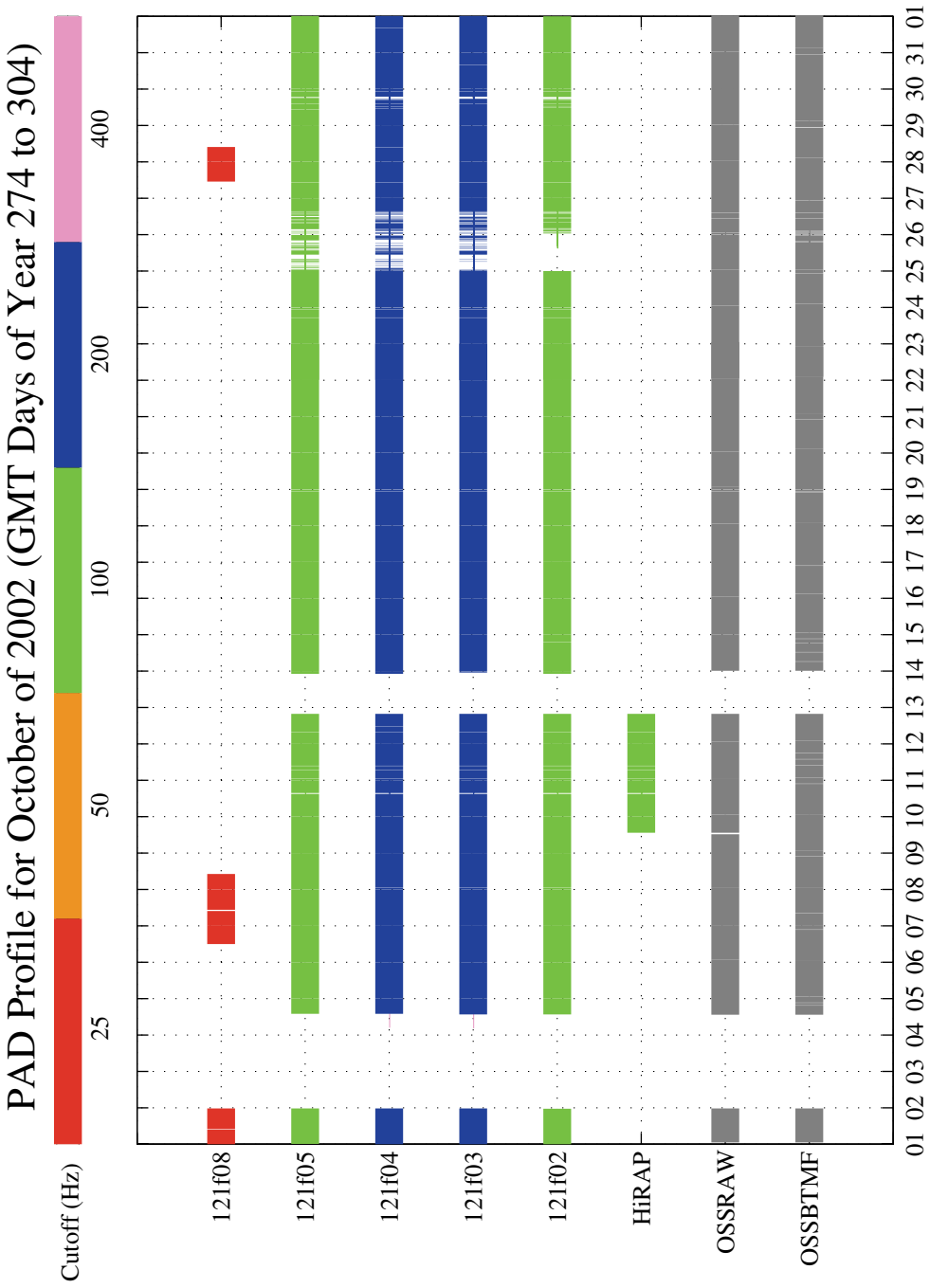

Figure 6-11 PAD Profile for October 2002

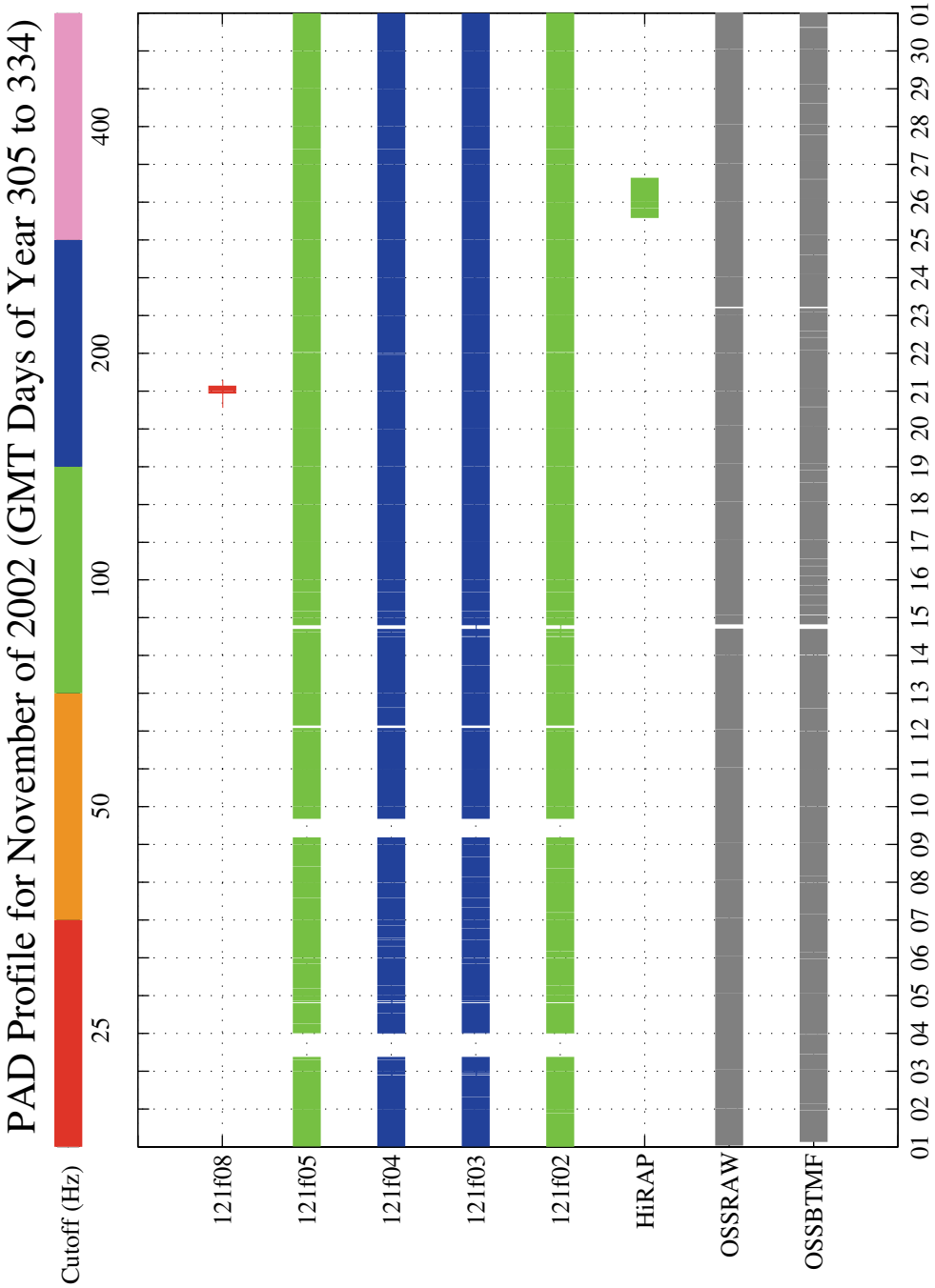

Figure 6-12 PAD Profile for November 2002

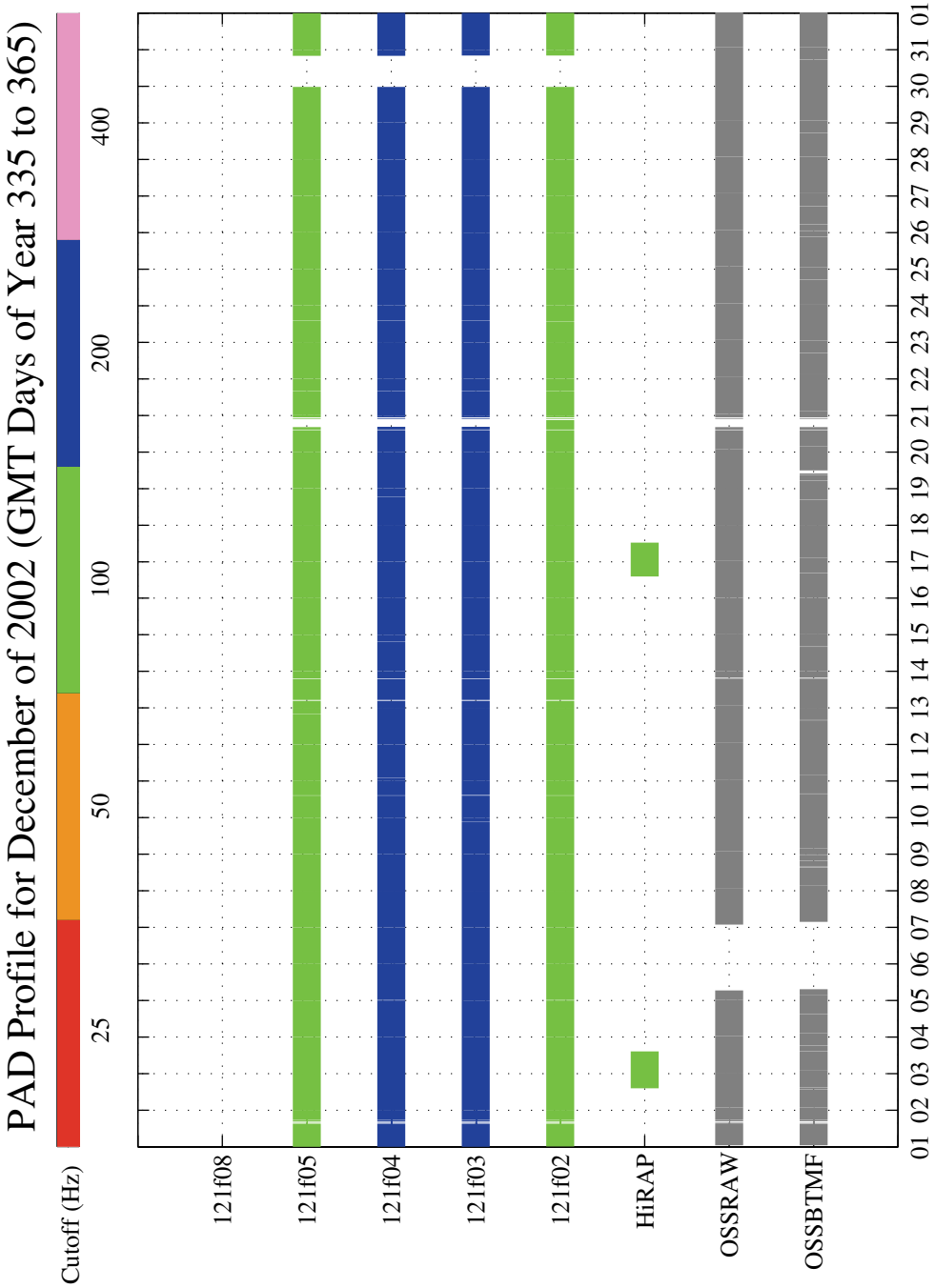

Figure 6-13 PAD Profile for December 2002

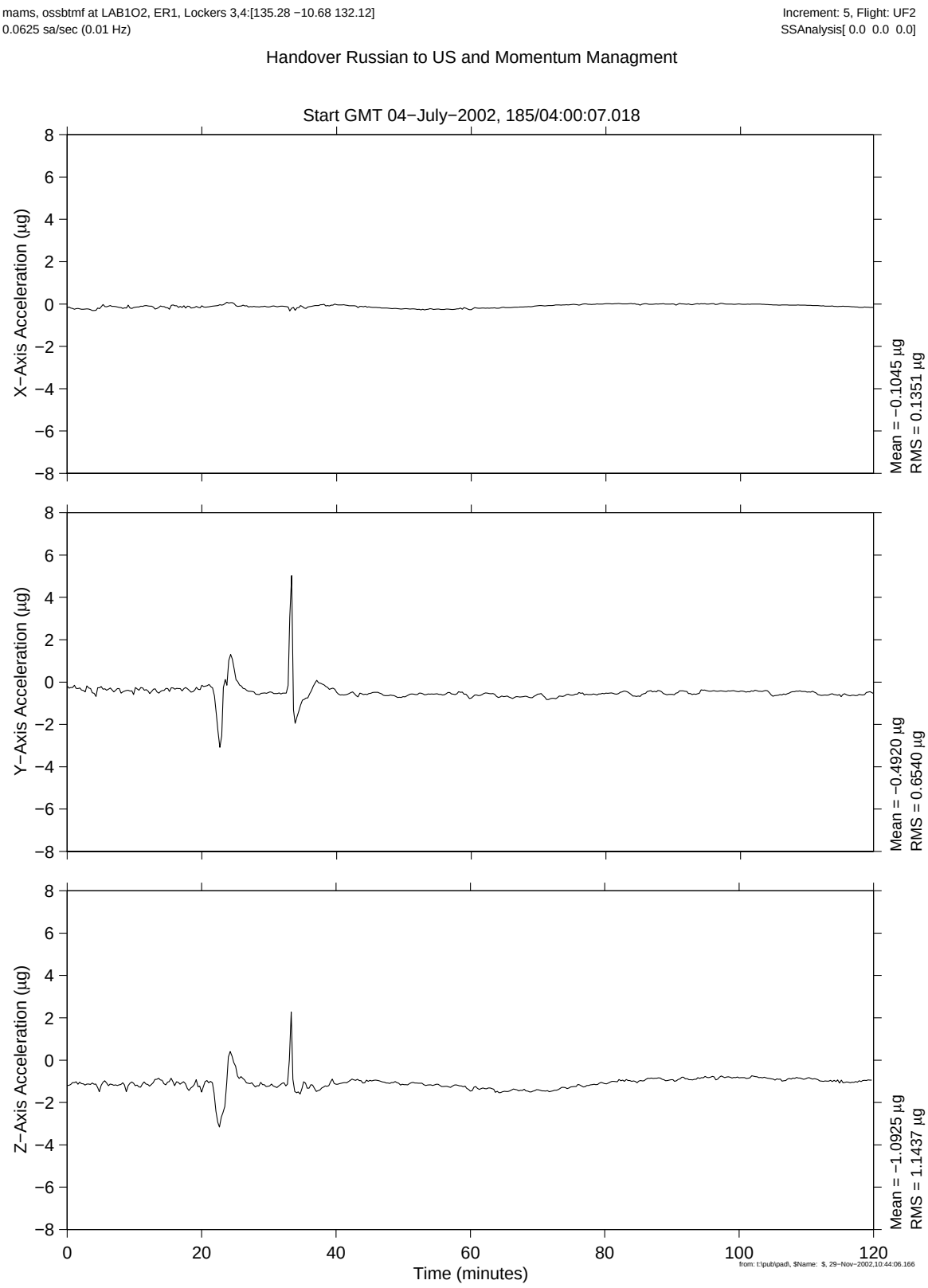

Figure 6-14 Time Series of Handover from Russian to US Attitude Control, GMT 314 (OSSBTMF)

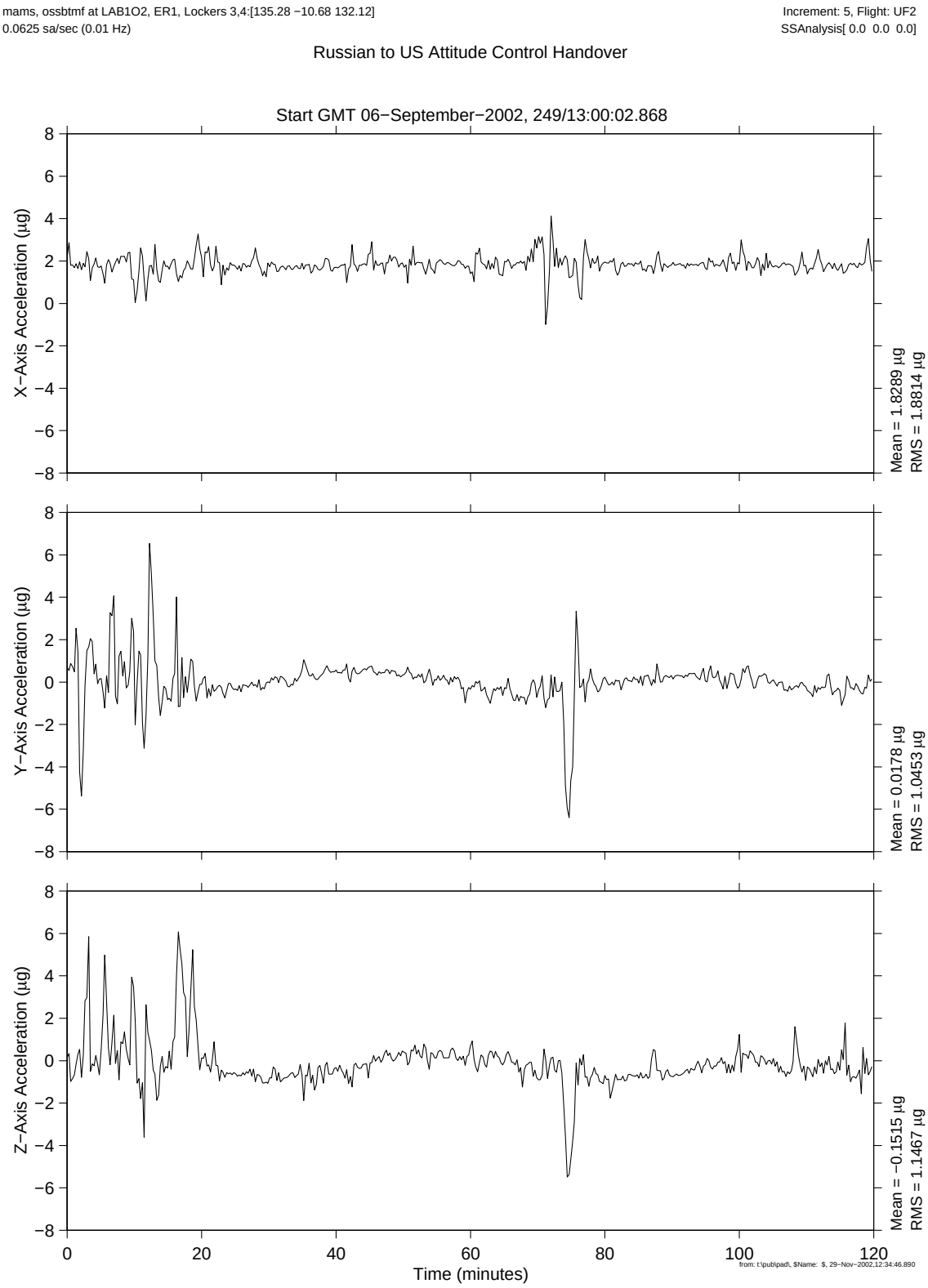

Figure 6-15 Time Series of Handover from Russian to US Attitude Control, GMT 249 (OSSBTMF)

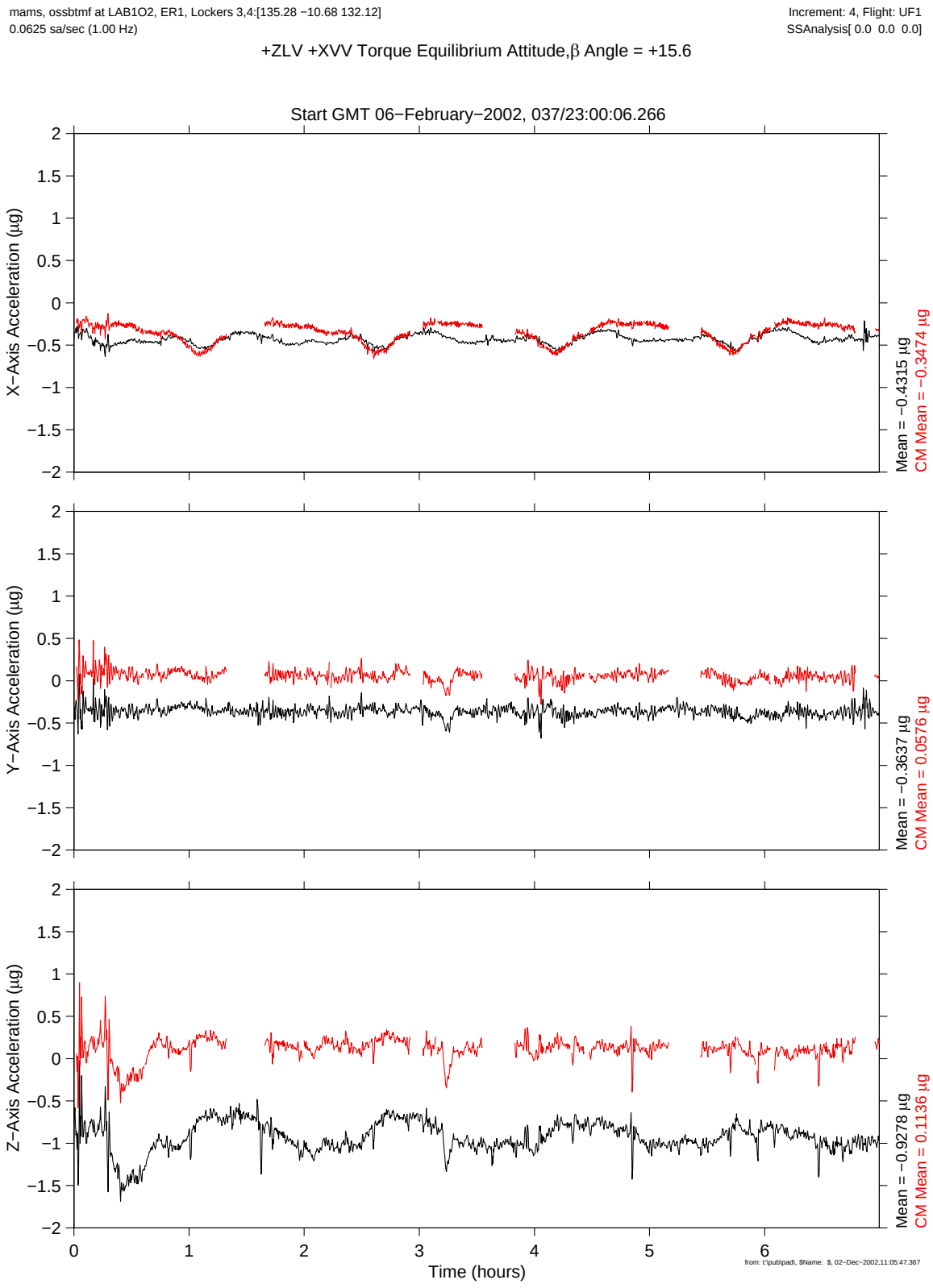

Figure 6-16 Time Series of TEA during Crew Sleep, GMT 037 (OSSBTMF)

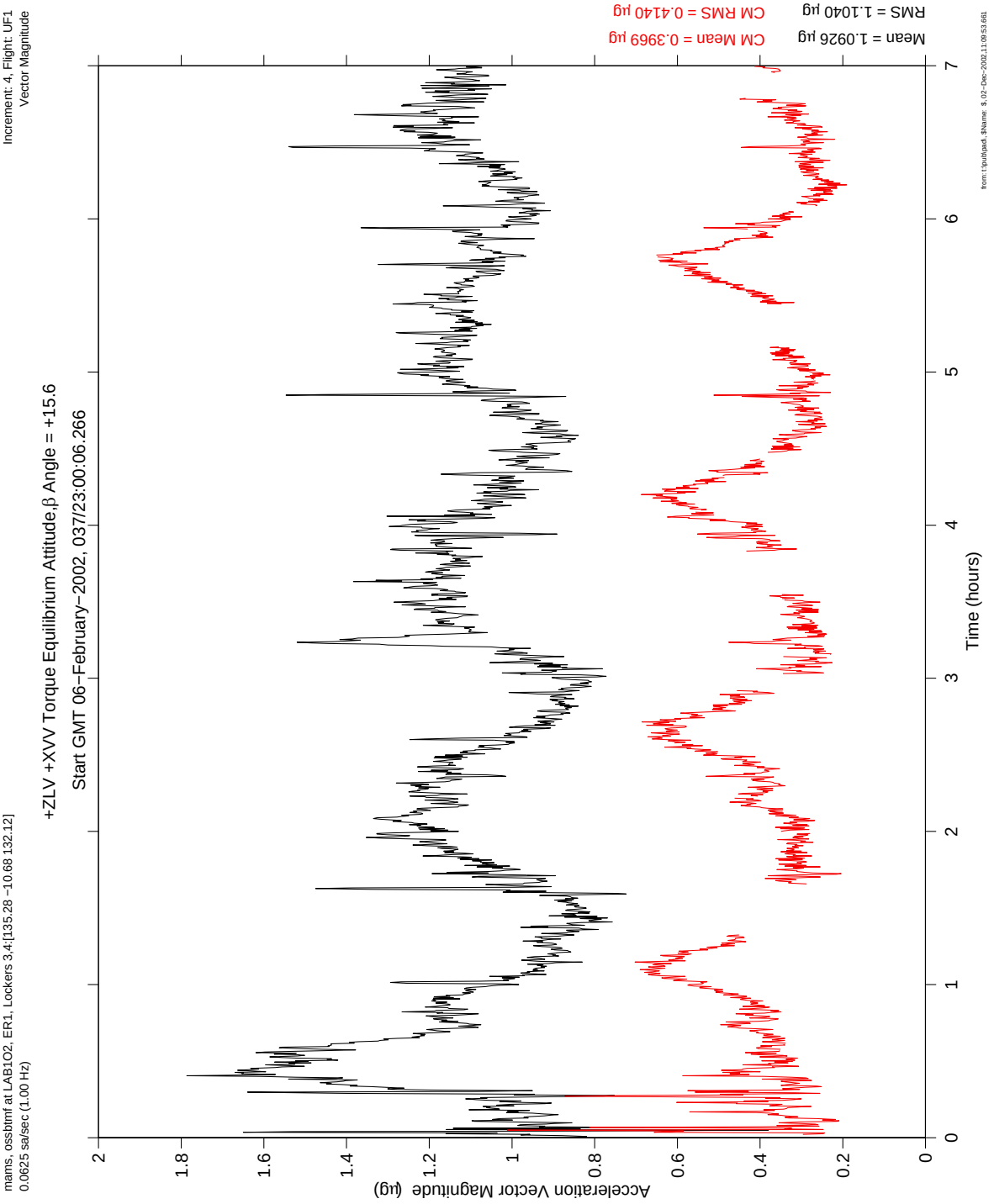

Figure 6-17 Acceleration Magnitude of TEA during Crew Sleep, GMT 037 (OSSBTMF)

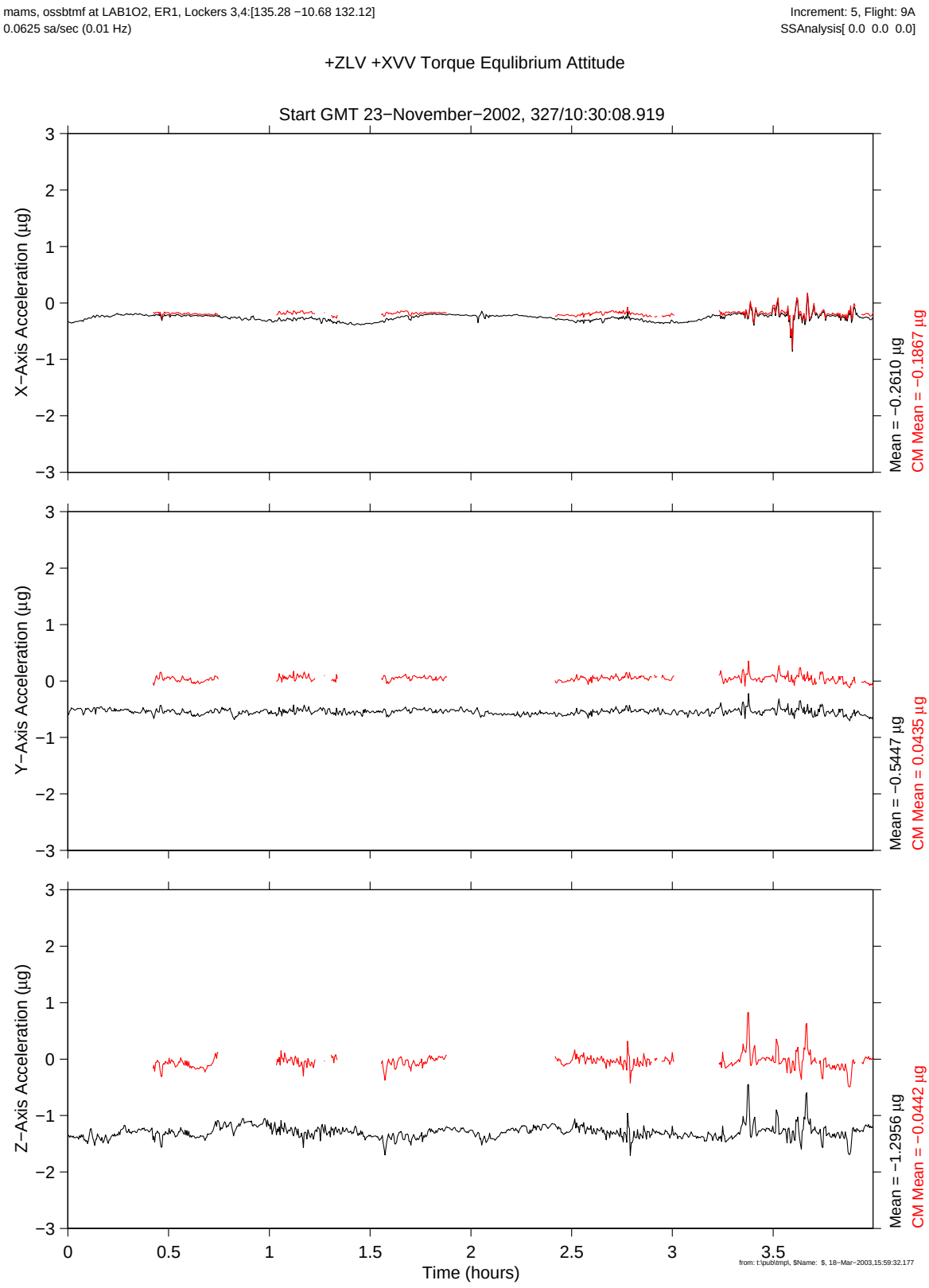

Figure 6-18 Time Series of TEA during Crew Sleep, GMT 327 (OSSBTMF)

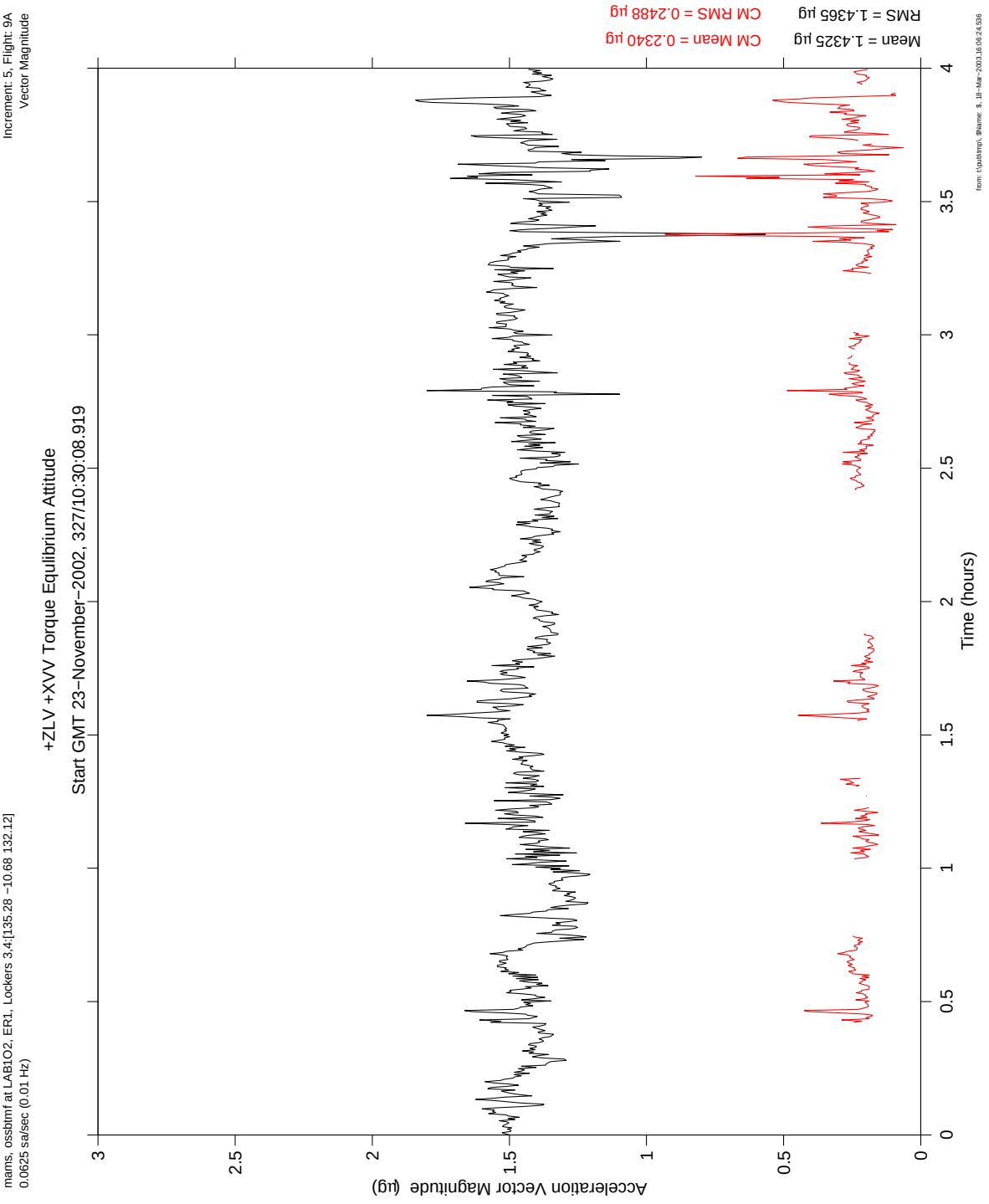

Figure 6-19 Acceleration Magnitude of TEA during Crew Sleep, GMT 327 (OSSBTMF)

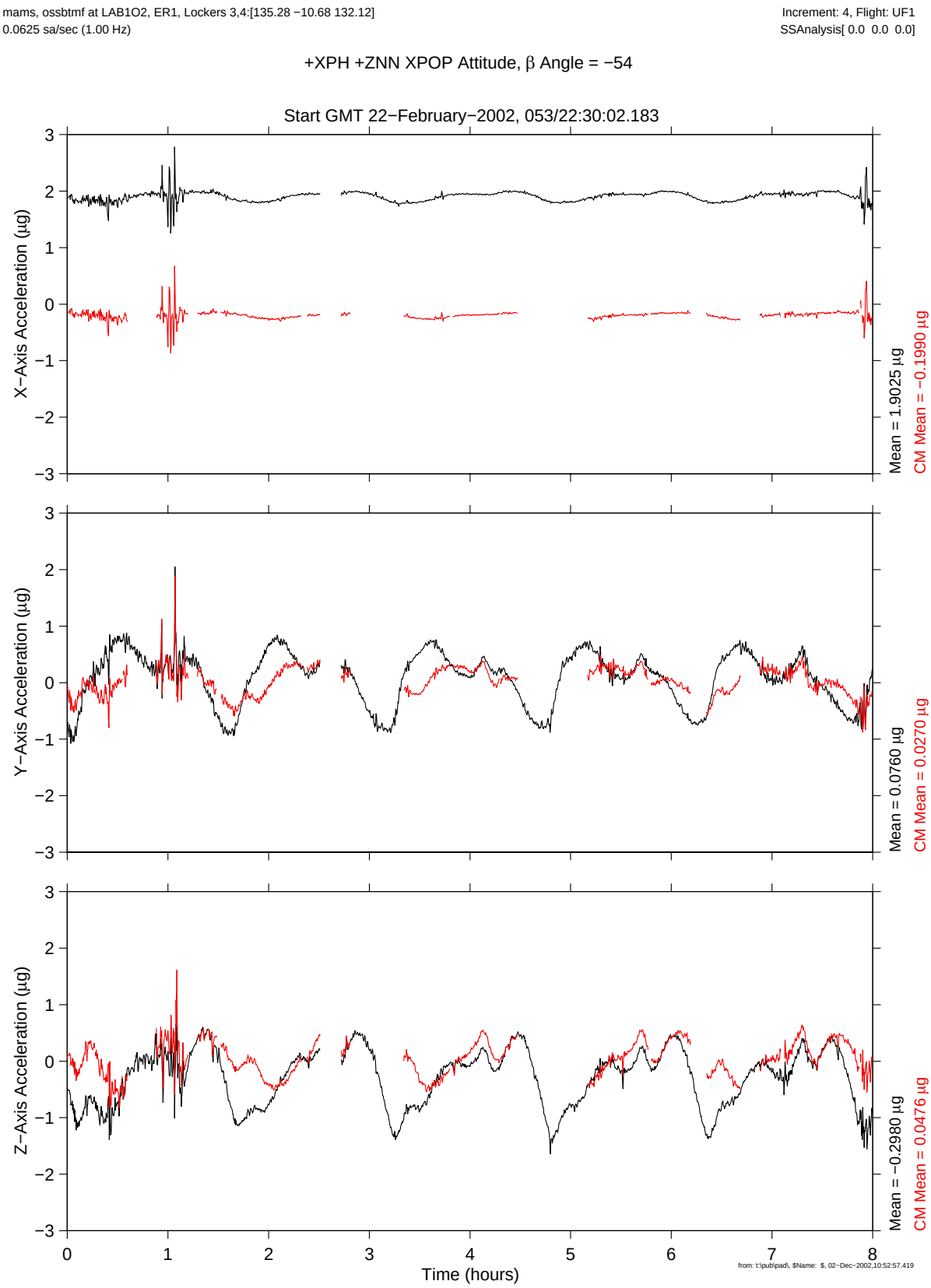

Figure 6-20 Time Series of XPOP Attitude during Crew Sleep, GMT 053 (OSSBTMF)

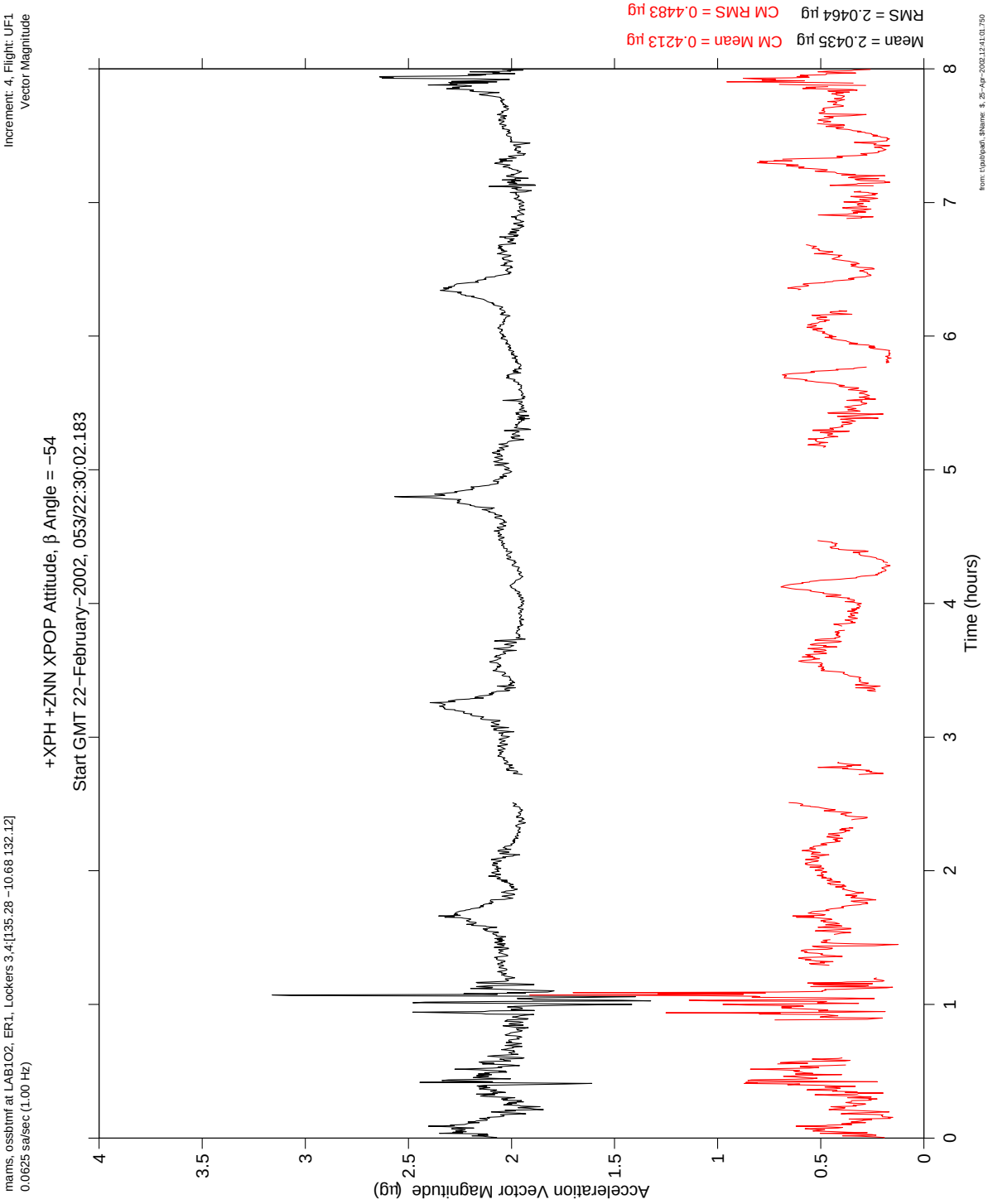

Figure 6-21 Acceleration Magnitude of XPOP Attitude during Crew Sleep, GMT 053 (OSSBTMF)

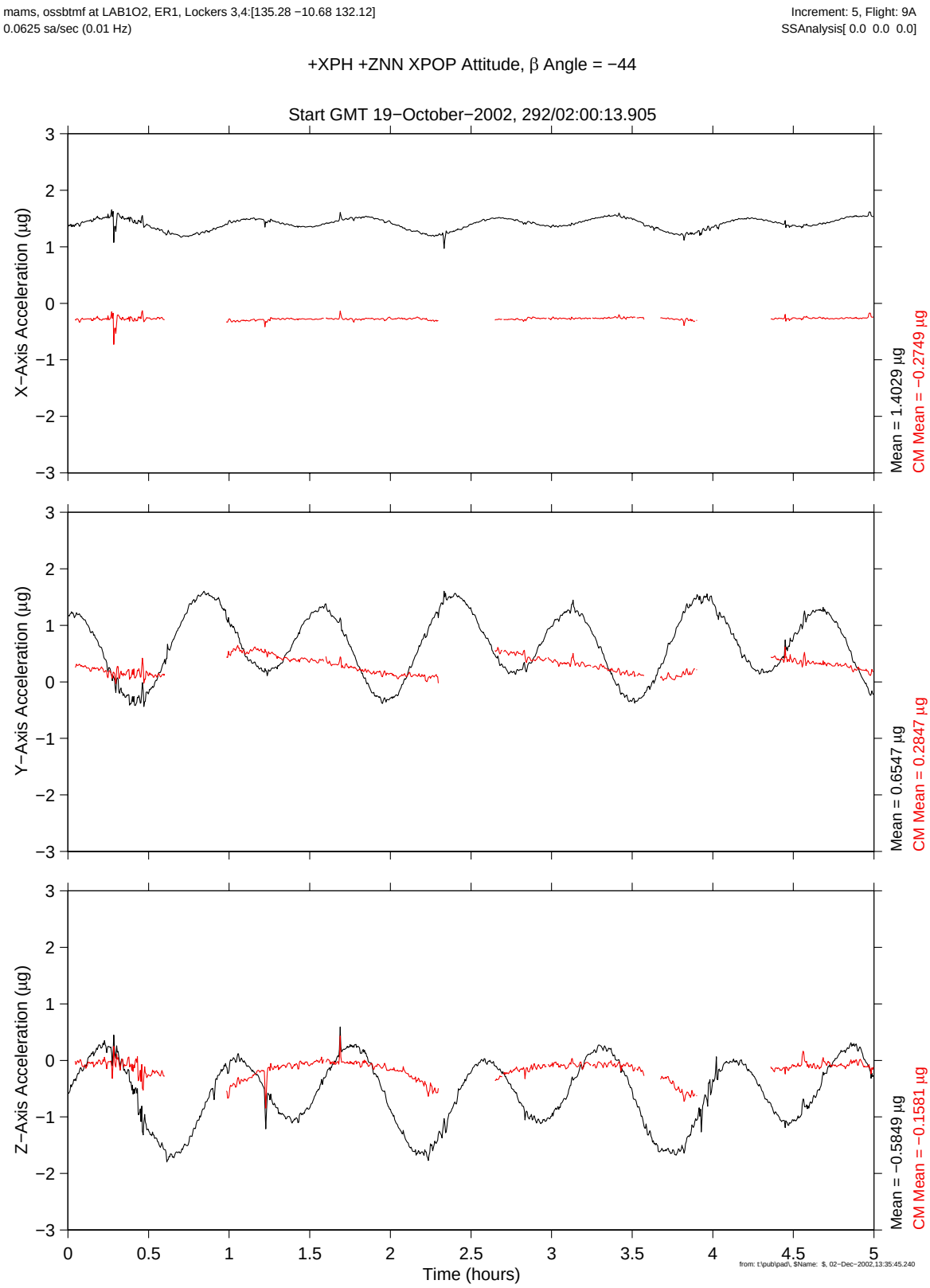

Figure 6-22 Time Series of XPOP Attitude during Crew Sleep, GMT 292 (OSSBTMF)

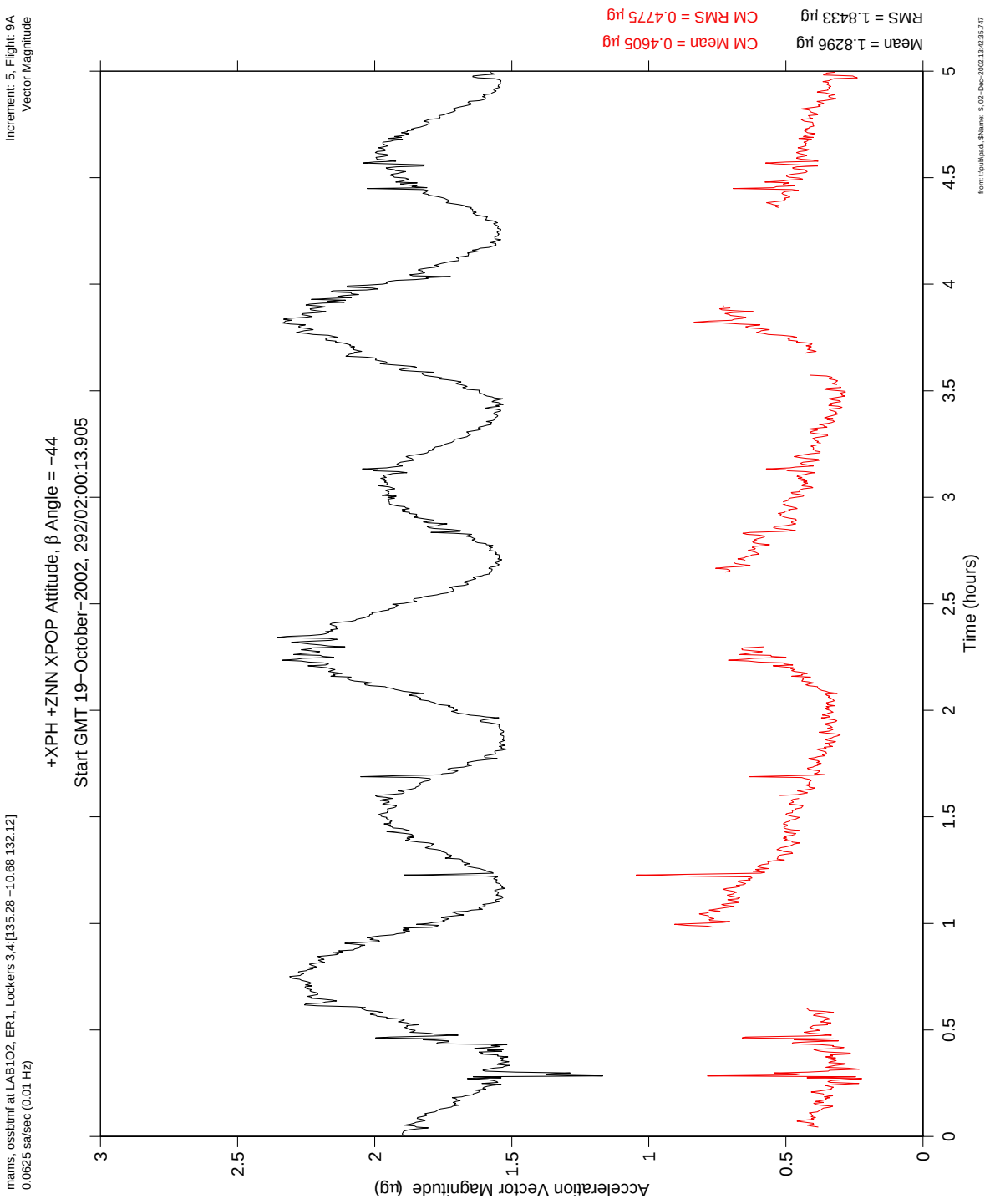

Figure 6-23 Acceleration Magnitude of XPOP Attitude during Crew Sleep, GMT 292 (OSSBTMF)

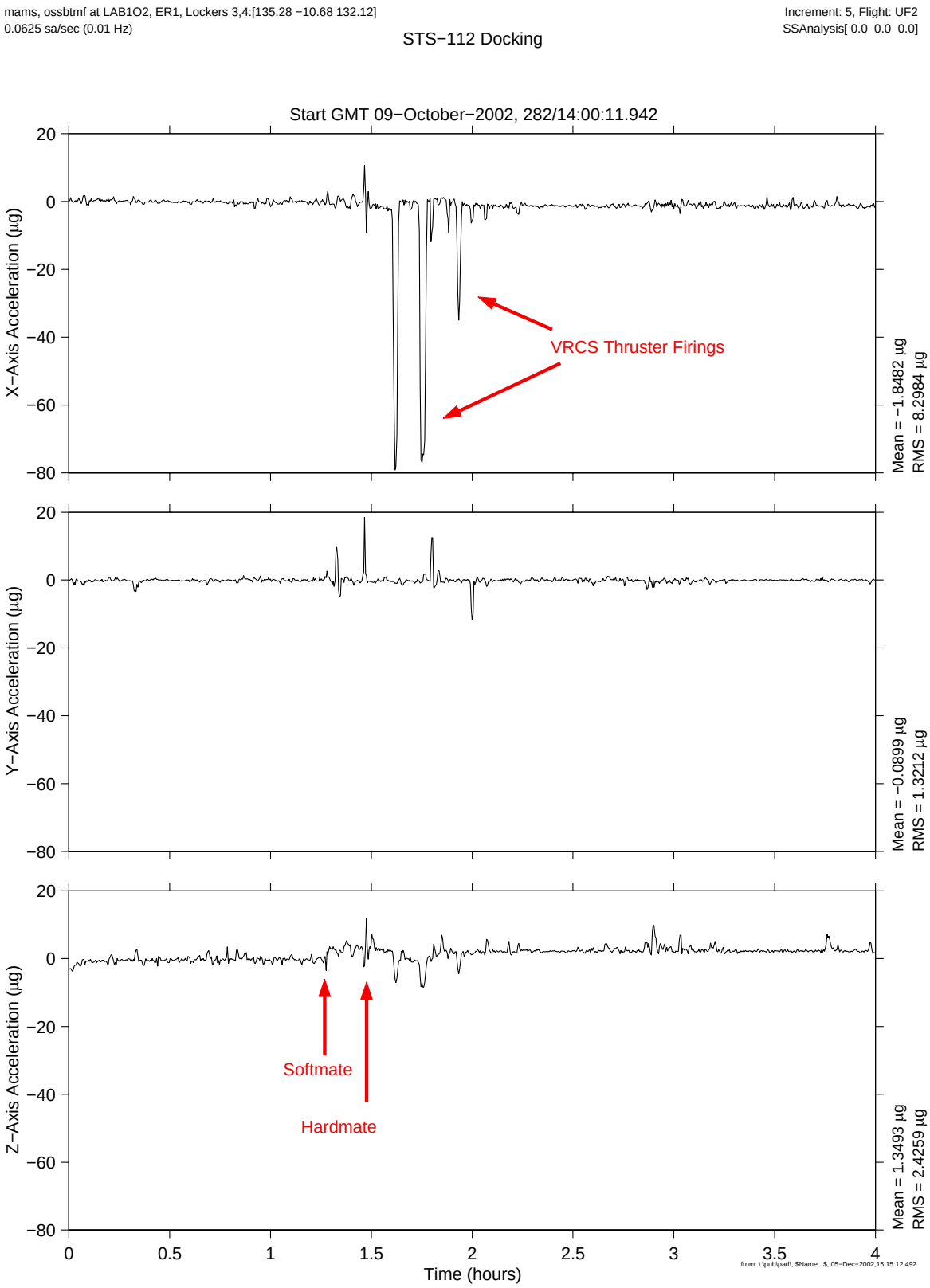

Figure 6-24 Time Series of STS-112 Docking (OSSBTMF)

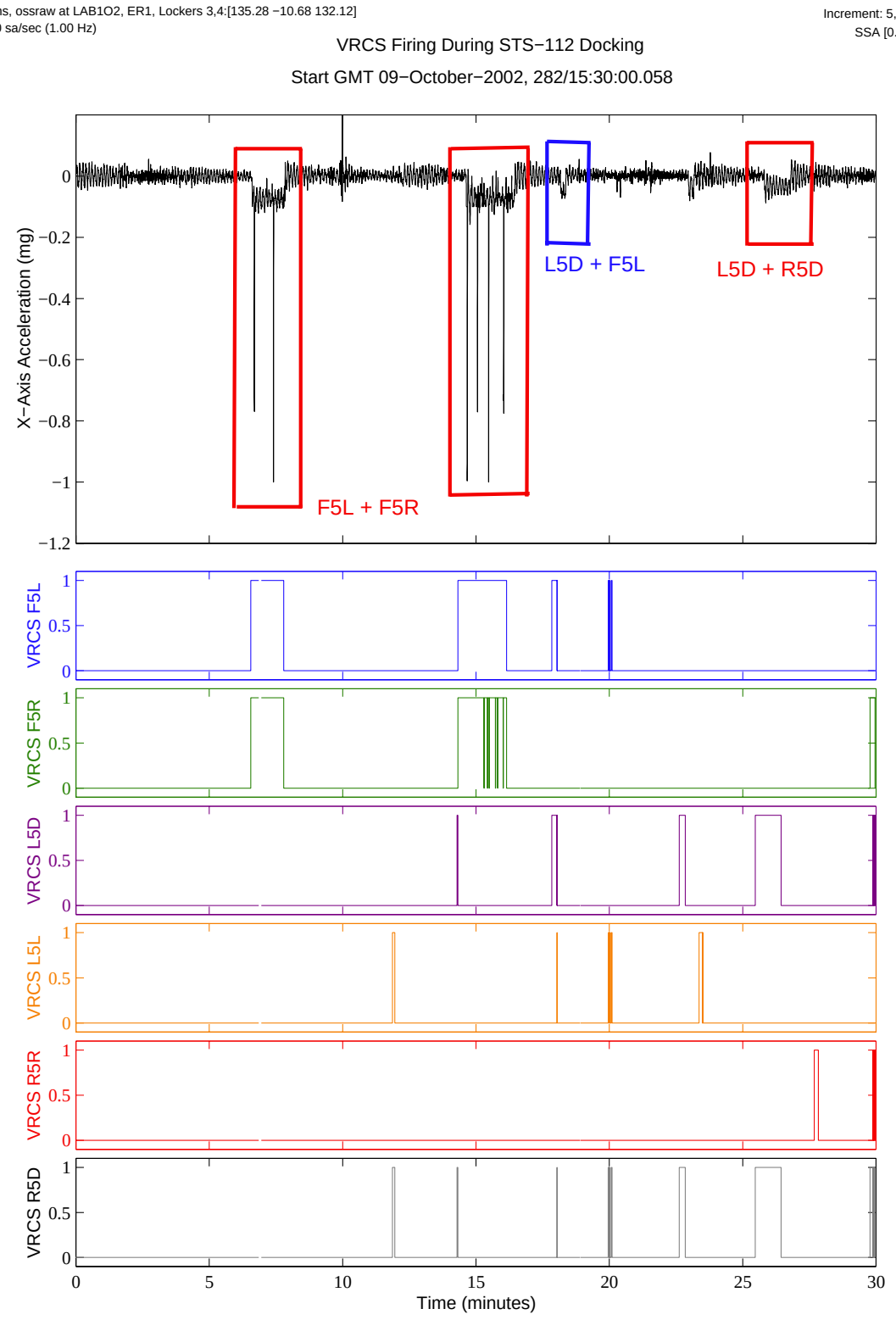

Figure 6-25 Time Series of X-Axis Accelerations Correlated with VRCS Firings (OSSBTMF)

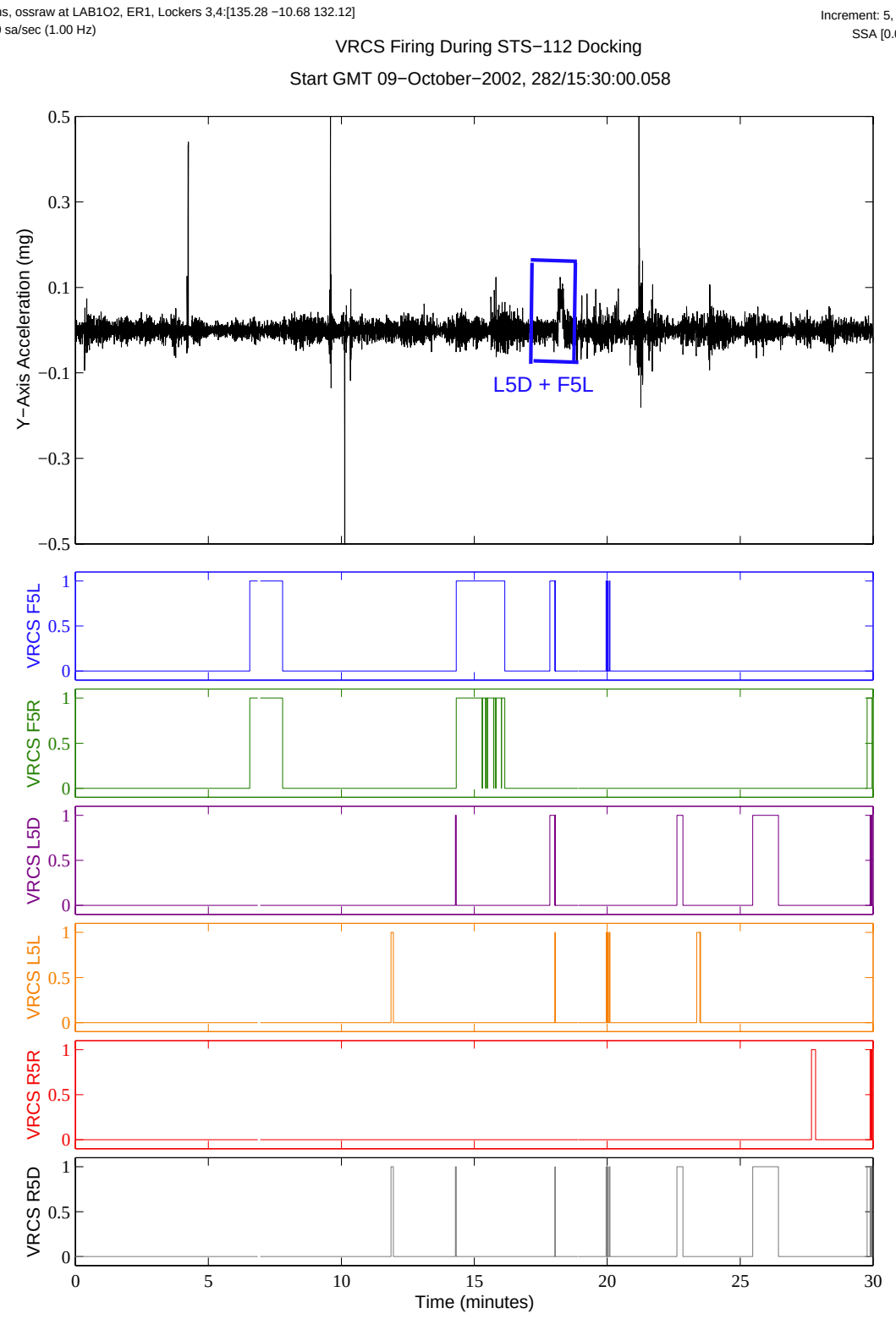

Figure 6-26 Time Series of Y-Axis Accelerations Correlated with VRCS Firings (OSSBTMF)

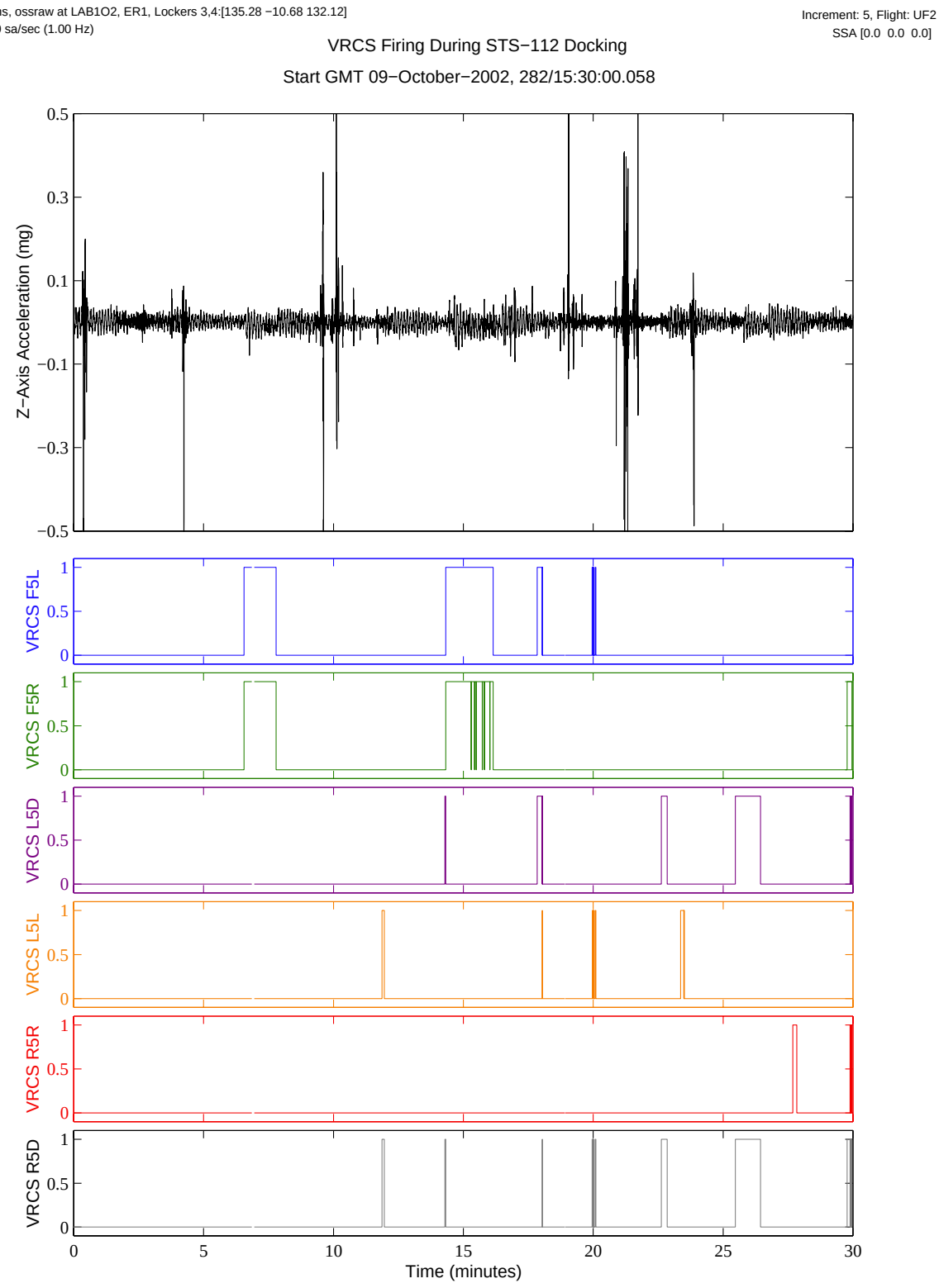

Figure 6-27 Time Series of Z-Axis Accelerations Correlated with VRCS Firings (OSSBTMF)

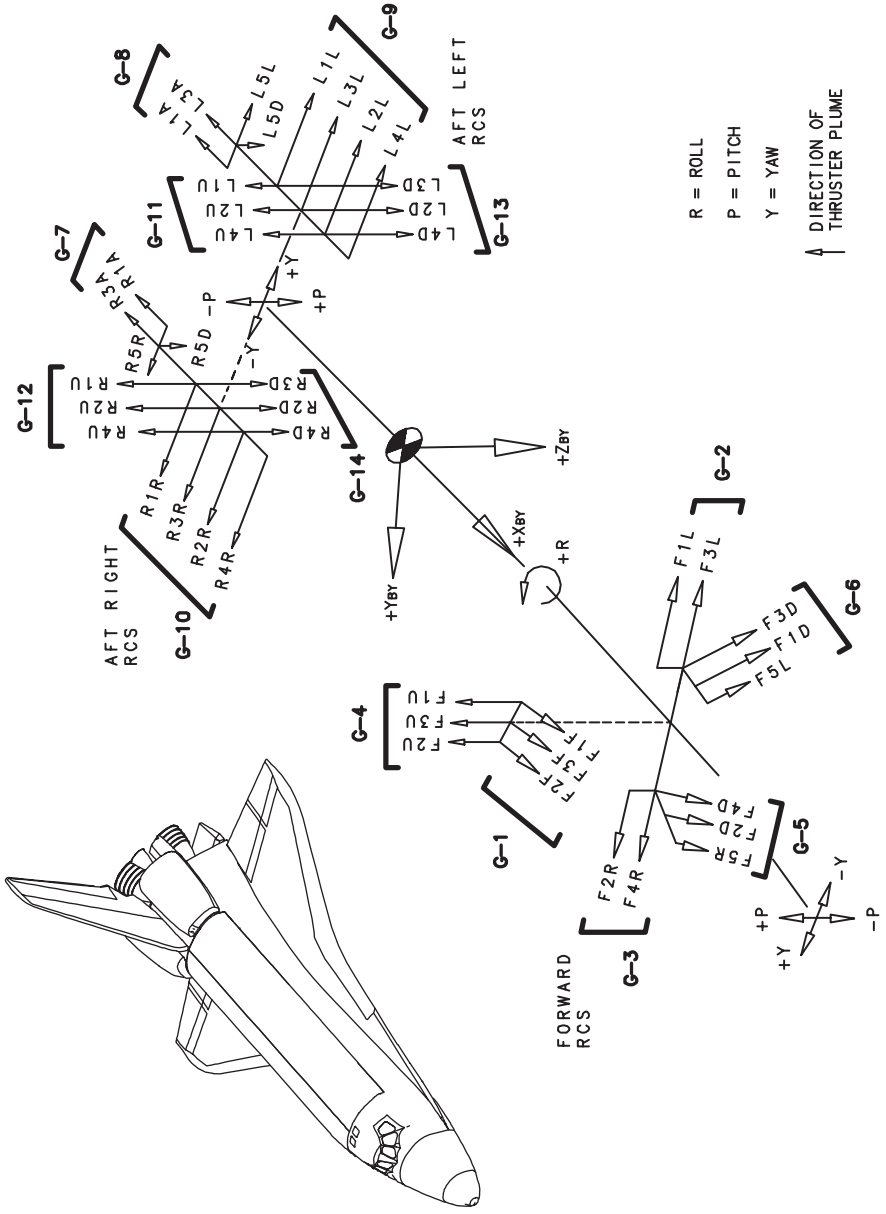

Figure 6-28 Reaction Control System Thruster Locations and Orientations

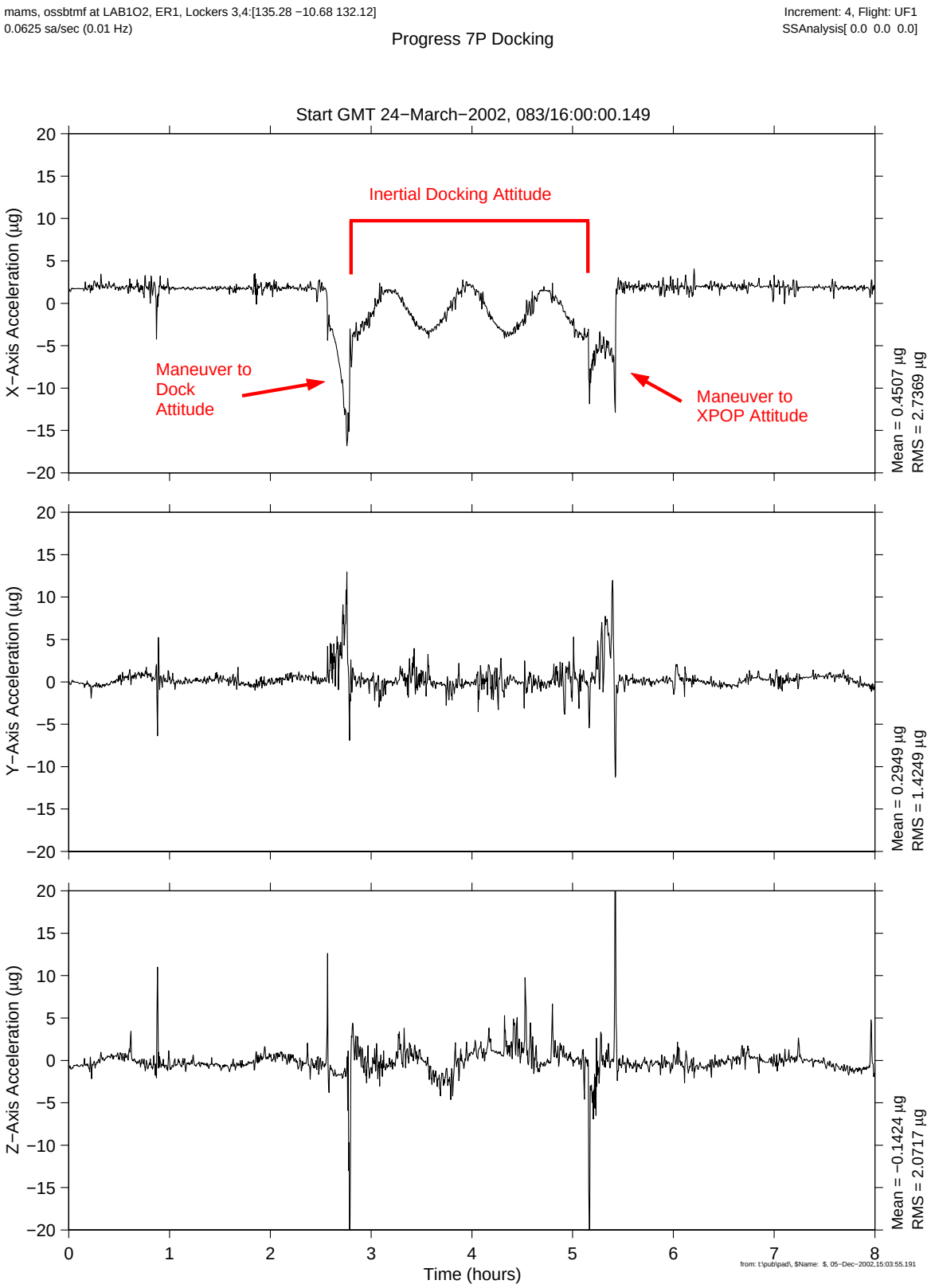

Figure 6-29 Time Series of Progress 7P Docking (OSSBTMF)

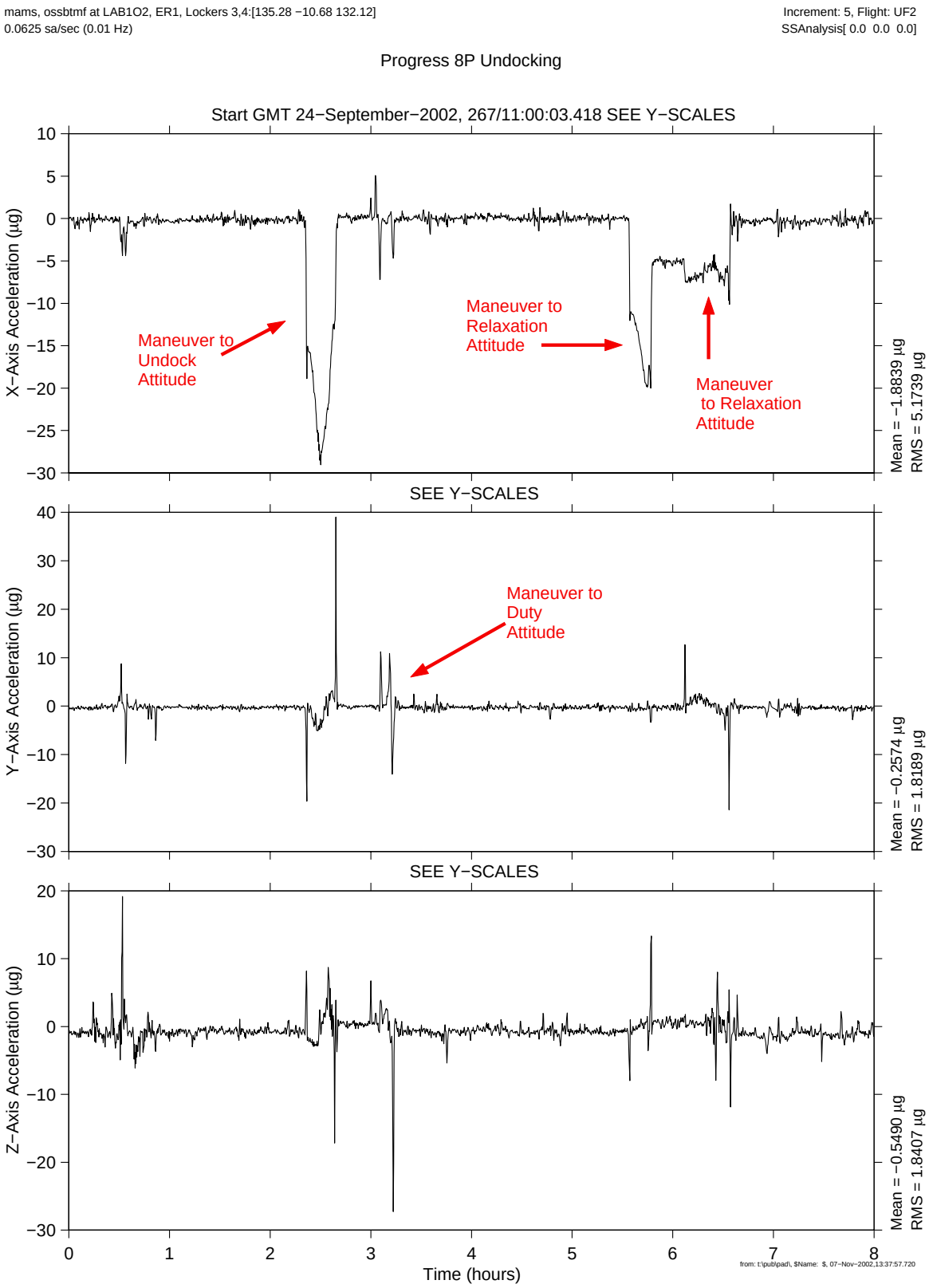

Figure 6-30 Time Series of Progress 8P Undocking (OSSBTMF)

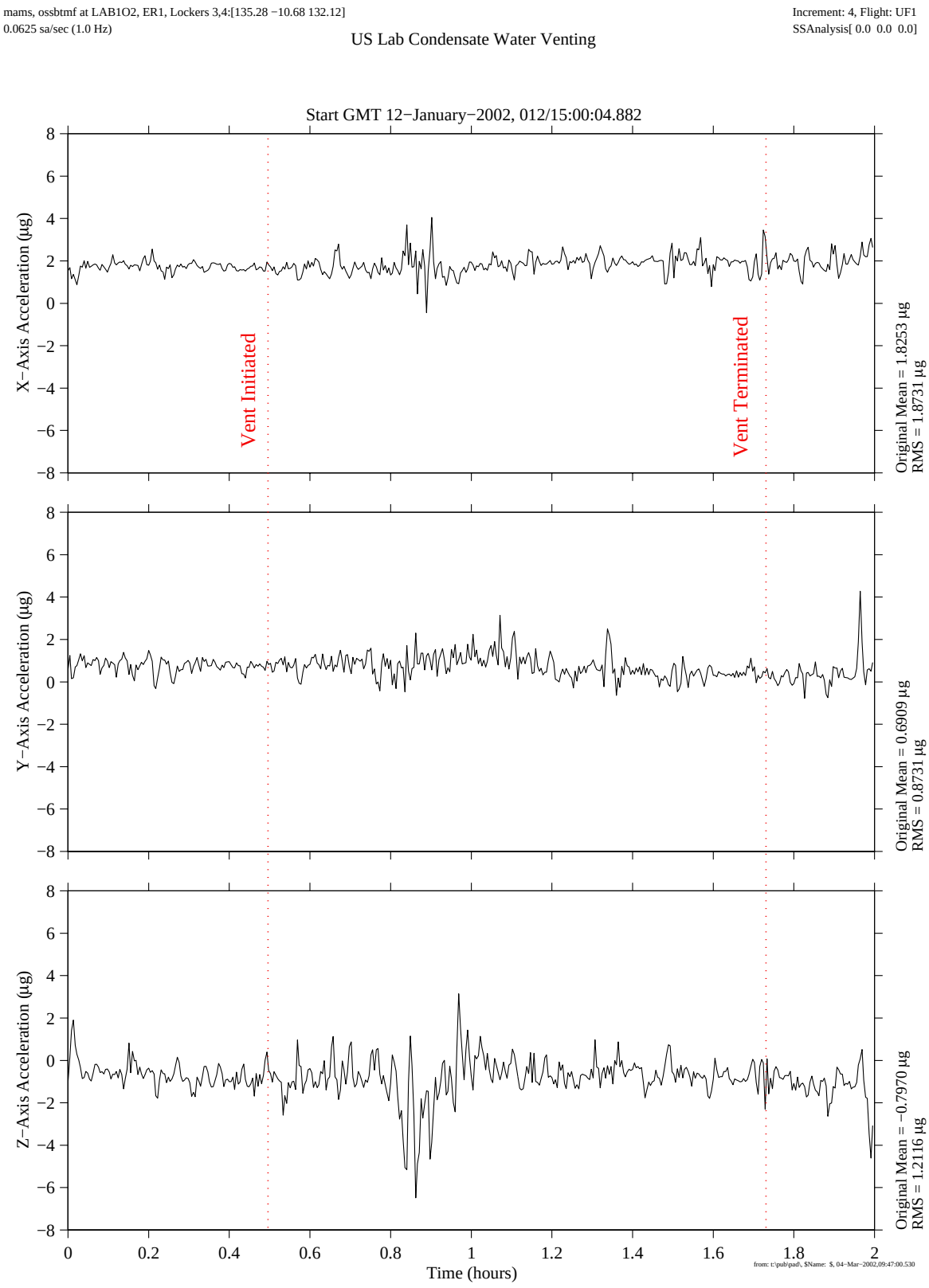

Figure 6-31 Time Series of USLAB Water Dump (OSSBTMF)

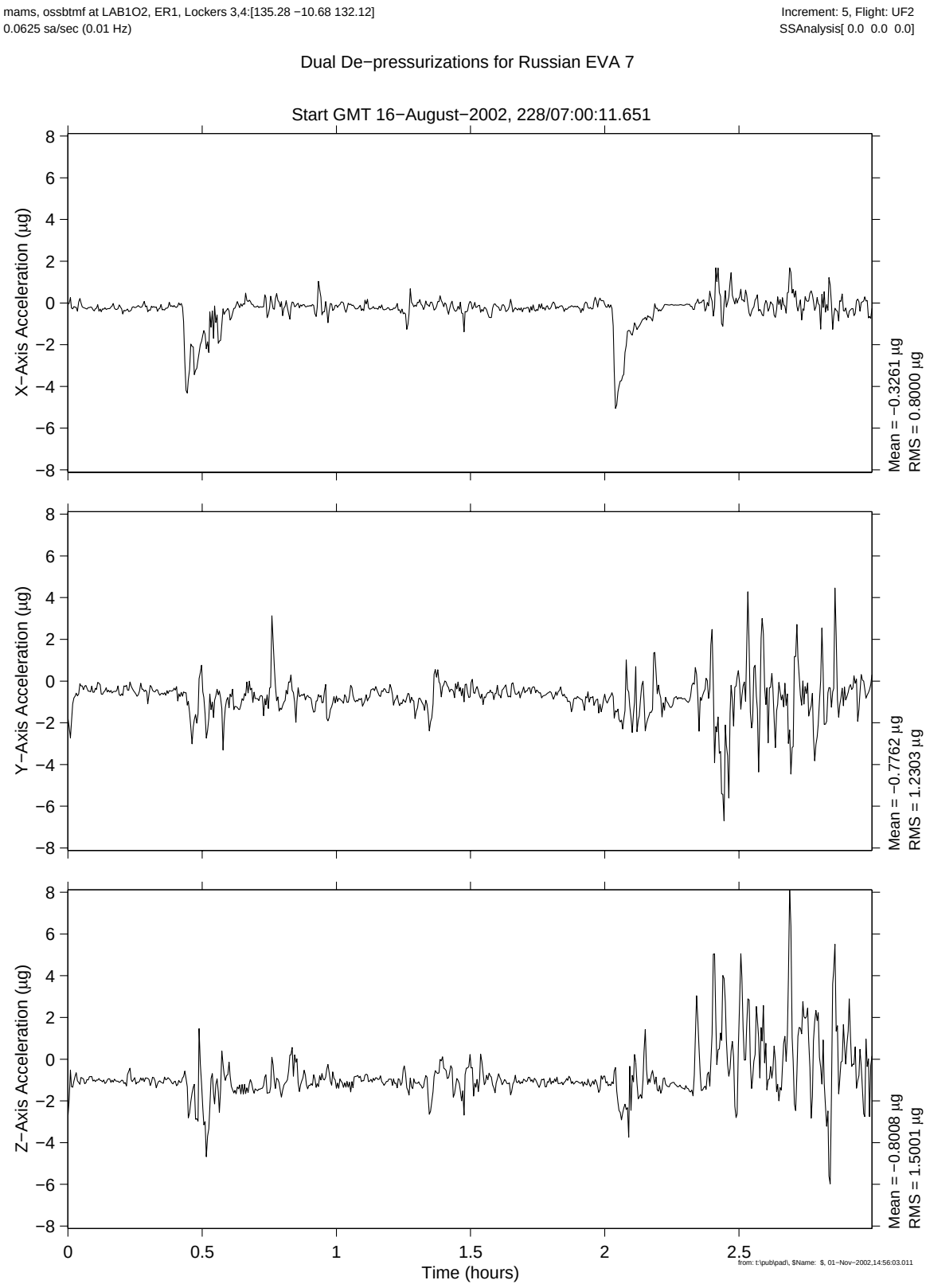

Figure 6-32 Time Series of DC-1 Dual-Depressurization (OSSBTMF)

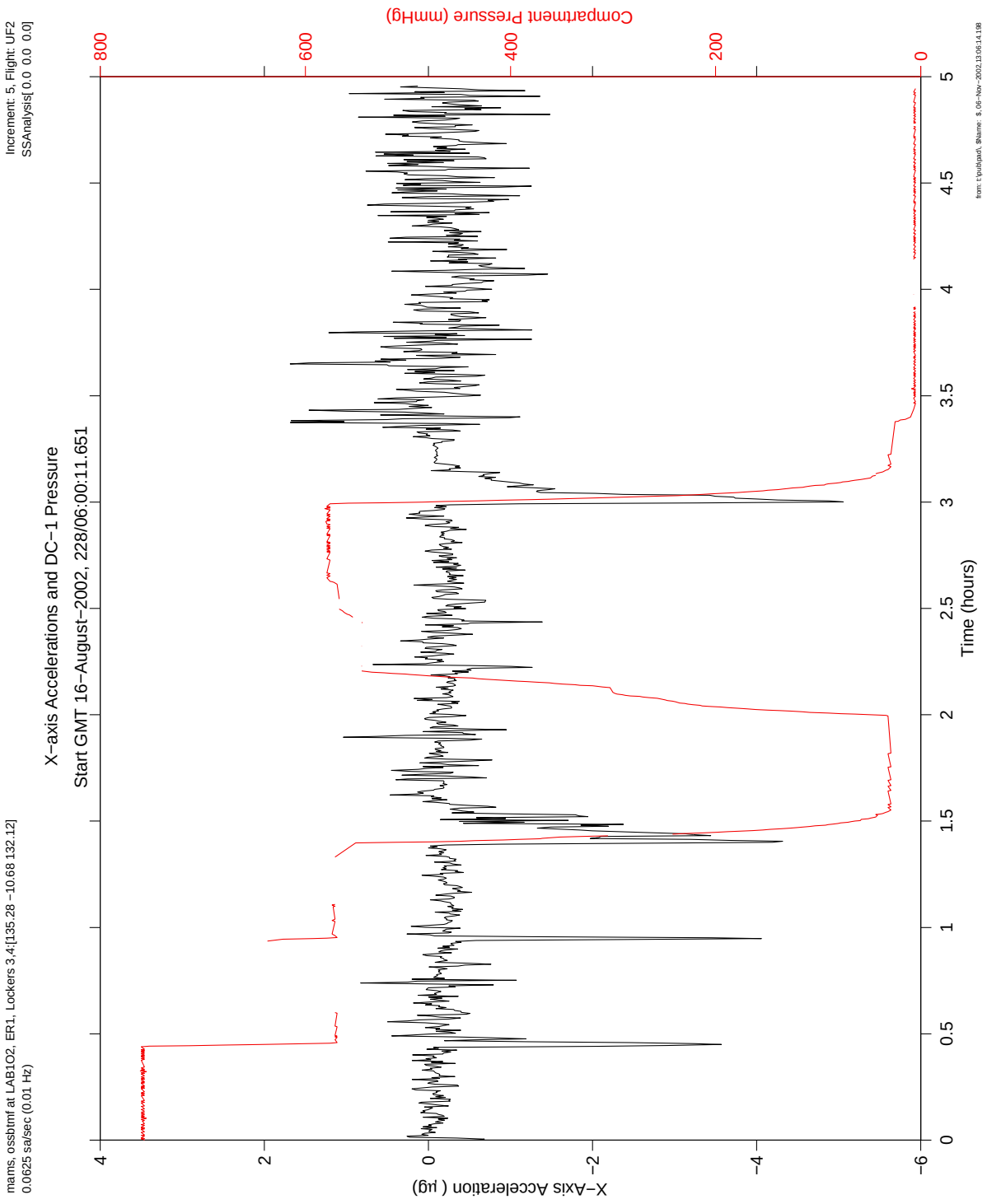

Figure 6-33 Time Series of DC-1 Pressure and X-axis Acceleration (OSSBTMF)

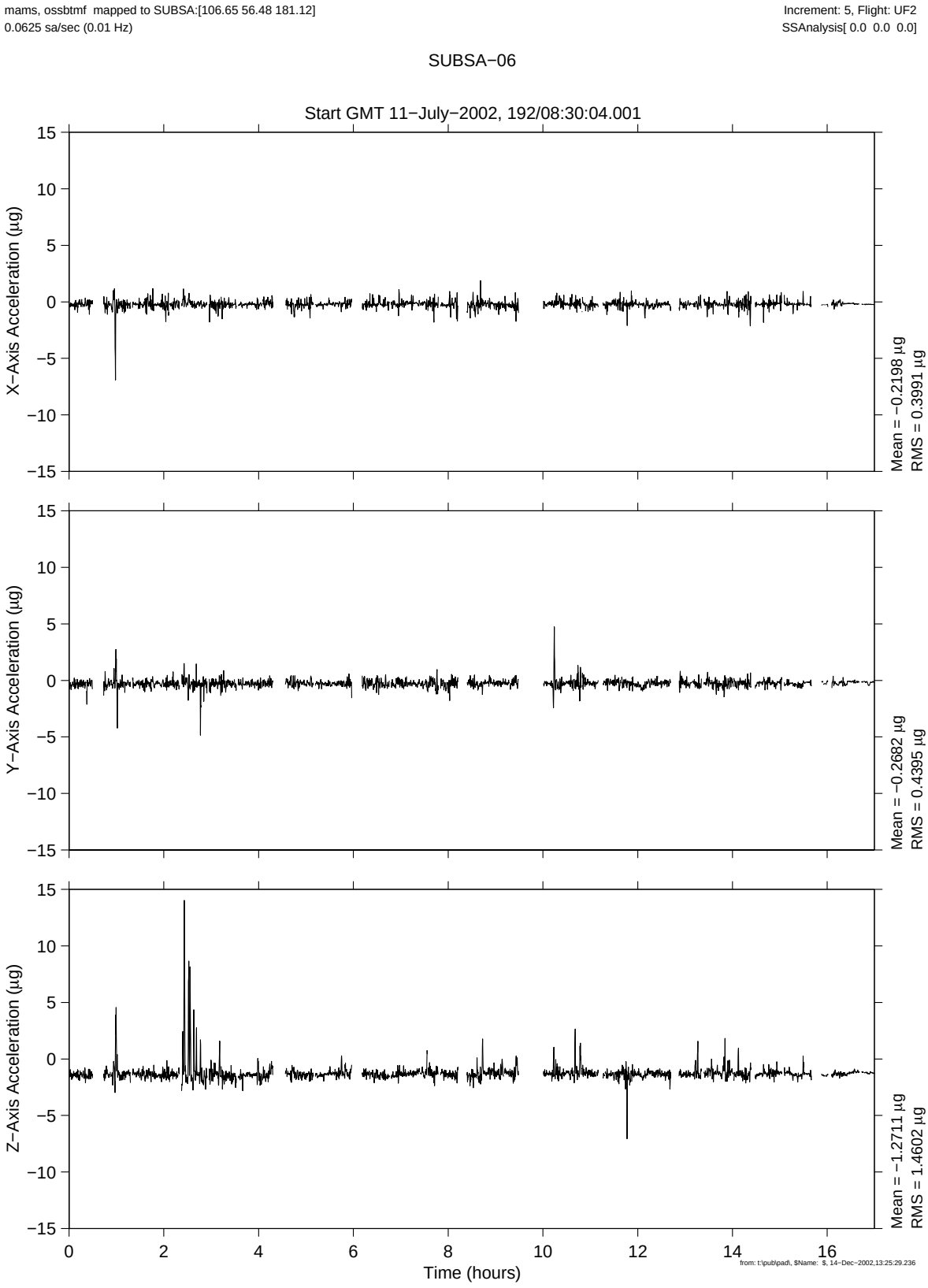

Figure 6-34 Time Series of SUBSA-06 Sample Run (OSSBTMF)

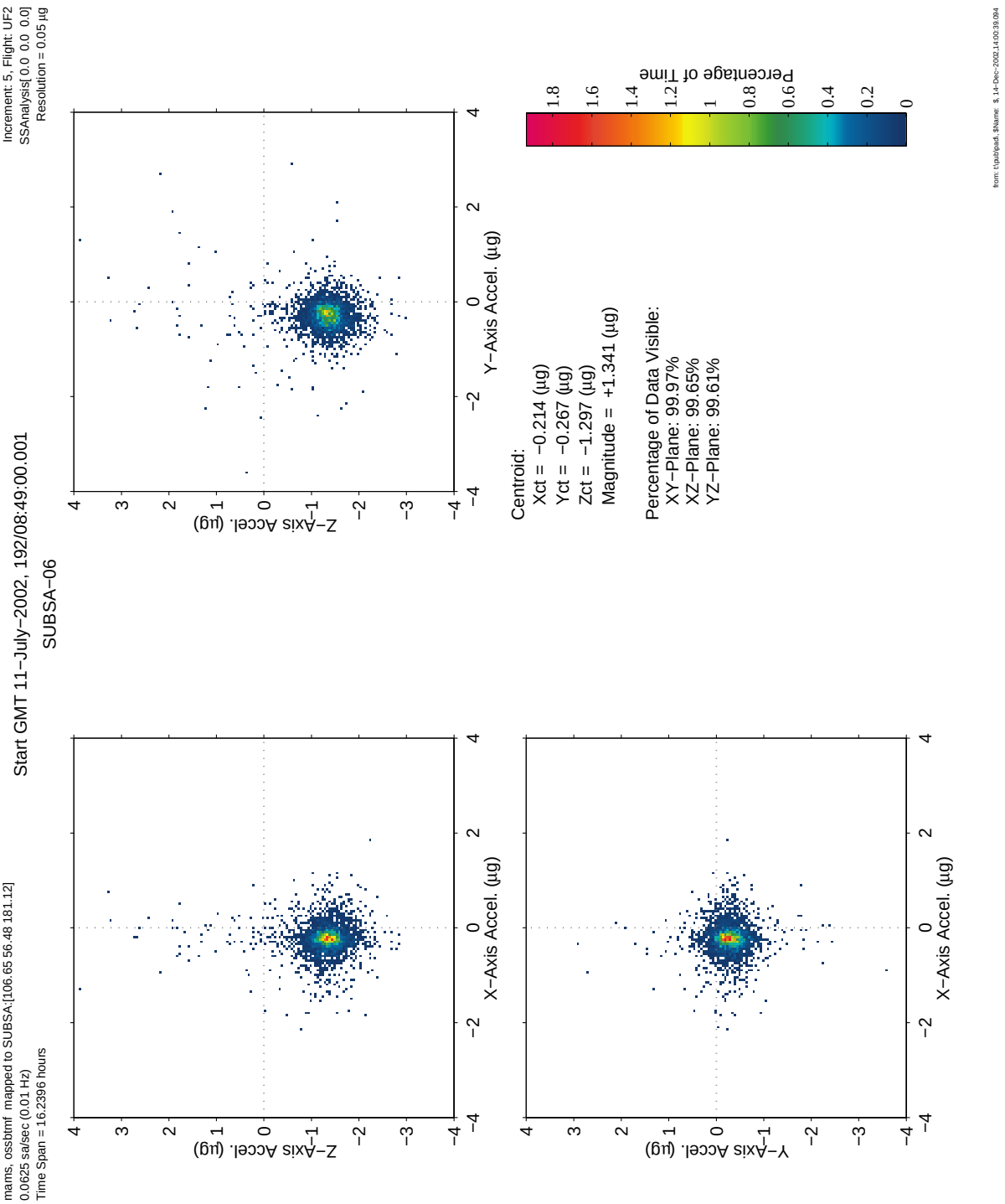

Figure 6-35 QTH of SUBSA-06 Sample Run (OSSBTMF)

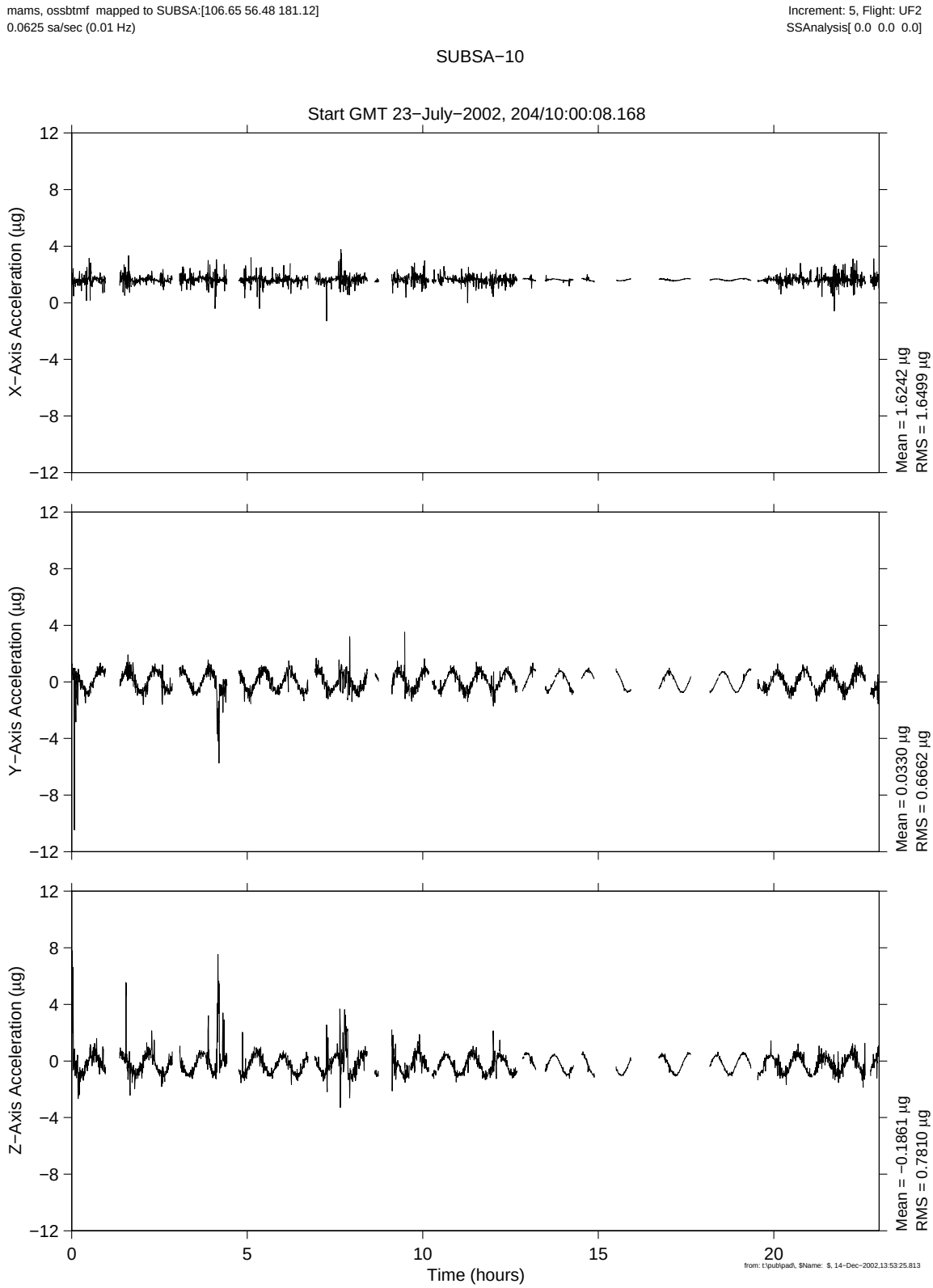

Figure 6-36 Time Series of SUBSA-10 Sample Run (OSSBTMF)

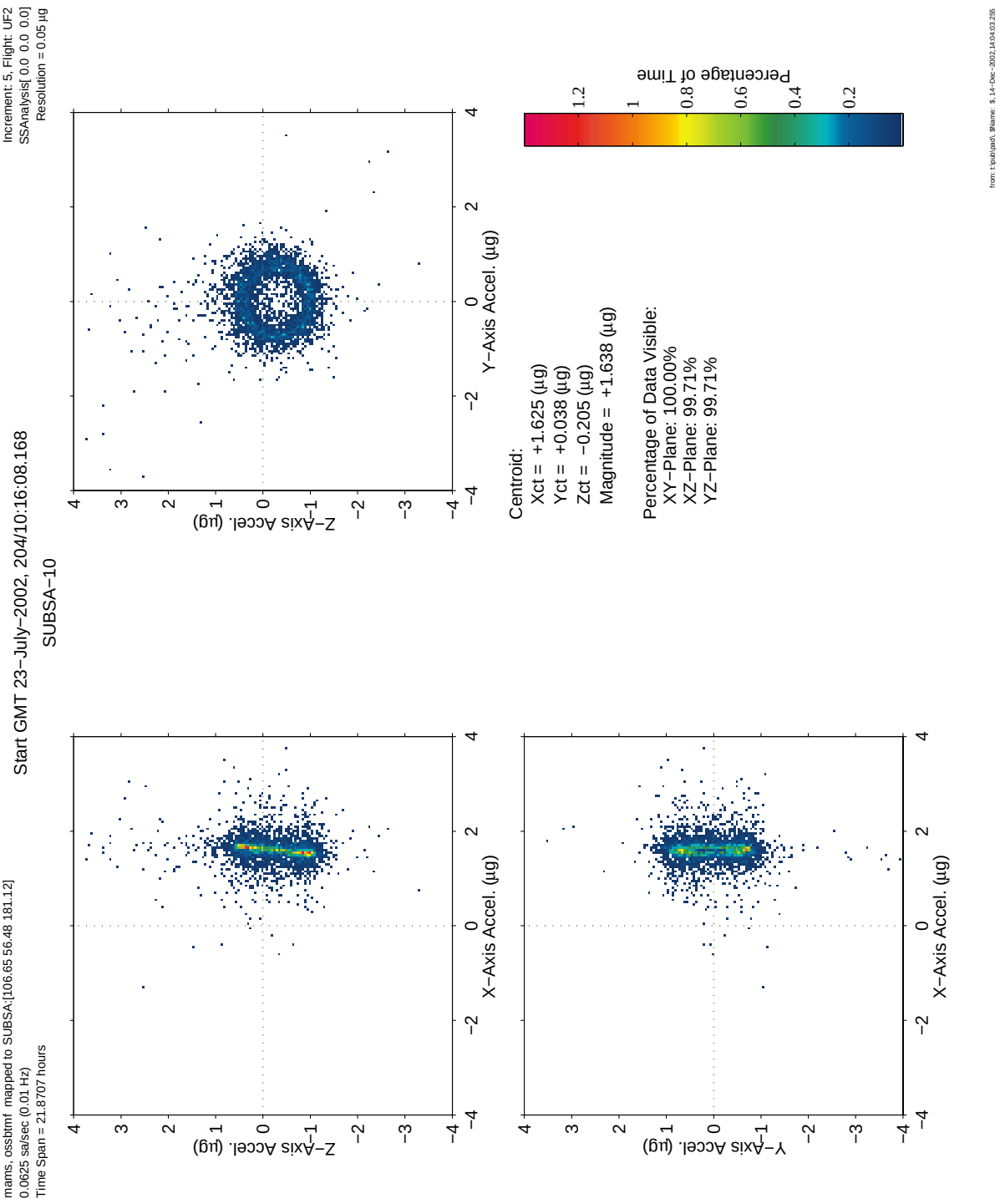

Figure 6-37 QTH of SUBSA-10 Sample Run (OSSBTMF)

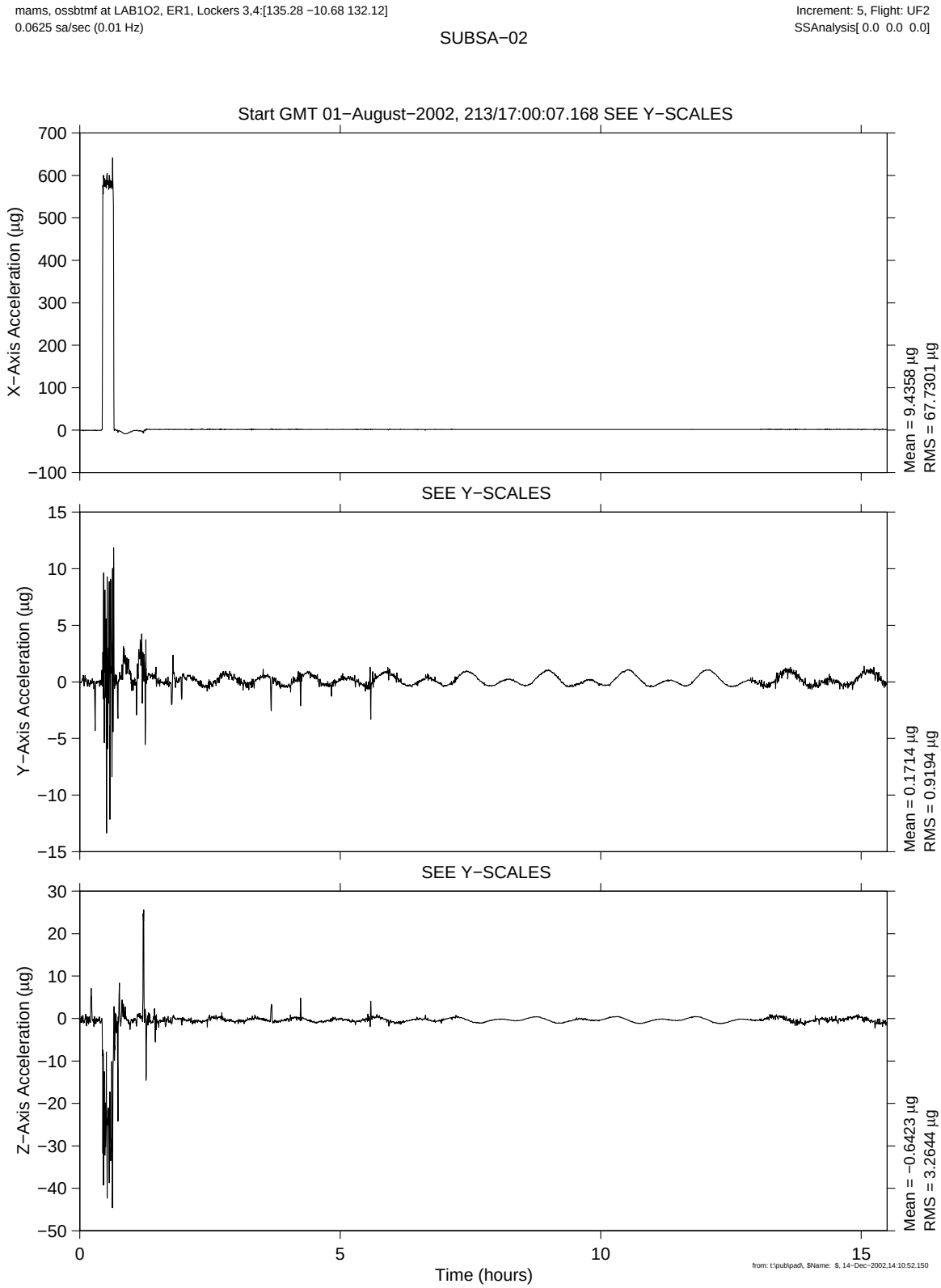

Figure 6-38 Time Series of SUBSA-02 Sample Run (OSSBTMF)

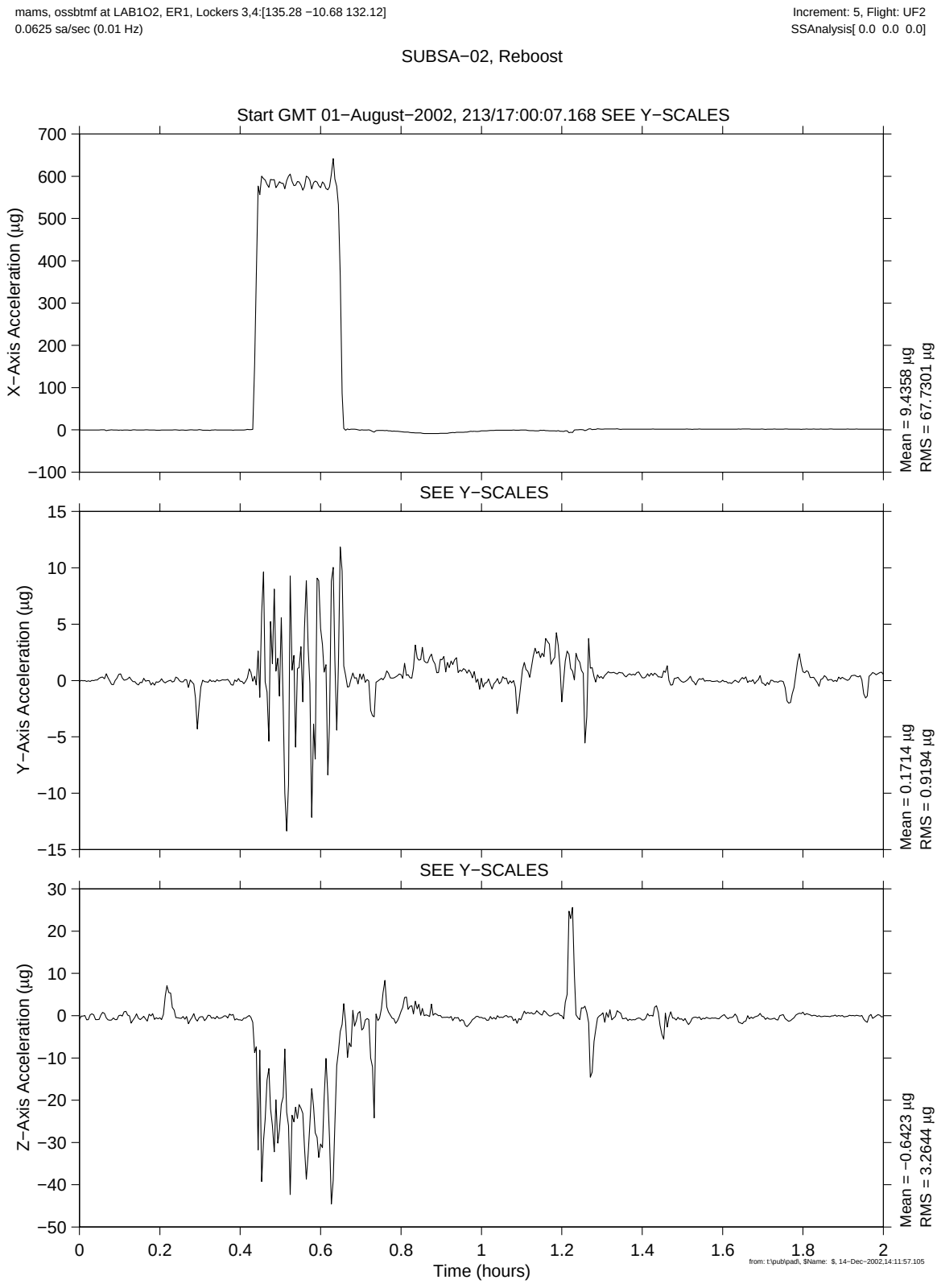

Figure 6-39 Time Series of Reboost during SUBSA-02 Sample Run (OSSBTMF)

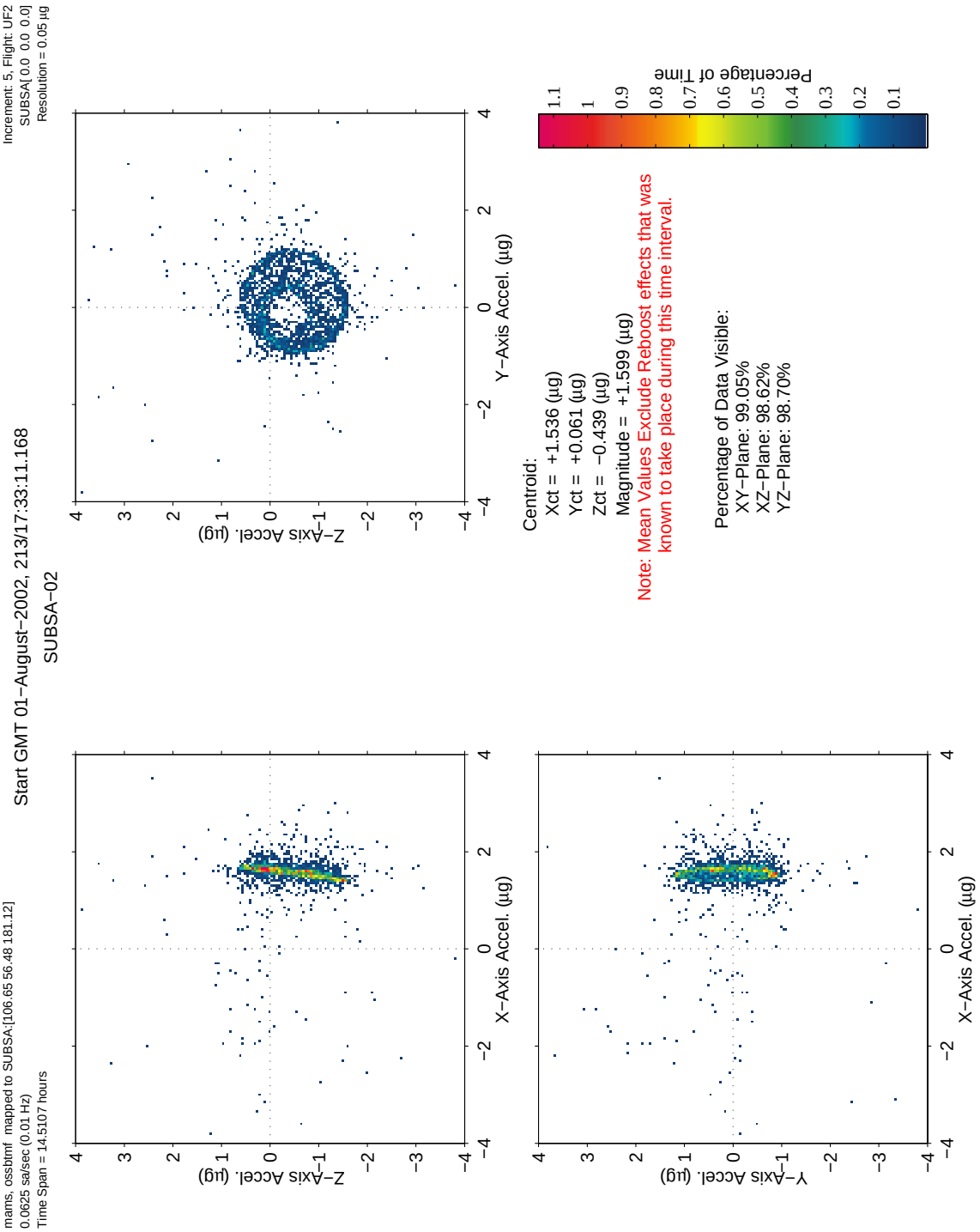

Figure 6-40 QTH of SUBSA-02 Sample Run (OSSBTMF)

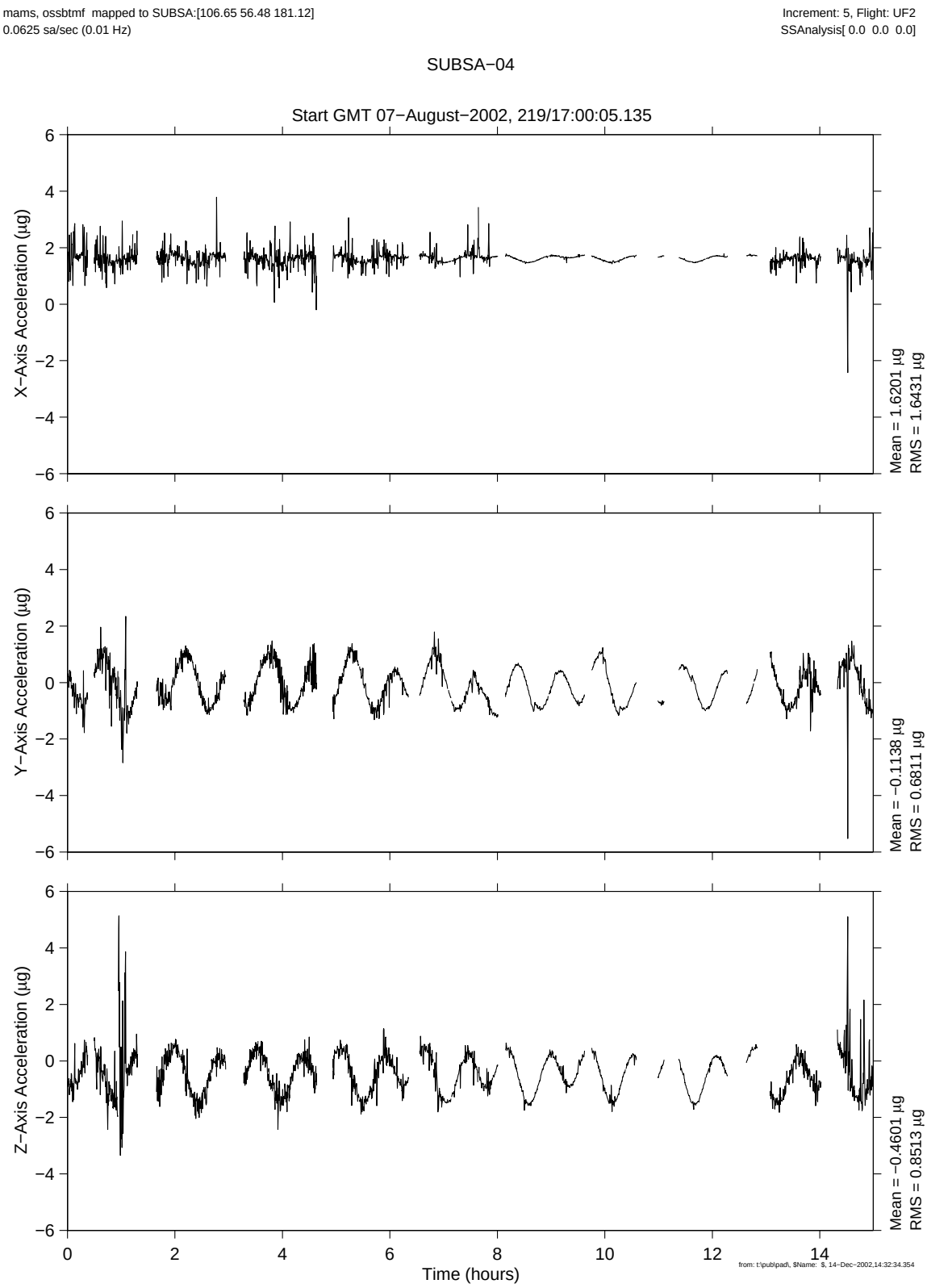

Figure 6-41 Time Series of SUBSA-04 Sample Run (OSSBTMF)

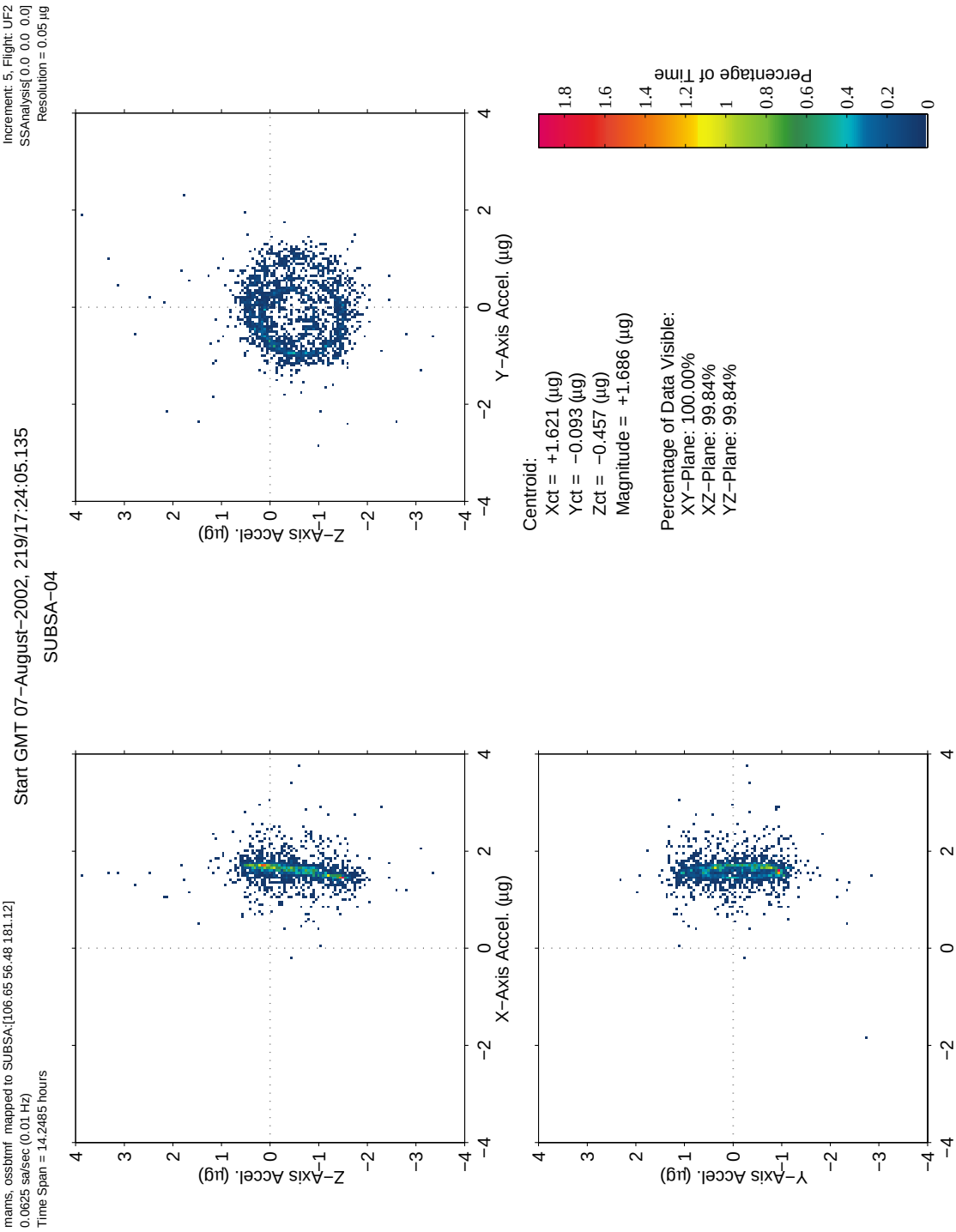

Figure 6-42 QTH of SUBSA-04 Sample Run (OSSBTMF)

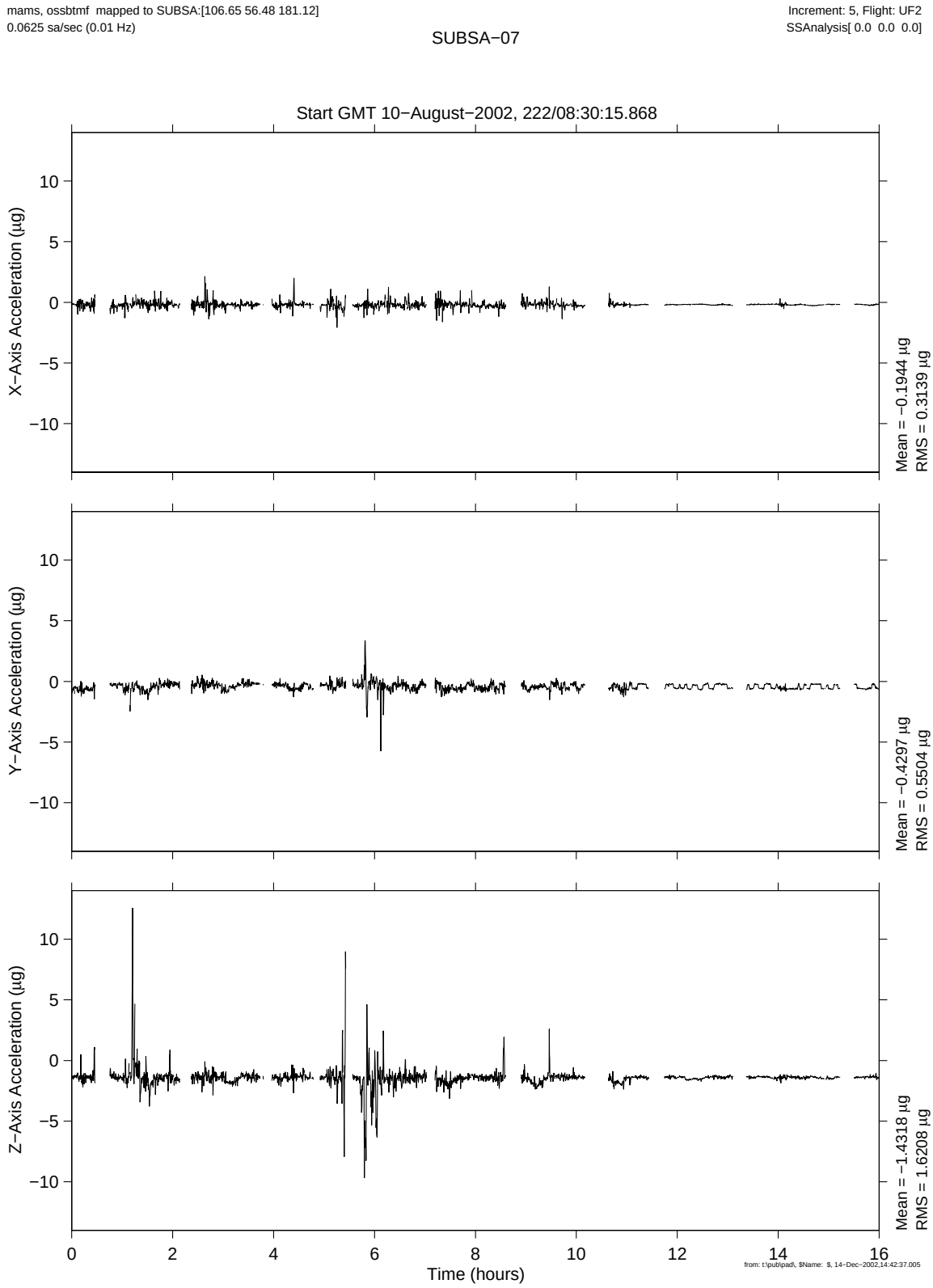

Figure 6-43 Time Series of SUBSA-07 Sample Run (OSSBTMF)

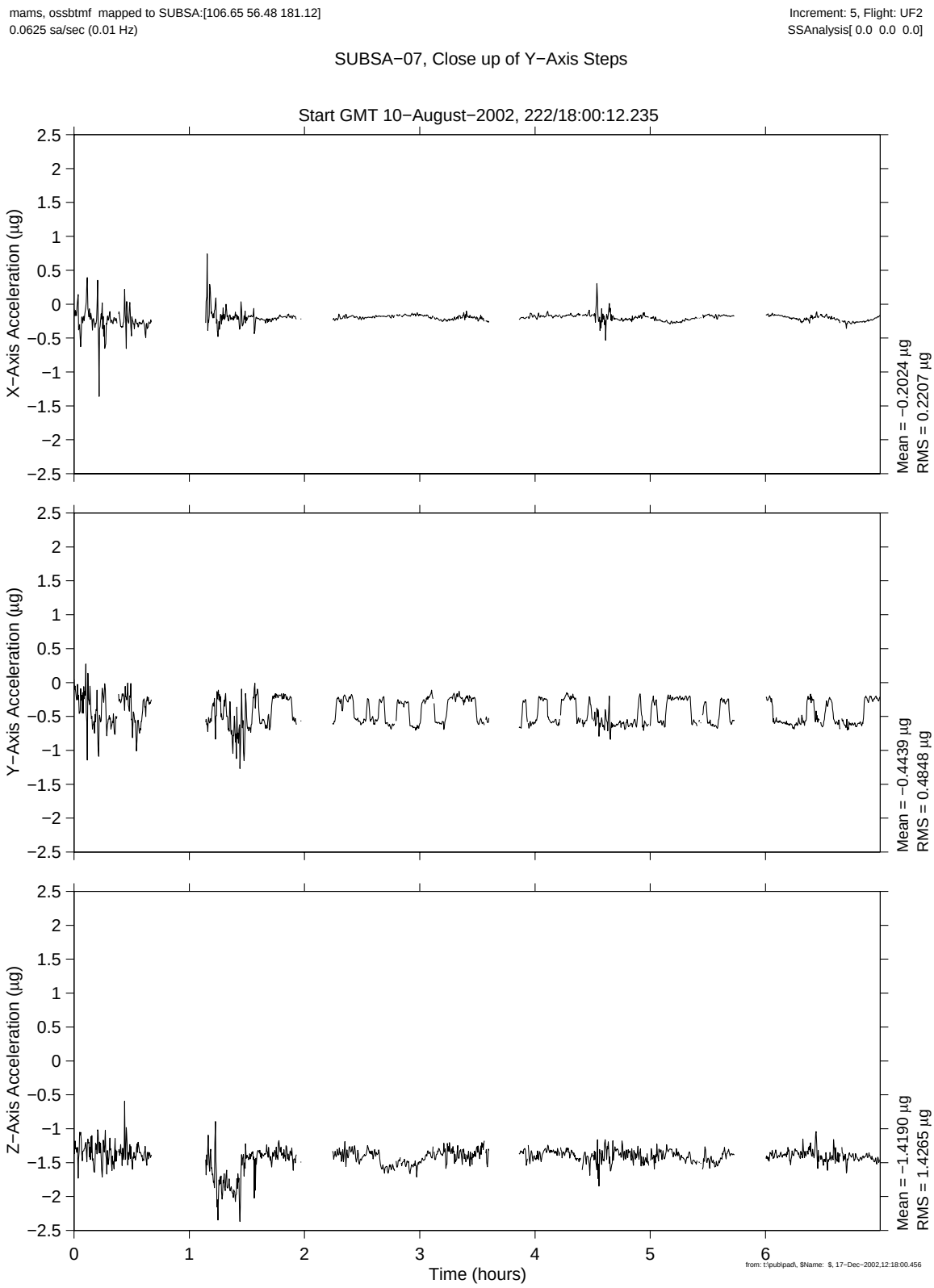

Figure 6-44 Time Series of SUBSA-07, Zoom on Y_A-Axis Steps (OSSBTMF)

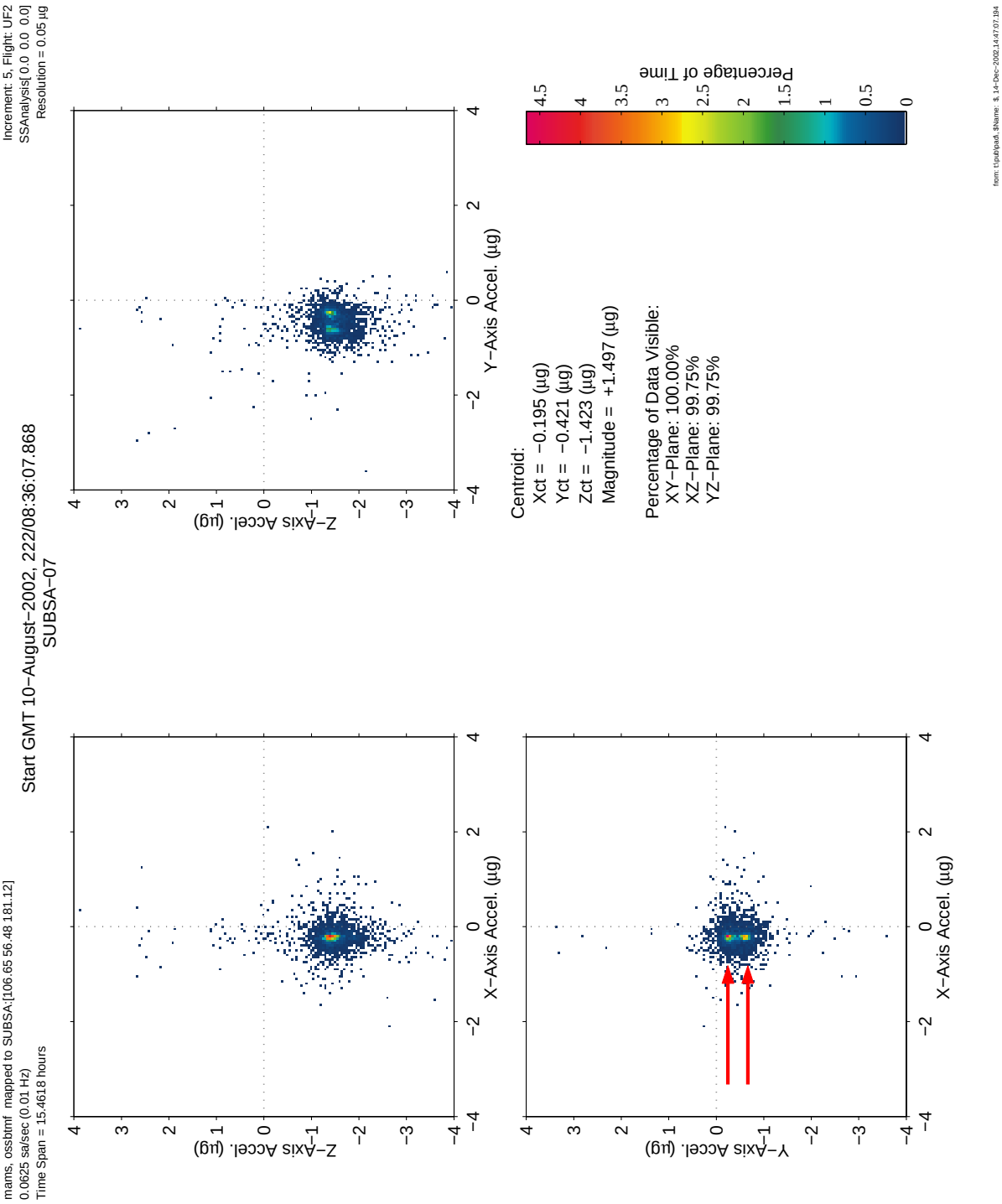

Figure 6-45 QTH of SUBSA-07 Sample Run (OSSBTMF)

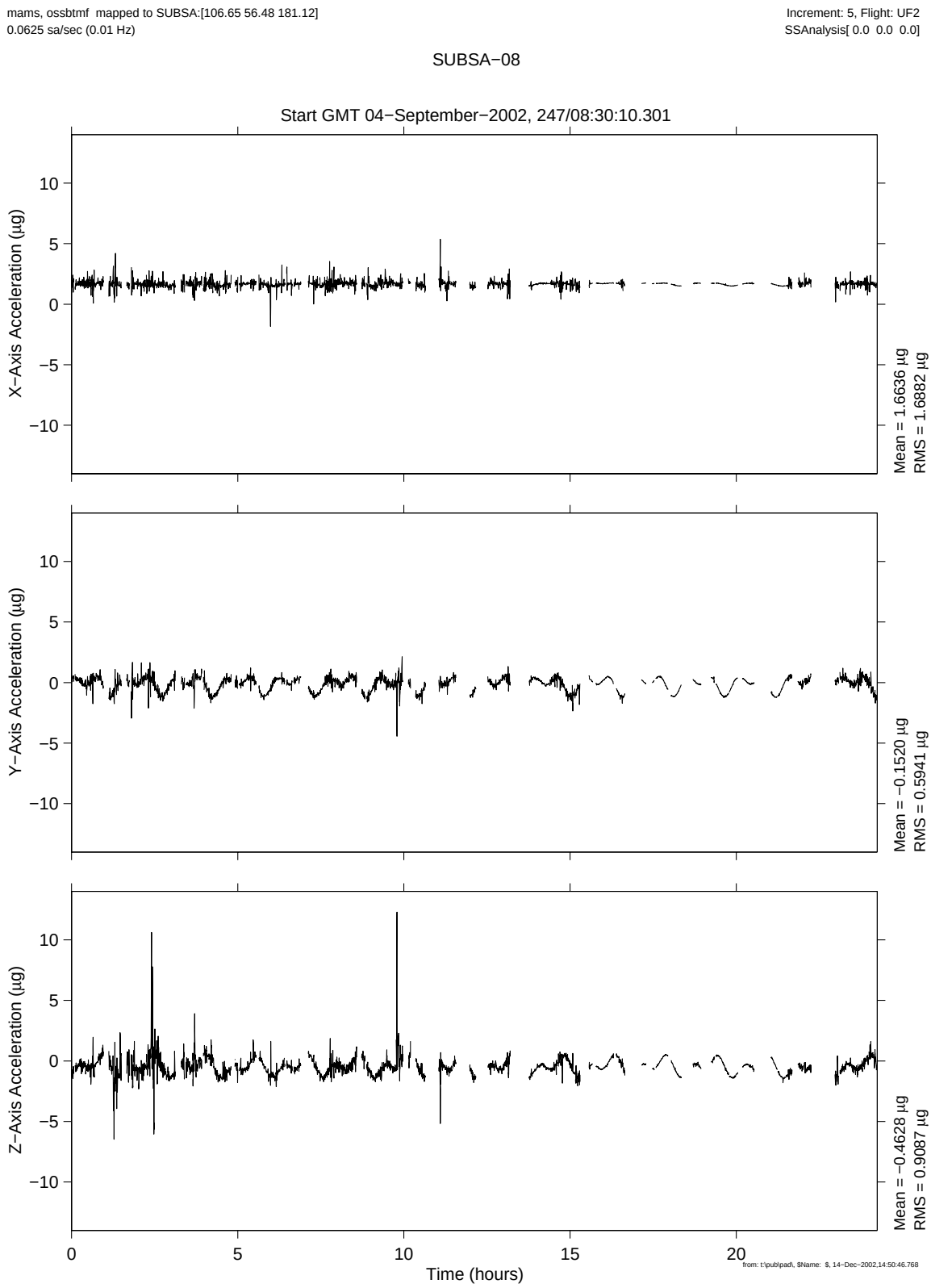

Figure 6-46 Time Series of SUBSA-08 Sample Run (OSSBTMF)

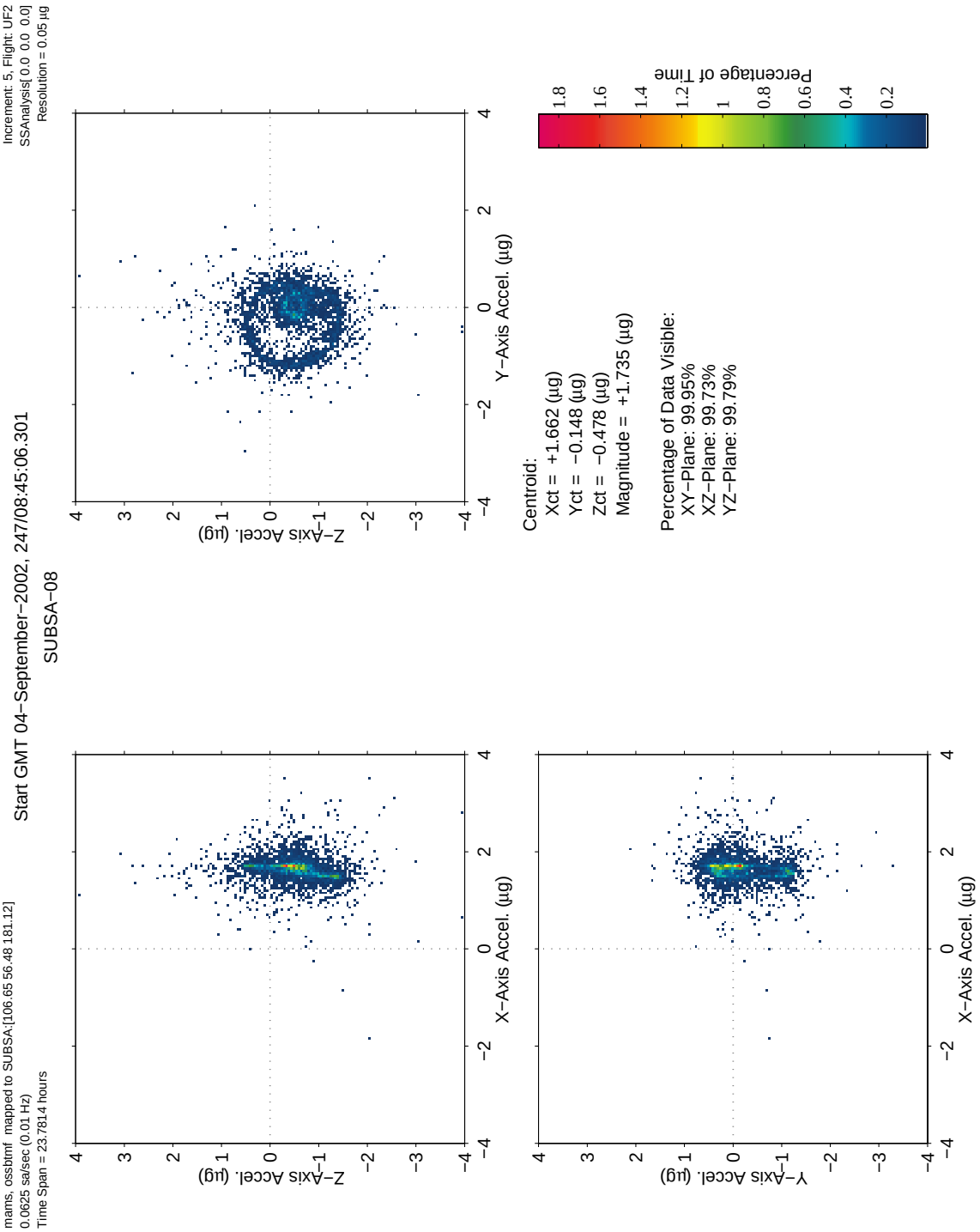

Figure 6-47 QTH of SUBSA-08 Sample Run (OSSBTMF)

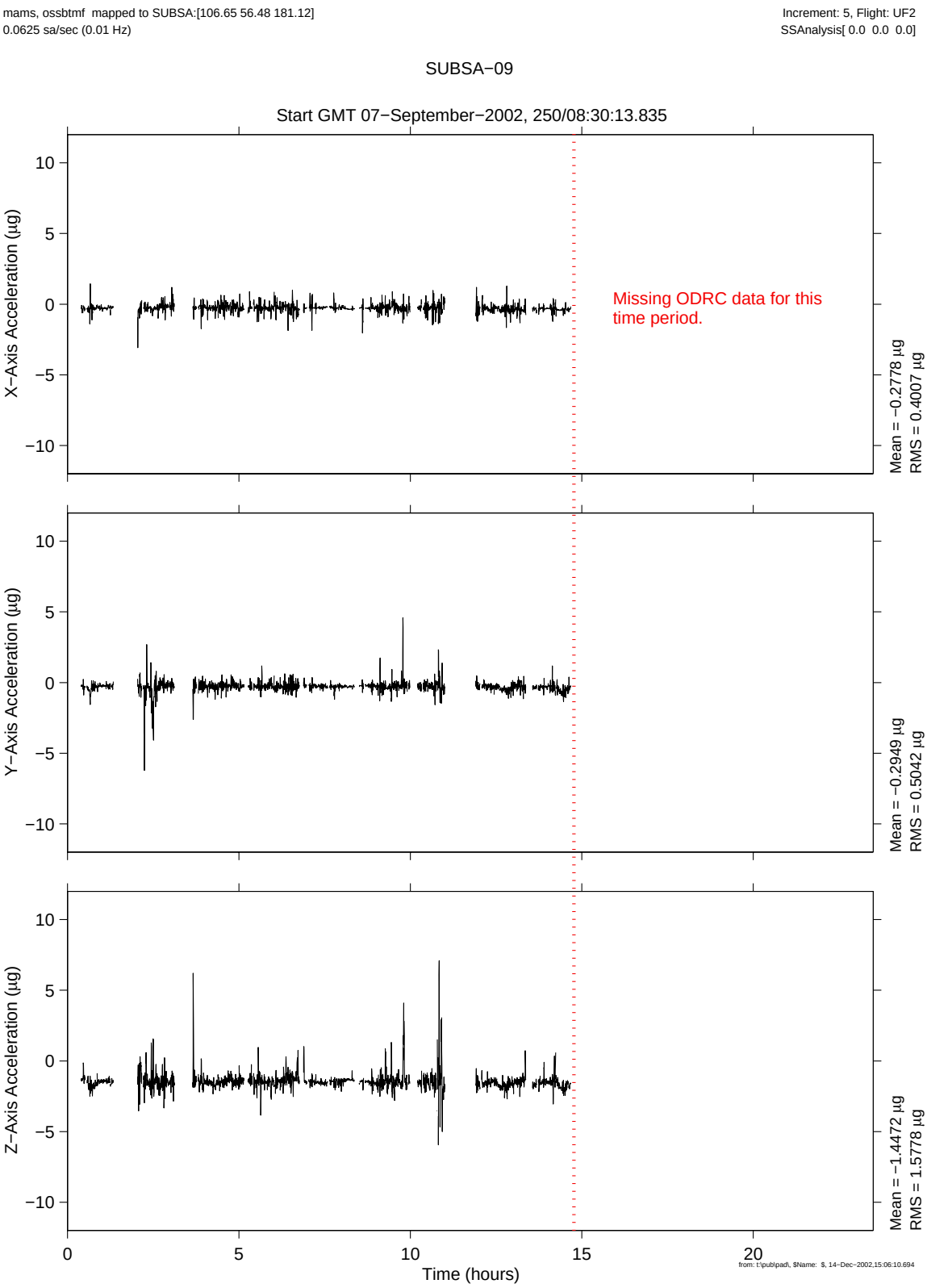

Figure 6-48 Time Series of SUBSA-09 Sample Run (OSSBTMF)

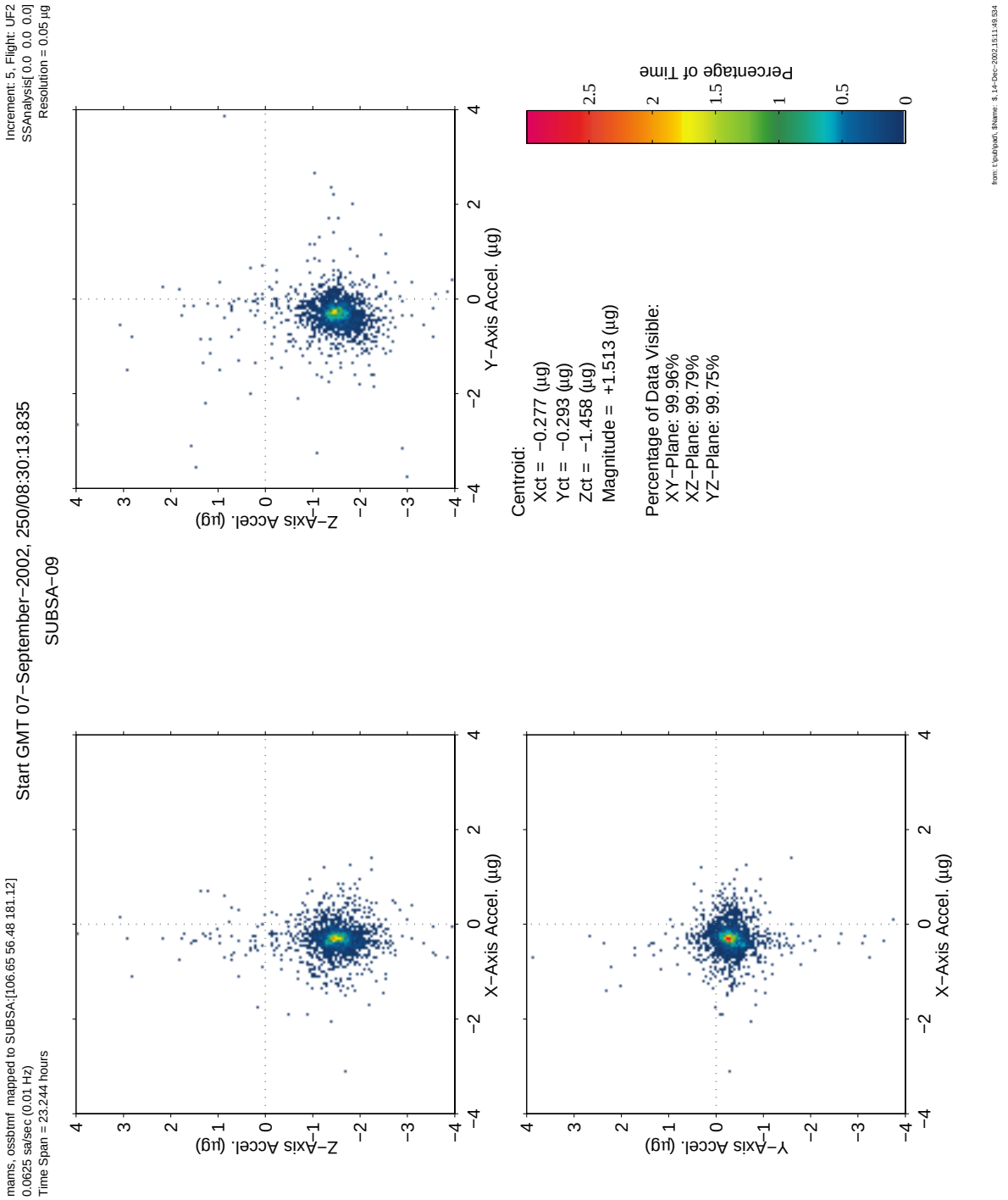

Figure 6-49 QTH of SUBSA-09 Sample Run (OSSBTMF)

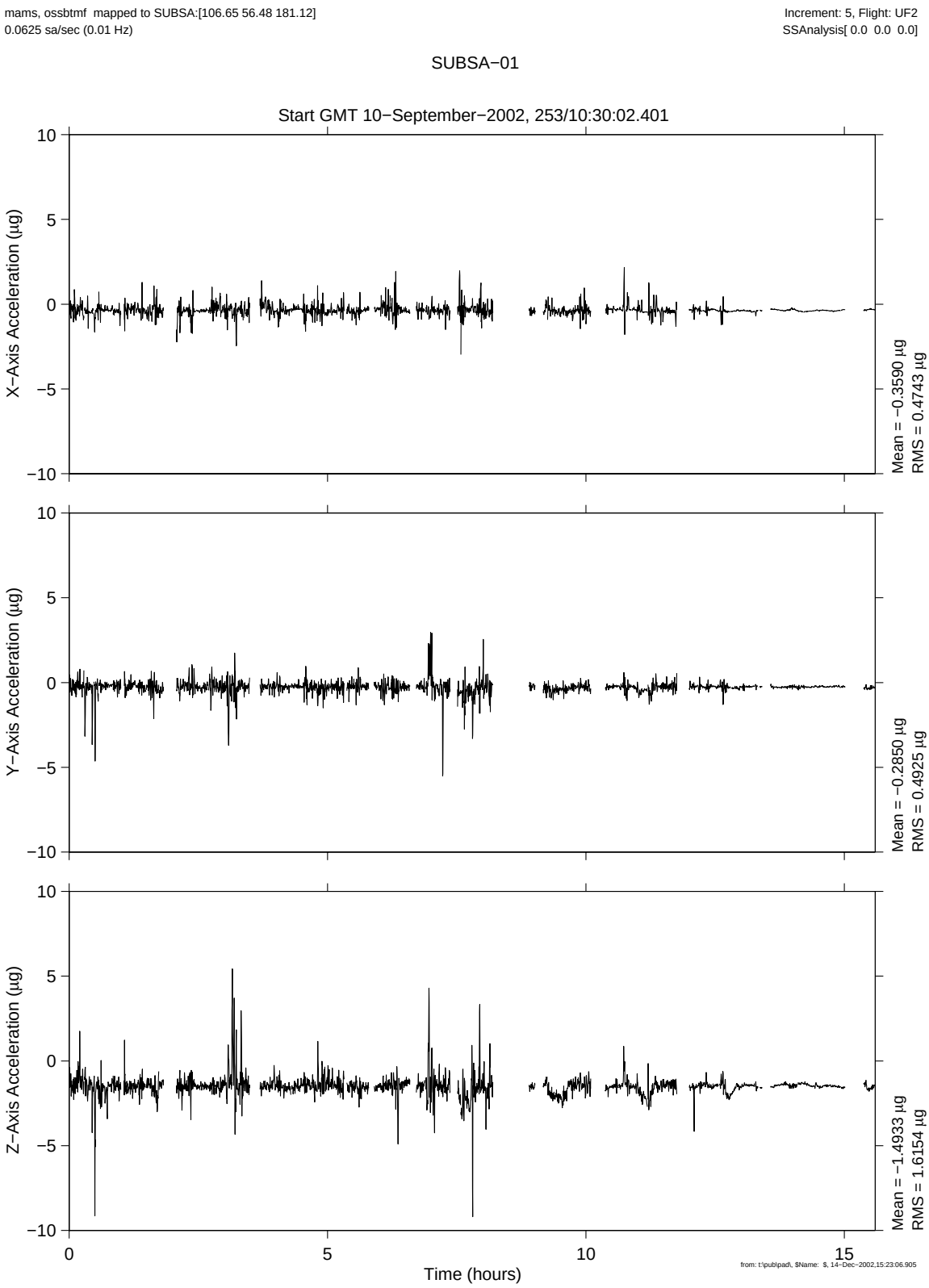

Figure 6-50 Time Series of SUBSA-01 Sample Run (OSSBTMF)

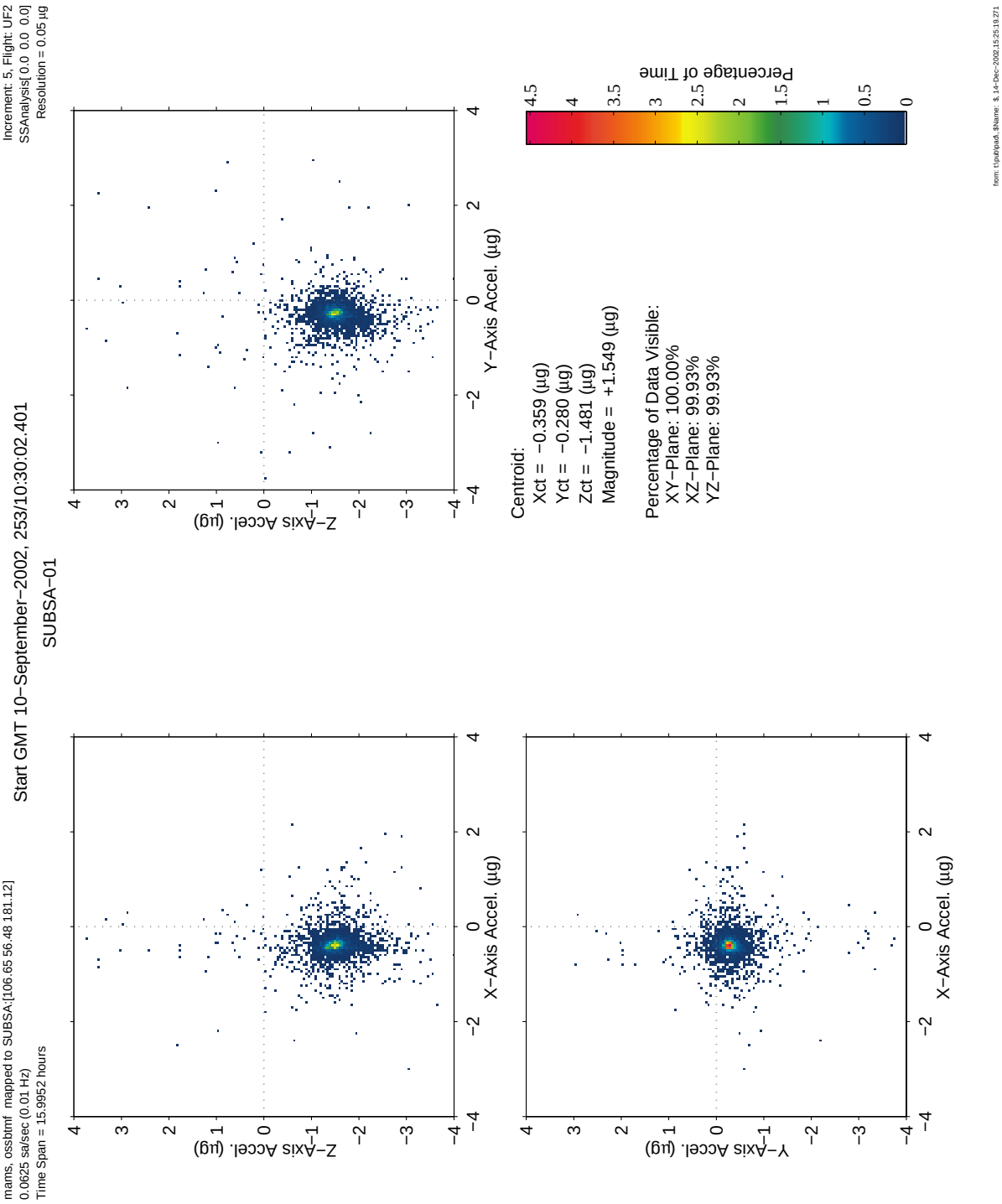

Figure 6-51 QTH of SUBSA-01 Sample Run (OSSBTMF)

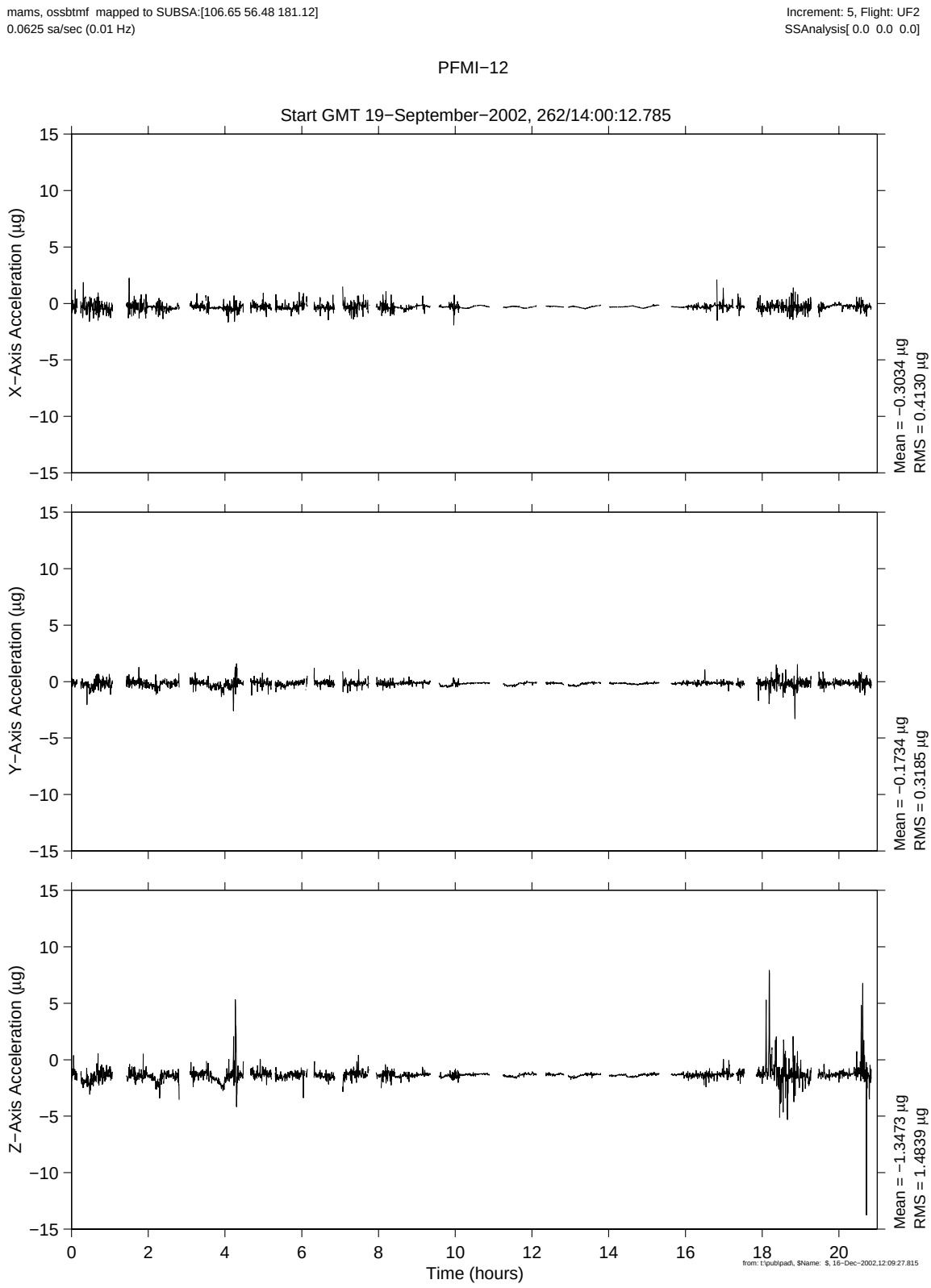

Figure 6-52 Time Series of PFMI-12 Sample Run (OSSBTMF)

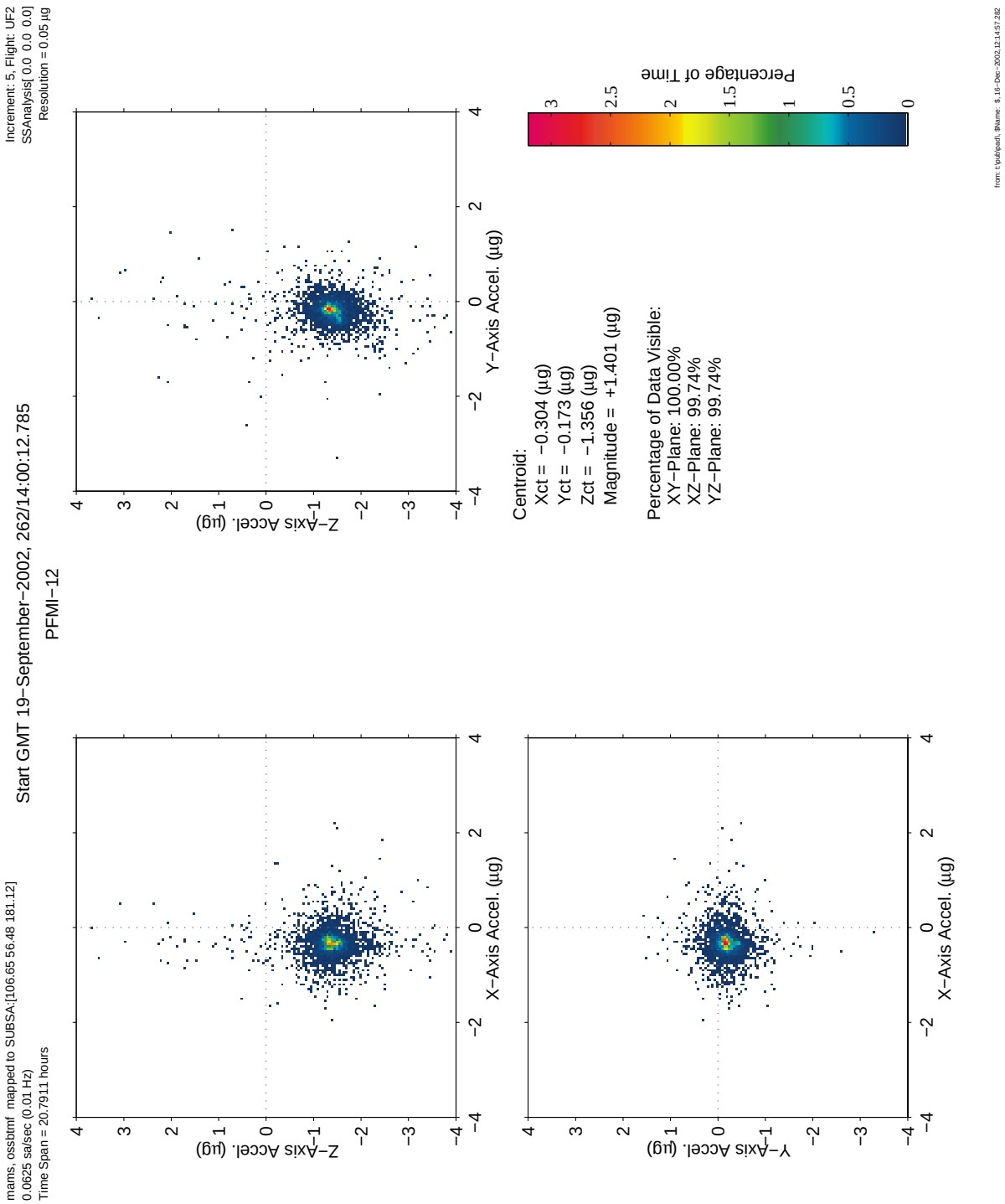

Figure 6-53 QTH of PFMI-12 Sample Run (OSSBTMF)

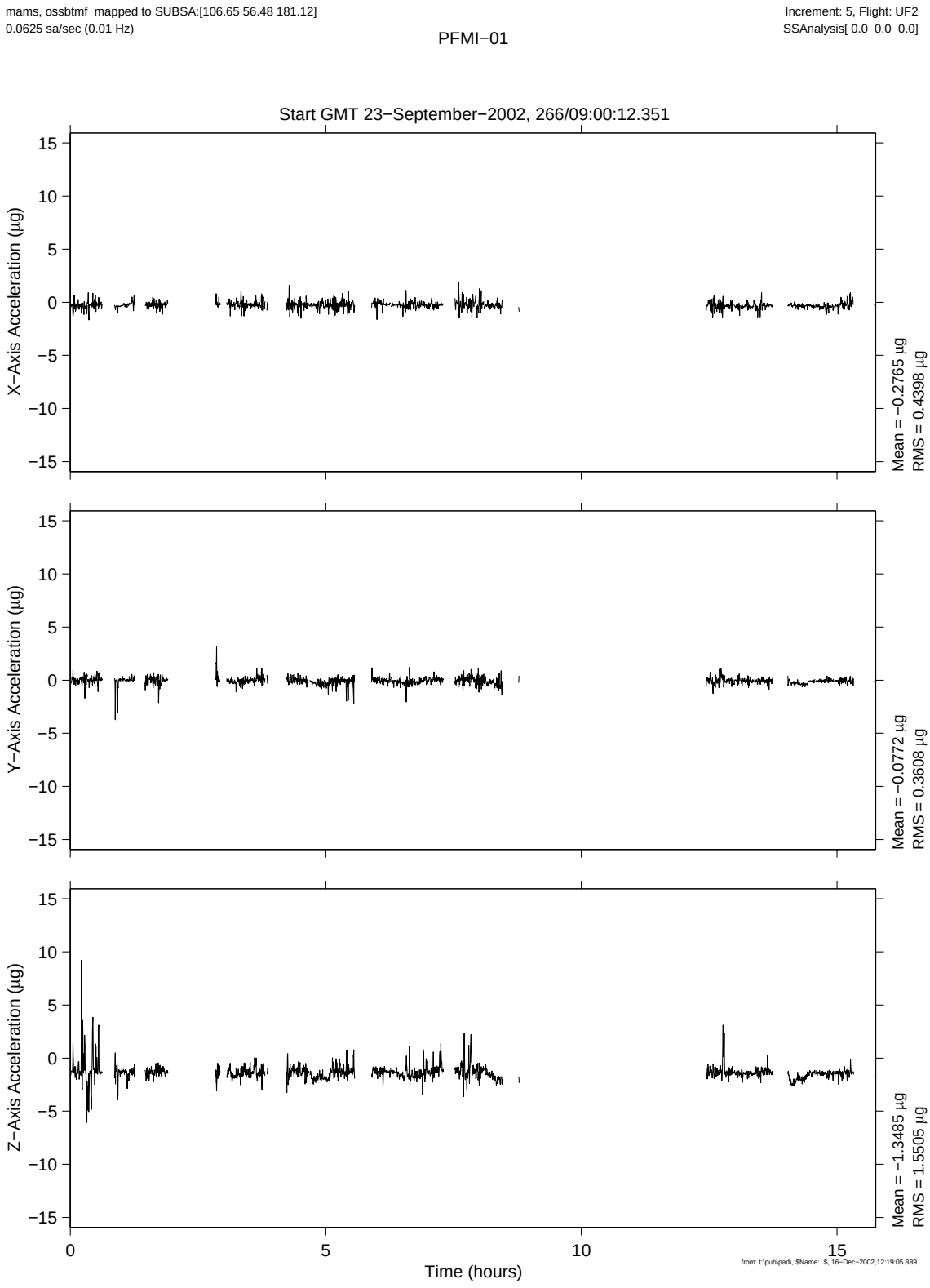

Figure 6-54 Time Series of PFMI-01 Sample Run (OSSBTMF)

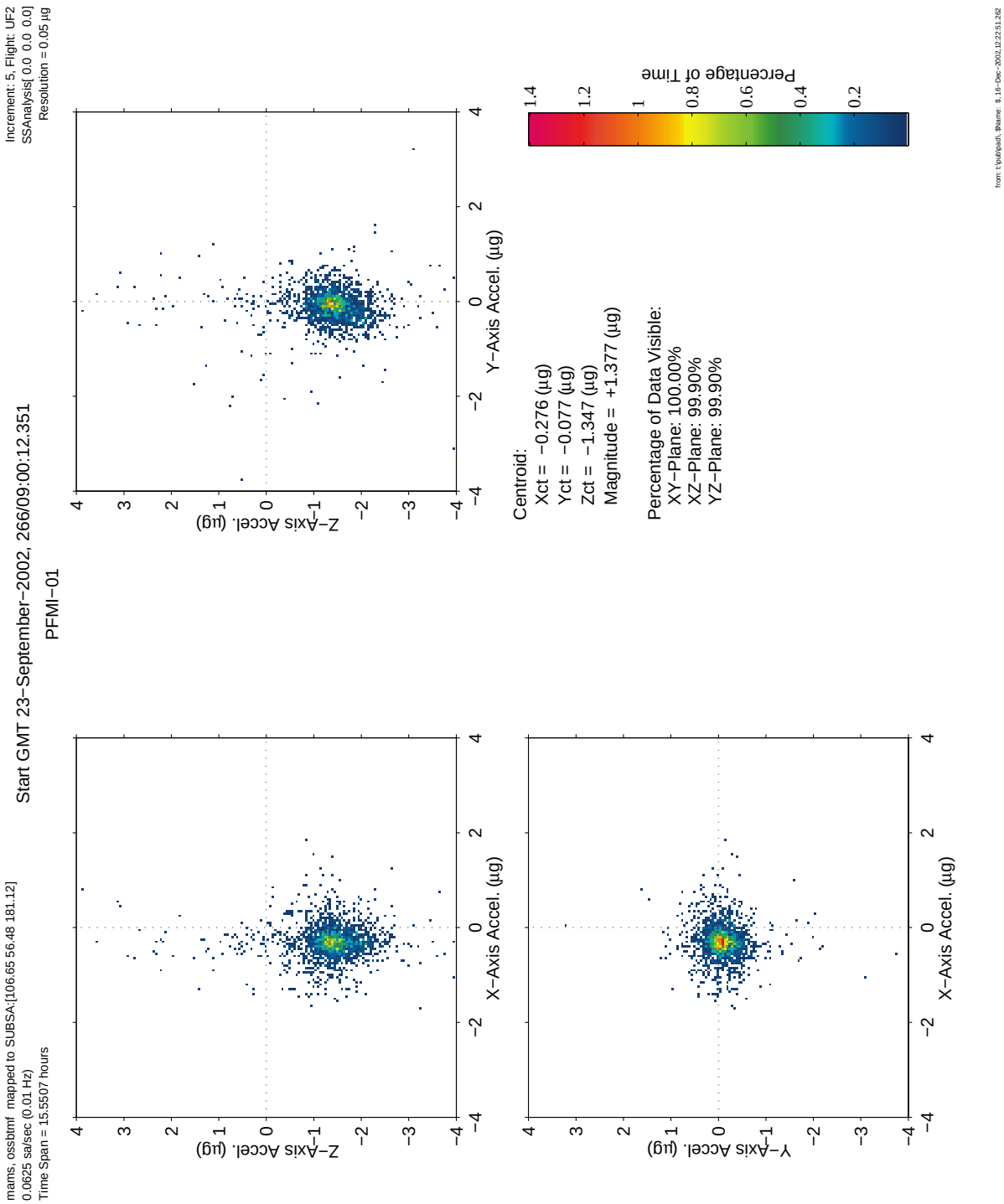

Figure 6-55 QTH of PFMI-01 Sample Run (OSSBTMF)

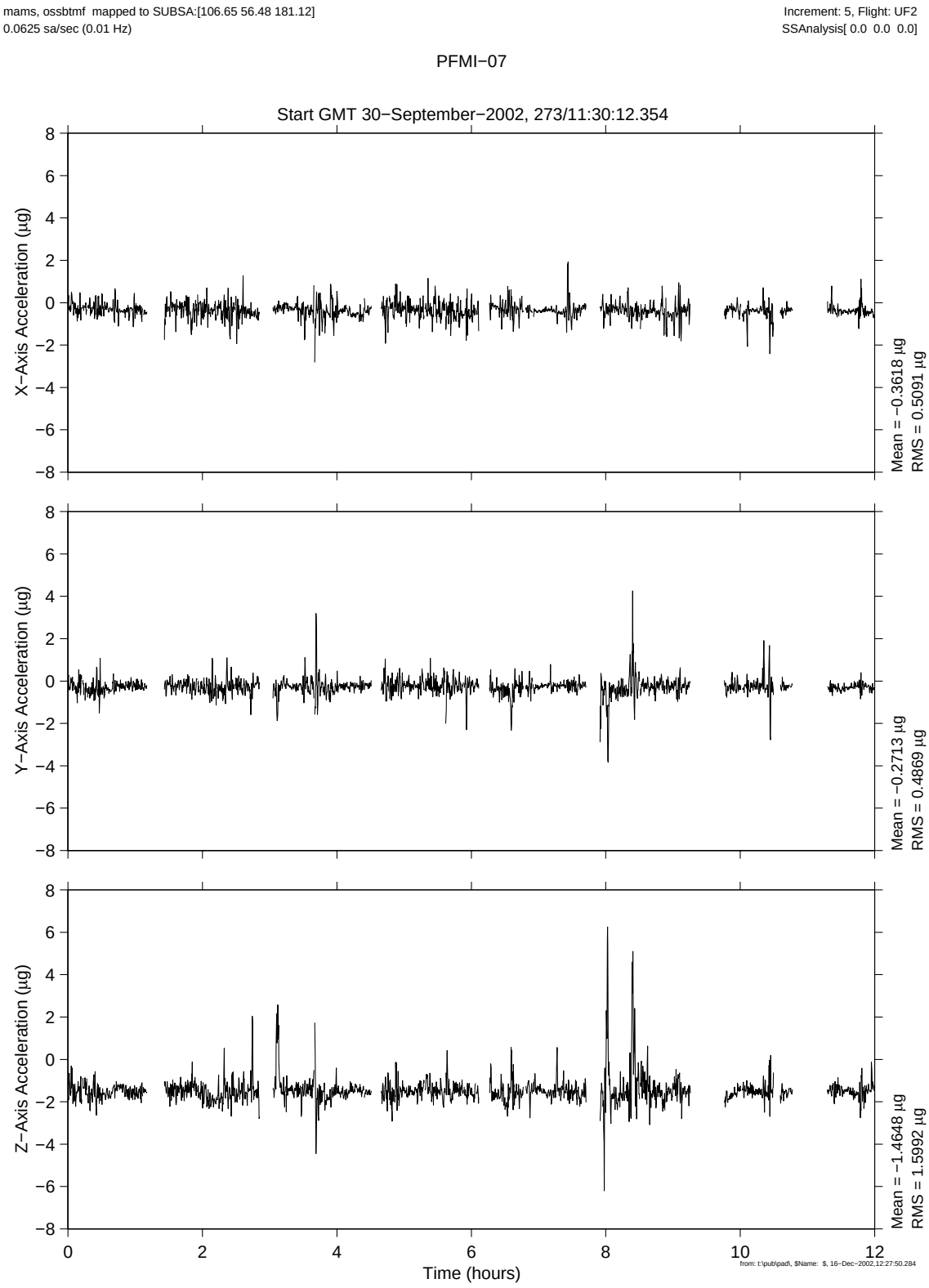

Figure 6-56 Time Series of PFMI-07 Sample Run (OSSBTMF)

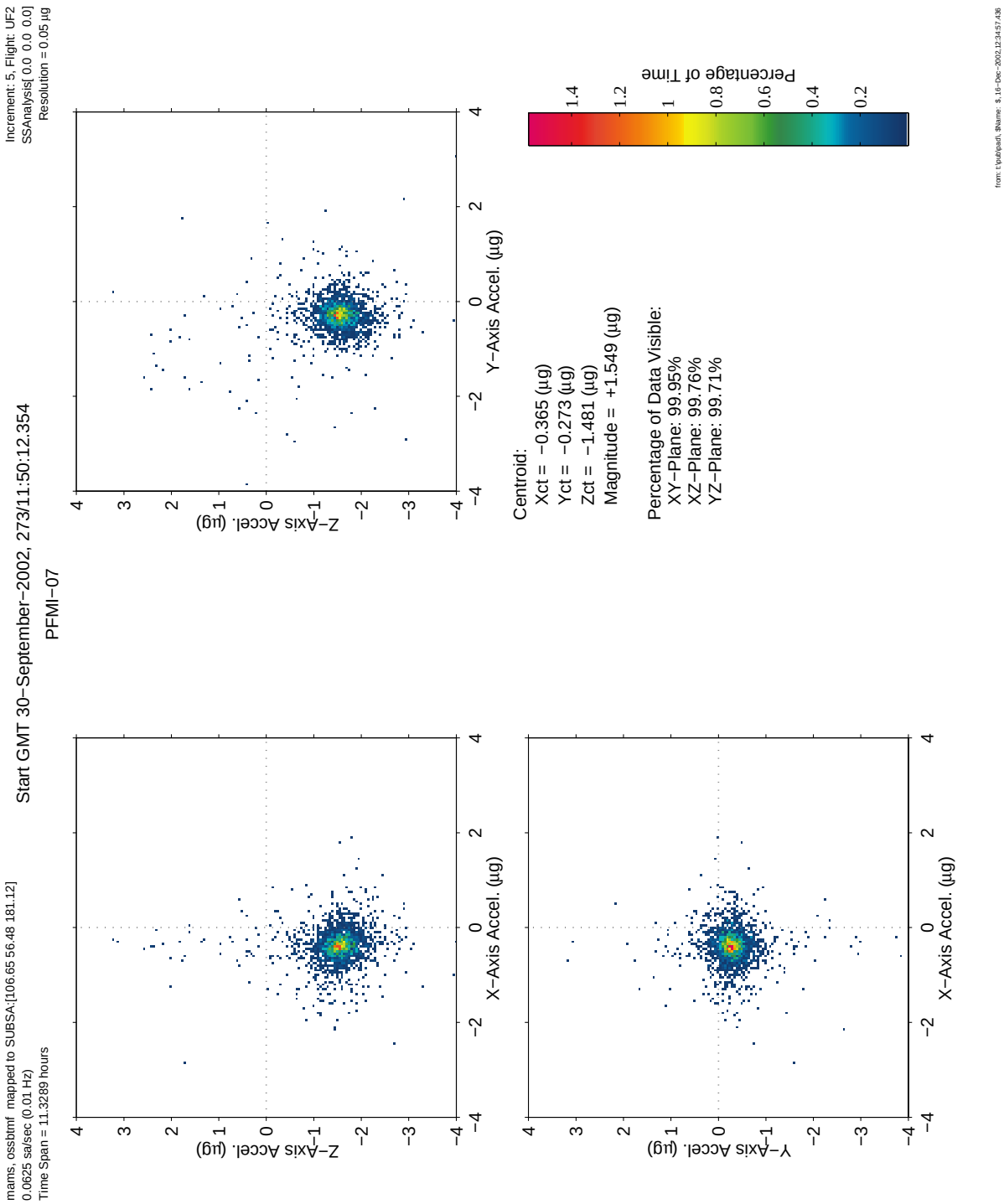

Figure 6-57 QTH of PFMI-07 Sample Run (OSSBTMF)

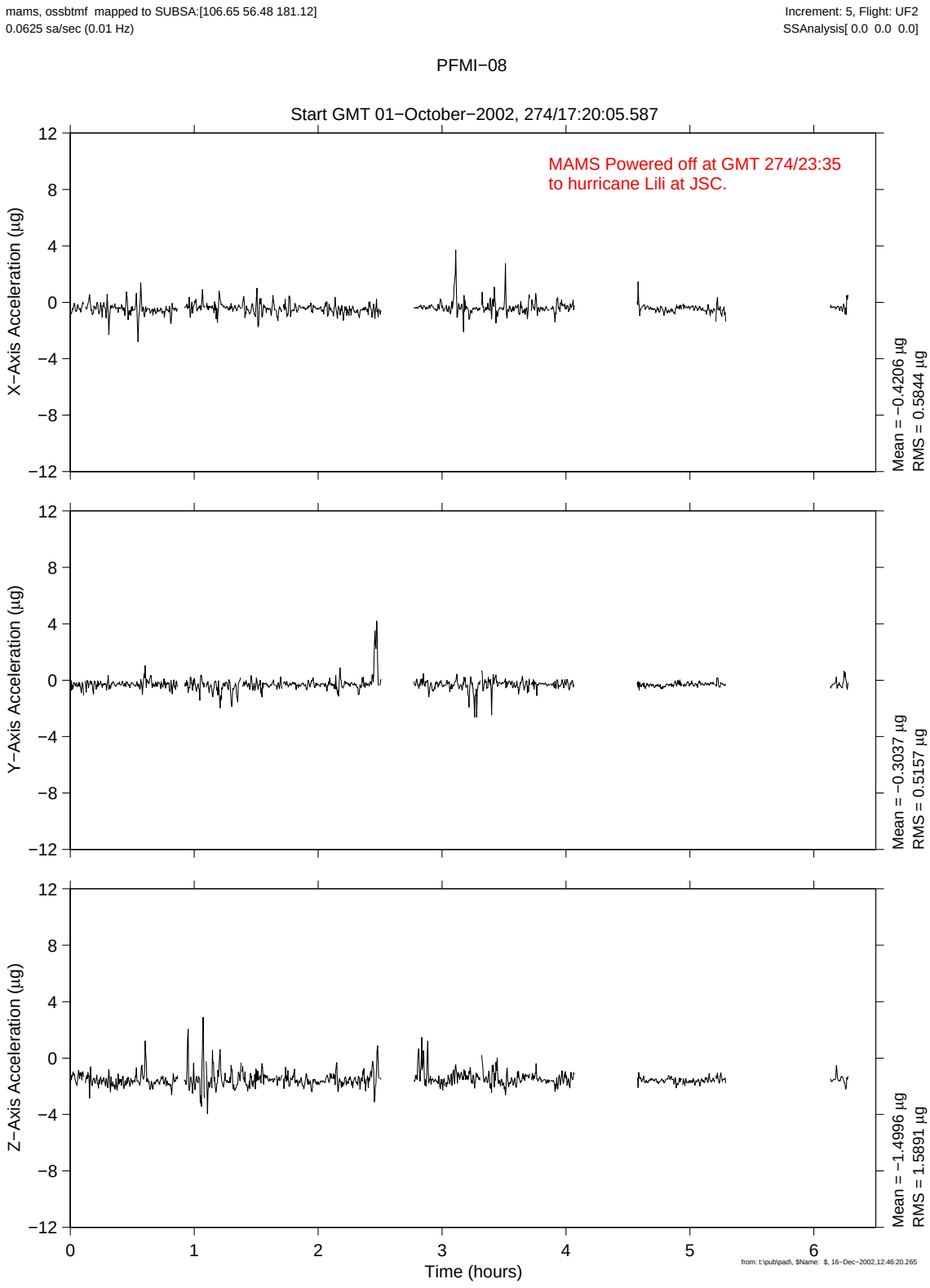

Figure 6-58 Time Series of PFMI-08 Sample Run (OSSBTMF)

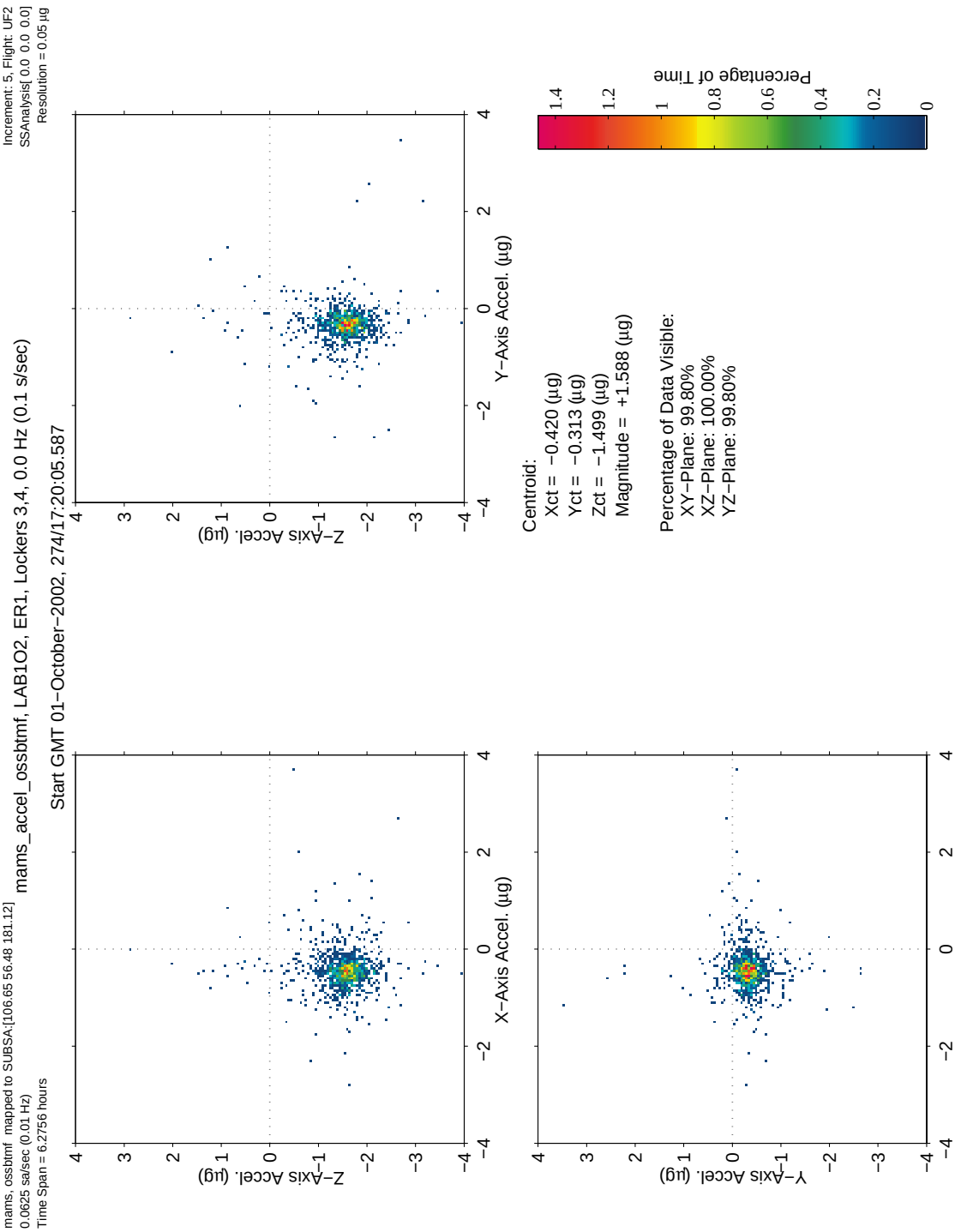

Figure 6-59 QTH of PFMI-08 Sample Run (OSSBTMF)

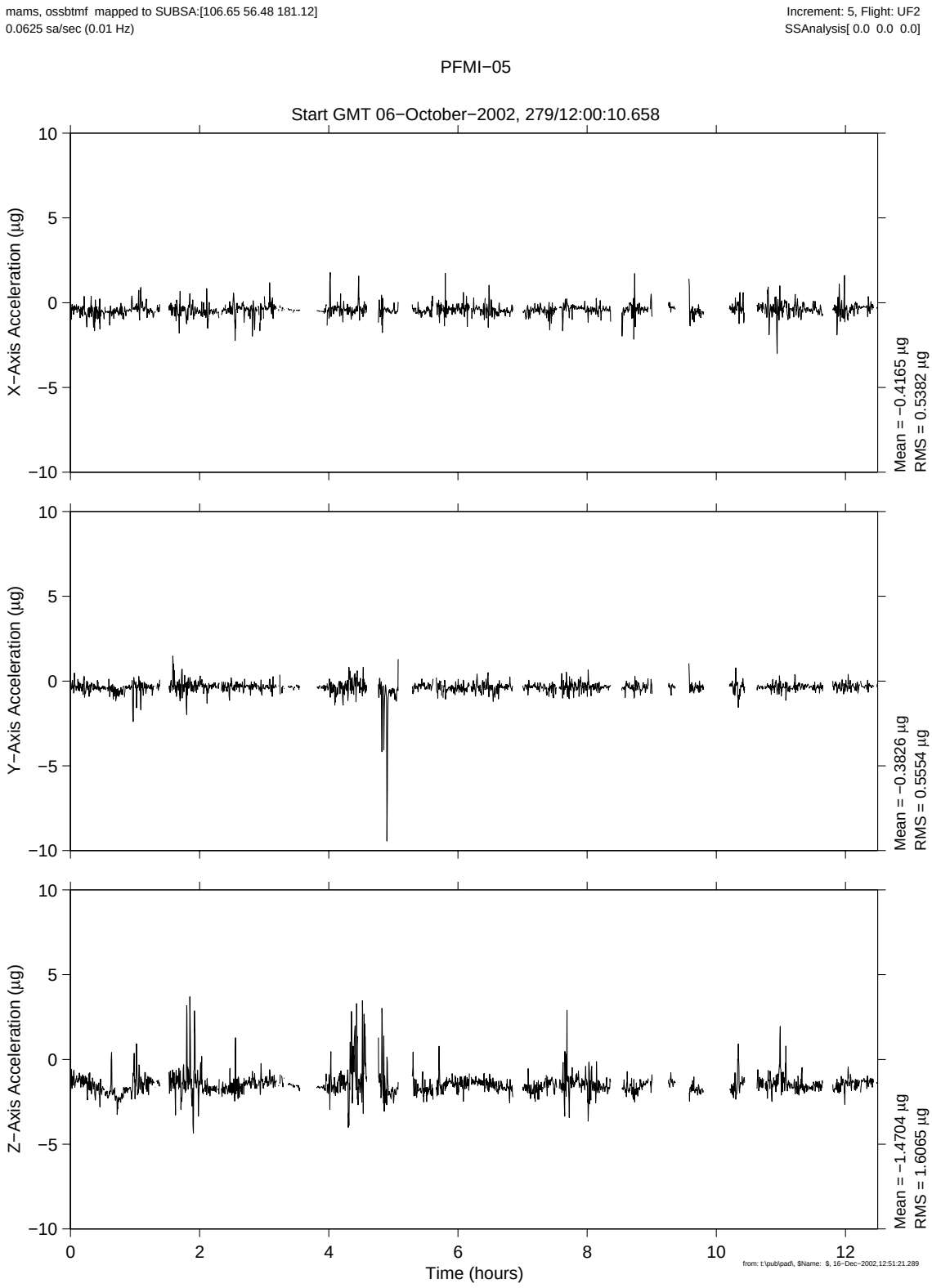

Figure 6-60 Time Series of PFMI-05 Sample Run (OSSBTMF)

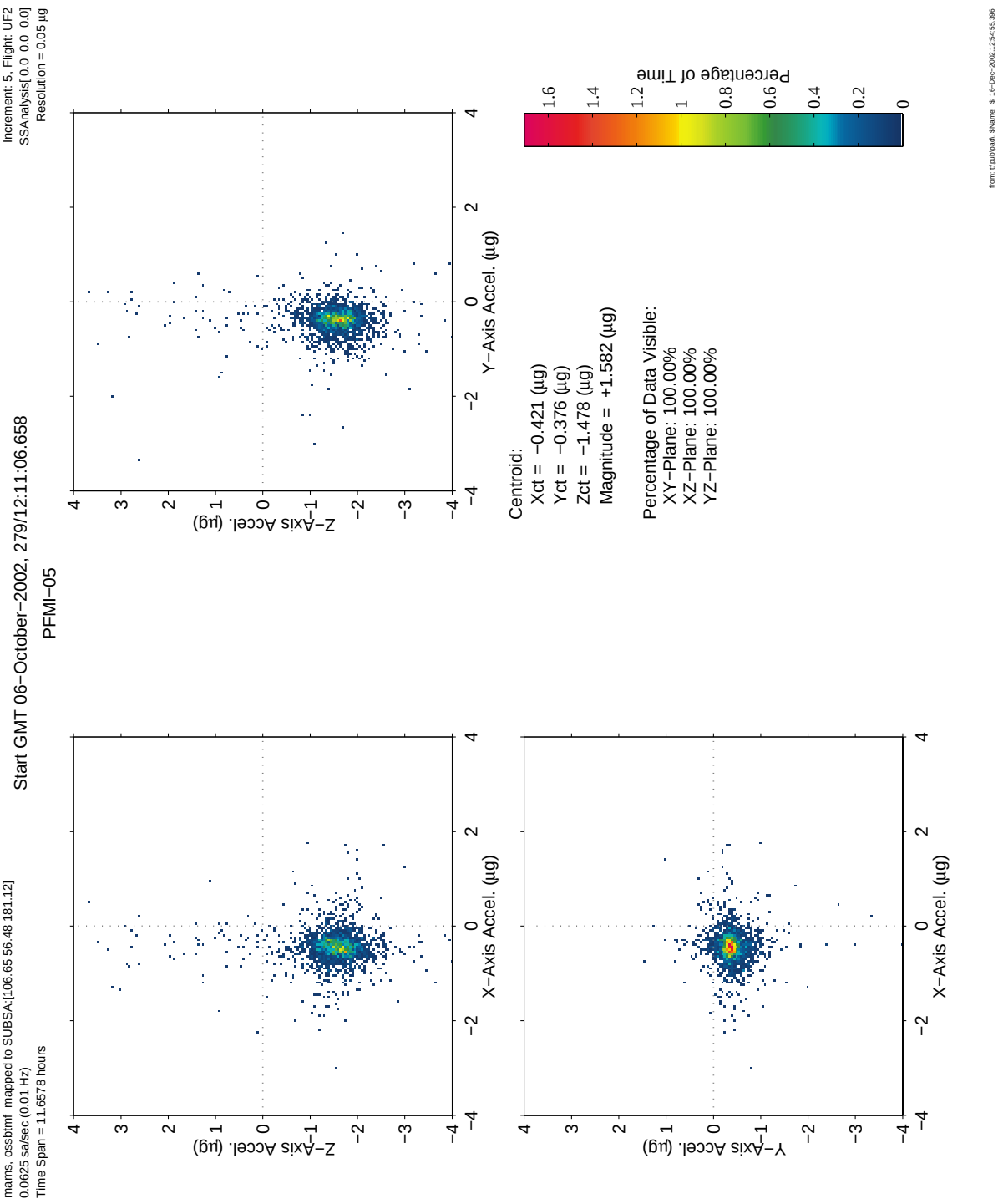

Figure 6-61 QTH of PFMI-05 Sample Run (OSSBTMF)

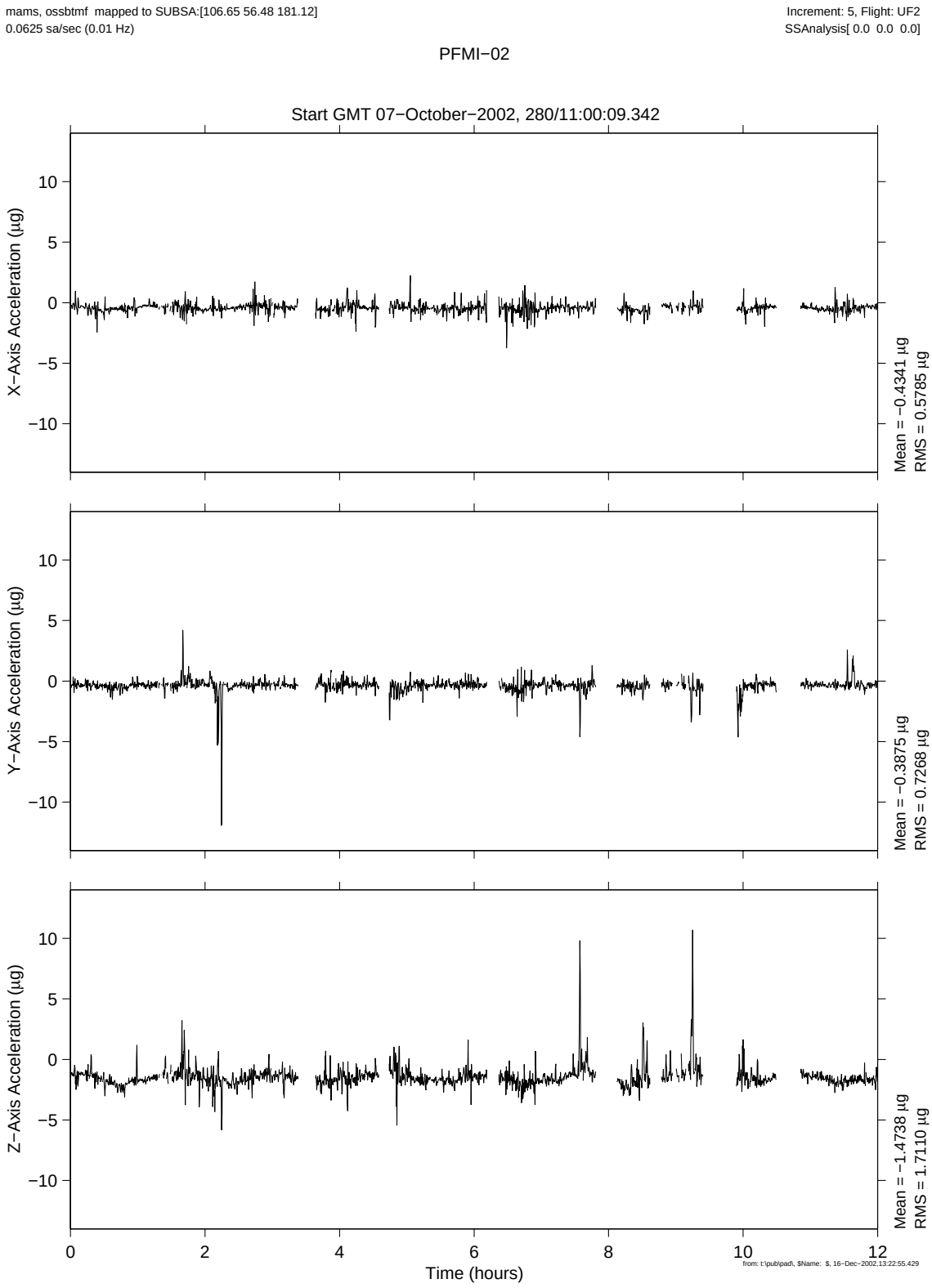

Figure 6-62 Time Series of PFMI-02 Sample Run (OSSBTMF)

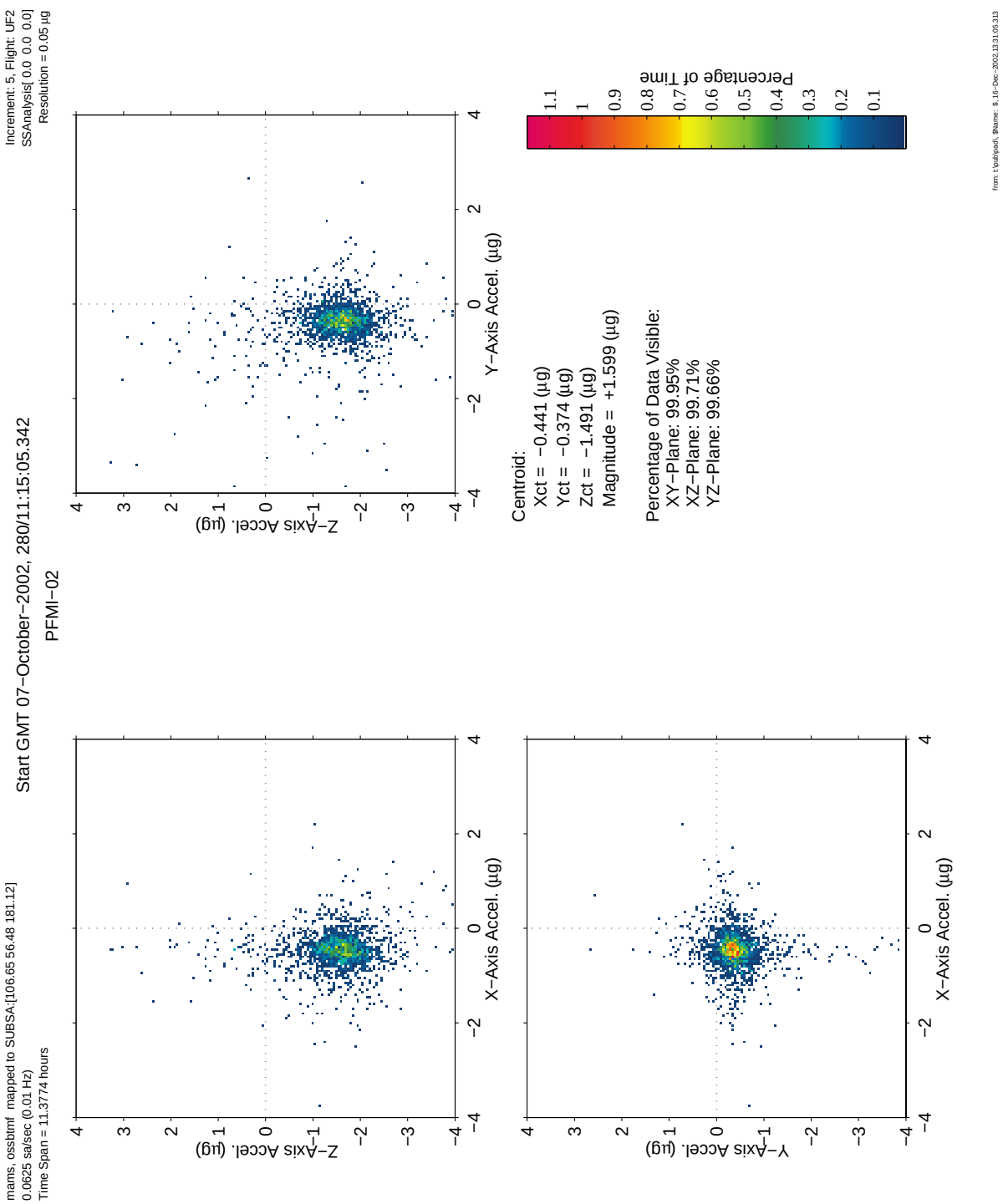

Figure 6-63 QTH of PFMI-02 Sample Run (OSSBTMF)

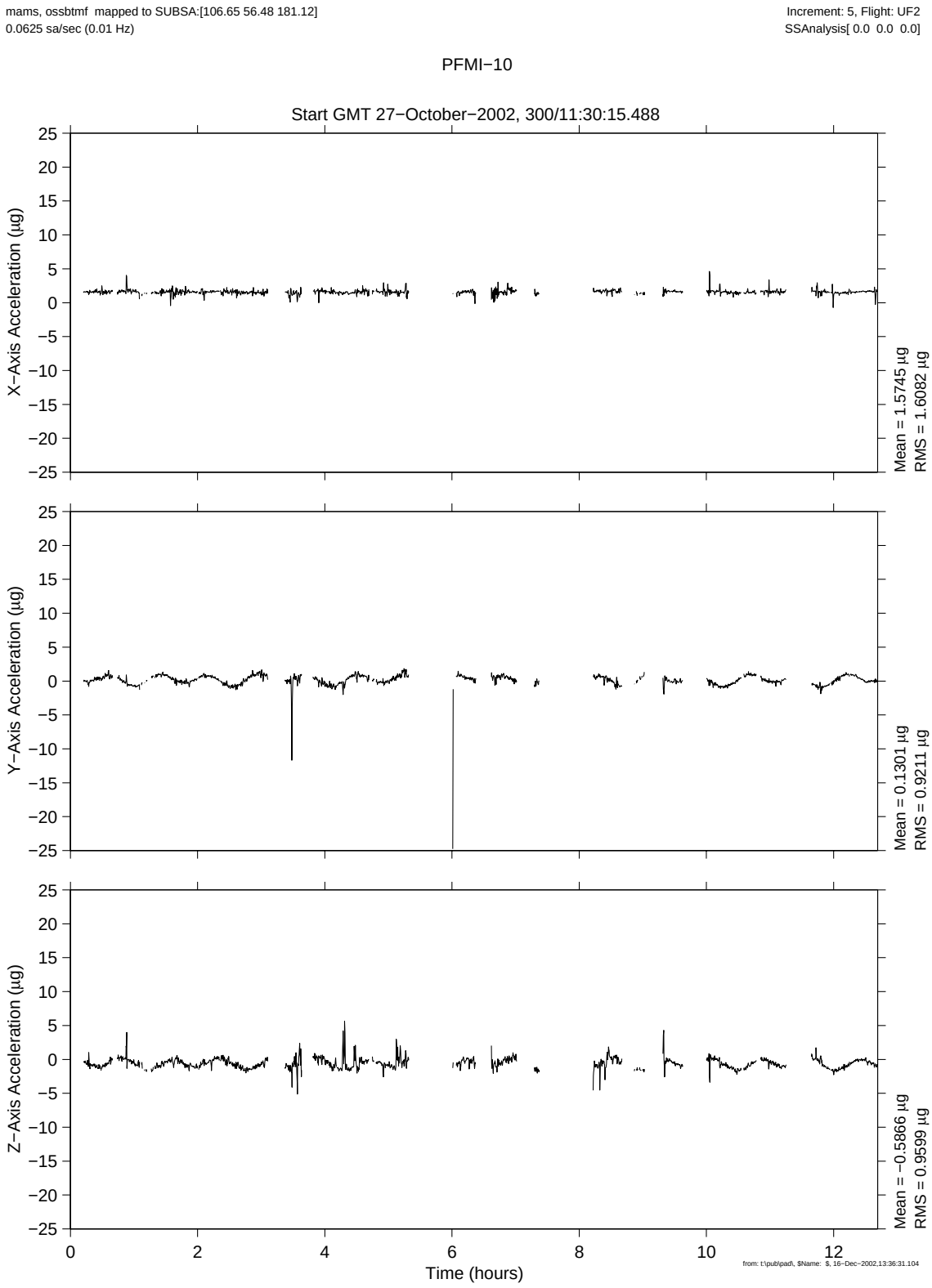

Figure 6-64 Time Series of PFMI-10 Sample Run (OSSBTMF)

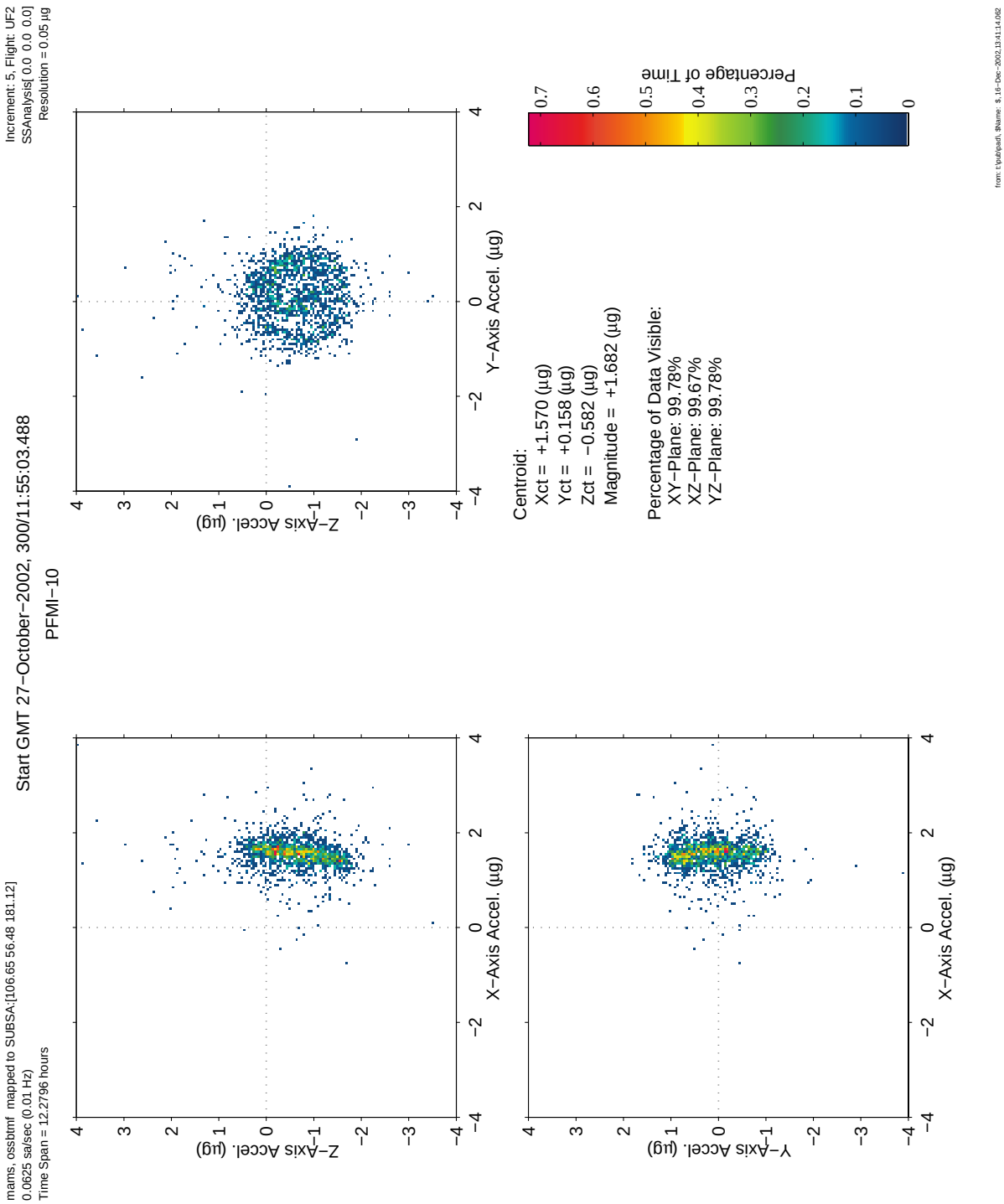

Figure 6-65 QTH of PFMI-10 Sample Run (OSSBTMF)

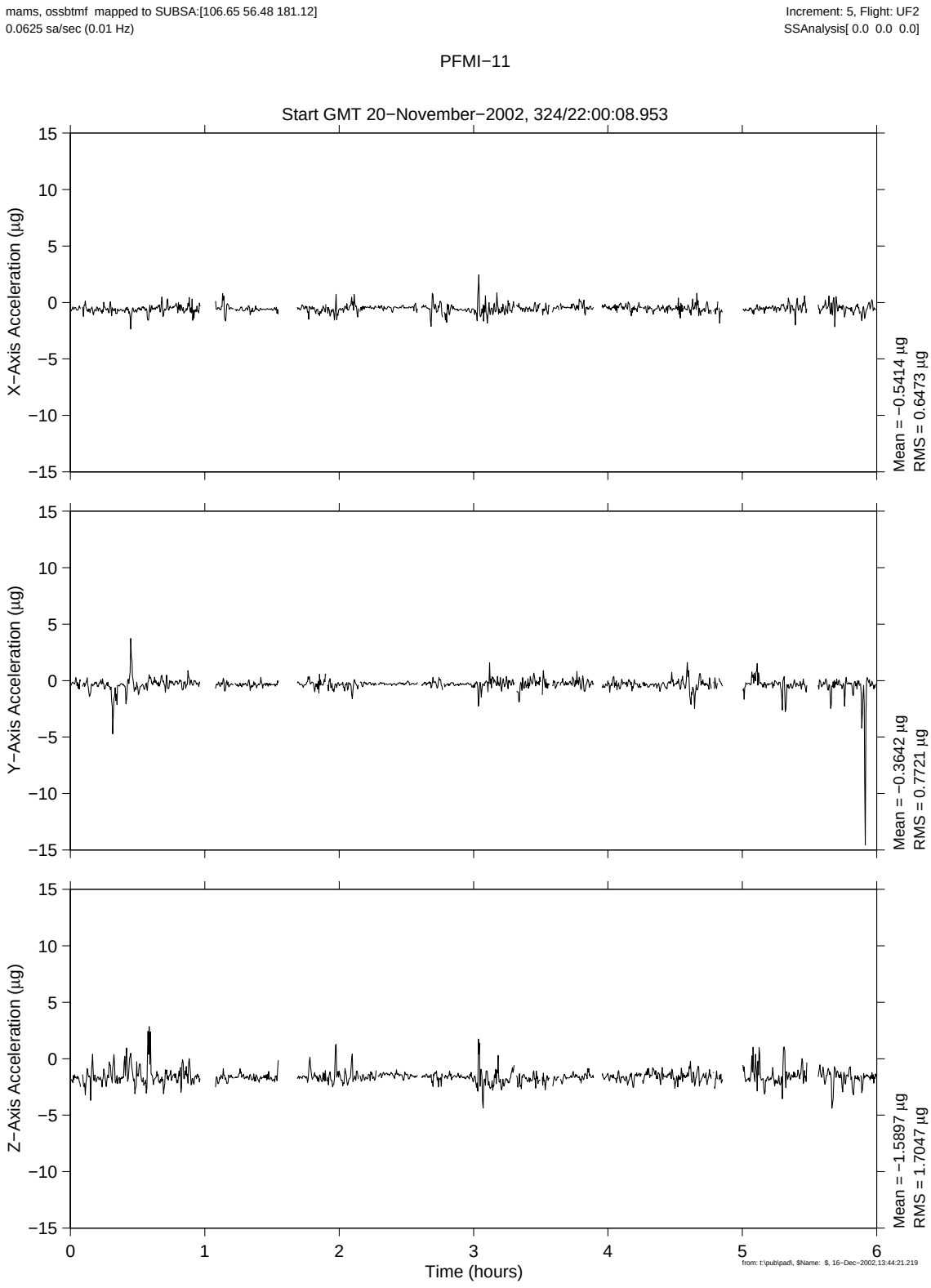

Figure 6-66 Time Series of PFMI-11 Sample Run (OSSBTMF)

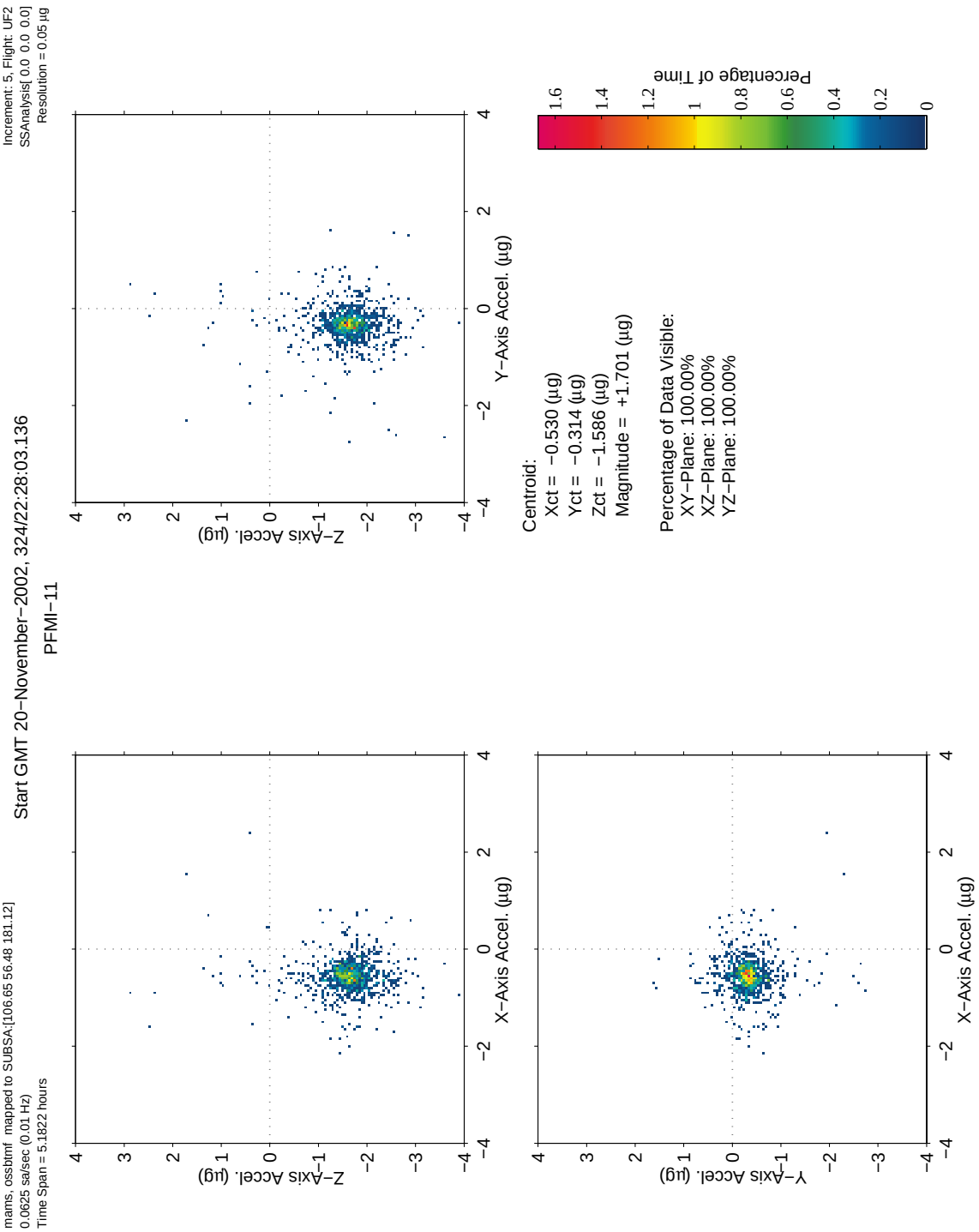

Figure 6-67 QTH of PFMI-11 Sample Run (OSSBTMF)

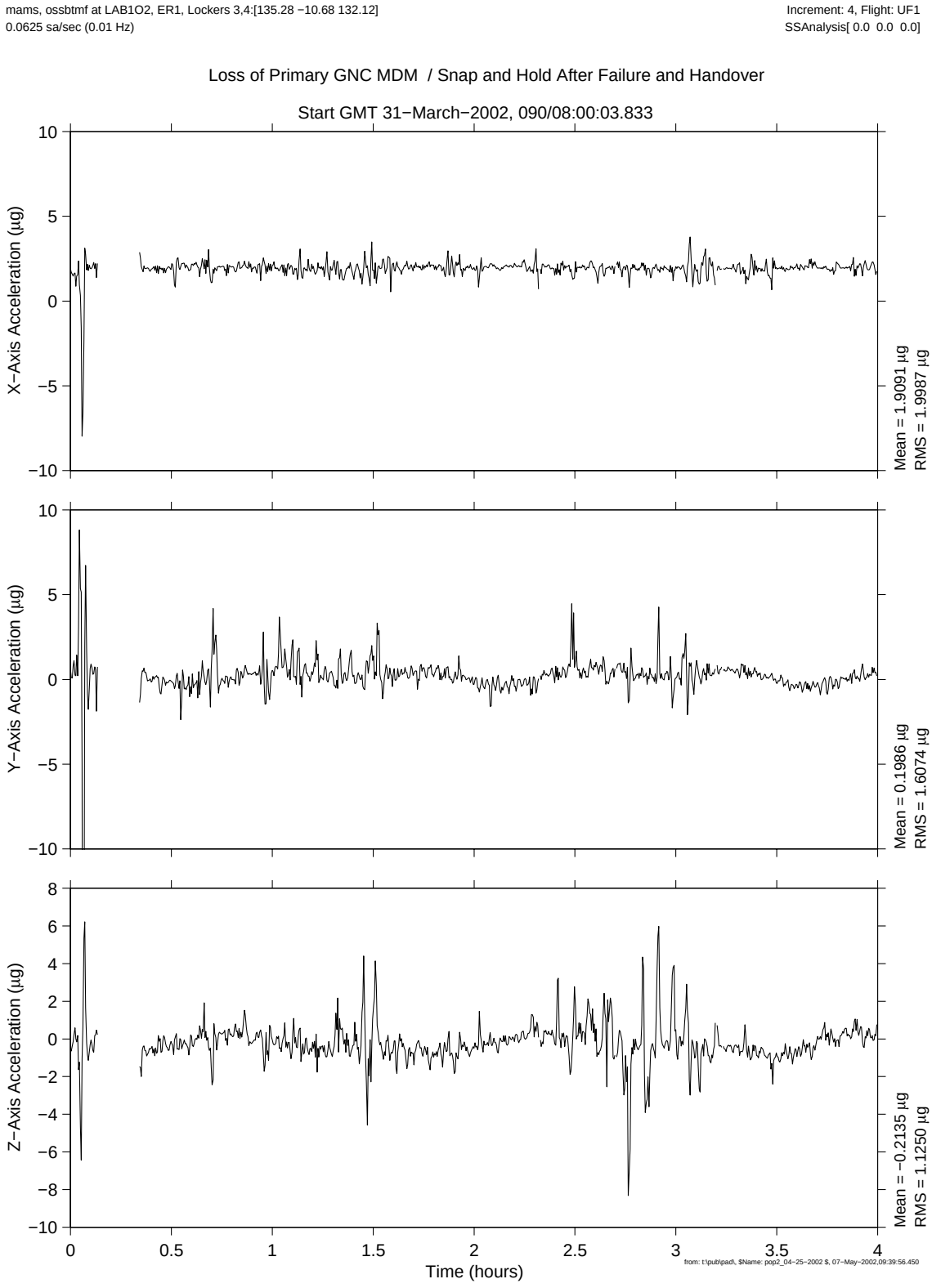

Figure 6-68 Time Series of Loss of Primary GNC MDM, GMT 090 (OSSBTMF)

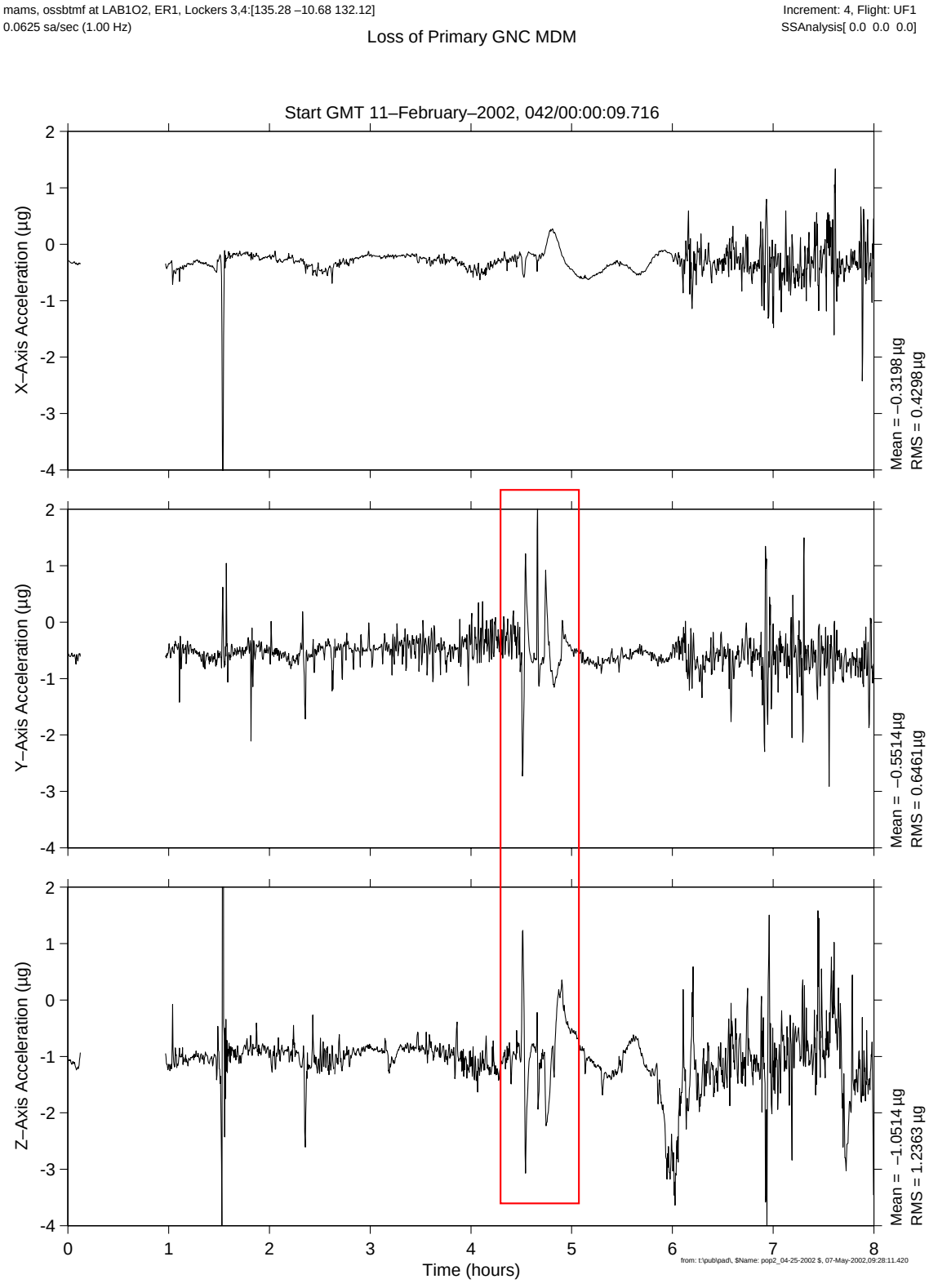

Figure 6-69 Time Series of Loss of Primary GNC MDM, GMT 042 (OSSBTMF)

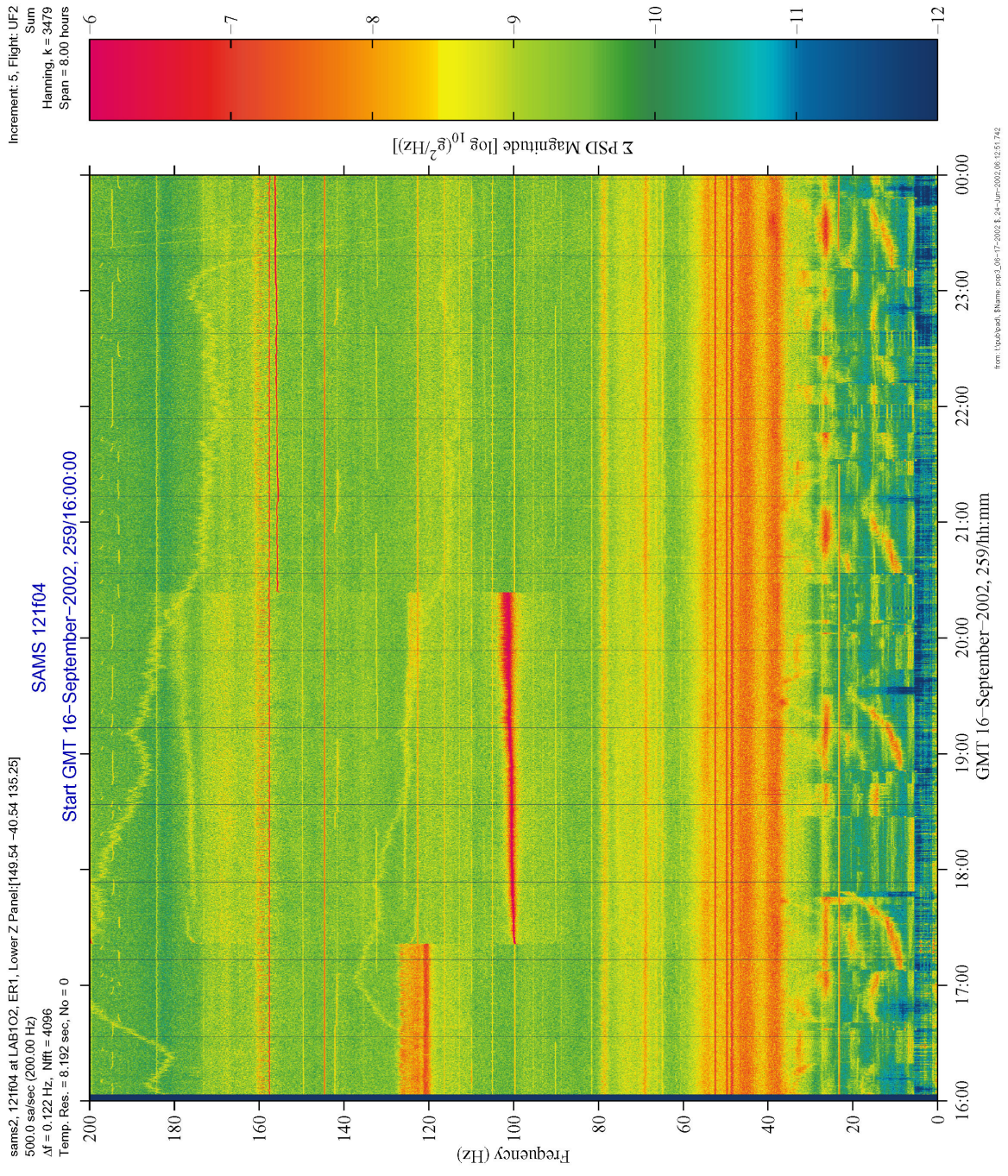

Figure 6-70 Spectrogram of Unknown Disturbance (121F04)

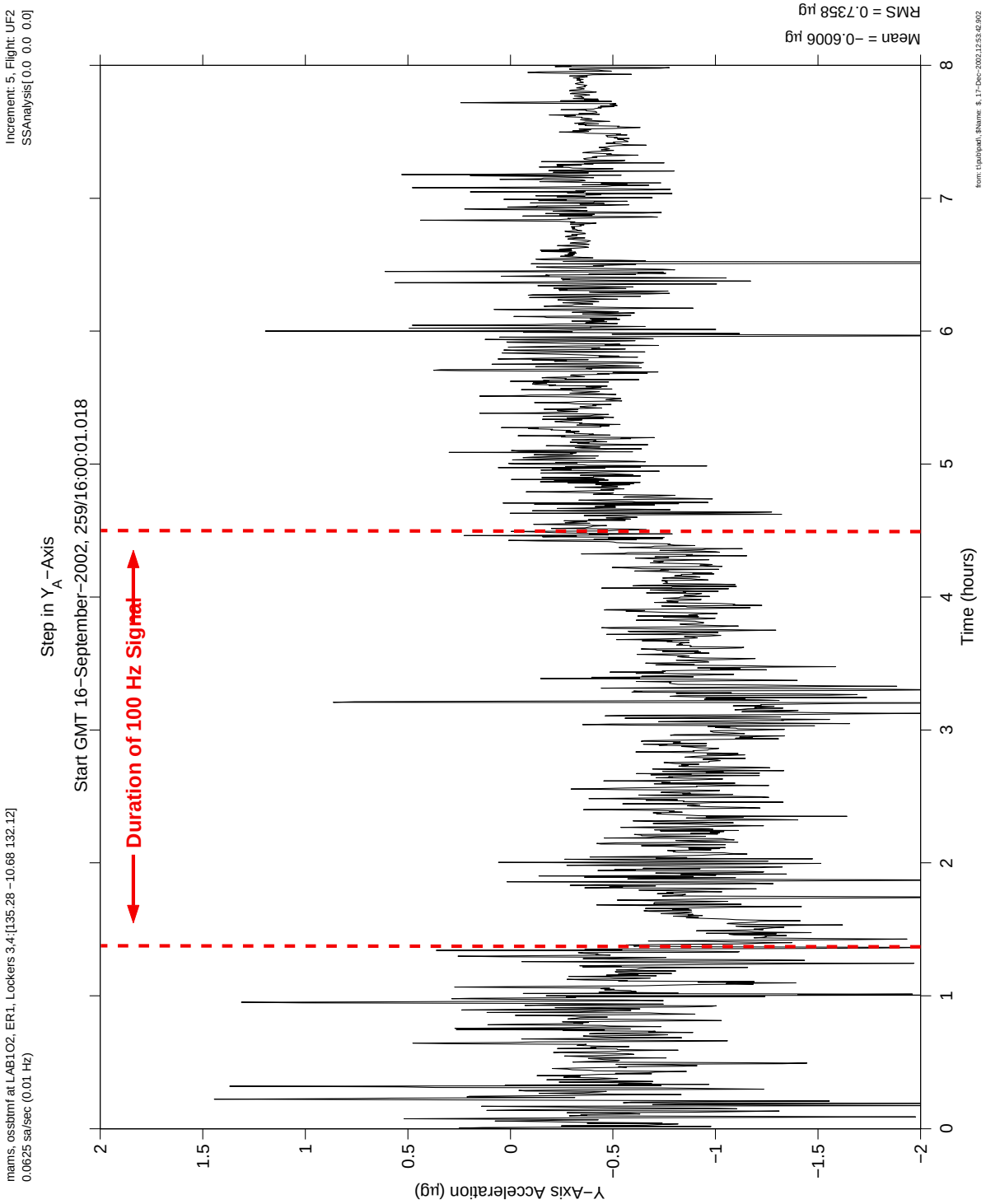

Figure 6-71 Time Series of Step in YA-axis during 100 Hz Signal (OSSBTMF)

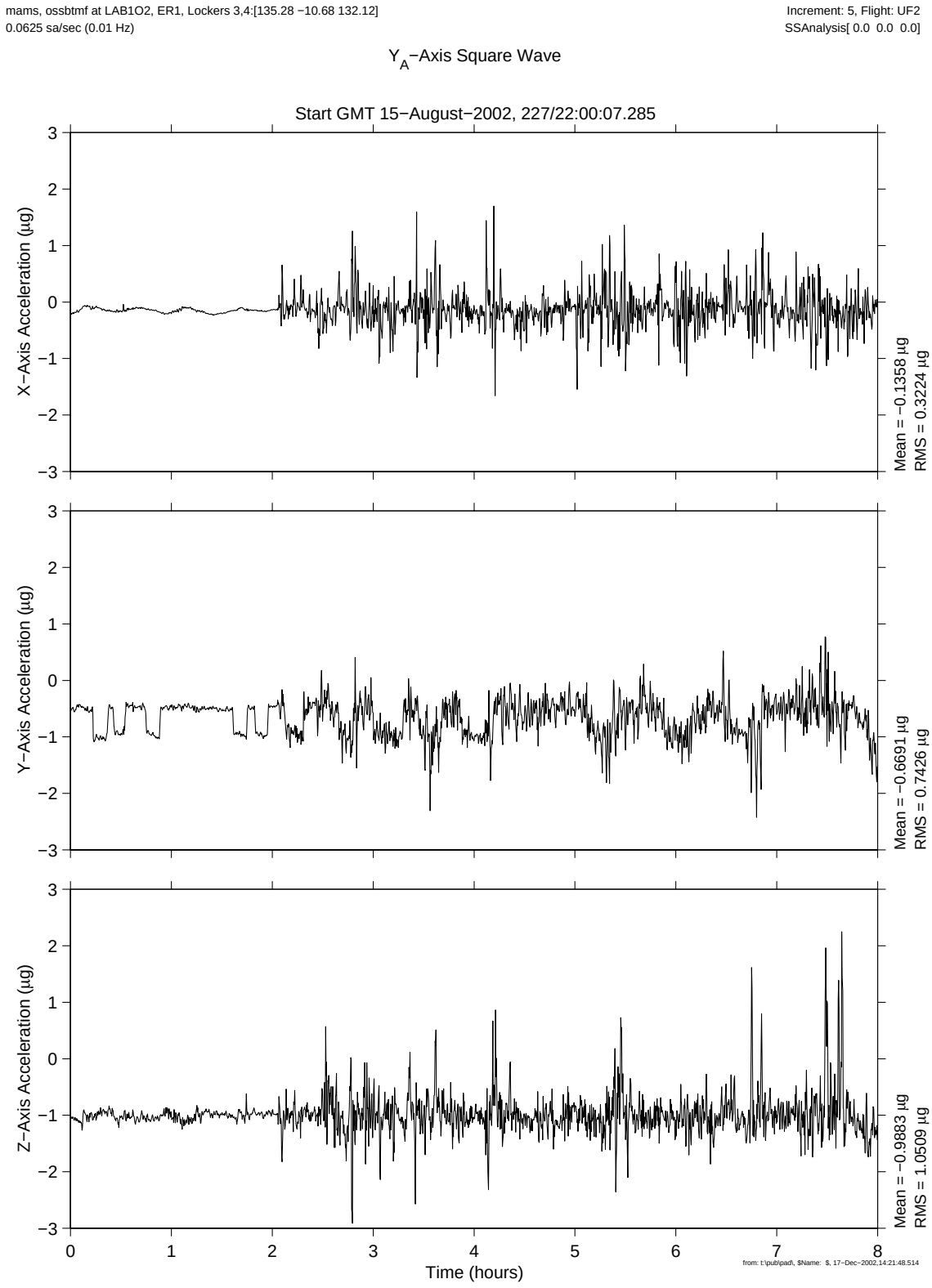

Figure 6-72 Time Series of Y_A-axis "Square Wave" (OSSBTMF)

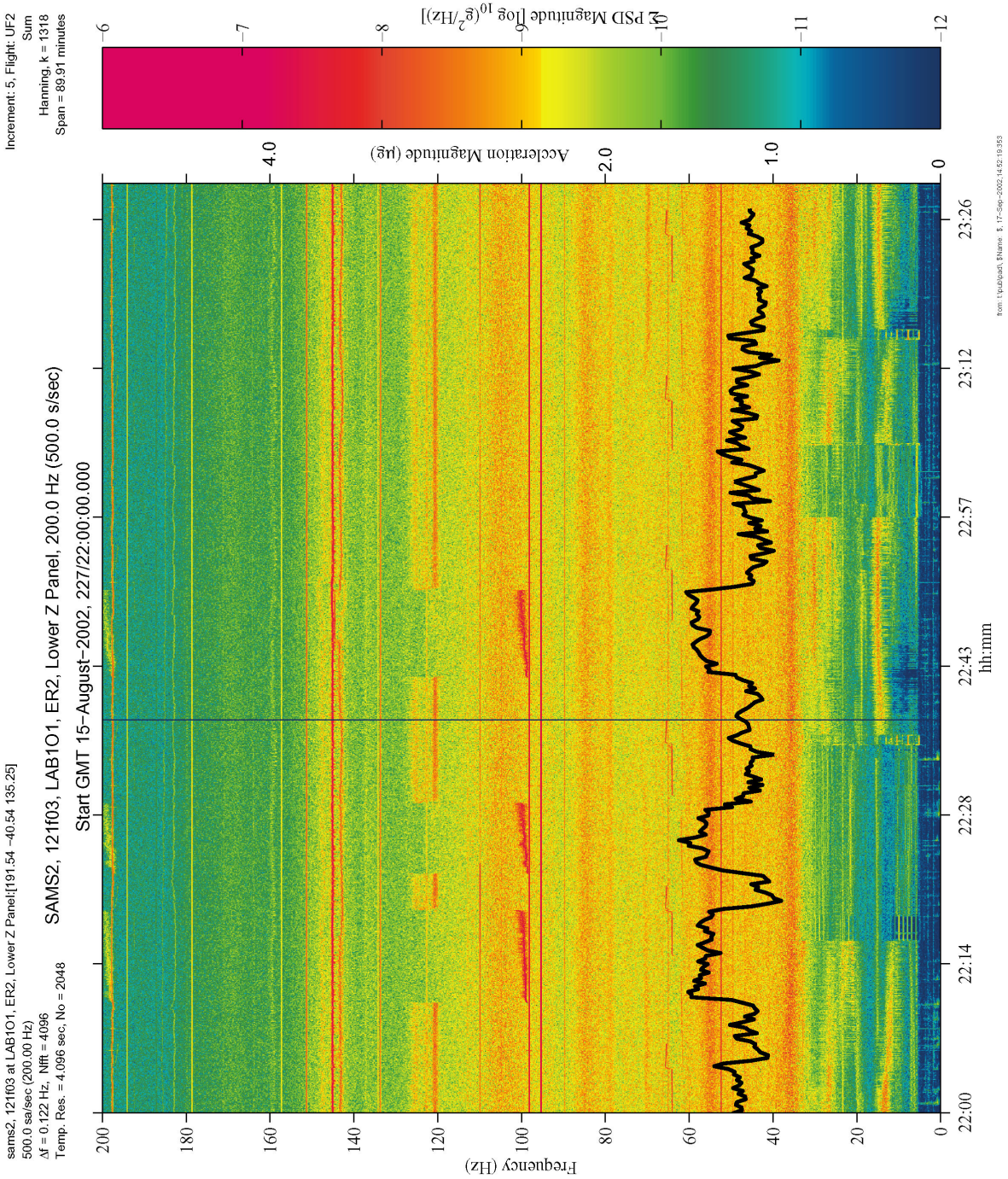

Figure 6-73 Spectrogram of Unknown Disturbance with OSS YA-axis Overlay (121F03)

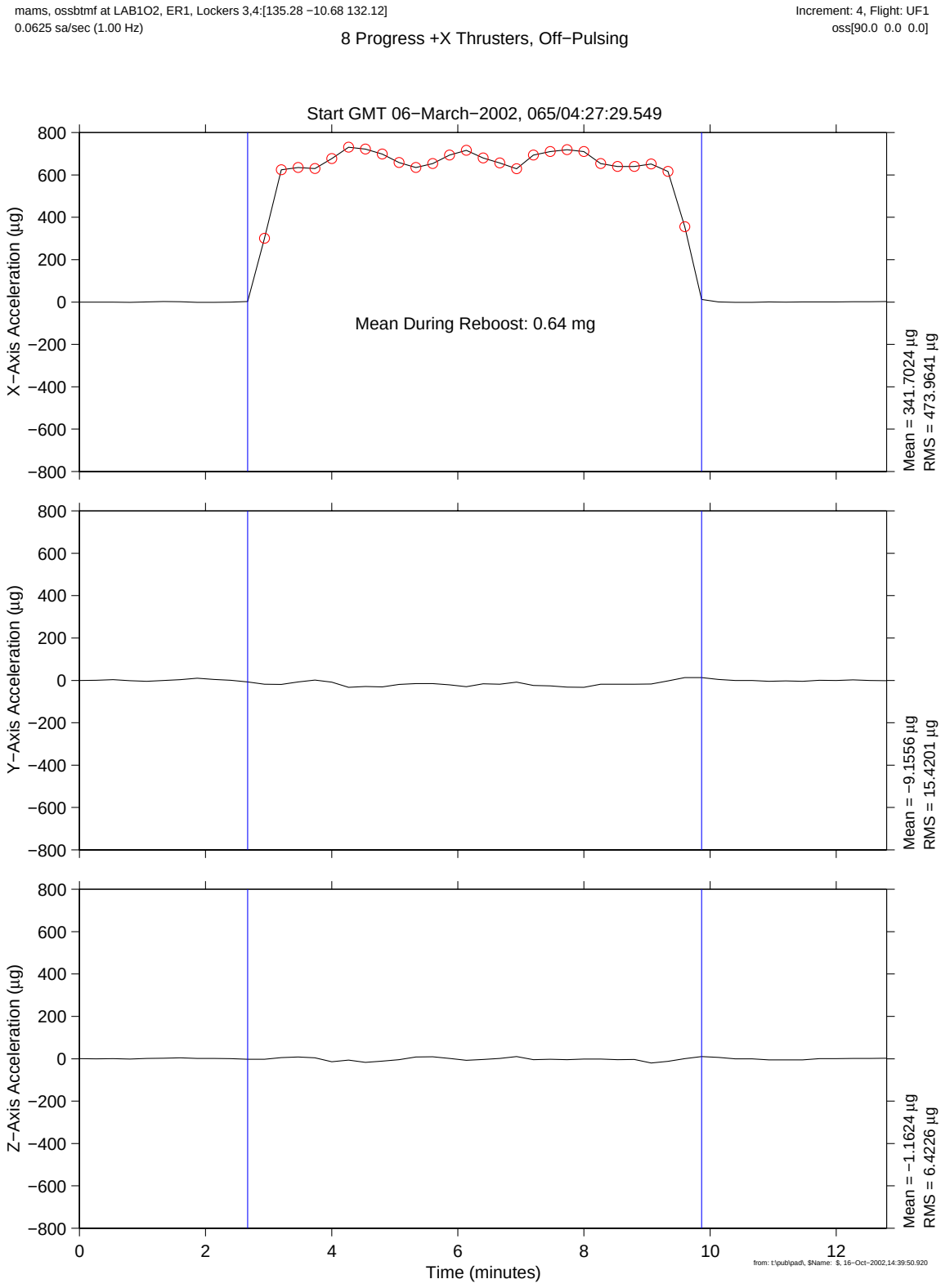

Figure 6-74 Time Series of Station Reboost (OSSBTMF)

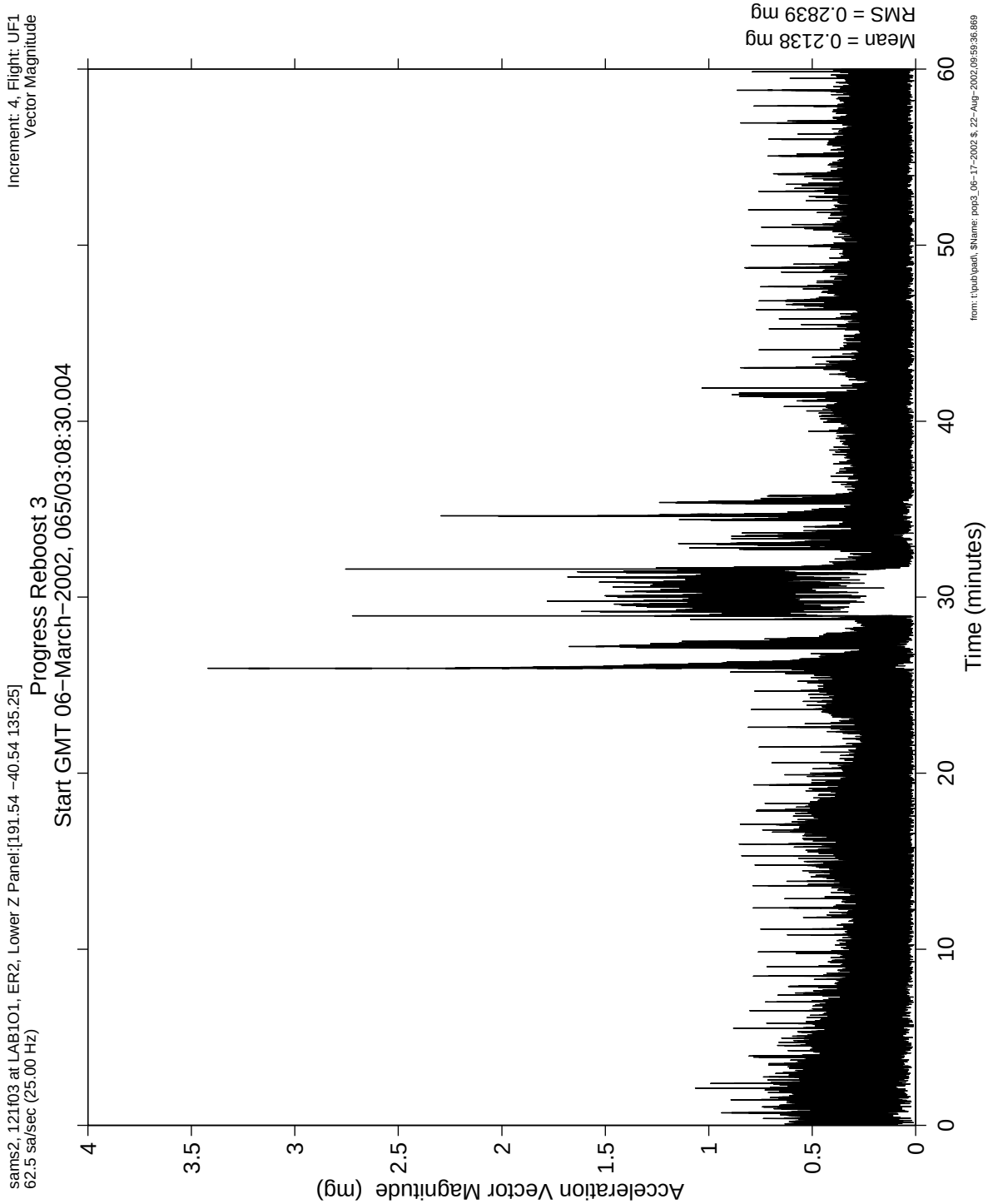

Figure 6-75 Acceleration Magnitude of Progress Reboost 3 (121f03)

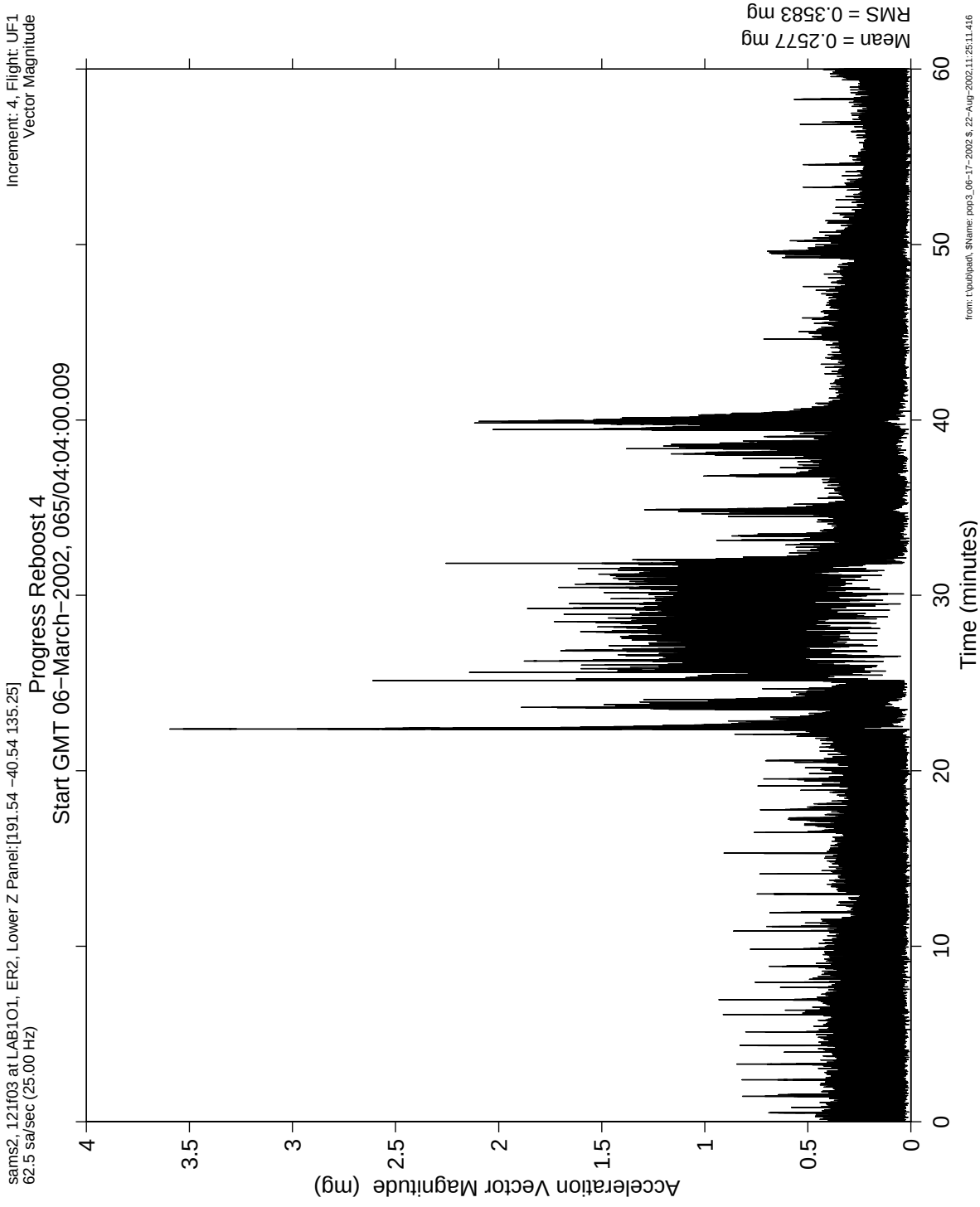

Figure 6-76 Acceleration Magnitude of Progress Reboost 4 (121f03)

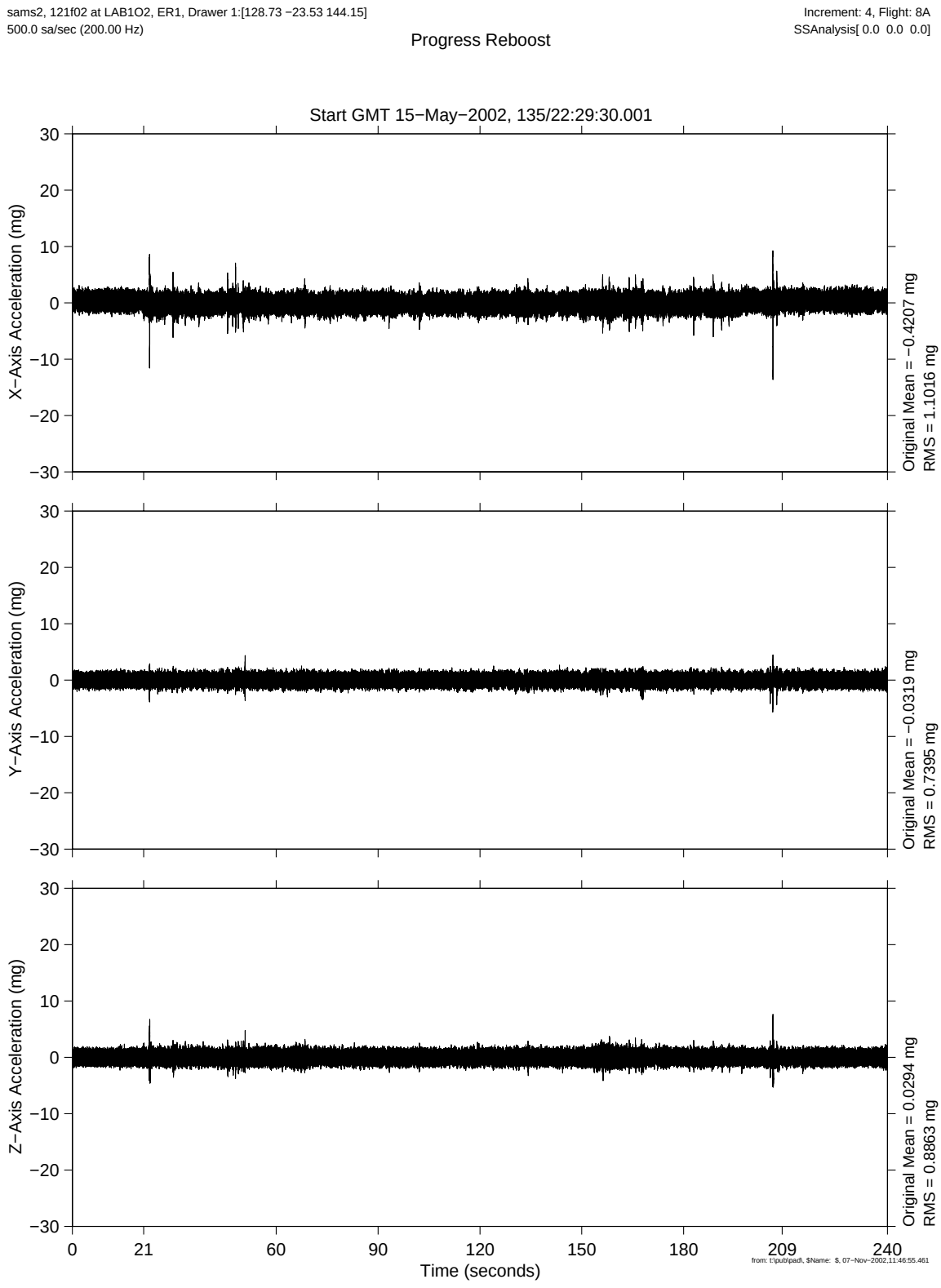

Figure 6-77 Time Series of Progress Reboost (121f02)

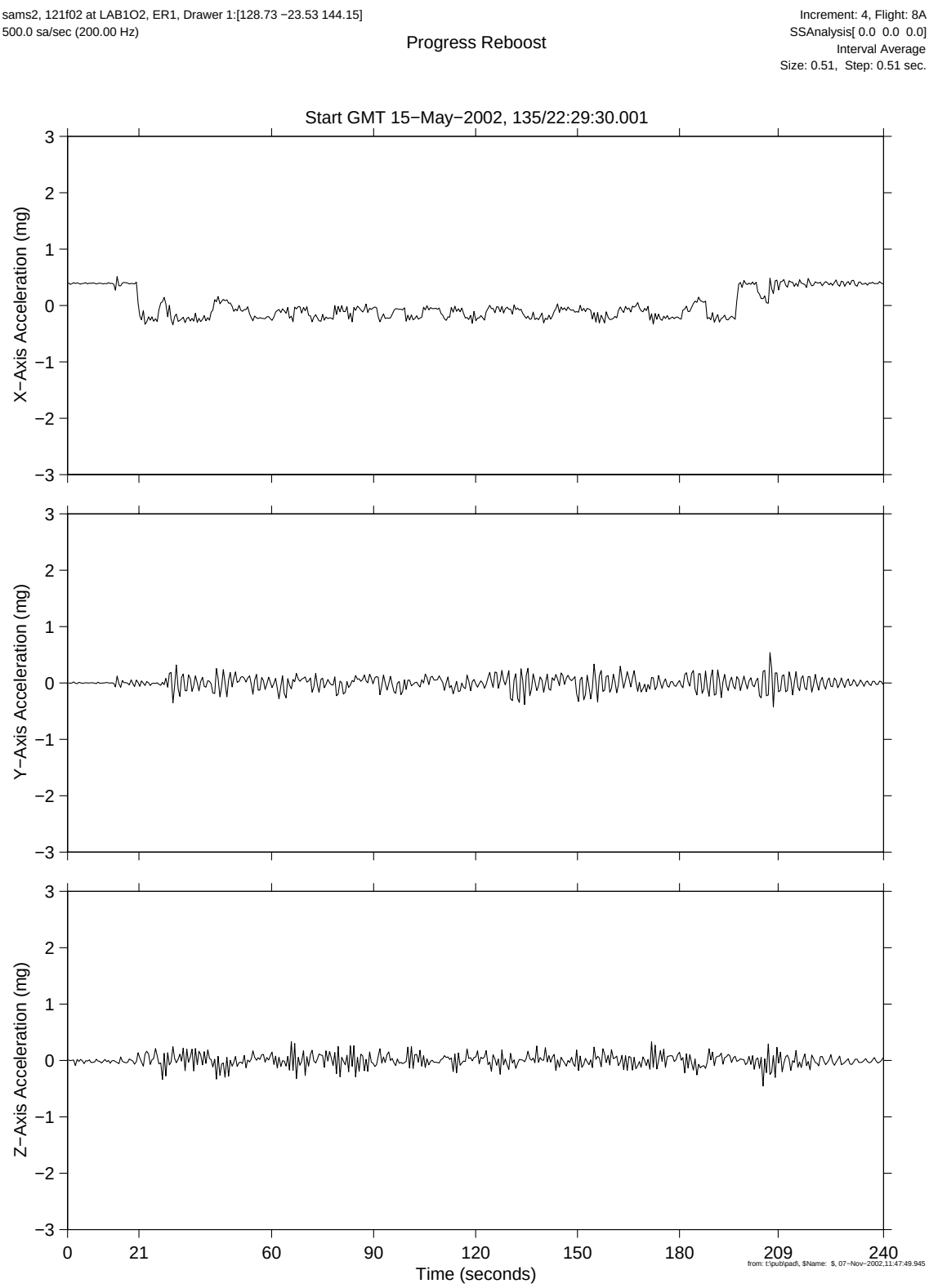

Figure 6-78 Interval Average of Progress Reboost (121f02)

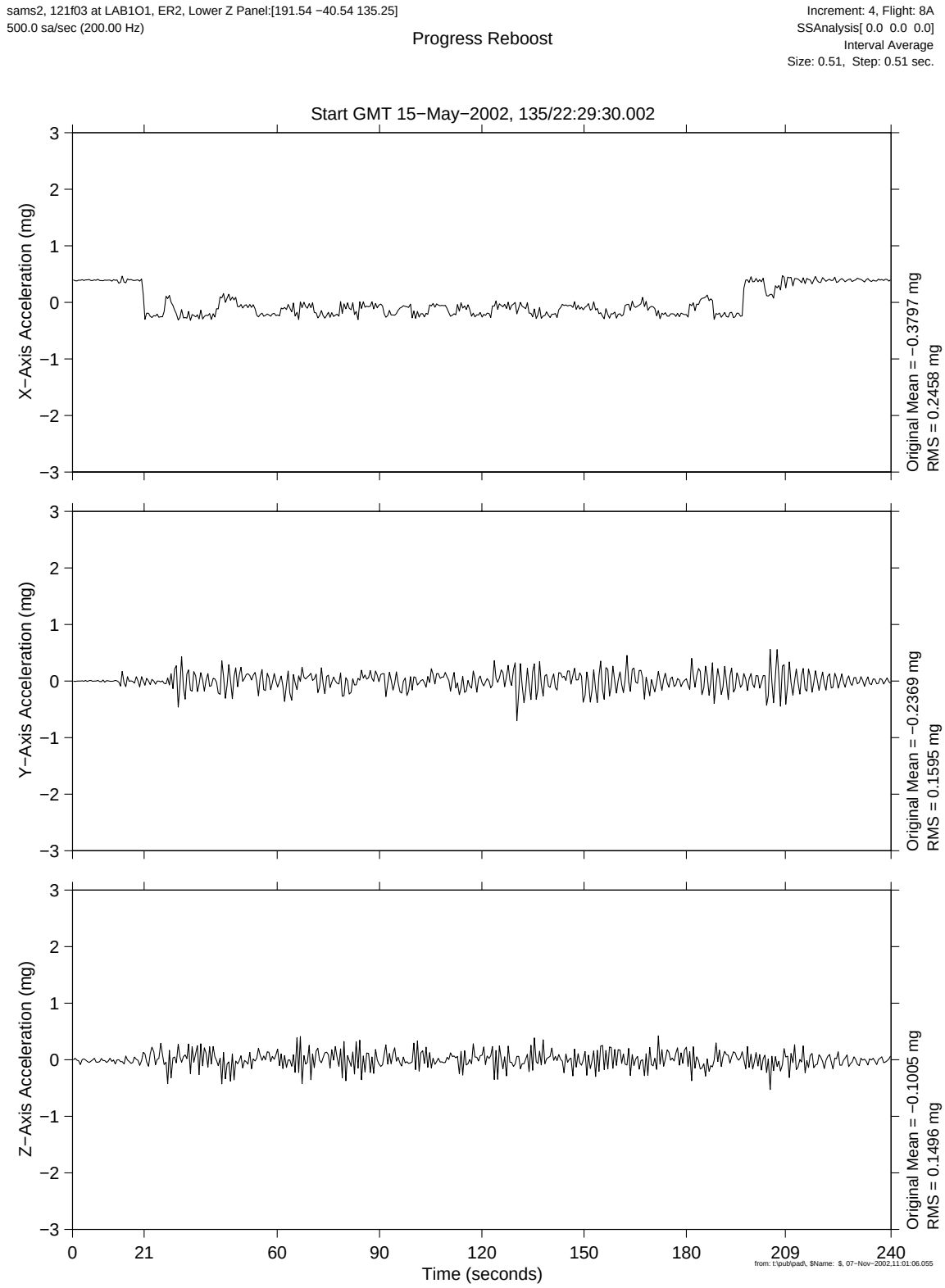

Figure 6-79 Interval Average of Progress Reboost (121f03)

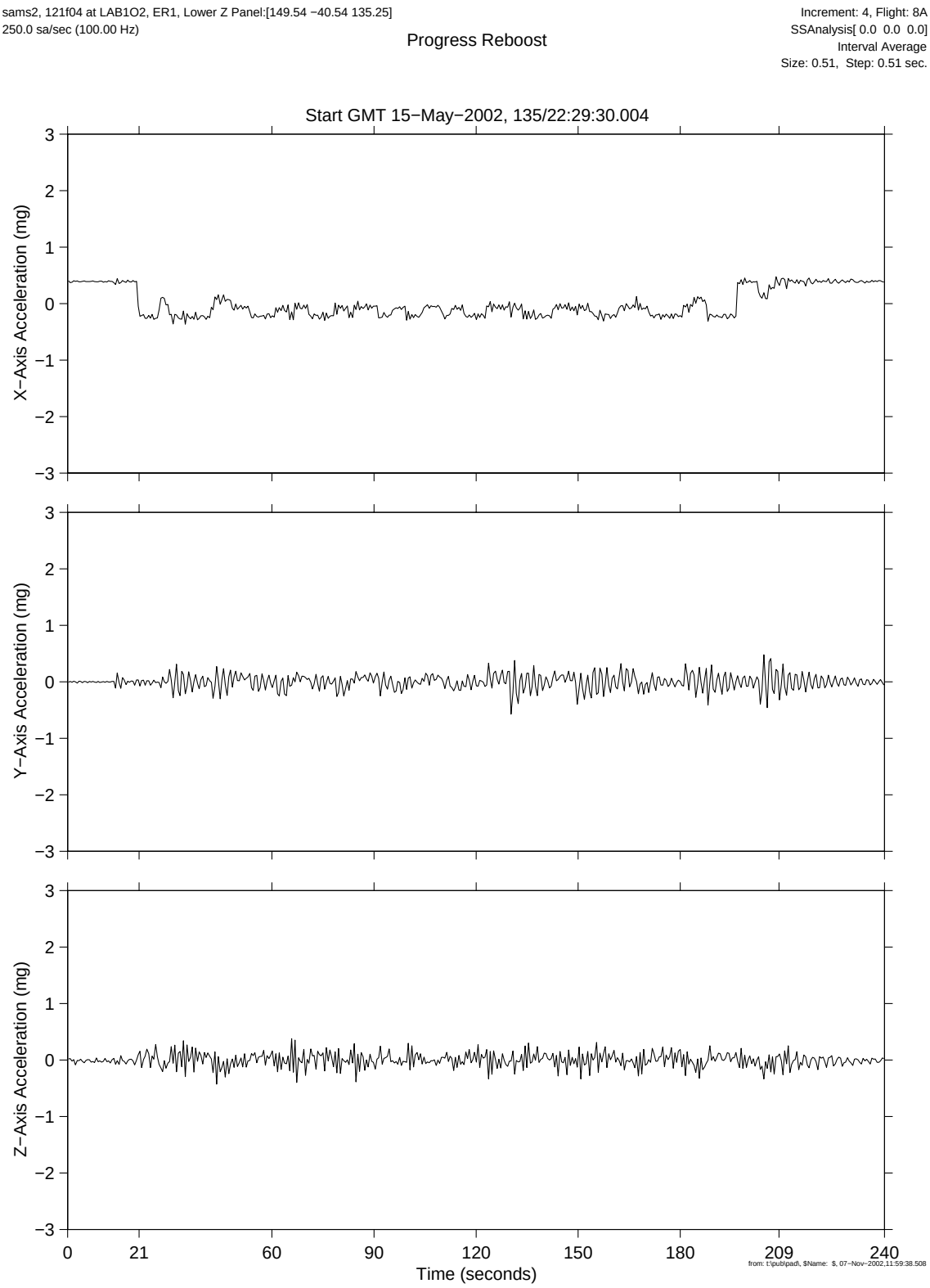

Figure 6-80 Interval Average of Progress Reboost (121f04)

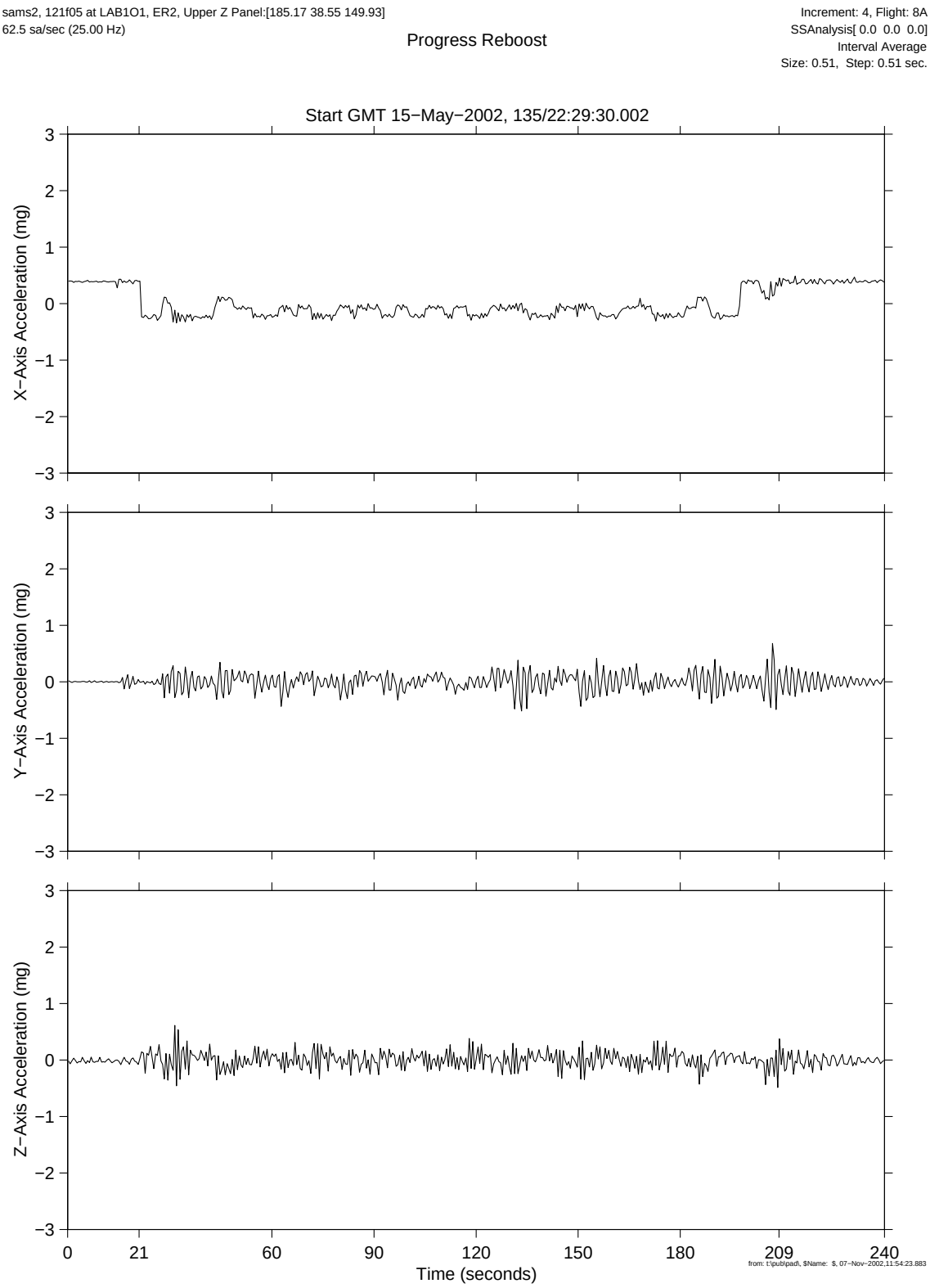

Figure 6-81 Interval Average of Progress Reboost (121f05)

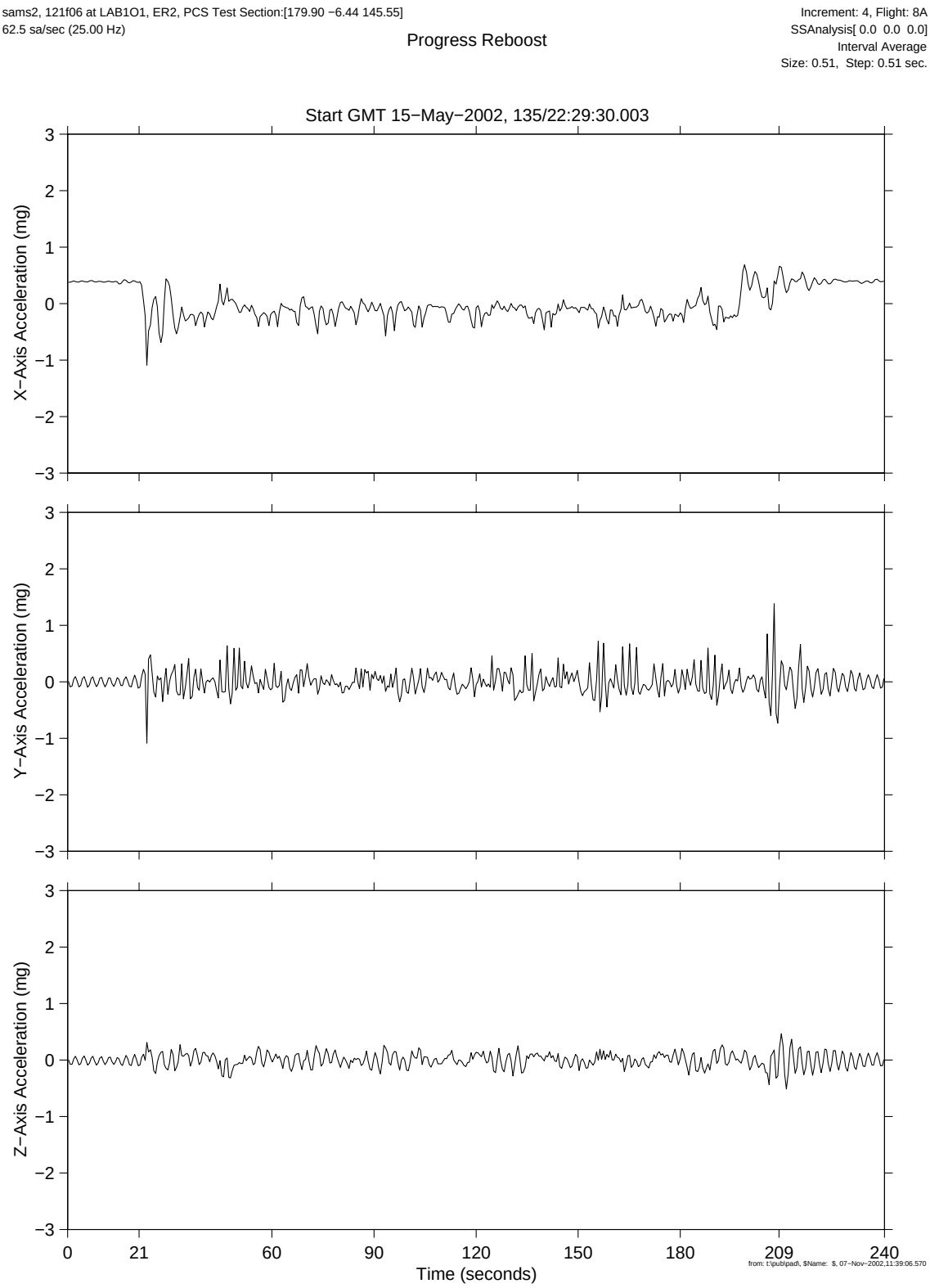

Figure 6-82 Interval Average of Progress Reboost (121f06)

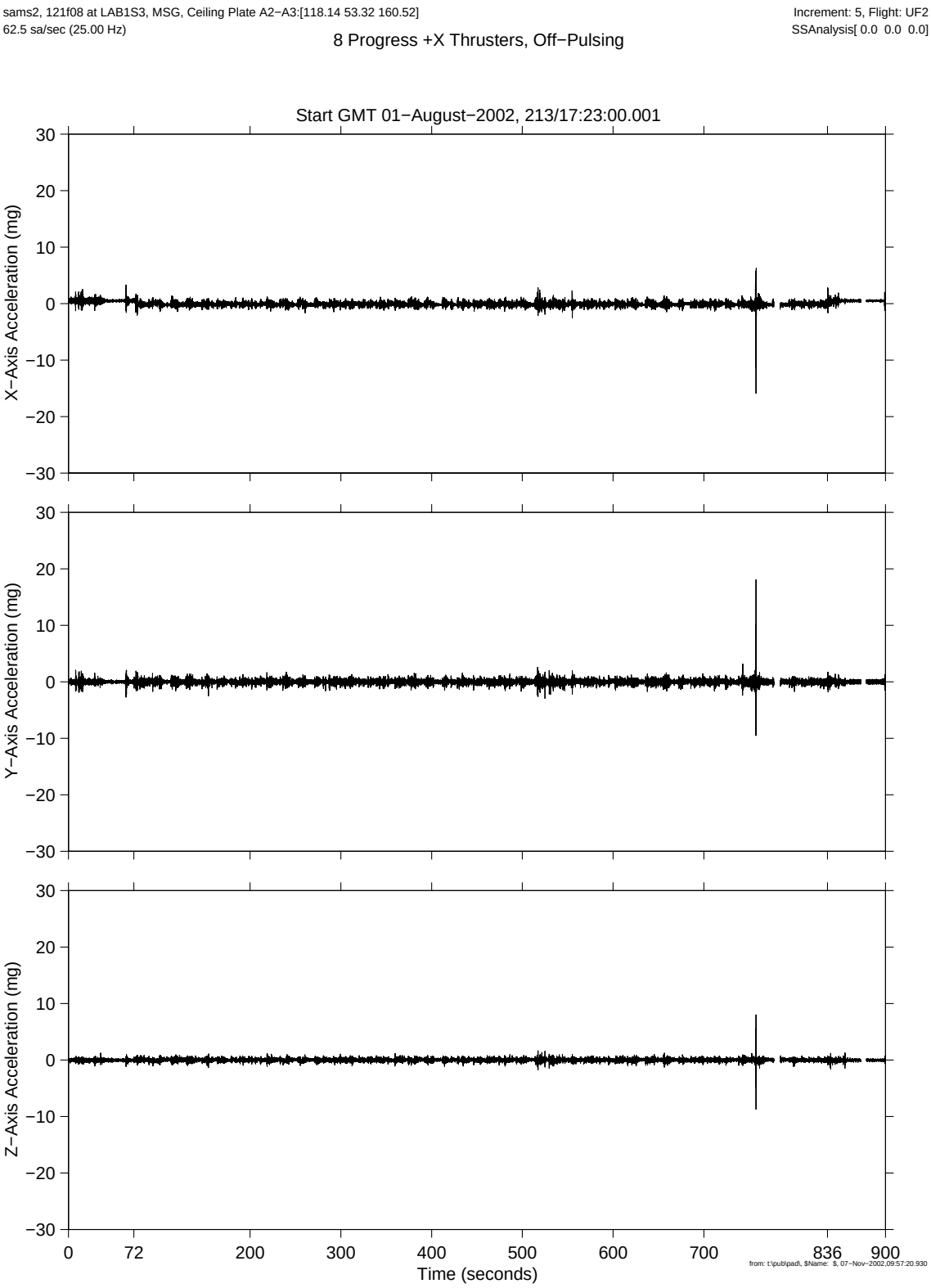

Figure 6-83 Time Series of Progress Reboost With Off Pulsing (121f08)

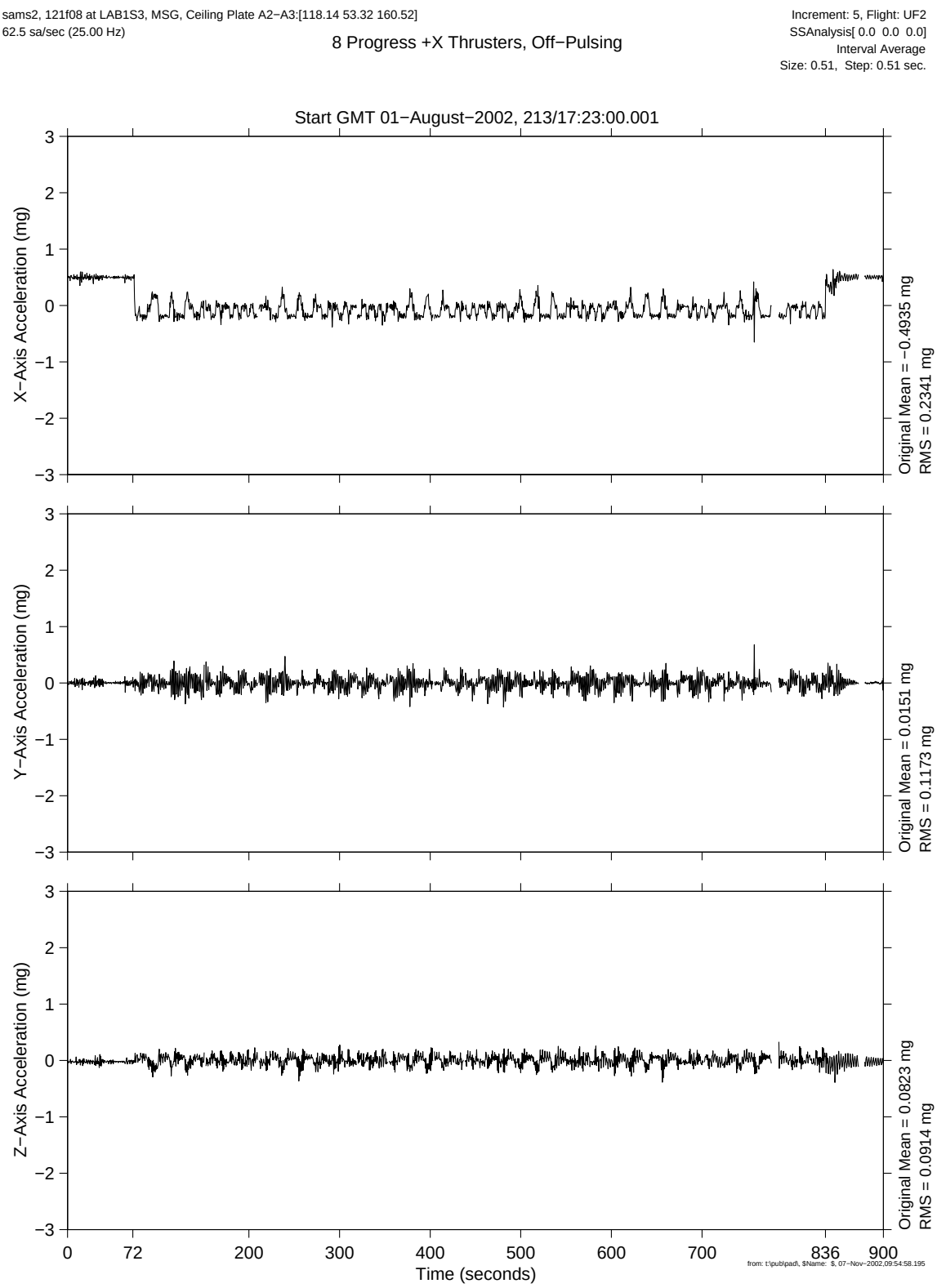

Figure 6-84 Interval Average of Progress Reboost With Off Pulsing (121f08)

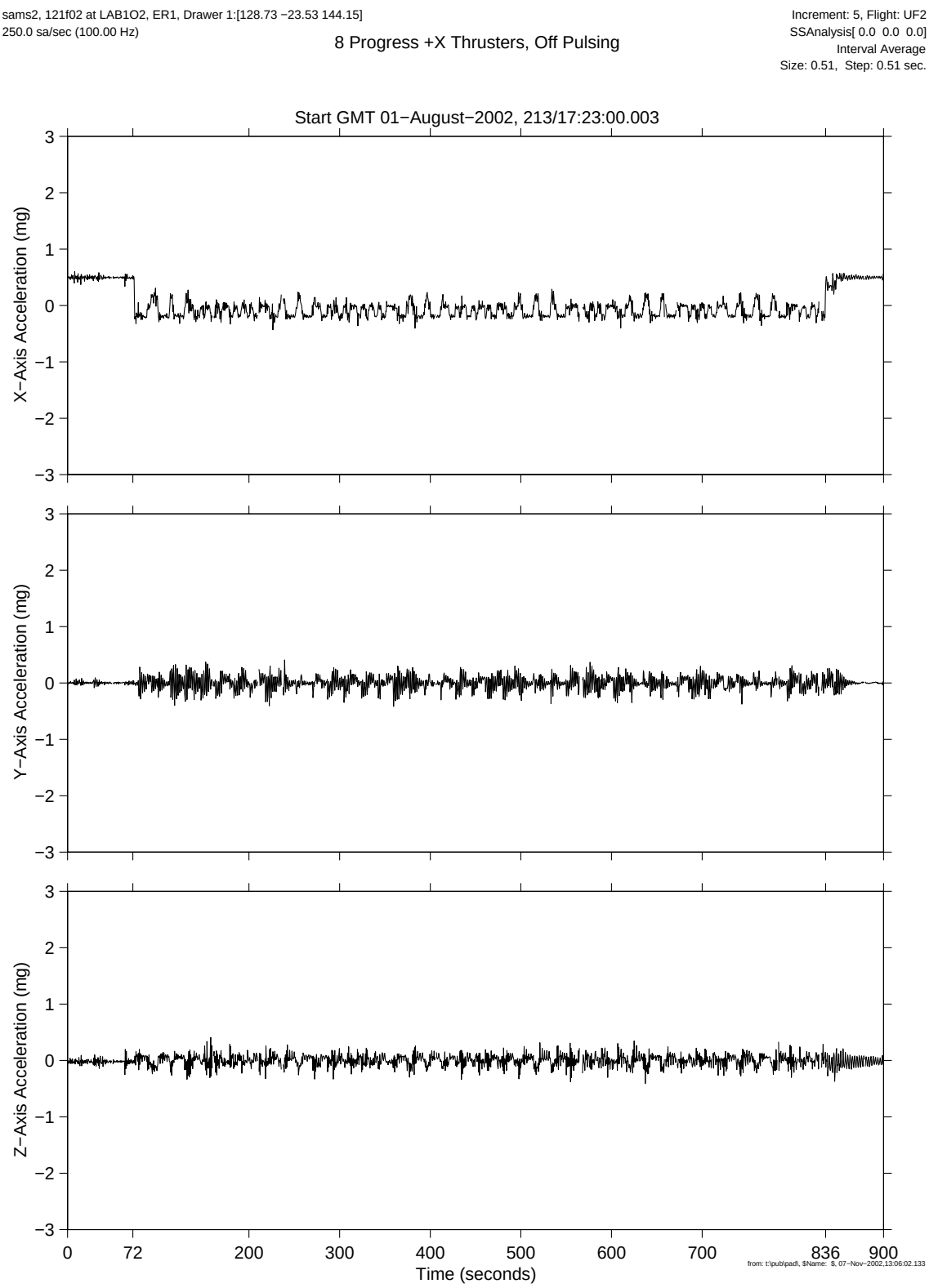

Figure 6-85 Interval Average of Progress Reboost With Off Pulsing (121f02)

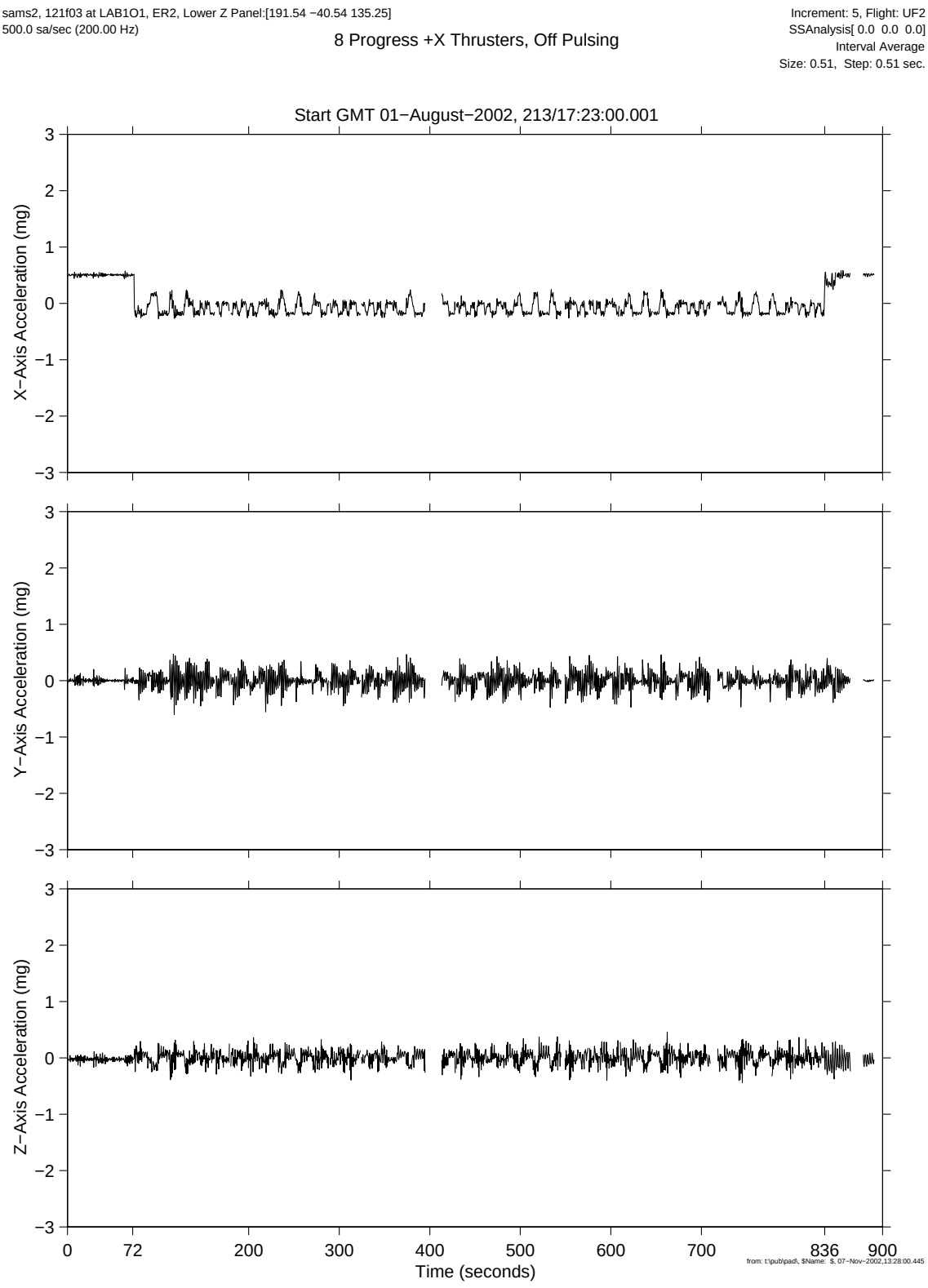

Figure 6-86 Interval Average of Progress Reboost With Off Pulsing (121f03)

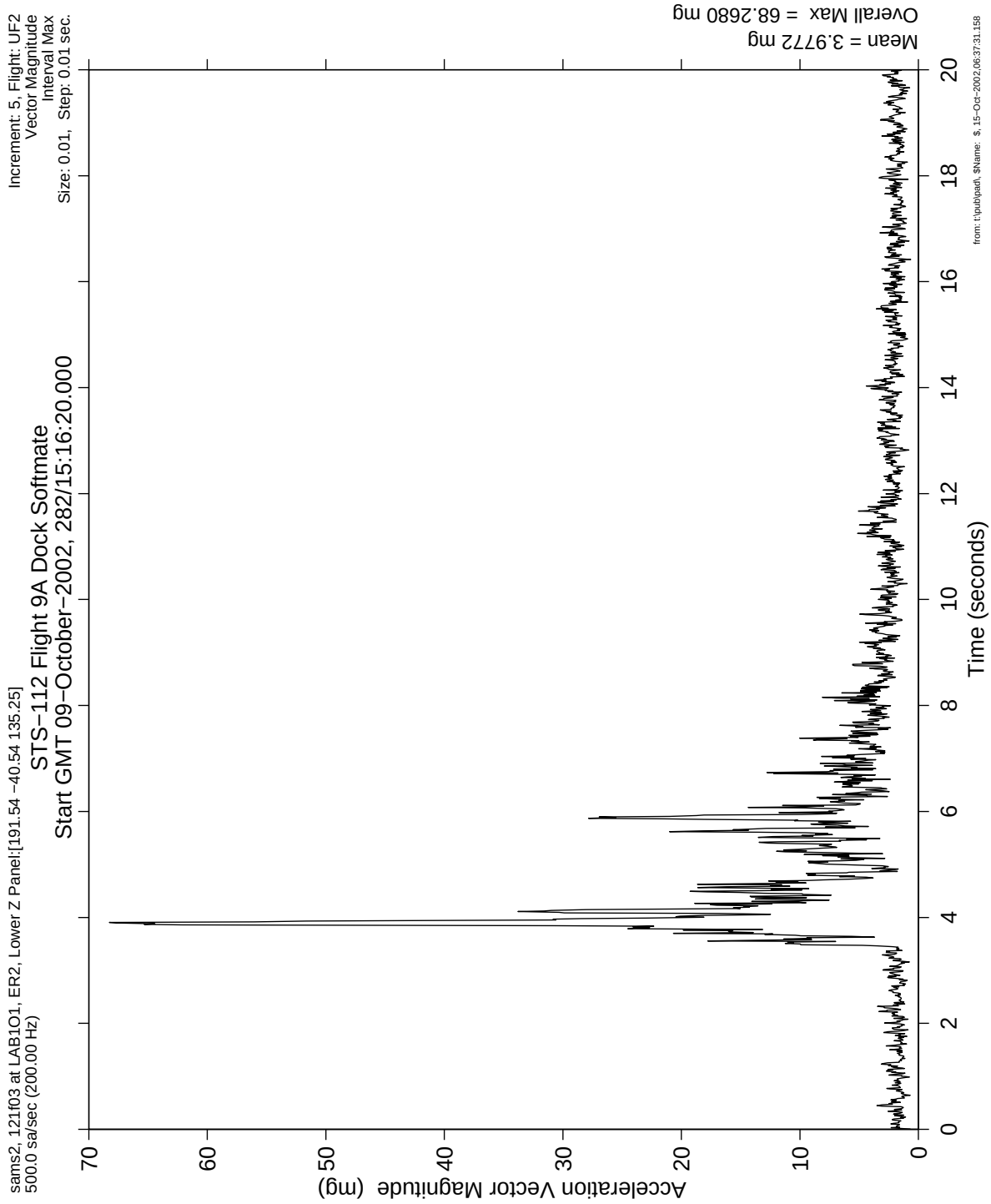

Figure 6-87 Interval Maximum of STS-112 Docking Softmate (121f03)

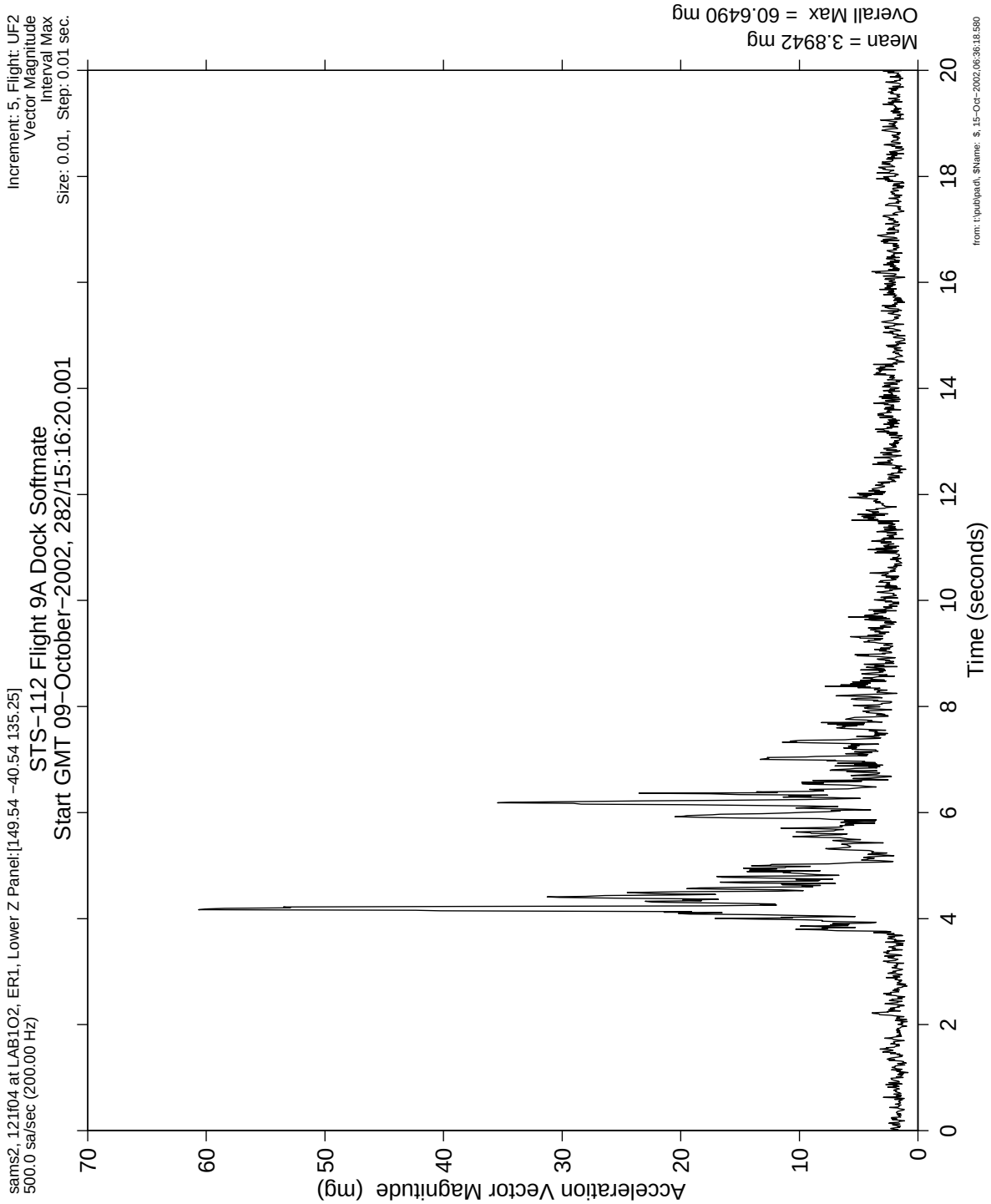

Figure 6-88 Interval Maximum of STS-112 Docking Softmate (121f04)

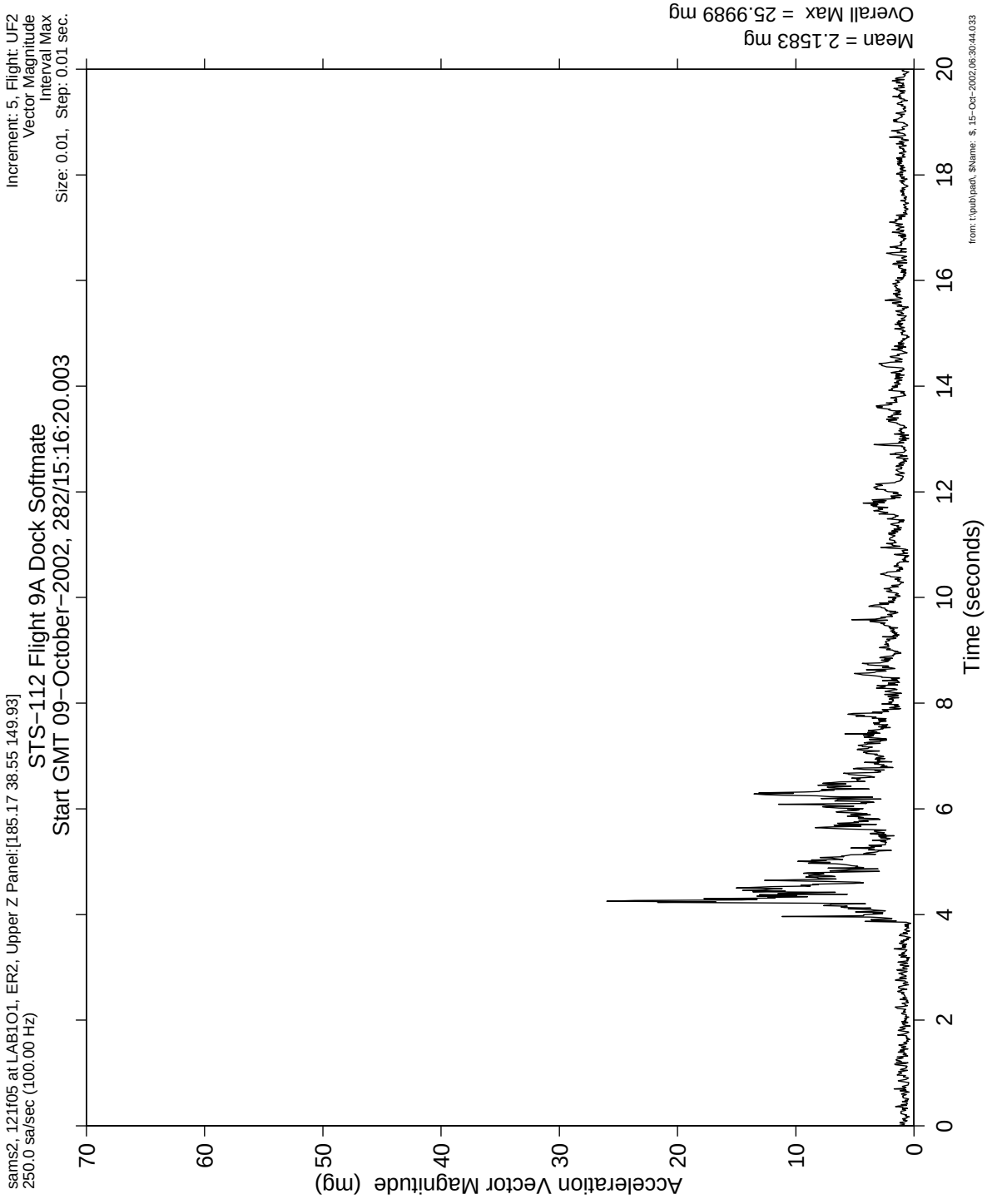

Figure 6-89 Interval Maximum of STS-112 Docking Softmate (121f05)

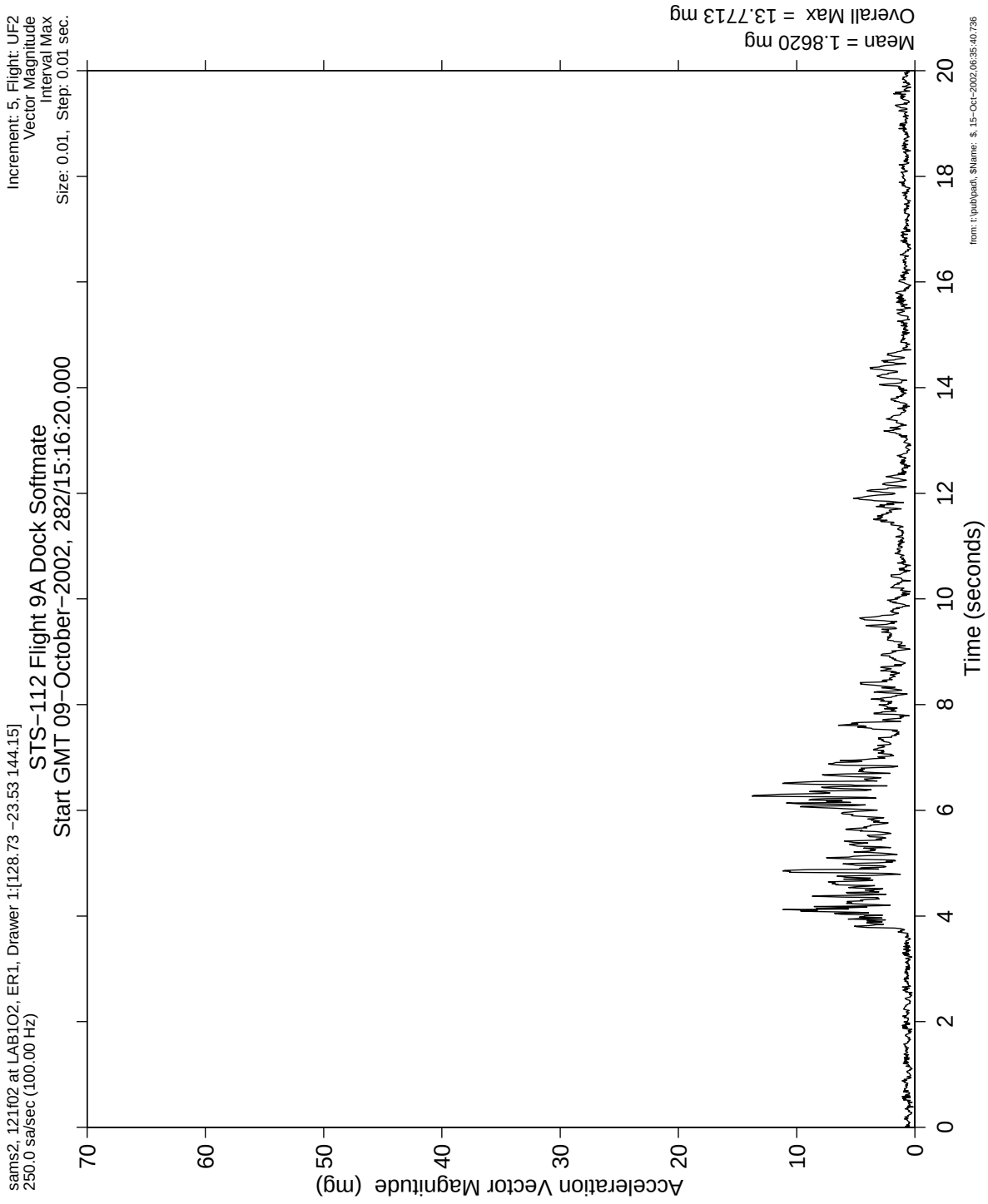

Figure 6-90 Interval Maximum of STS-112 Docking Softmate (121f02)

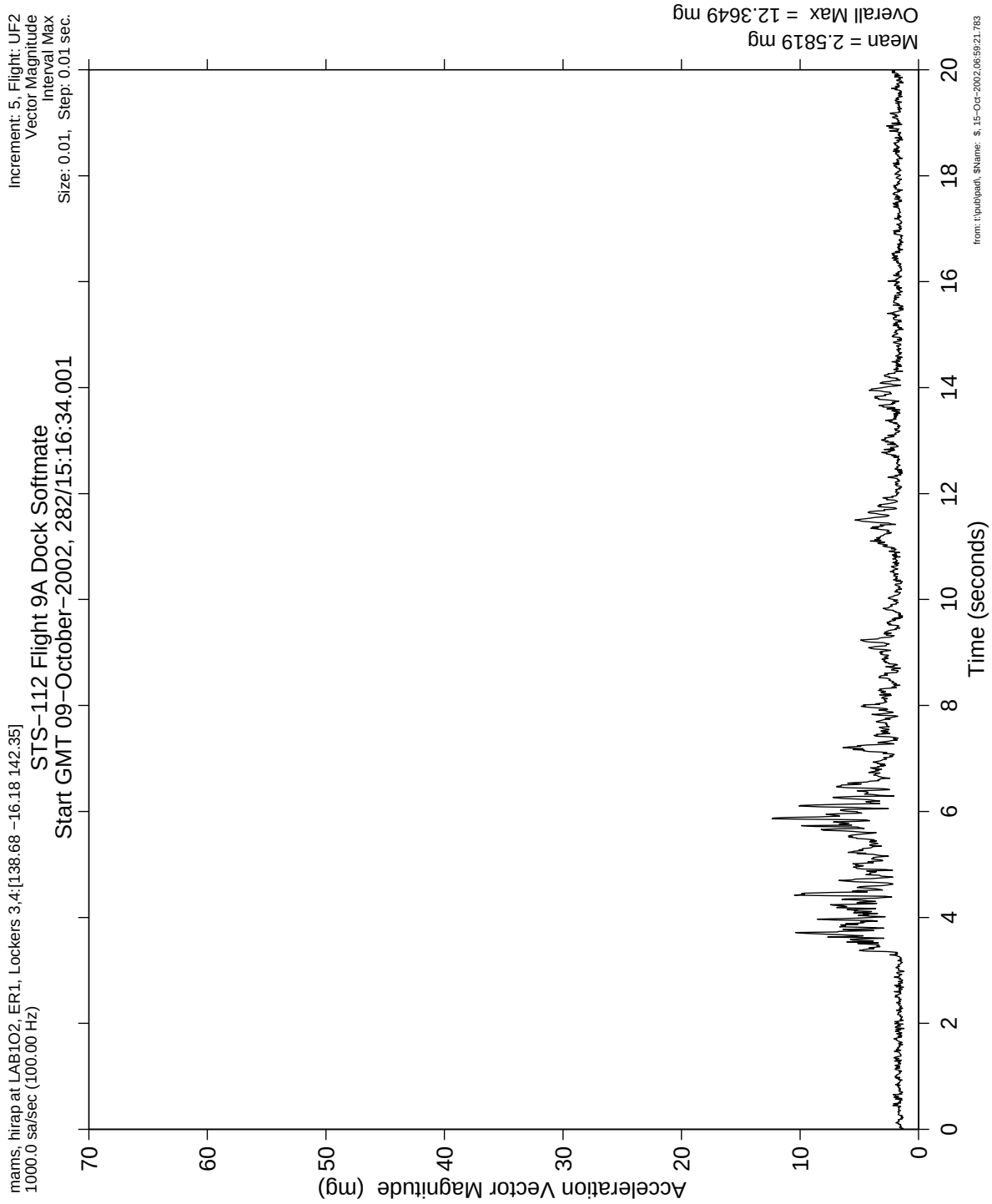

Figure 6-91 Interval Maximum of STS-112 Docking Softmate (HiRAP)

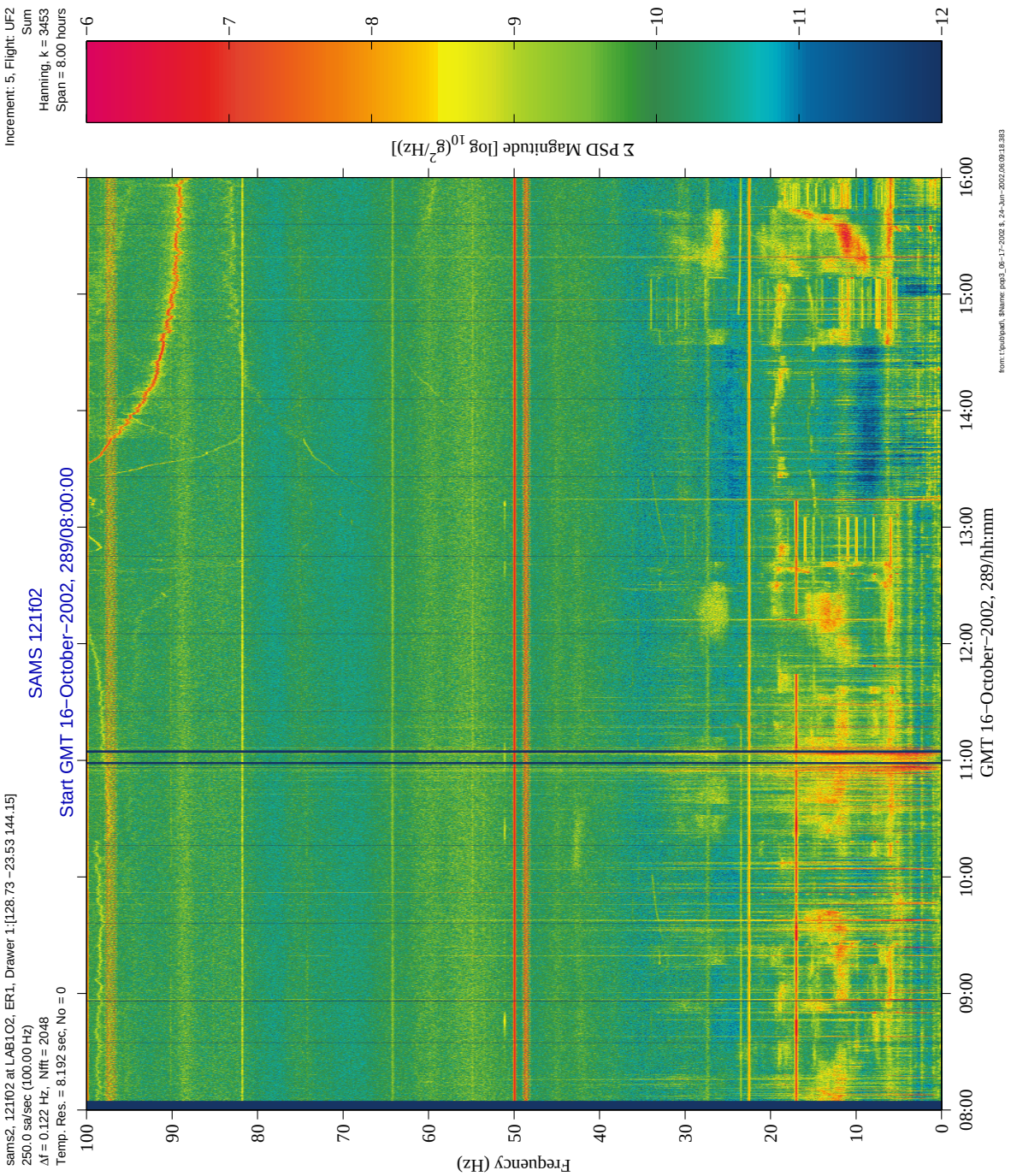

Figure 6-92 Spectrogram of STS-112 Undocking (121f02)

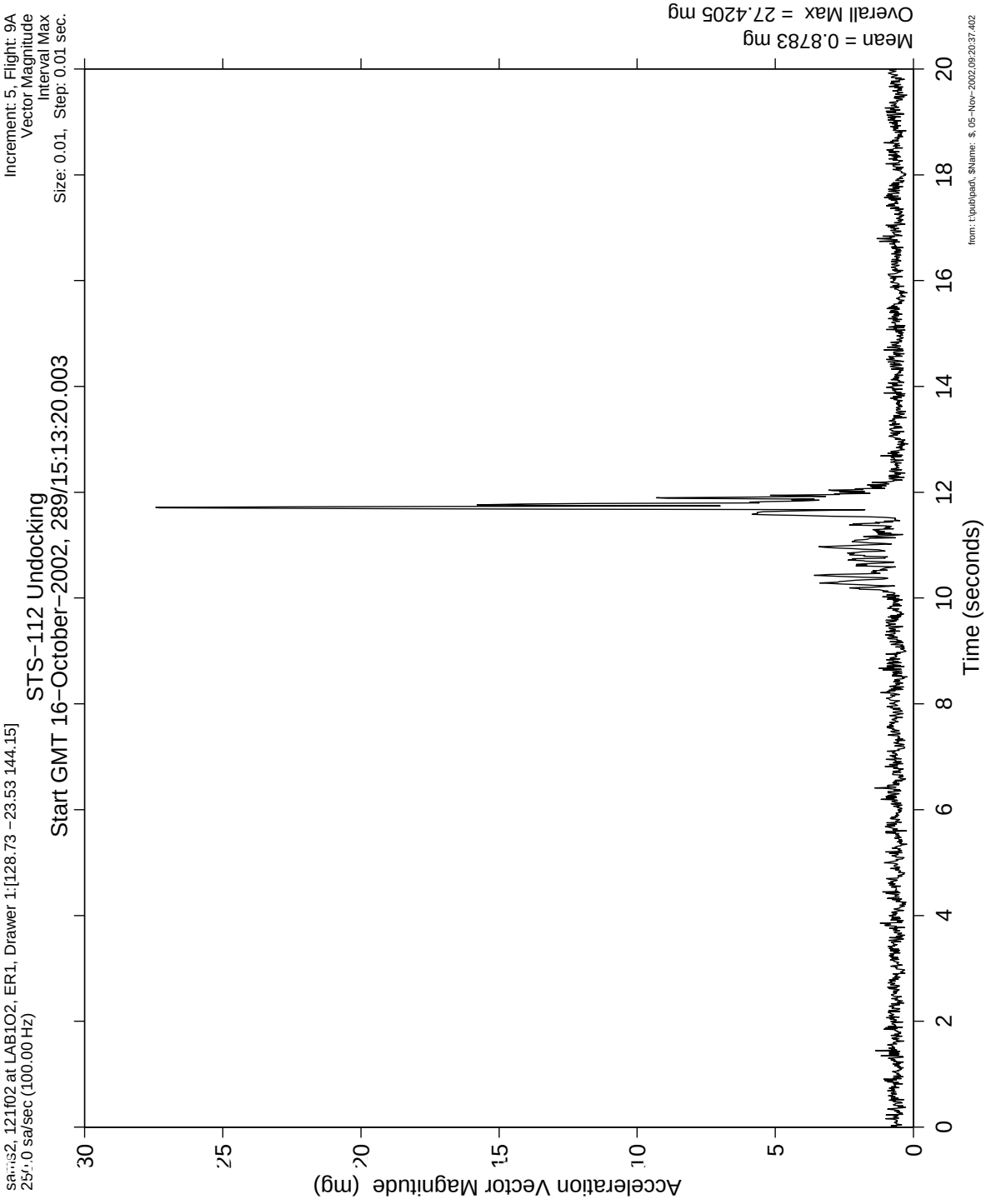

Figure 6-93 Interval Maximum of STS-112 Undocking (121f02)

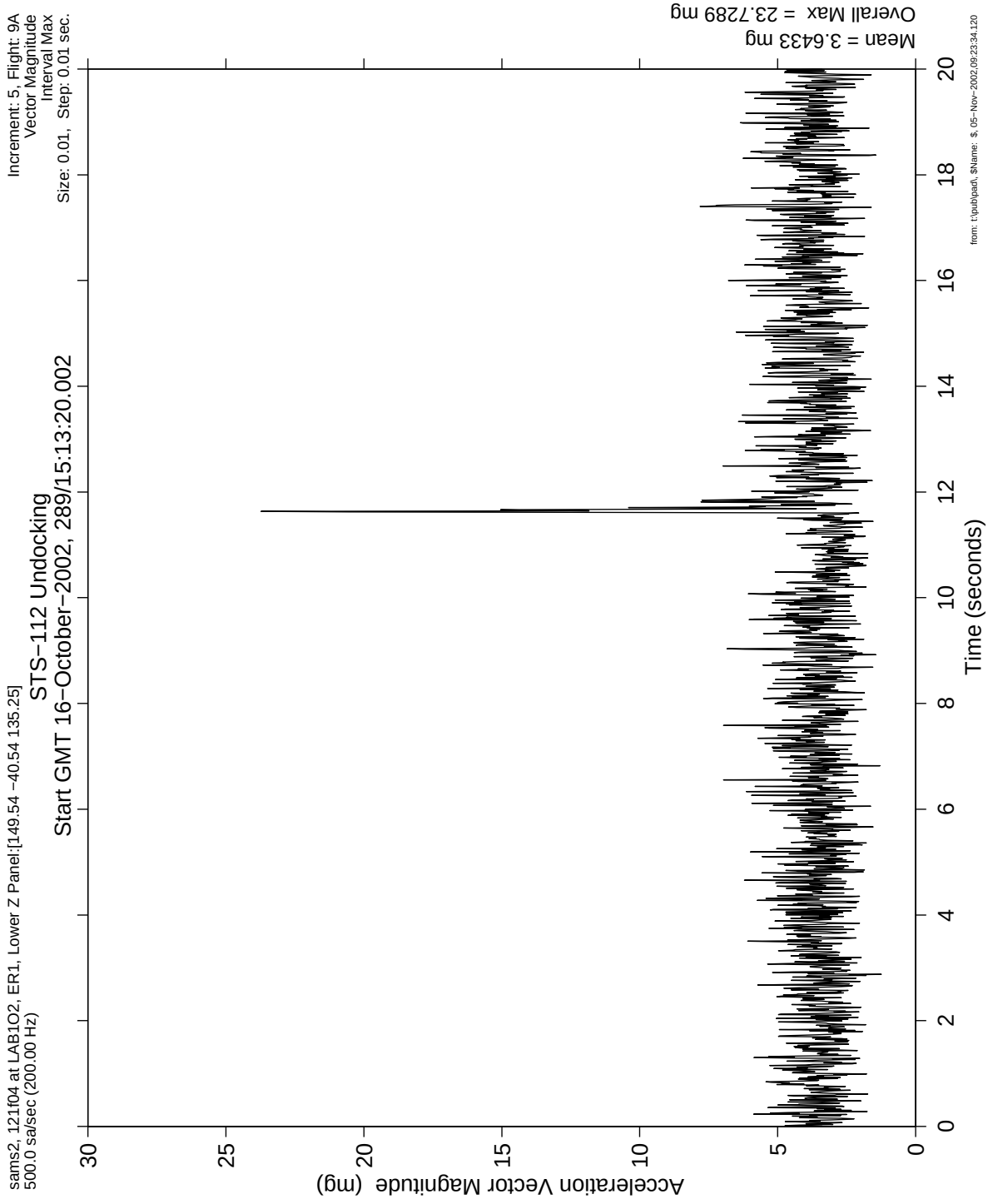

Figure 6-94 Interval Maximum of STS-112 Undocking (121f04)

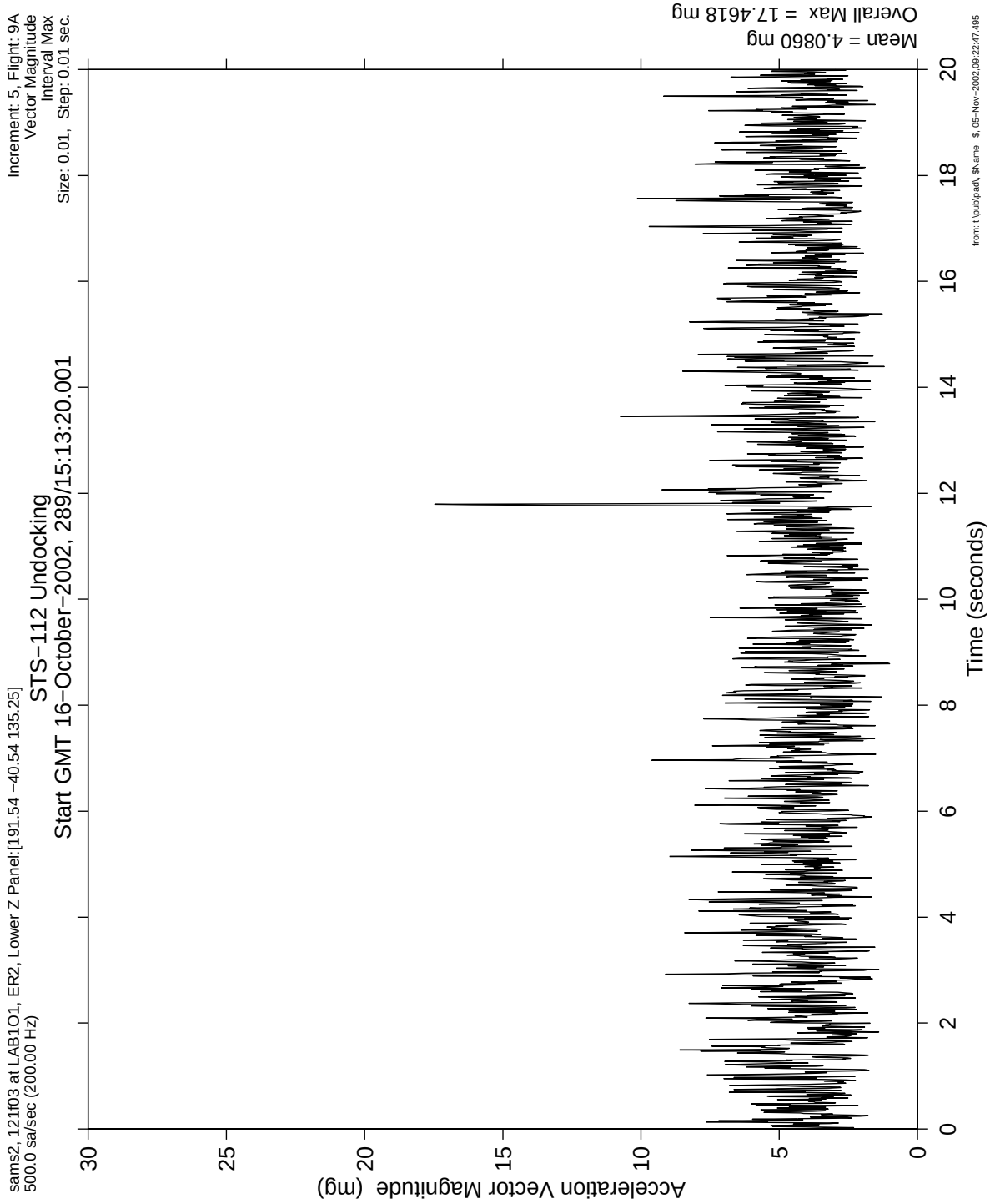

Figure 6-95 Interval Maximum of STS-112 Undocking (121f03)

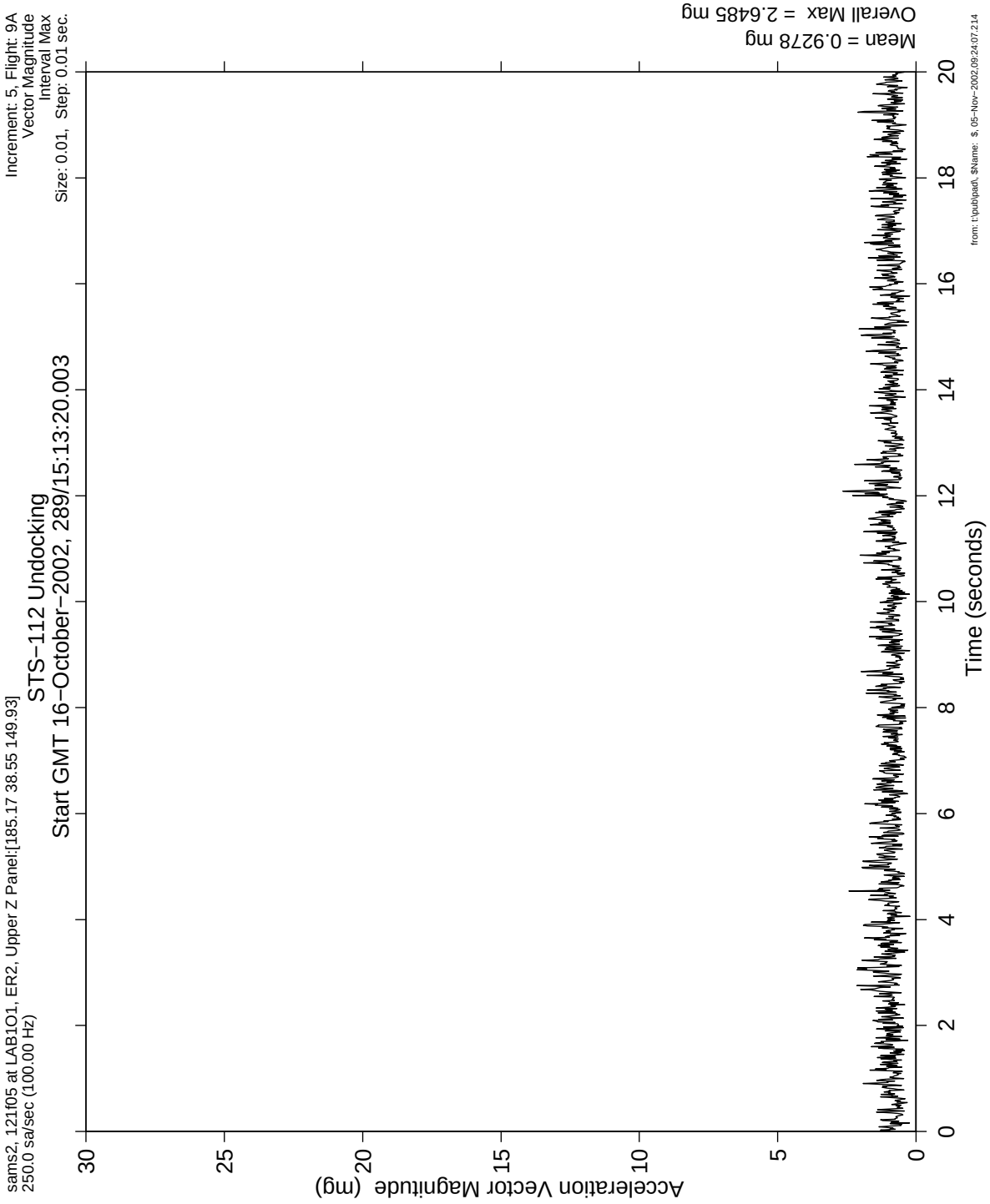

Figure 6-96 Interval Maximum of STS-112 Undocking (121f05)

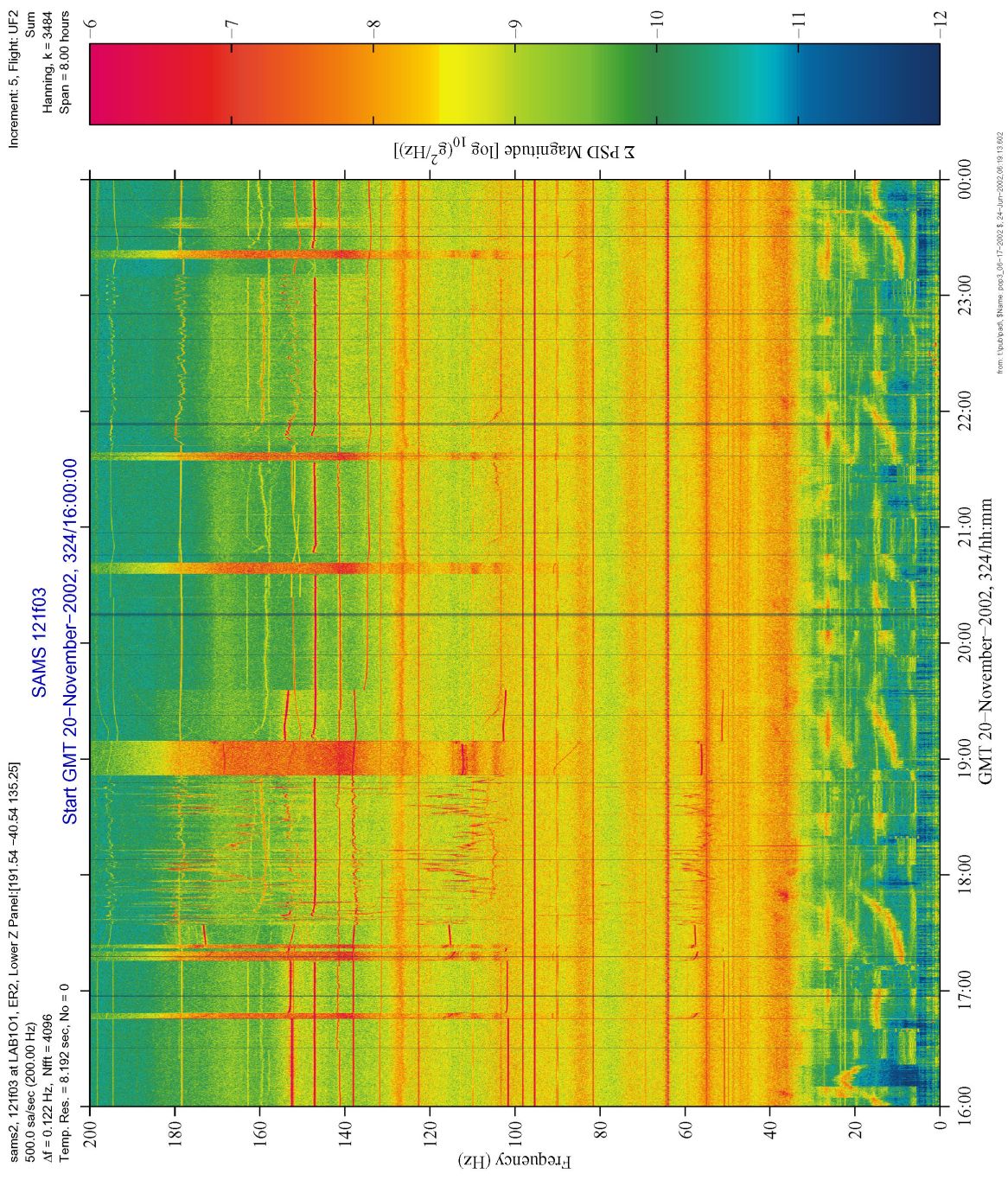

Figure 6-97 Spectrogram of ARIS Transitions (121f03)

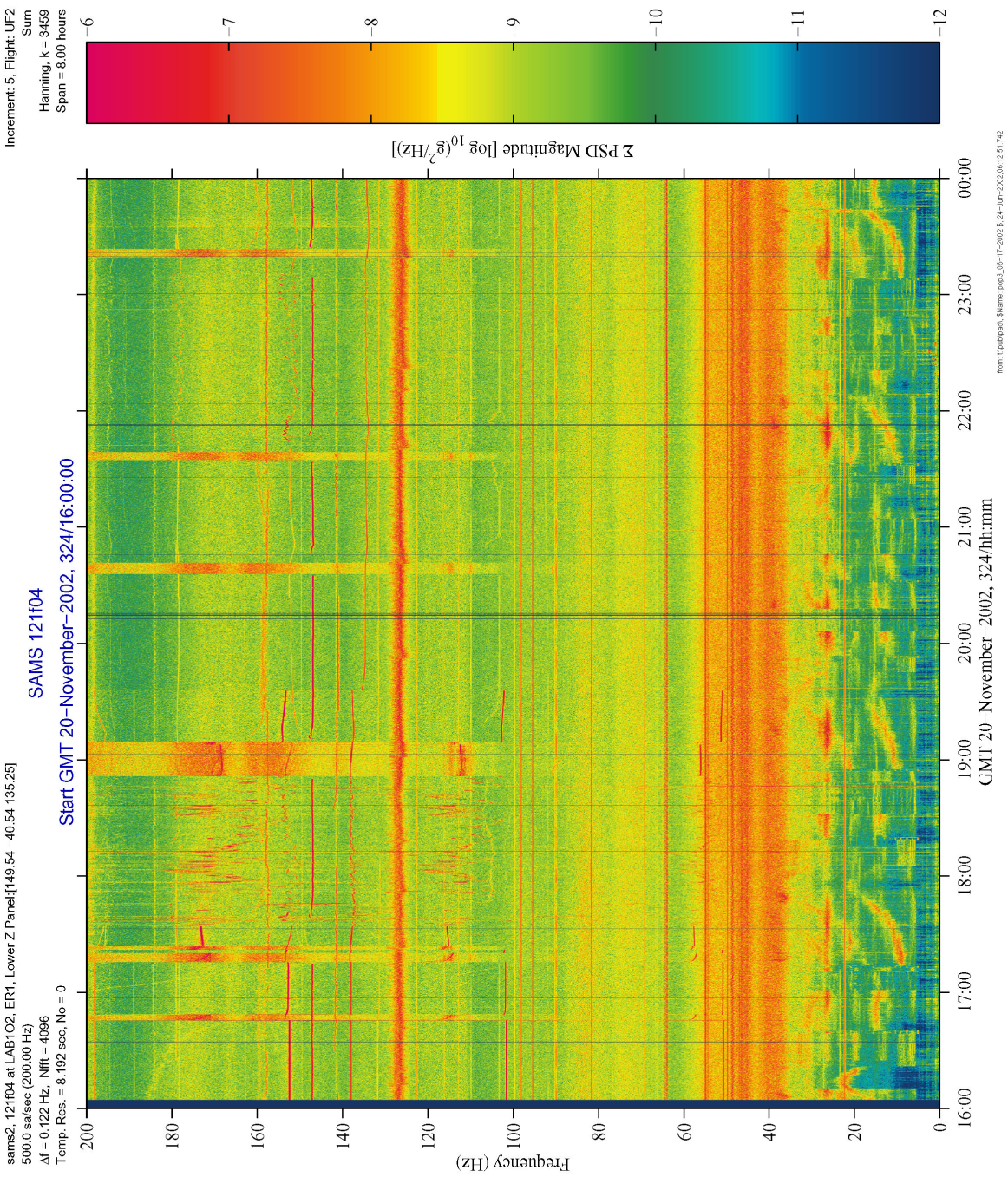

Figure 6-98 Spectrogram of ARIS Transitions (121f04)

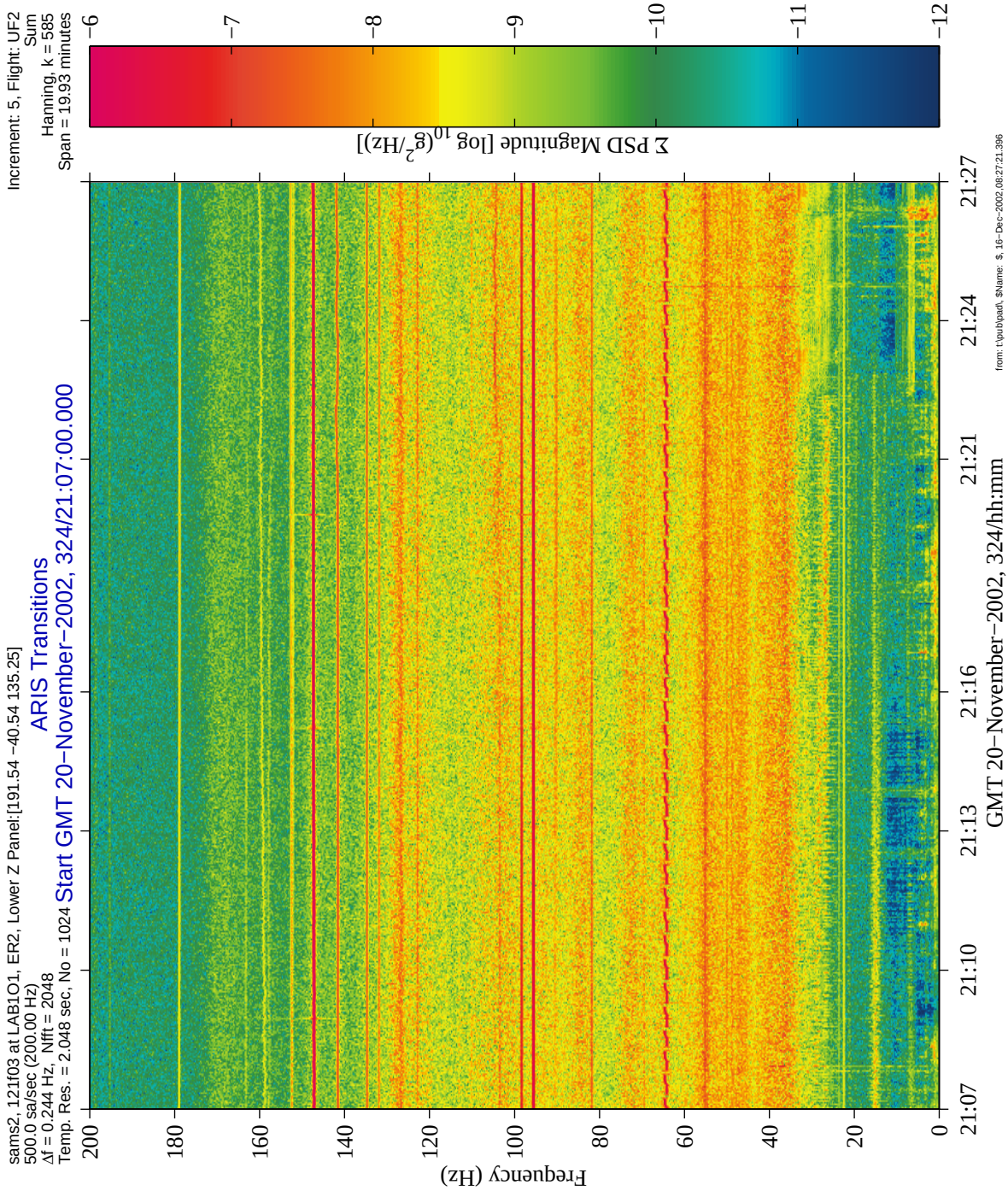

Figure 6-99 Spectrogram of ARIS HOLD and ACTIVE Transitions (121f03)

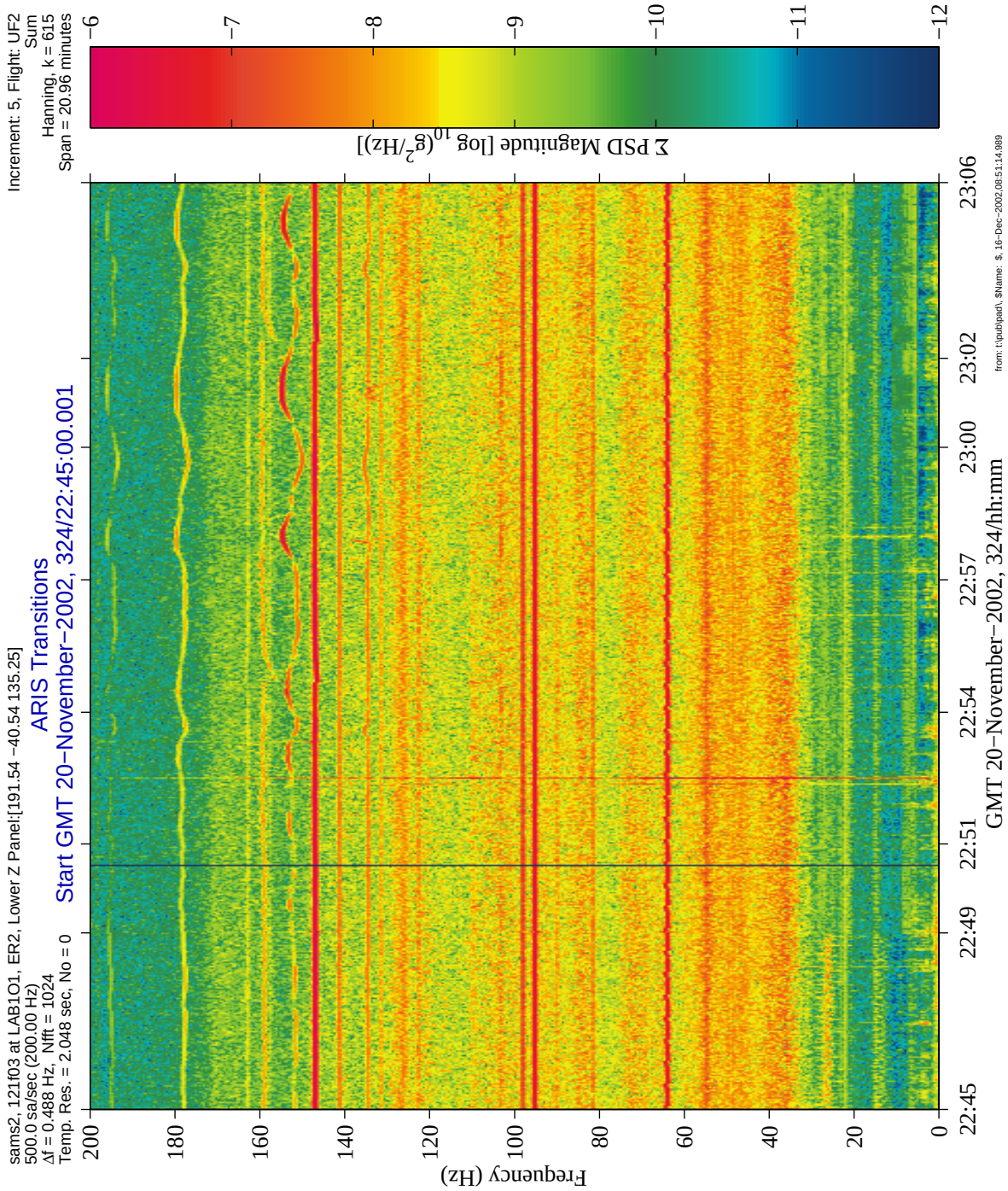

Figure 6-100 Spectrogram of ARIS REST and IDLE Transitions (121f03)

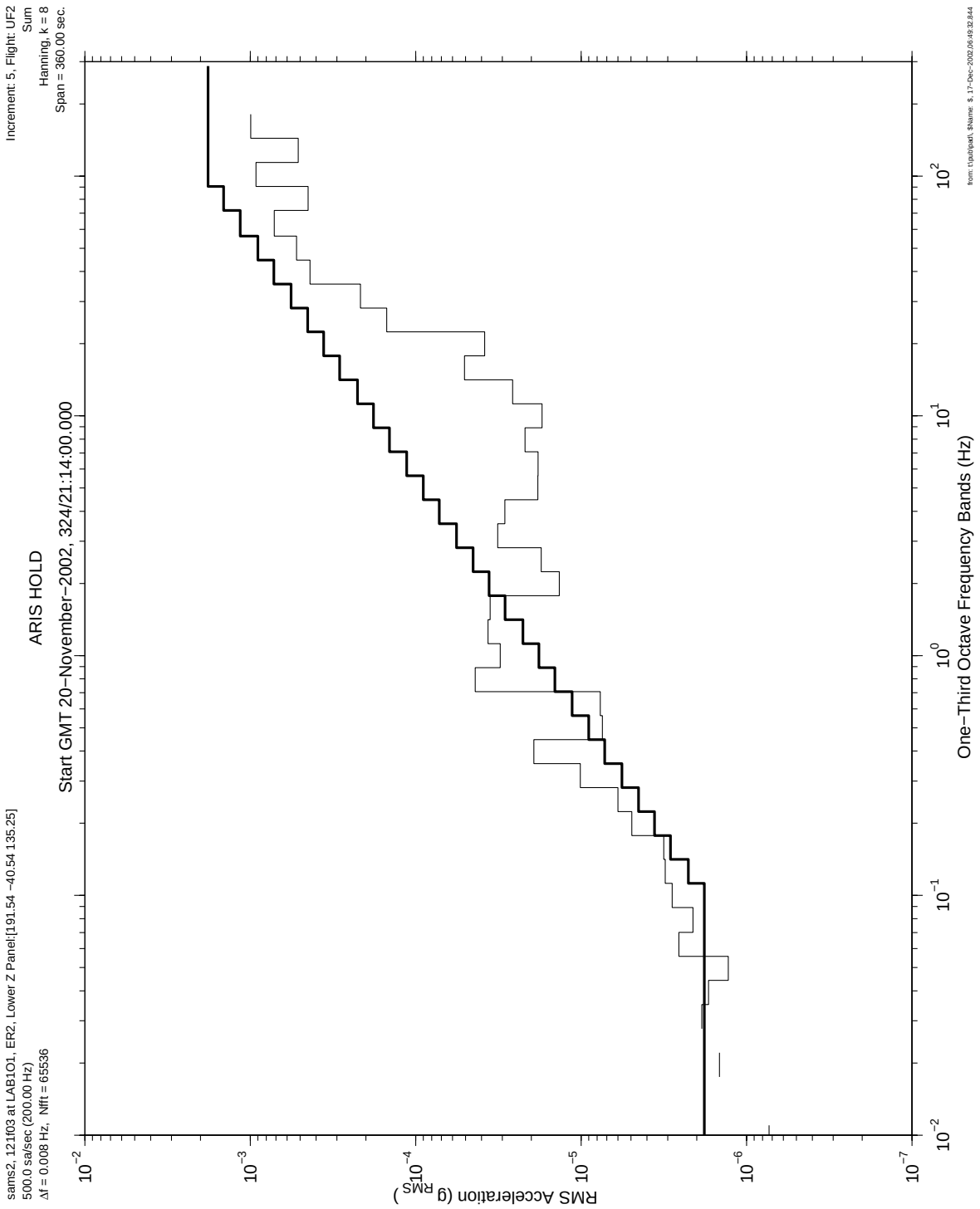

Figure 6-101 One-Third Octave RMS of ARIS HOLD (121f03)

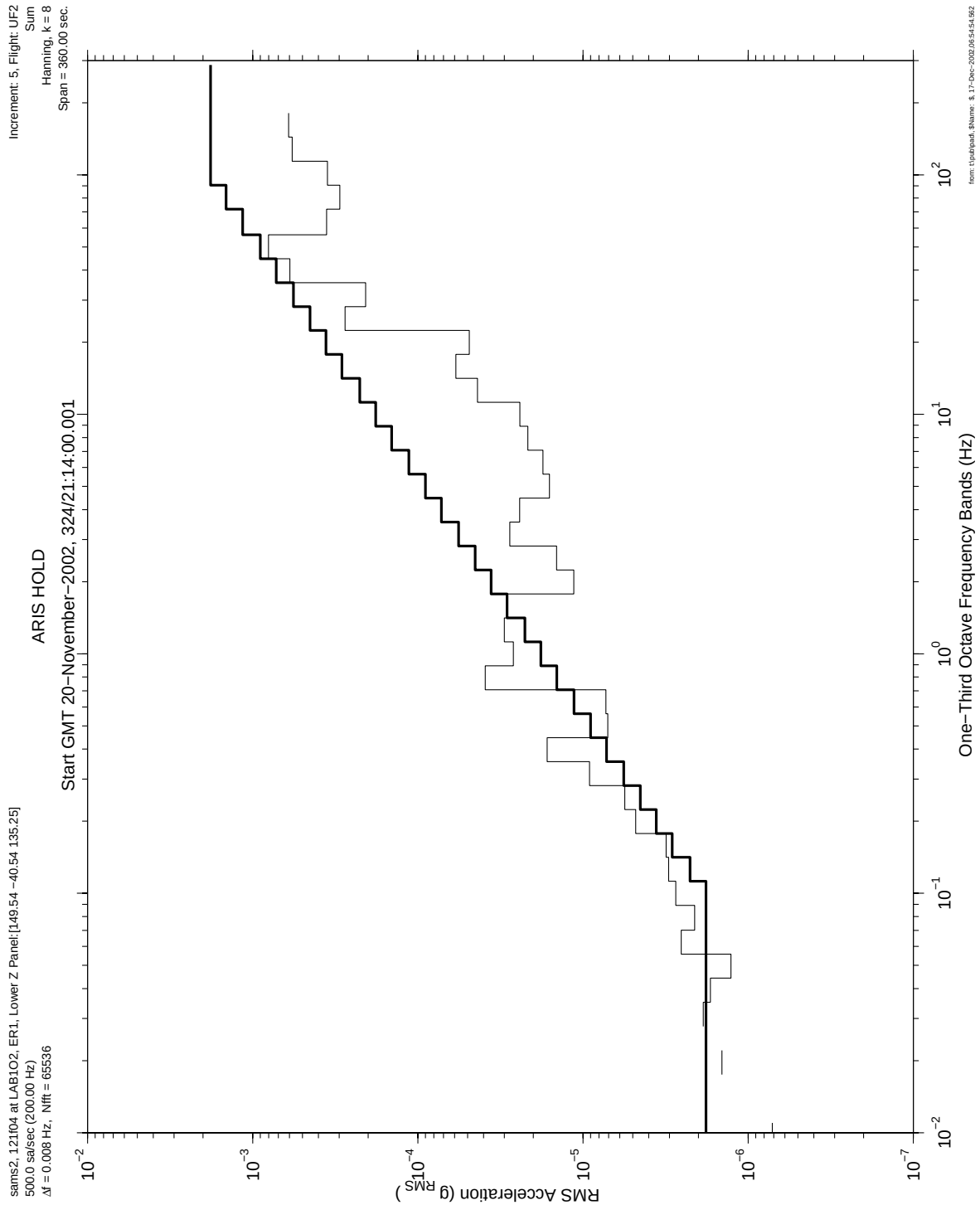

Figure 6-102 One-Third Octave RMS of ARIS HOLD (121f04)

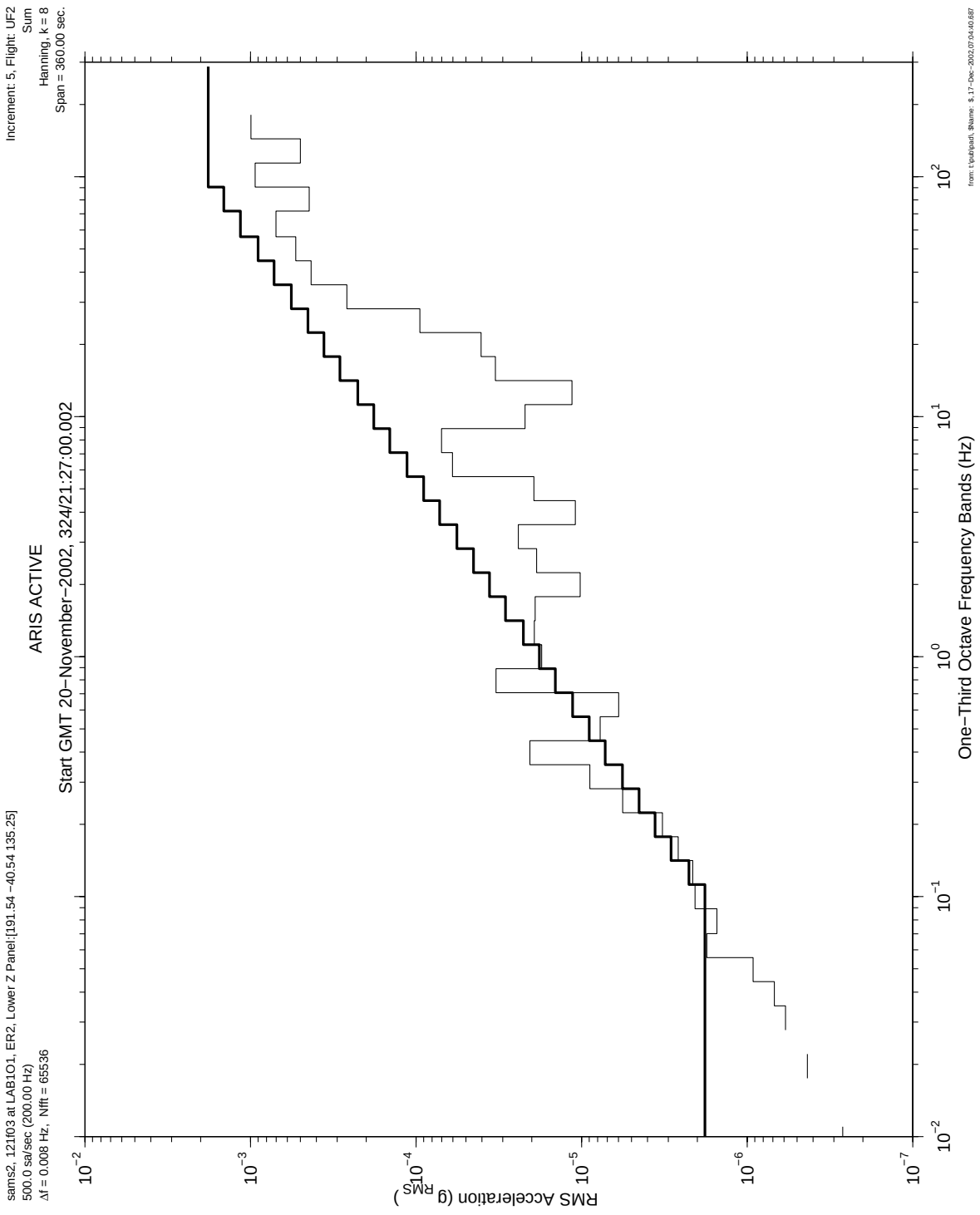

Figure 6-103 One-Third Octave RMS of ARIS ACTIVE (121f03)

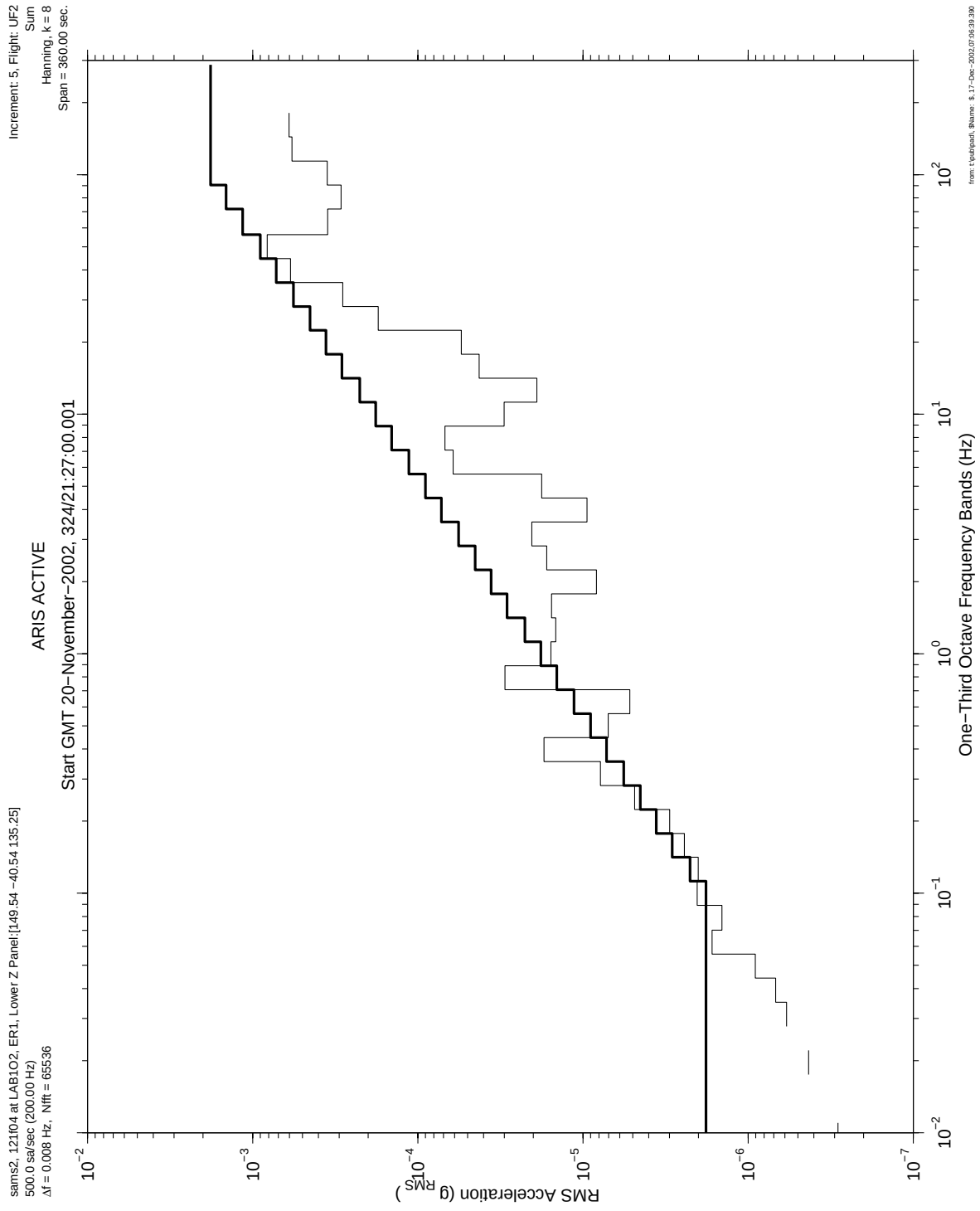

Figure 6-104 One-Third Octave RMS of ARIS ACTIVE (121f04)

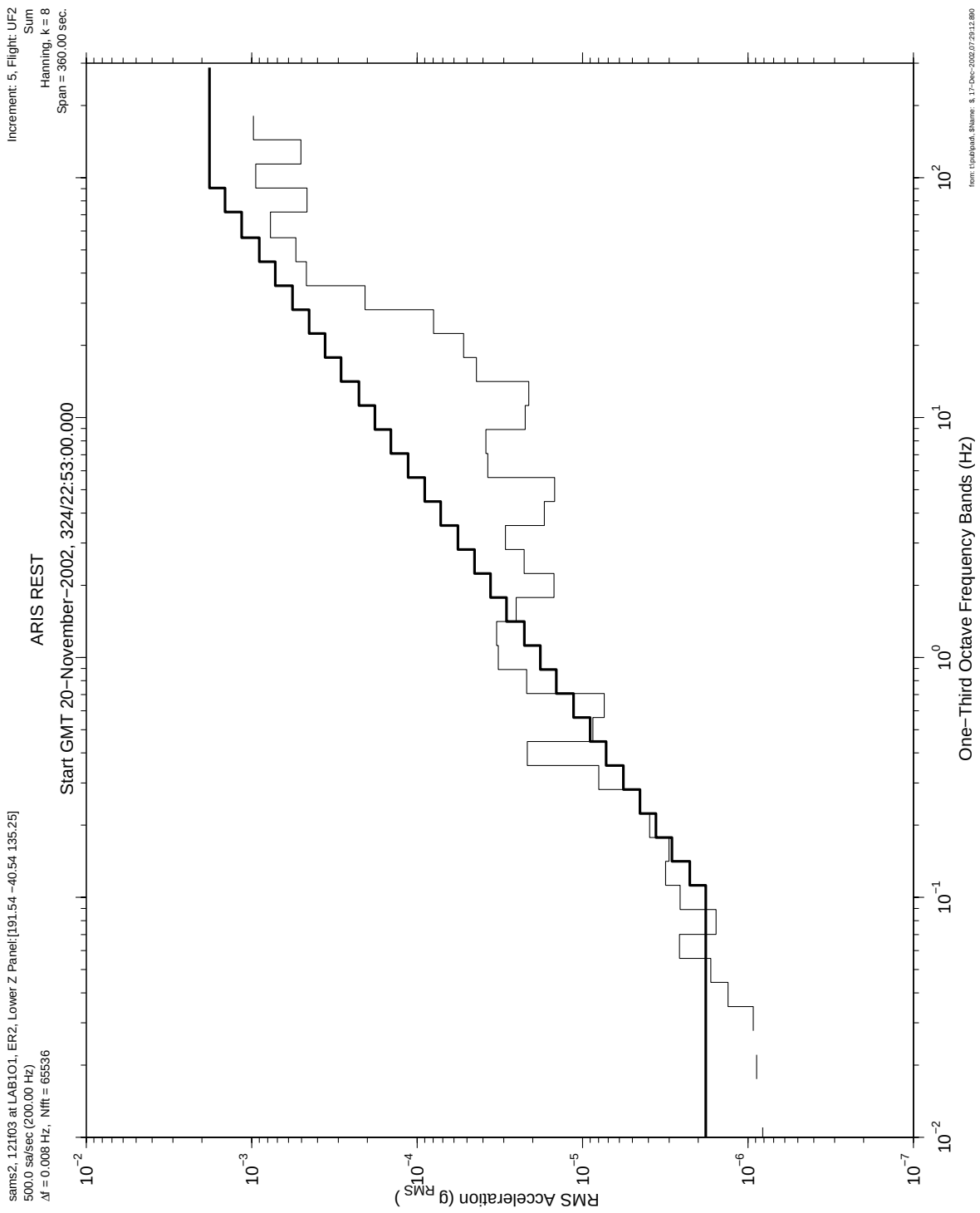

Figure 6-105 One-Third Octave RMS of ARIS REST (121f03)

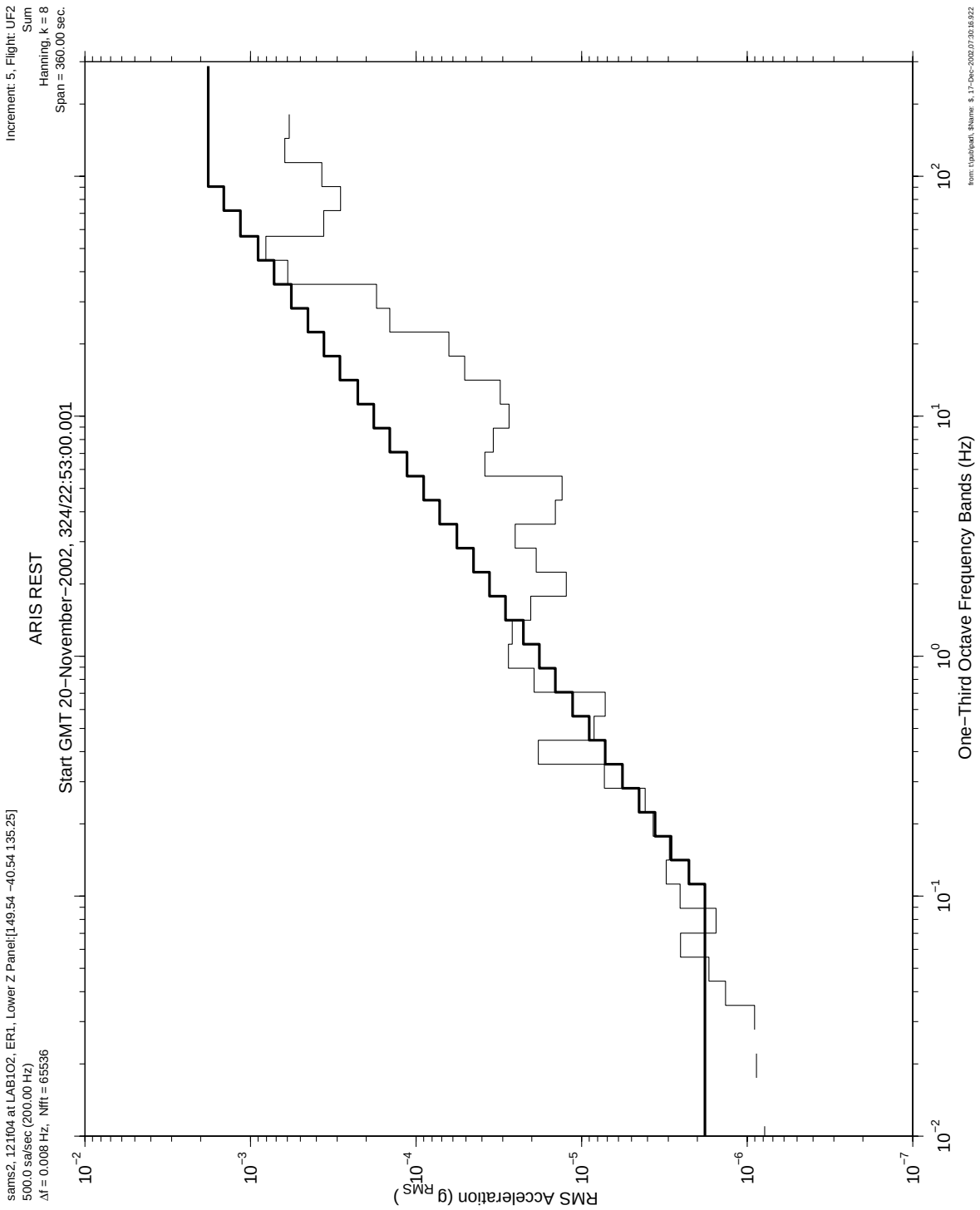

Figure 6-106 One-Third Octave RMS of ARIS REST (121f04)

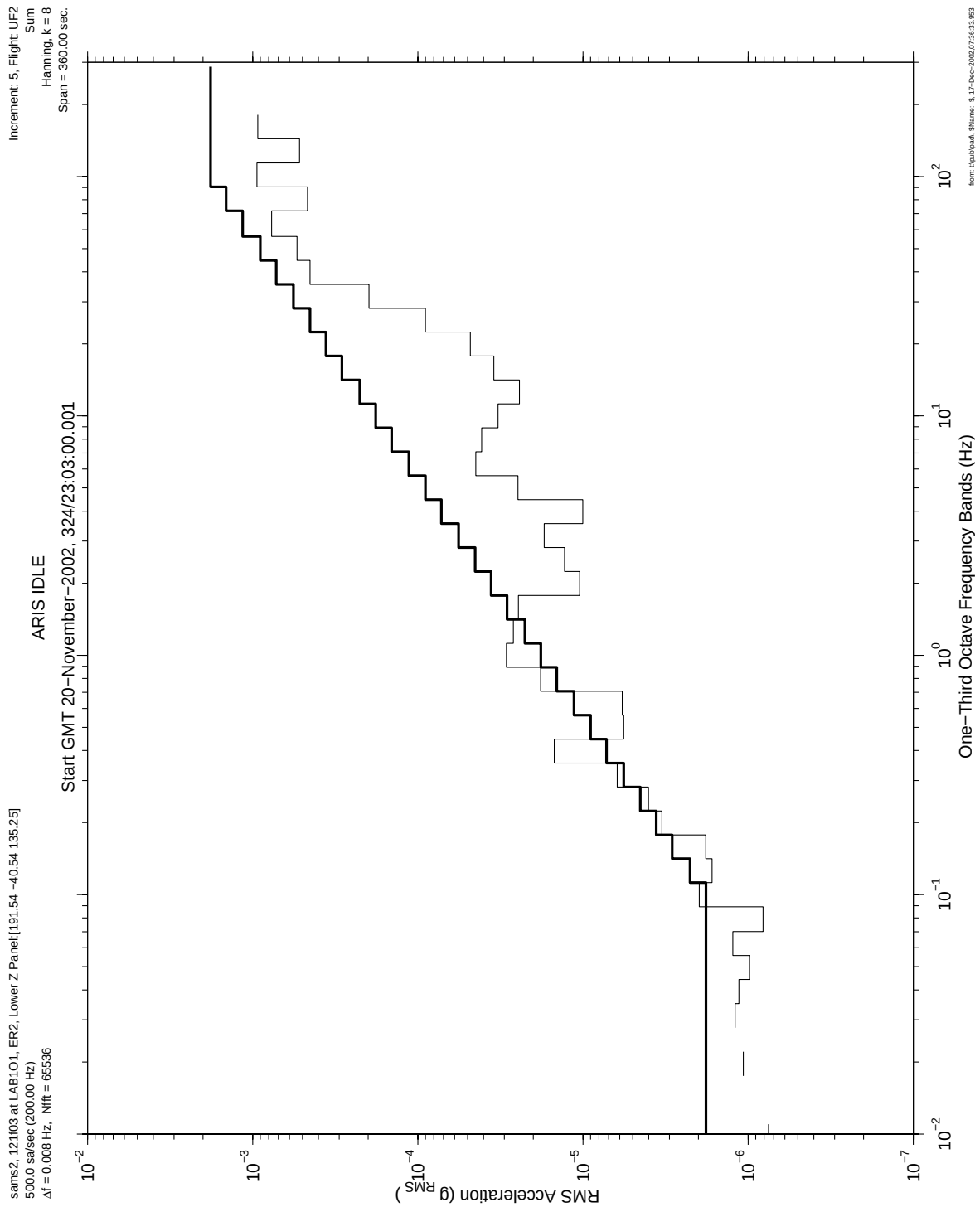

Figure 6-107 One-Third Octave RMS of ARIS IDLE (121f03)

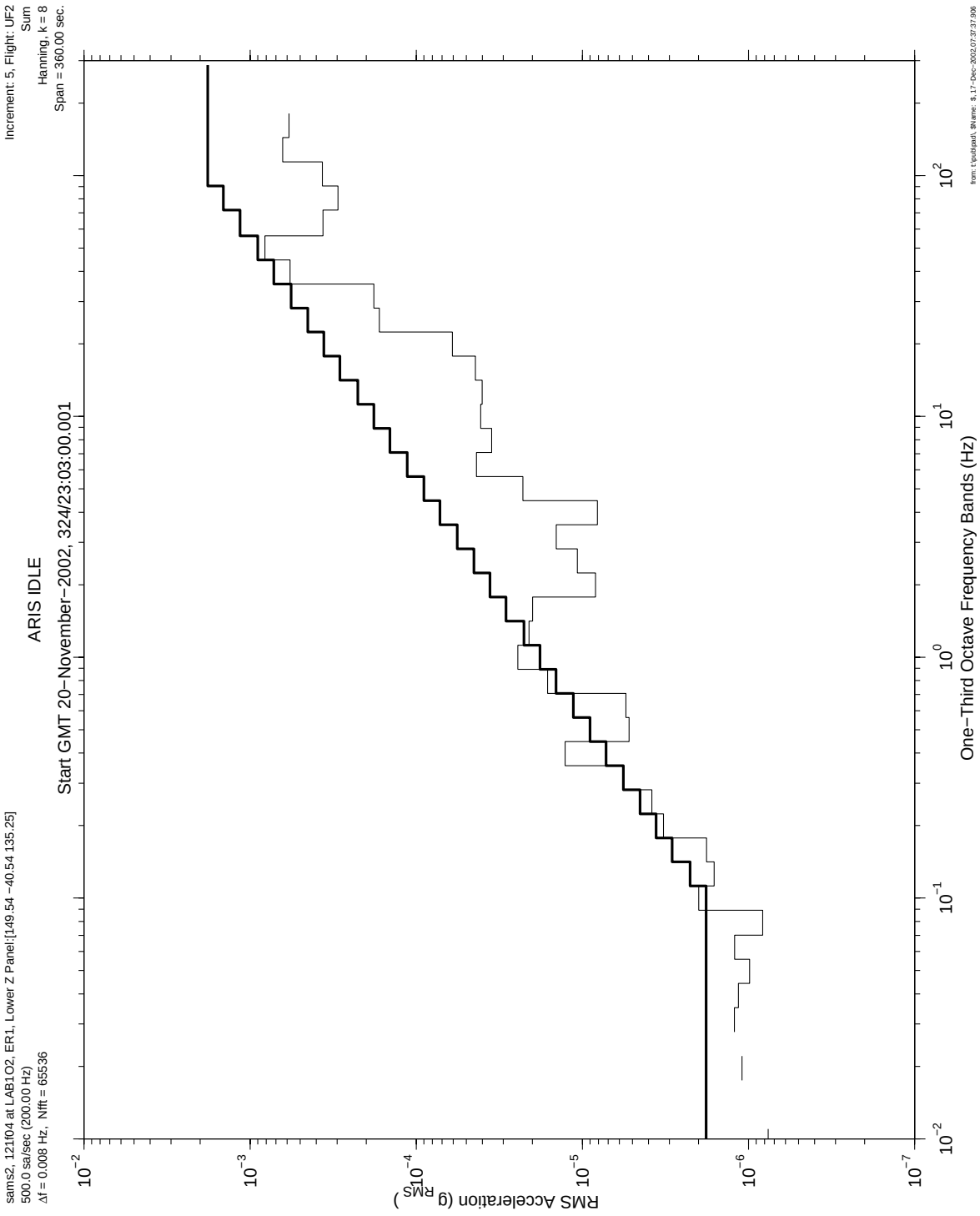

Figure 6-108 One-Third Octave RMS of ARIS IDLE (121f04)

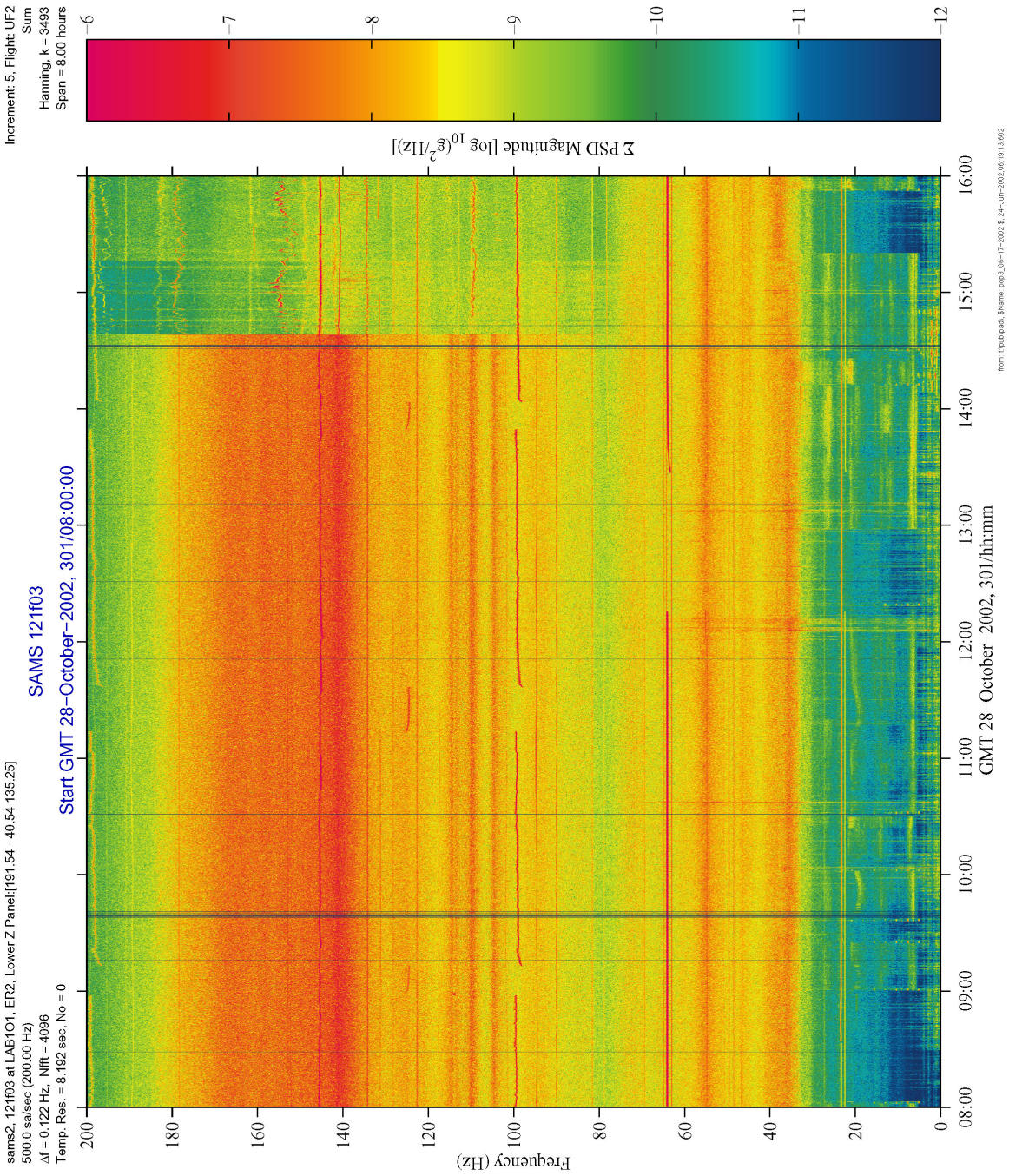

Figure 6-109 Spectrogram of ARIS Transition from HOLD to ACTIVE Mode (121f03)

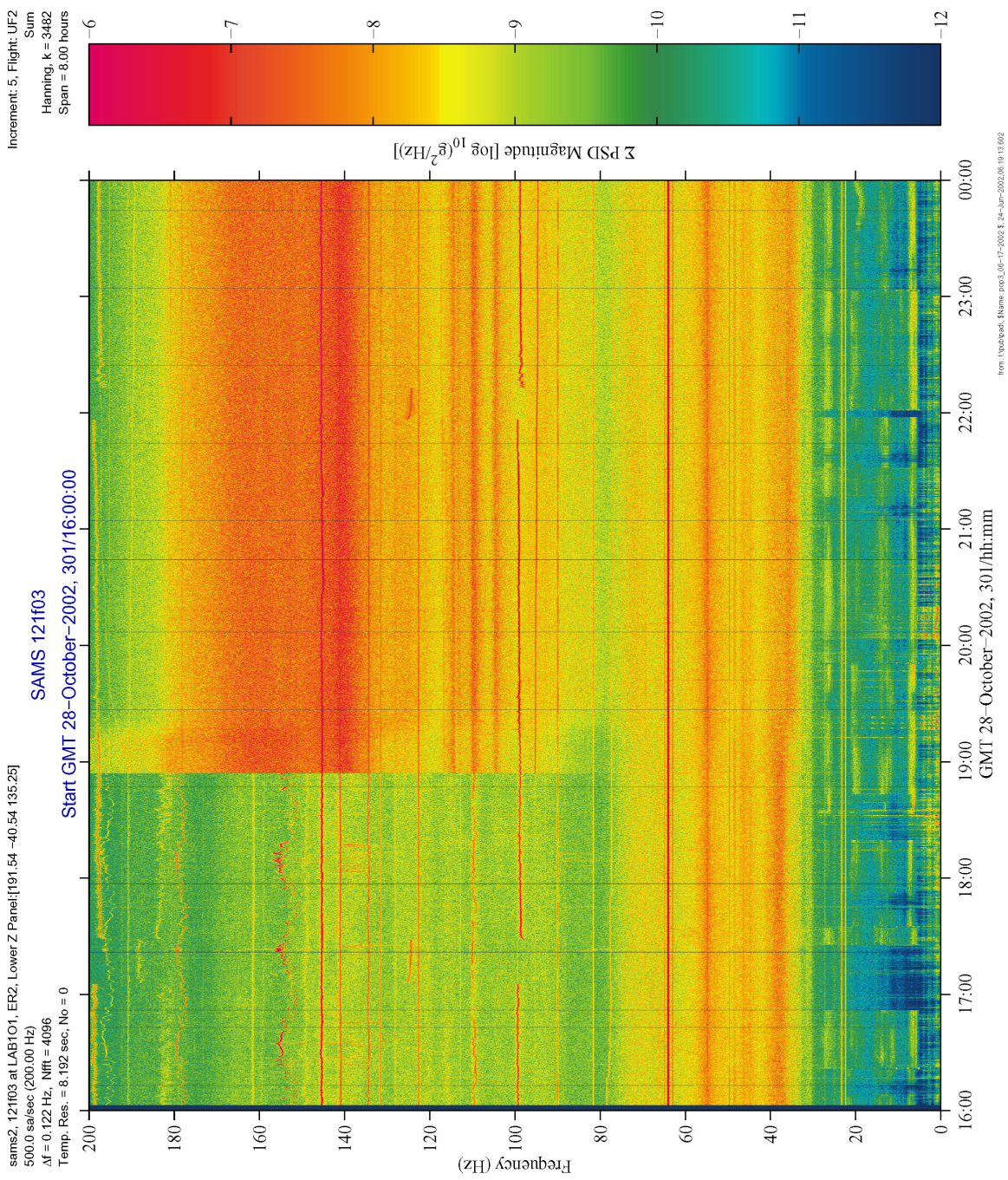

Figure 6-110 Spectrogram of ARIS Transition from ACTIVE to HOLD Mode (121f03)

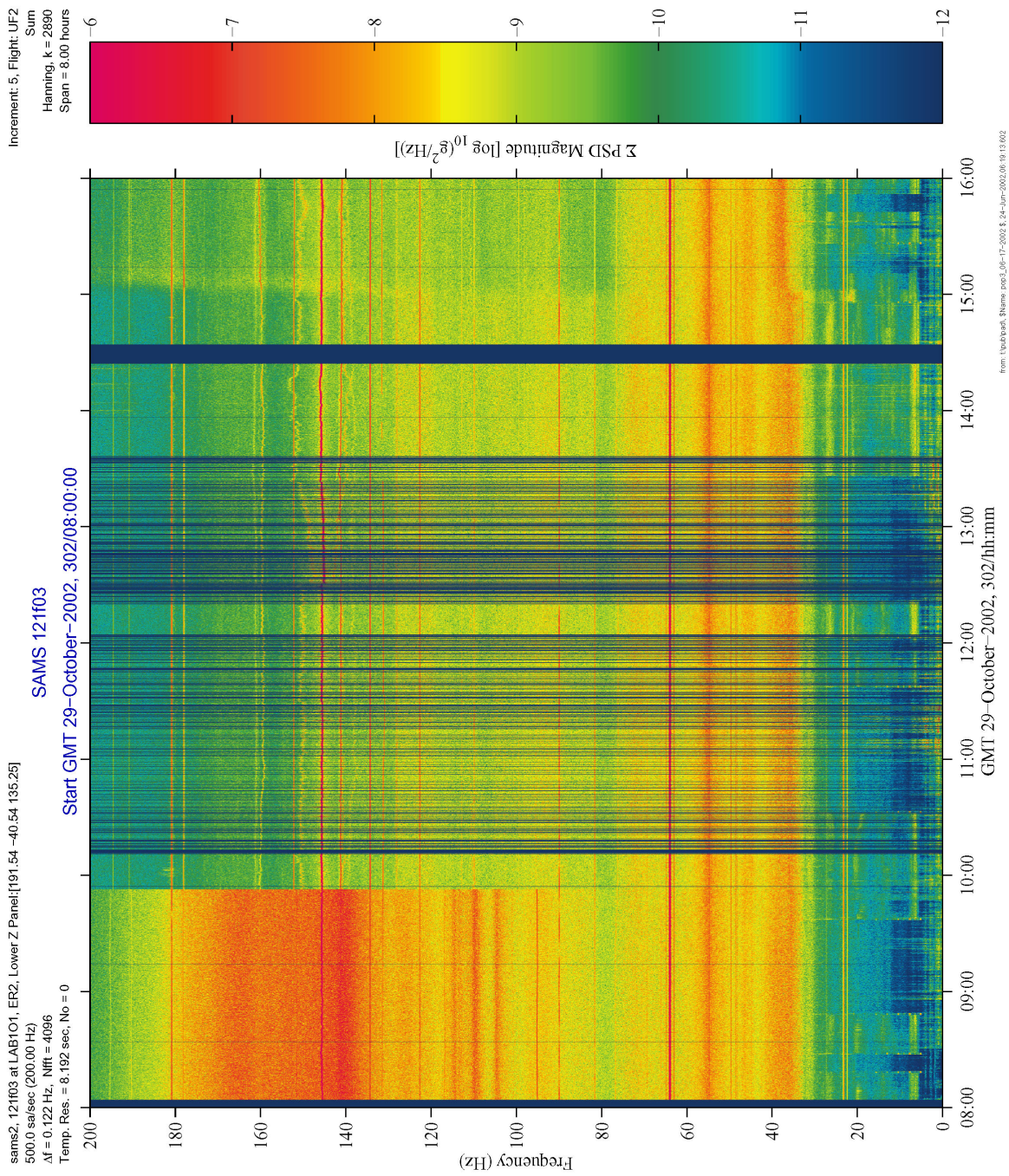

Figure 6-111 Spectrogram of ARIS Transition from HOLD to IDLE Mode (121f03)

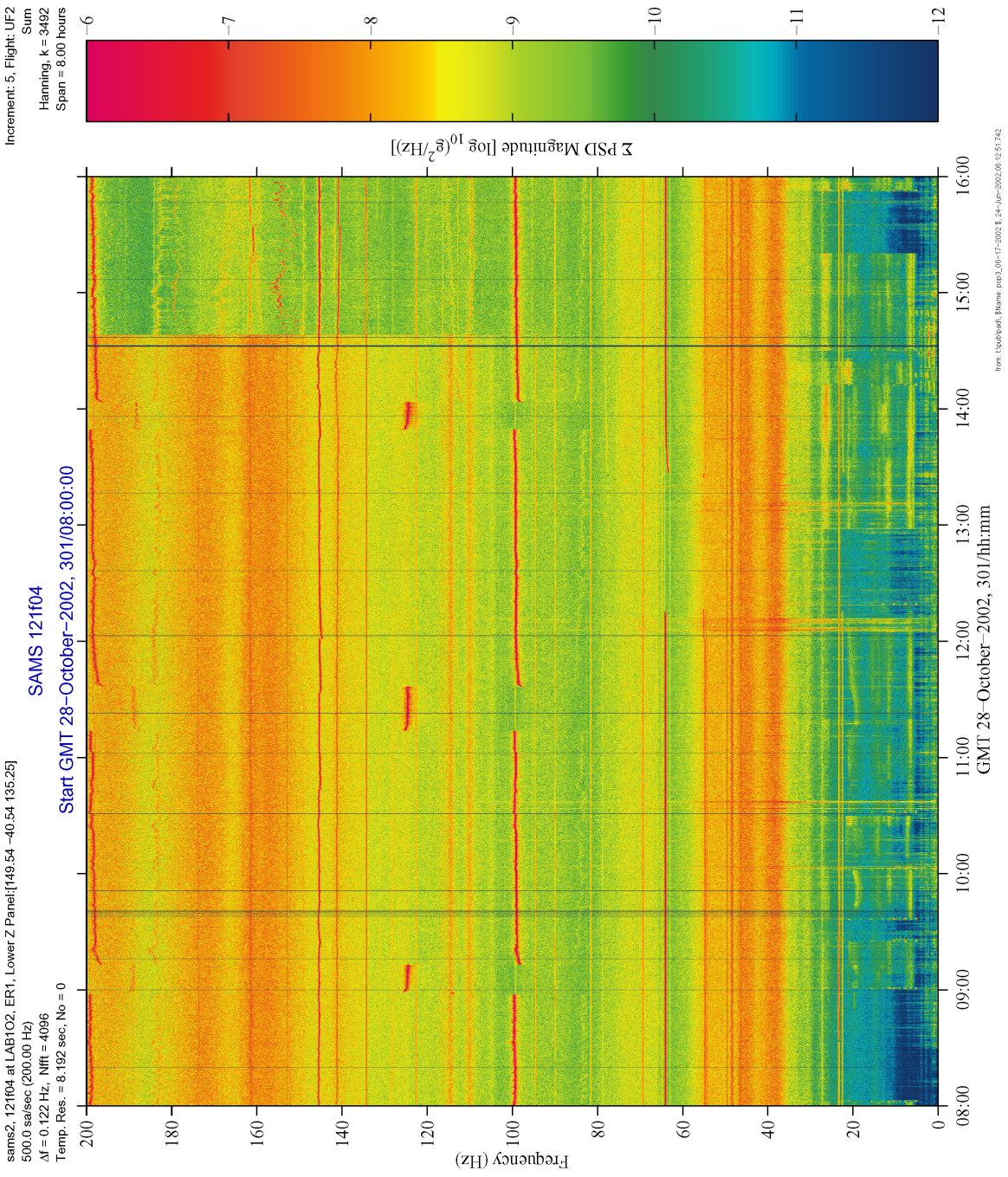

Figure 6-112 Spectrogram of ARIS Transition from HOLD to ACTIVE Mode (121f04)

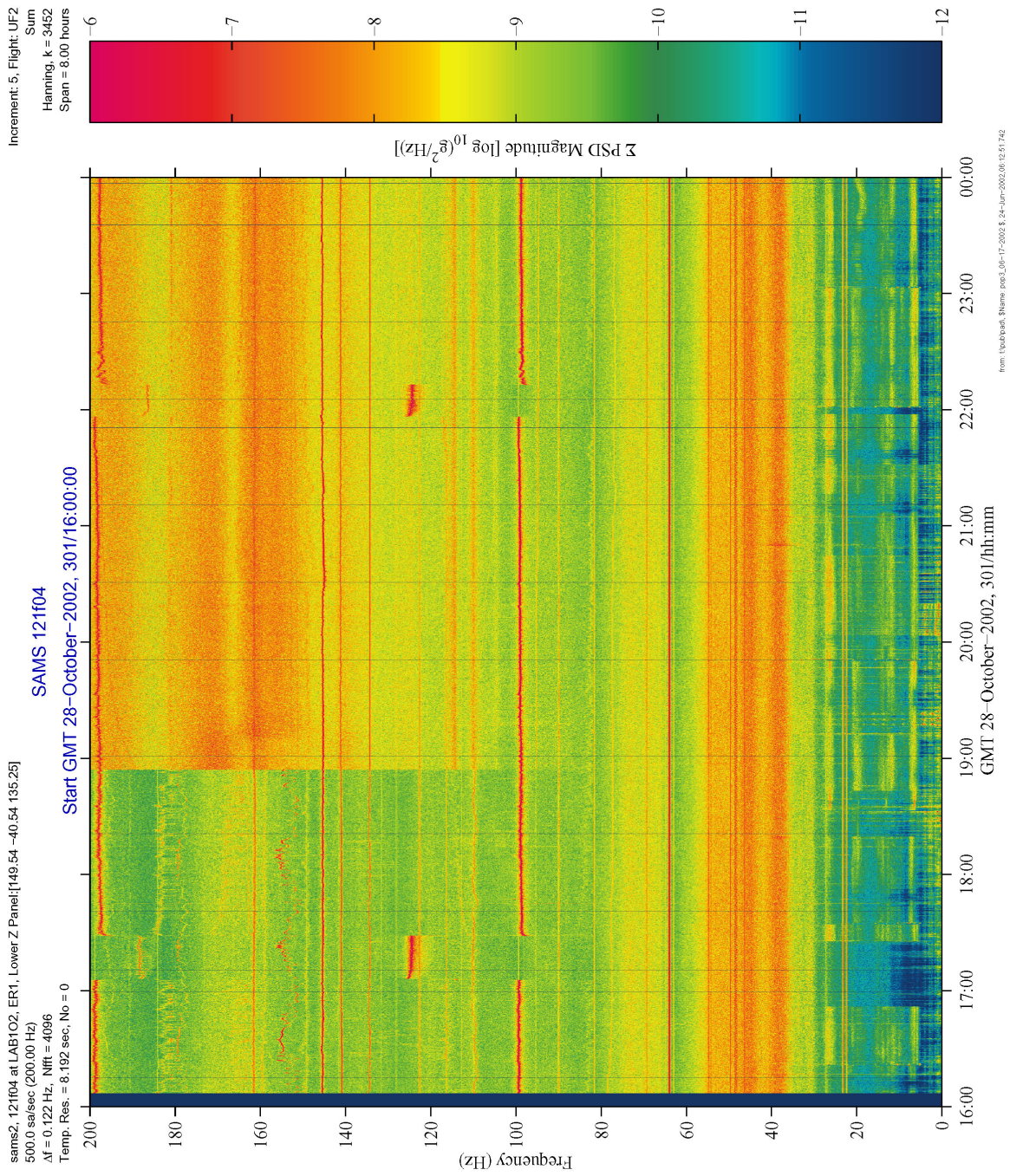

Figure 6-113 Spectrogram of ARIS Transition from ACTIVE to HOLD Mode (121f04)

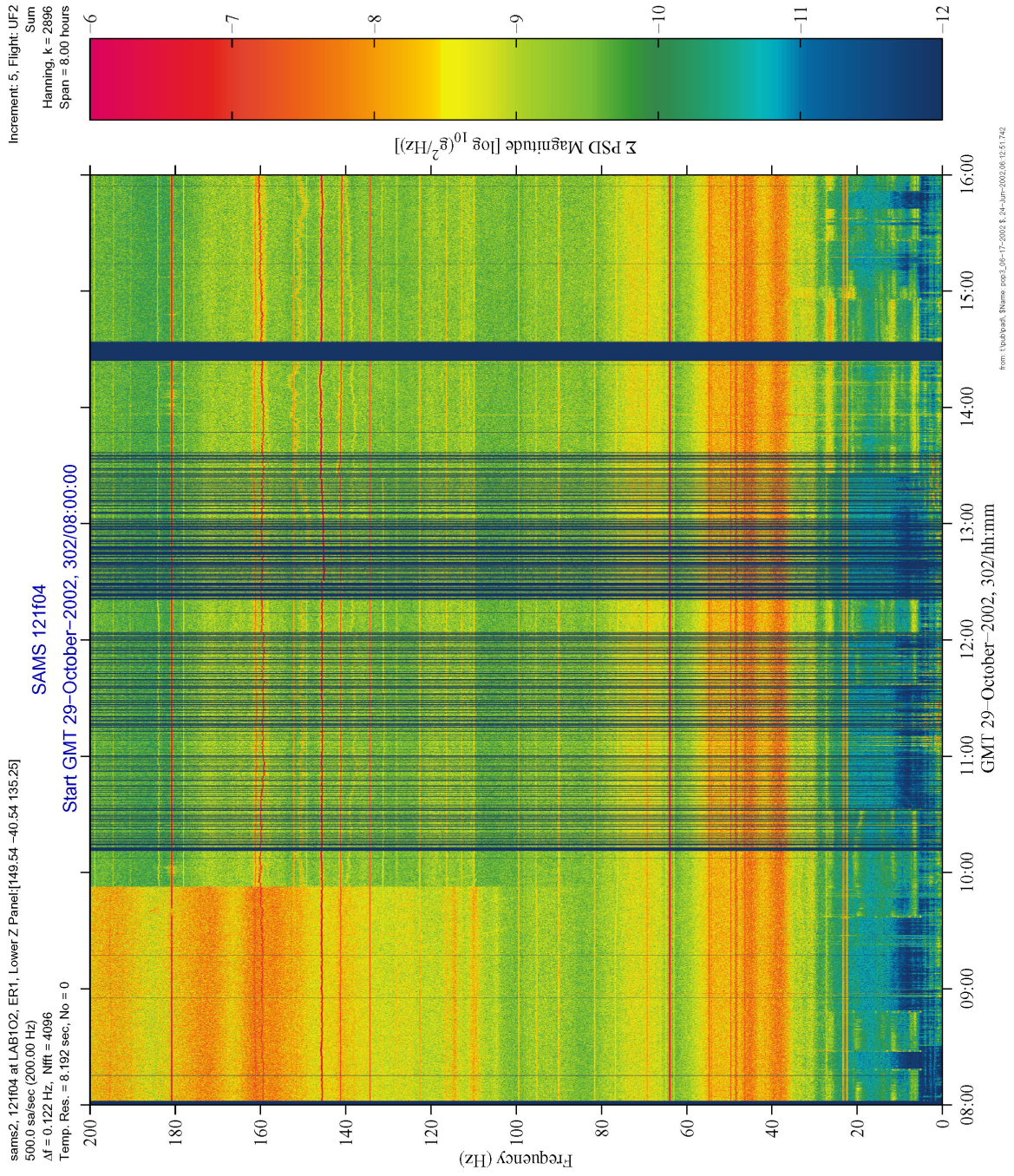

Figure 6-114 Spectrogram of ARIS Transition from HOLD to IDLE Mode (121f04)

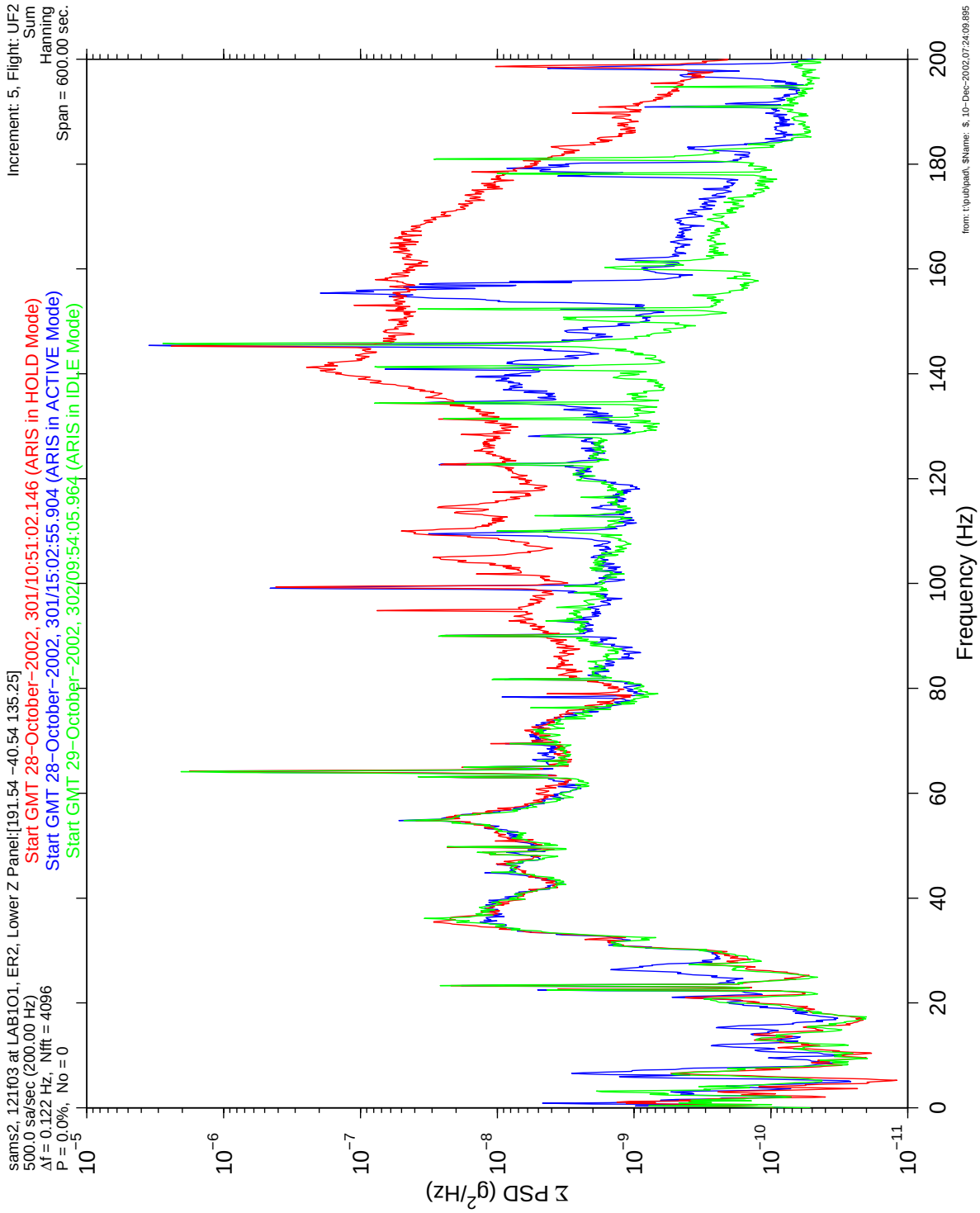

Figure 6-115 PSD of ARIS HOLD, ACTIVE, and IDLE Modes (121f03)

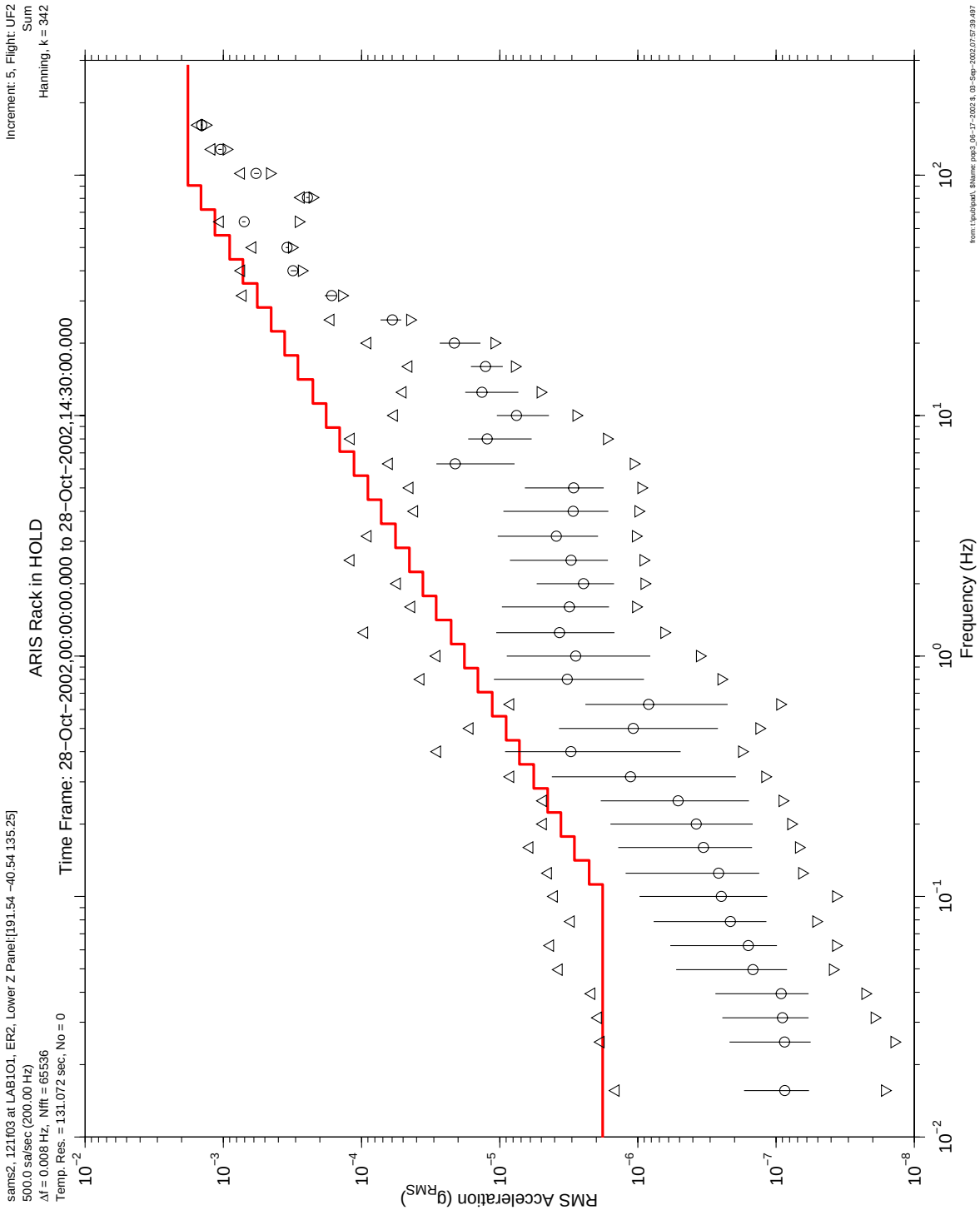

Figure 6-116 One-Third Octave Quartile of ARIS HOLD (121f03)

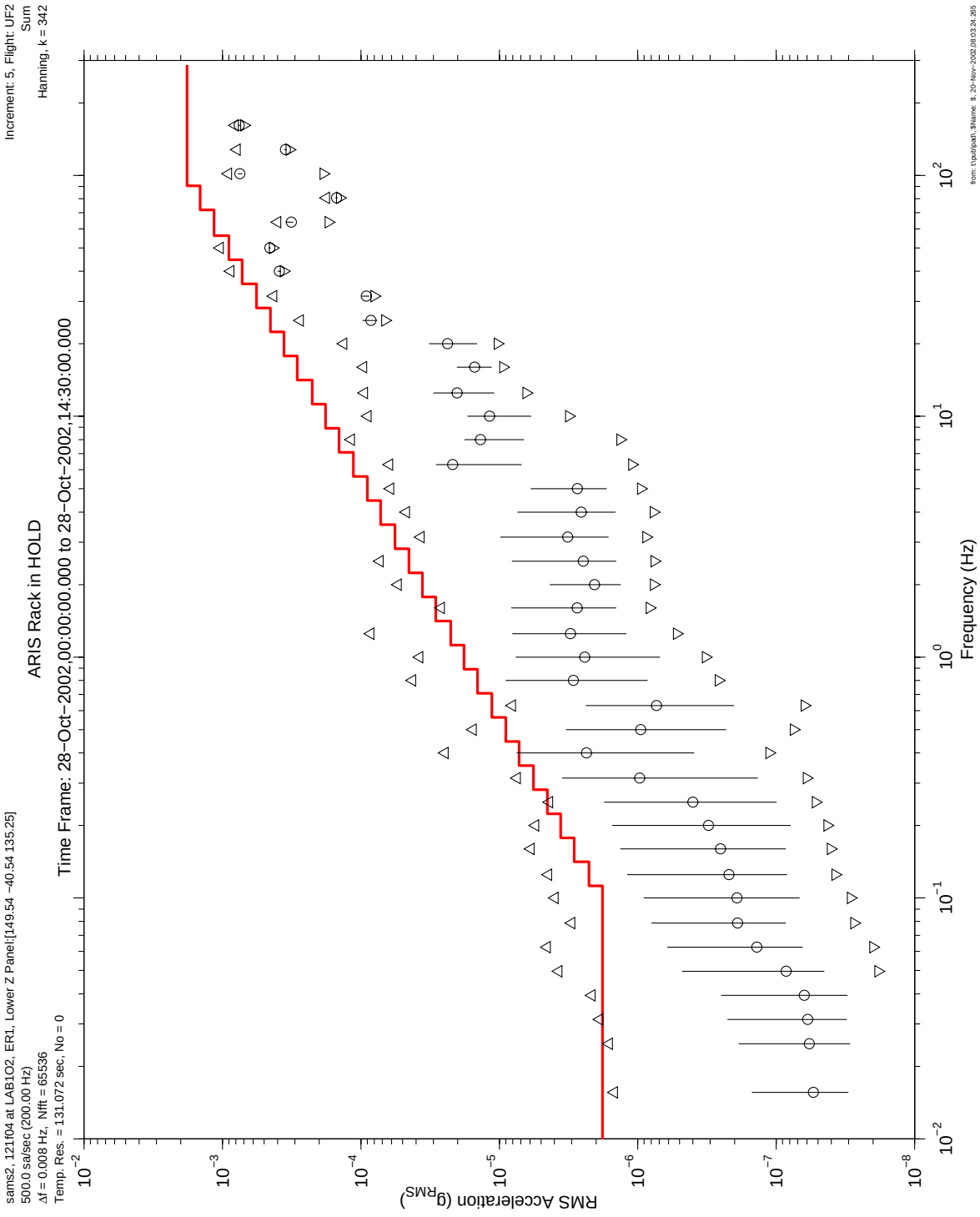

Figure 6-117 One-Third Octave Quartile of ARIS HOLD (121f04)

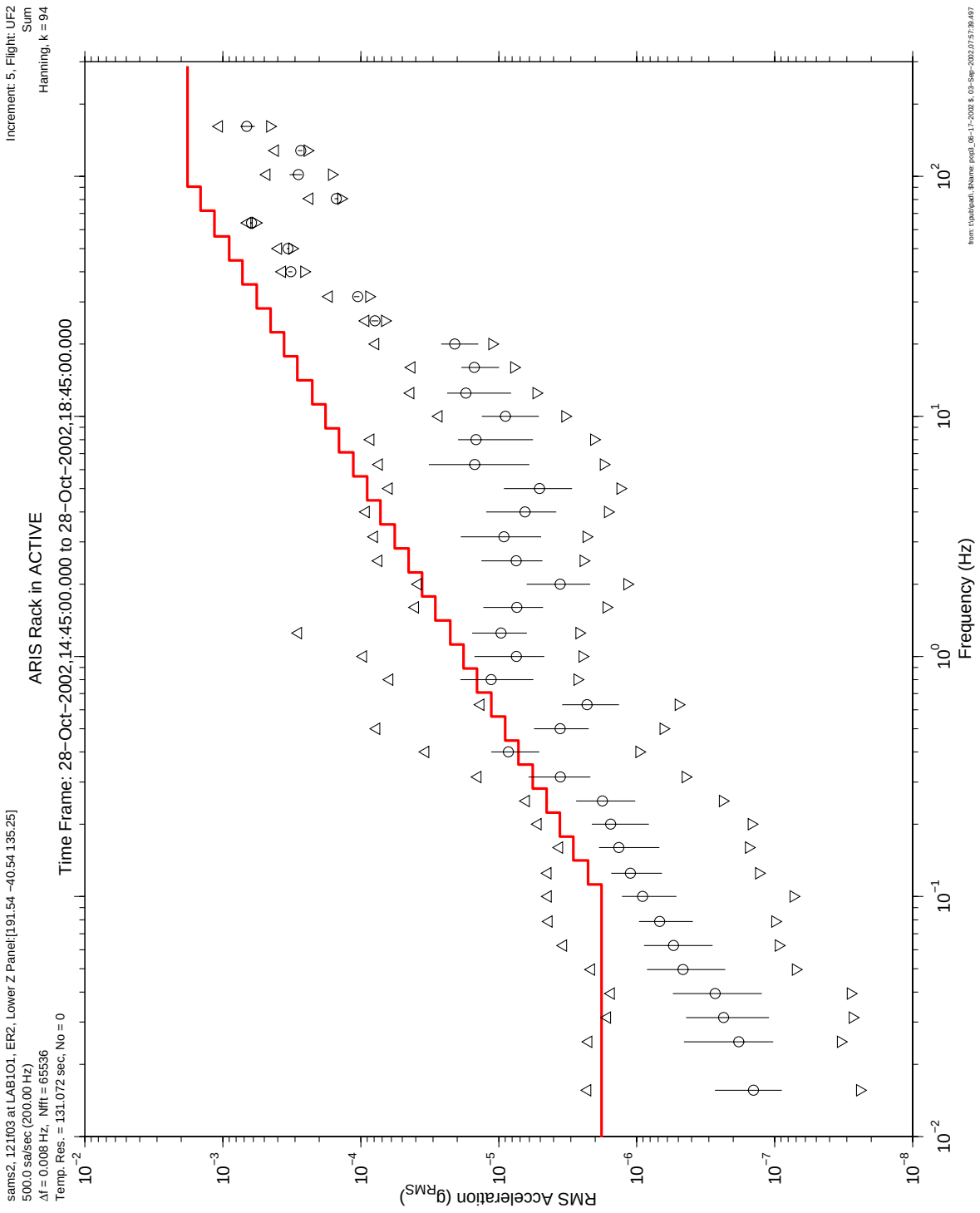

Figure 6-118 One-Third Octave Quartile of ARIS ACTIVE (121f03)

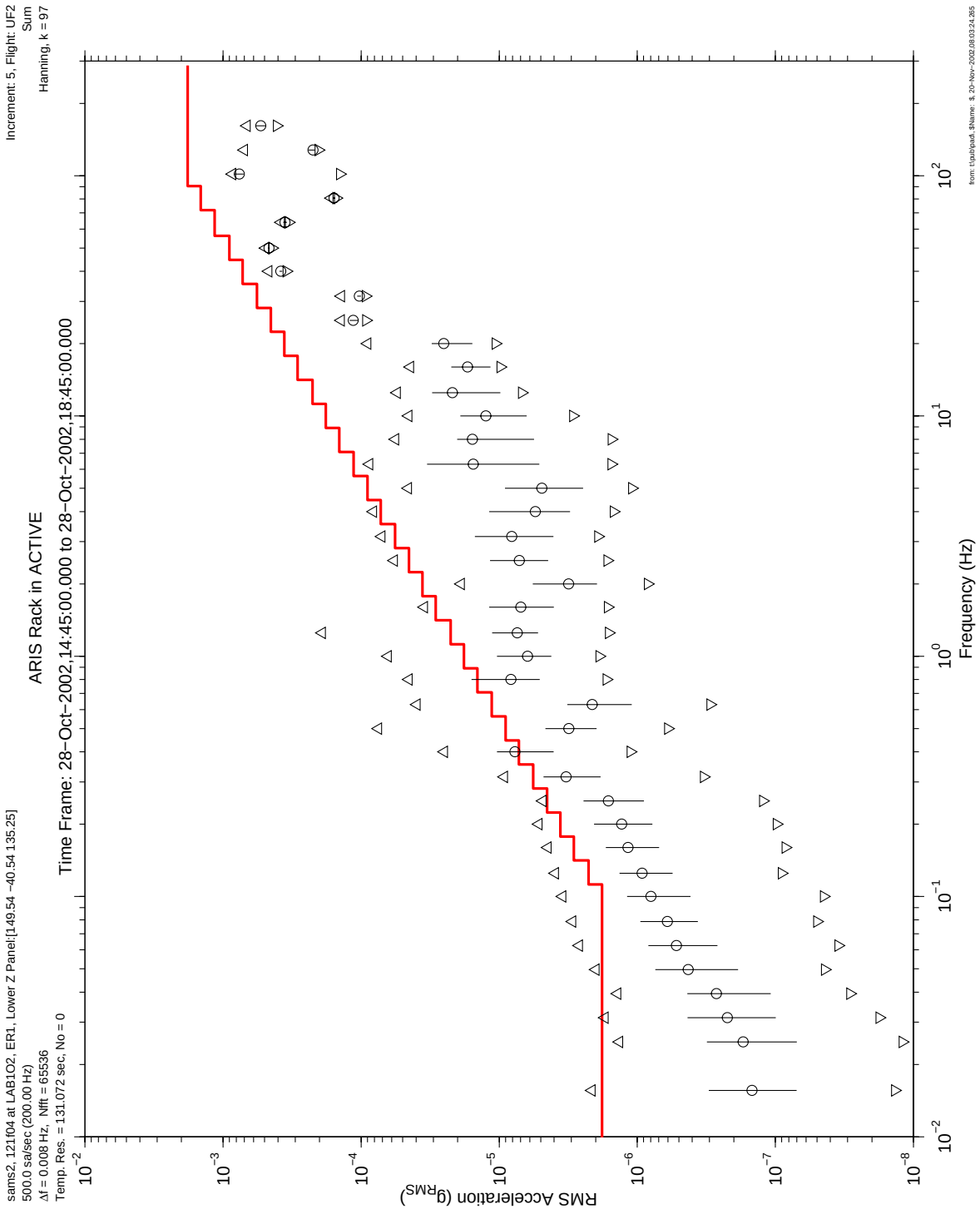

Figure 6-119 One-Third Octave Quartile of ARIS ACTIVE (121f04)

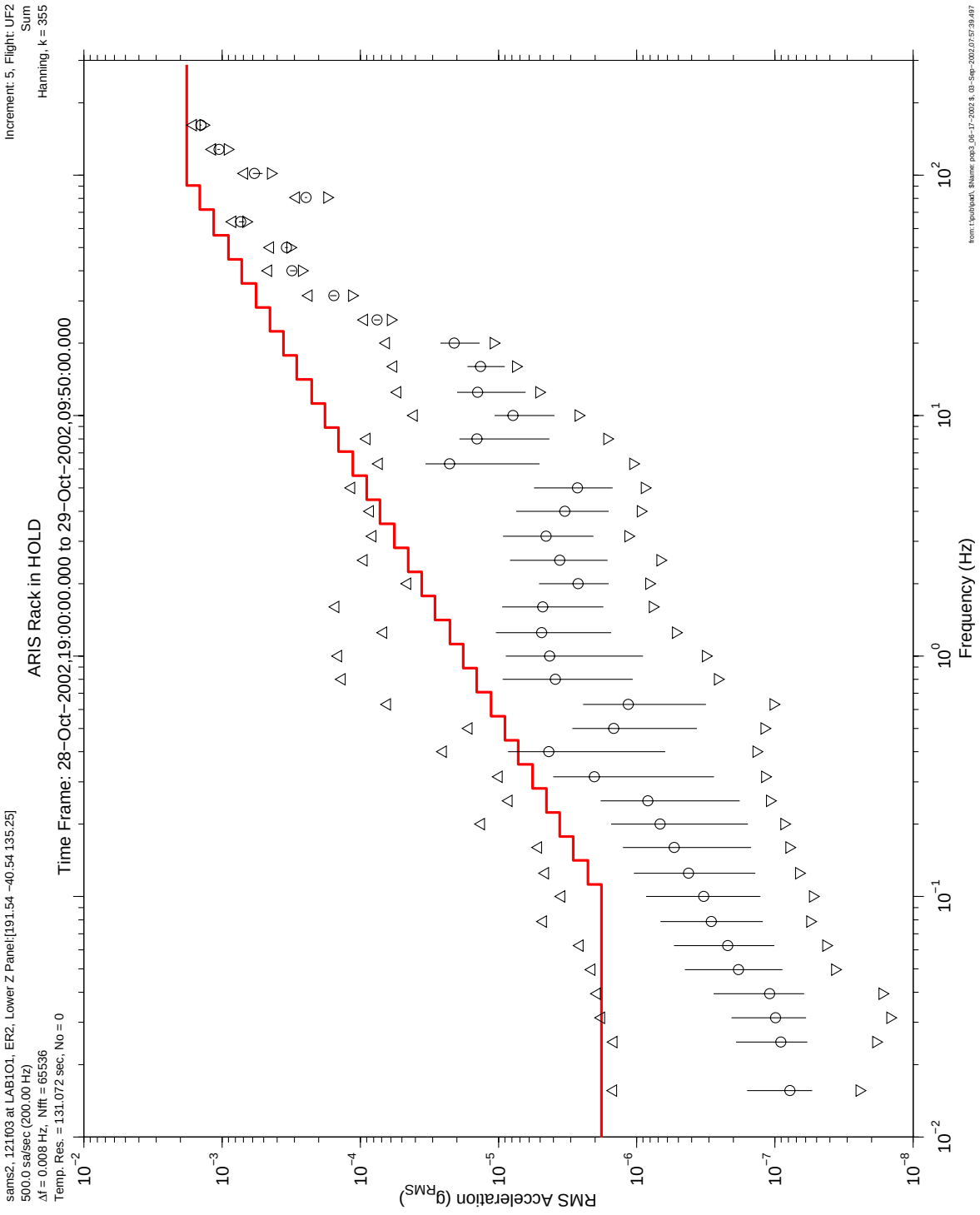

Figure 6-120 One-Third Octave Quartile of ARIS HOLD (121f03)

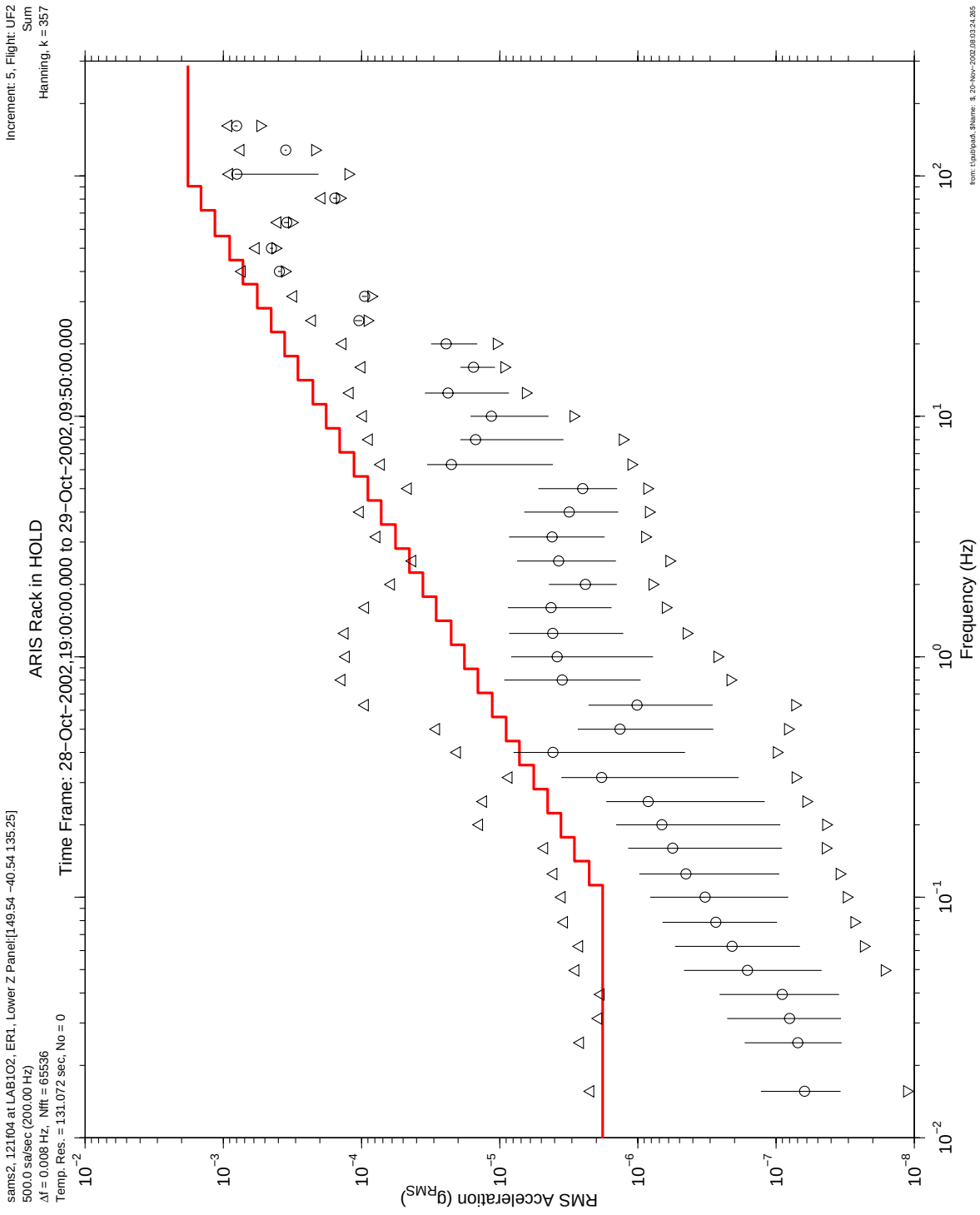

Figure 6-121 One-Third Octave Quartile of ARIS HOLD (121f04)

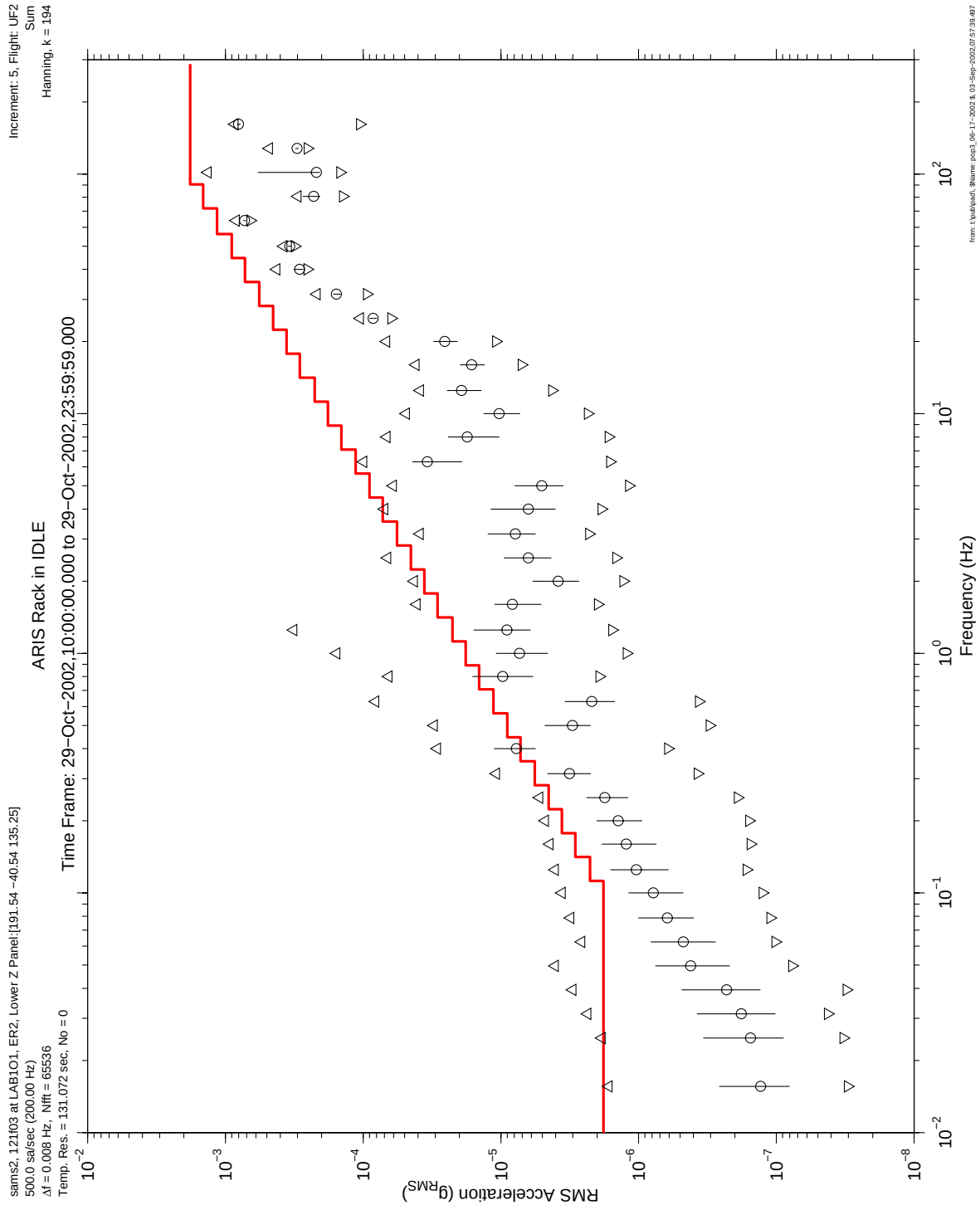

Figure 6-122 One-Third Octave Quartile of ARIS IDLE (121f03)

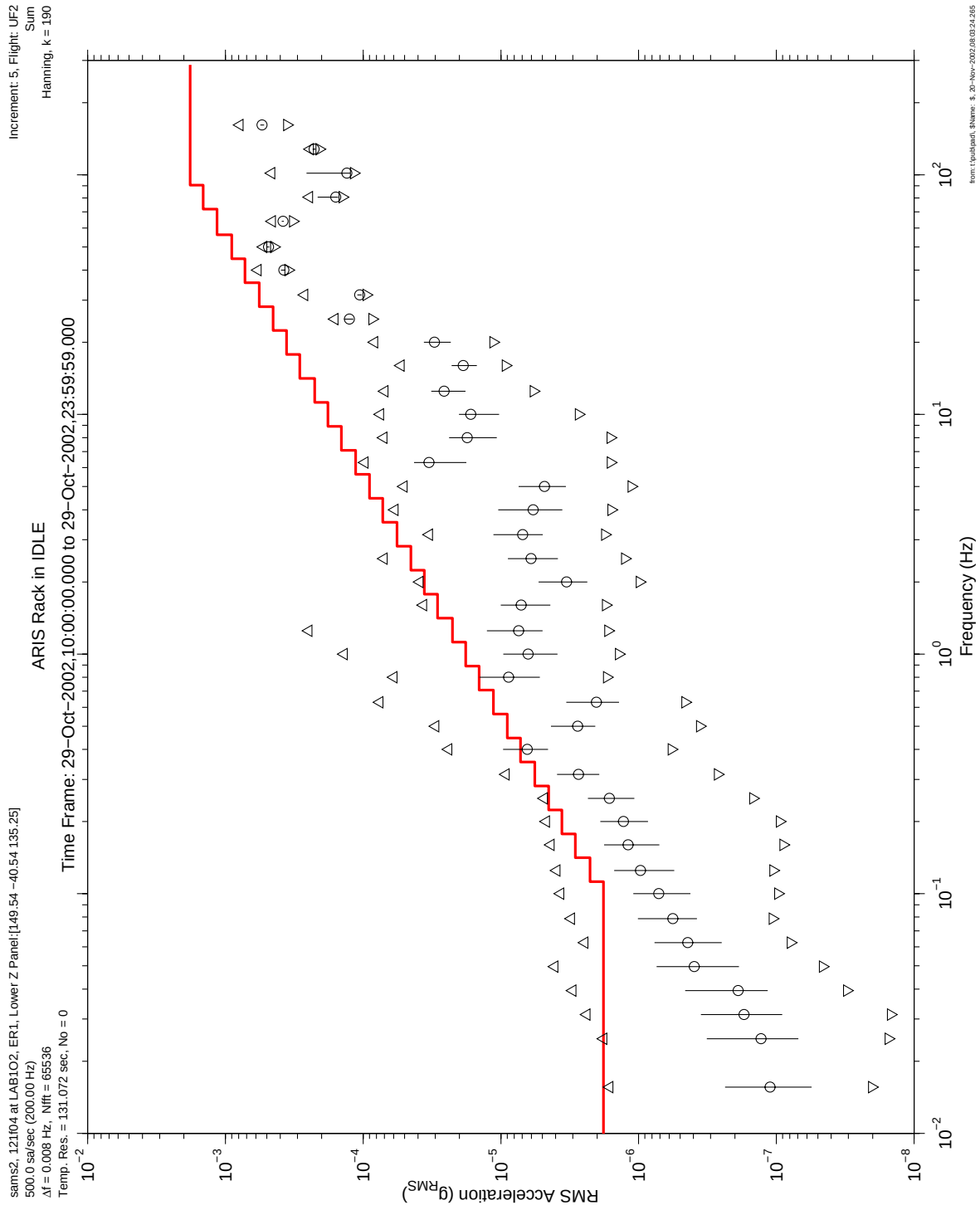

Figure 6-123 One-Third Octave Quartile of ARIS IDLE (121f04)

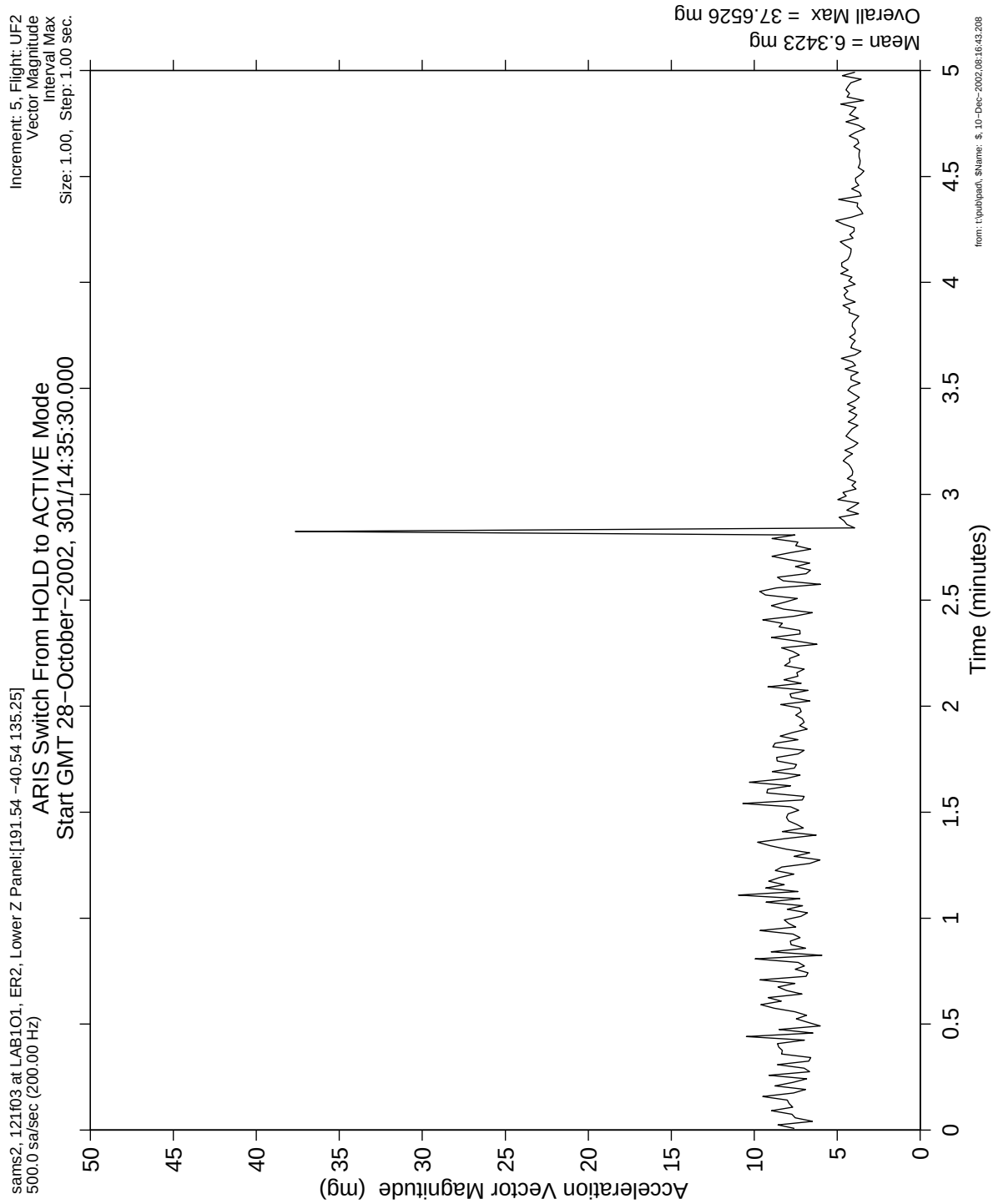

Figure 6-124 Interval Maximum of ARIS Transient from HOLD to ACTIVE (121f03)

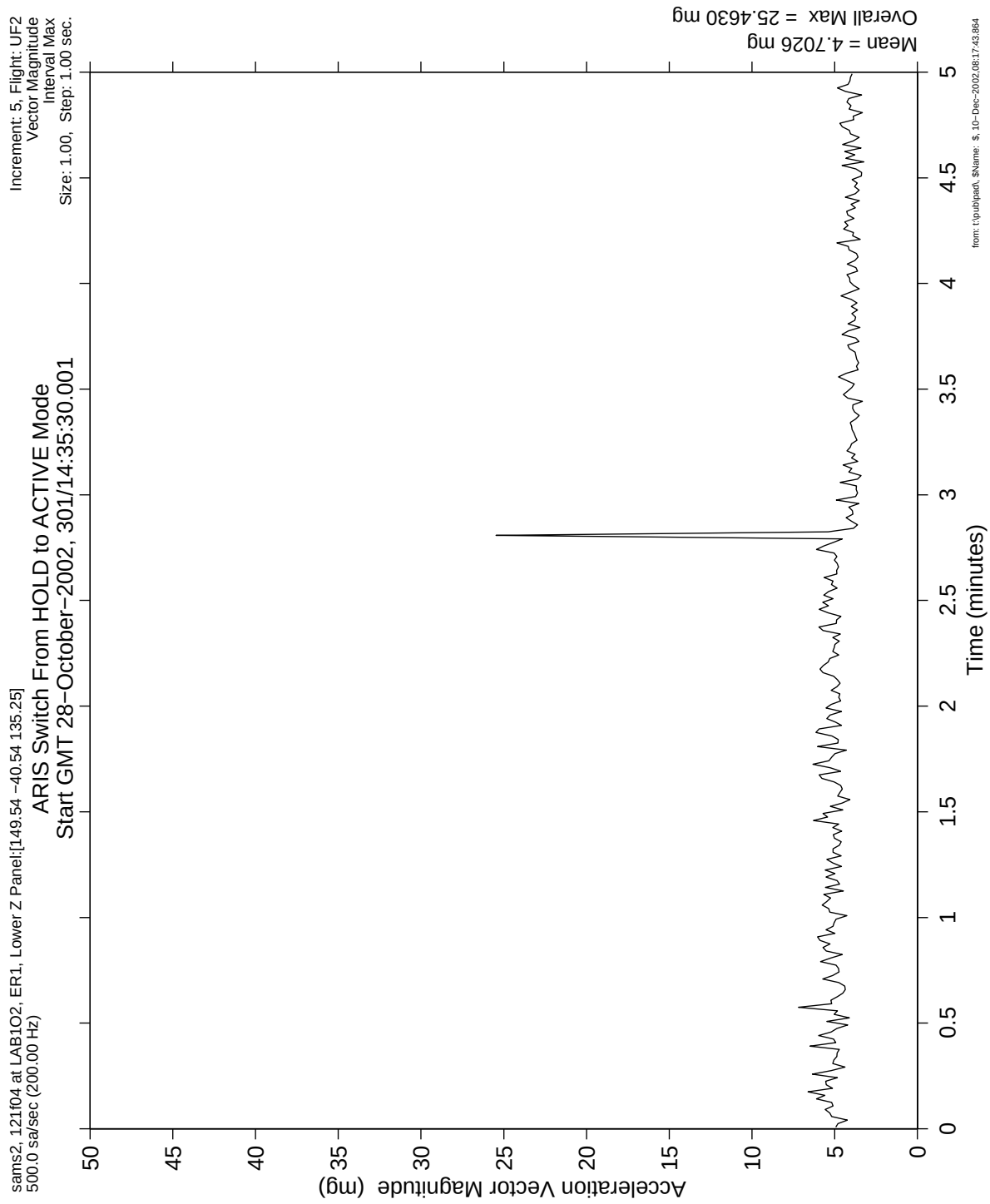

Figure 6-125 Interval Maximum of ARIS Transient from HOLD to ACTIVE (121f04)

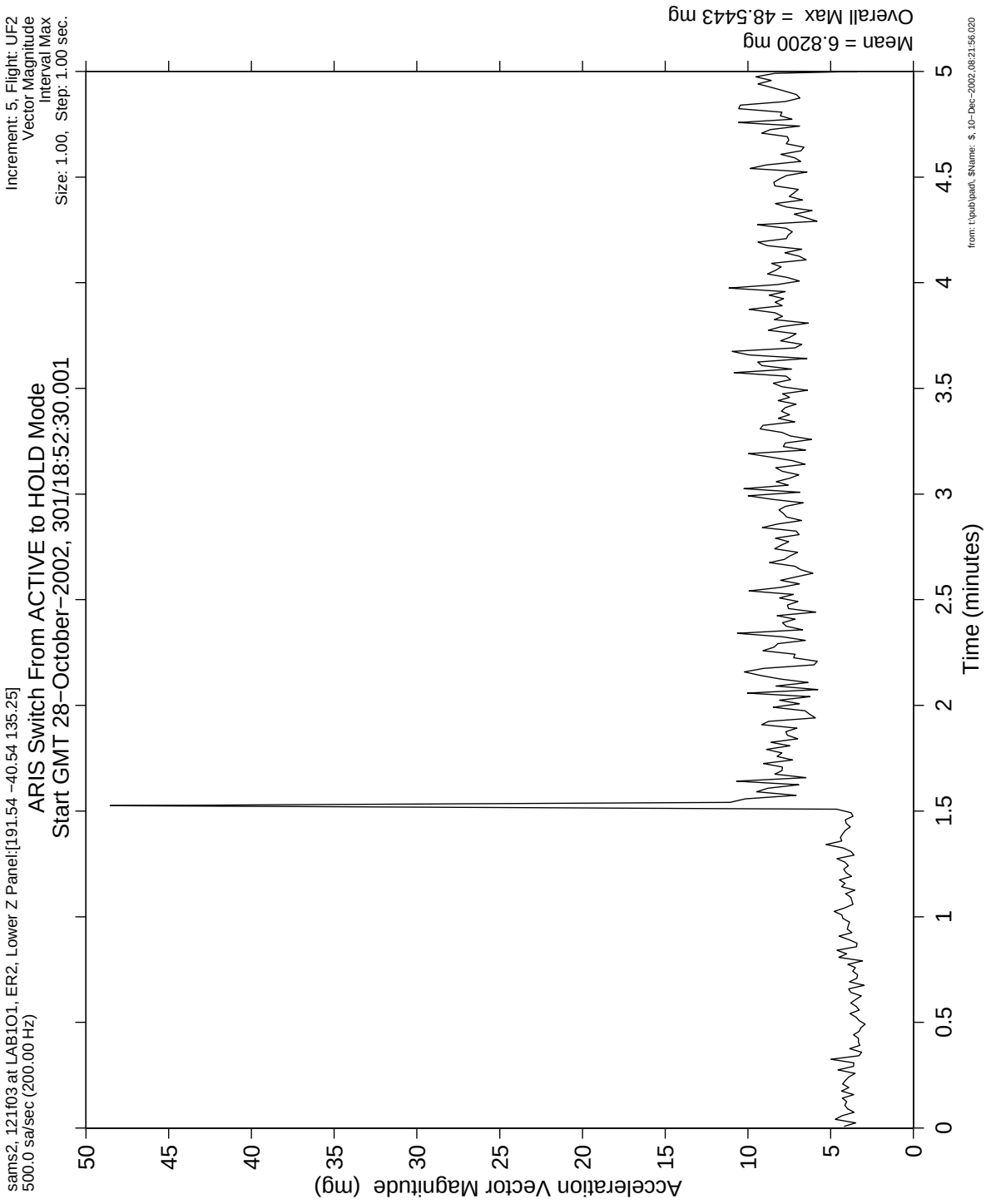

Figure 6-126 Interval Maximum of ARIS Transient from ACTIVE to HOLD (121f03)

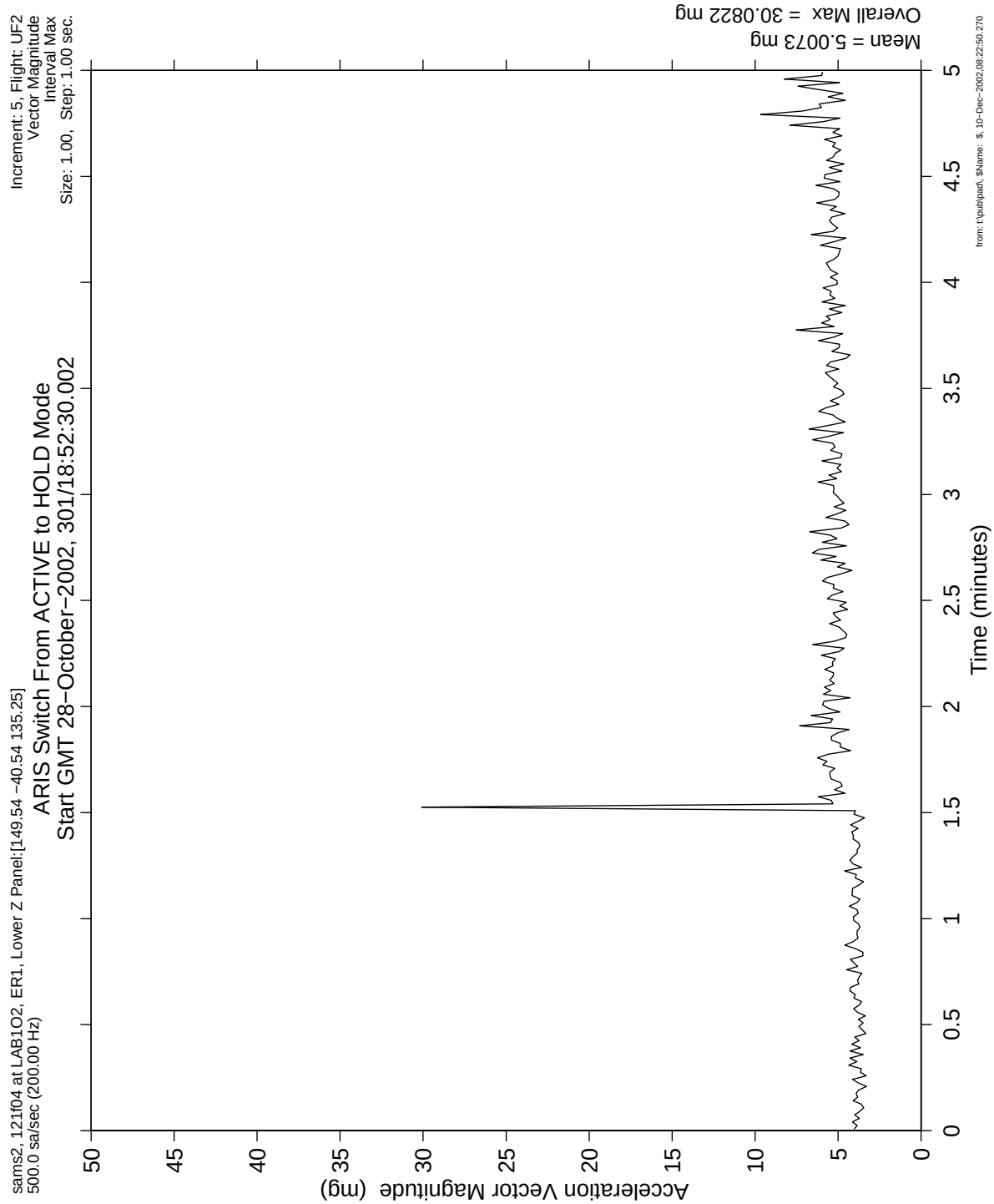

Figure 6-127 Interval Maximum of ARIS Transient from ACTIVE to HOLD (121f04)

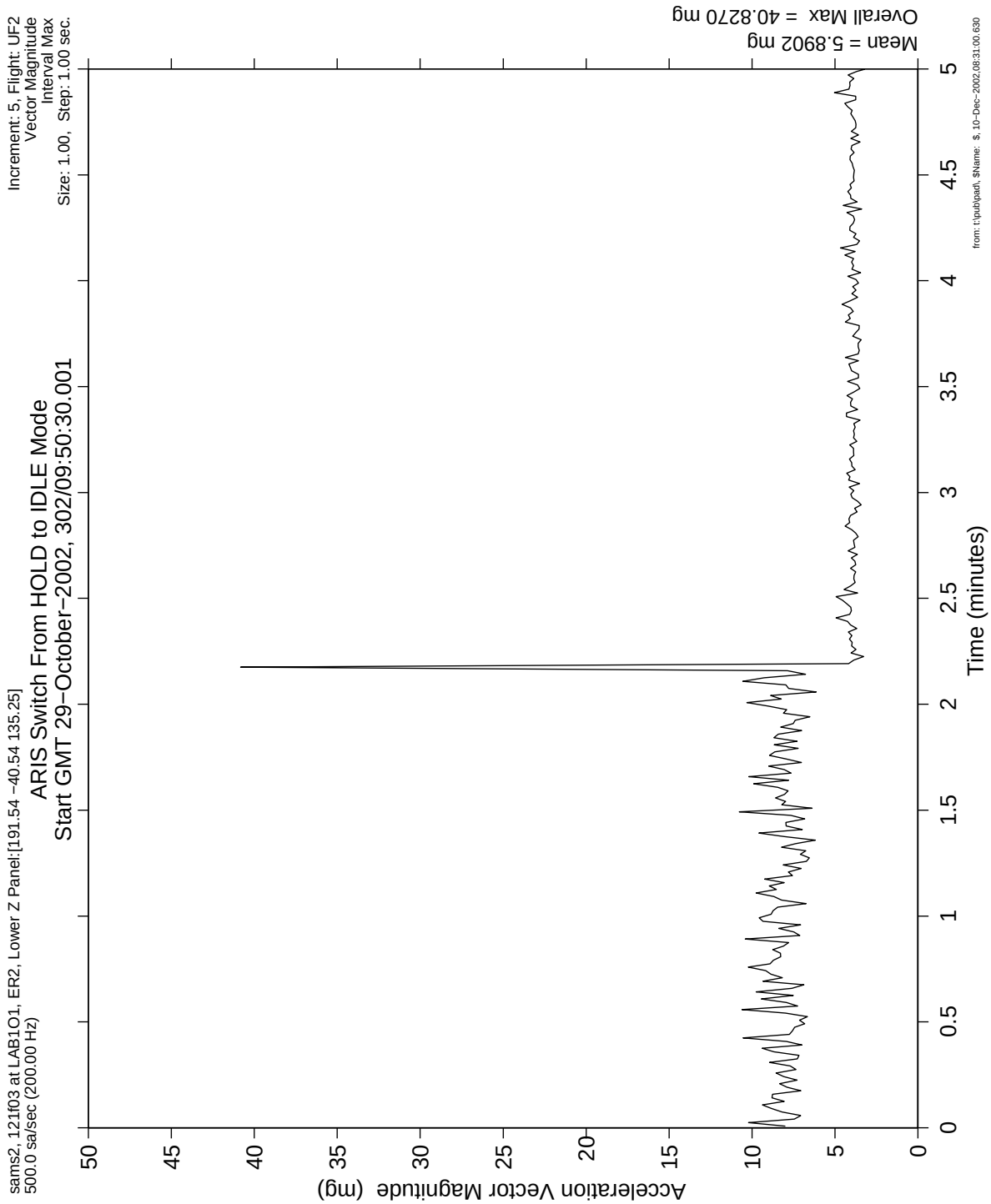

Figure 6-128 Interval Maximum of ARIS Transient from HOLD to IDLE (121f03)

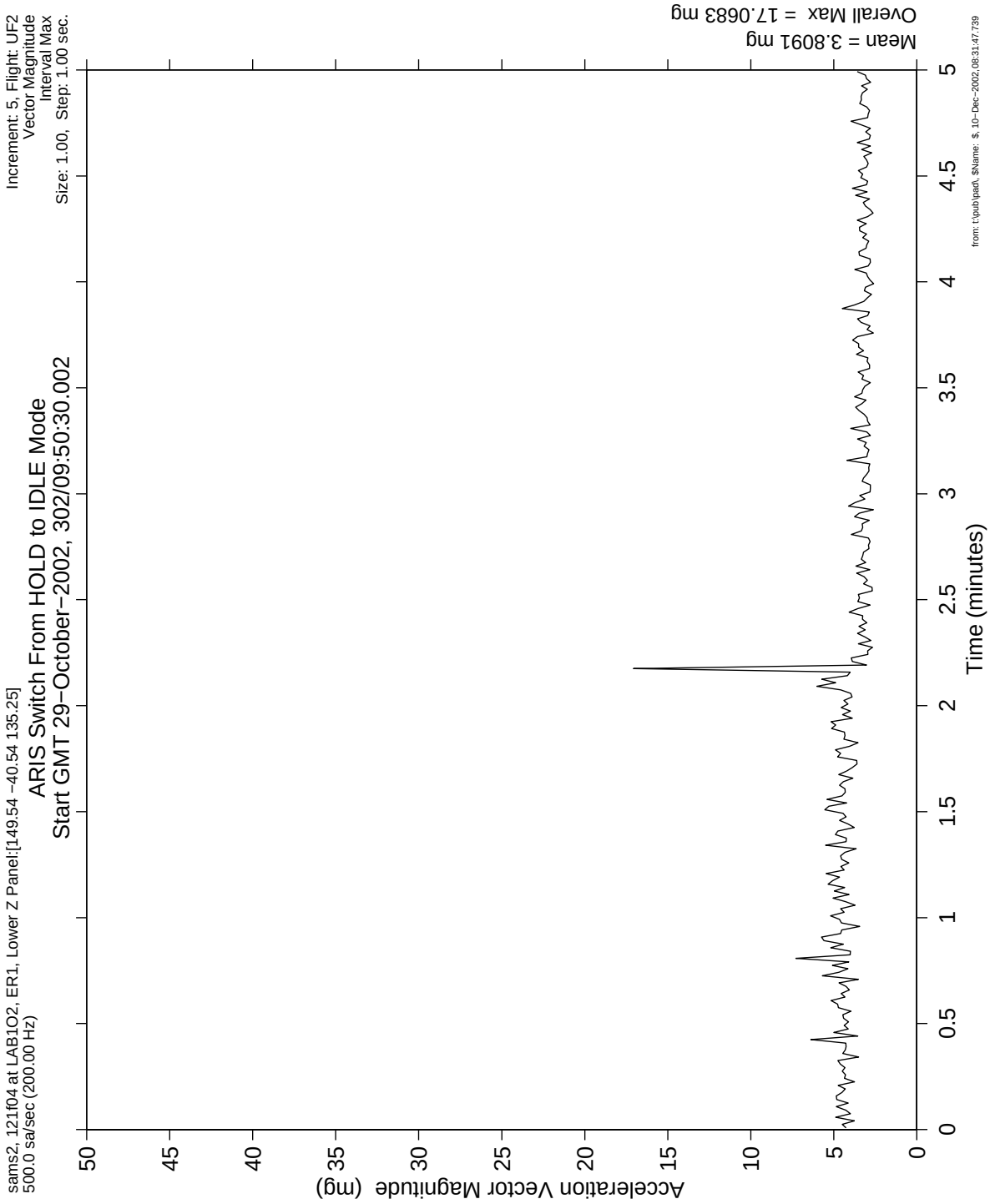

Figure 6-129 Interval Maximum of ARIS Transient from HOLD to IDLE (121f04)

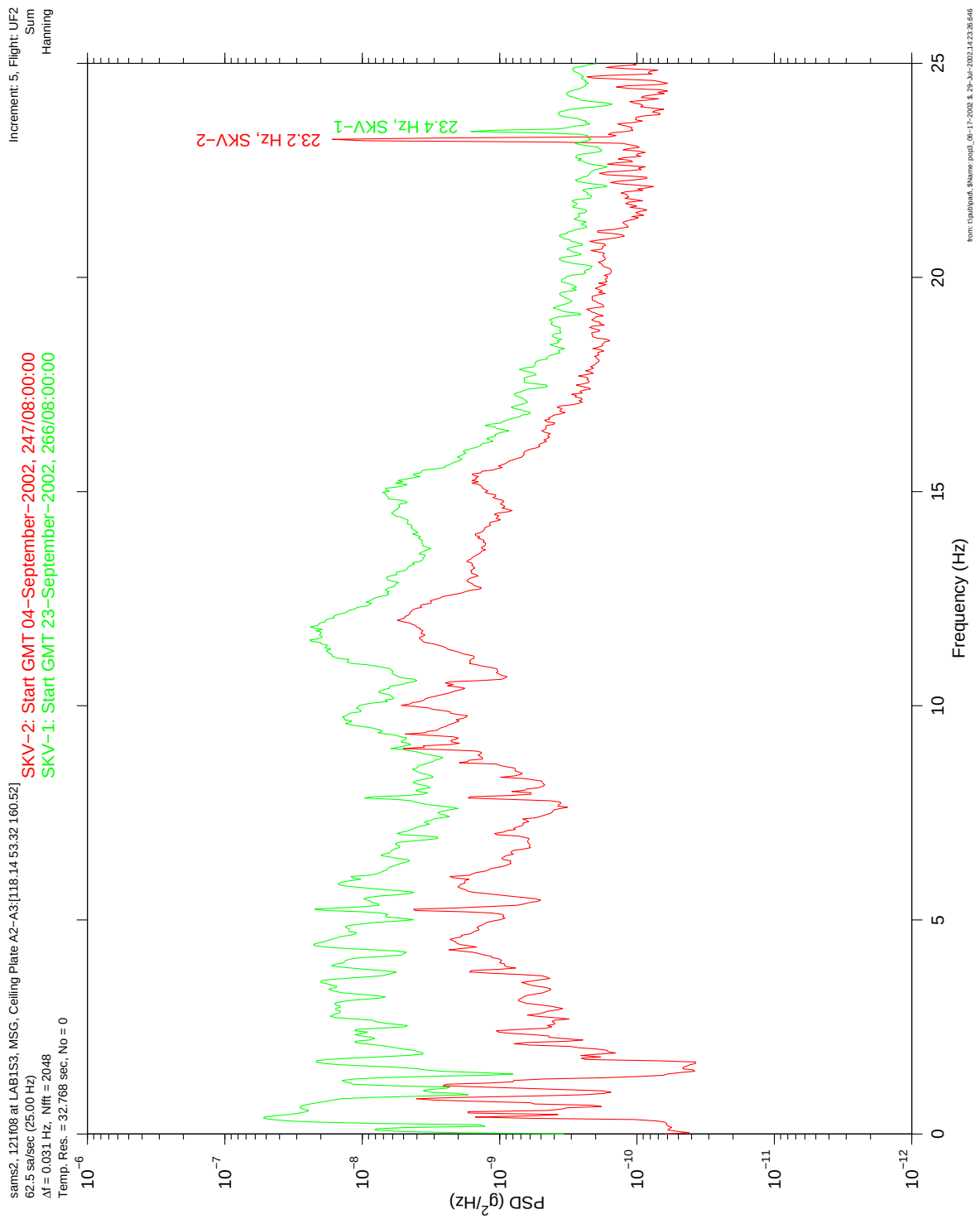

Figure 6-130 PSD of SKVs (121f08)

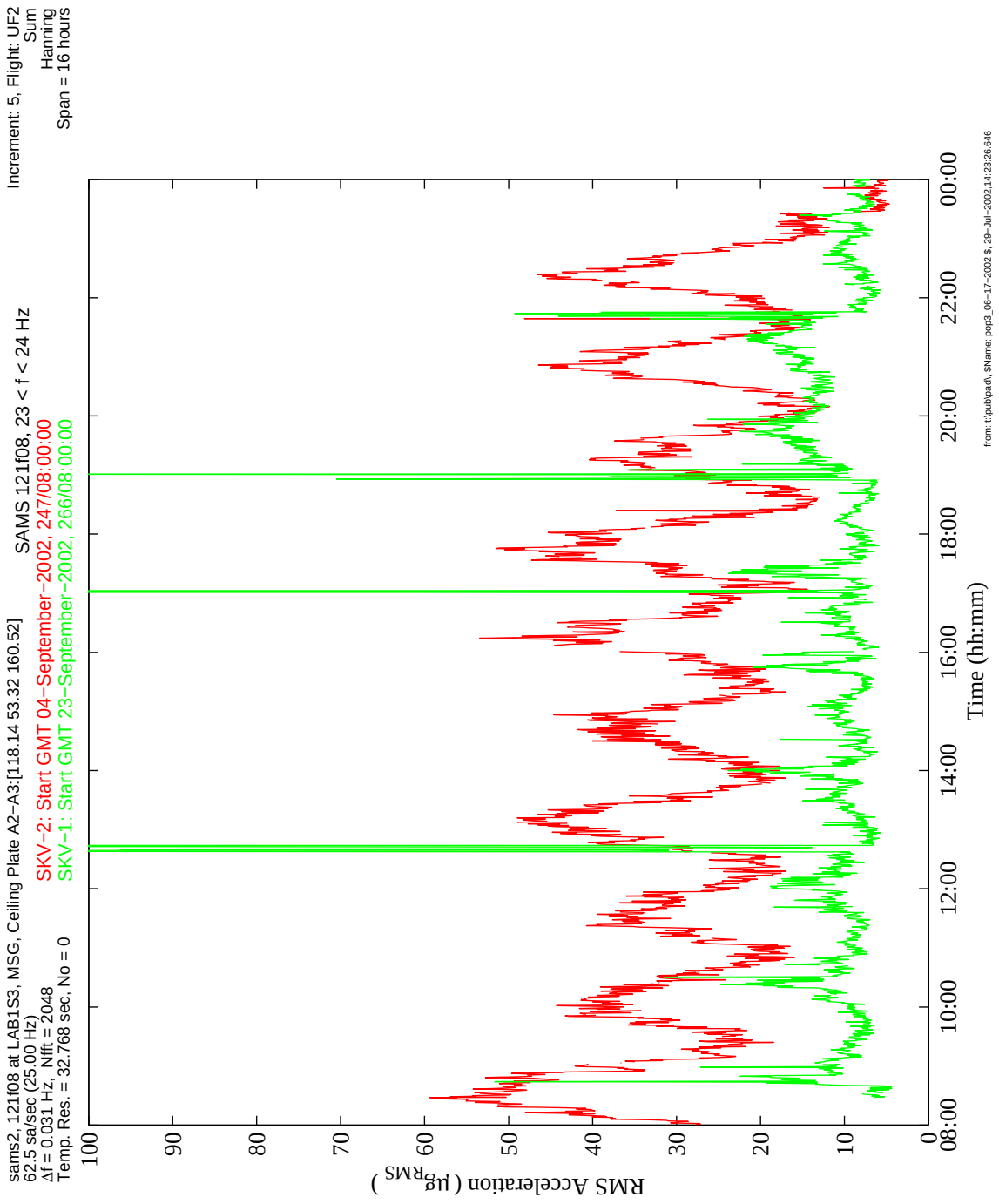

Figure 6-131 Interval RMS of SKV (121f08)

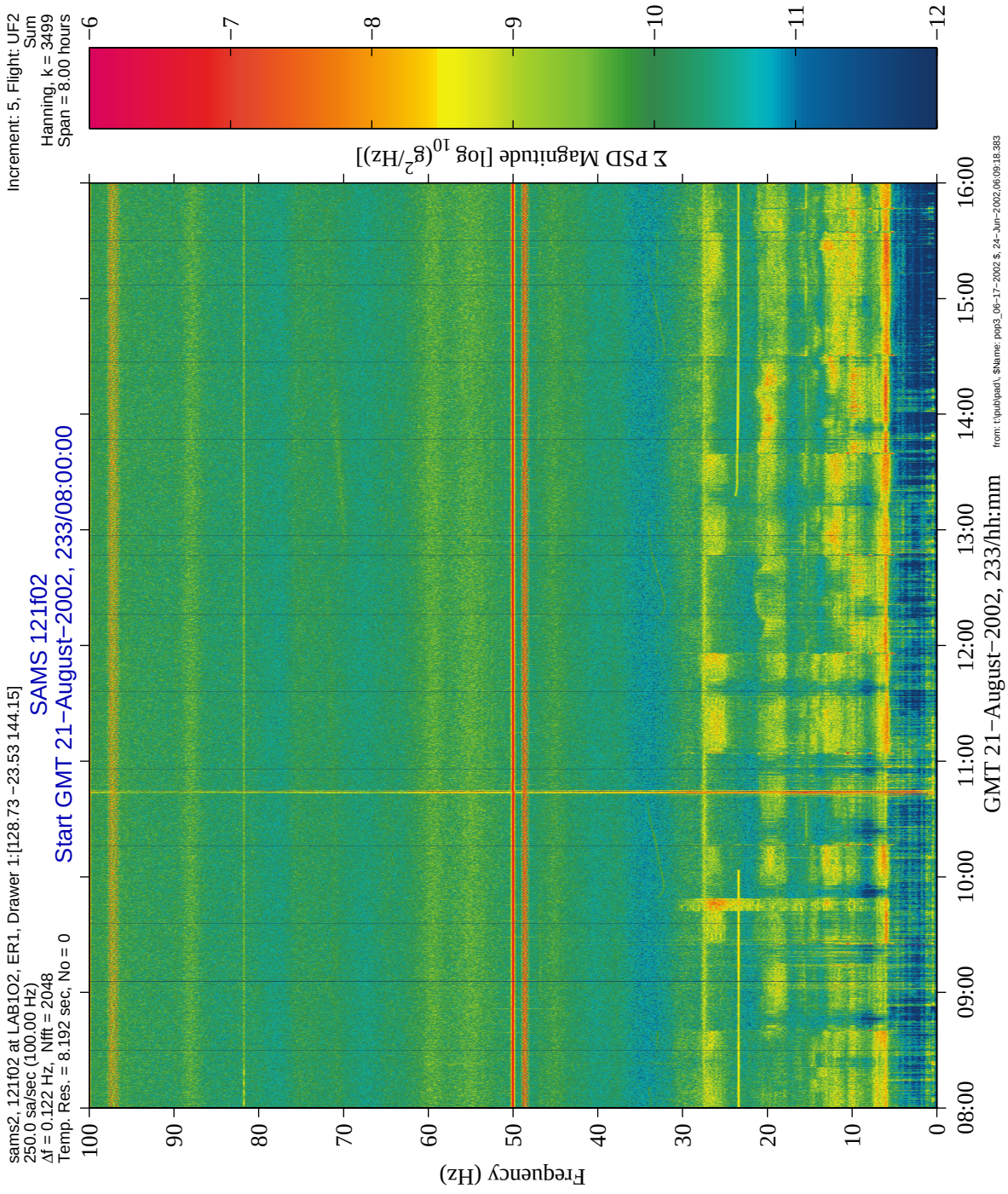

Figure 6-132 Spectrogram of SKV-1 (121f02)

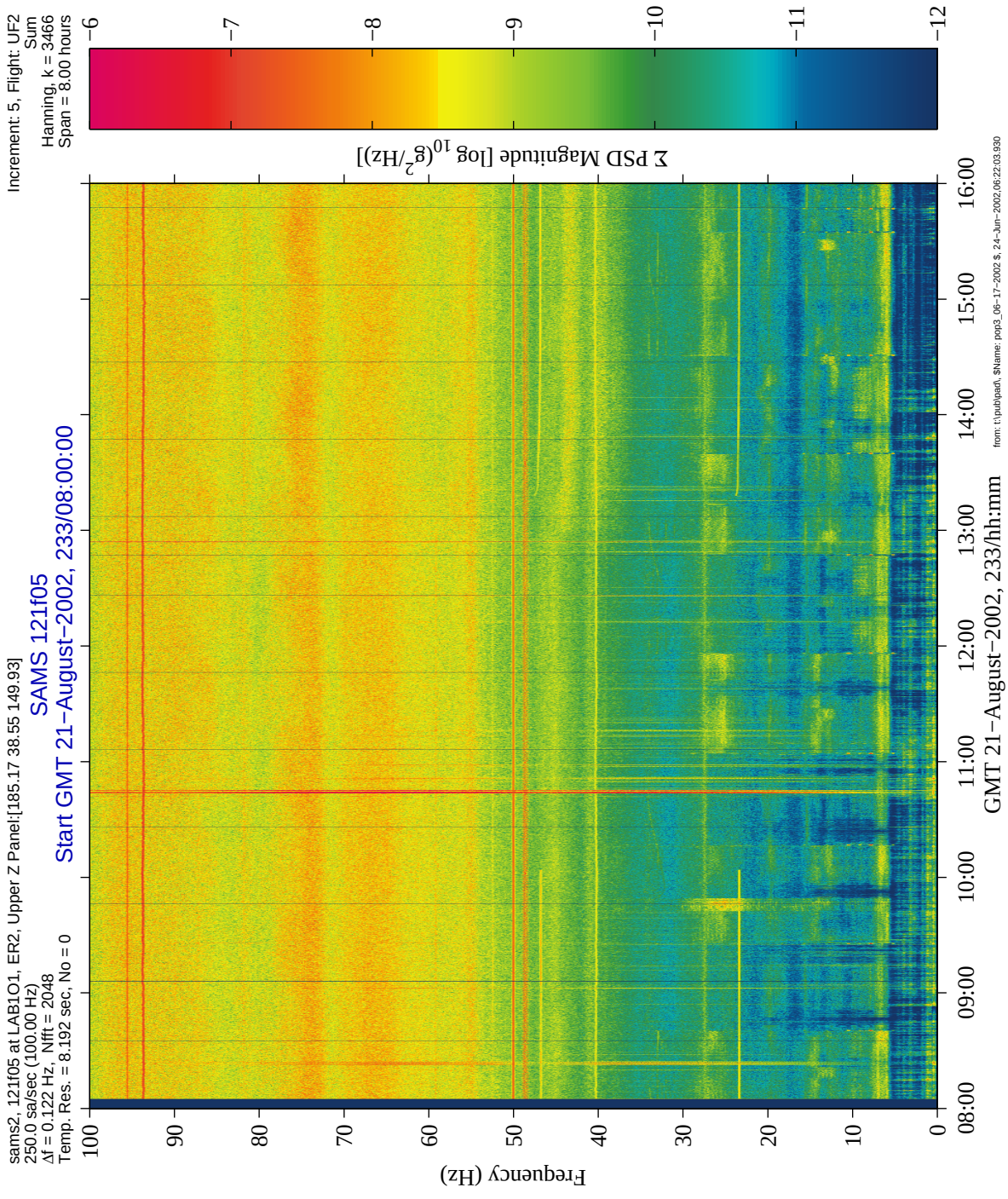

Figure 6-133 Spectrogram of SKV-1 (121f05)

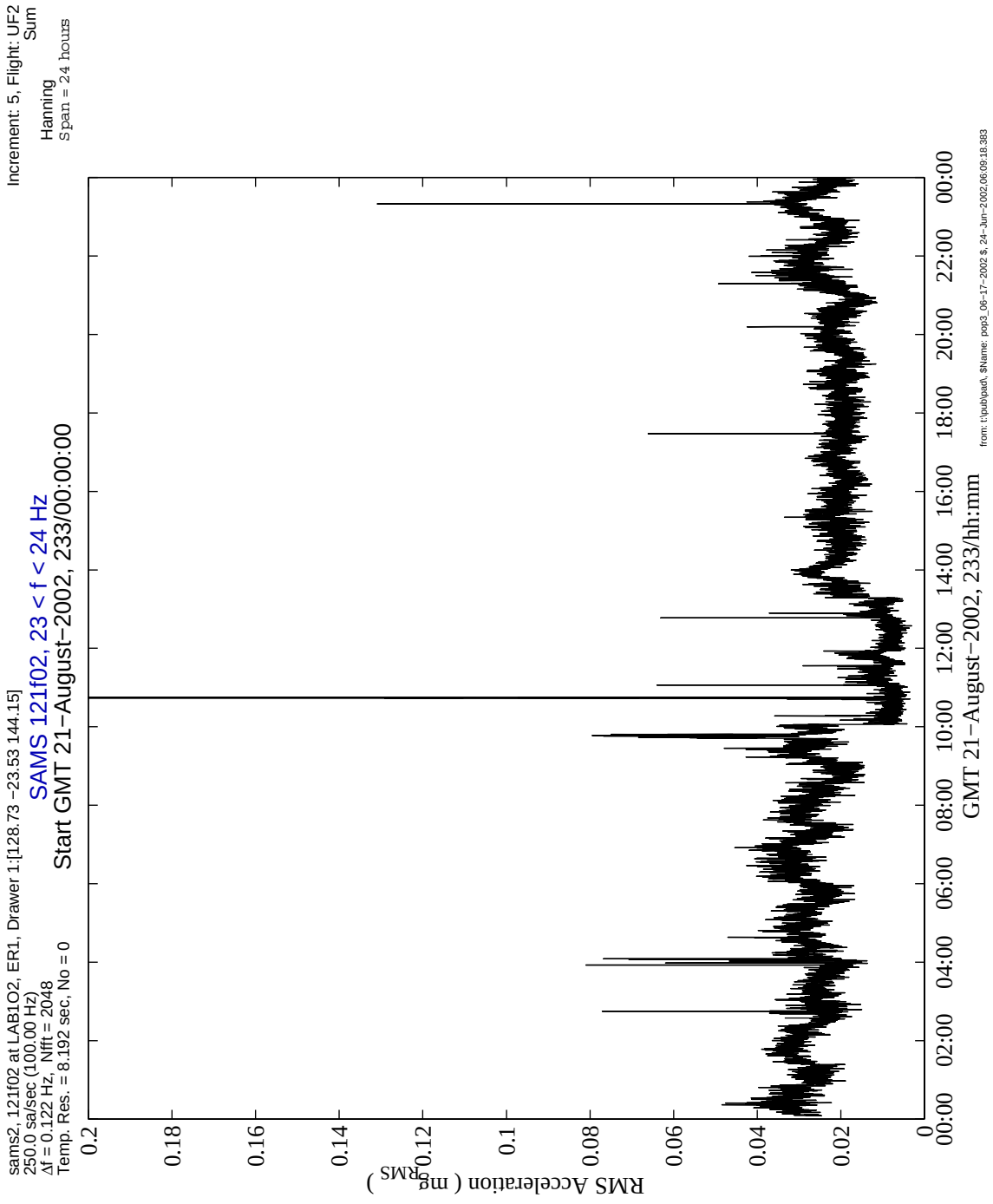

Figure 6-134 Interval RMS of SKV-1 (121f02)

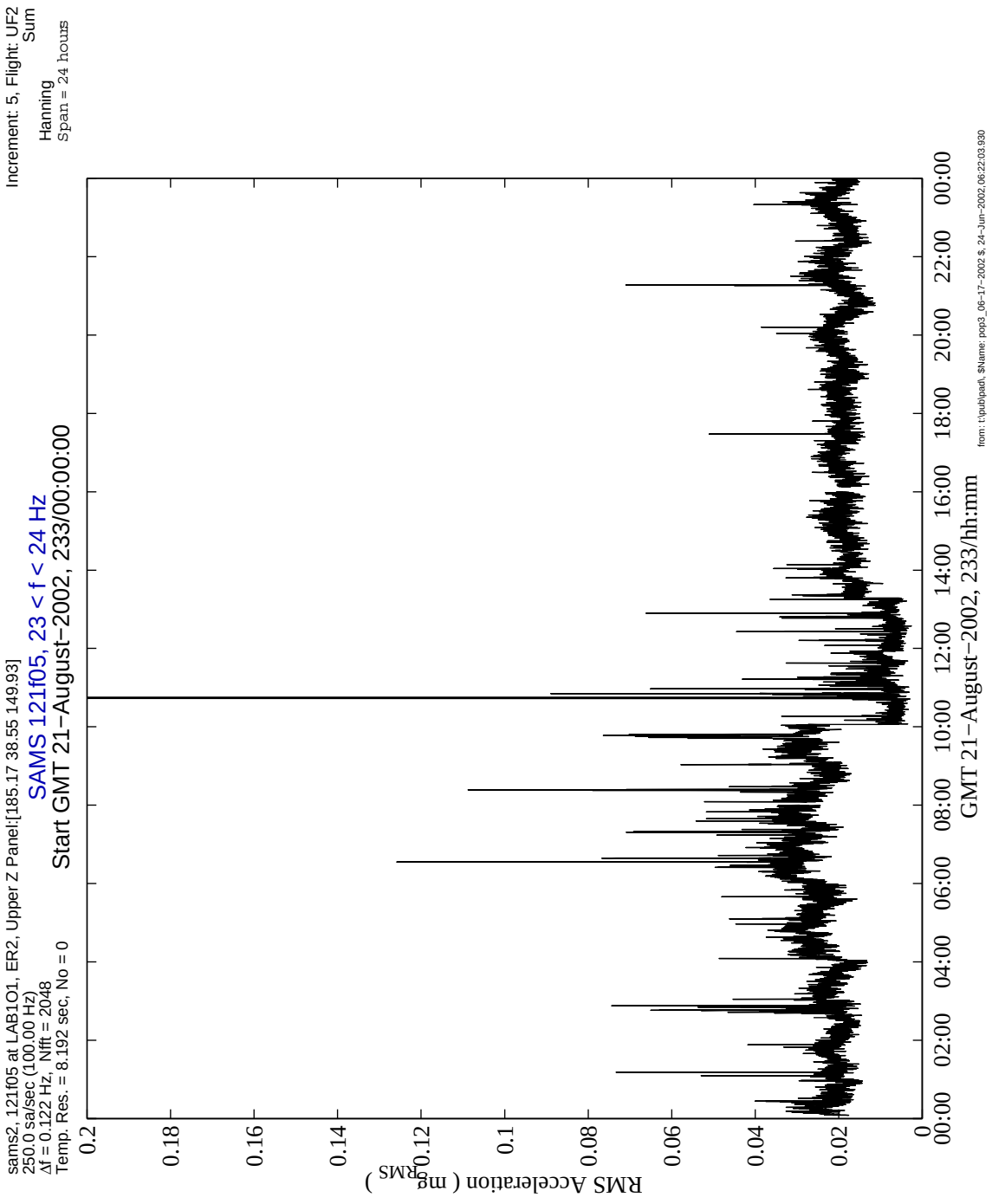

Figure 6-135 Interval RMS of SKV-1 (121f05)

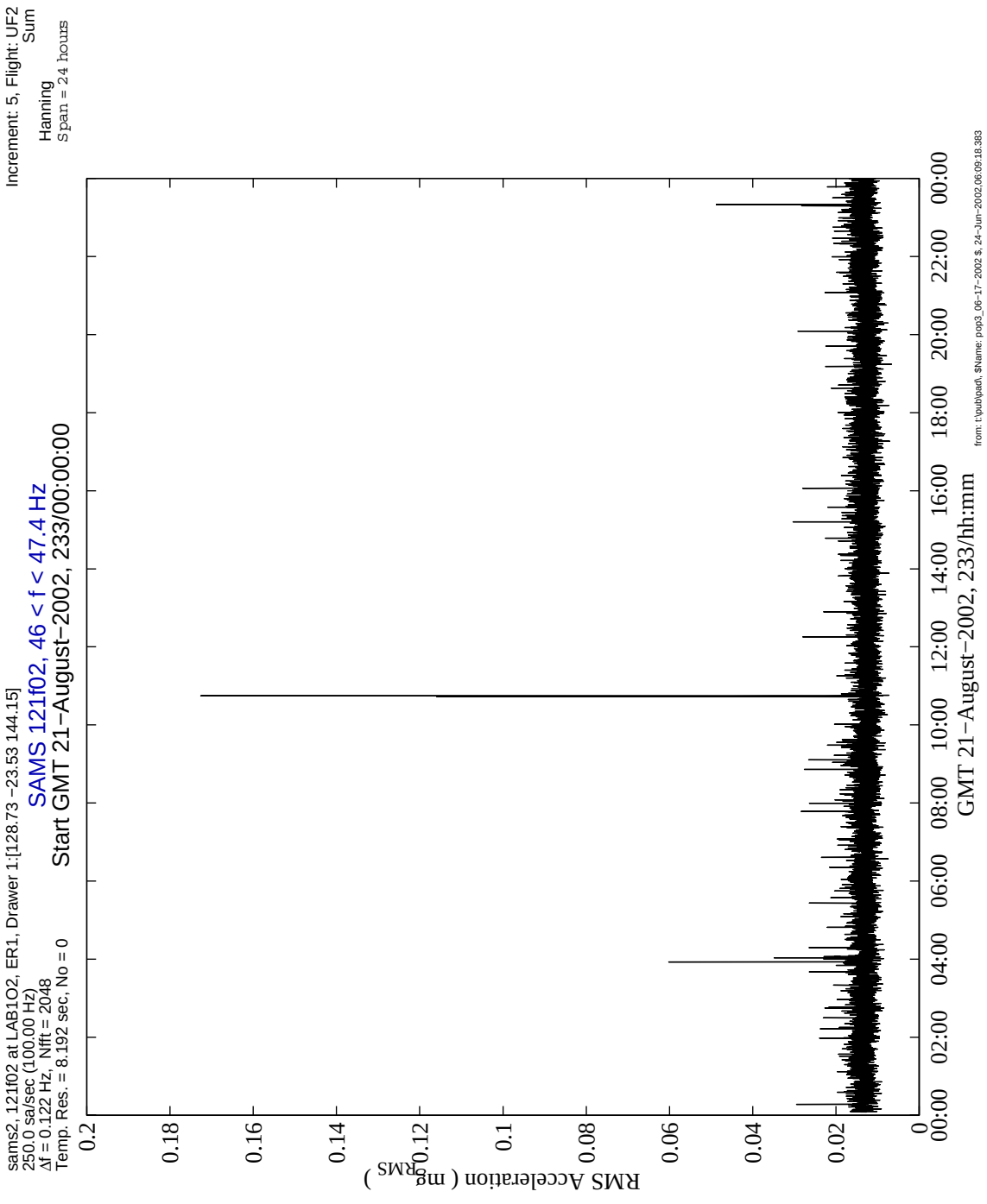

Figure 6-136 Interval RMS of SKV-1 Second Harmonic (121f02)

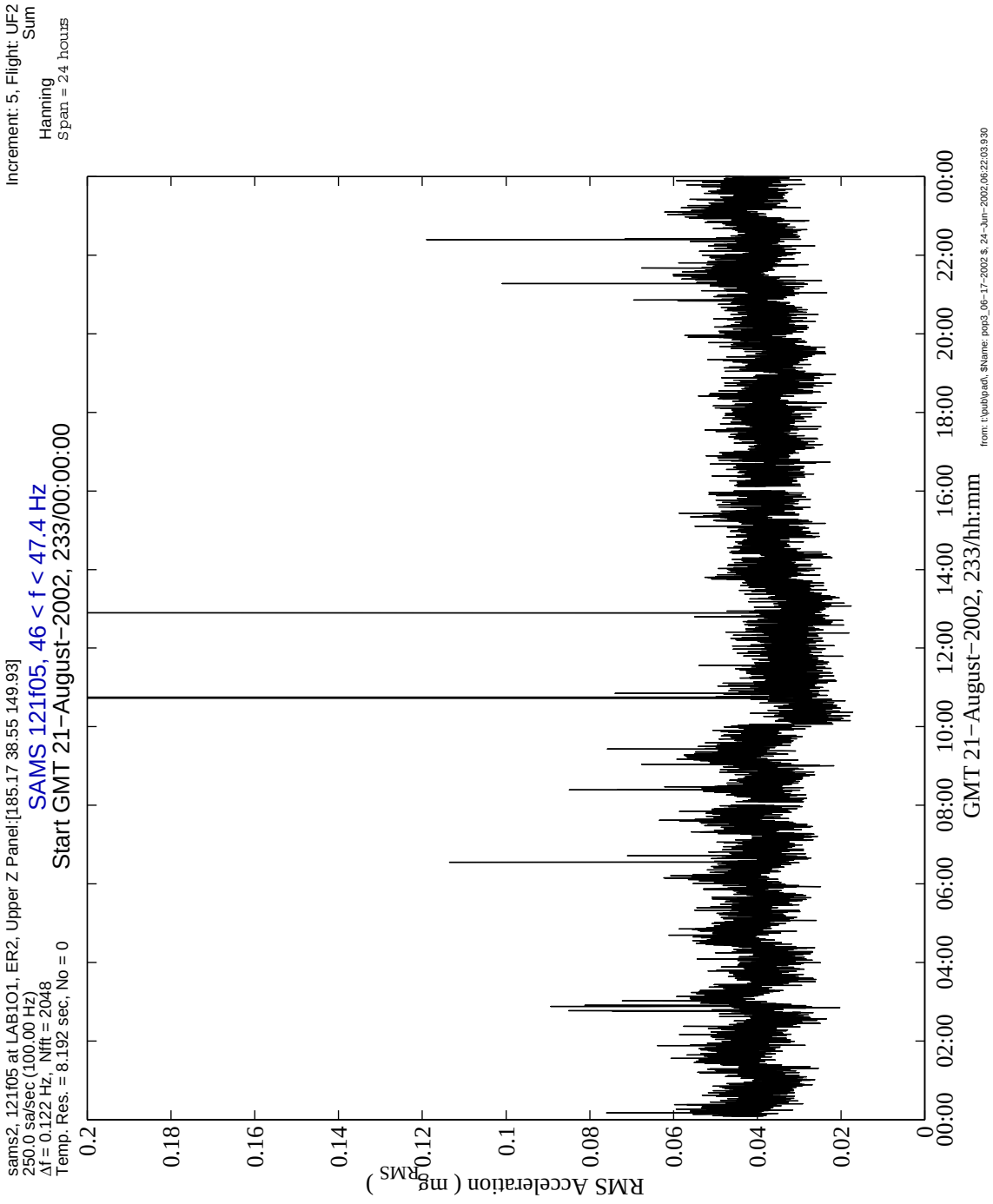

Figure 6-137 Interval RMS of SKV-1 Second Harmonic (121f05)

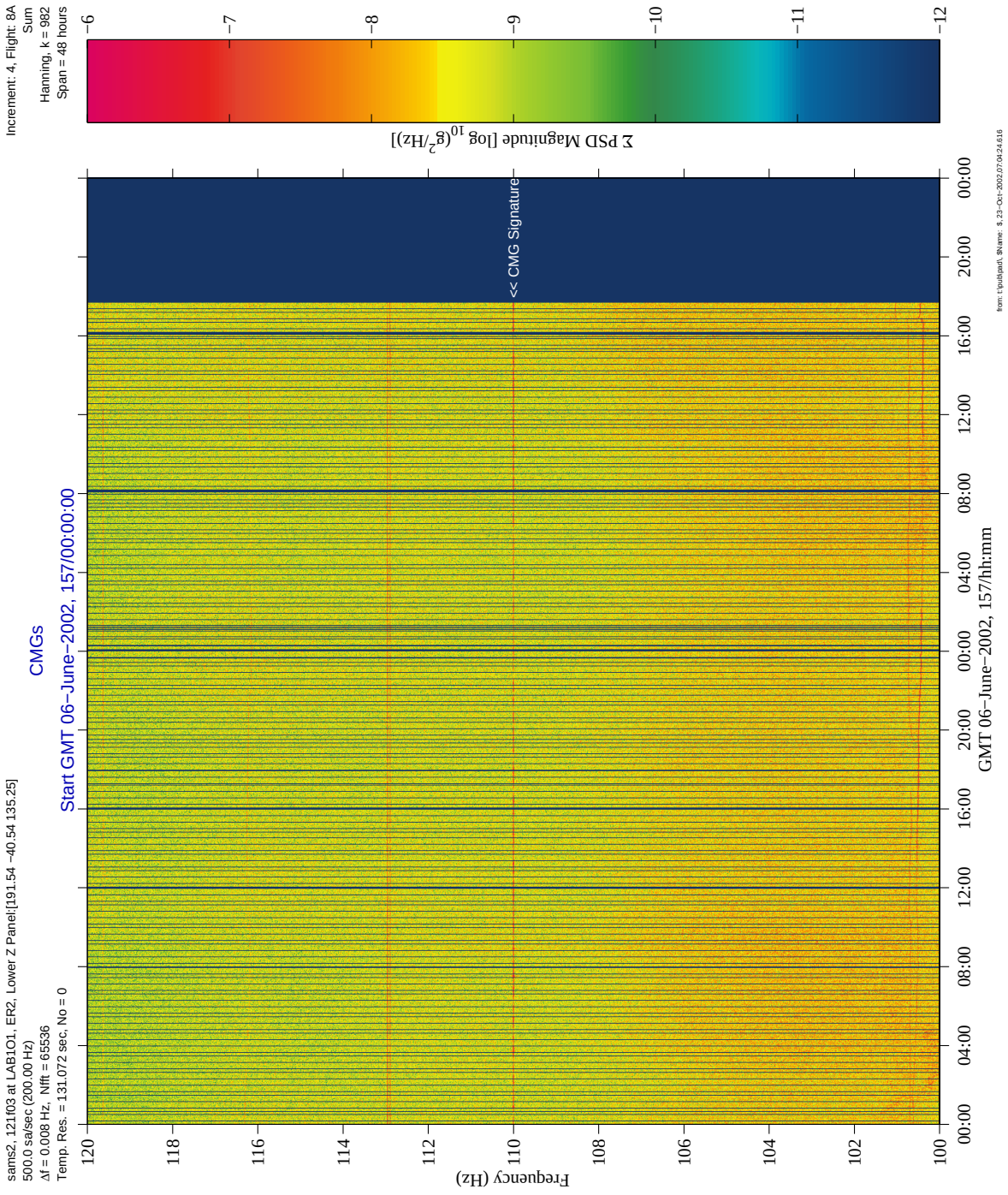

Figure 6-138 Spectrogram of CMGs Operating (121f03)

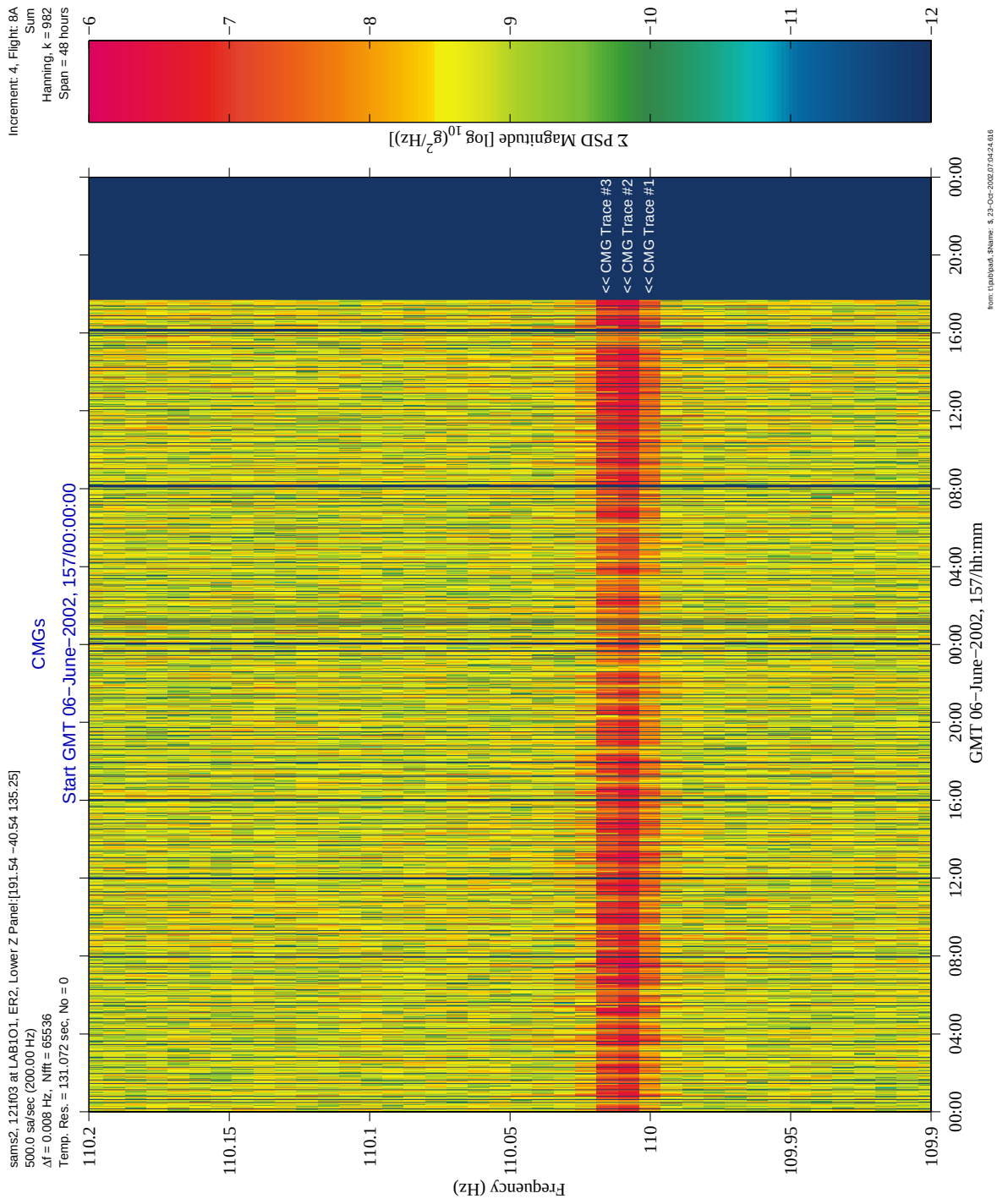

Figure 6-139 Spectrogram of CMGs Zoom Around Rotational Rate (121f03)

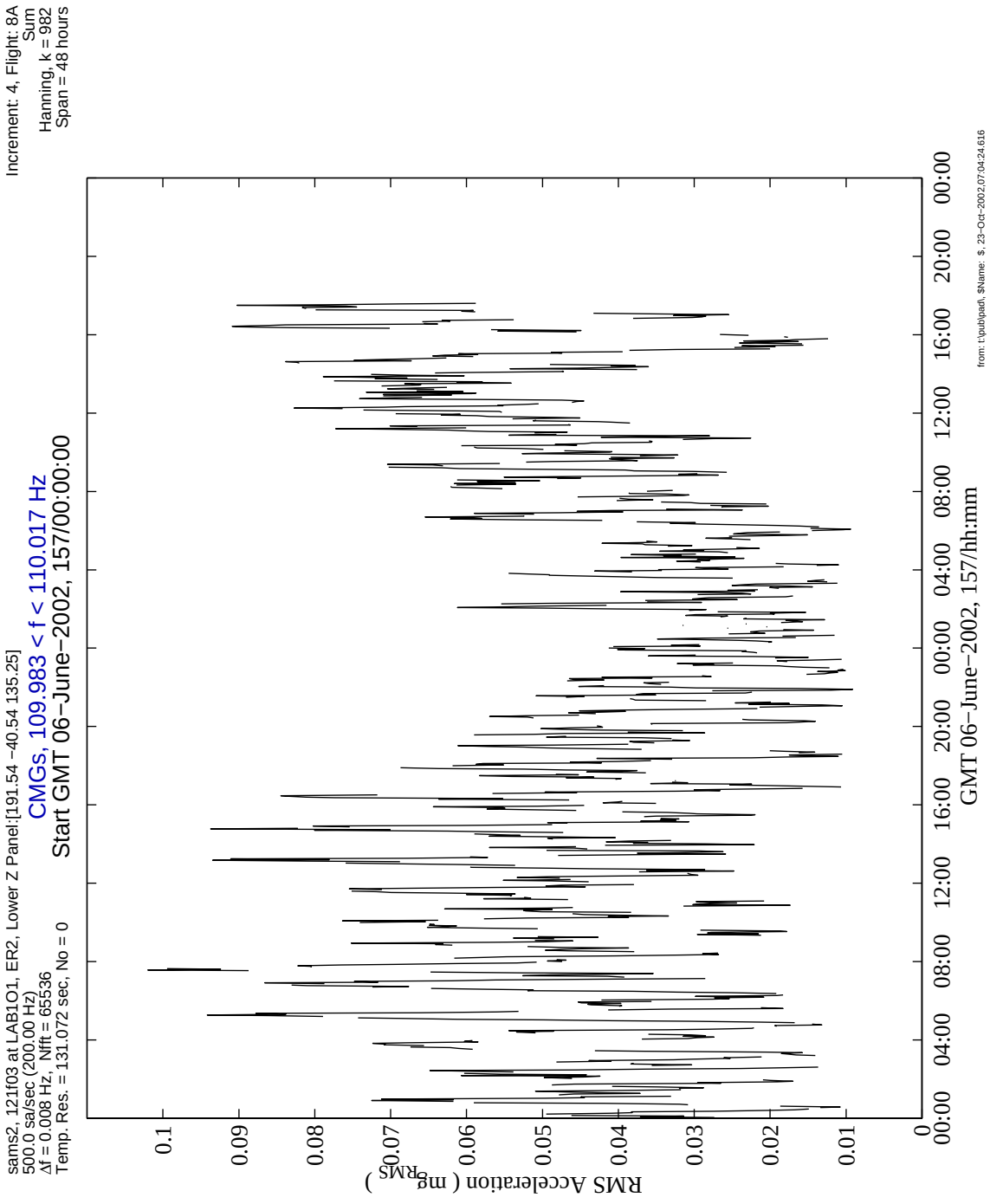

Figure 6-140 Interval RMS of CMGs Operating (121f03)

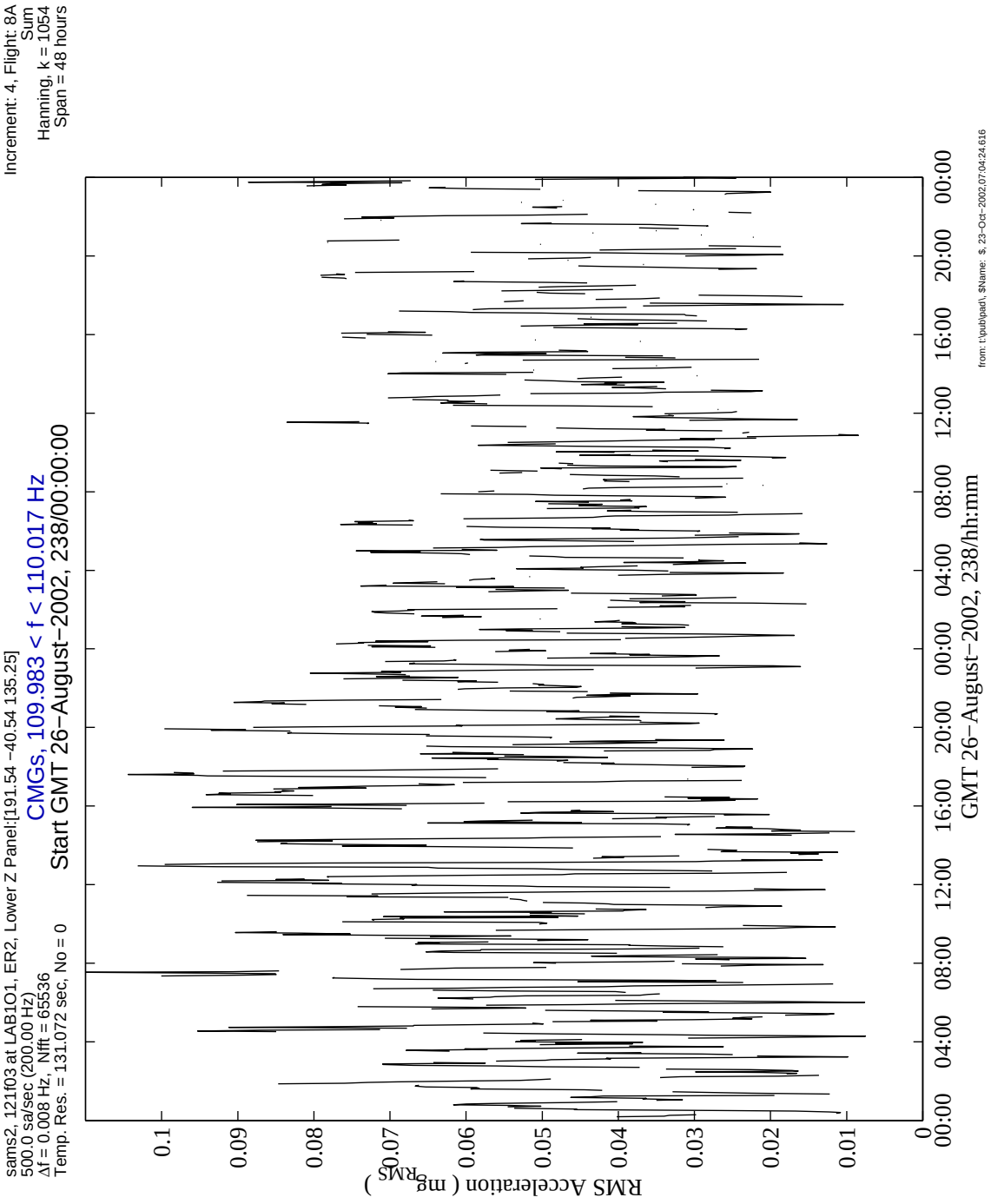

Figure 6-141 Interval RMS of CMGs Operating (121f03)

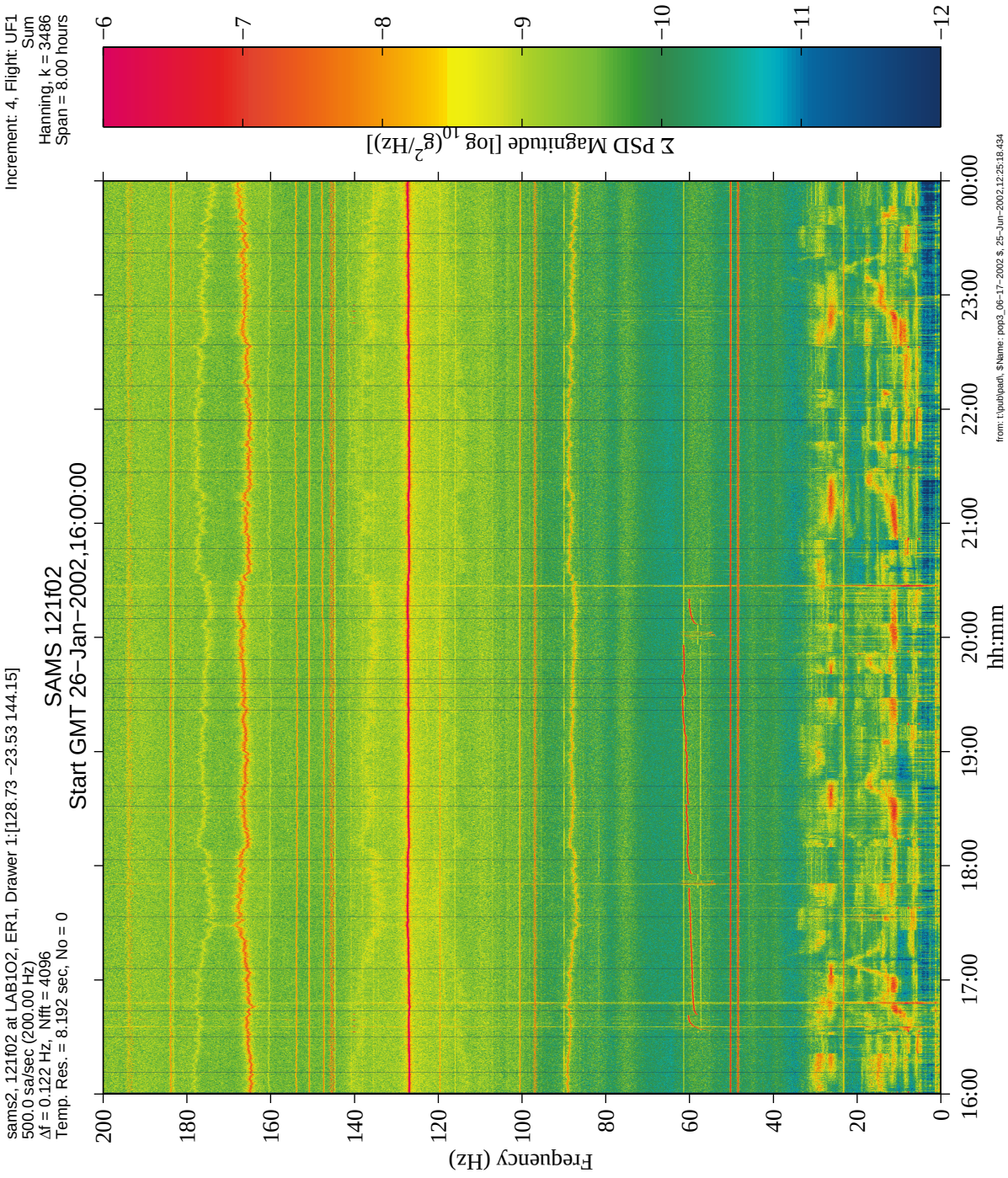

Figure 6-142 Spectrogram of GASMAP Equipment Operations (121f02)

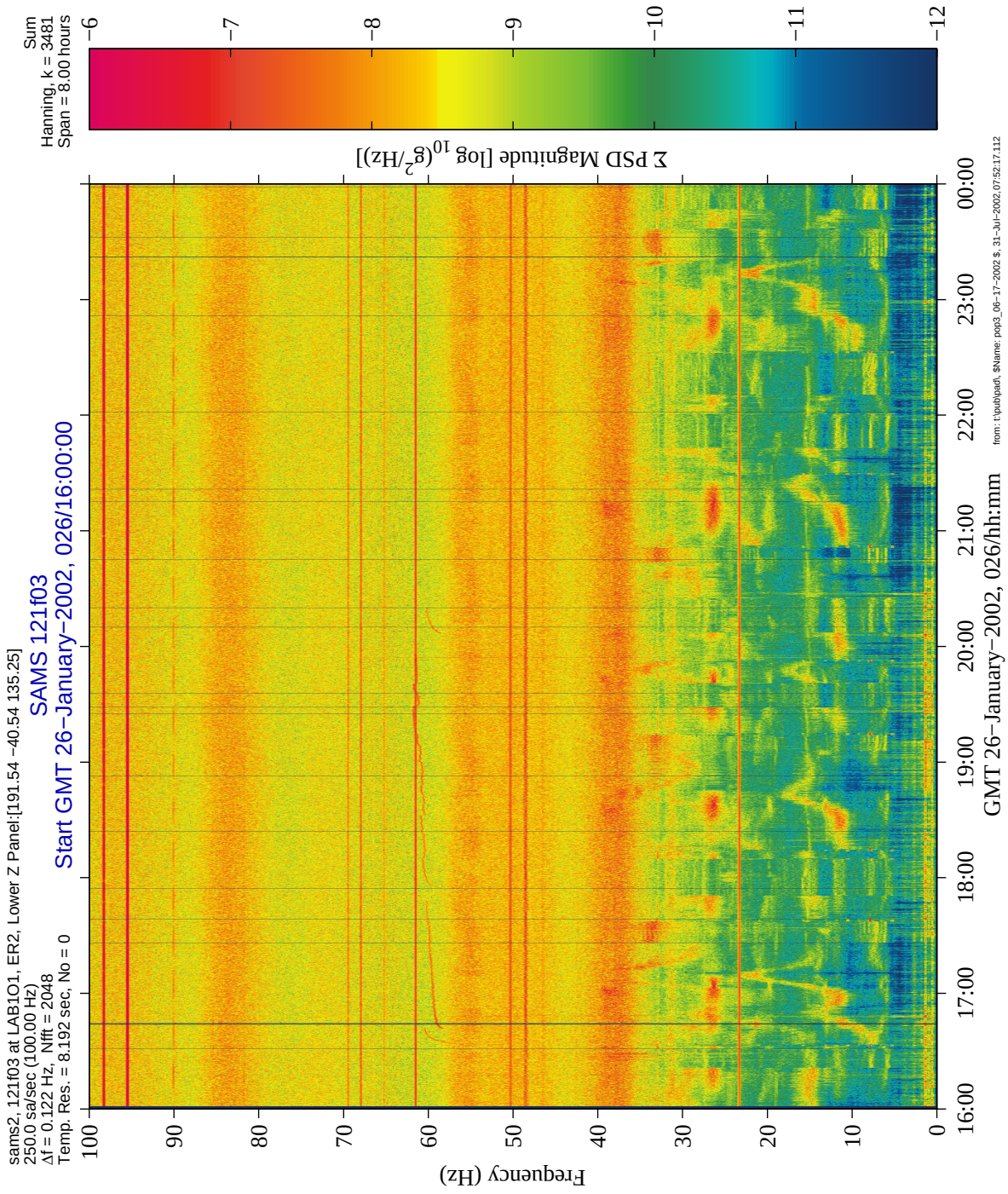

Figure 6-143 Spectrogram of GASMAP Equipment Operations (121f03)

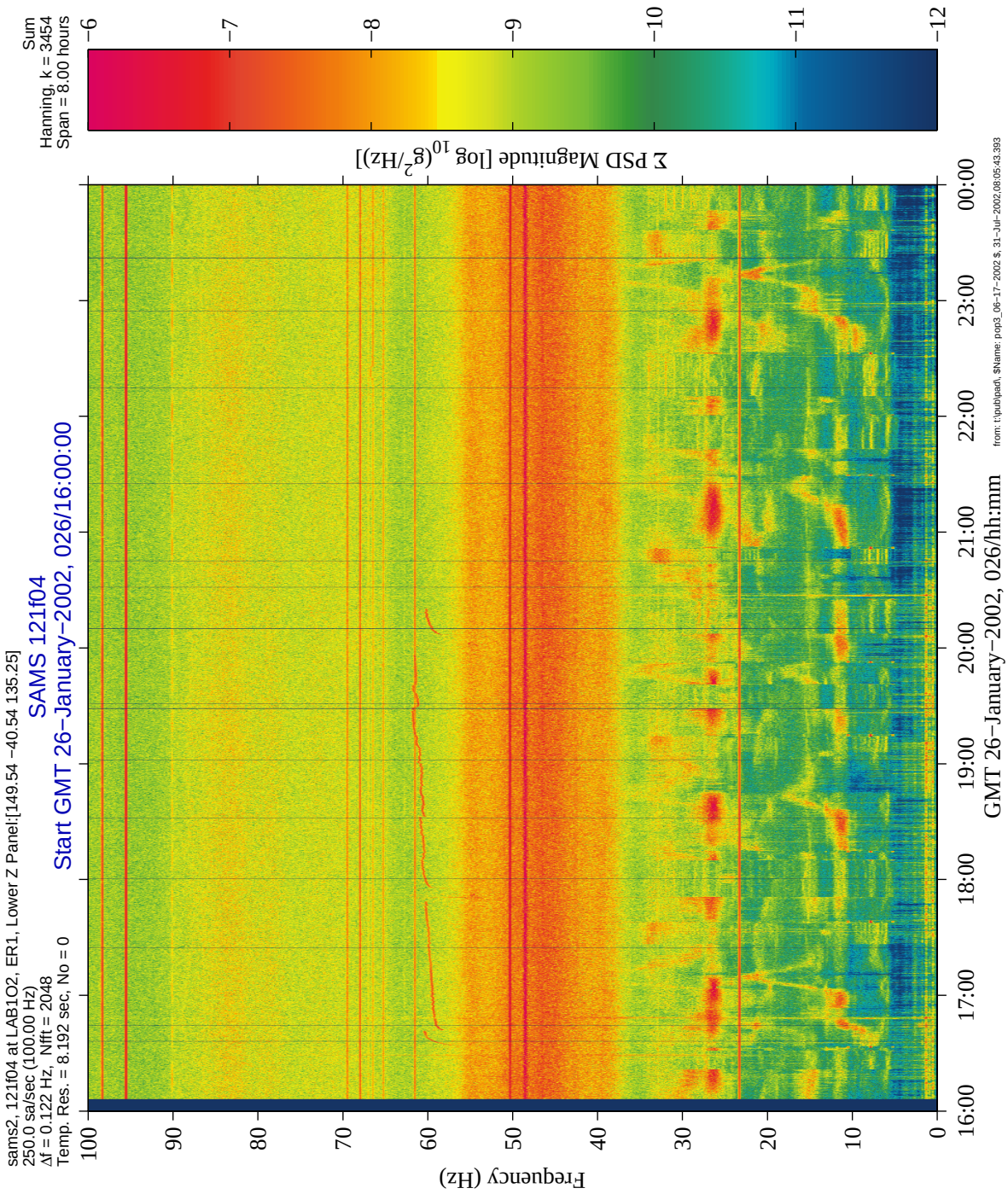

Figure 6-144 Spectrogram of GASMAP Equipment Operations (121f04)

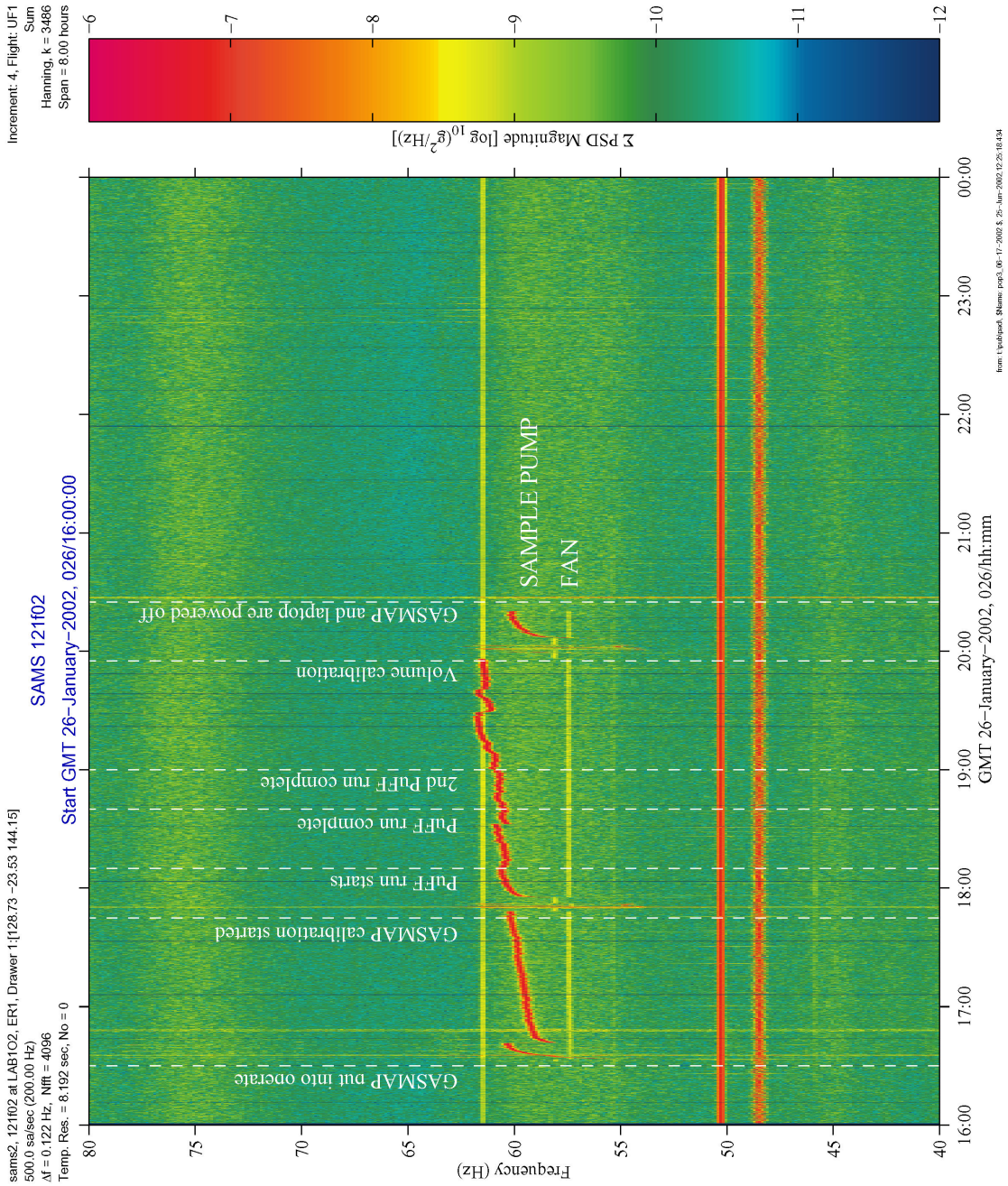

Figure 6-145 Spectrogram Zoom of GASMAP Equipment Operations (121f02)

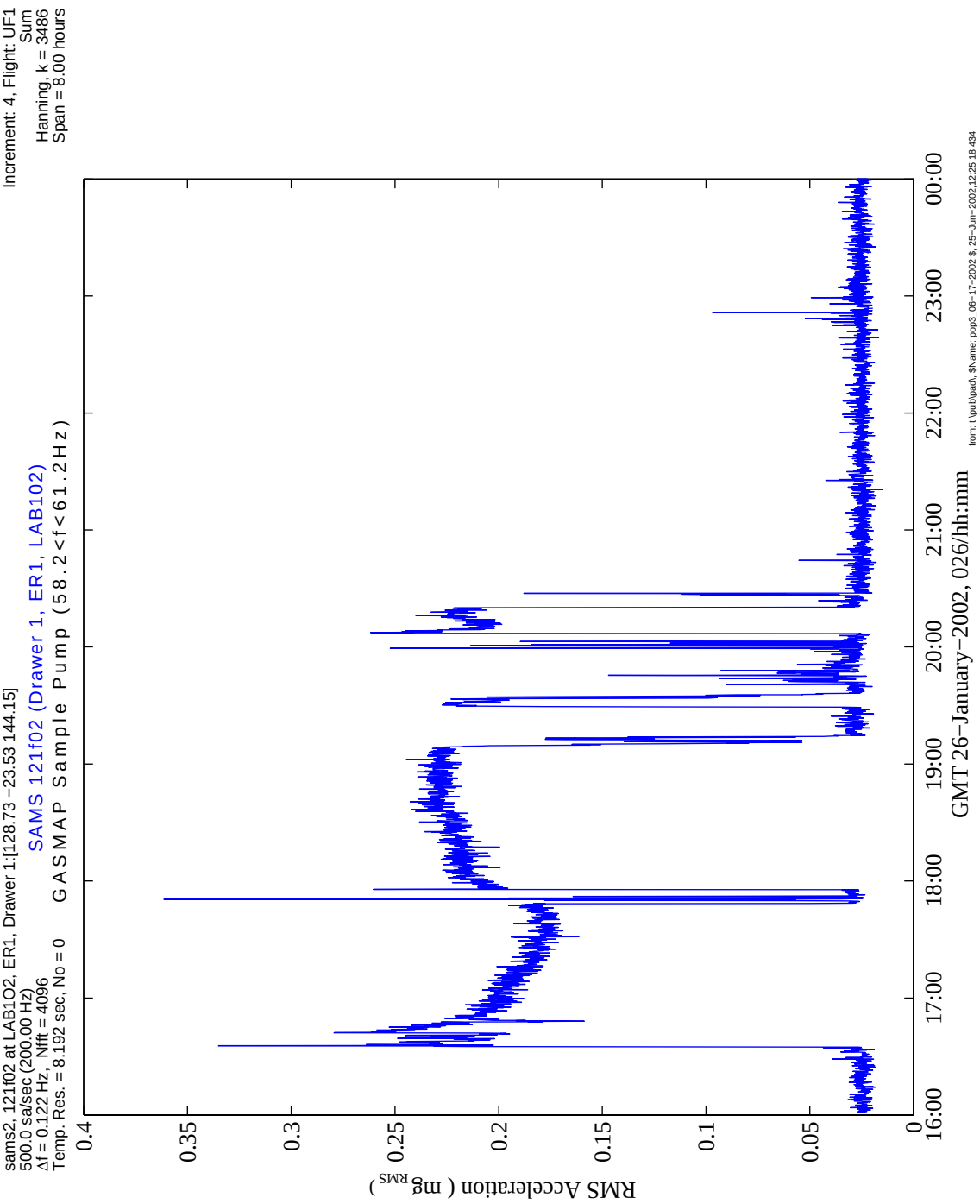

Figure 6-146 Interval RMS of GASMAP Sample Pump (121f02)

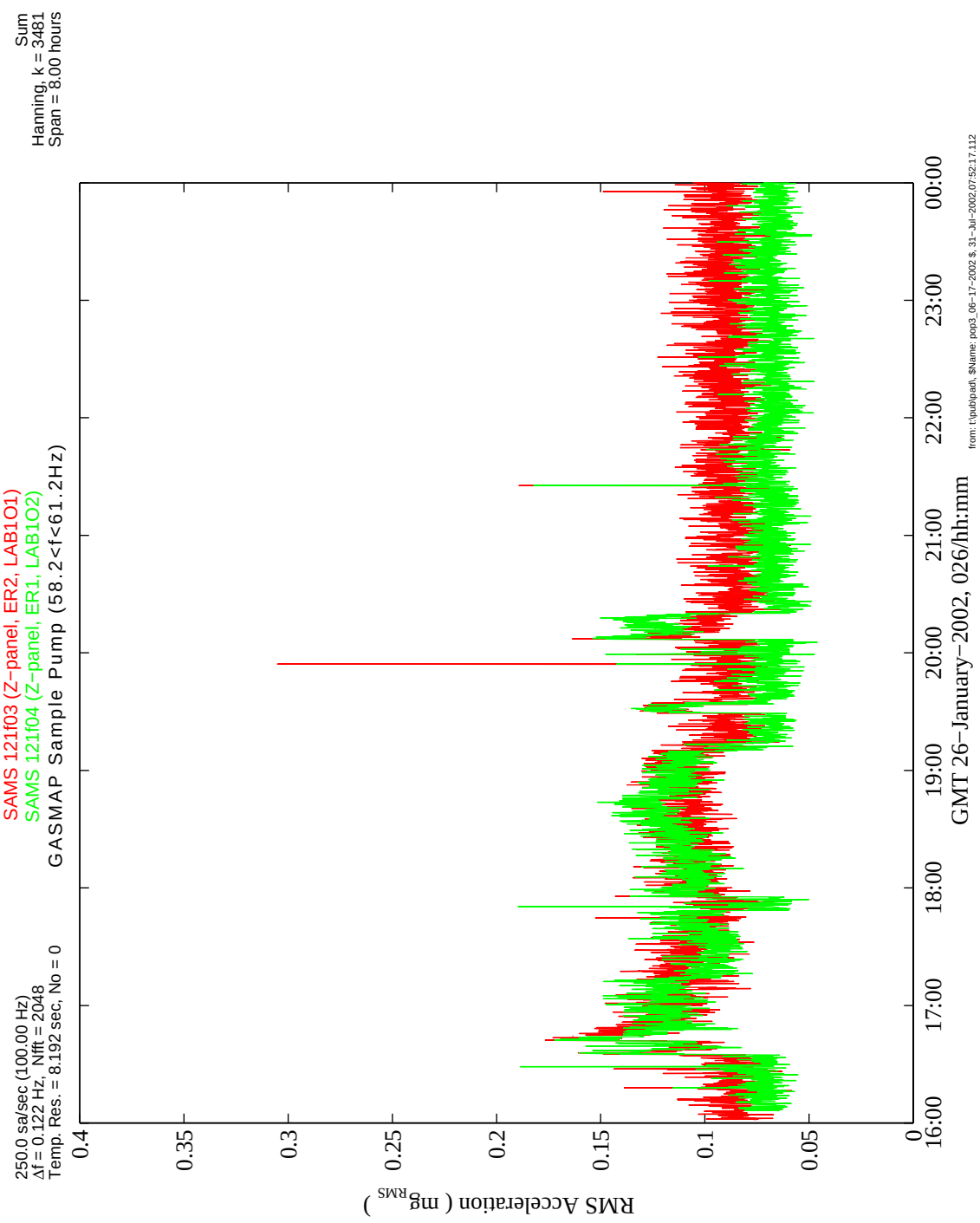

Figure 6-147 Interval RMS of GASMAP Sample Pump (121f03, 121f04)

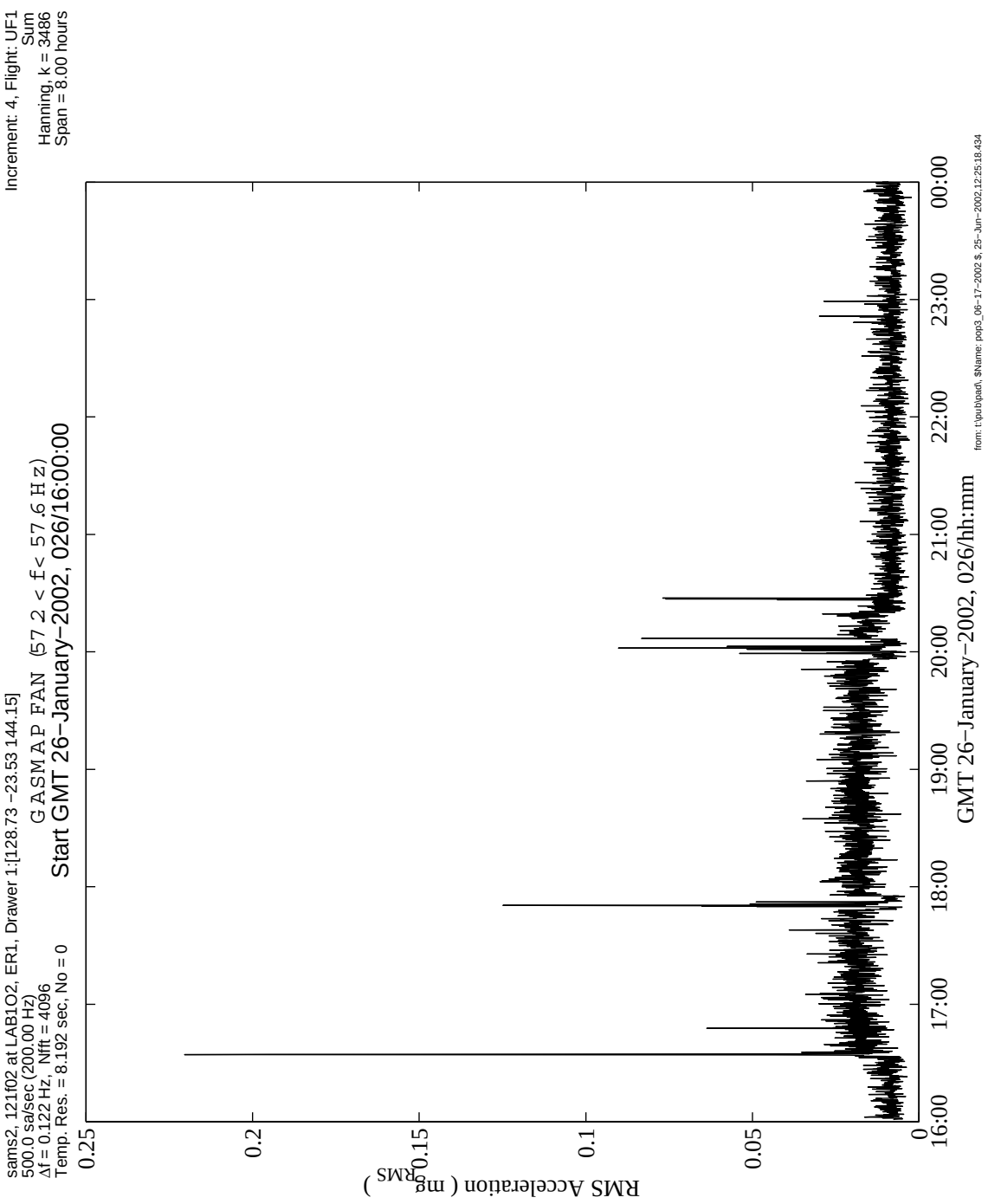

Figure 6-148 Interval RMS of GASMAP Fan (121f02)

Front View of MEPS Hardware Installed in Express Rack Locker (front panels removed)

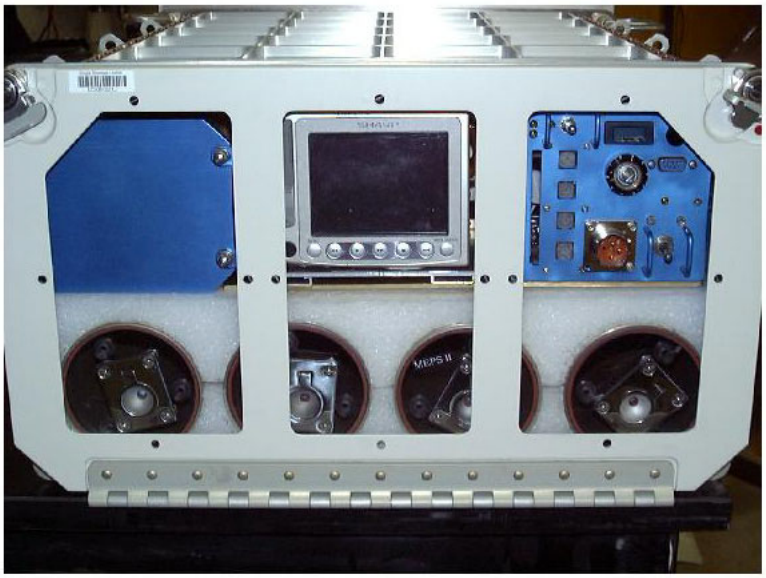

Figure 6-149 MEPS Chassis Configuration in an EXPRESS Rack Locker with Door Closed

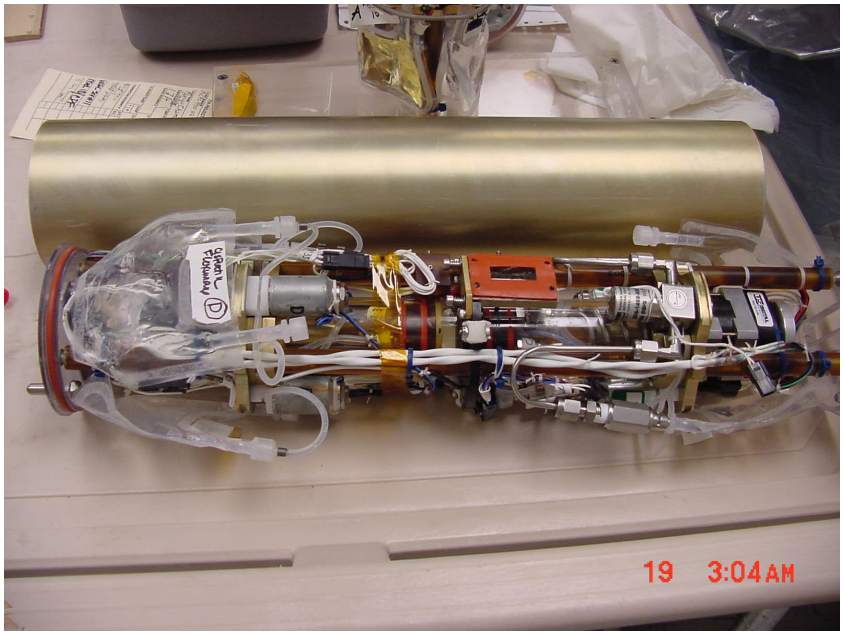

Figure 6-150 PCM Outside Of Housing

Figure 6-151 MEPS Chassis Unit with the EXPRESS Rack Locker Door Open

Figure 6-152 MEPS Close Up Of Door

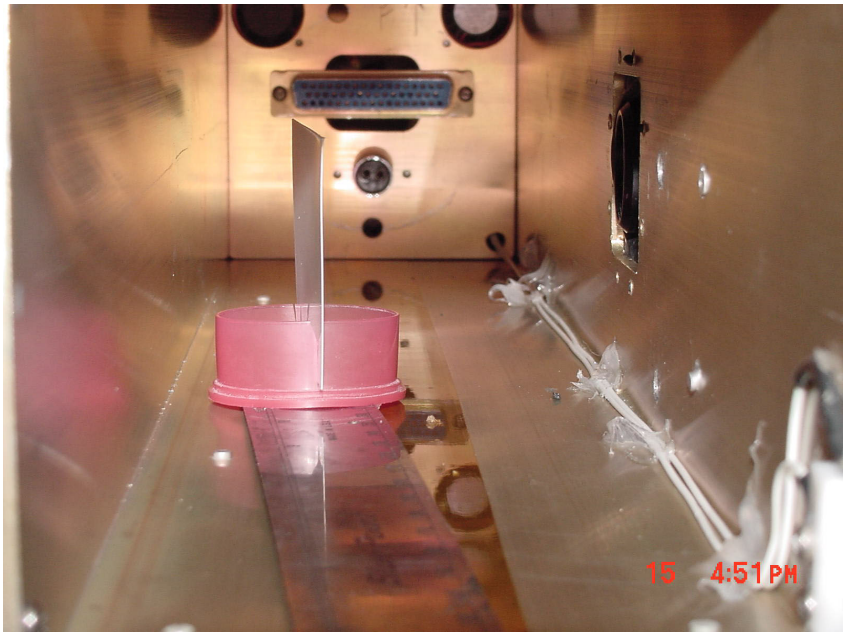

Figure 6-153 Interior of PCM Housing

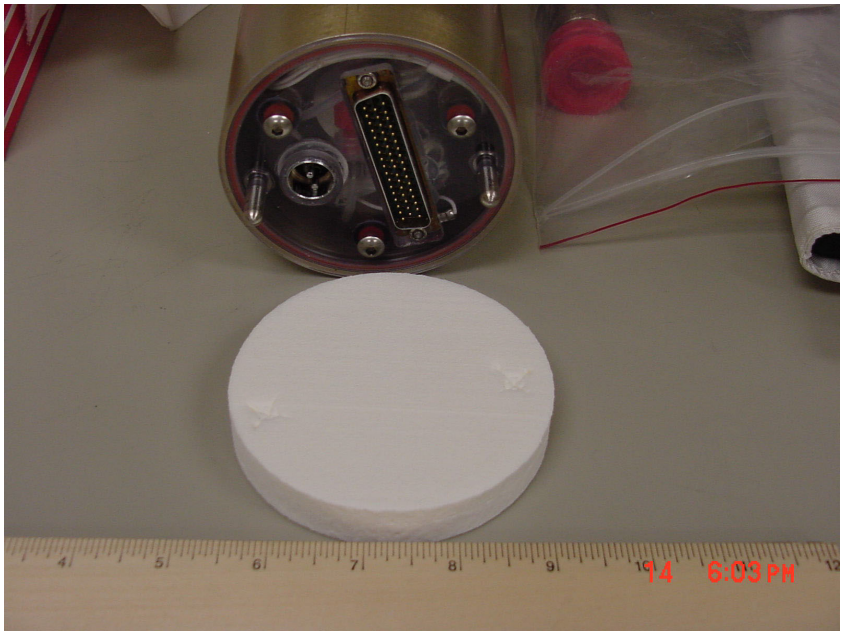

Figure 6-154 PCM End Showing Connector

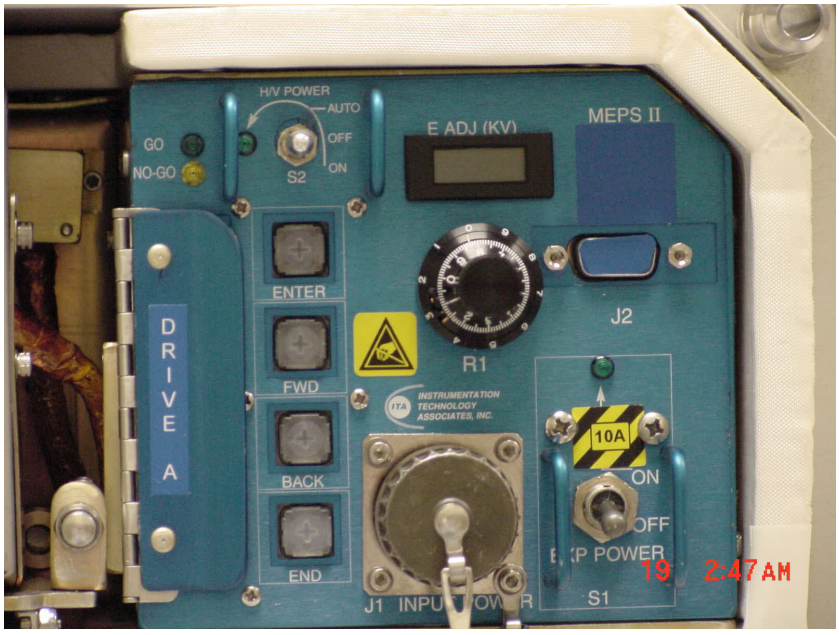

Figure 6-155 Right Front Panel of Chassis Unit Shows PCMCIA Slot

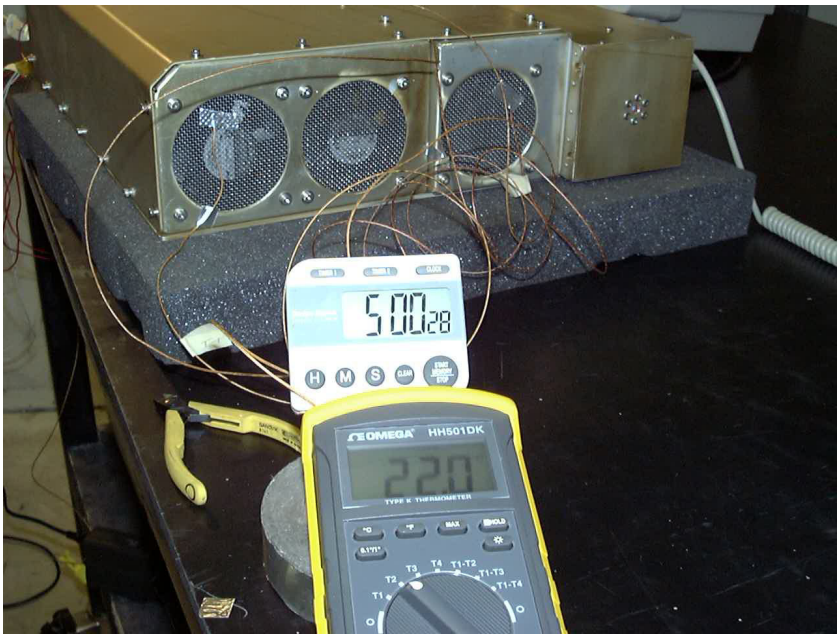

Figure 6-156 MEPS Fans to Circulate Cooling Air

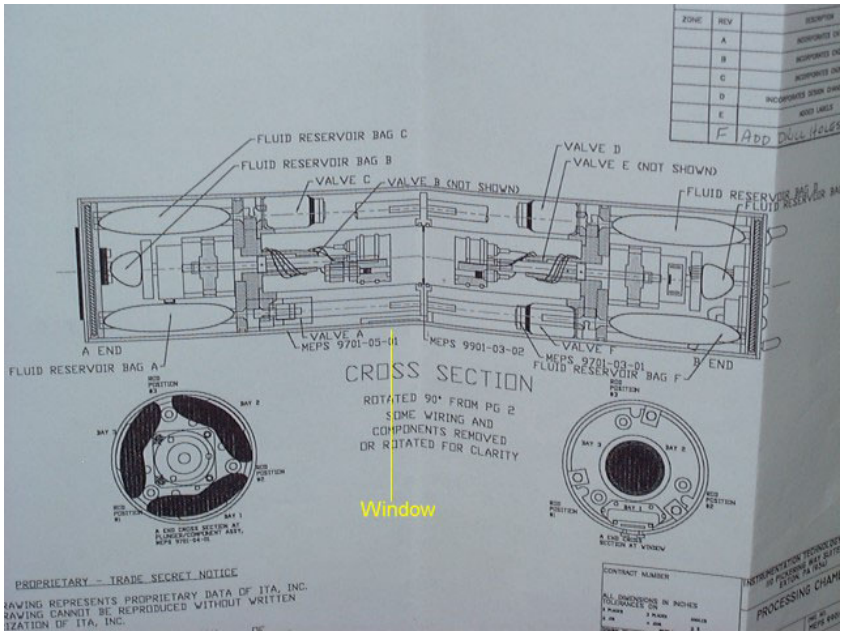

Figure 6-157 Top-Level Assembly of PCM

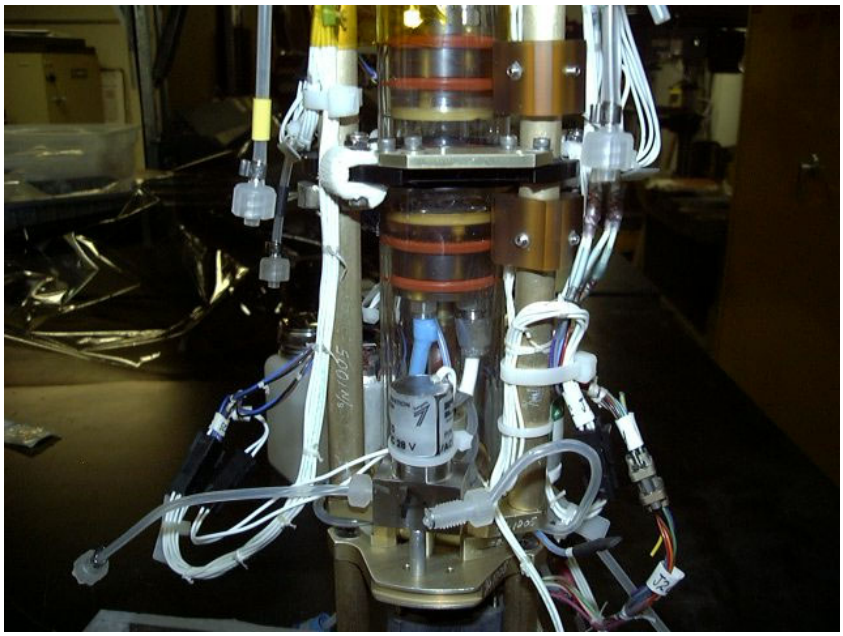

Figure 6-158 MEPS Hardware, Plungers and One of the Solenoid Valves

Figure 6-159 MEPS Blow Up of Plunger Area

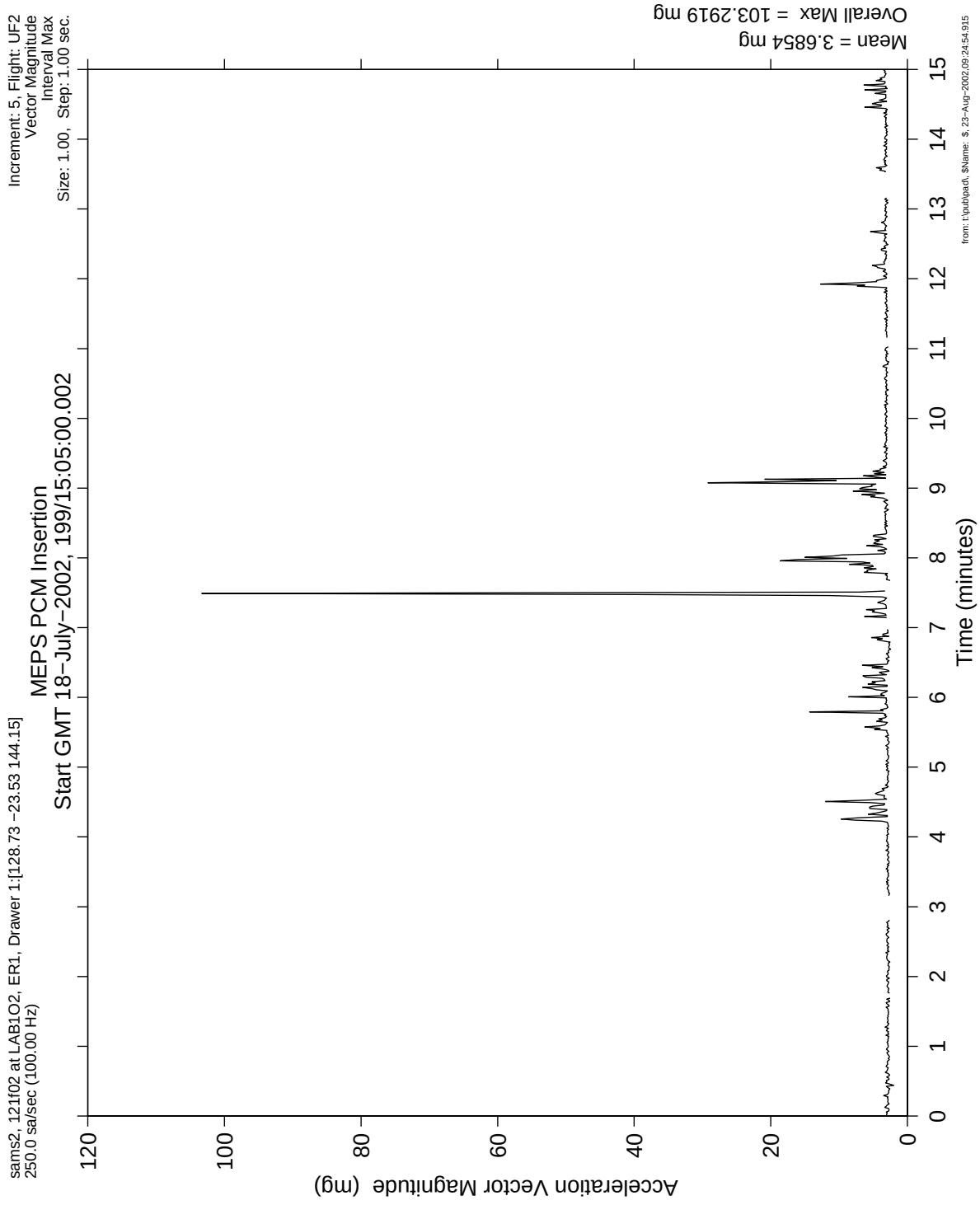

Figure 6-160 Interval Maximum of MEPS PCM Insertion (121f02)

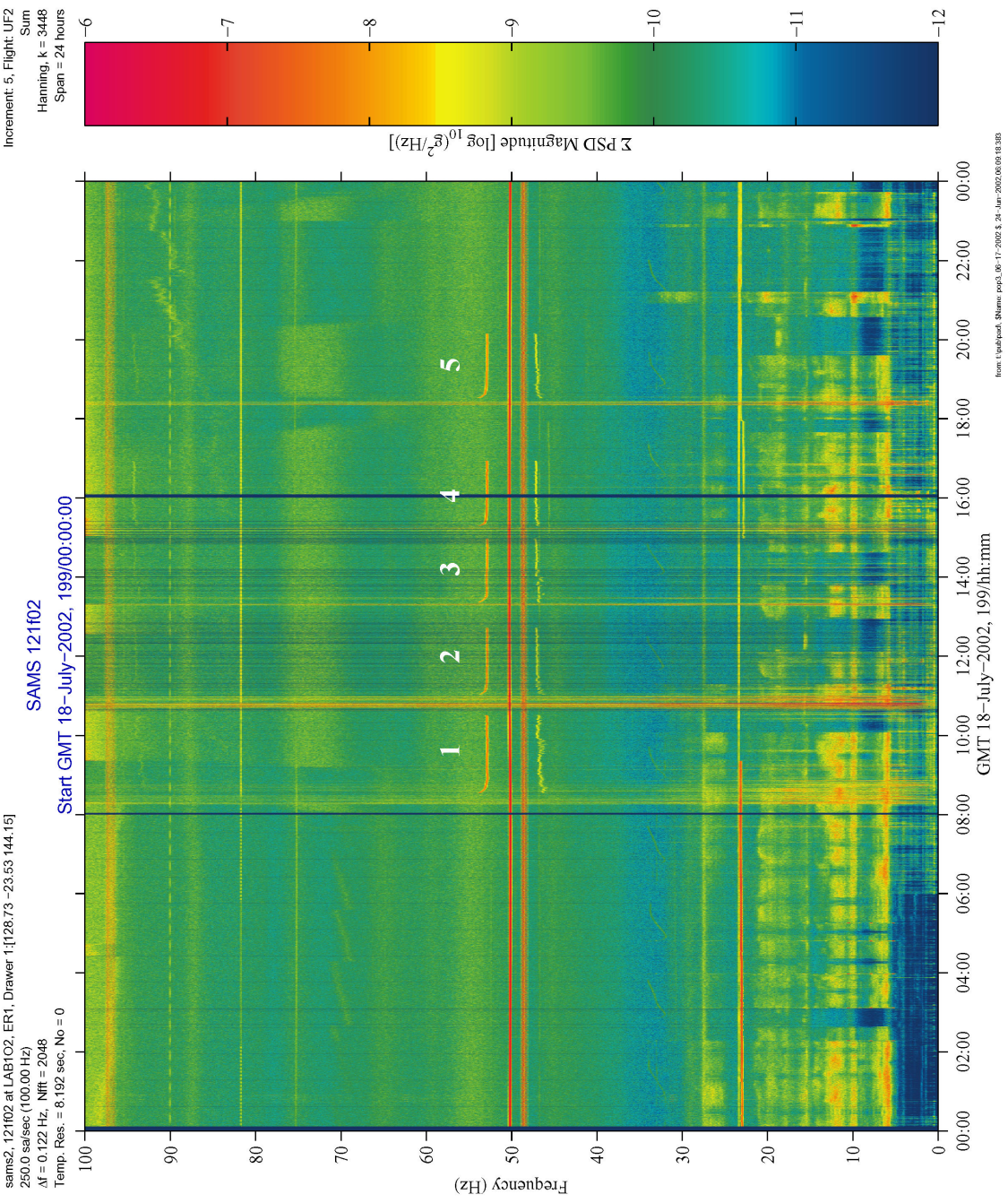

Figure 6-161 Spectrogram of 5 MEPS Runs (121f02)

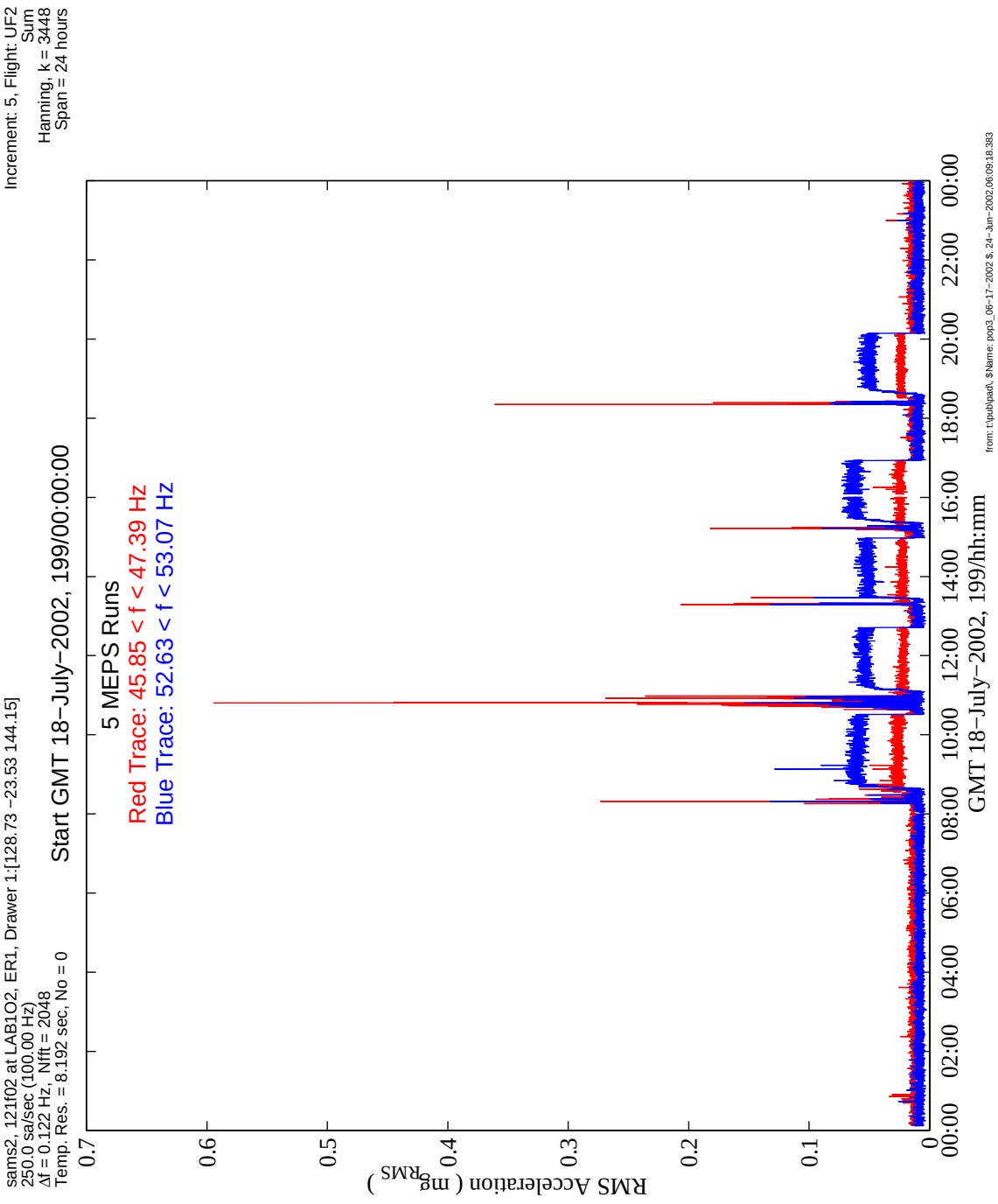

Figure 6-162 Interval RMS of 5 MEPS Runs (121f02)

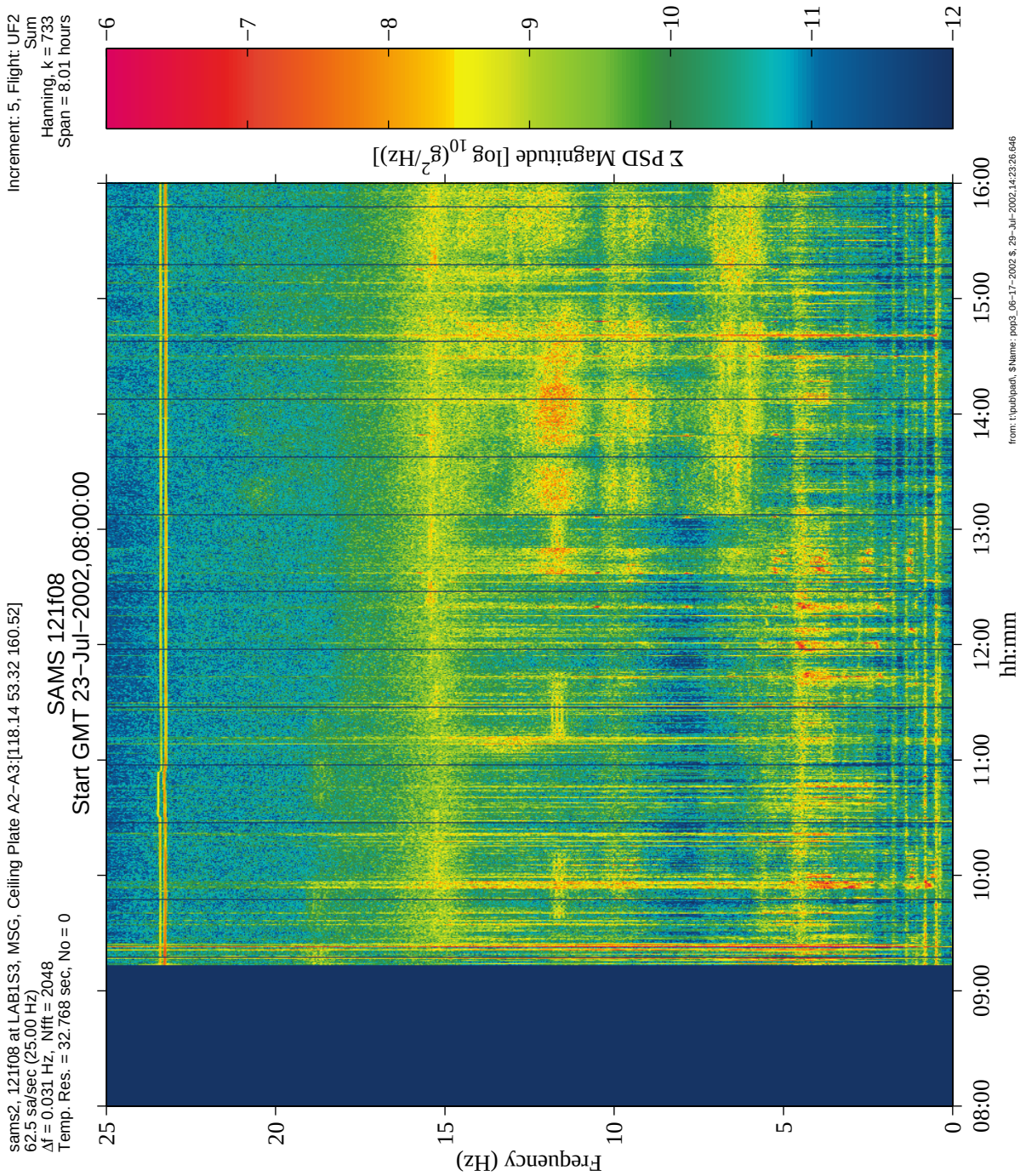

Figure 6-163 Spectrogram of SUBSA-10 (121f08)

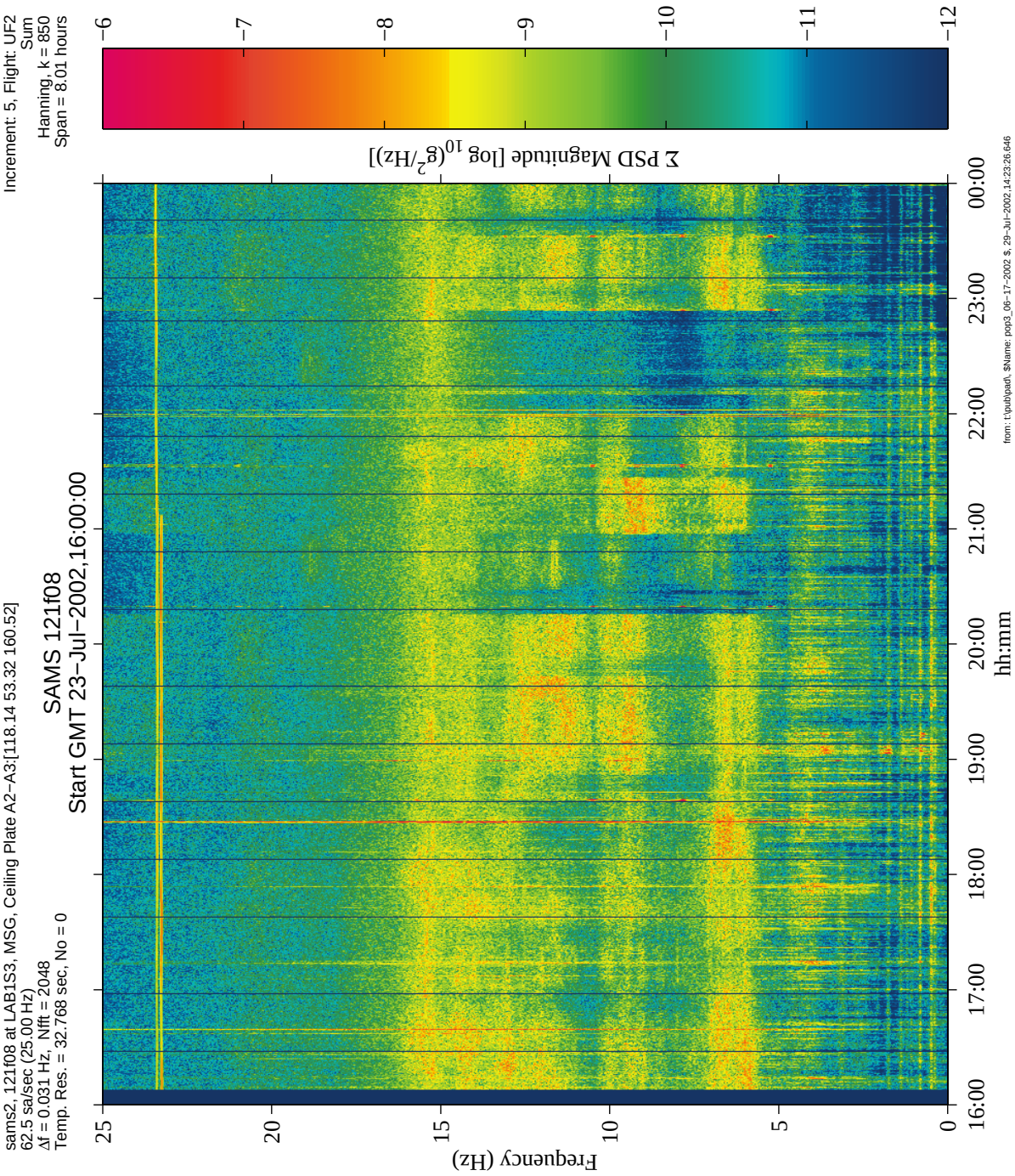

Figure 6-164 Spectrogram of SUBSA-10 (121f08)

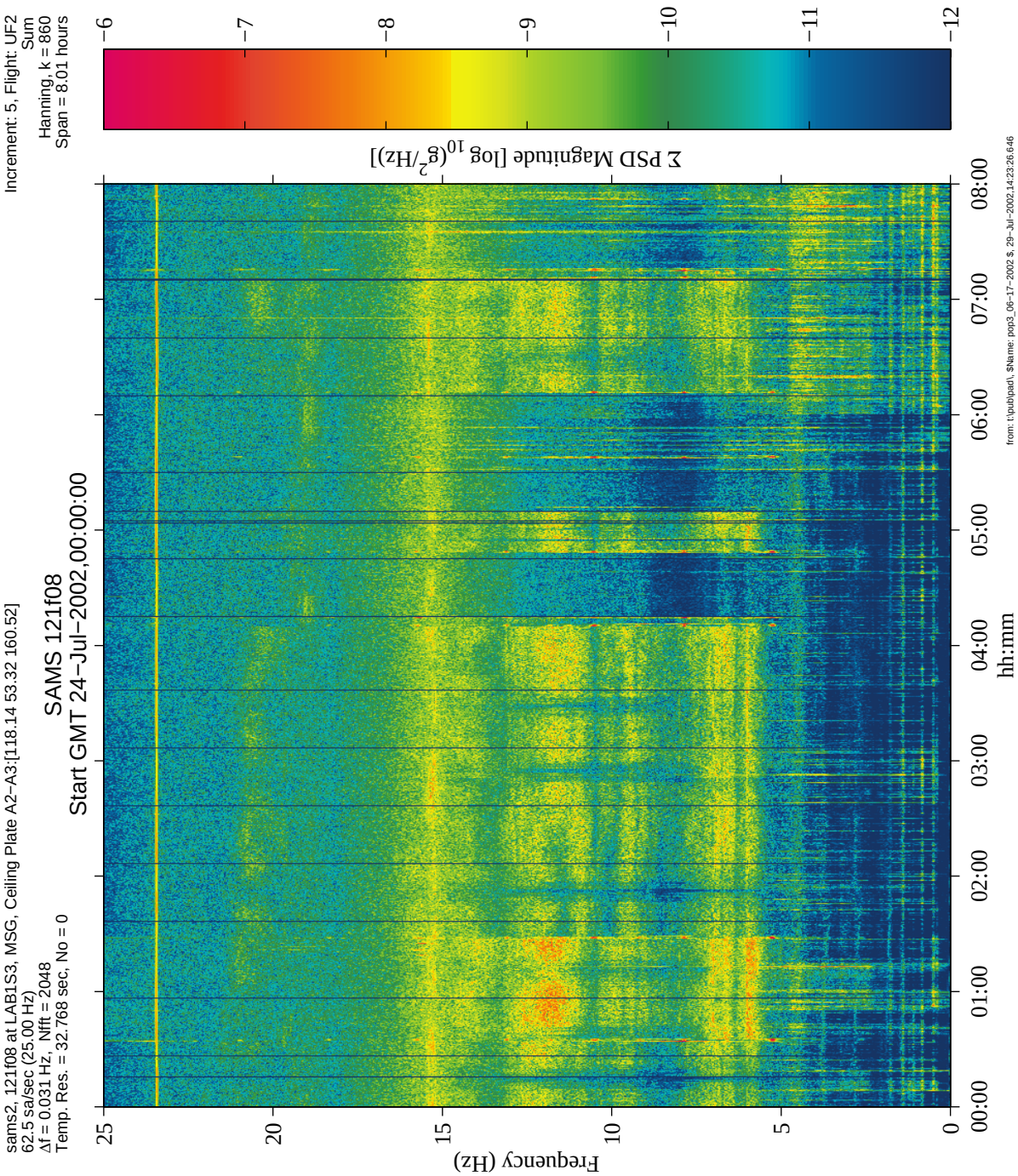

Figure 6-165 Spectrogram of SUBSA-10 (121f08)

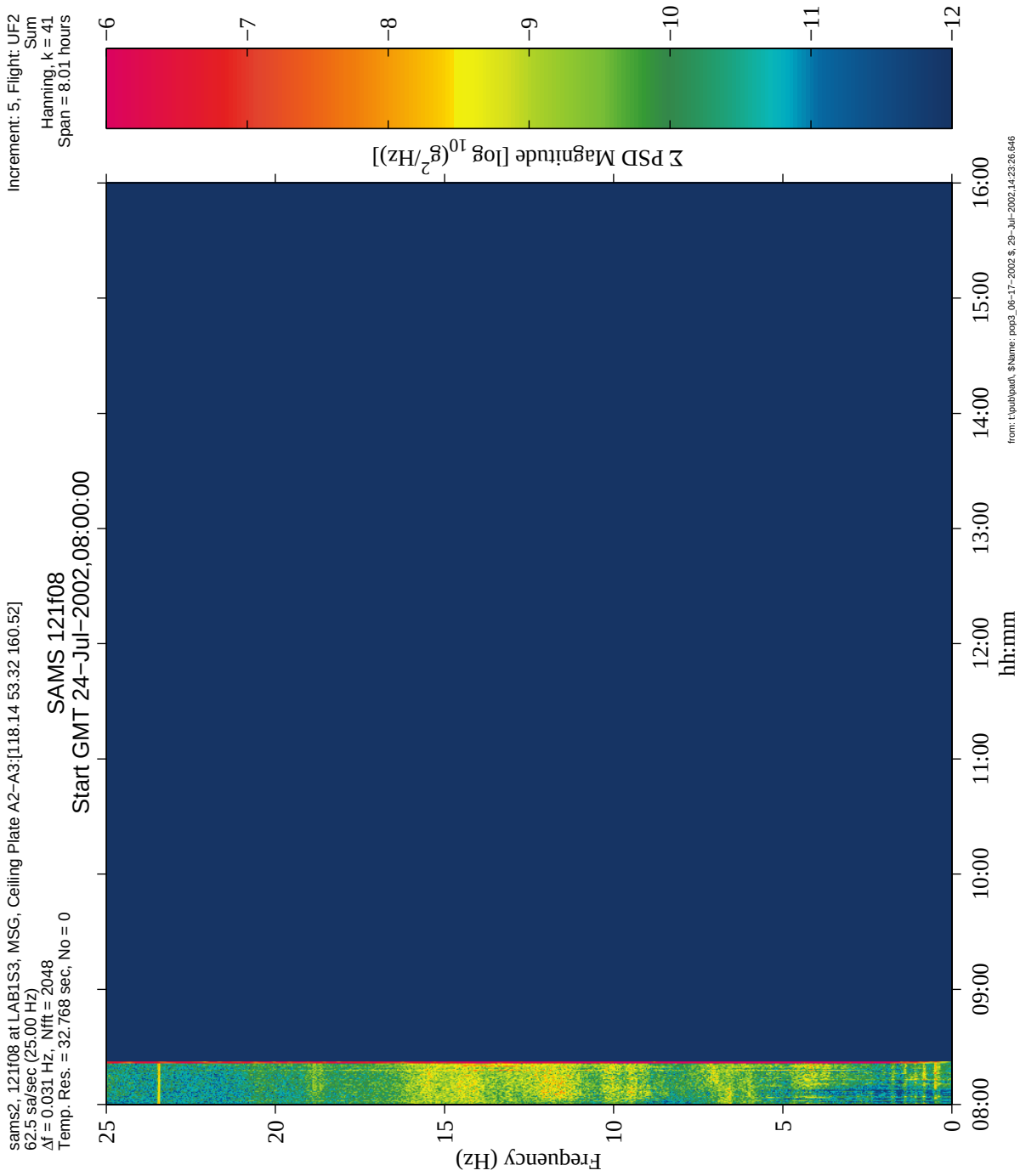

Figure 6-166 Spectrogram of SUBSA-10 (121f08)

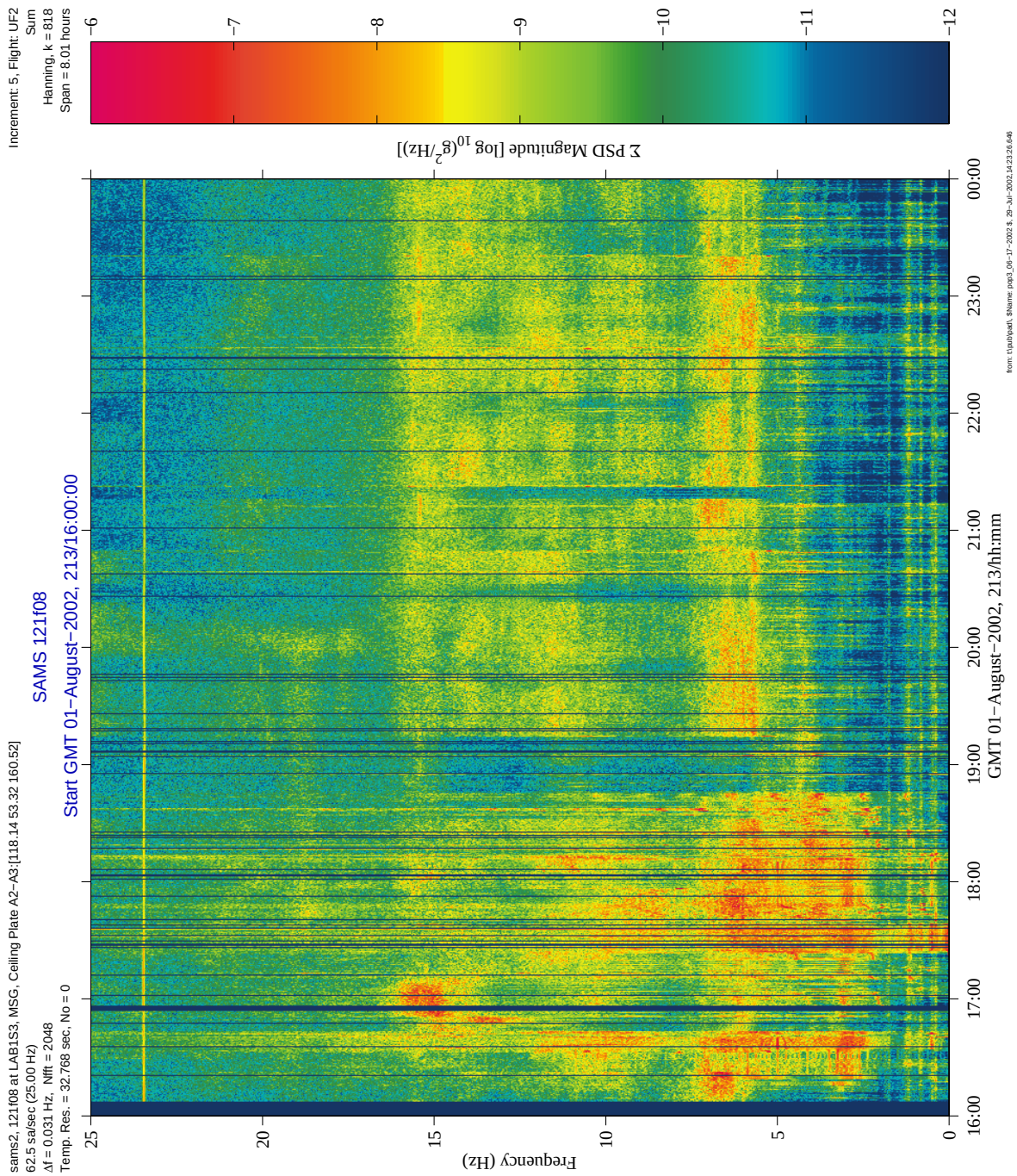

Figure 6-167 Spectrogram of SUBSA-02 (121f08)

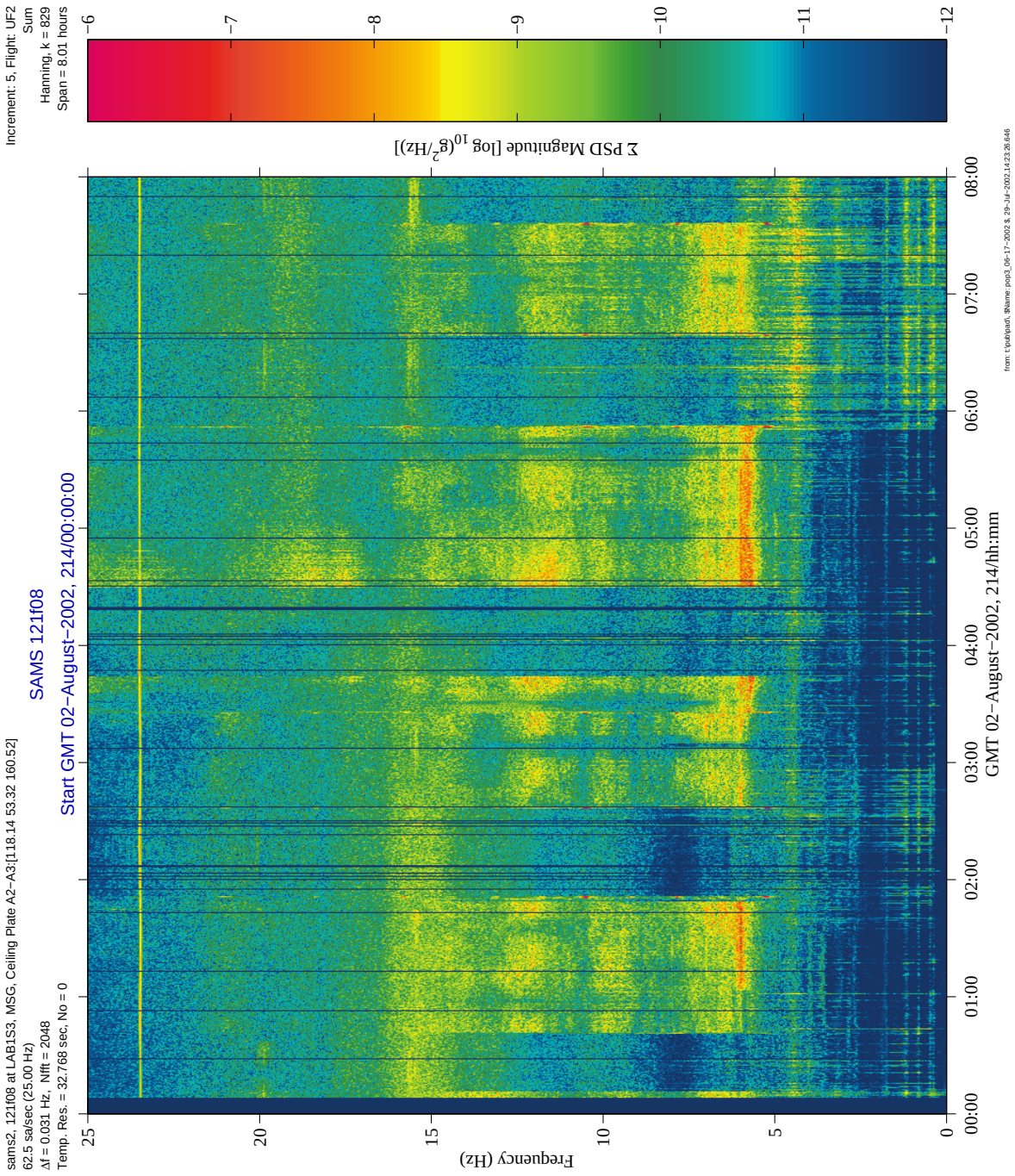

Figure 6-168 Spectrogram of SUBSA-02 (121f08)

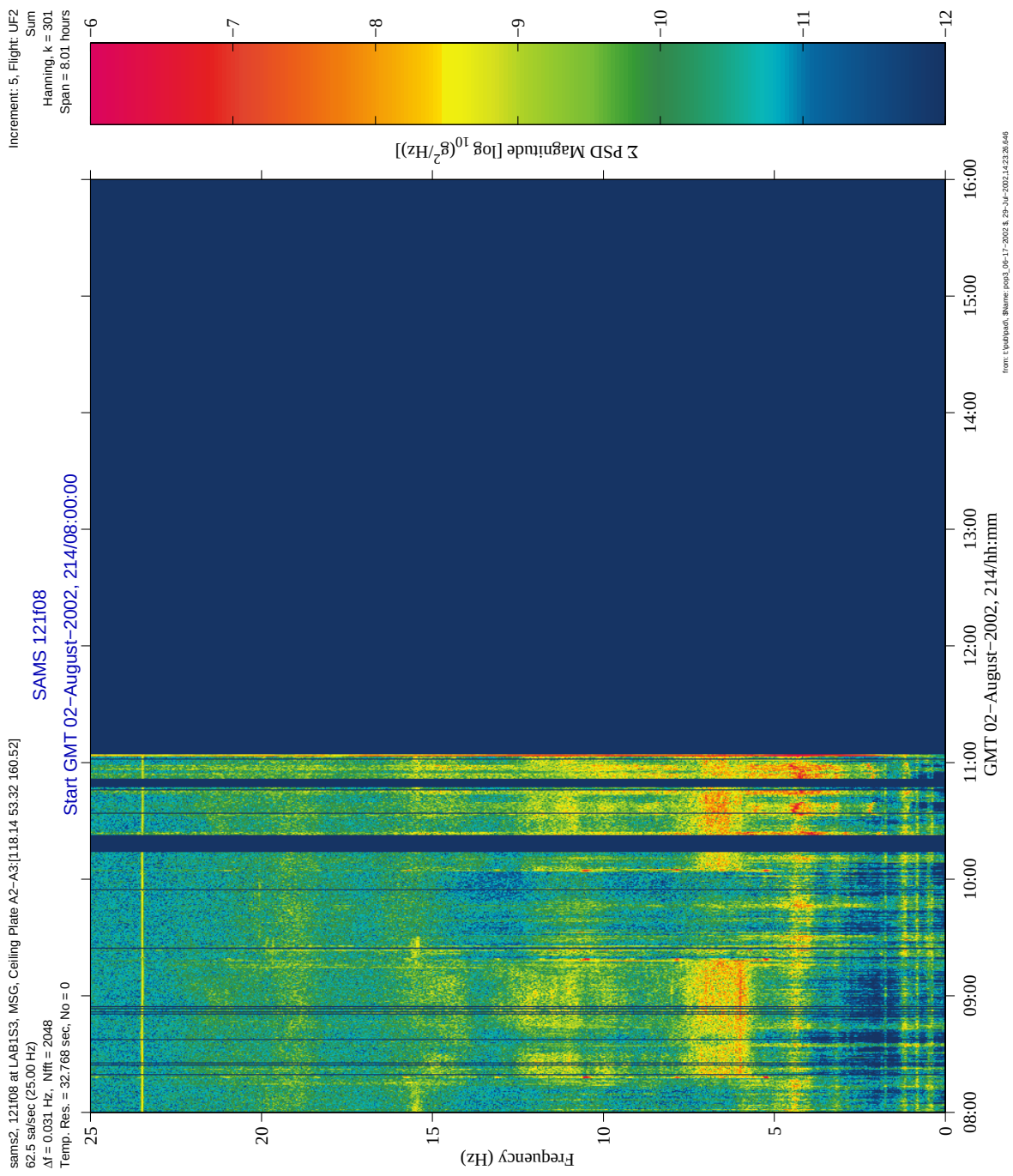

Figure 6-169 Spectrogram of SUBSA-02 (121f08)

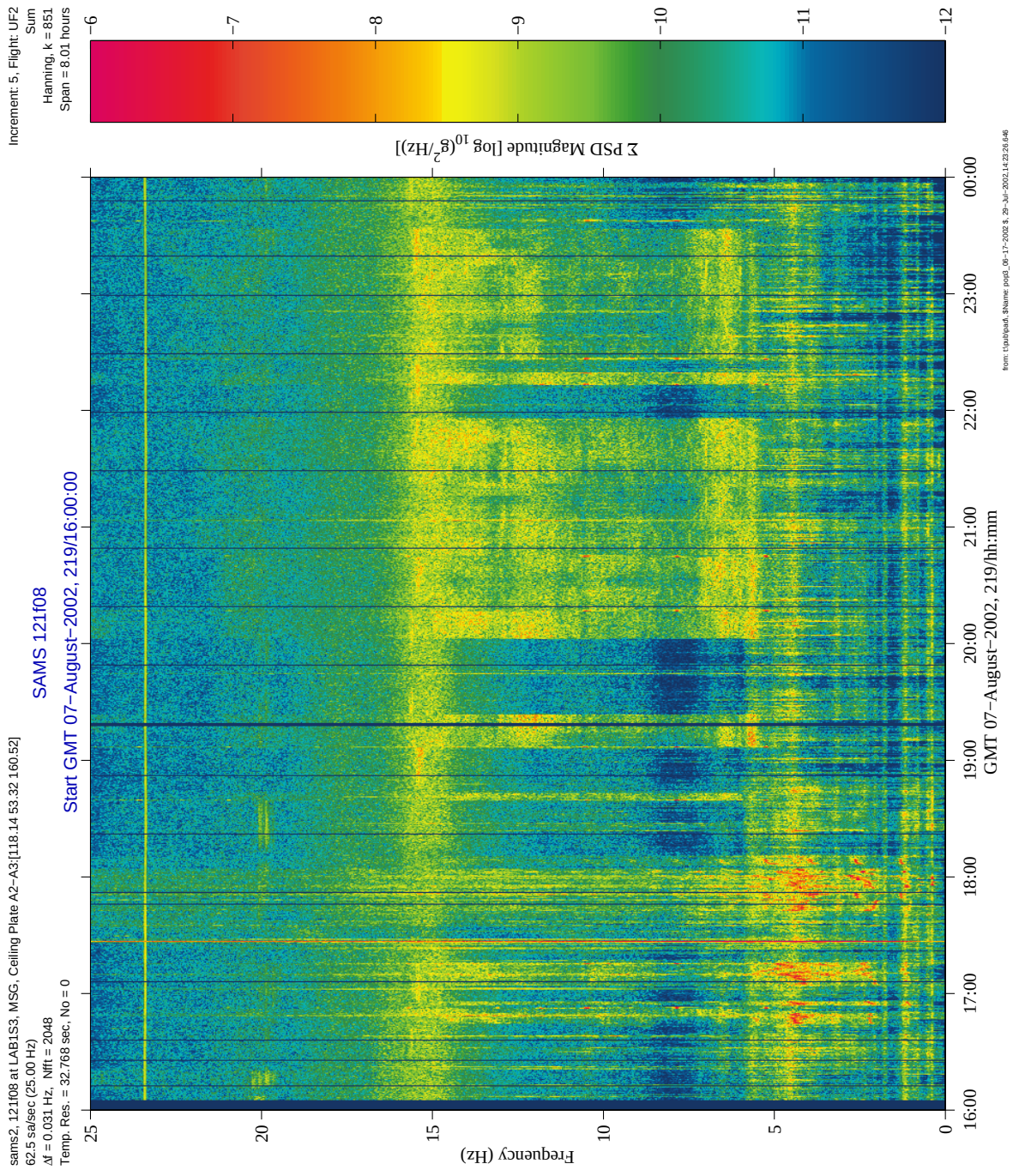

Figure 6-170 Spectrogram of SUBSA-04 (121f08)

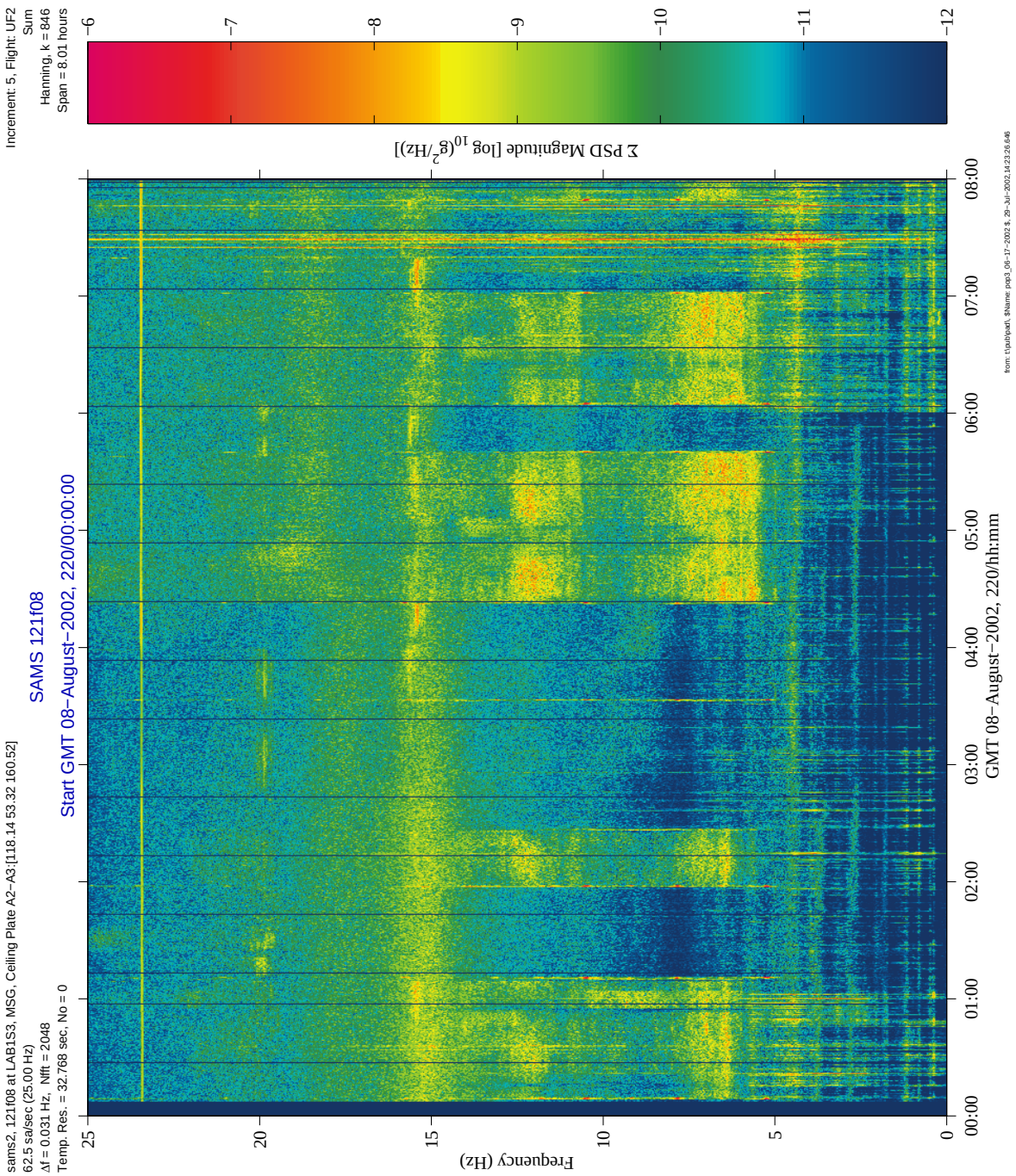

Figure 6-171 Spectrogram of SUBSA-04 (121f08)

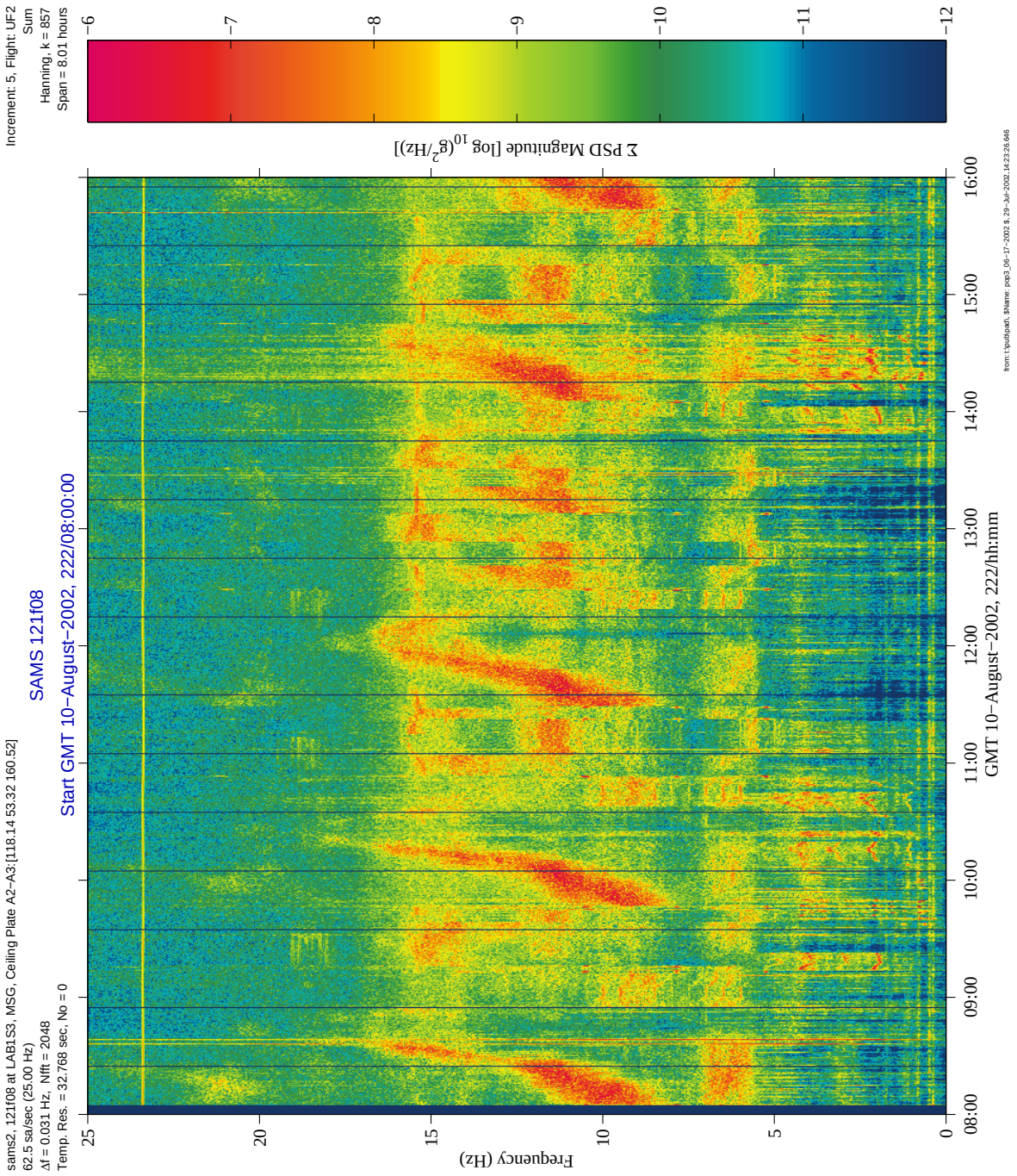

Figure 6-172 Spectrogram of SUBSA-07 (121f08)

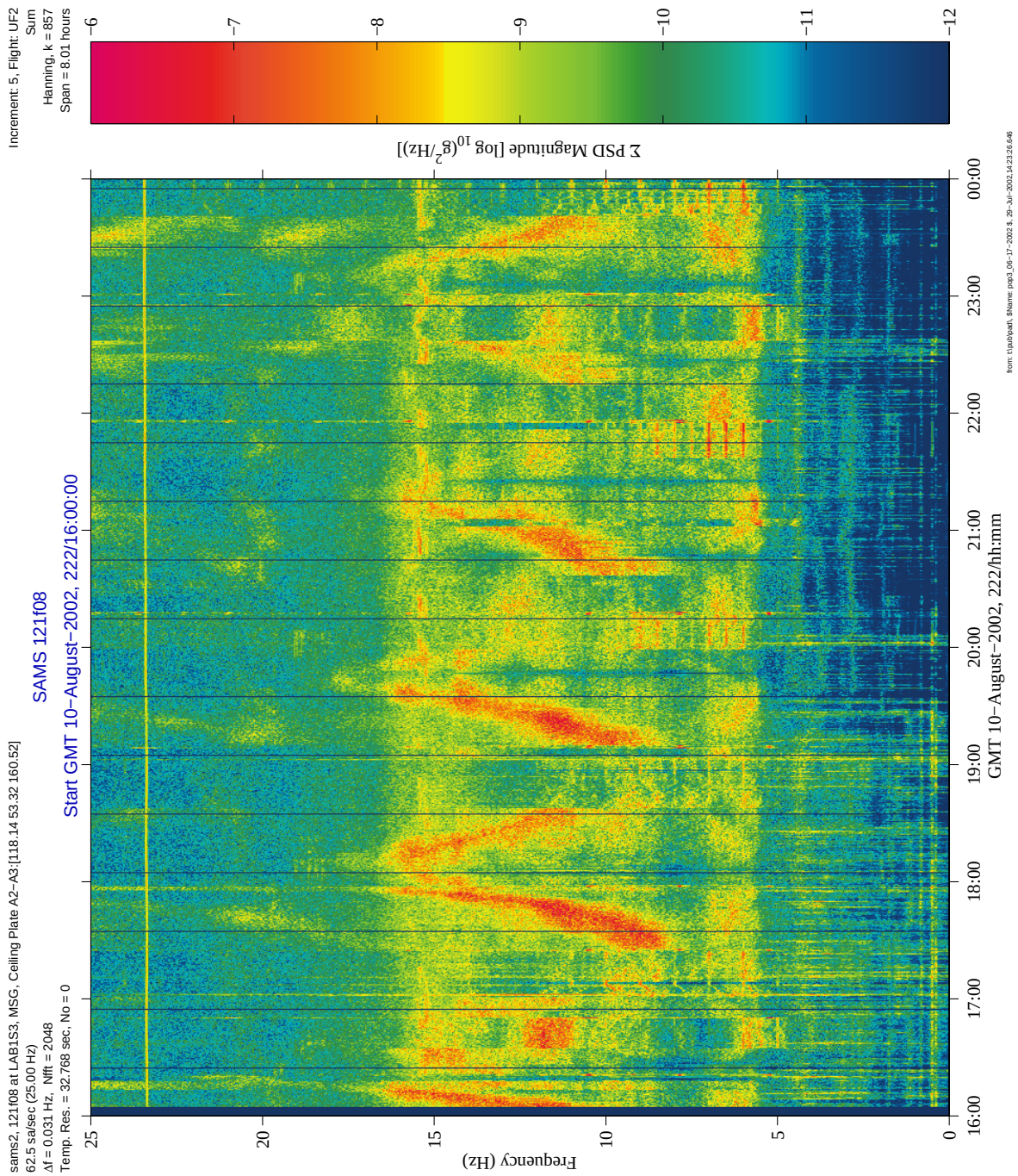

Figure 6-173 Spectrogram of SUBSA-07 (121f08)

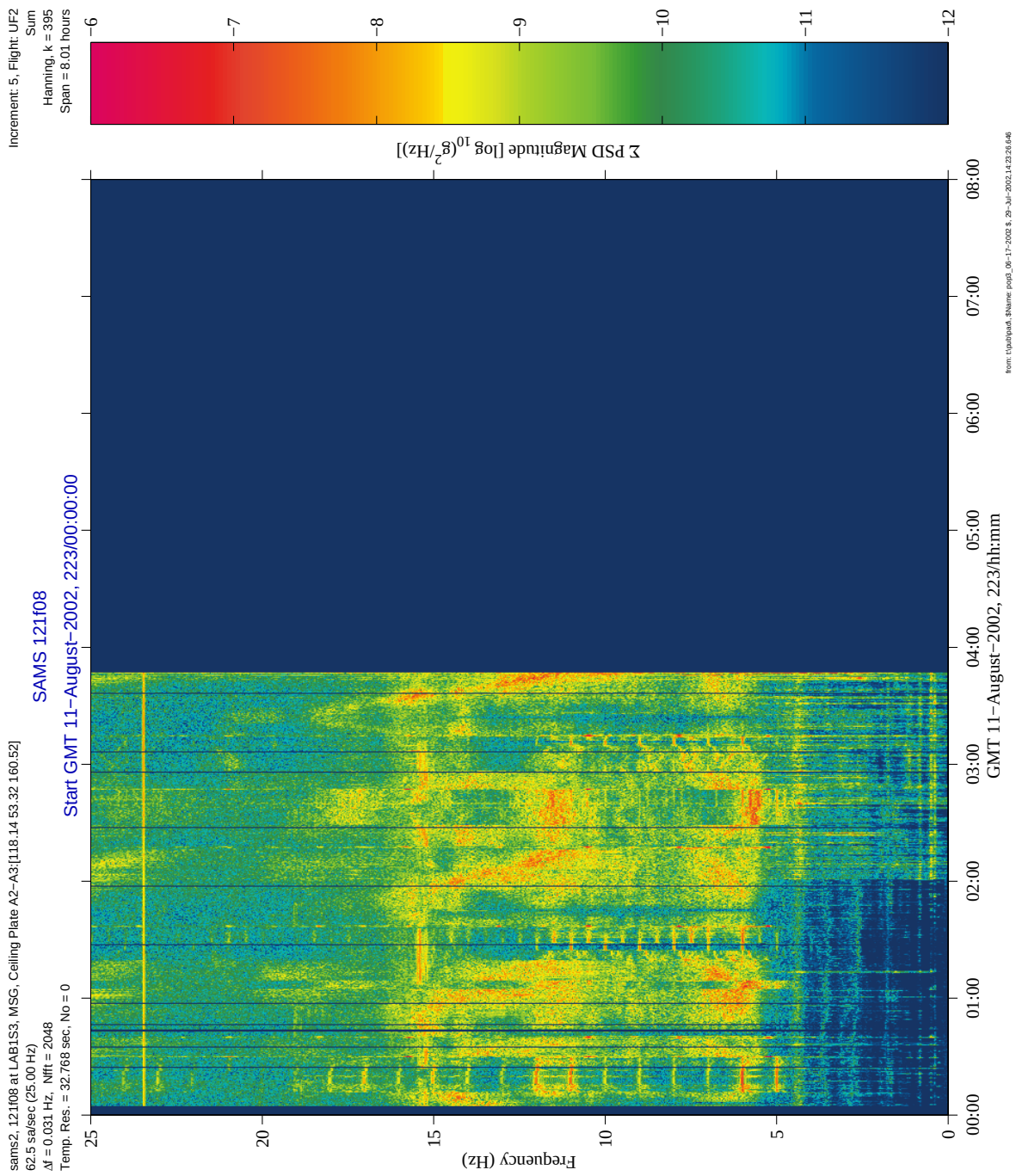

Figure 6-174 Spectrogram of SUBSA-07 (121f08)

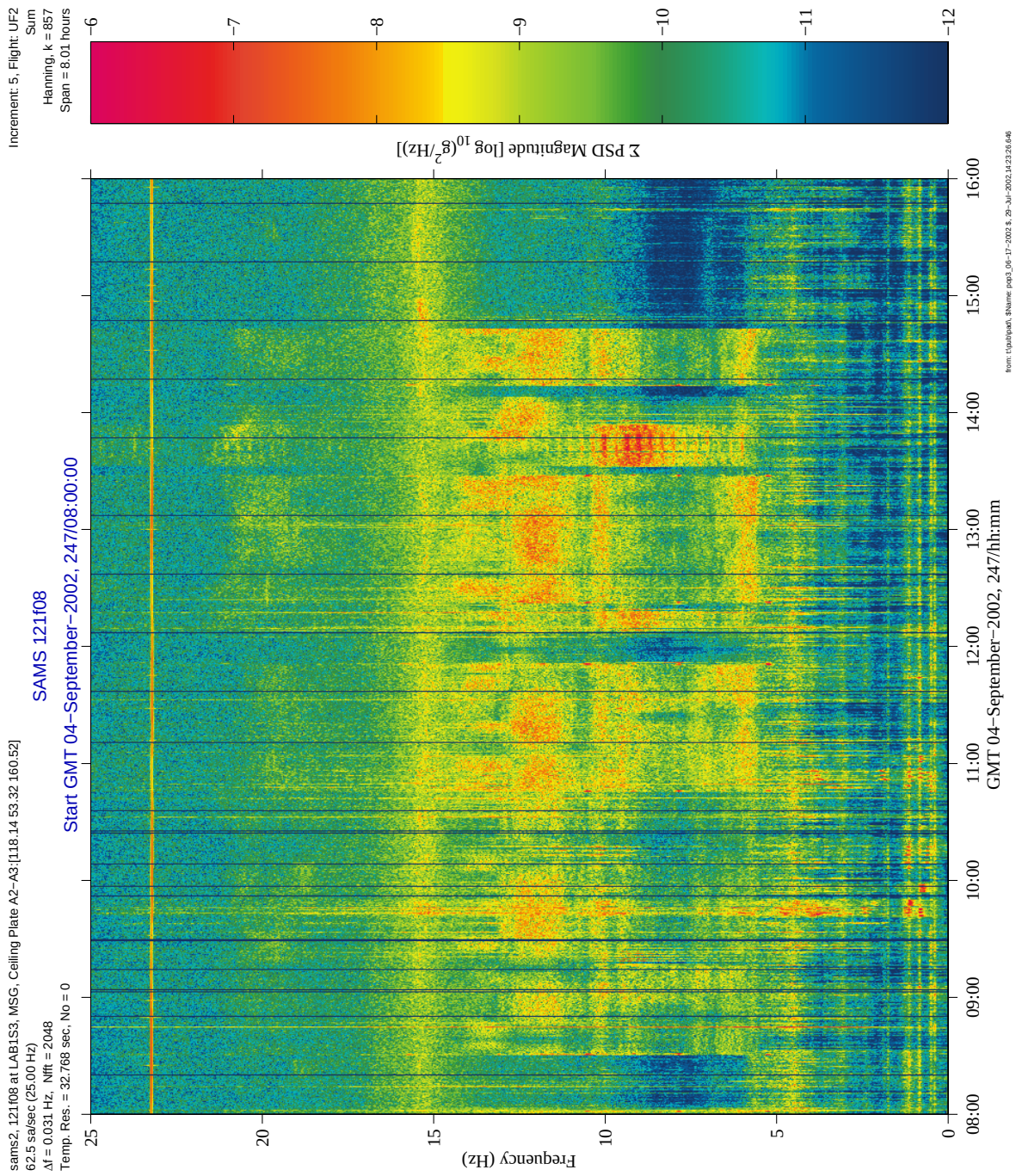

Figure 6-175 Spectrogram of SUBSA-08 (121f08)

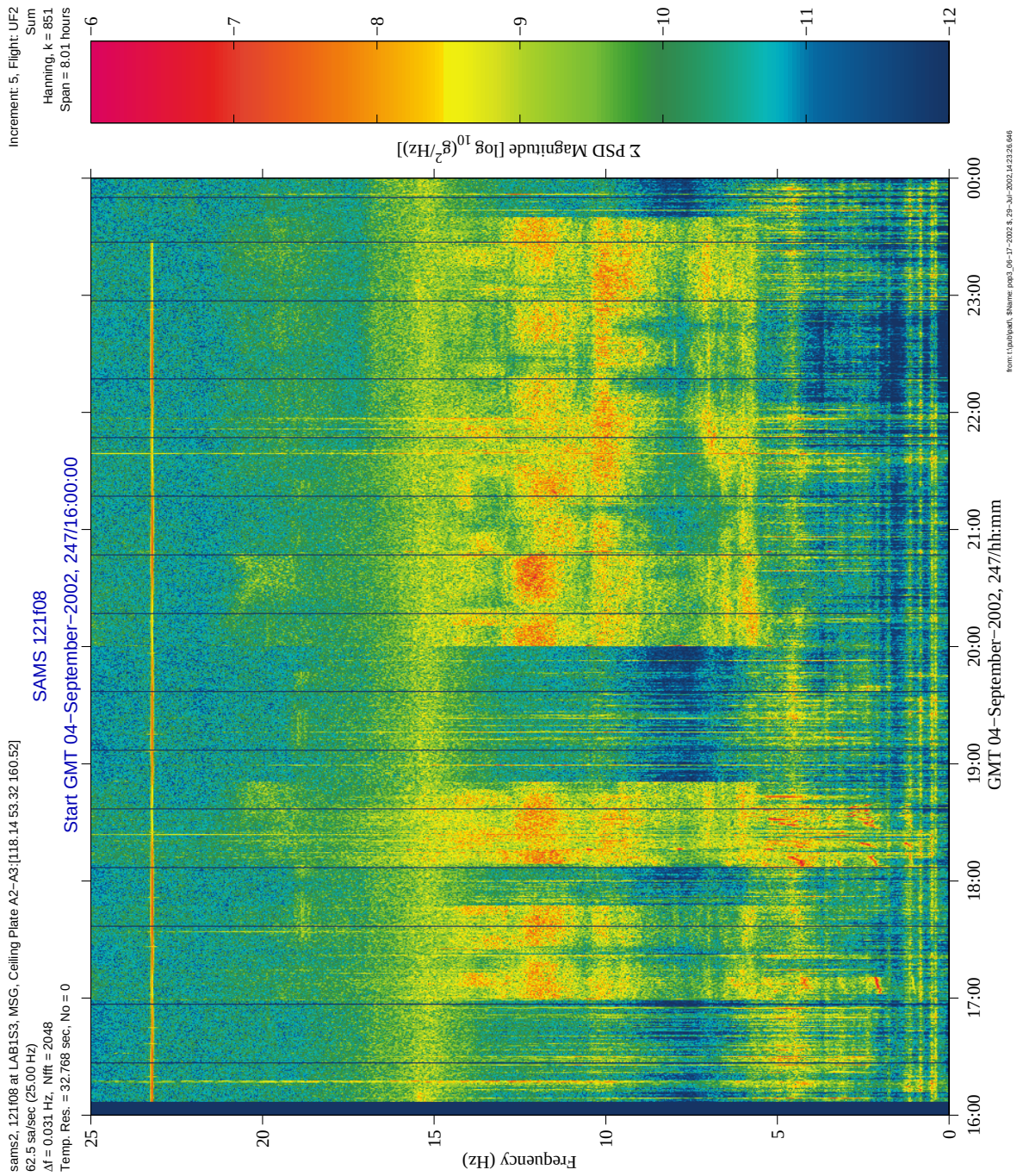

Figure 6-176 Spectrogram of SUBSA-08 (121f08)

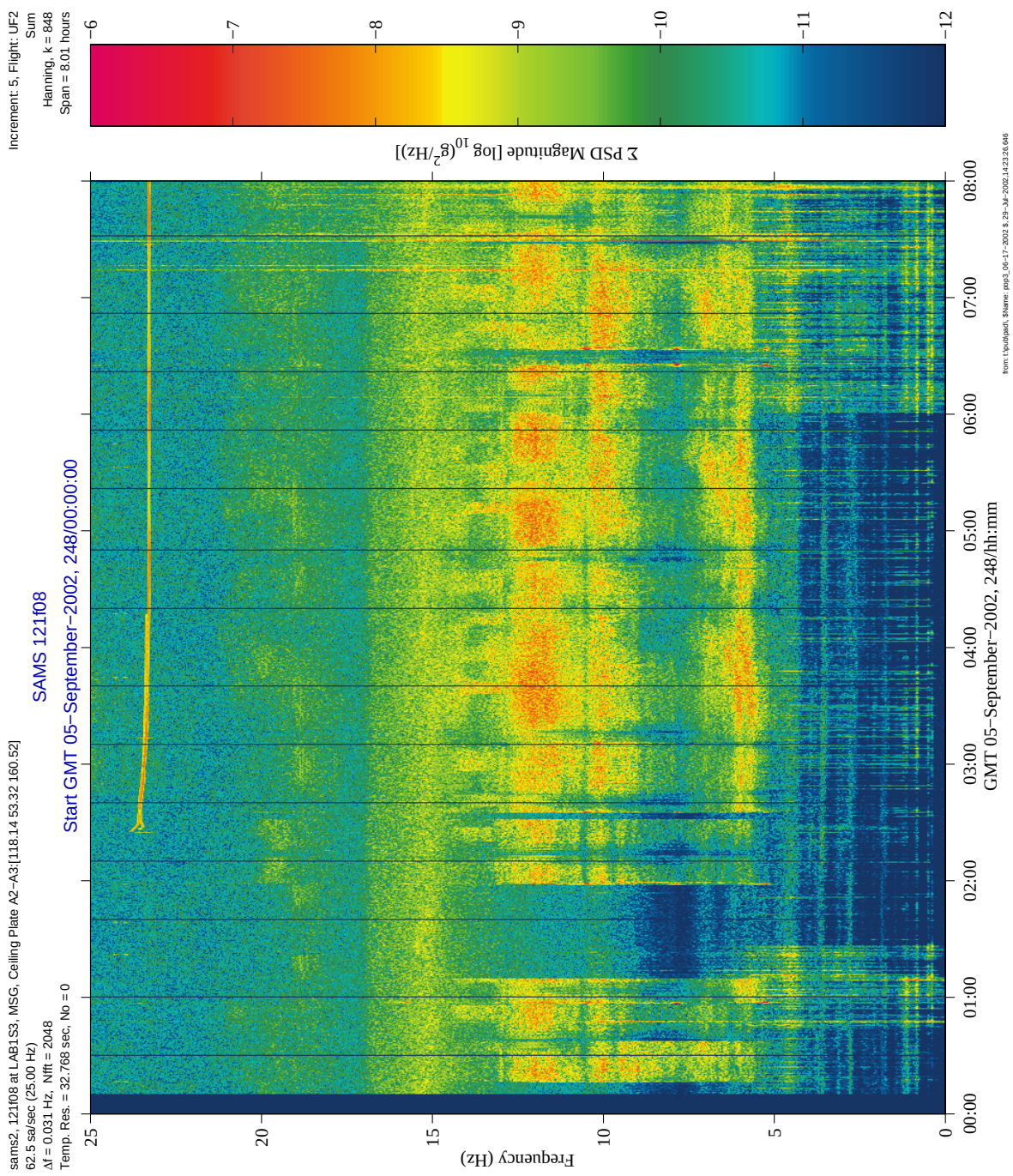

Figure 6-177 Spectrogram of SUBSA-08 (121f08)

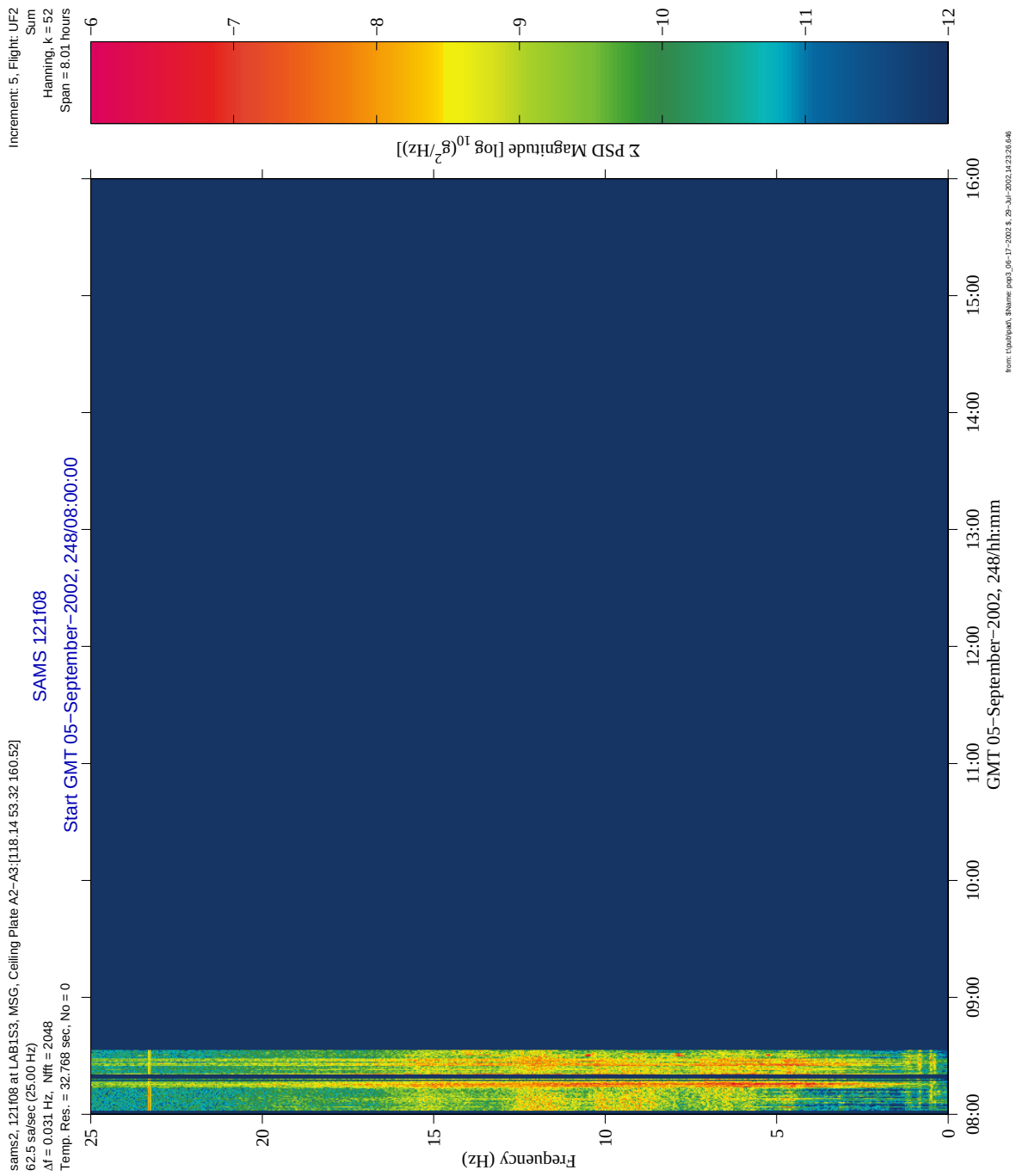

Figure 6-178 Spectrogram of SUBSA-08 (121f08)

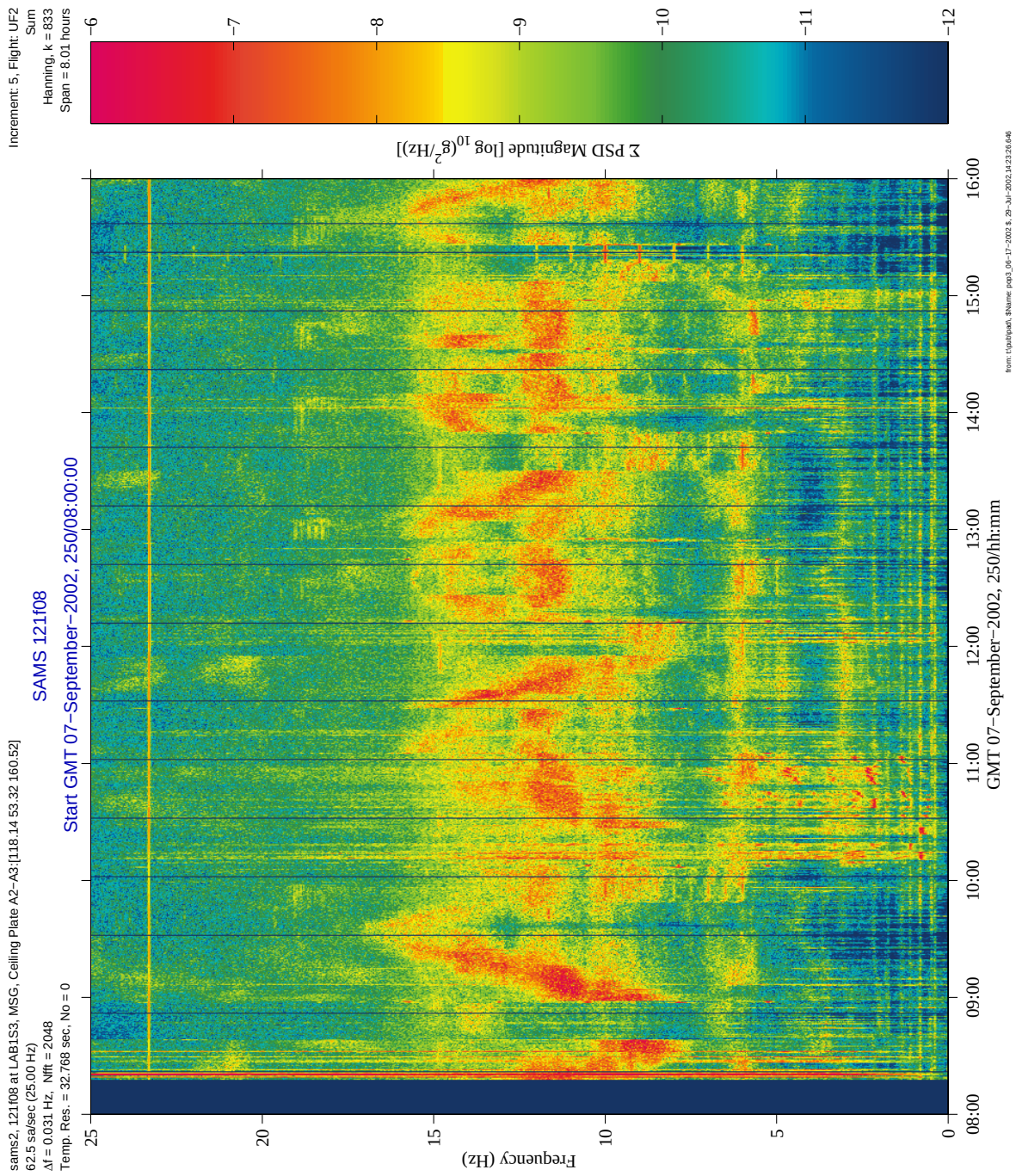

Figure 6-179 Spectrogram of SUBSA-09 (121f08)

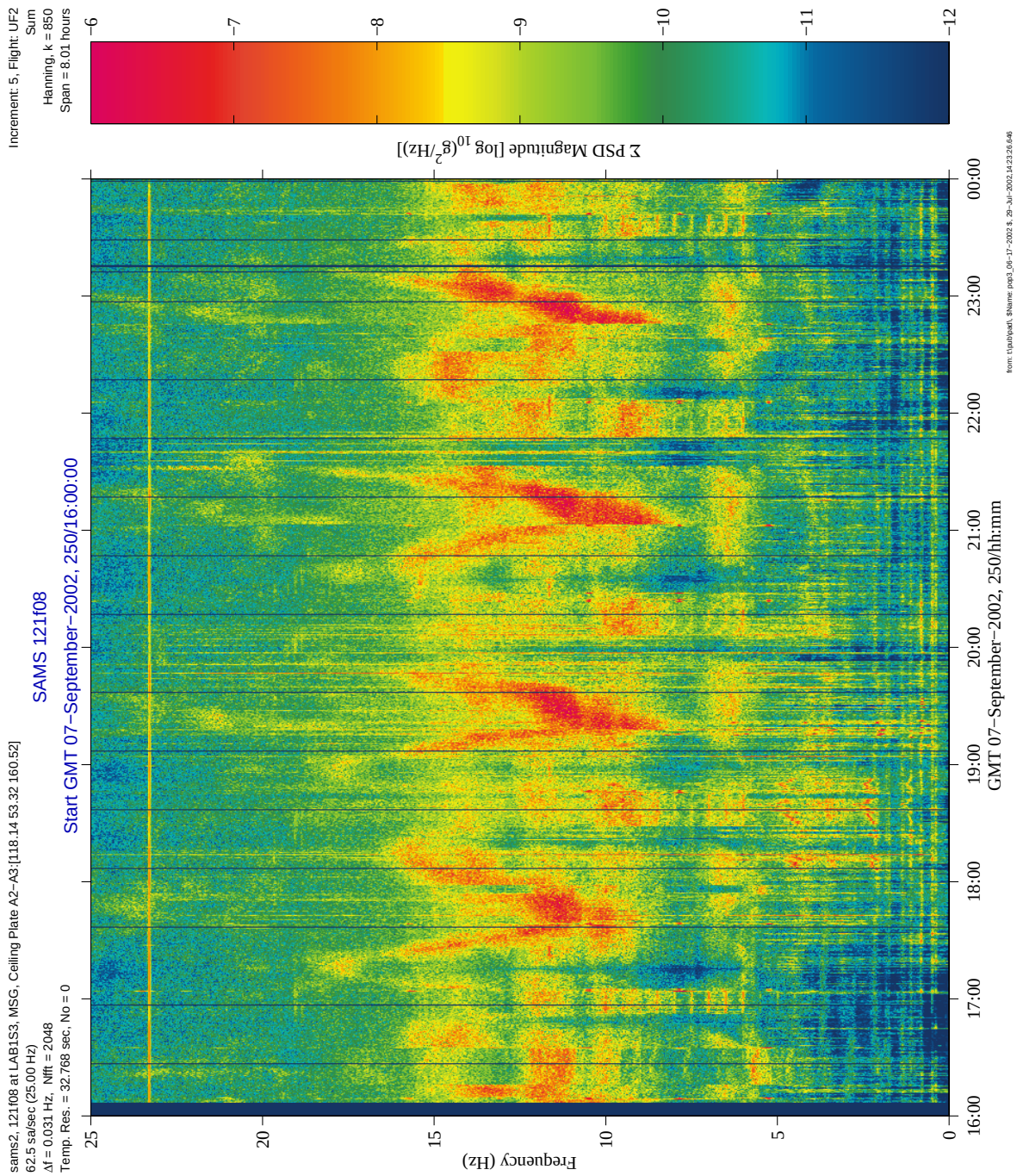

Figure 6-180 Spectrogram of SUBSA-09 (121f08)

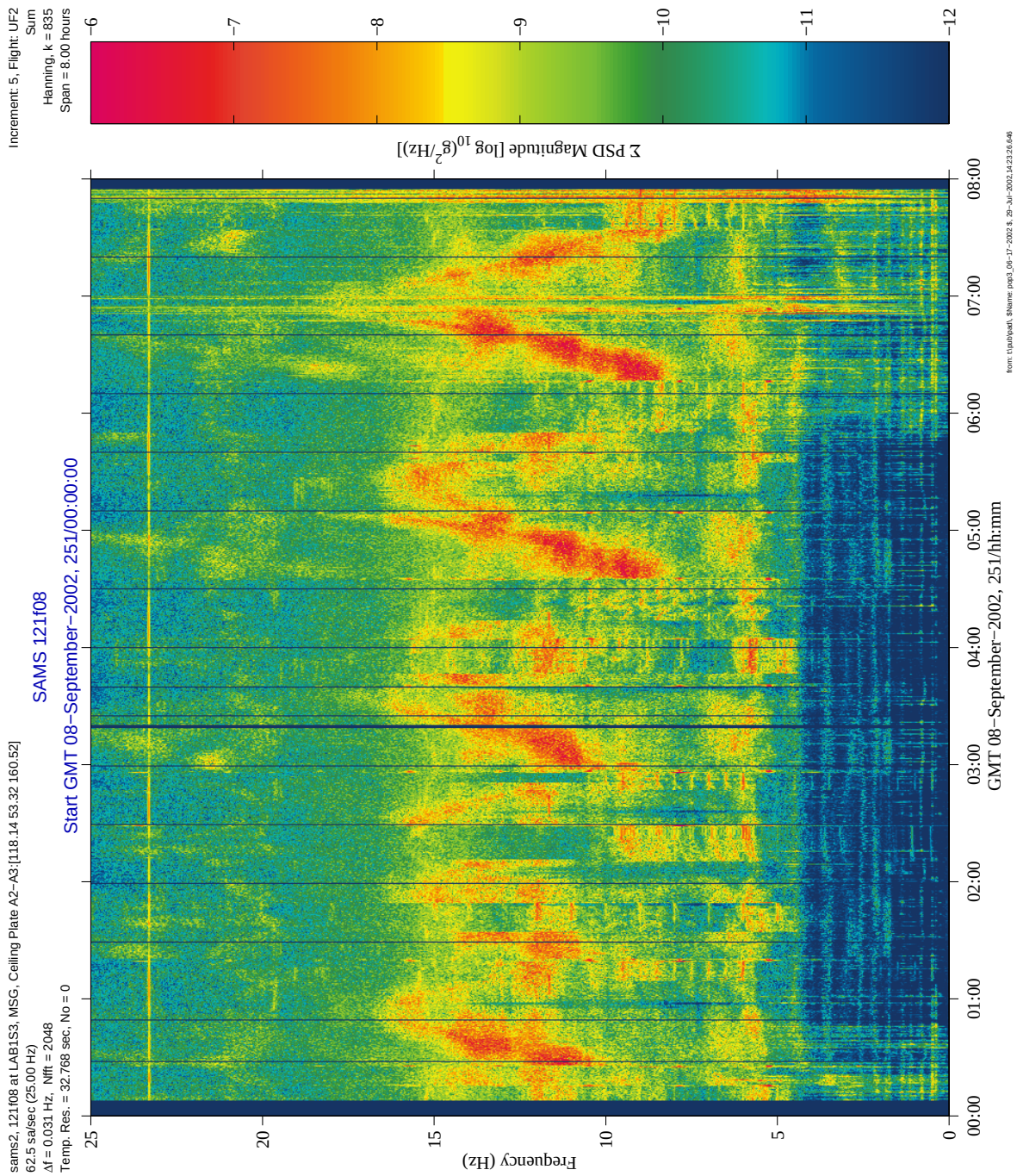

Figure 6-181 Spectrogram of SUBSA-09 (121f08)

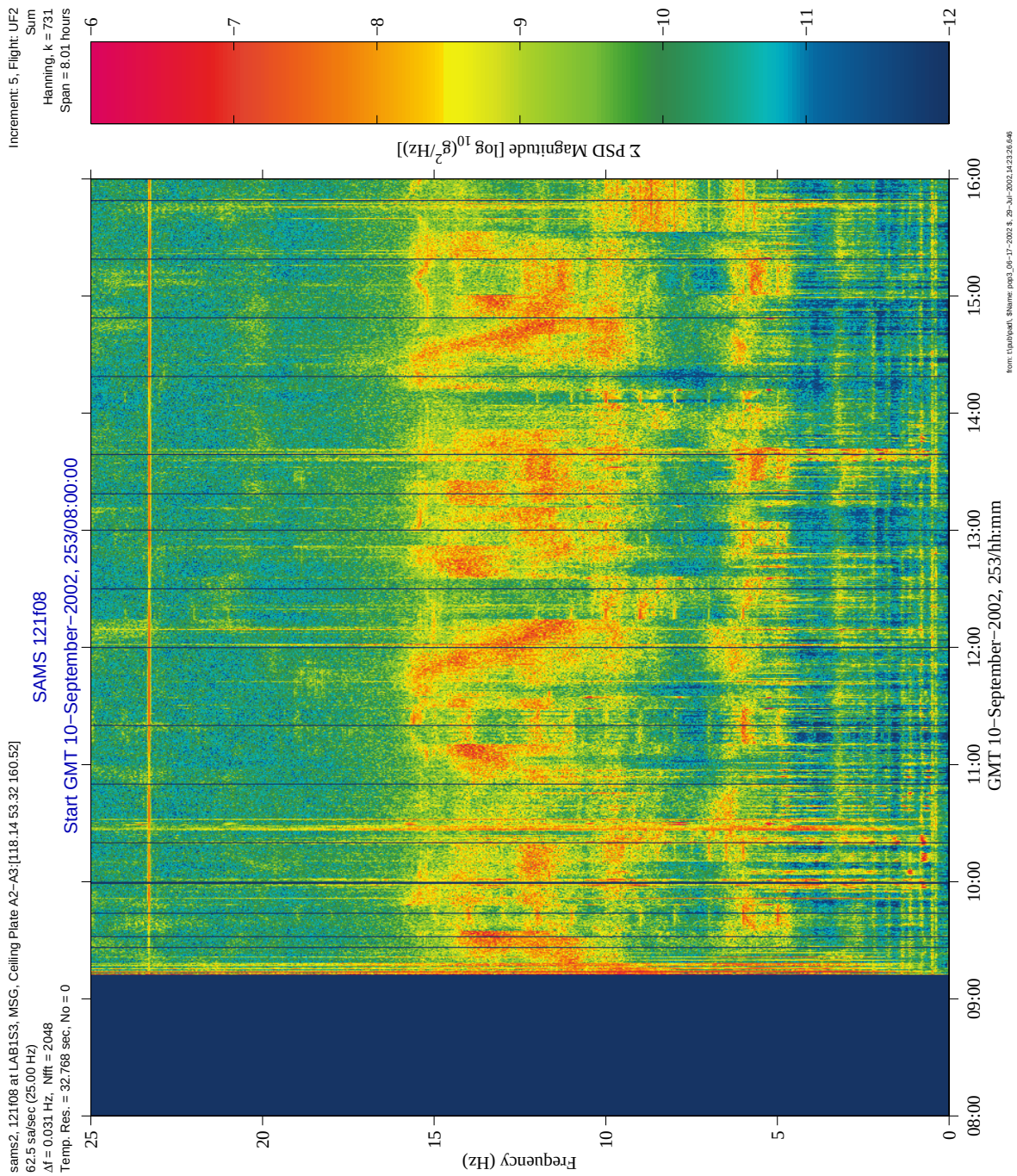

Figure 6-182 Spectrogram of SUBSA-01 (121f08)

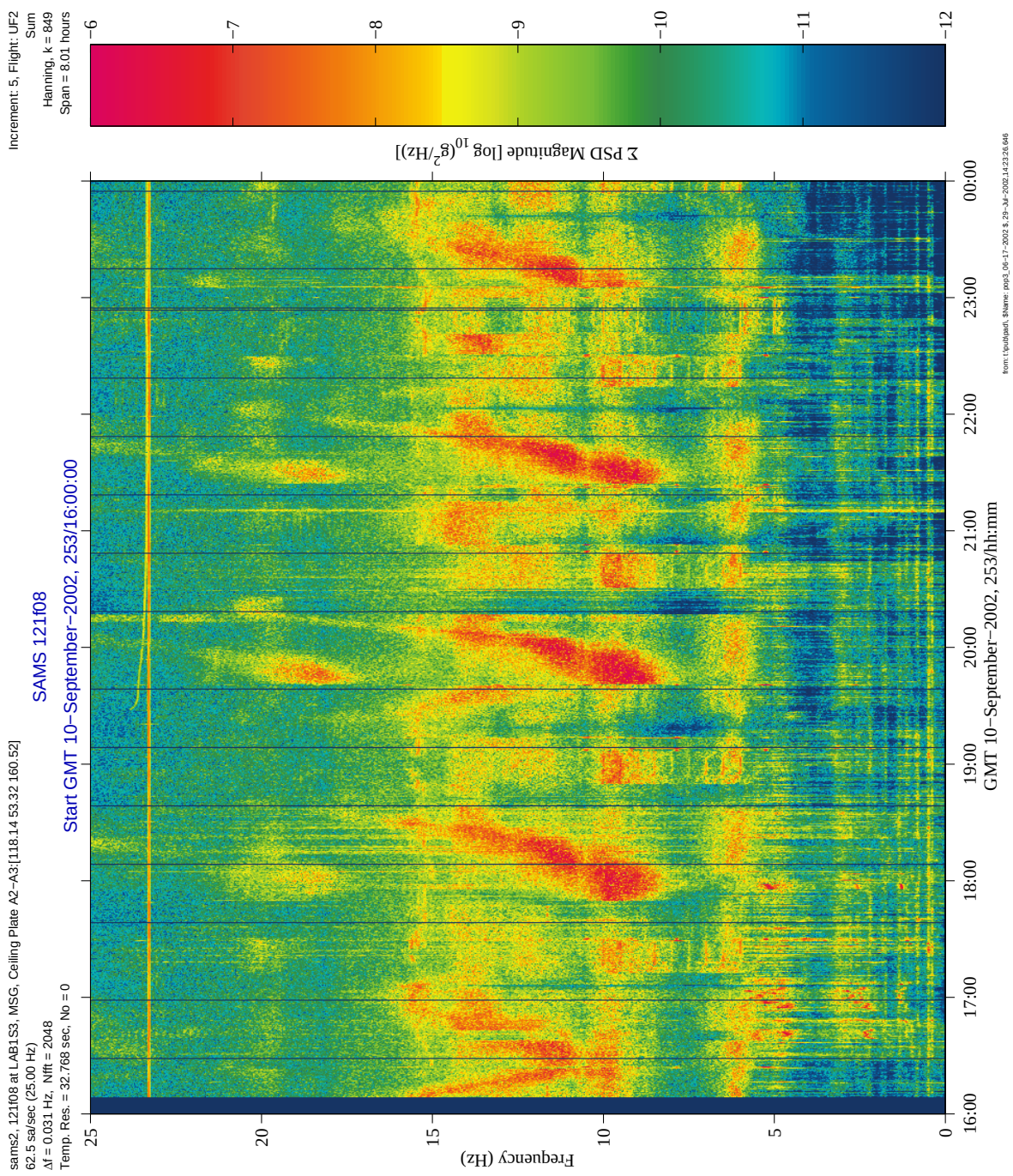

Figure 6-183 Spectrogram of SUBSA-01 (121f08)

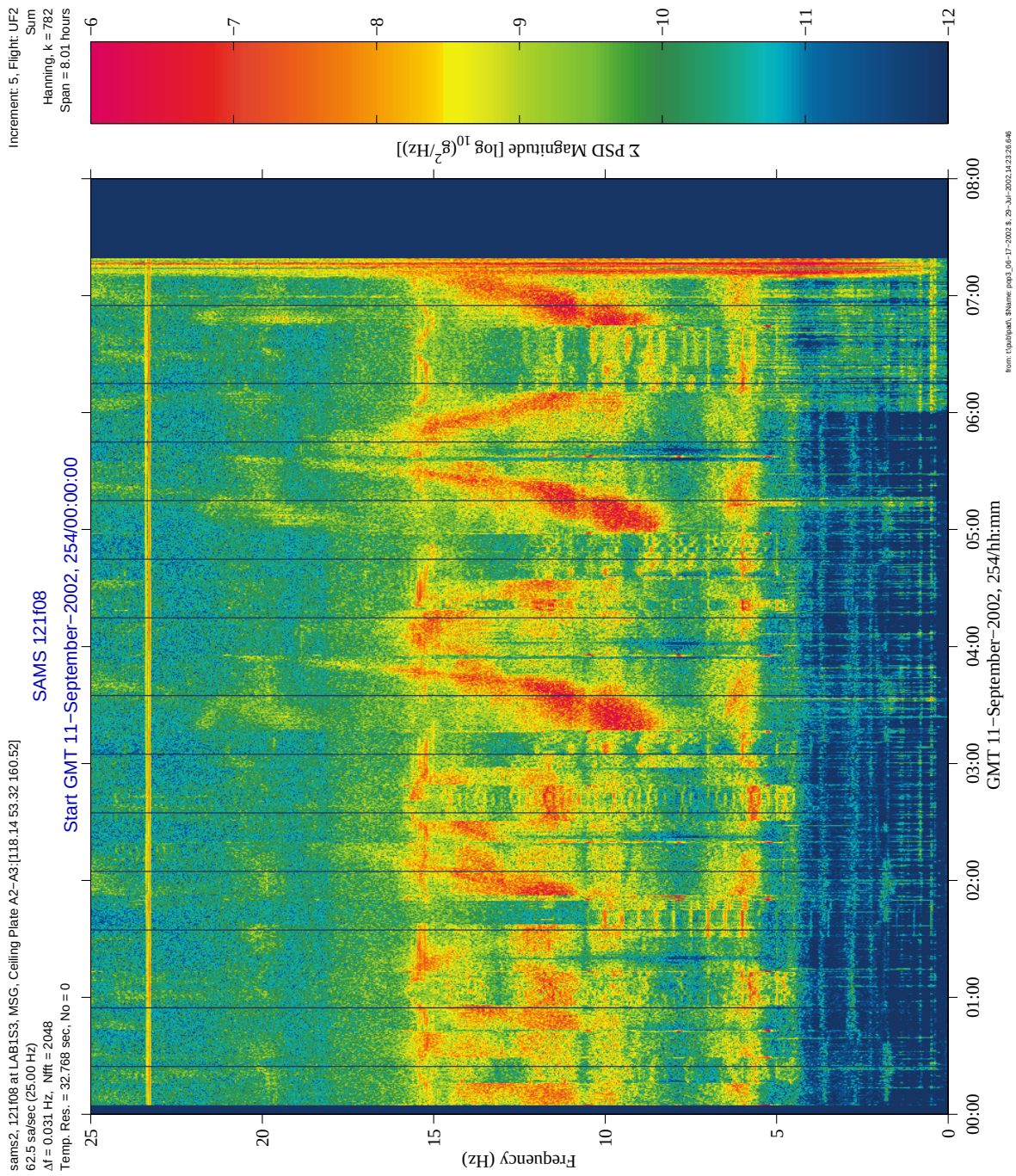

Figure 6-184 Spectrogram of SUBSA-01 (121f08)

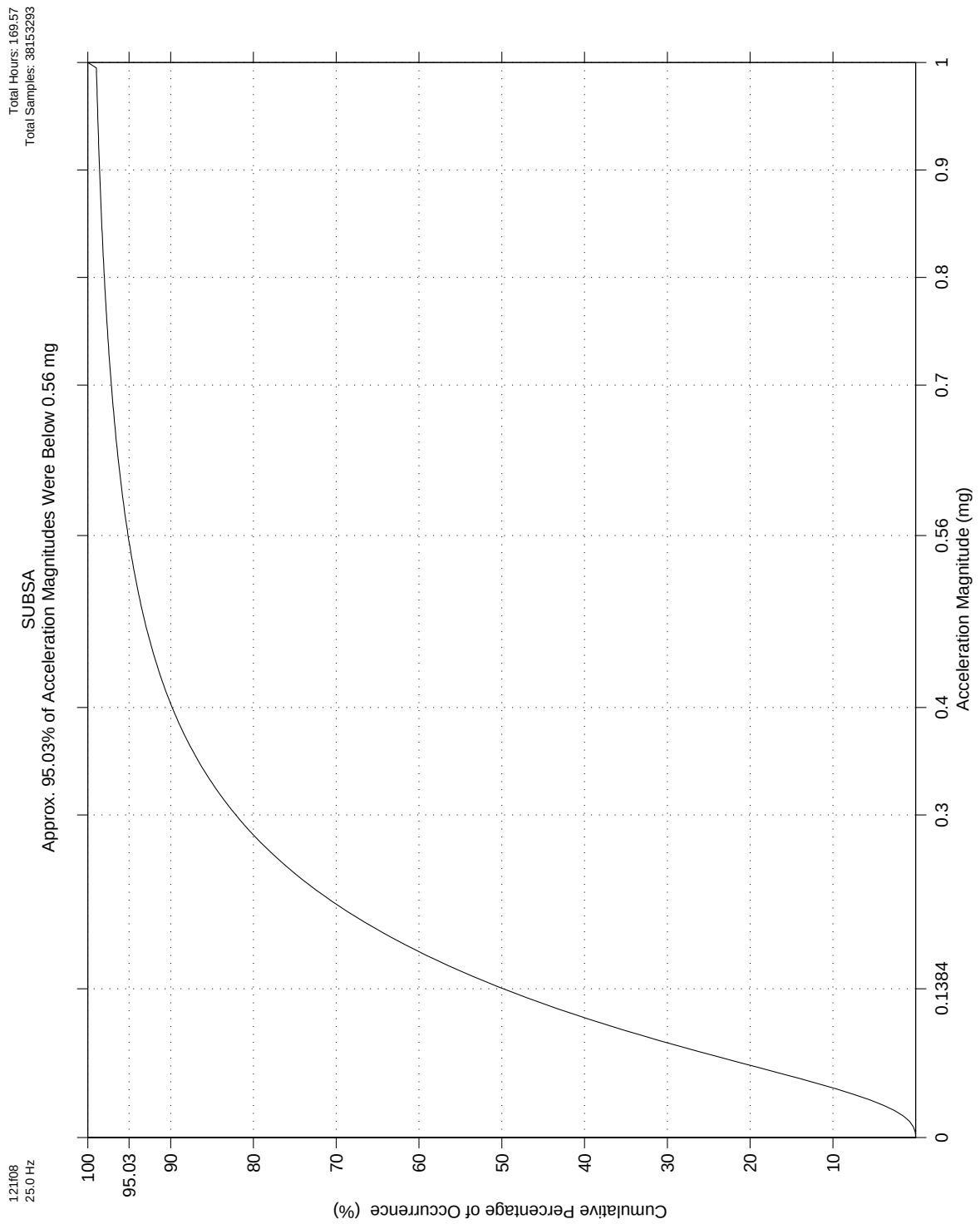

Figure 6-185 Magnitude Cumulative Percentage of SUBSA (121f08)

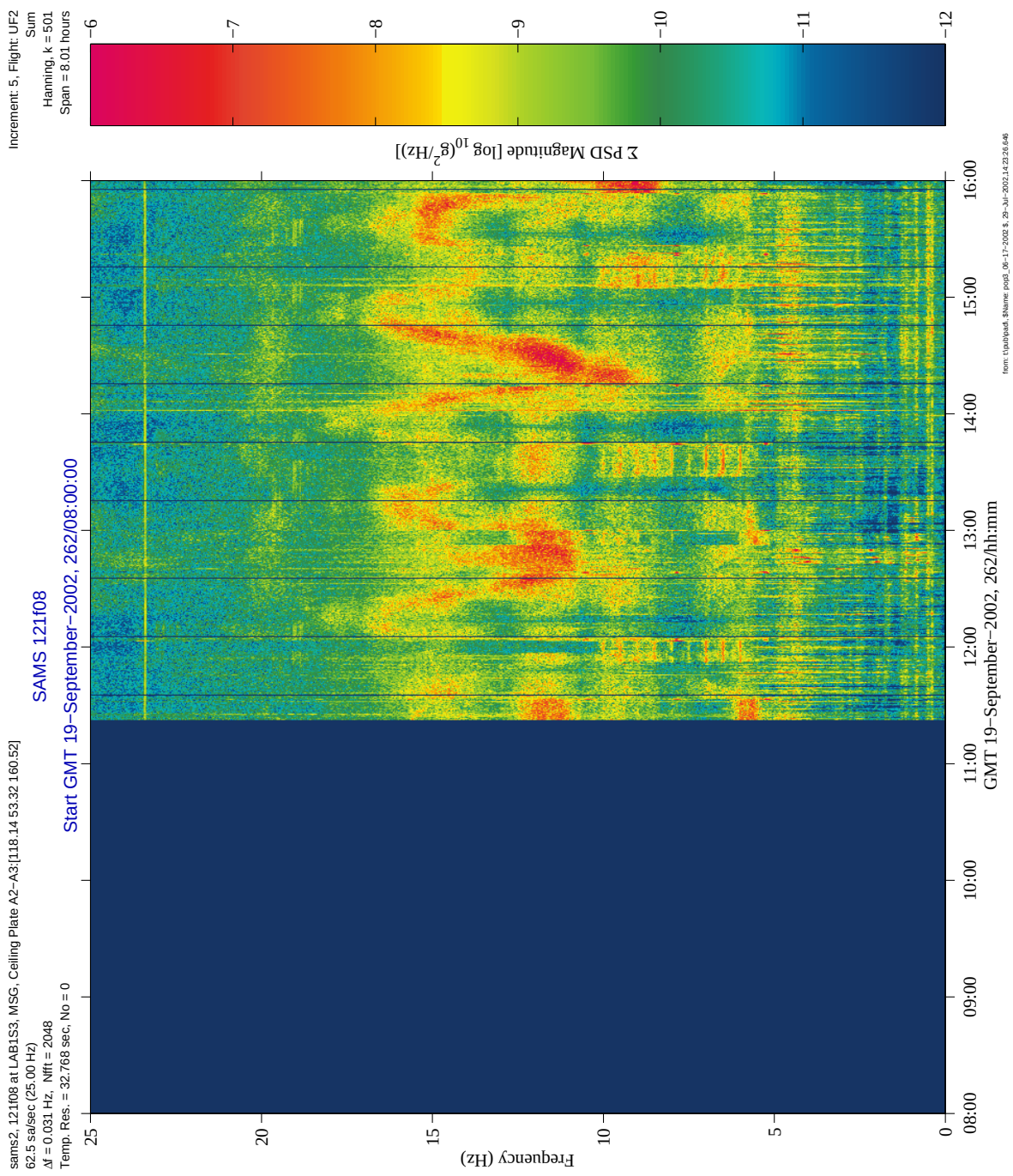

Figure 6-186 Spectrogram of PFMI-12 (121f08)

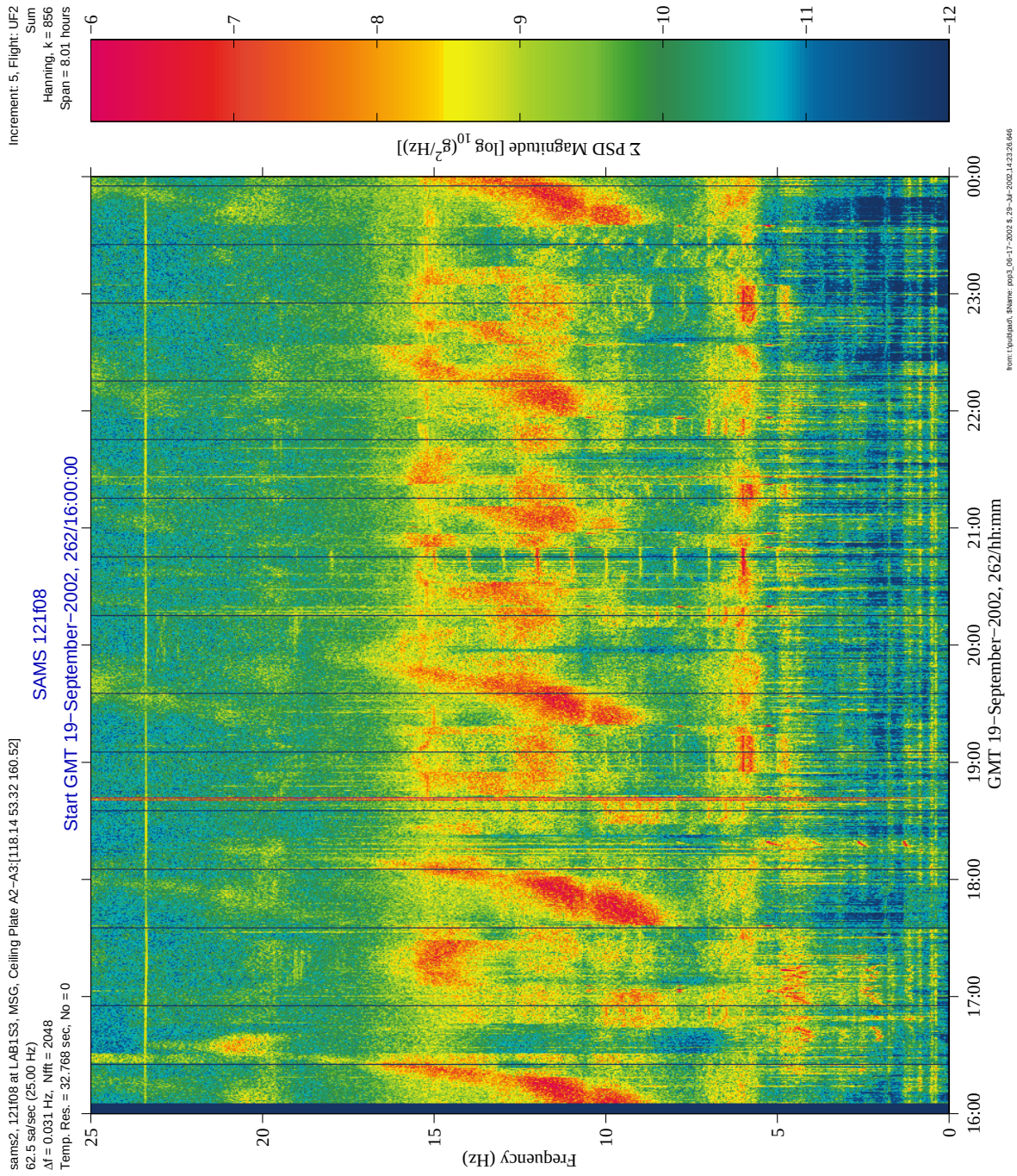

Figure 6-187 Spectrogram of PFMI-12 (121f08)

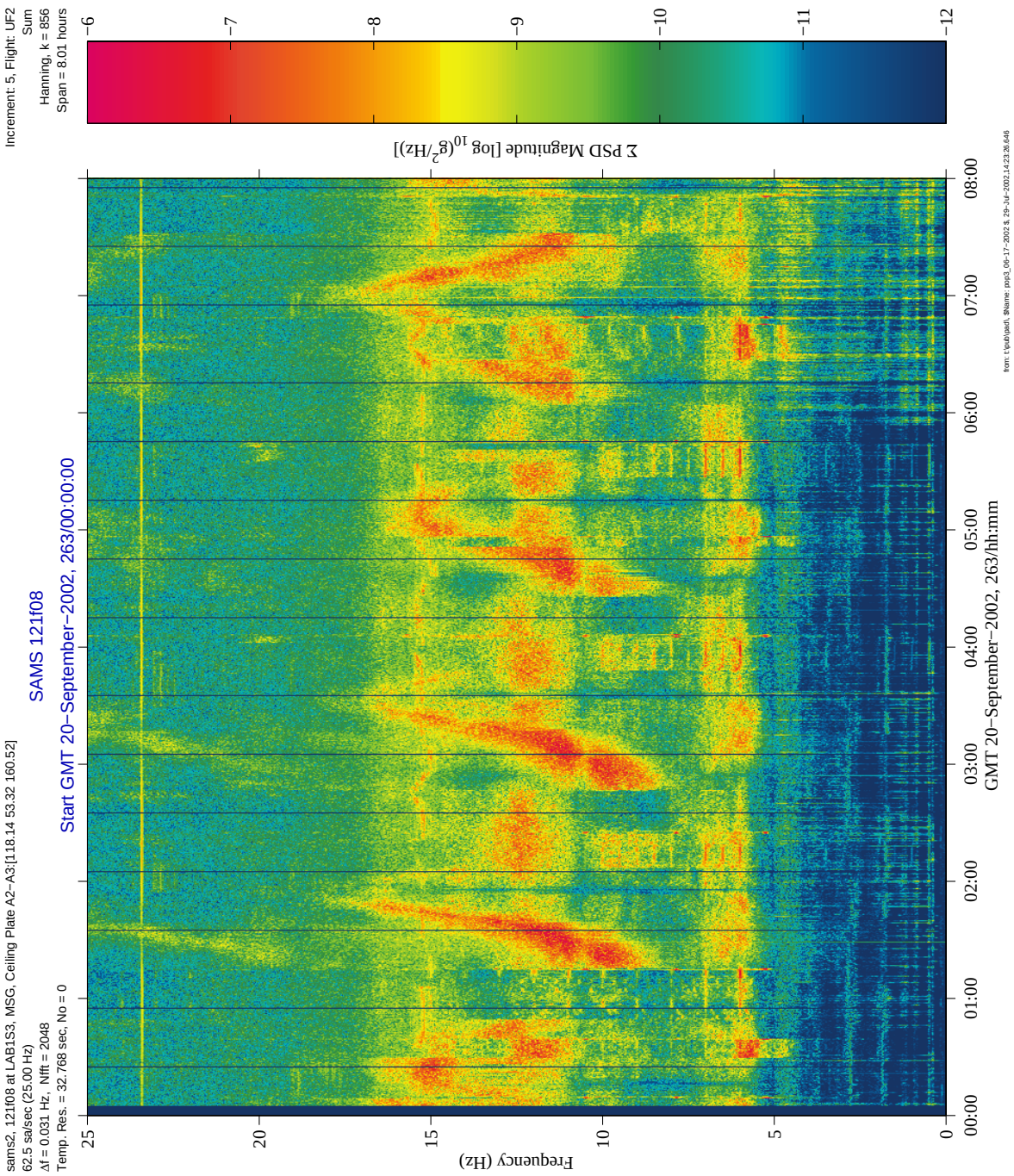

Figure 6-188 Spectrogram of PFMI-12 (121f08)

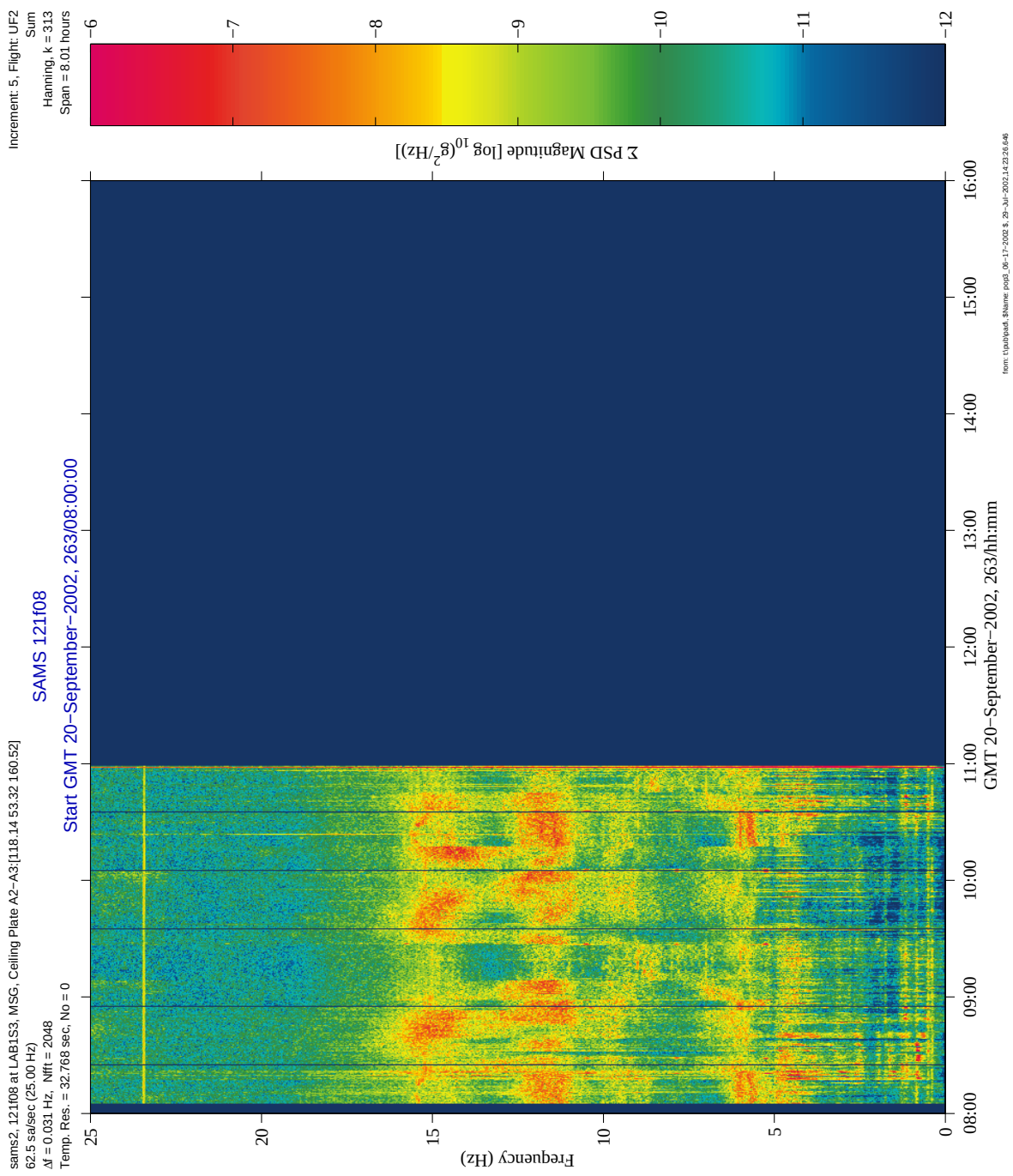

Figure 6-189 Spectrogram of PFMI-12 (121f08)

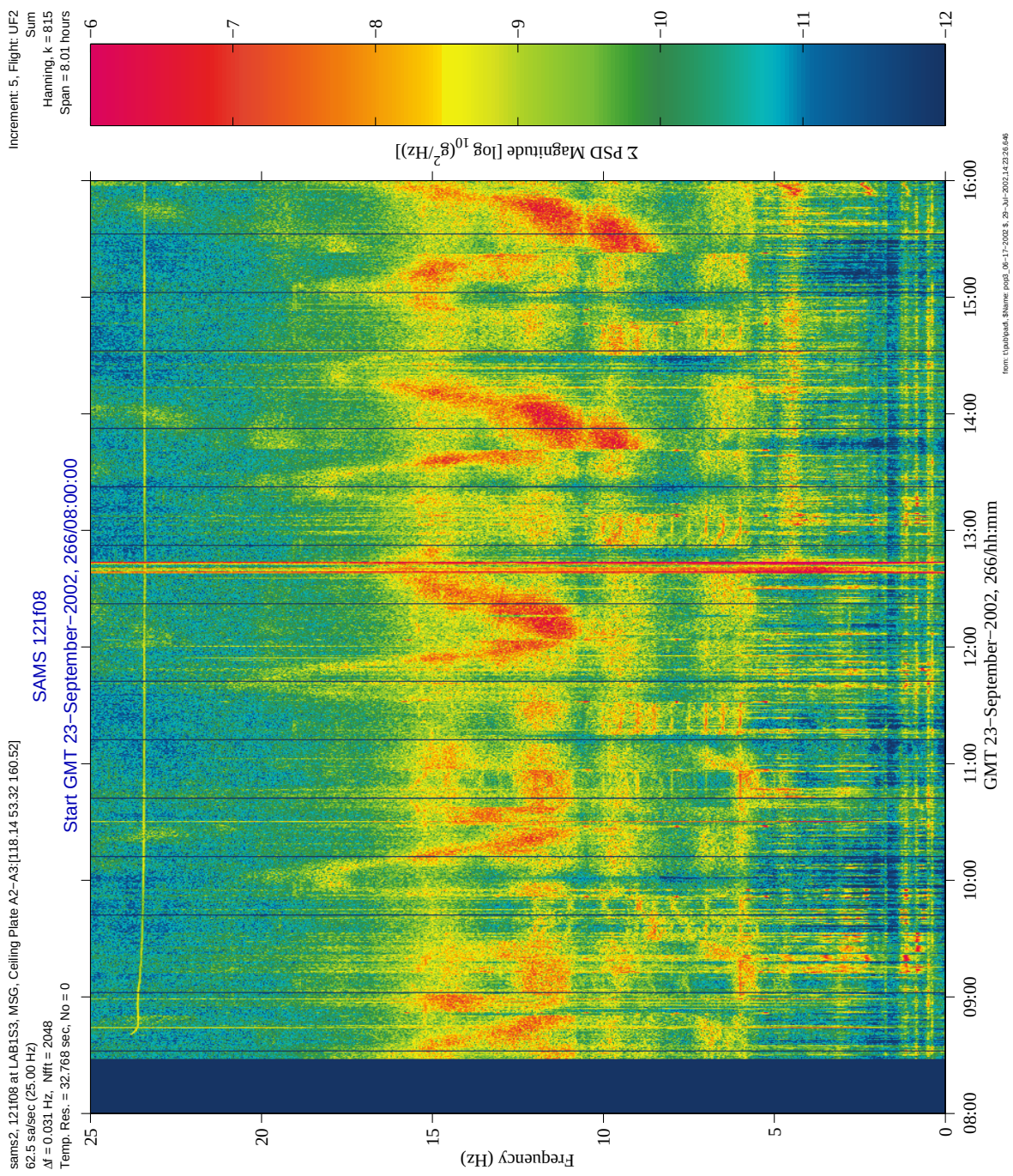

Figure 6-190 Spectrogram of PFMI-01 (121f08)

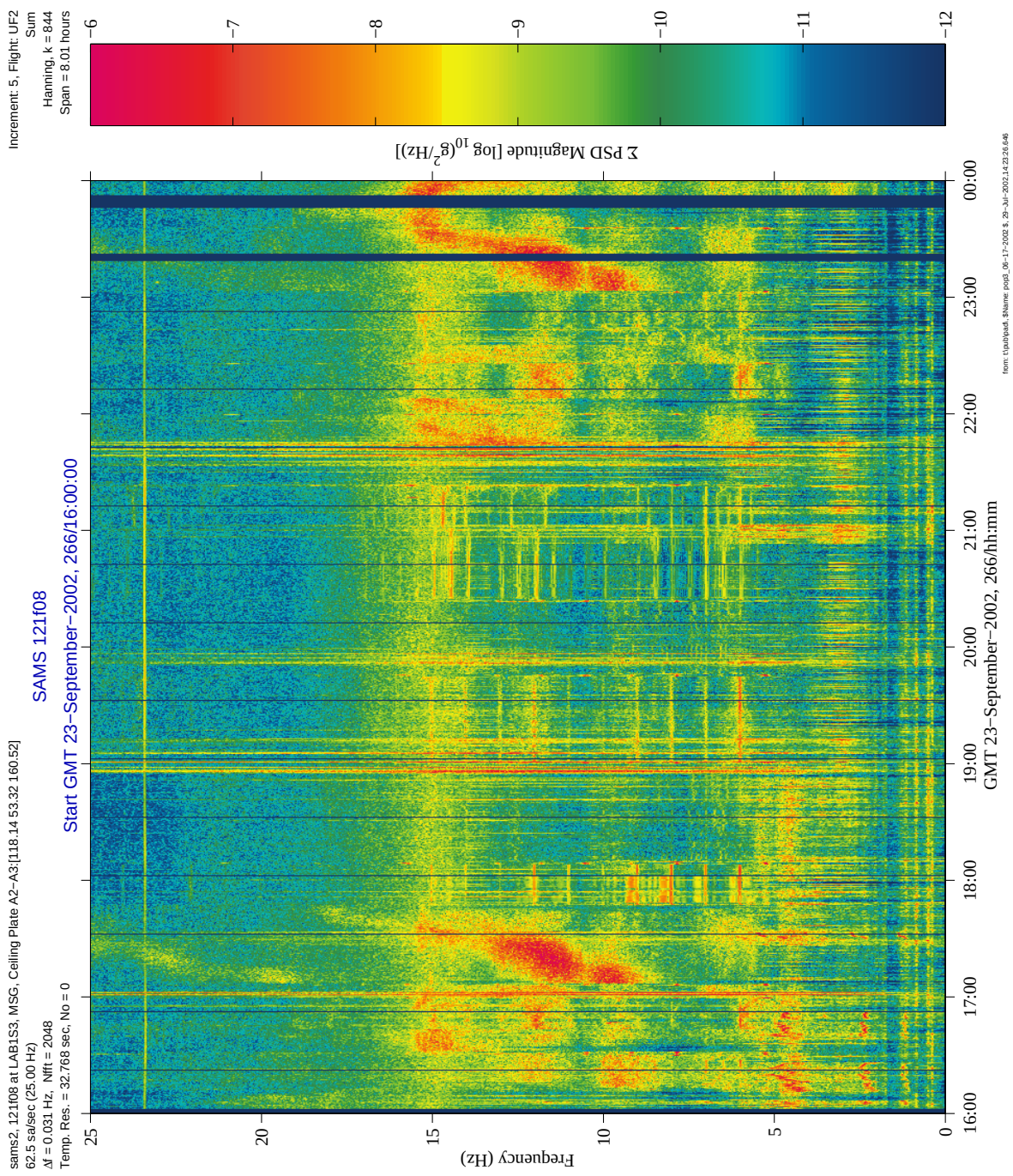

Figure 6-191 Spectrogram of PFMI-01 (121f08)

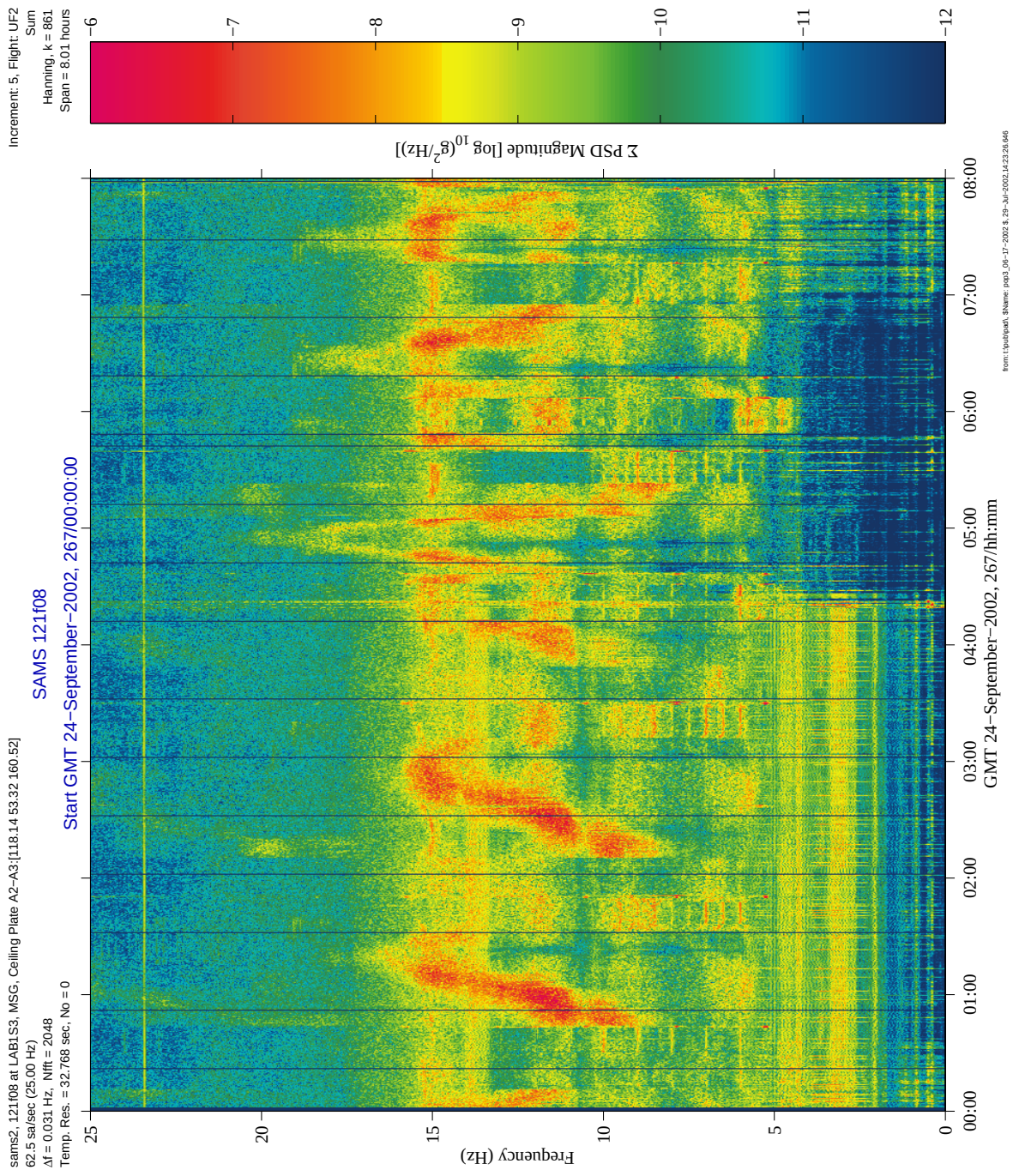

Figure 6-192 Spectrogram of PFMI-01 (121f08)

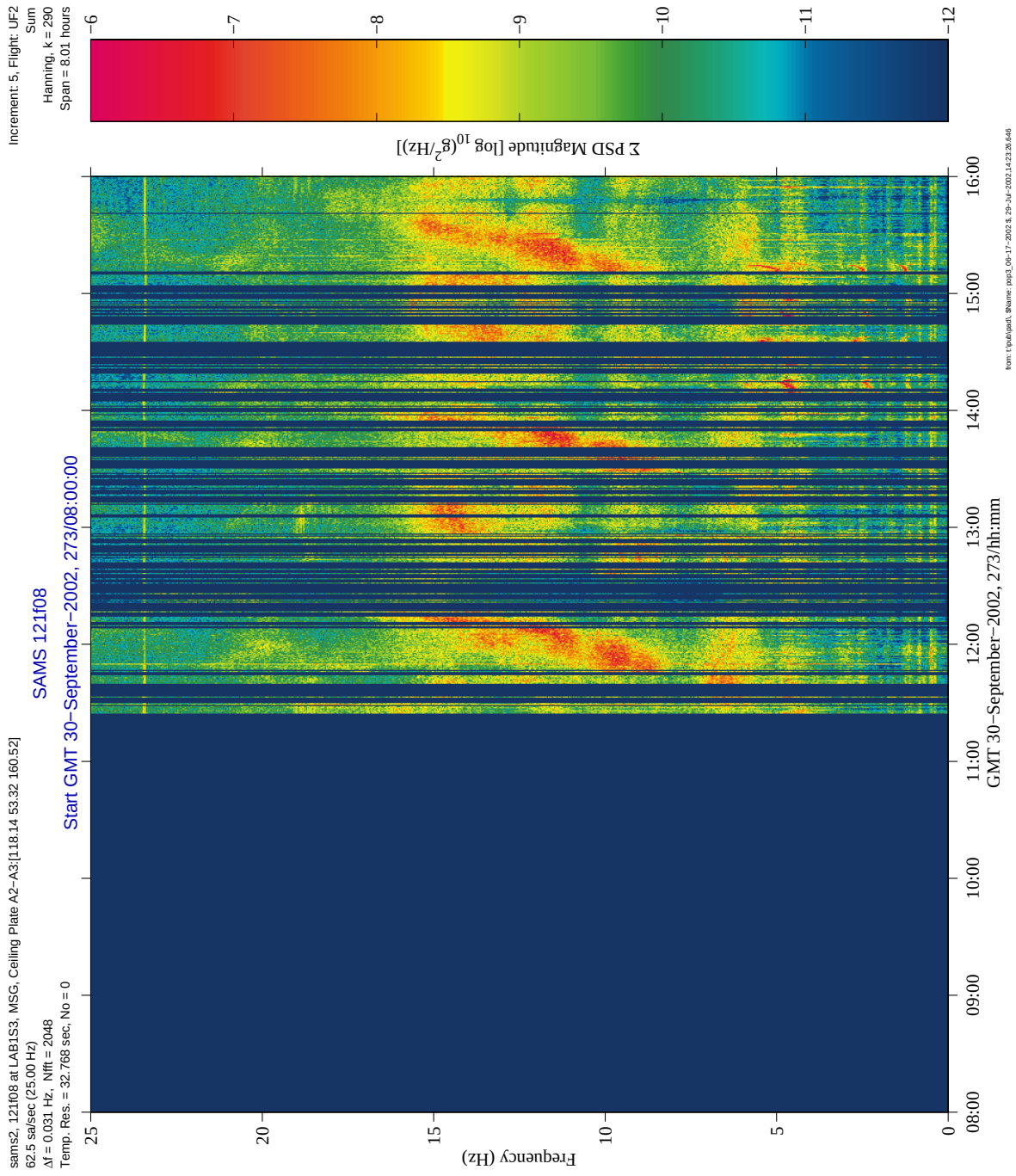

Figure 6-193 Spectrogram of PFMI-07 (121f08)

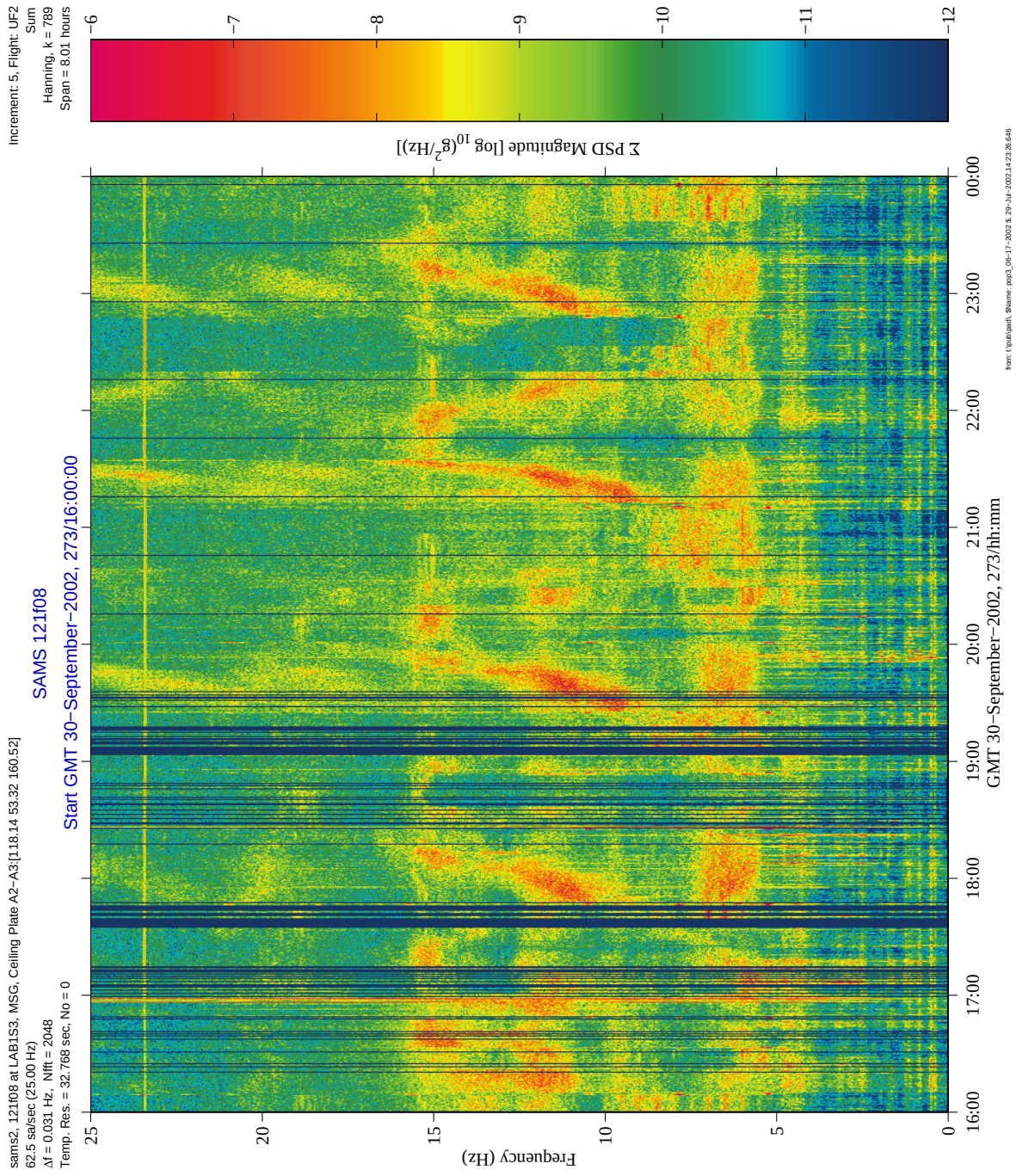

Figure 6-194 Spectrogram of PFMI-07 (121f08)

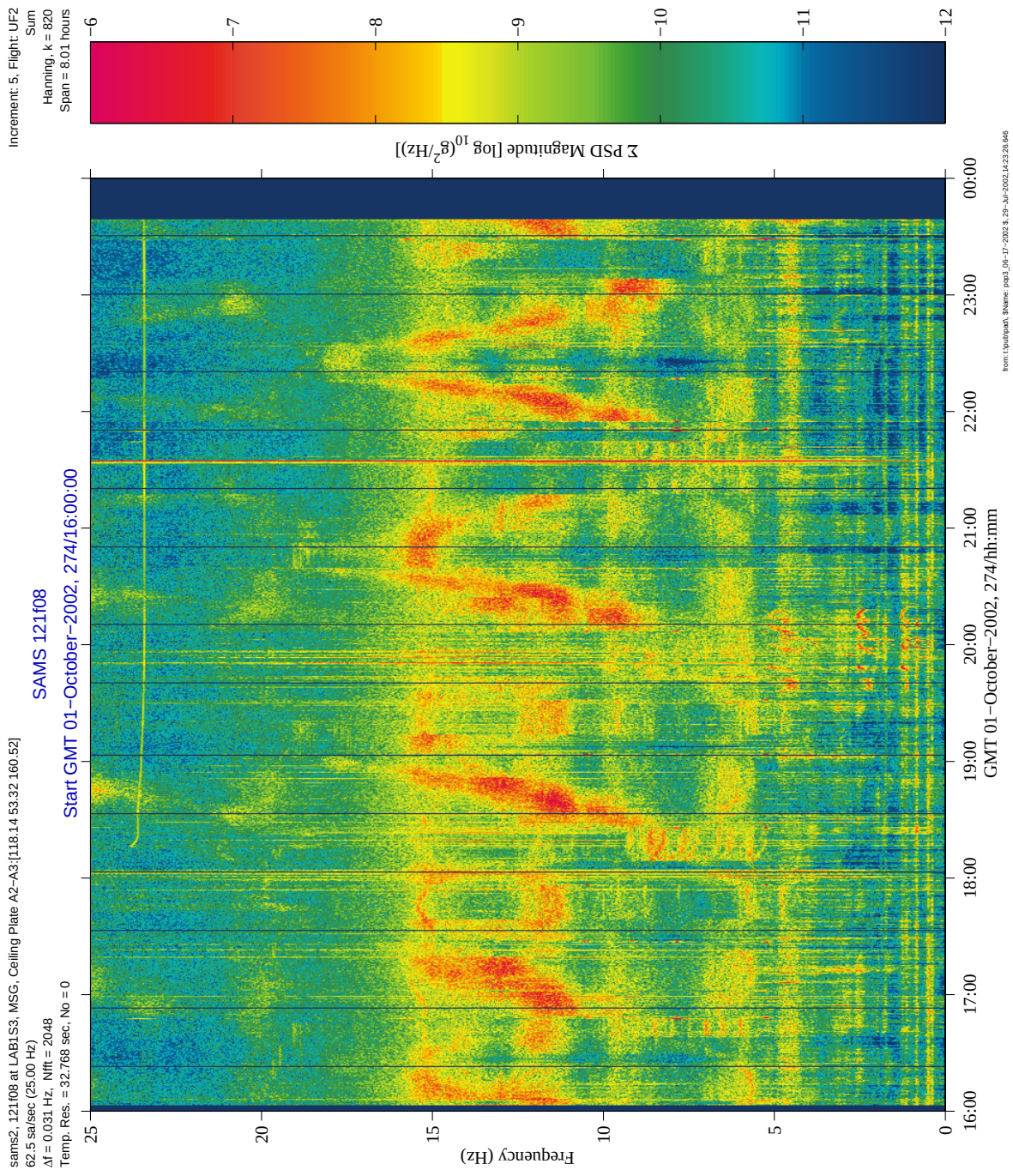

Figure 6-195 Spectrogram of PFMI-08 (121f08)

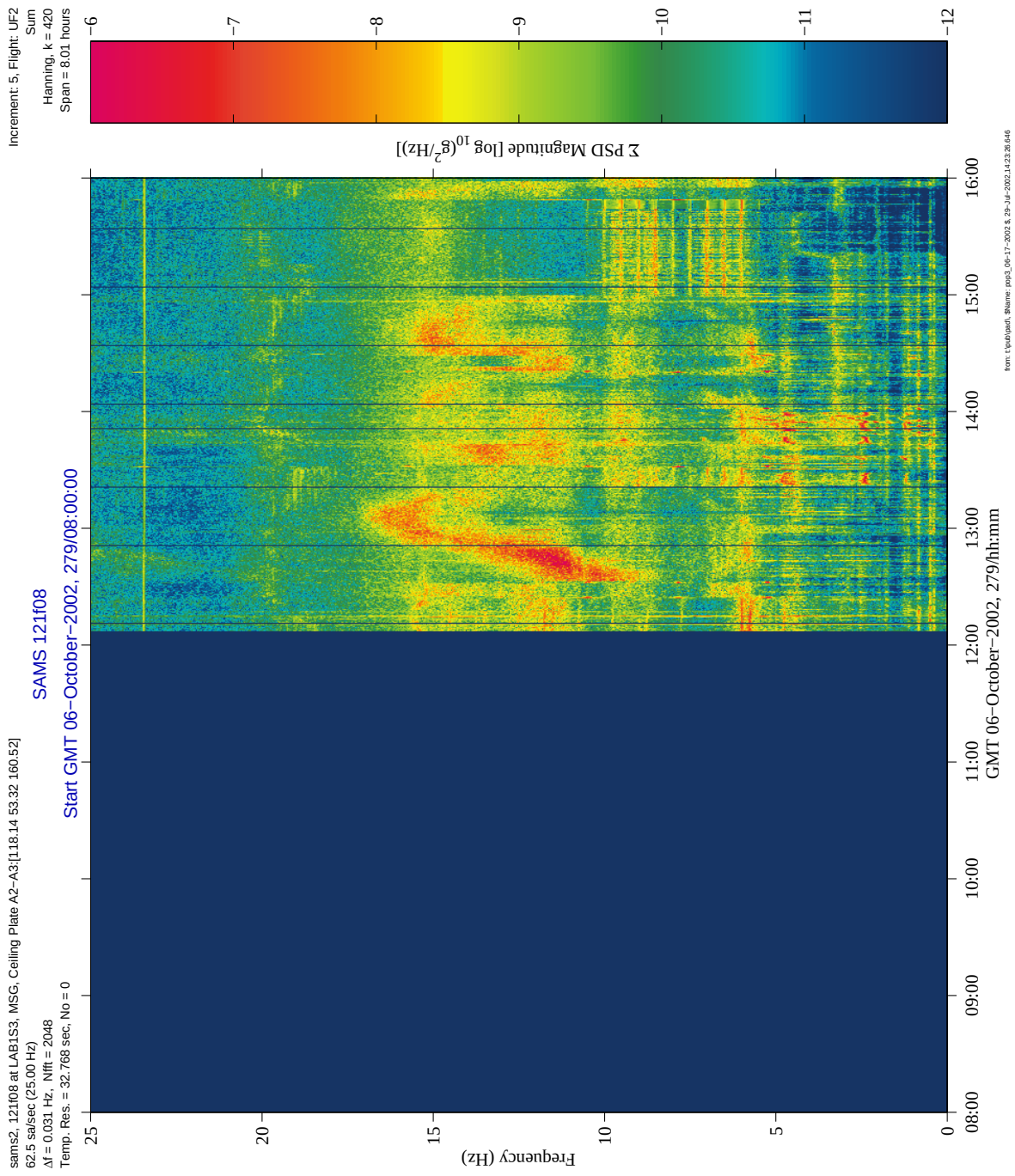

Figure 6-196 Spectrogram of PFMI-05 (121f08)

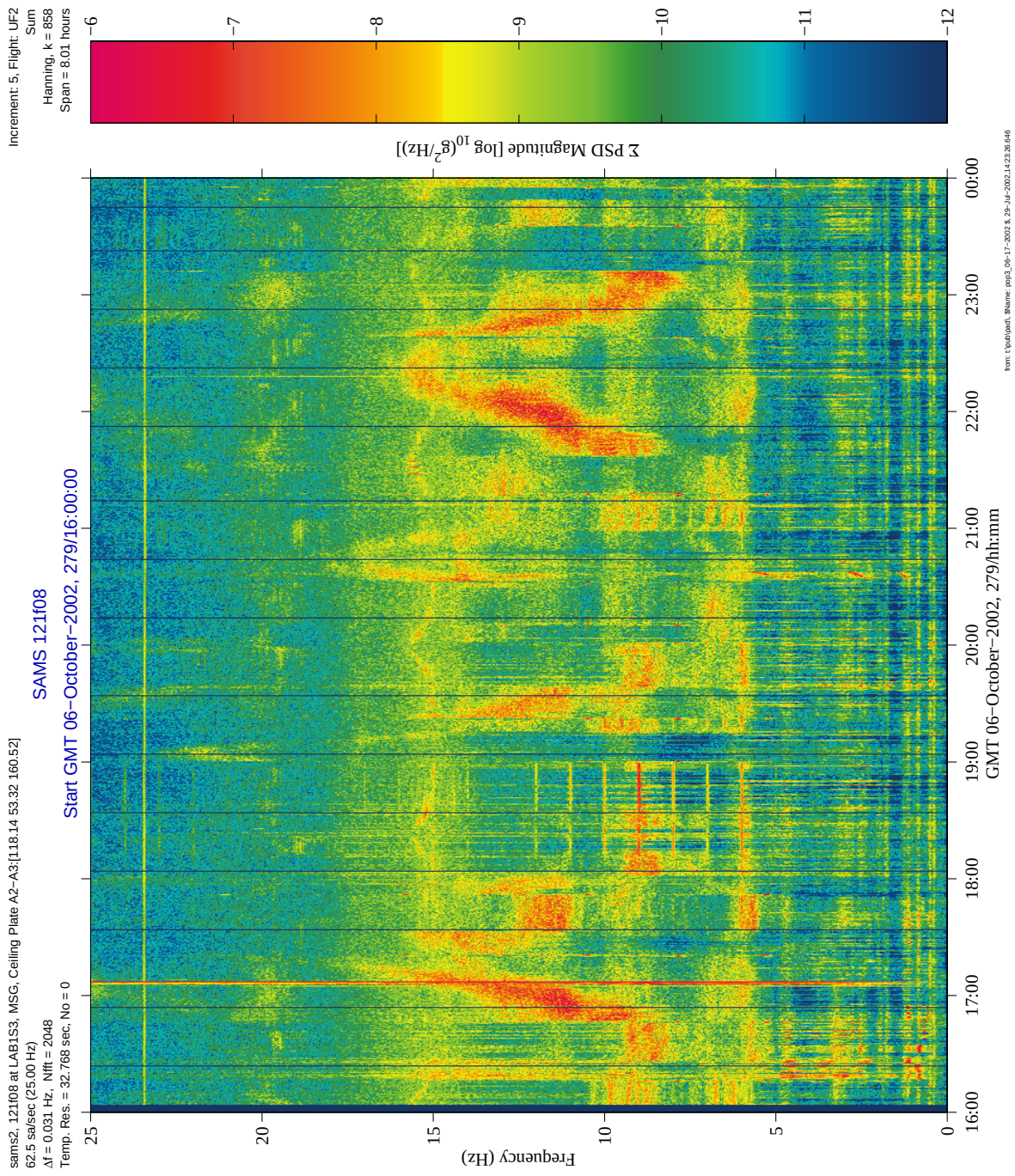

Figure 6-197 Spectrogram of PFMI-05 (121f08)

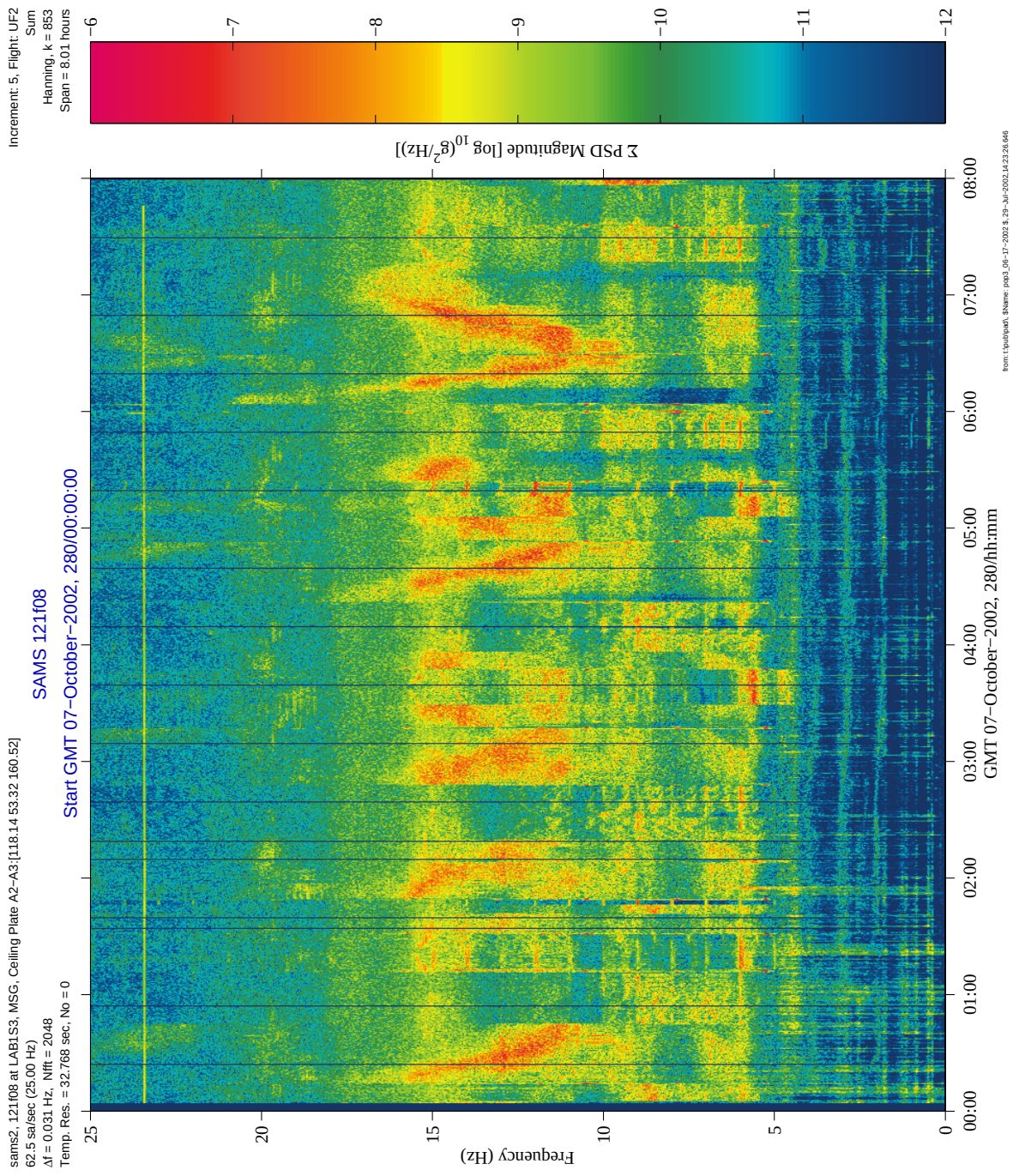

Figure 6-198 Spectrogram of PFMI-05 (121f08)

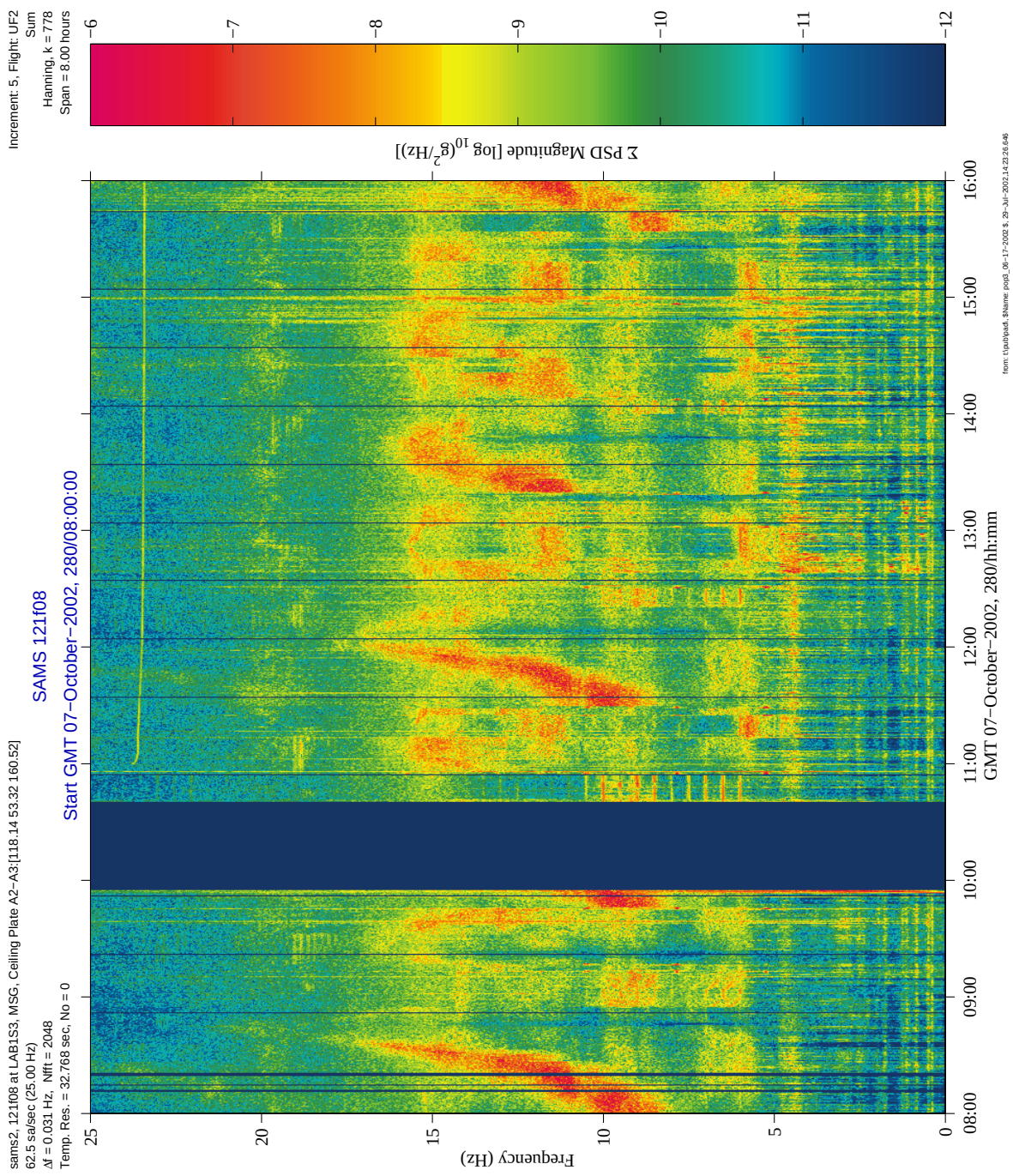

Figure 6-199 Spectrogram of PFMI-02 (121f08)

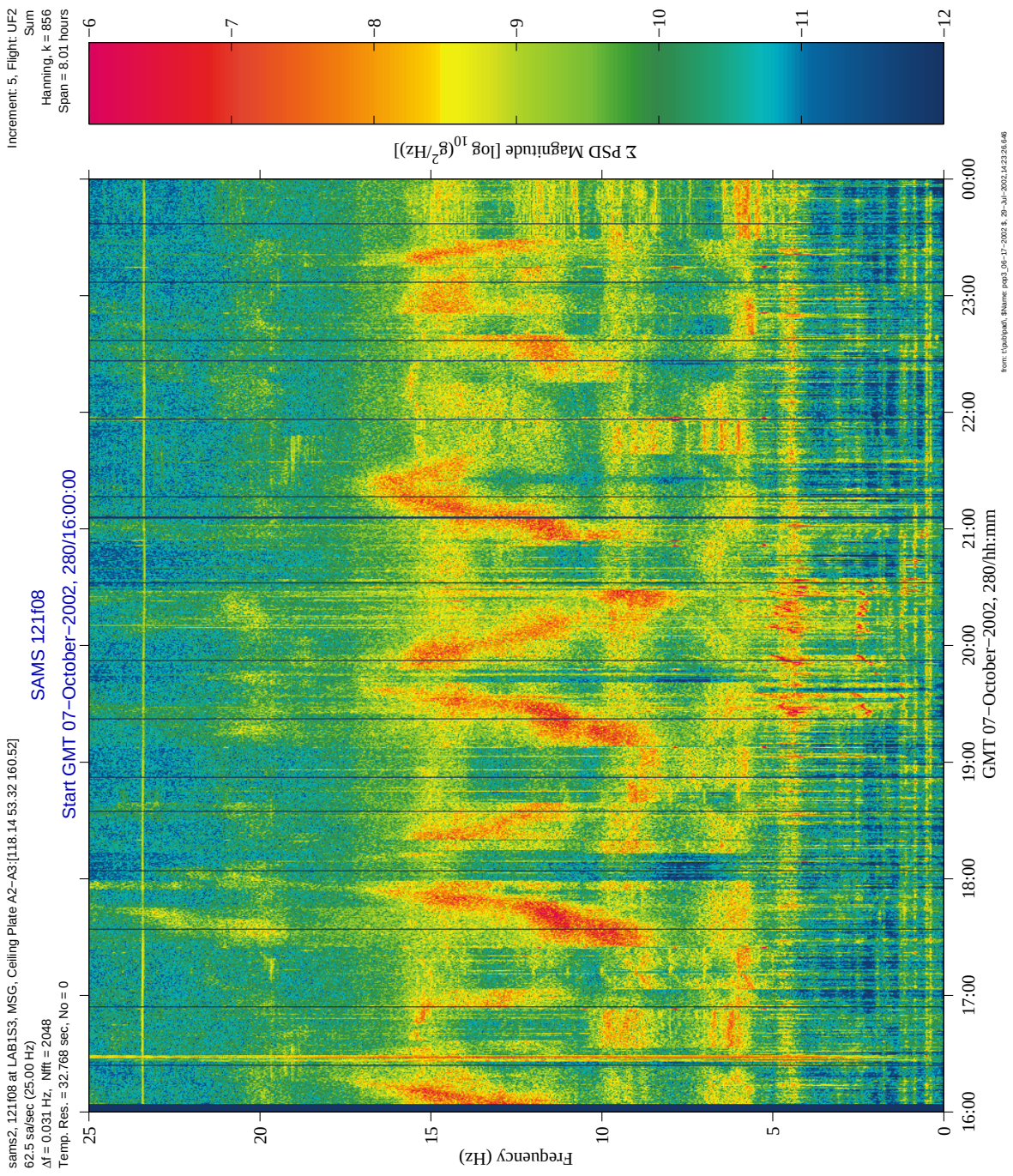

Figure 6-200 Spectrogram of PFMI-02 (121f08)

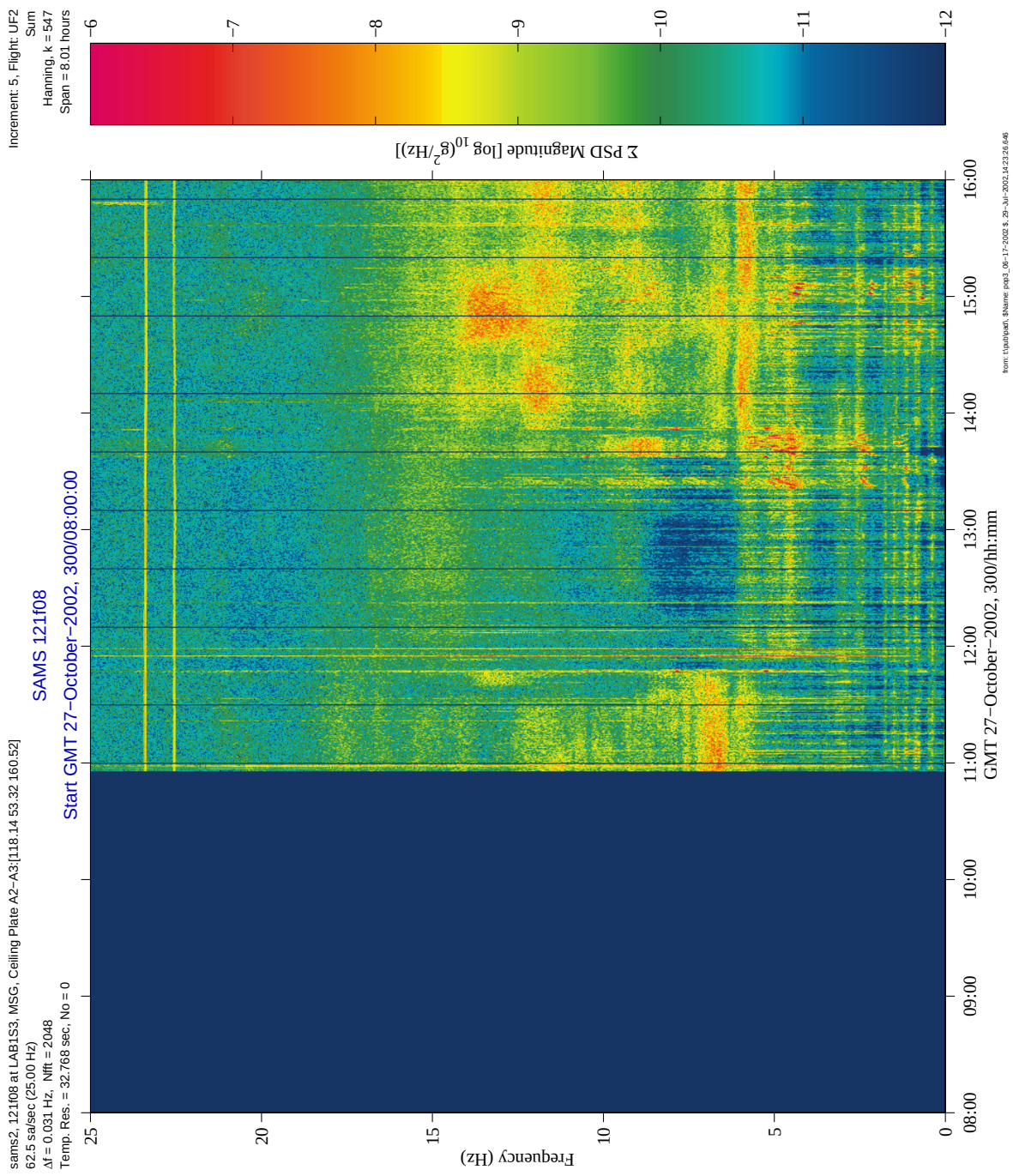

Figure 6-201 Spectrogram of PFMI-10 (121f08)

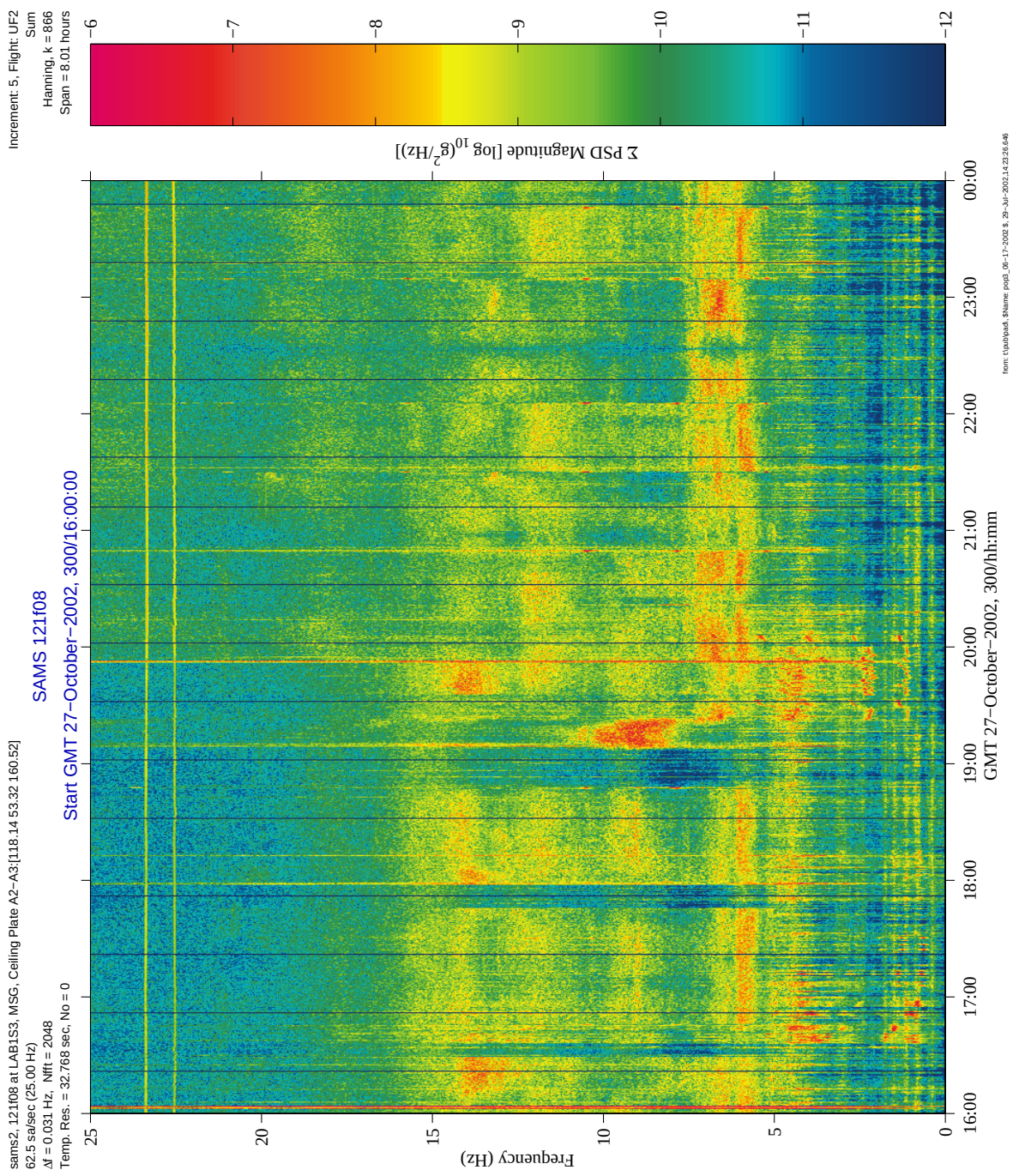

Figure 6-202 Spectrogram of PFMI-10 (121f08)

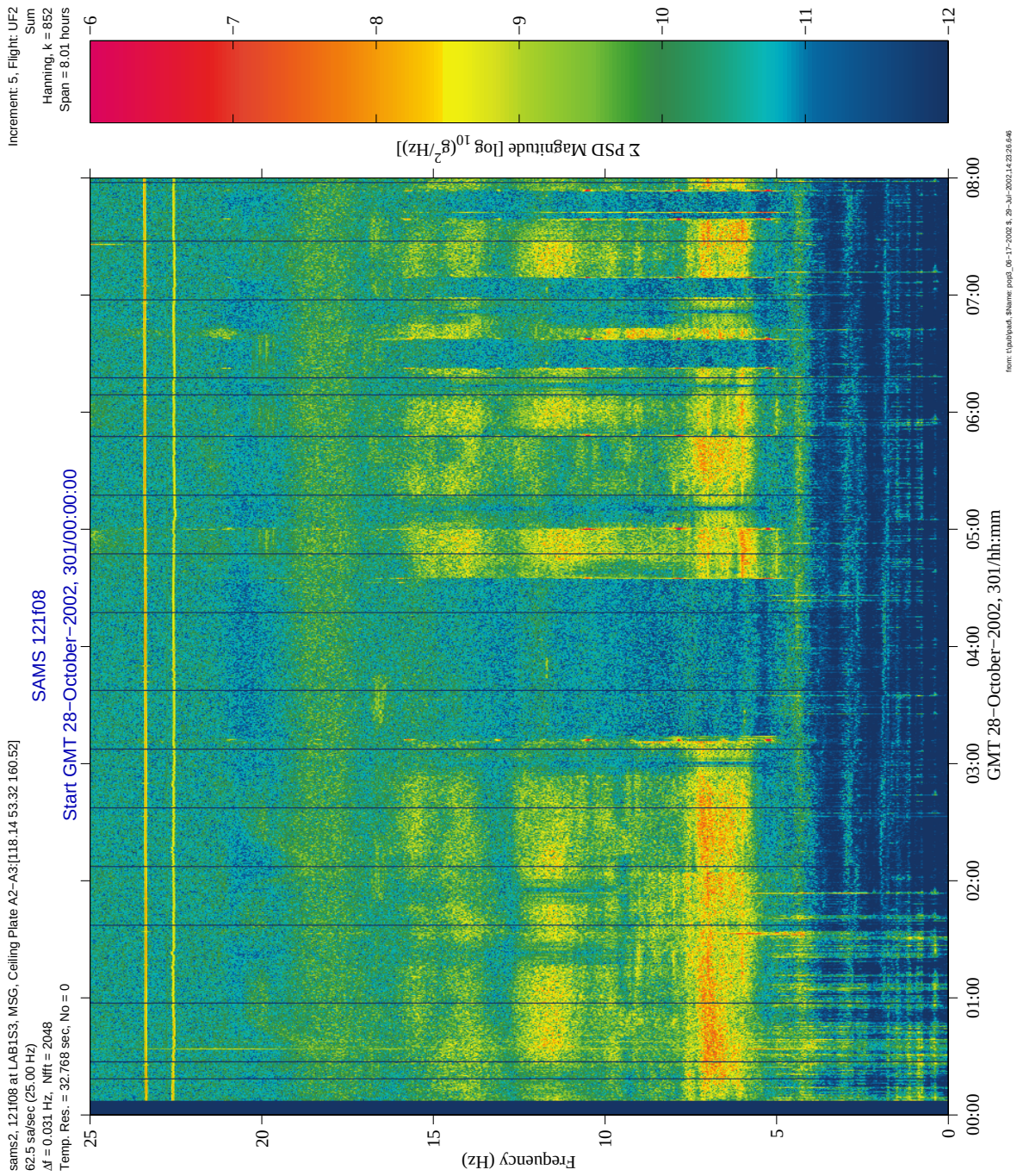

Figure 6-203 Spectrogram of PFMI-10 (121f08)

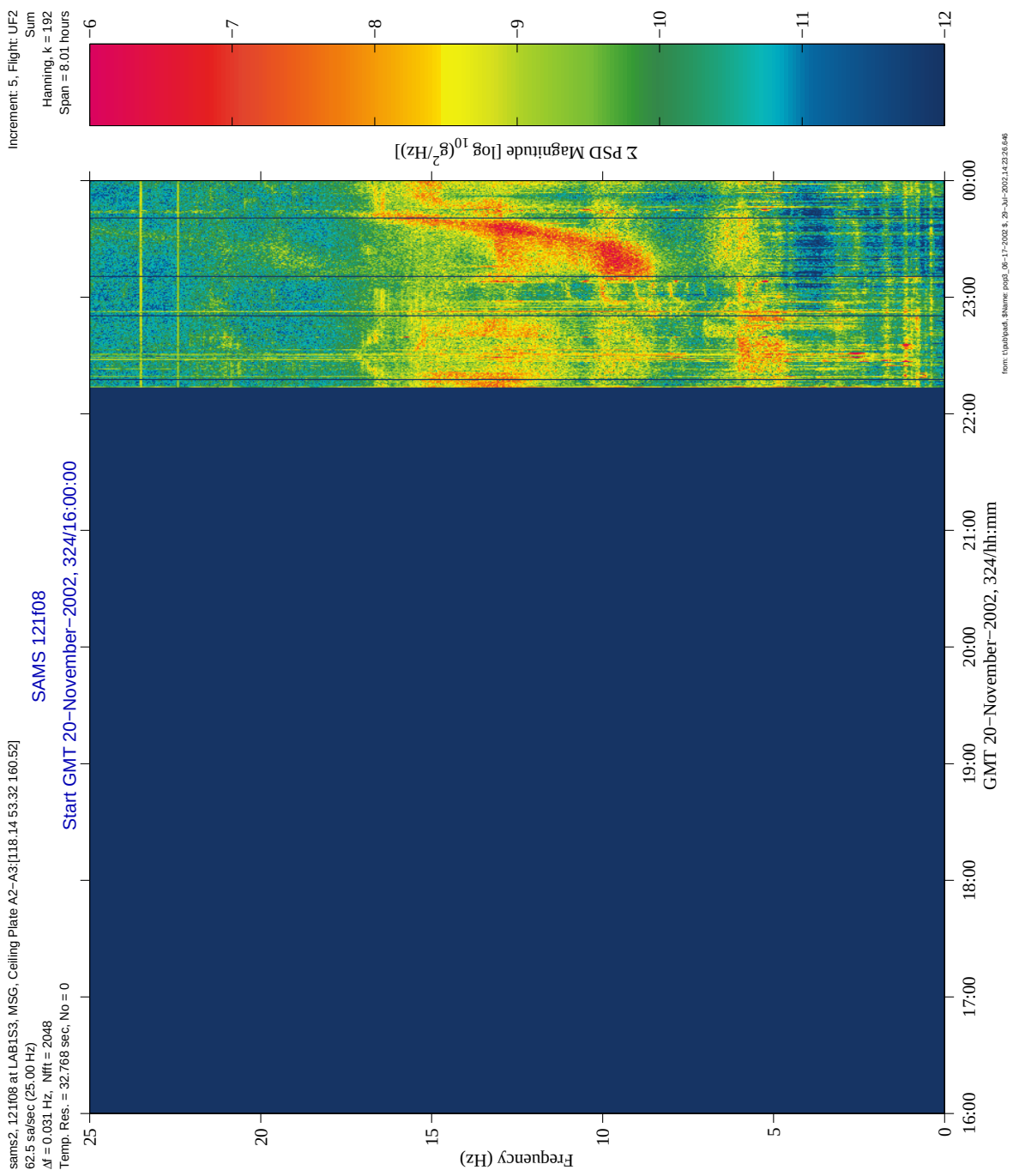

Figure 6-204 Spectrogram of PFMI-11 (121f08)

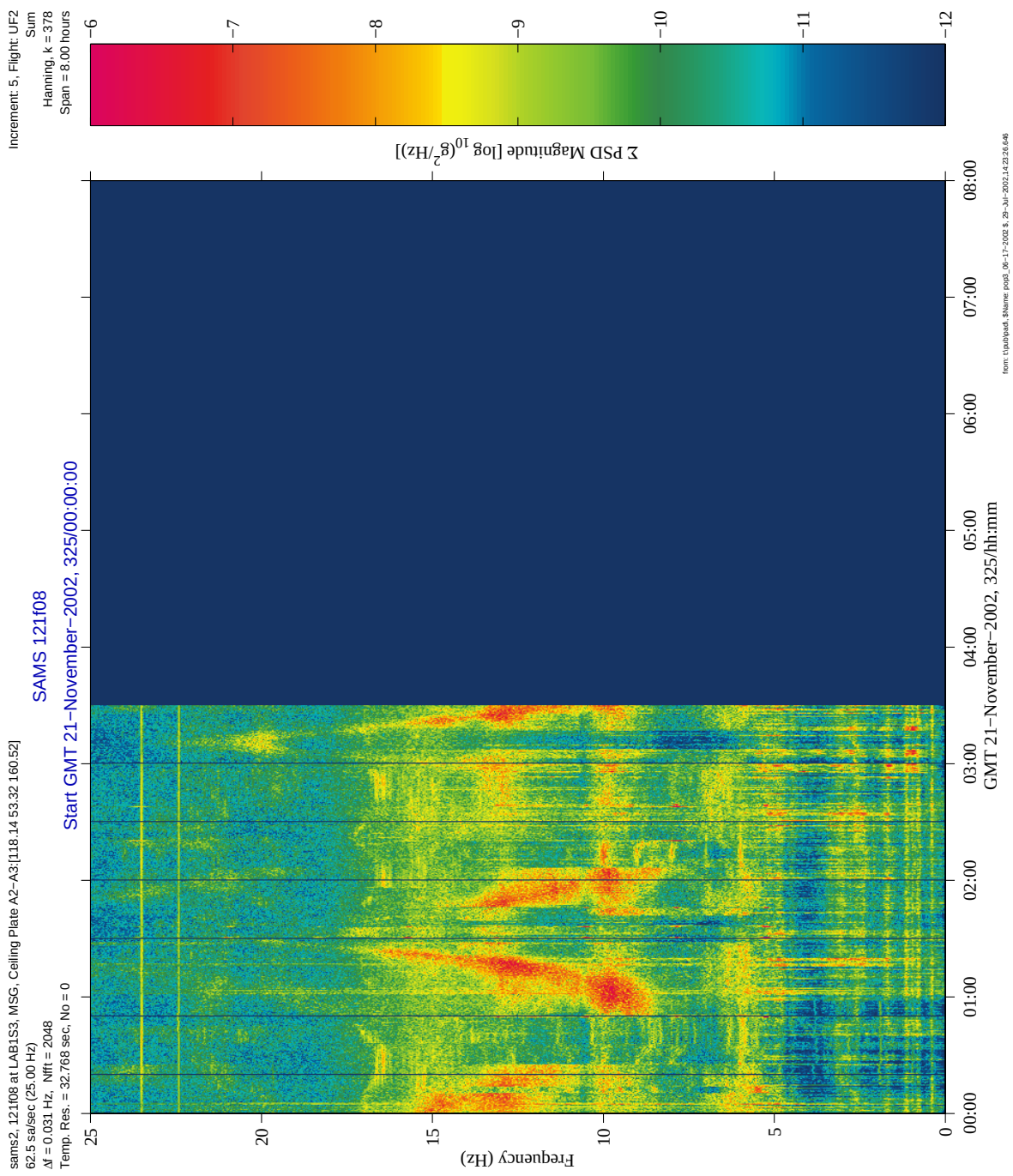

Figure 6-205 Spectrogram of PFMI-11 (121f08)

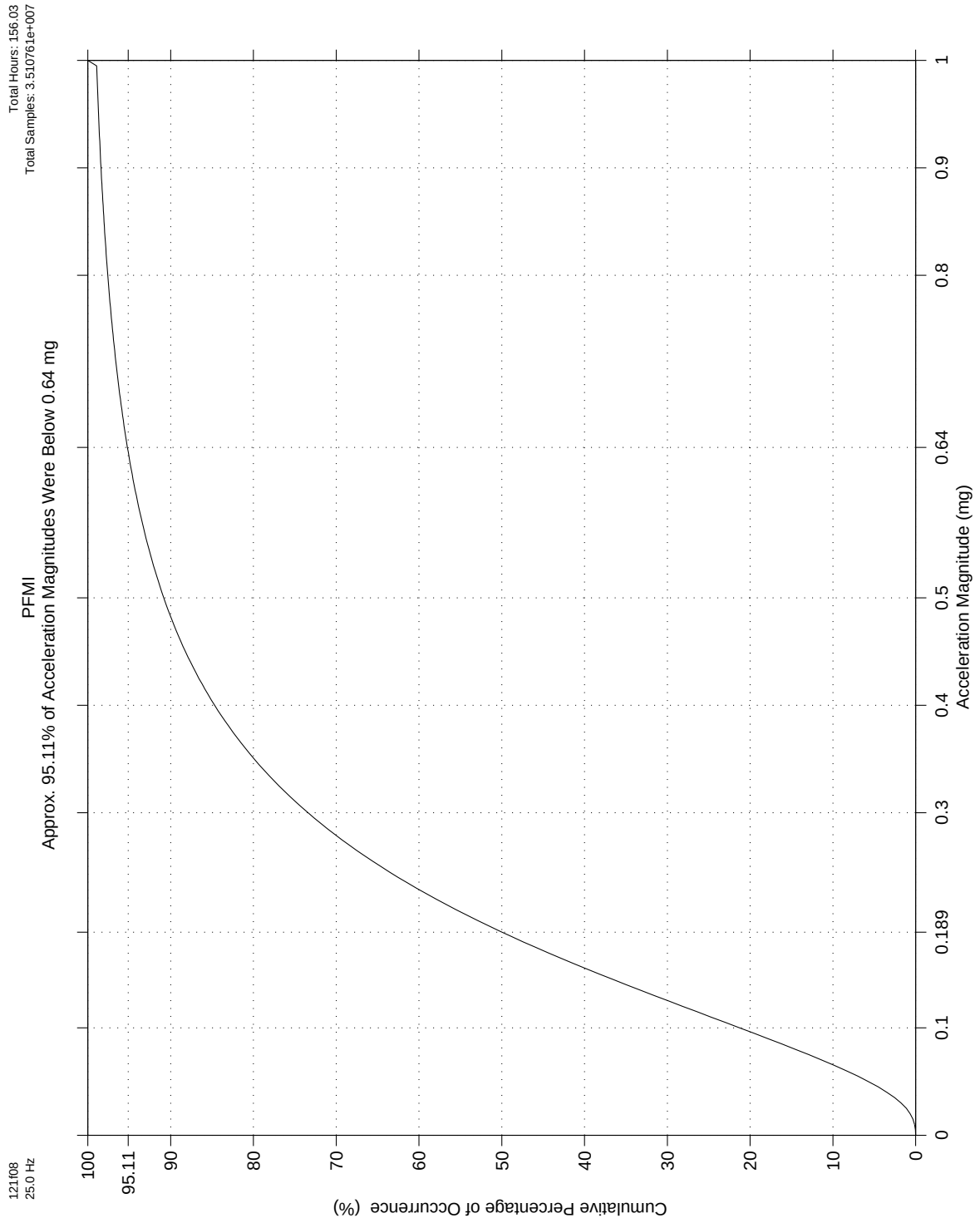

Figure 6-206 Magnitude Cumulative Percentage of PFMI (121f08)

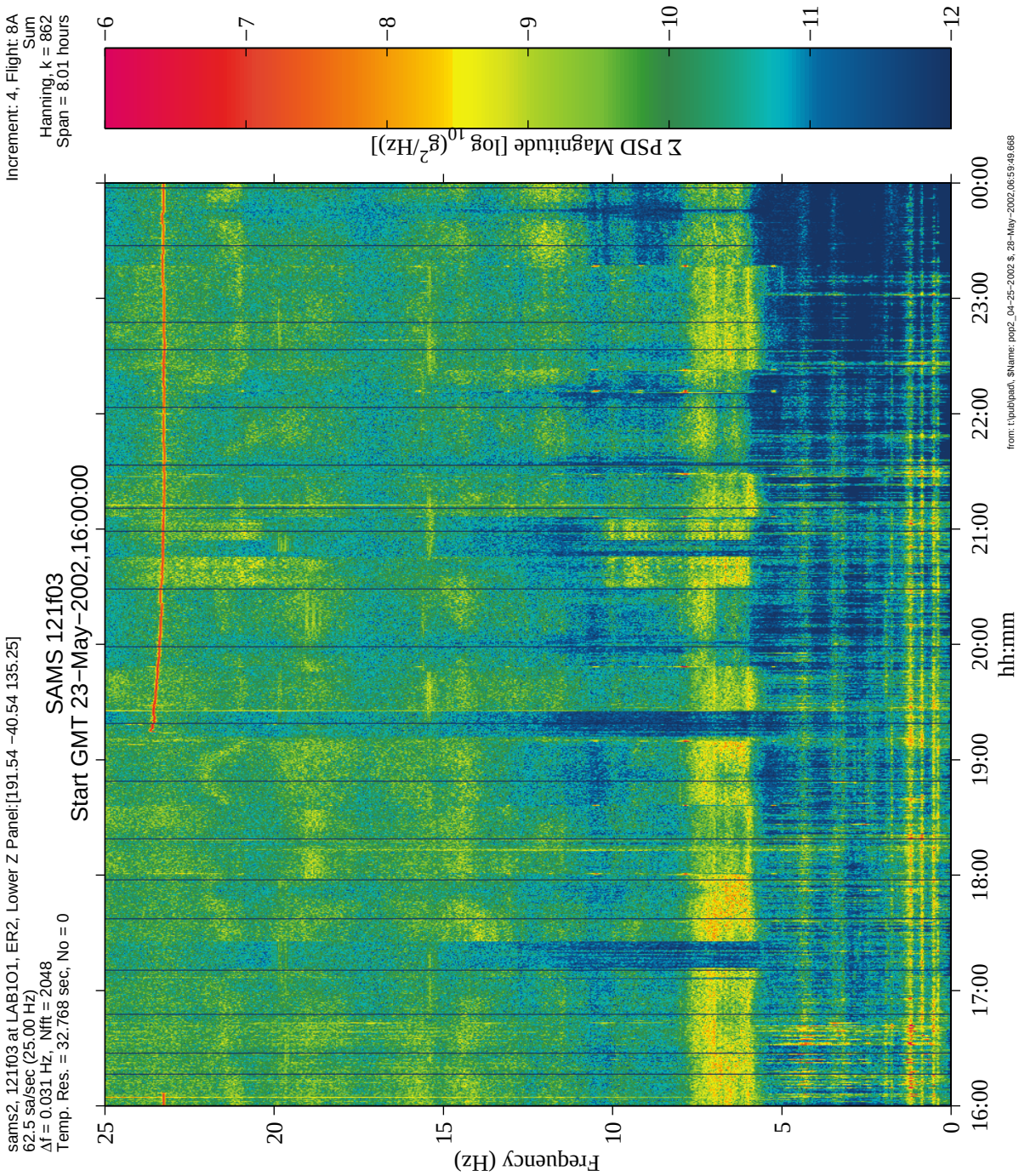

Figure 6-207 Spectrogram of TVIS Exercise Period (121f03)

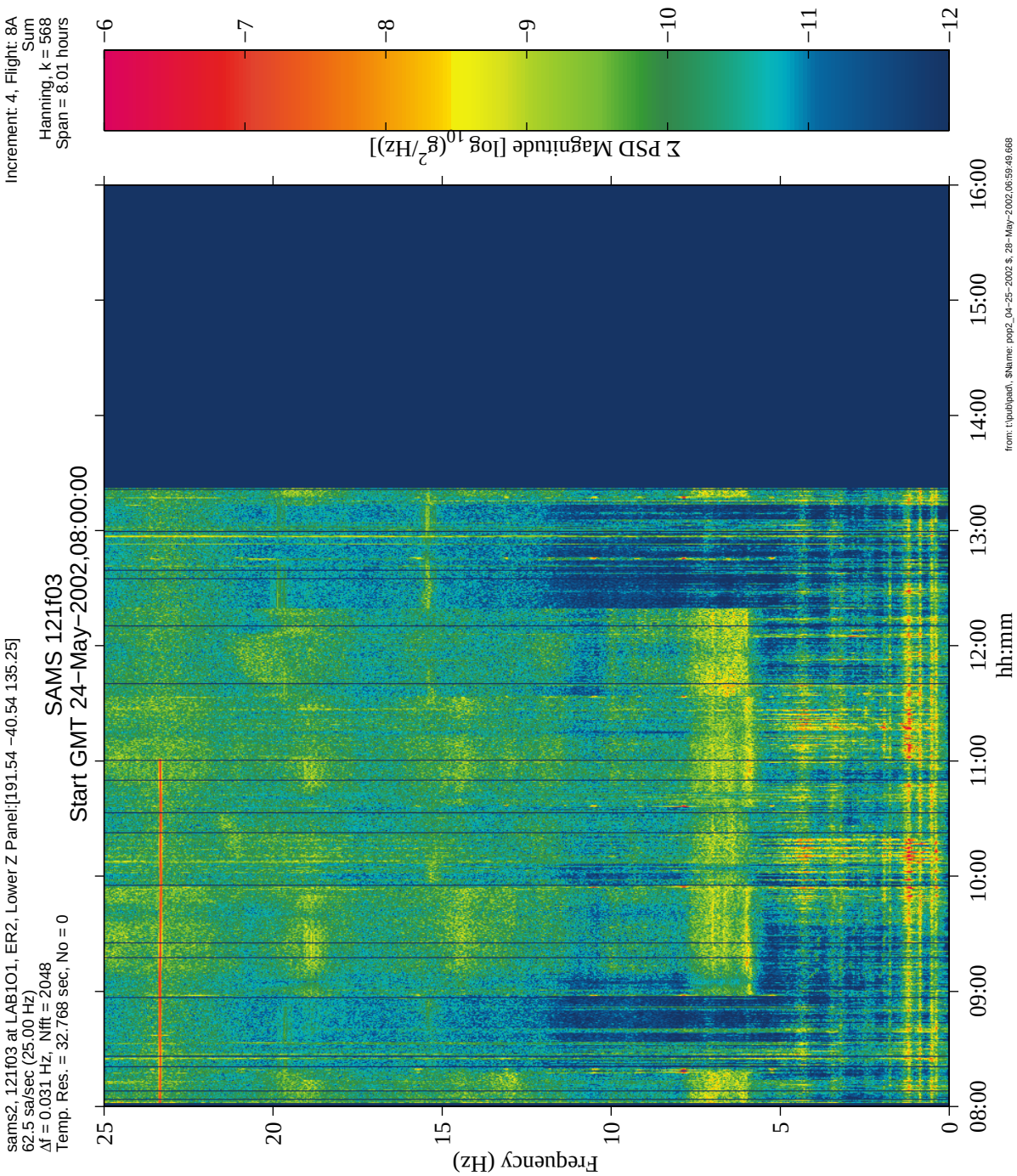

Figure 6-208 Spectrogram of TVIS Exercise Period (121f03)

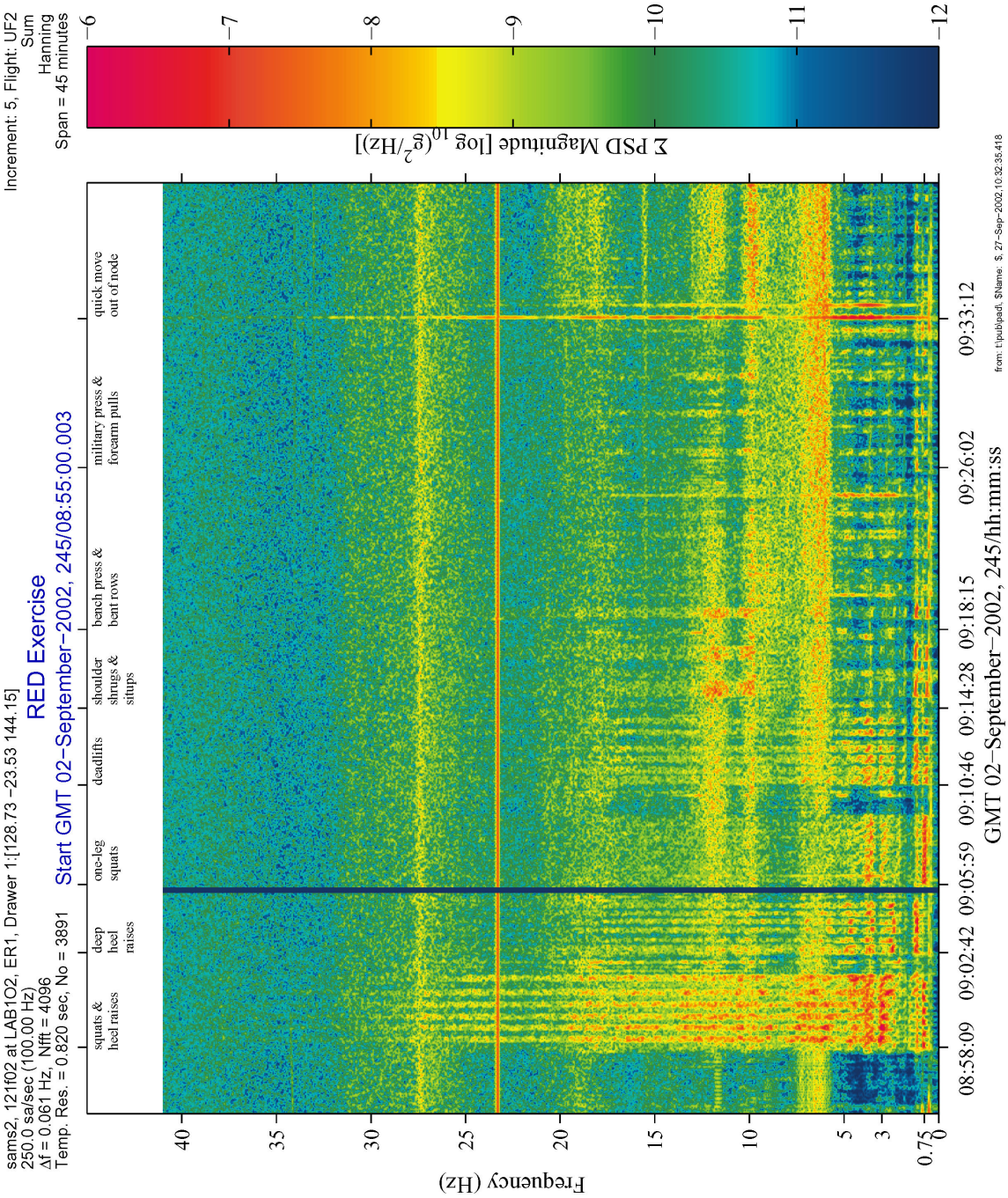

Figure 6-209 Spectrogram of RED Exercise Period (121f02)

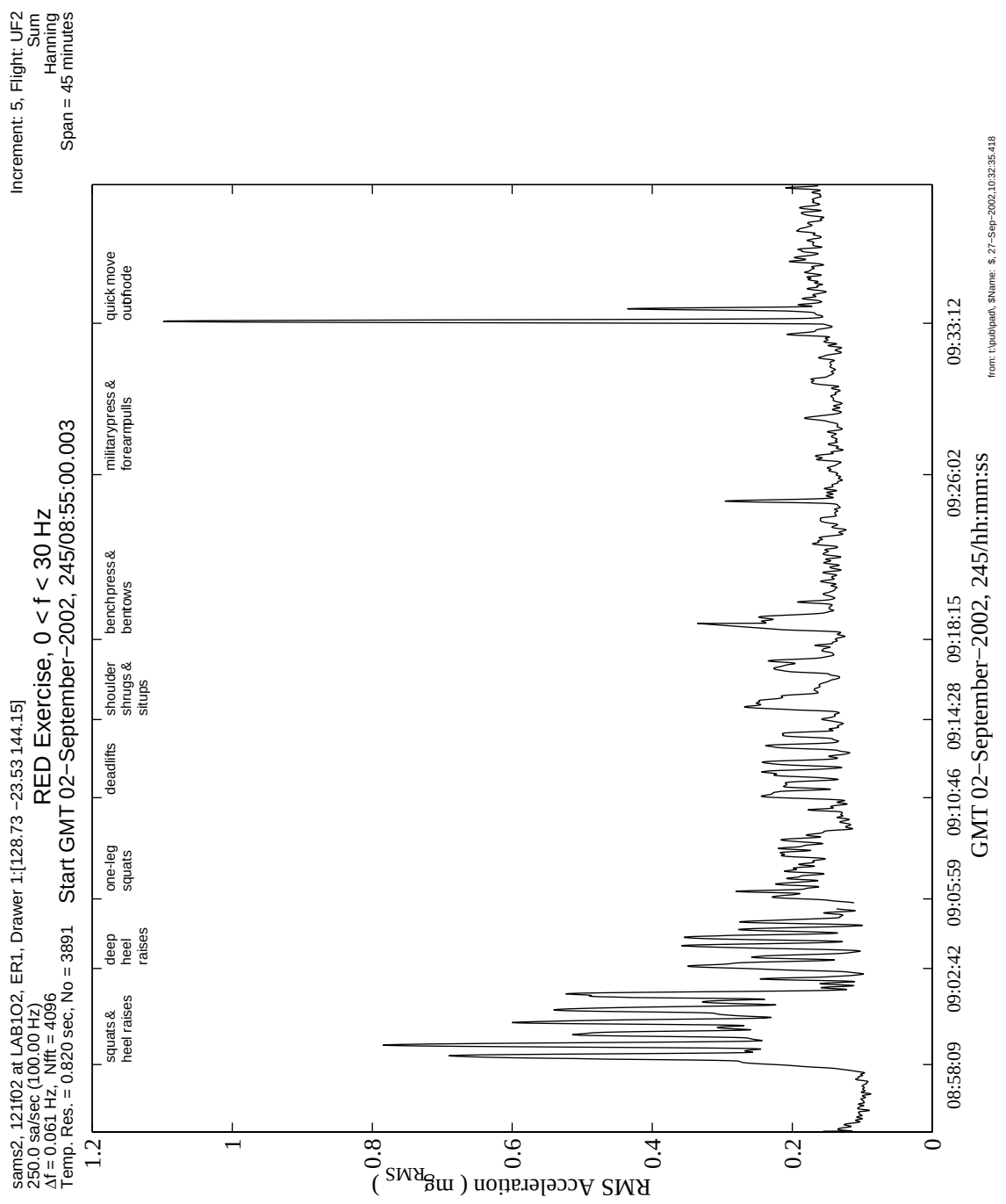

Figure 6-210 Interval RMS of RED Exercise Period (121f02)

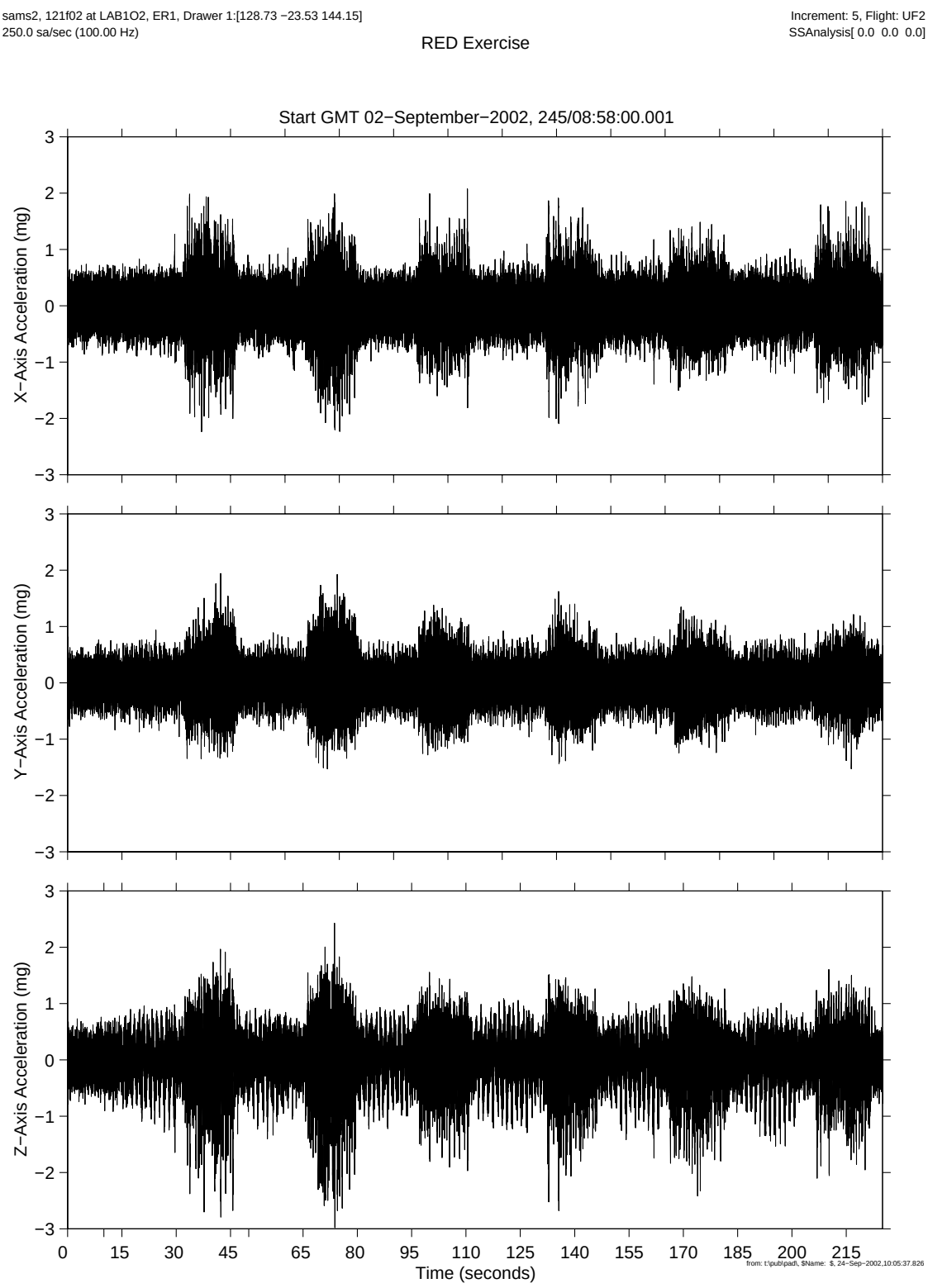

Figure 6-211 Time Series of RED Exercise Period (121f02)

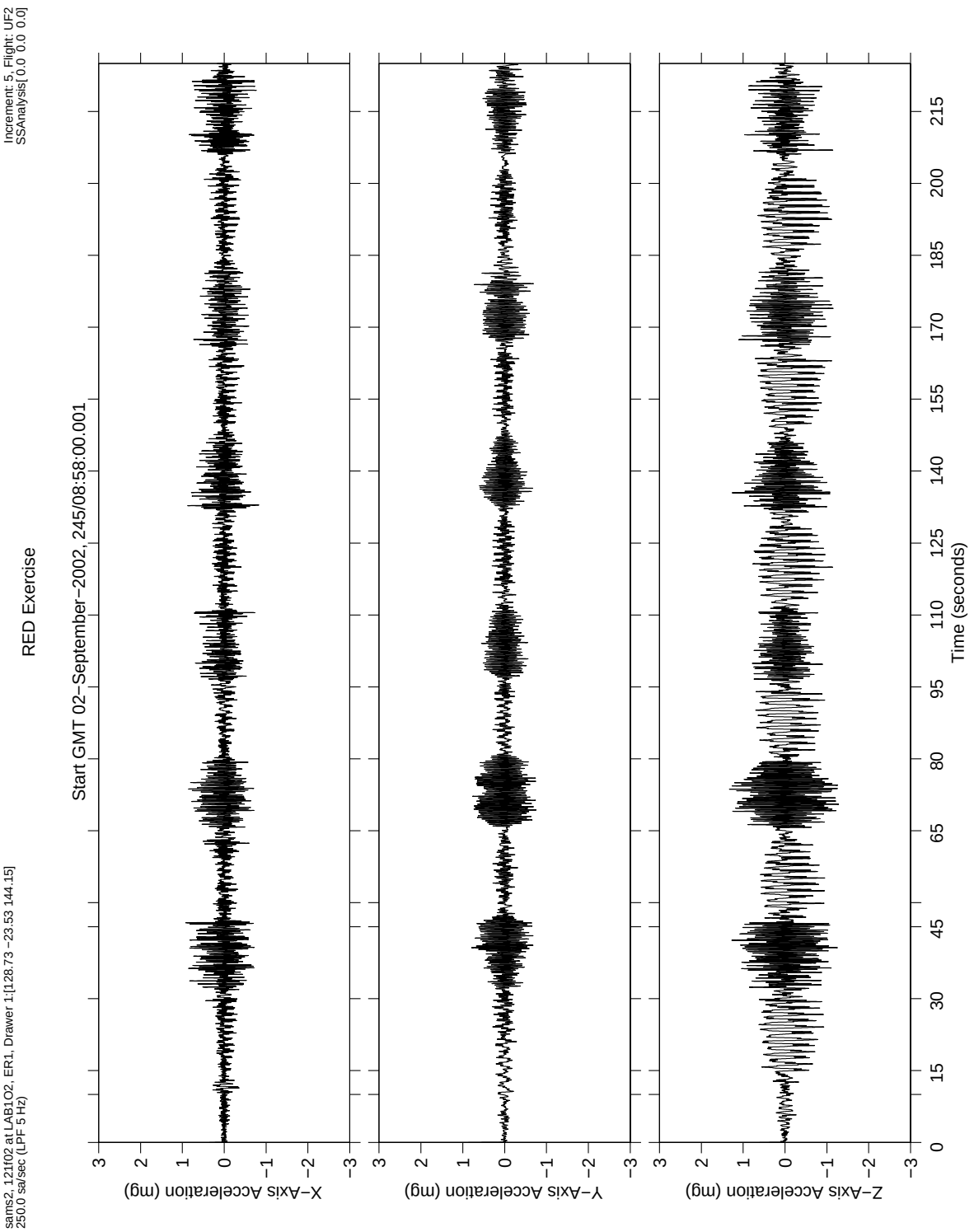

Figure 6-212 Lowpass Filtered Time Series of RED Exercise Period (121f02)

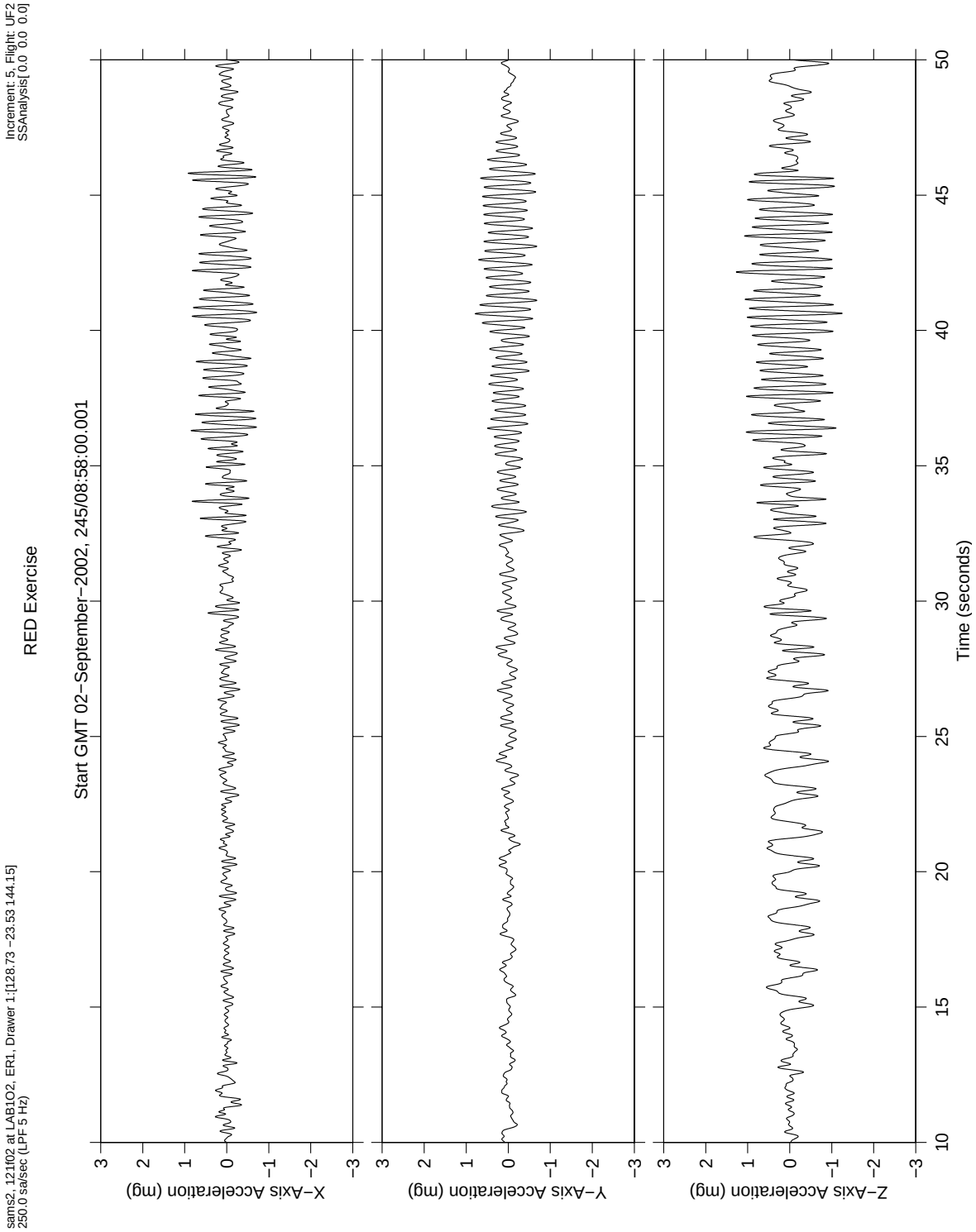

Figure 6-213 Lowpass Filtered Time Series Zoom of RED Exercise Period (121f02)

Figure 6-214 Digital Image of CEVIS Exercise

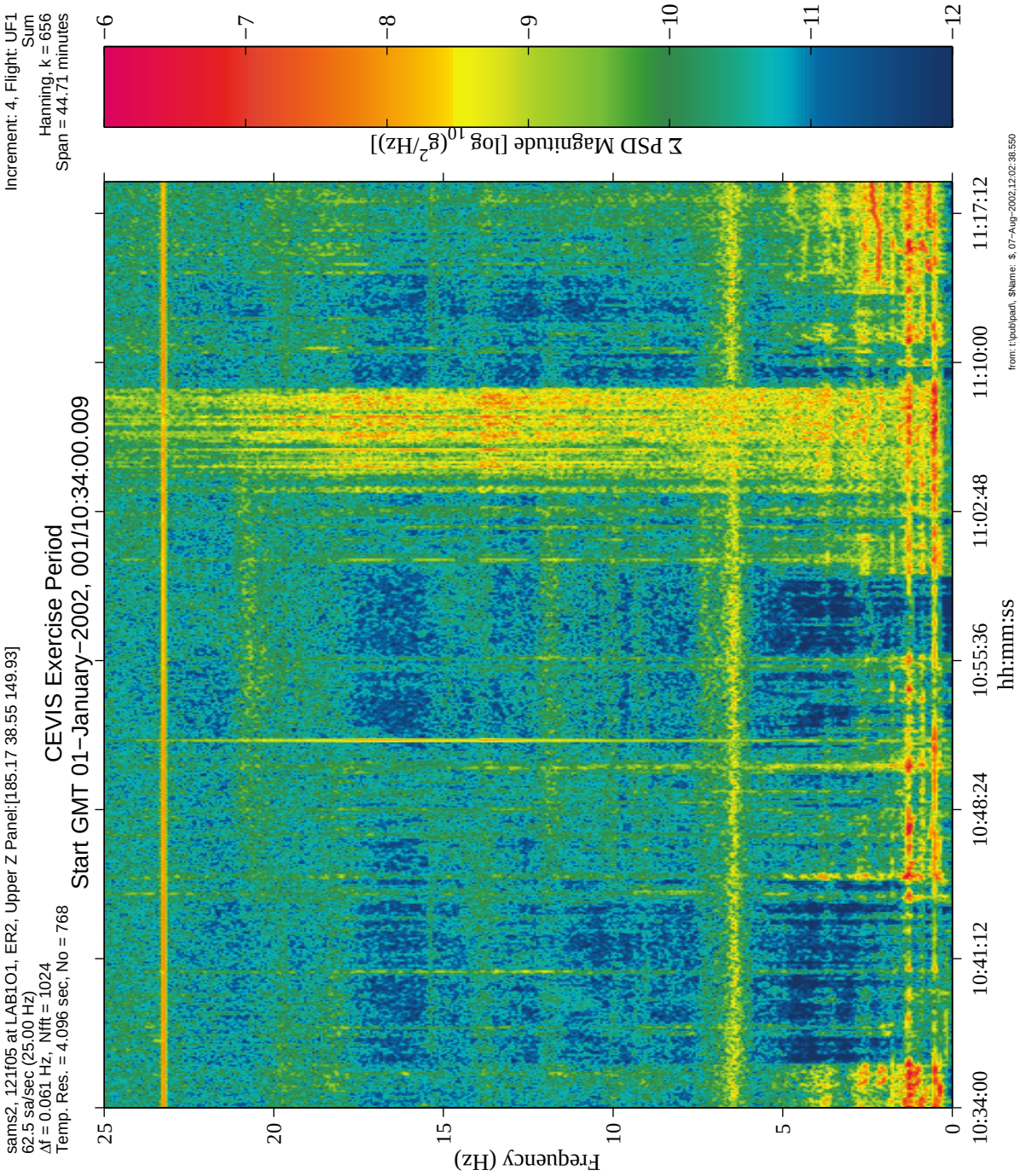

Figure 6-215 Spectrogram of CEVIS Exercise Period (121f05)

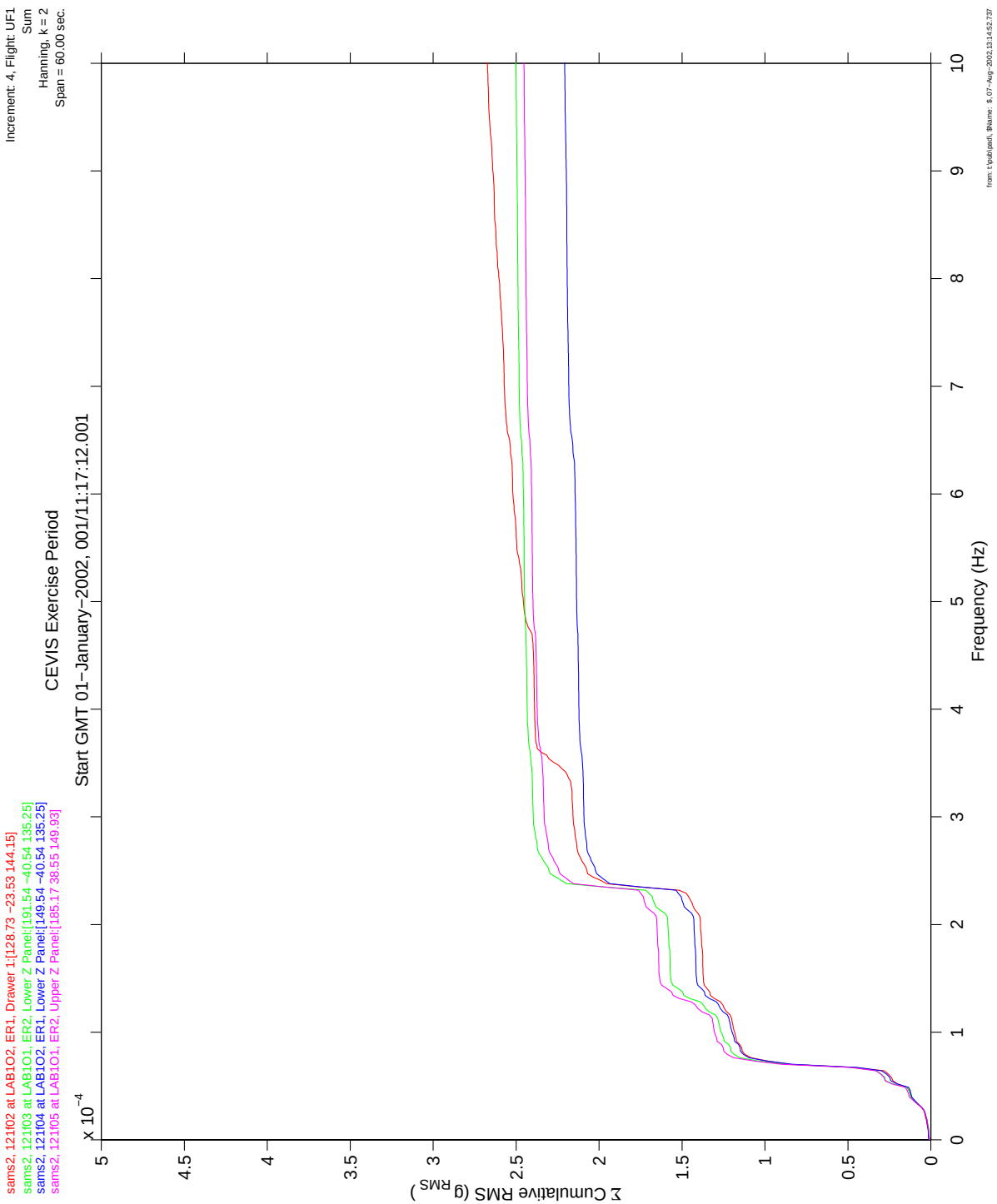

Figure 6-216 Cumulative RMS of CEVIS Exercise Period (121f02, 121f03, 121f04, 121f05)

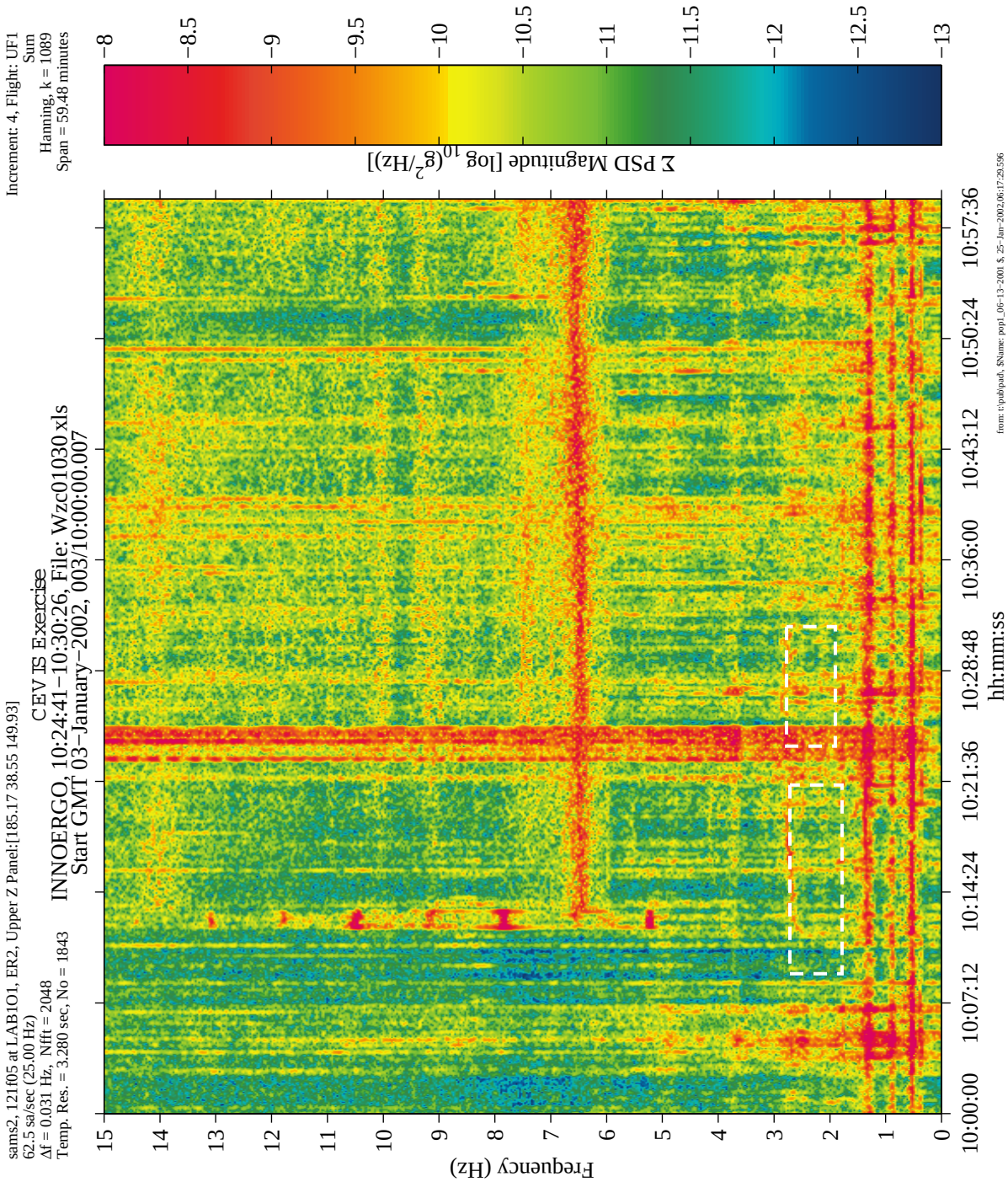

Figure 6-217 Spectrogram of CEVIS Exercise Period (121f05)

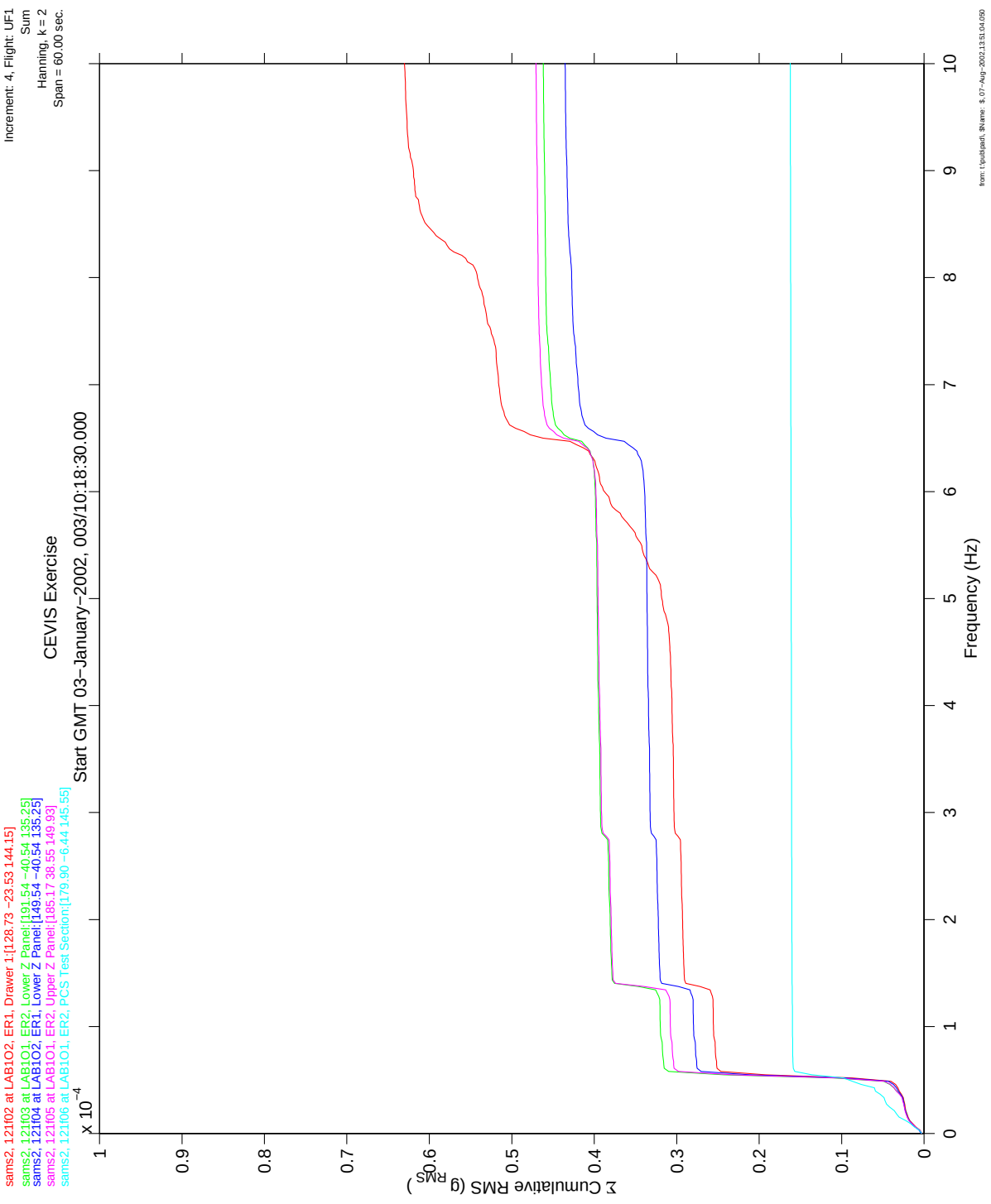

Figure 6-218 Cumulative RMS of CEVIS Exercise Period (121f02, 121f03, 121f04, 121f05)

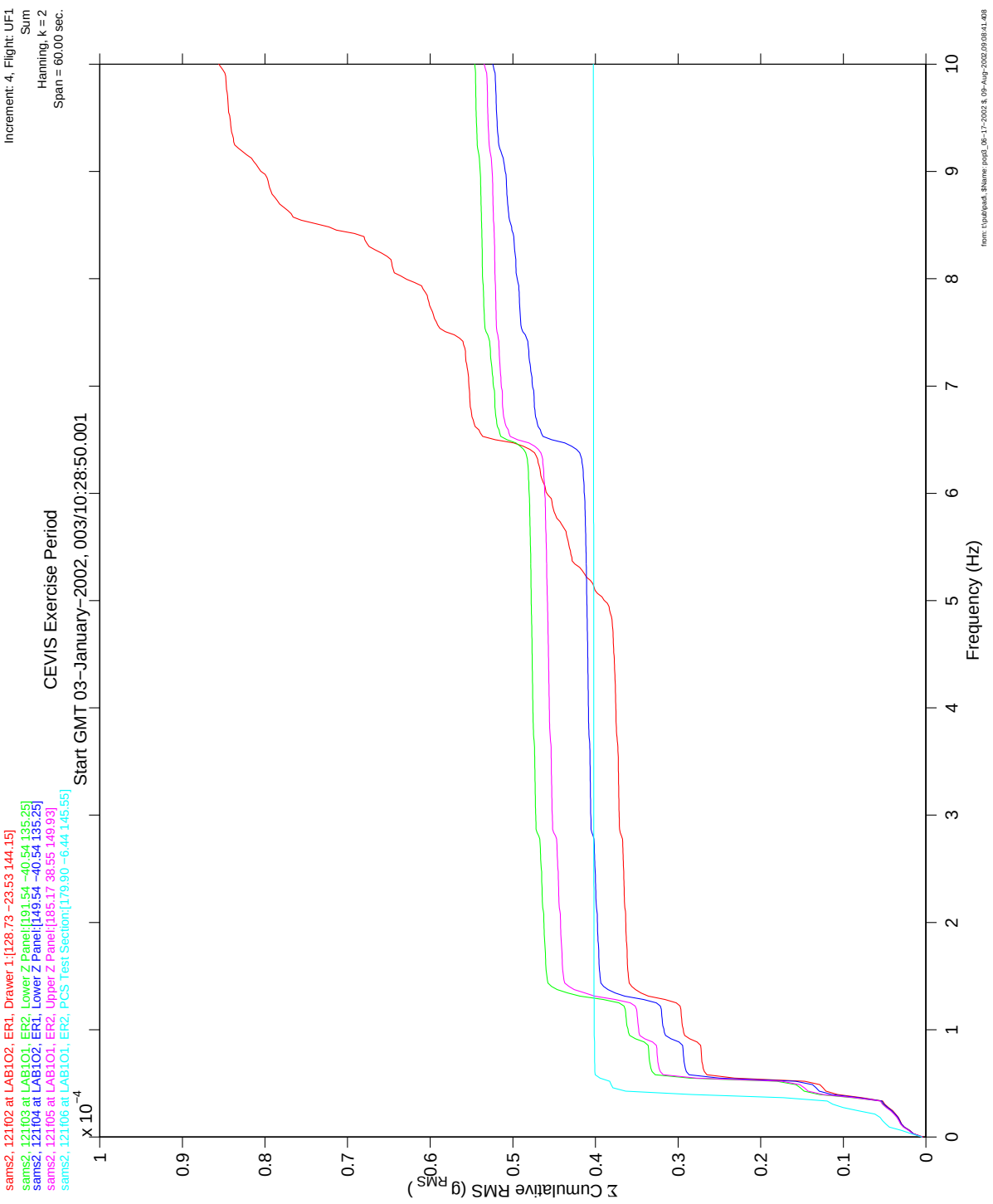

Figure 6-219 Cumulative RMS of CEVIS Exercise Period (121f02, 121f03, 121f04, 121f05)

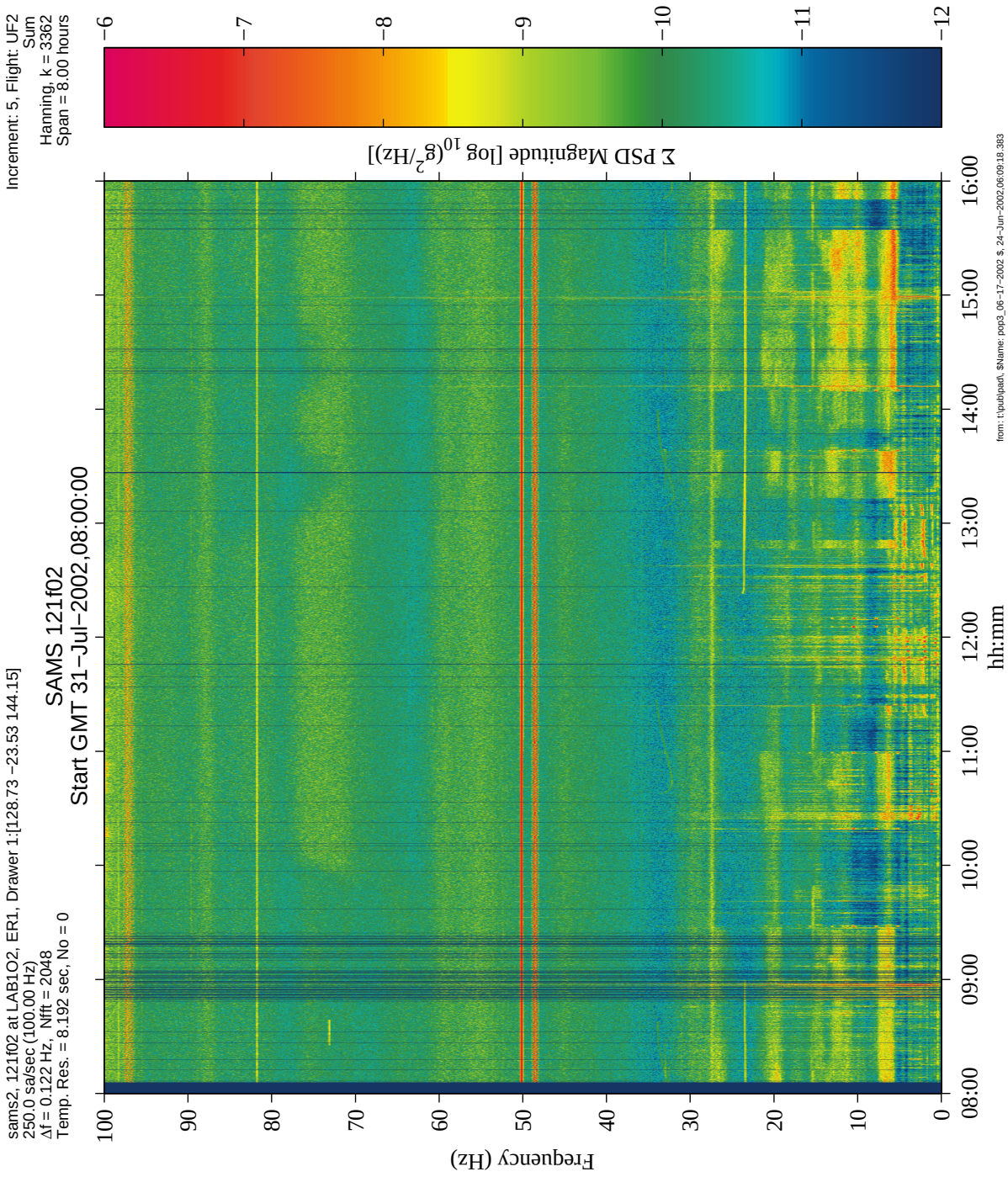

Figure 6-220 Spectrogram of VELO Exercise Periods (121f02)

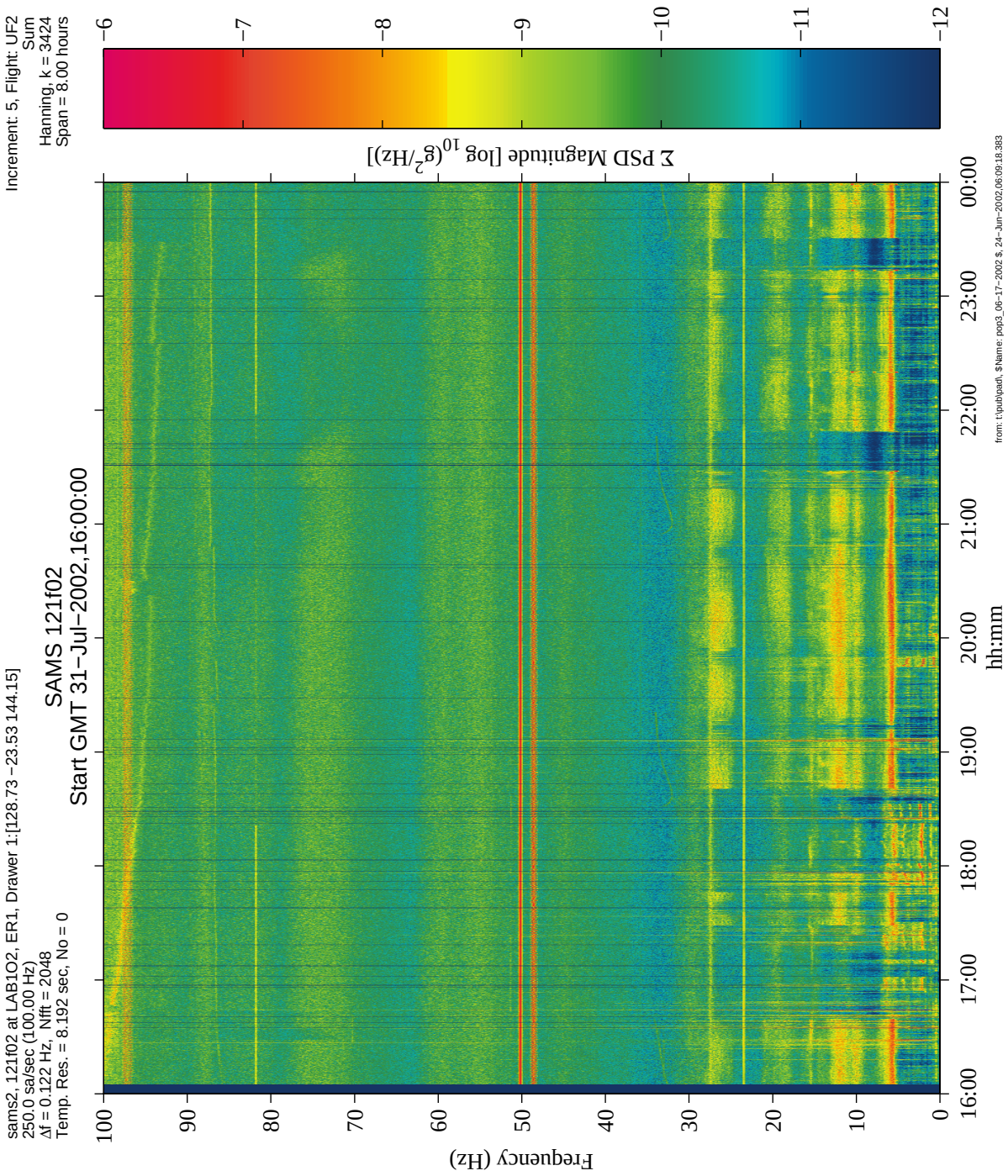

Figure 6-221 Spectrogram of VELO Exercise Periods (121f02)

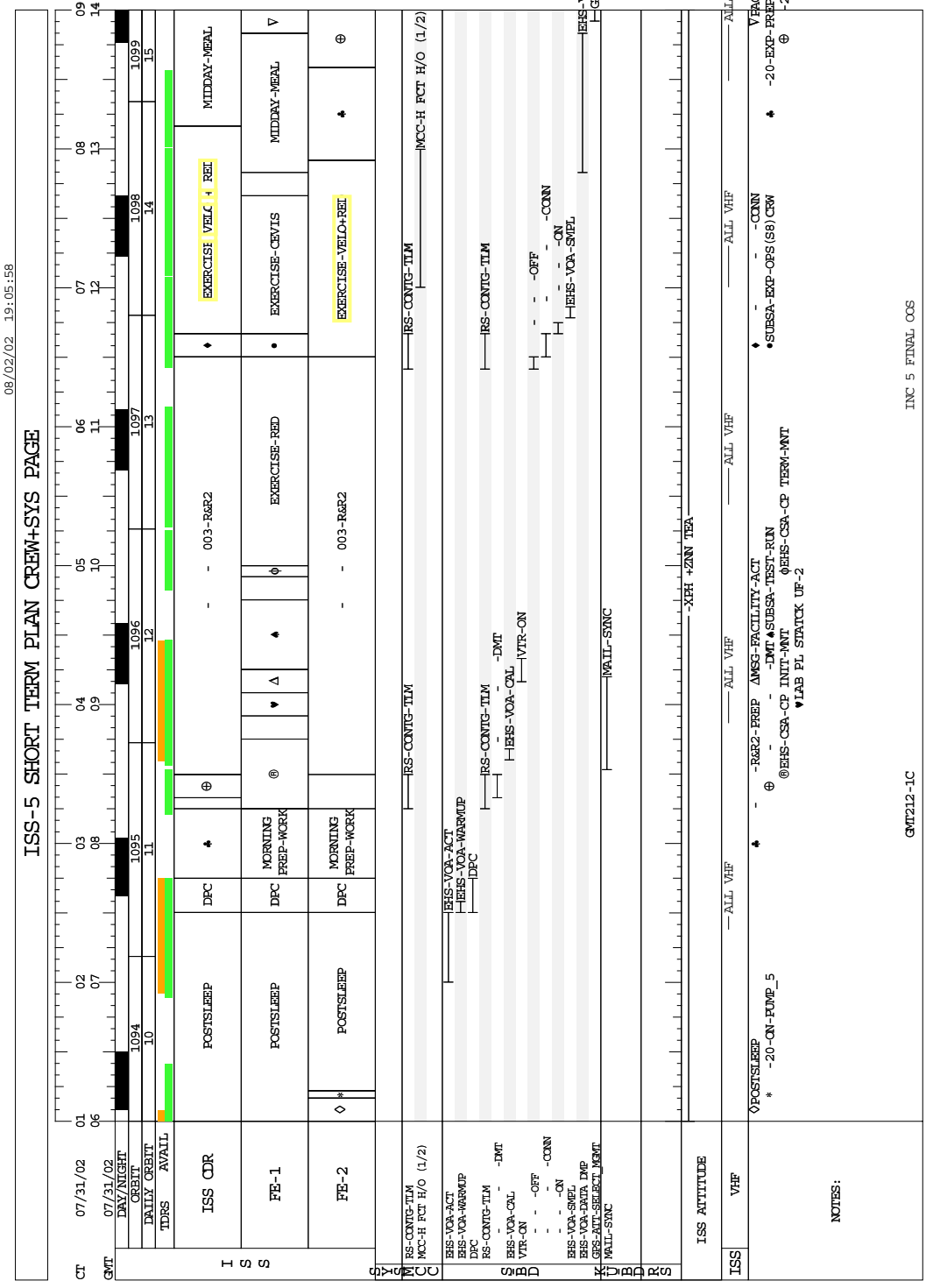

Figure 6-222 Short-Term Plan Excerpt for GMT 31-Jul-2002, 06:00 - 14:00

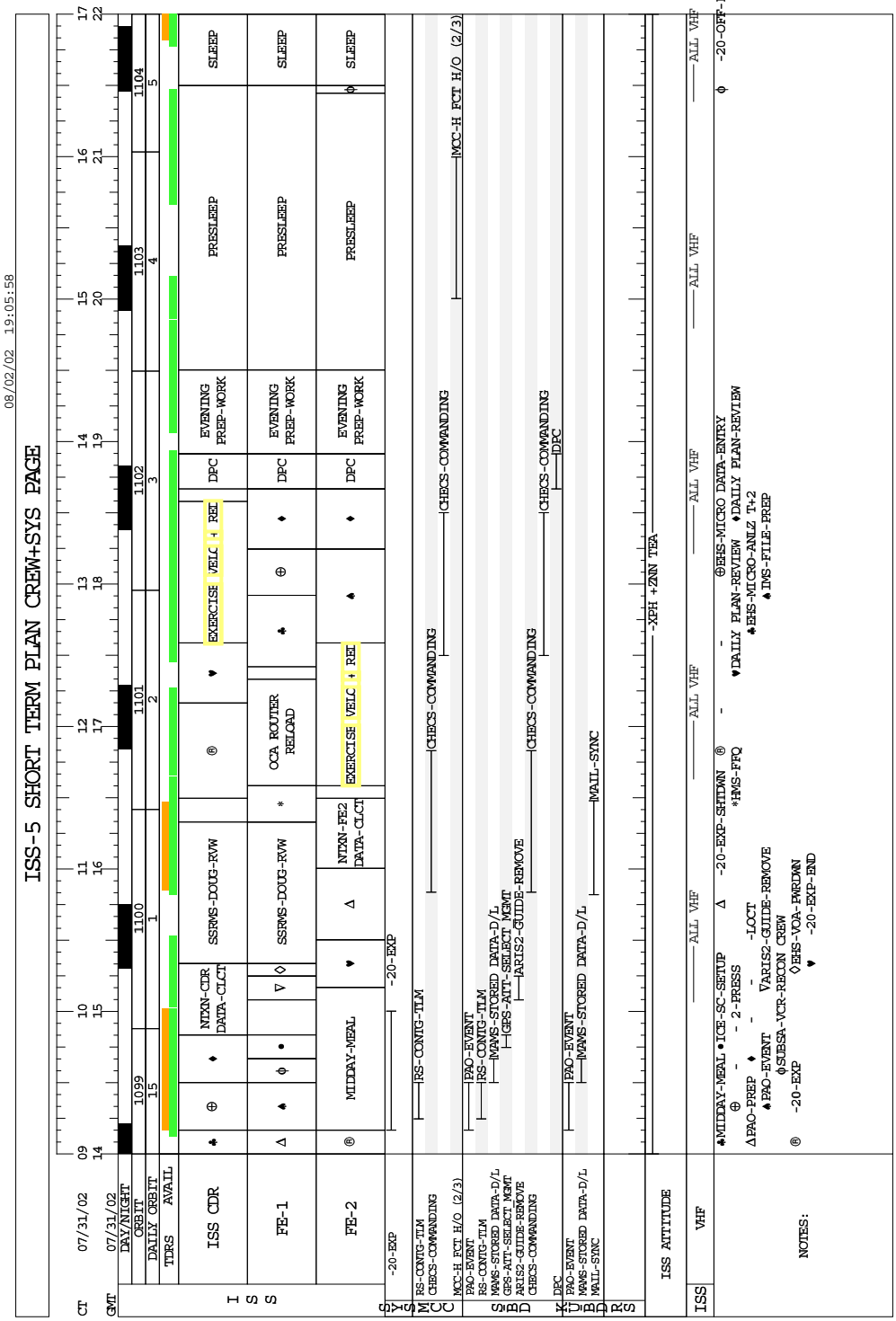

Figure 6-223 Short-Term Plan Excerpt for GMT 31-Jul-2002, 14:00 - 22:00

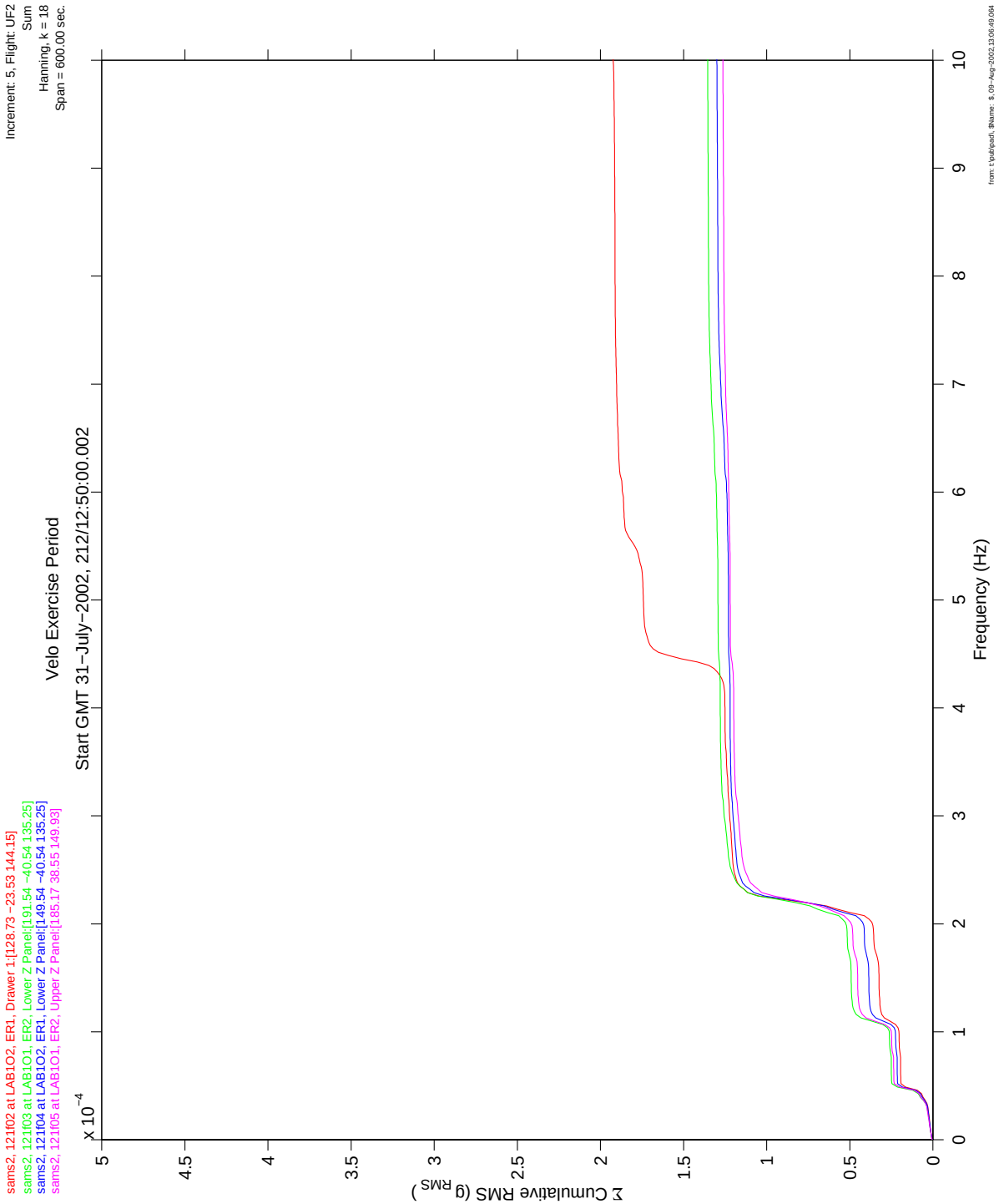

Figure 6-224 Cumulative RMS of VELO Exercise Period (121f02, 121f03, 121f04, 121f05)

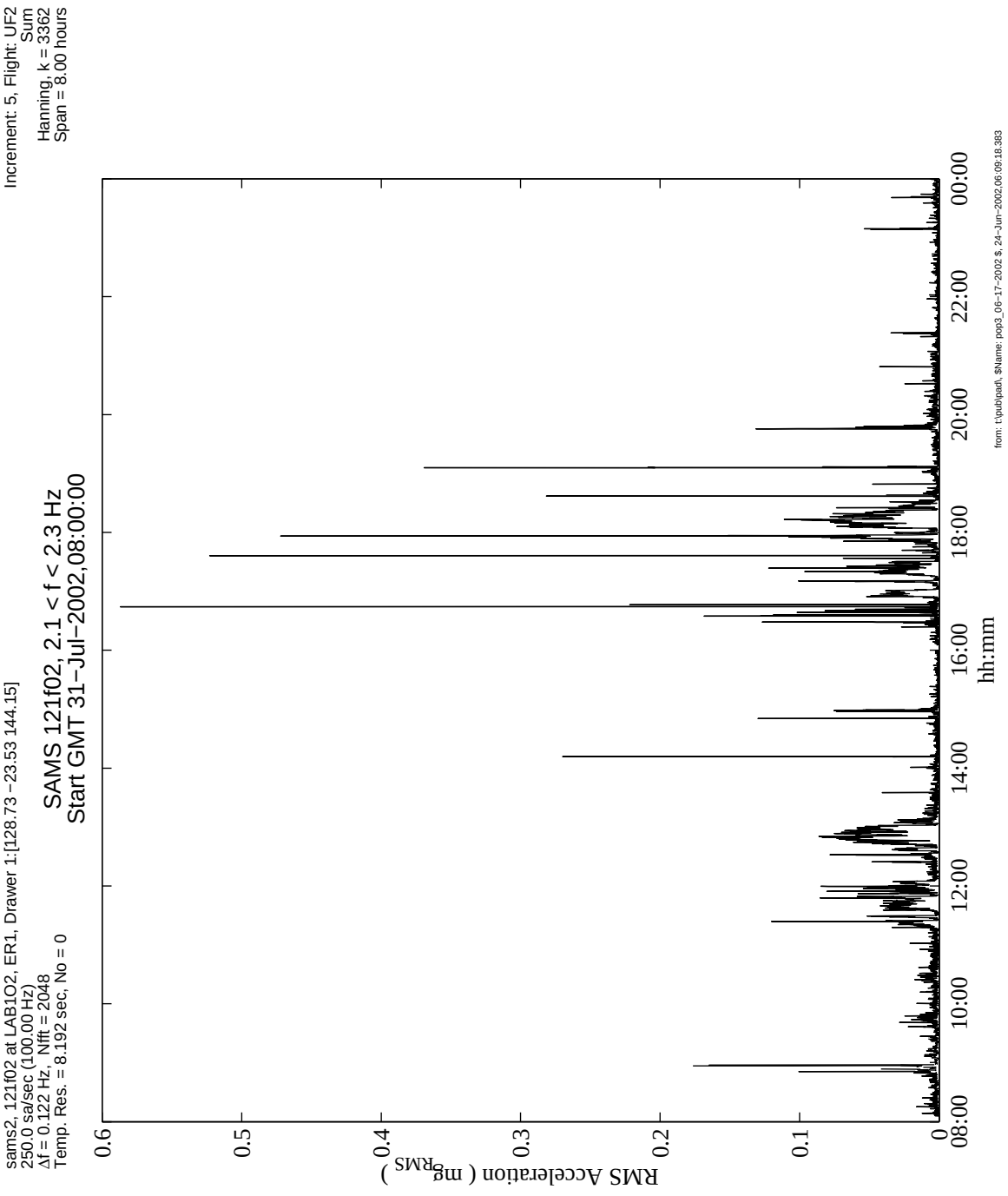

Figure 6-225 Interval RMS of VELO Exercise Periods (121f02)

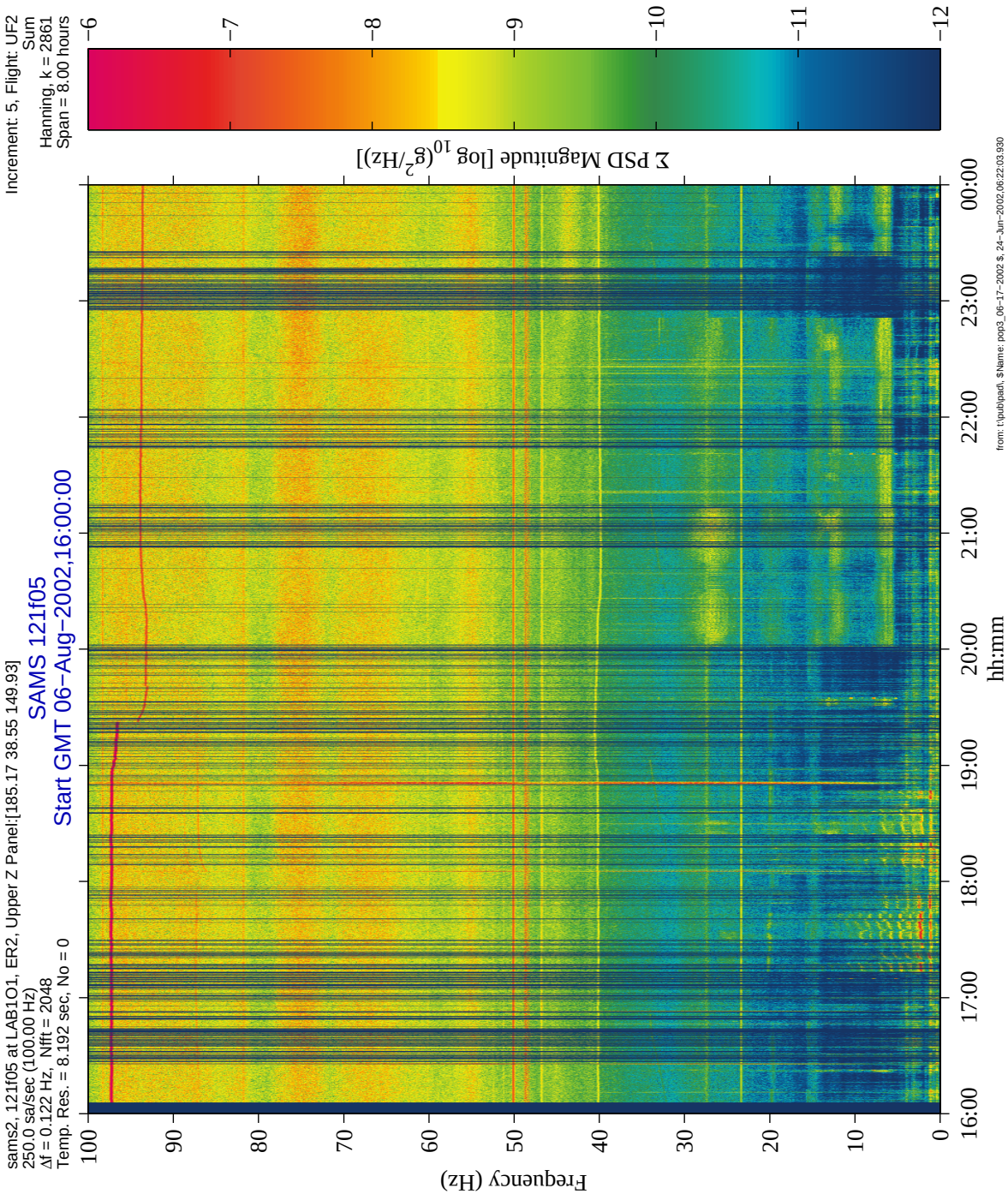

Figure 6-226 Spectrogram of VELO Exercise Period (121f05)

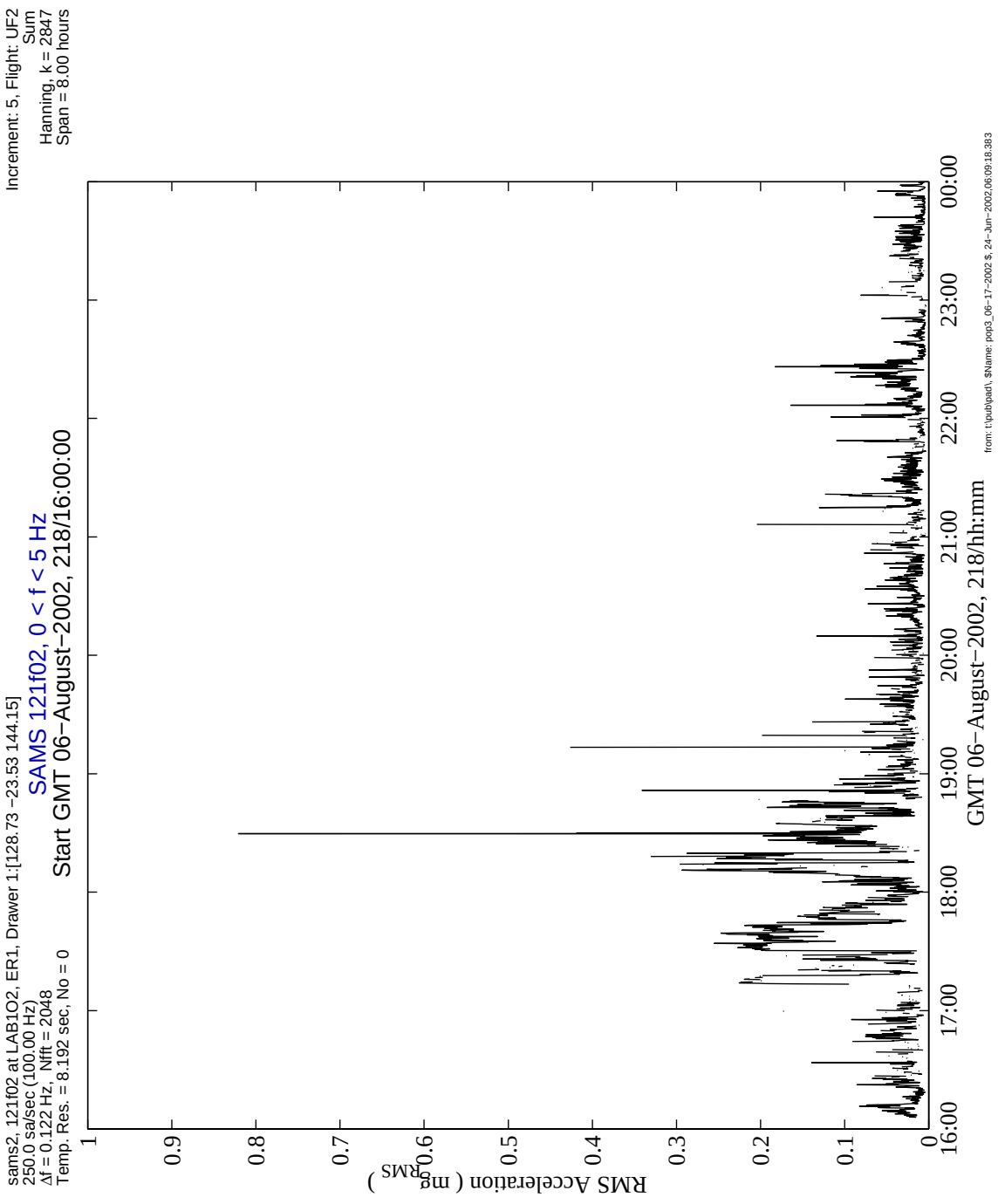

Figure 6-227 Interval RMS of VELO Exercise Period (121f02)

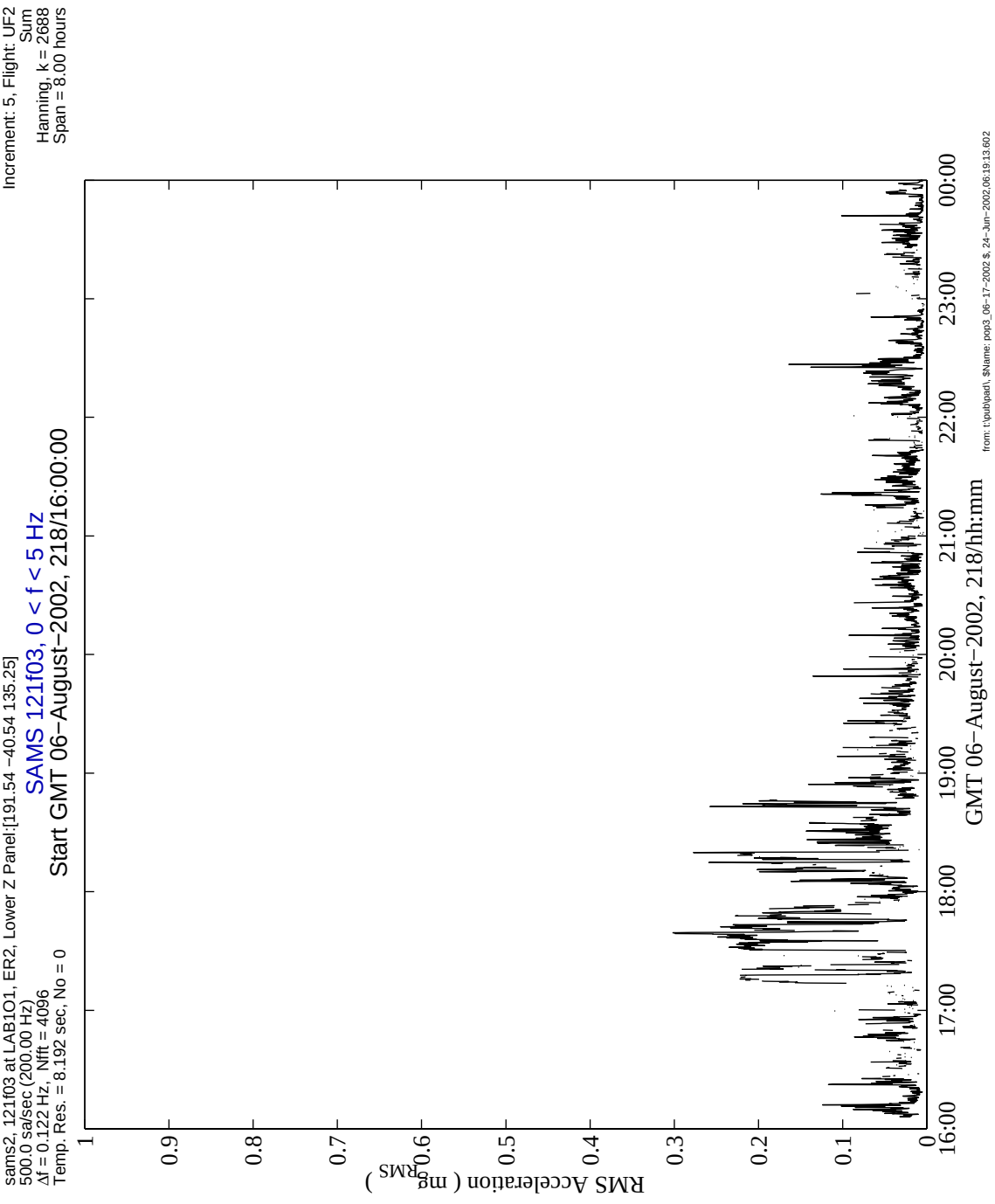

Figure 6-228 Interval RMS of VELO Exercise Period (121f03)

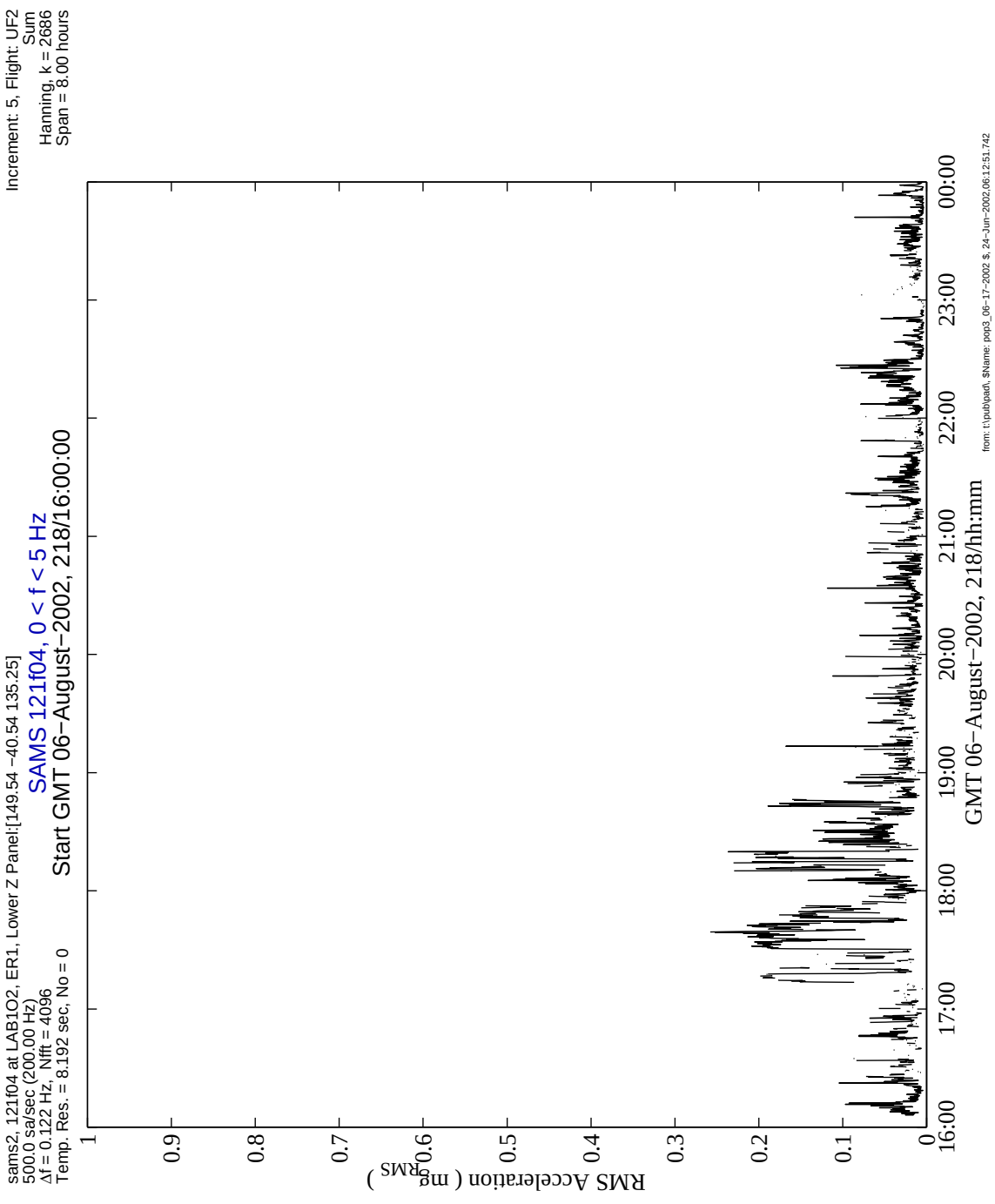

Figure 6-229 Interval RMS of VELO Exercise Period (121f04)

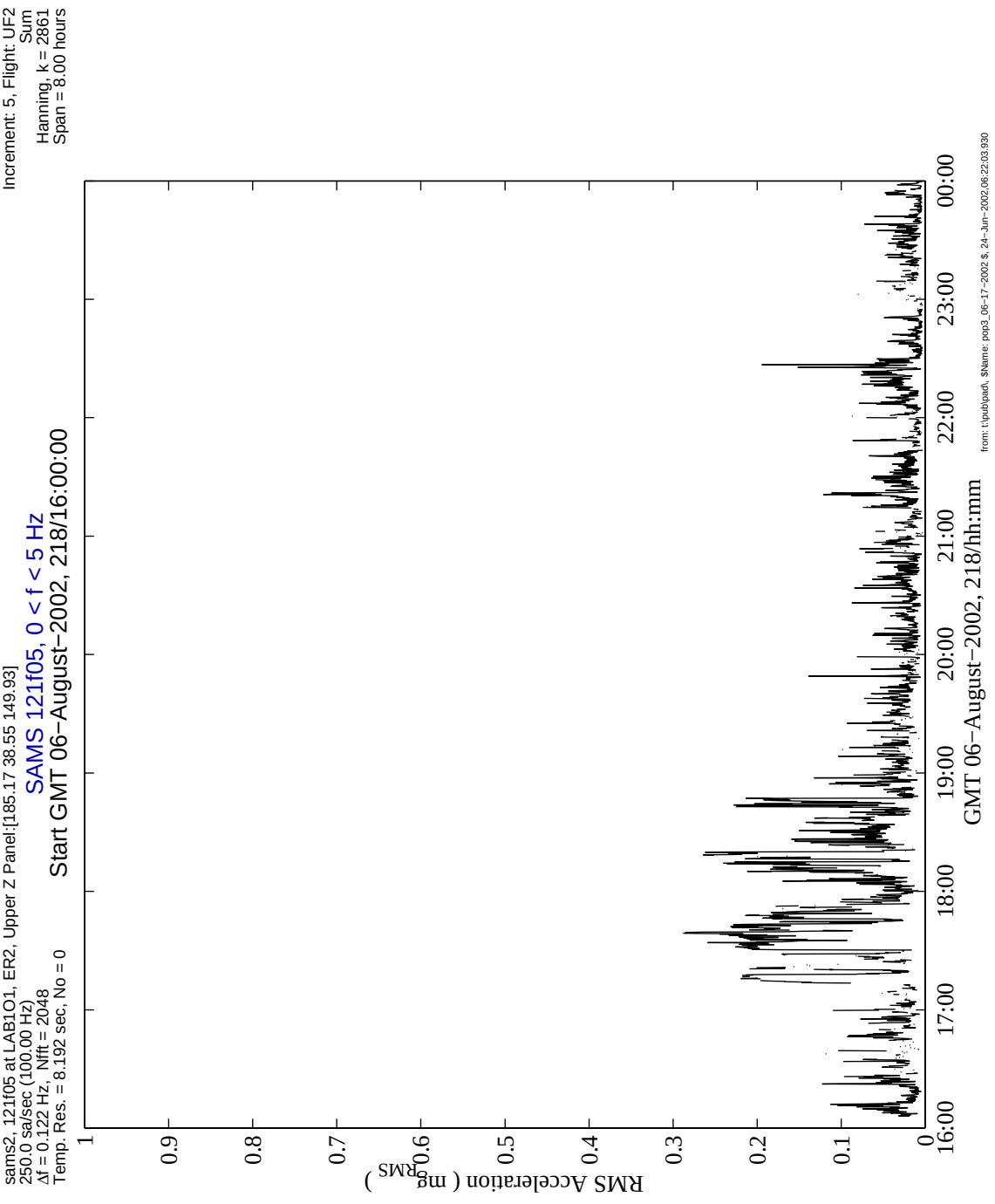

Figure 6-230 Interval RMS of VELO Exercise Period (121f05)

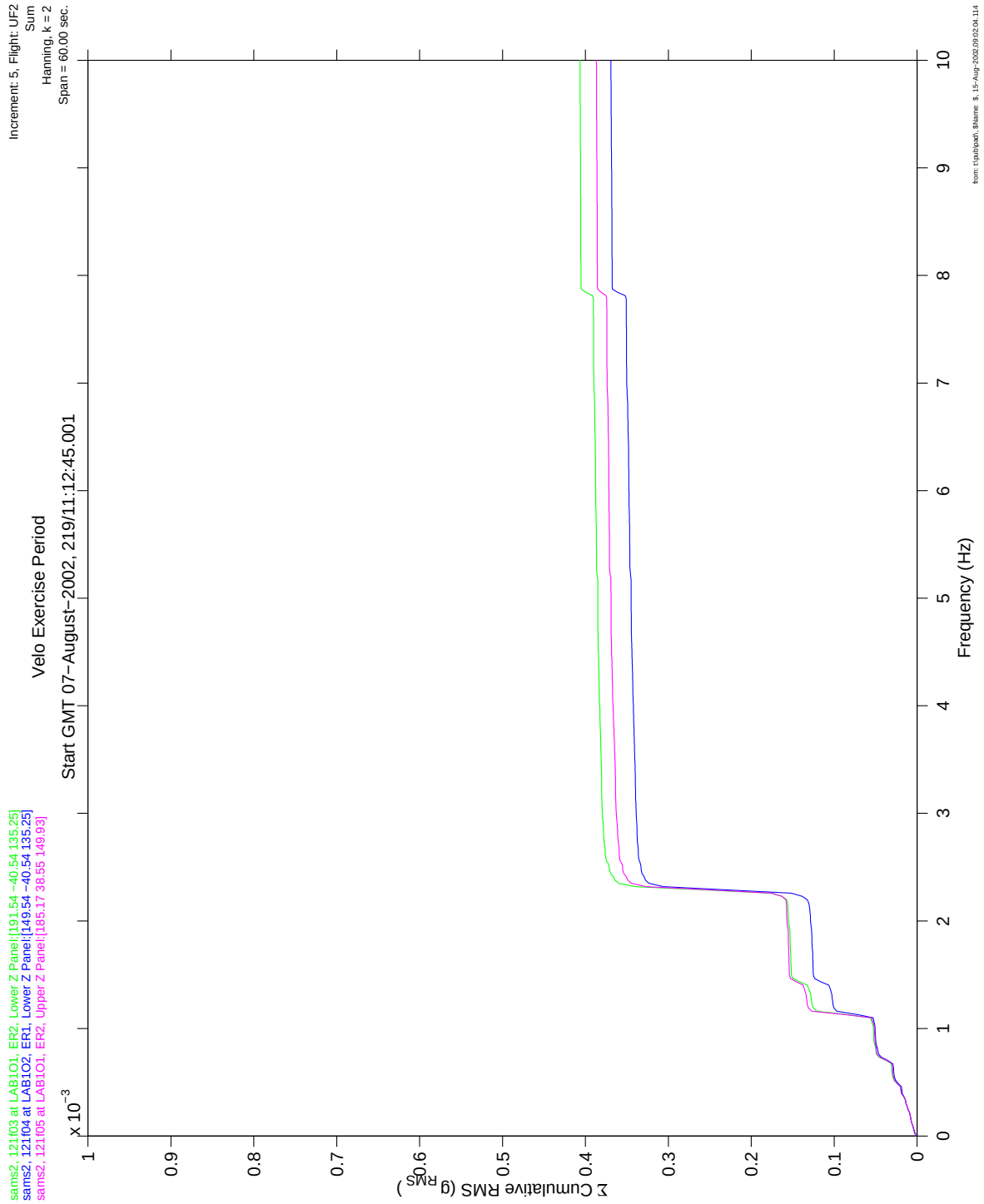

Figure 6-231 Cumulative RMS of VELO Exercise Period (121f03, 121f04, 121f05)

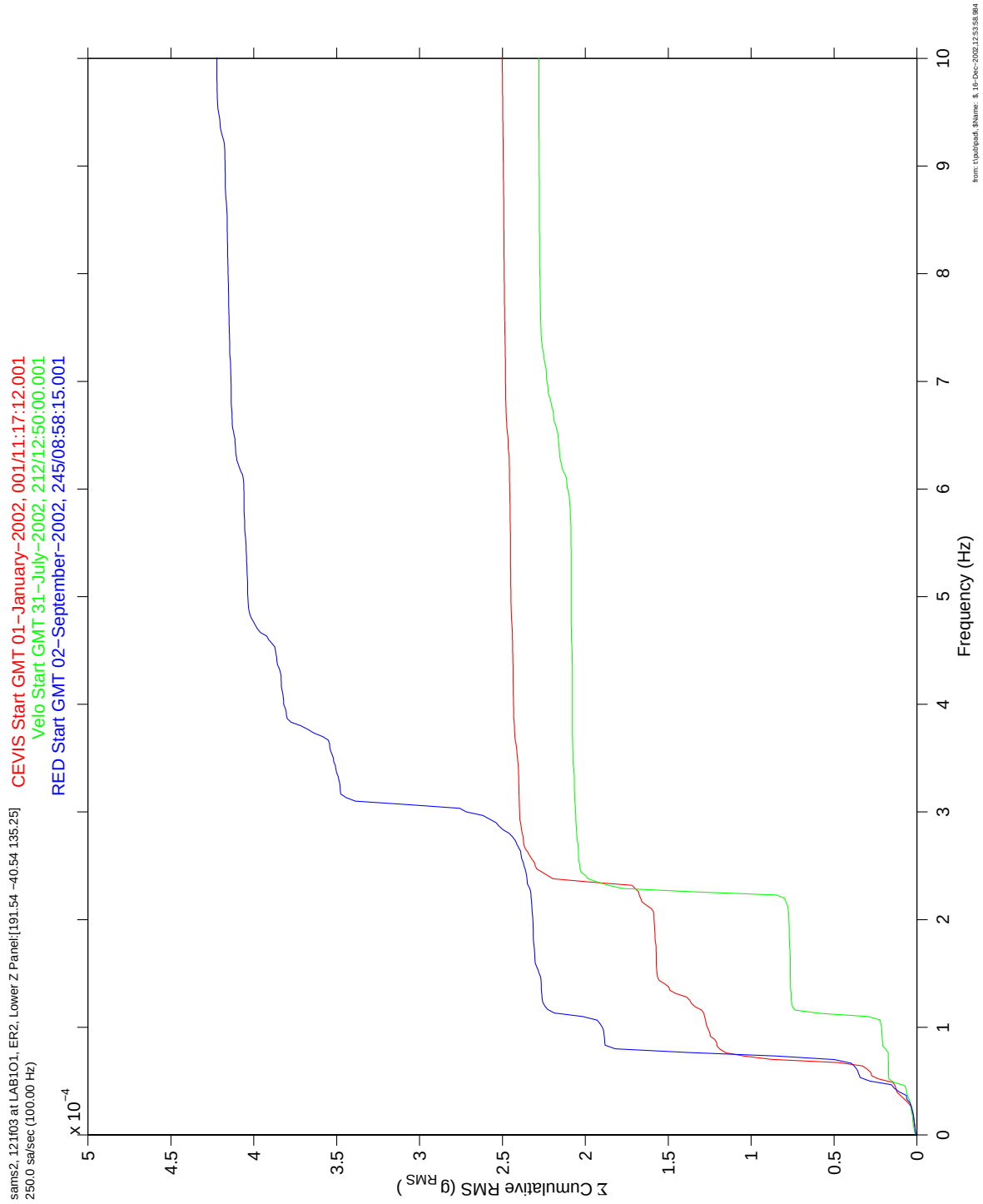

Figure 6-232 Cumulative RMS of CEVIS, VELO, & RED Exercise Comparison (121f03)

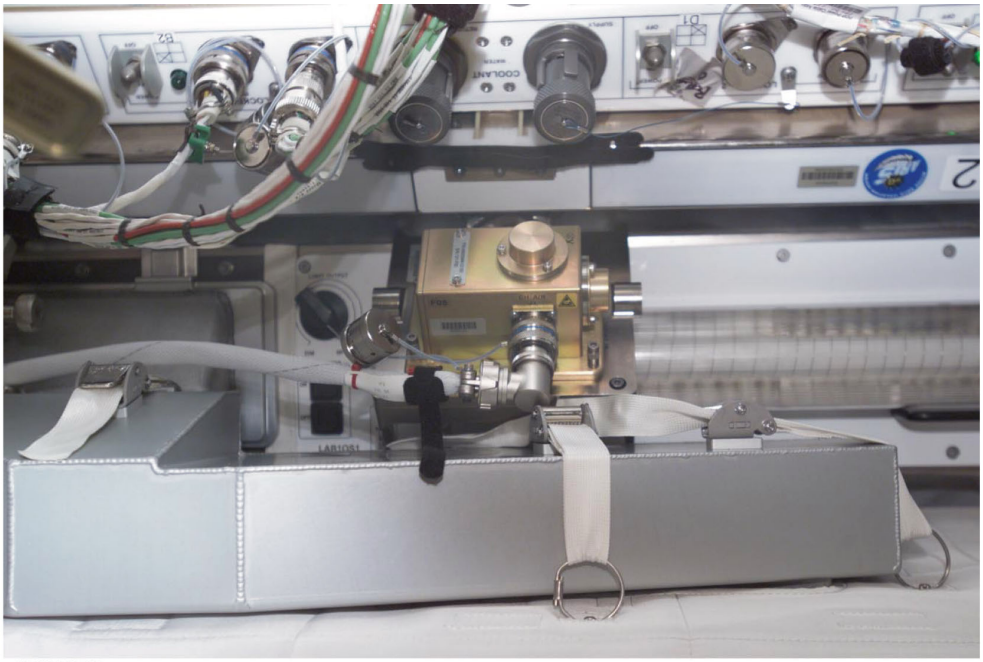

ISS004E8403

FRONT VIEW OF TeSS VENT, STRAP BUCKLE, AND SAMS SE 121F05

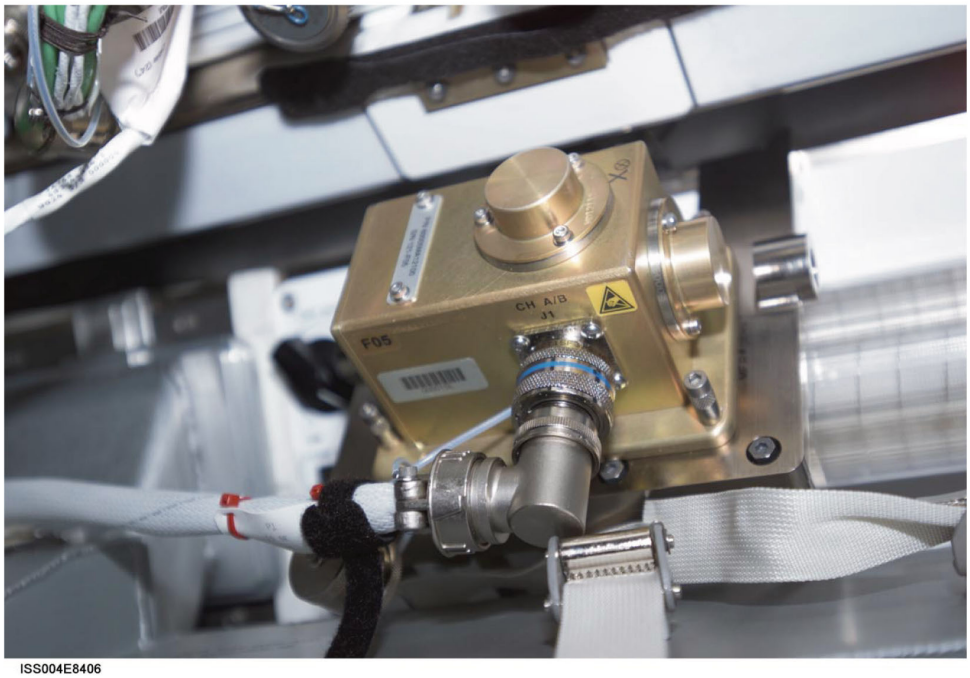

ISS004E8406

CLOSE UP OF TeSS STRAP BUCKLE BELOW SAMS SE 121F05

Figure 6-233 Photos of SAMS Sensor Located Near TeSS (121f05)

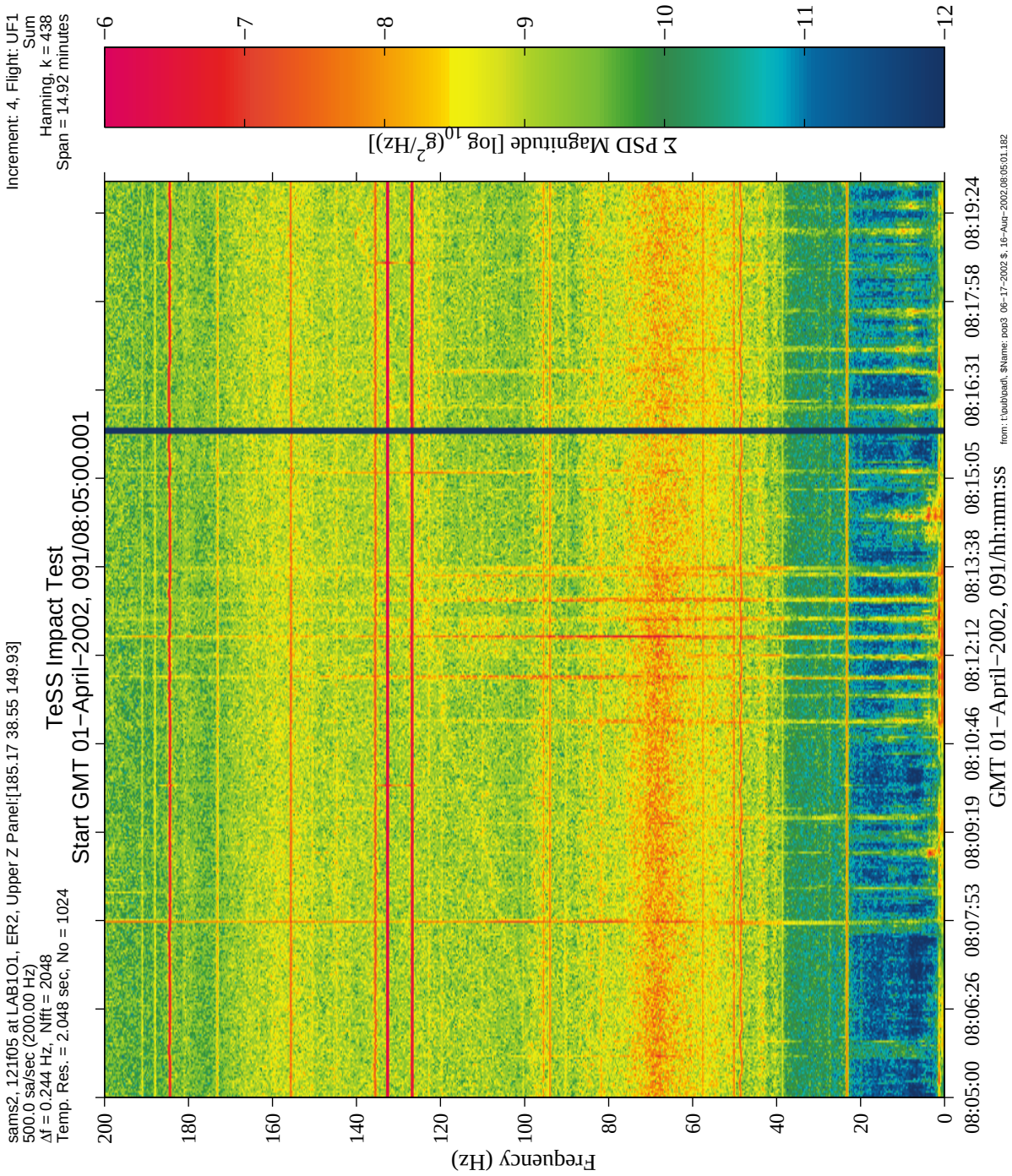

Figure 6-234 Spectrogram of TeSS Impact Test (121f05)

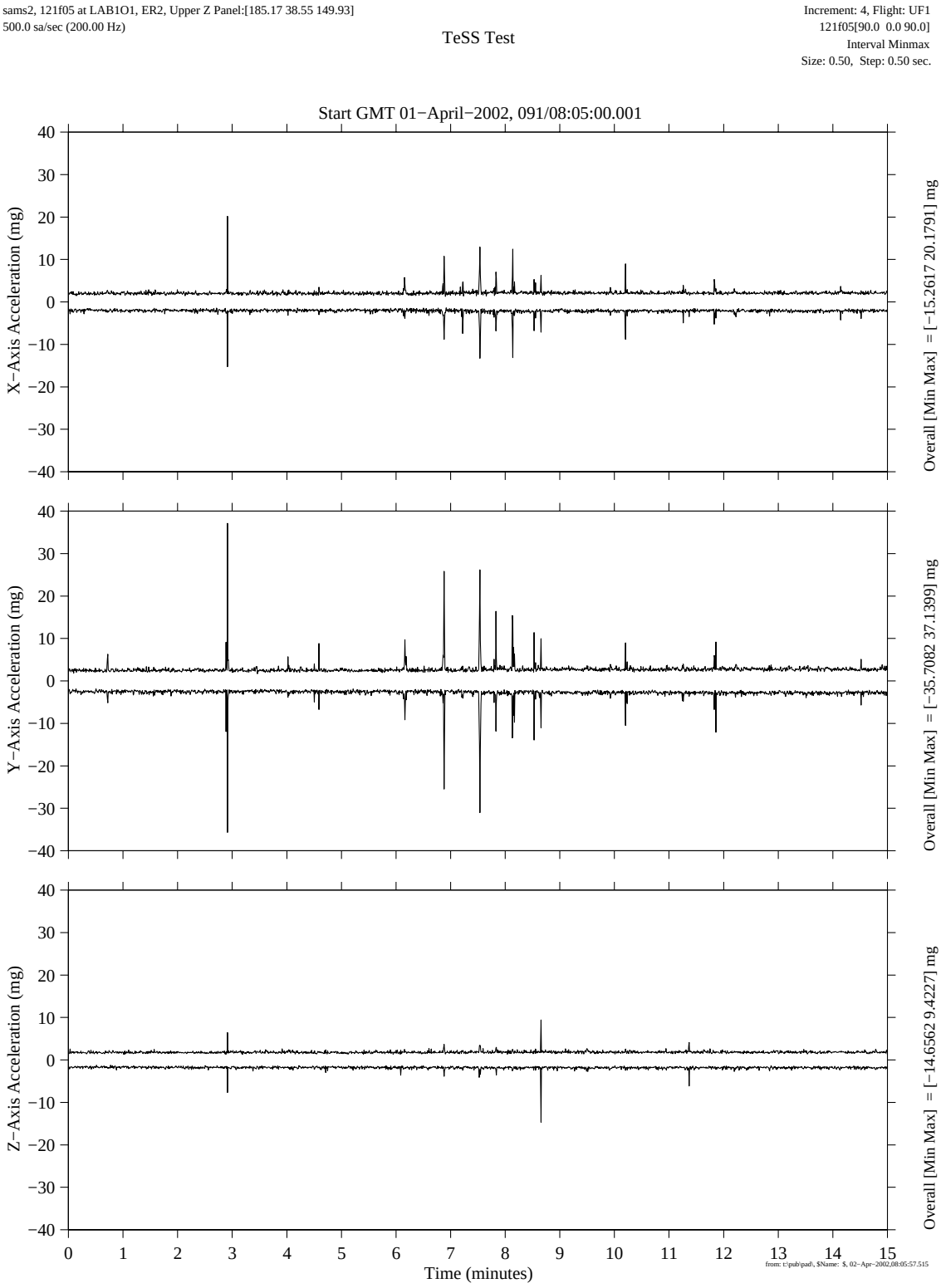

Figure 6-235 Interval Min/Max of TeSS Impact Test (121f05)

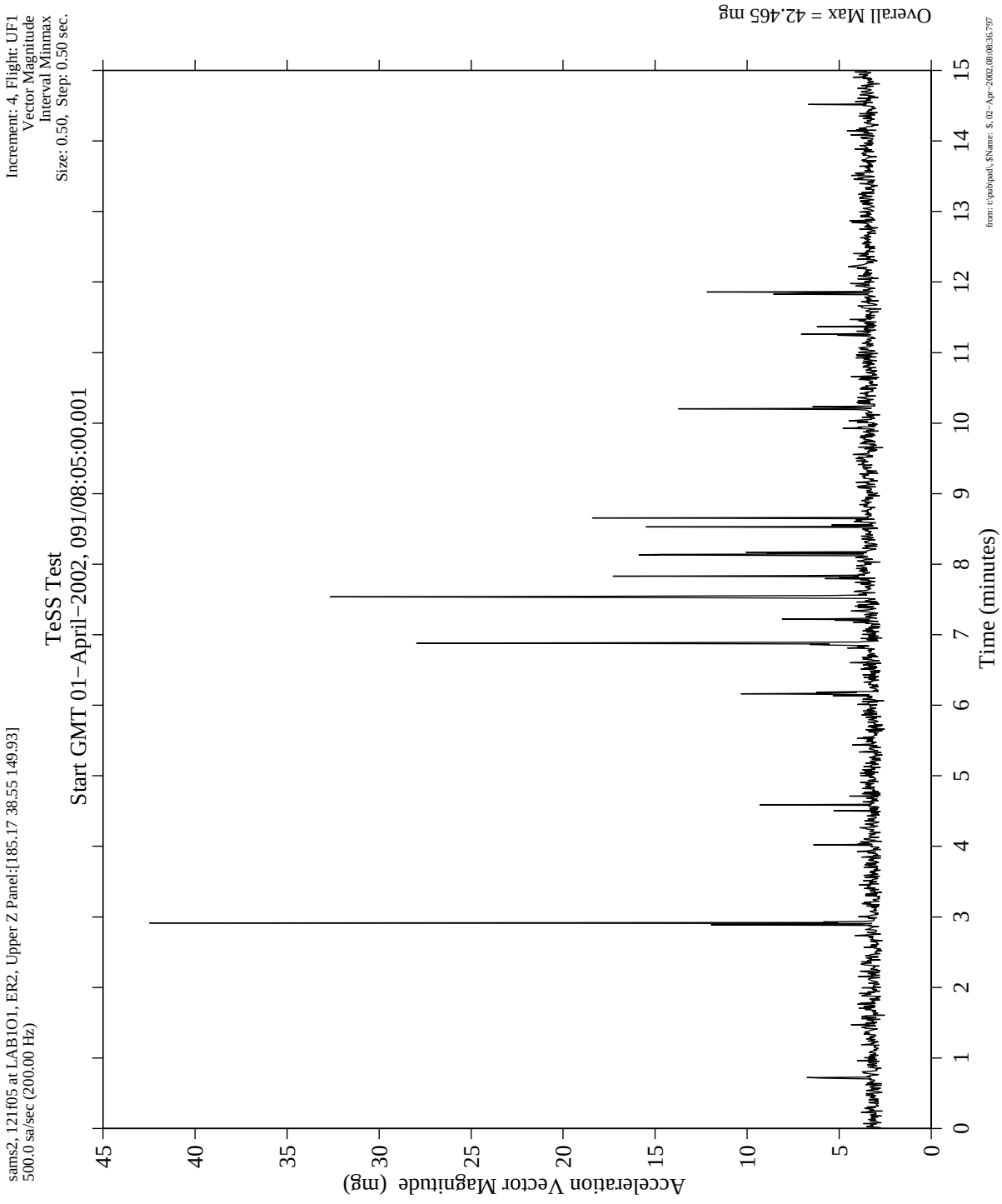

Figure 6-236 Interval Magnitude of TeSS Impact Test (121f05)

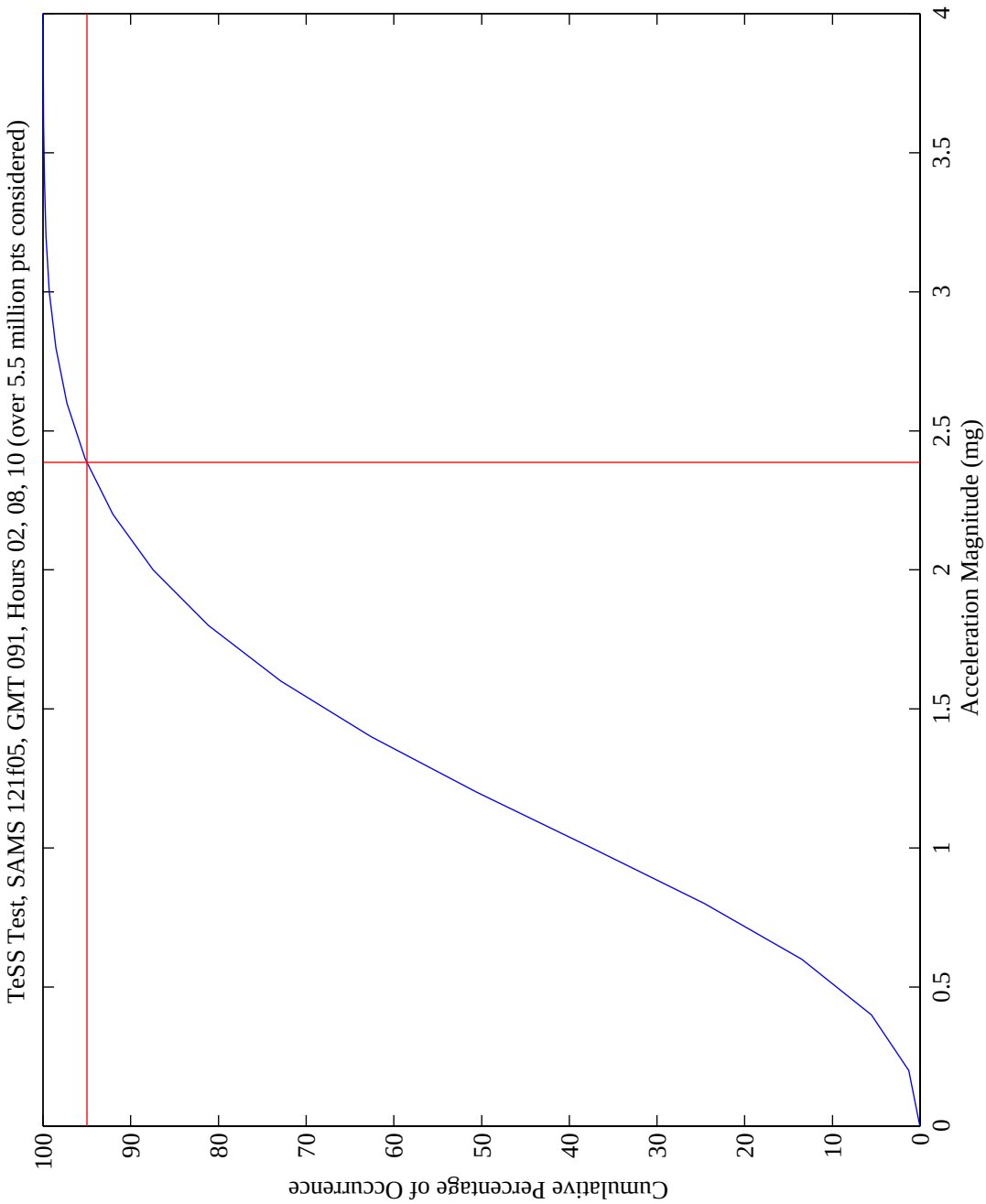

Figure 6-237 Cumulative Occurrence of Magnitudes of TeSS Impact Test (121f05)

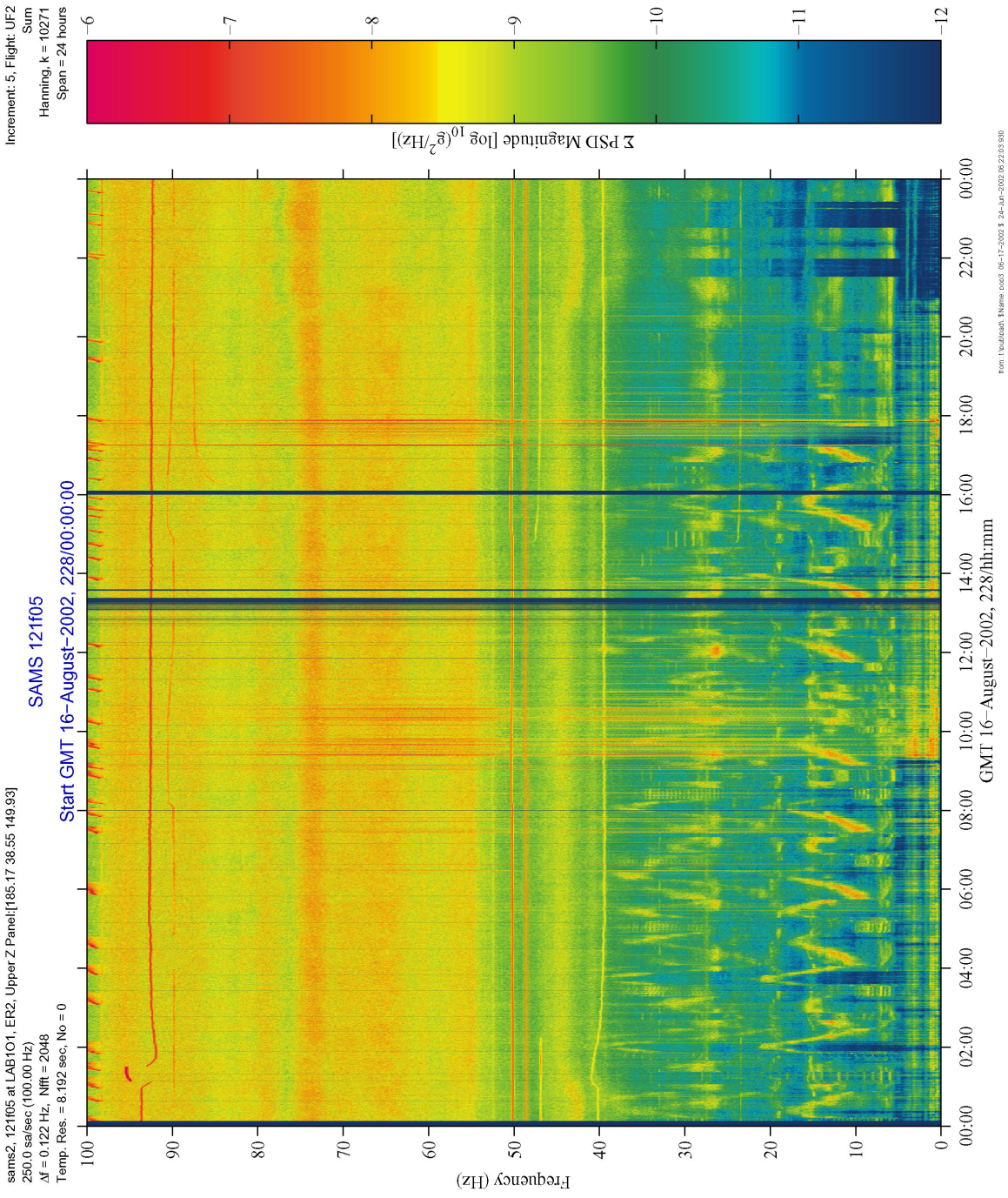

Figure 6-238 Spectrogram of EVA-7 (121f05)

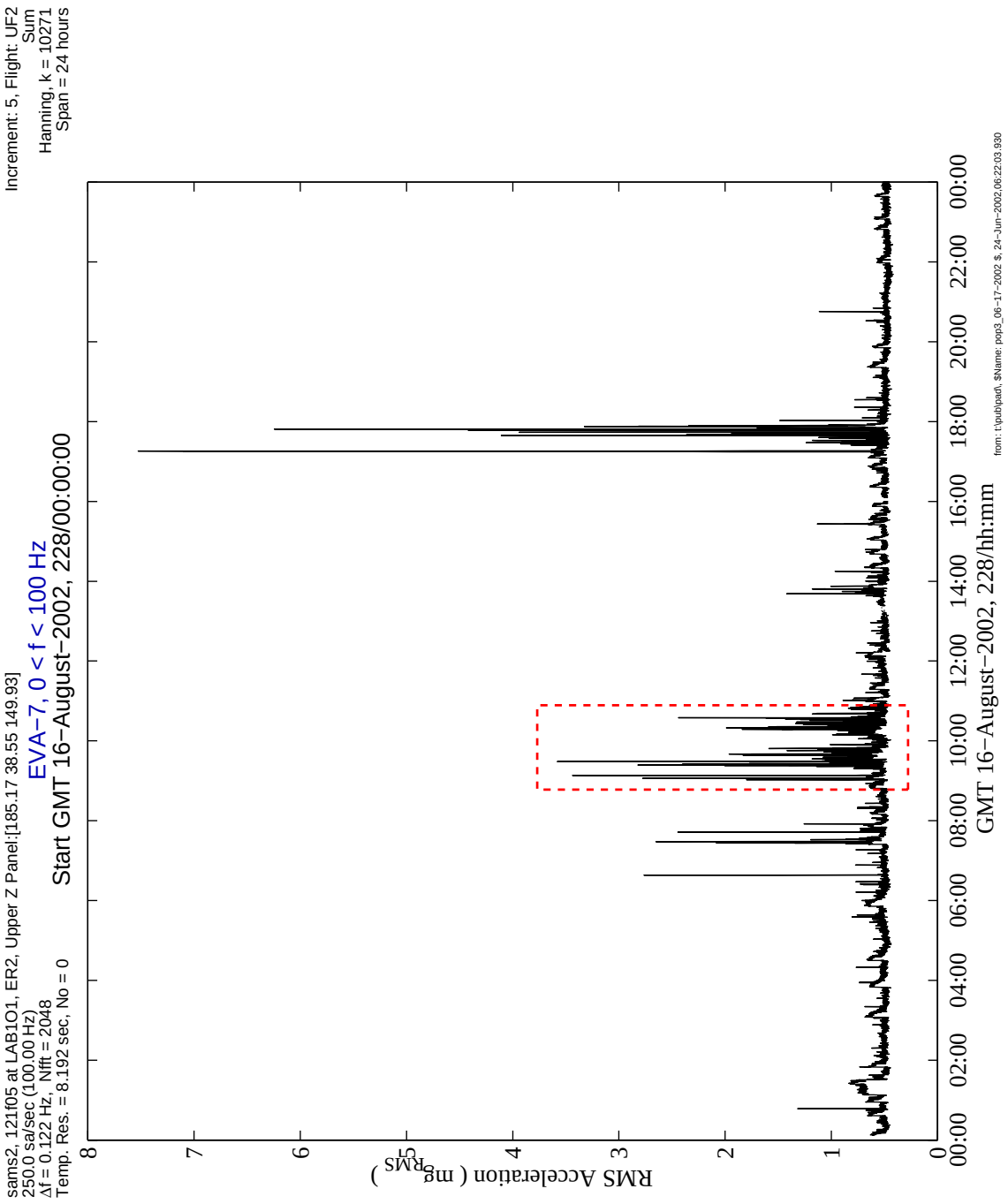

Figure 6-239 Interval RMS of EVA-7 (121f05)

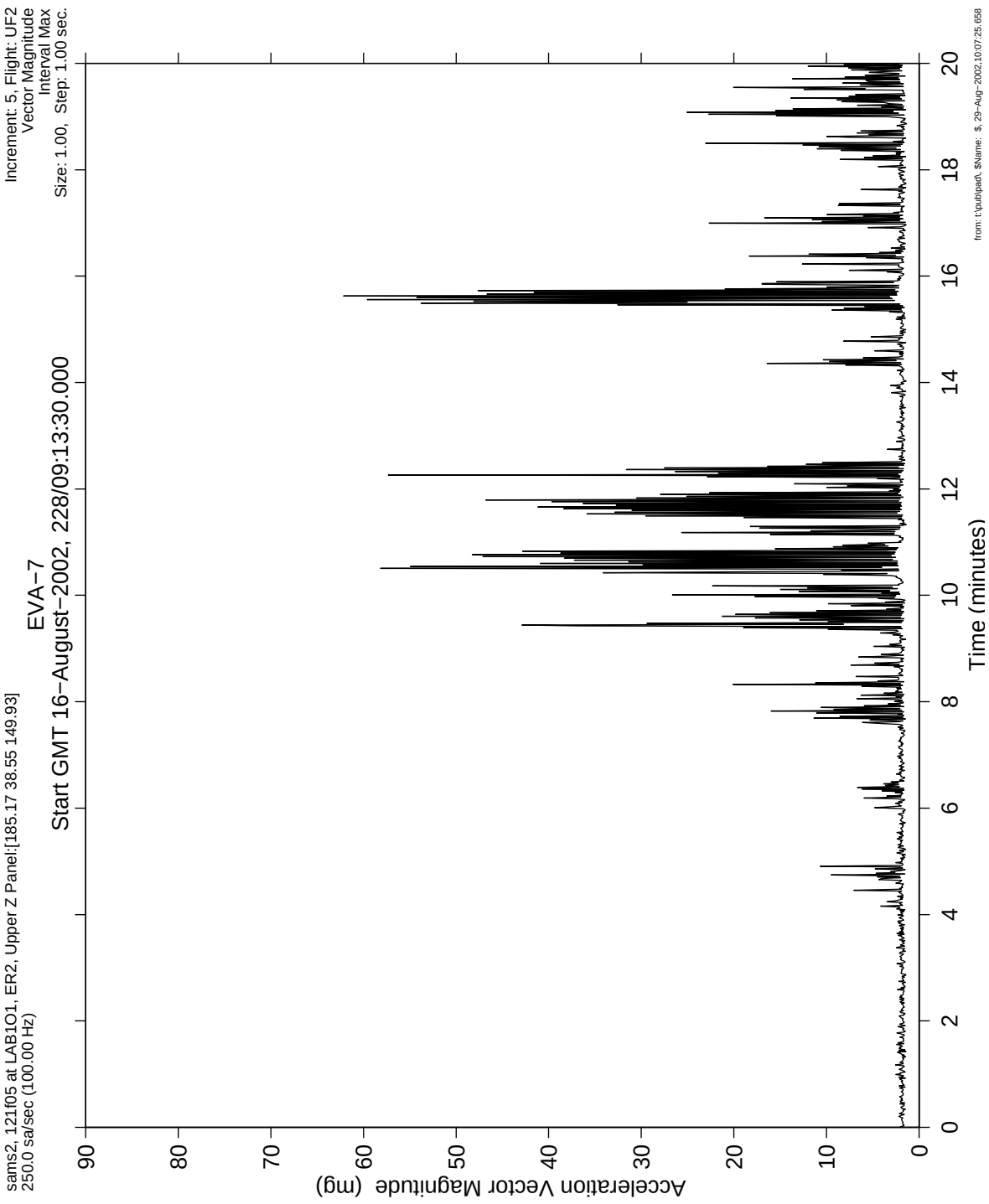

Figure 6-240 Interval Maximum of EVA-7 (121f05)

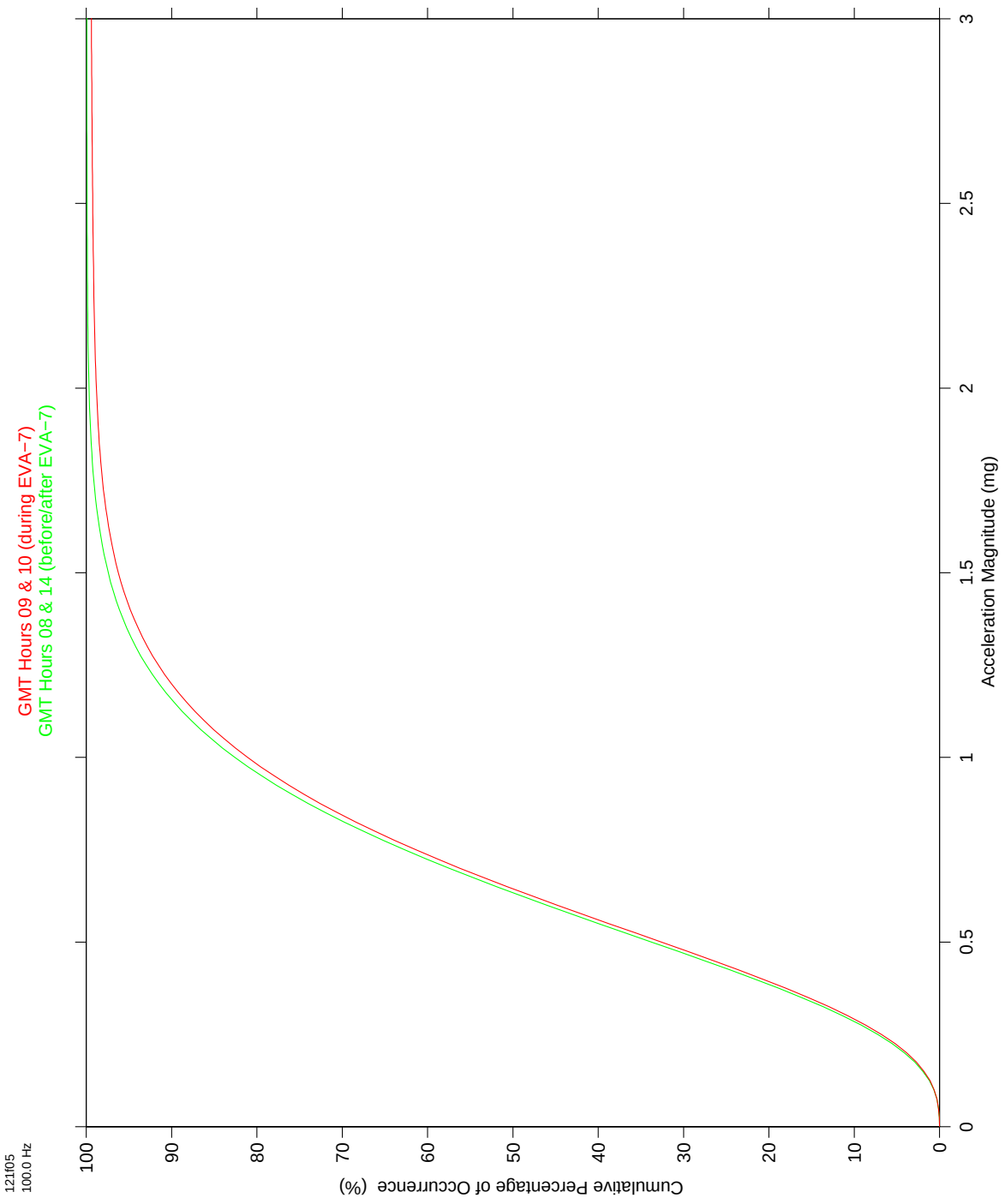

Figure 6-241 Cumulative Occurrence of Magnitudes of EVA-7 (121f05)

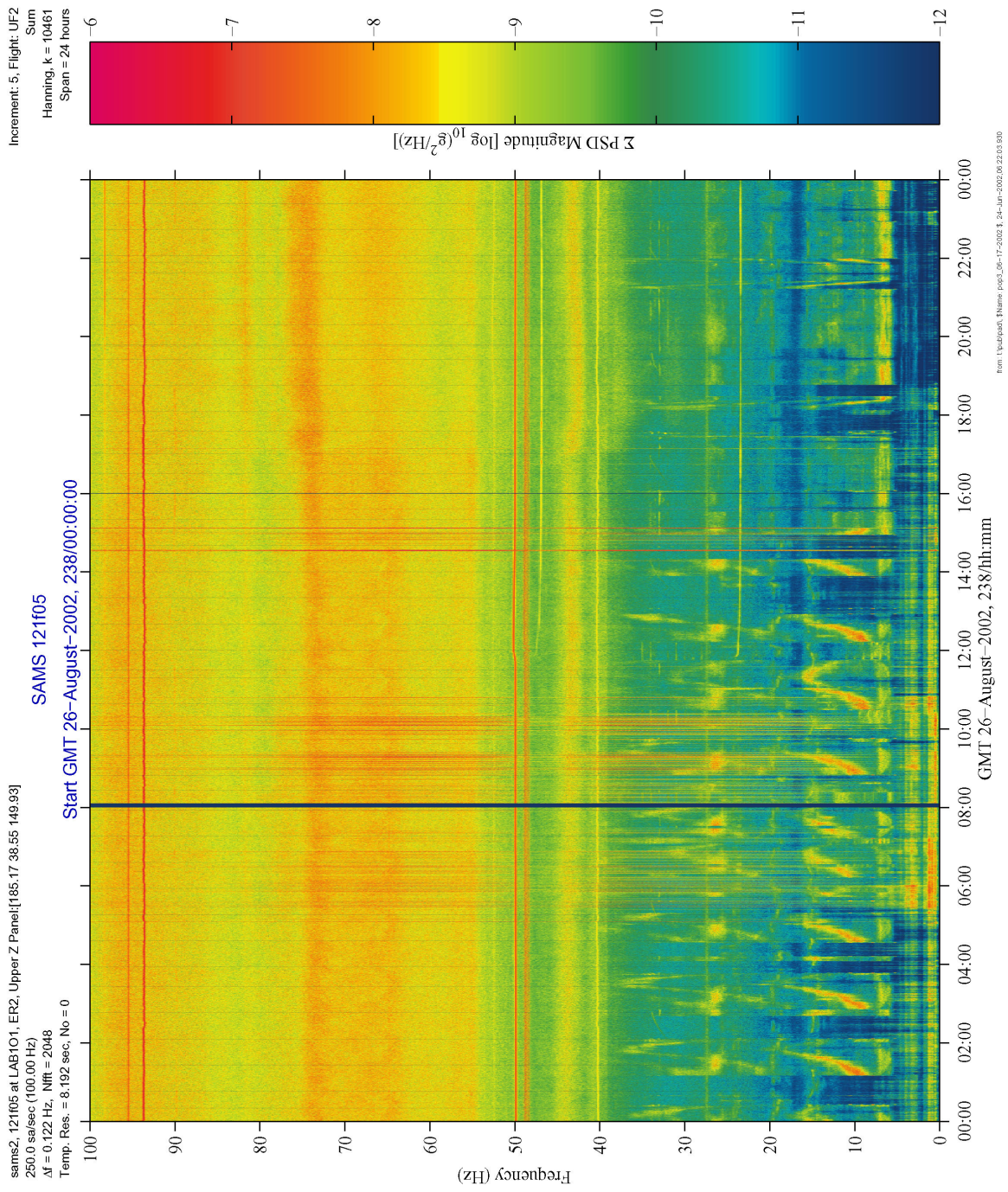

Figure 6-242 Spectrogram of EVA-8 (121f05)

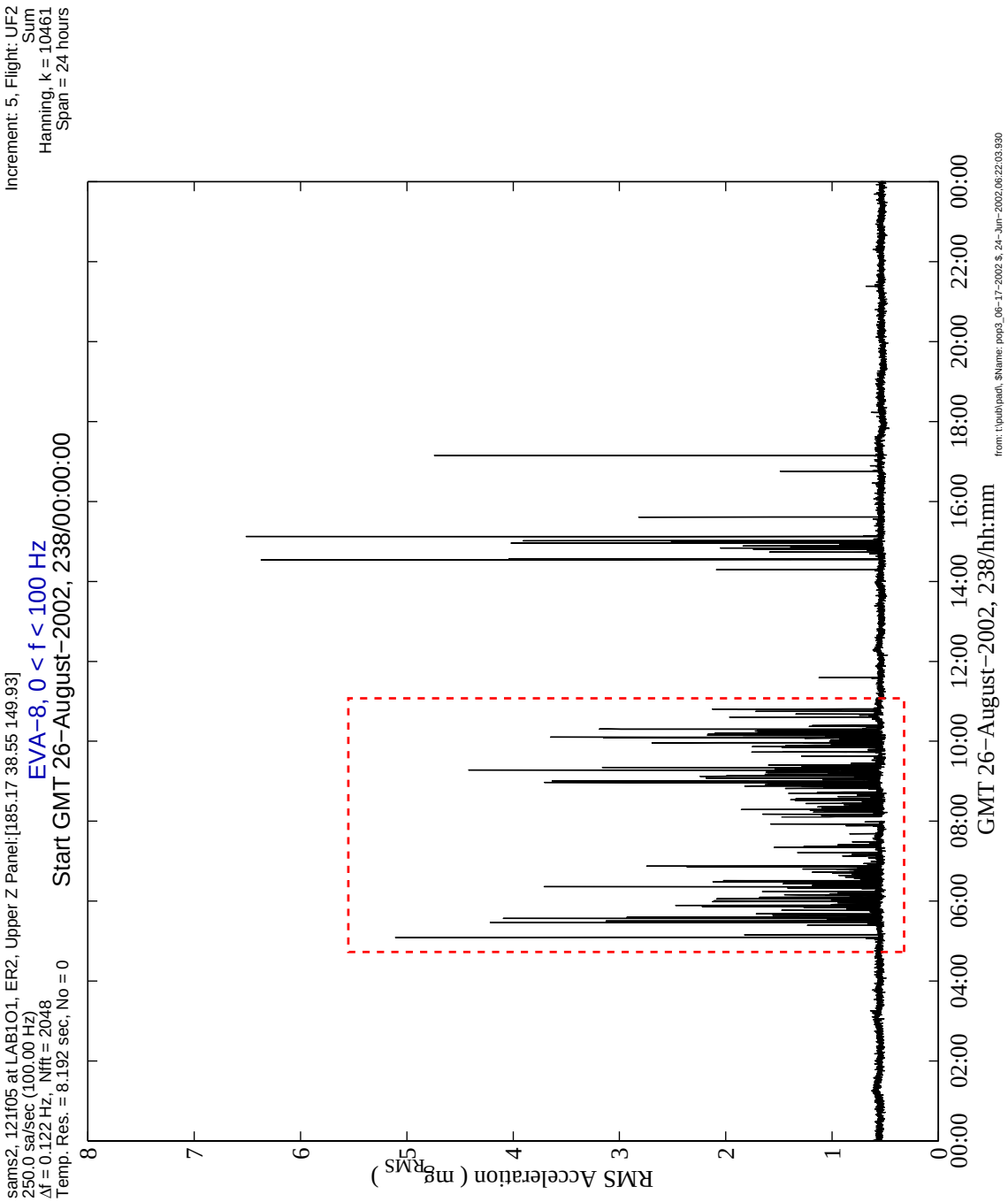

Figure 6-243 Interval RMS of EVA-8 (121f05)

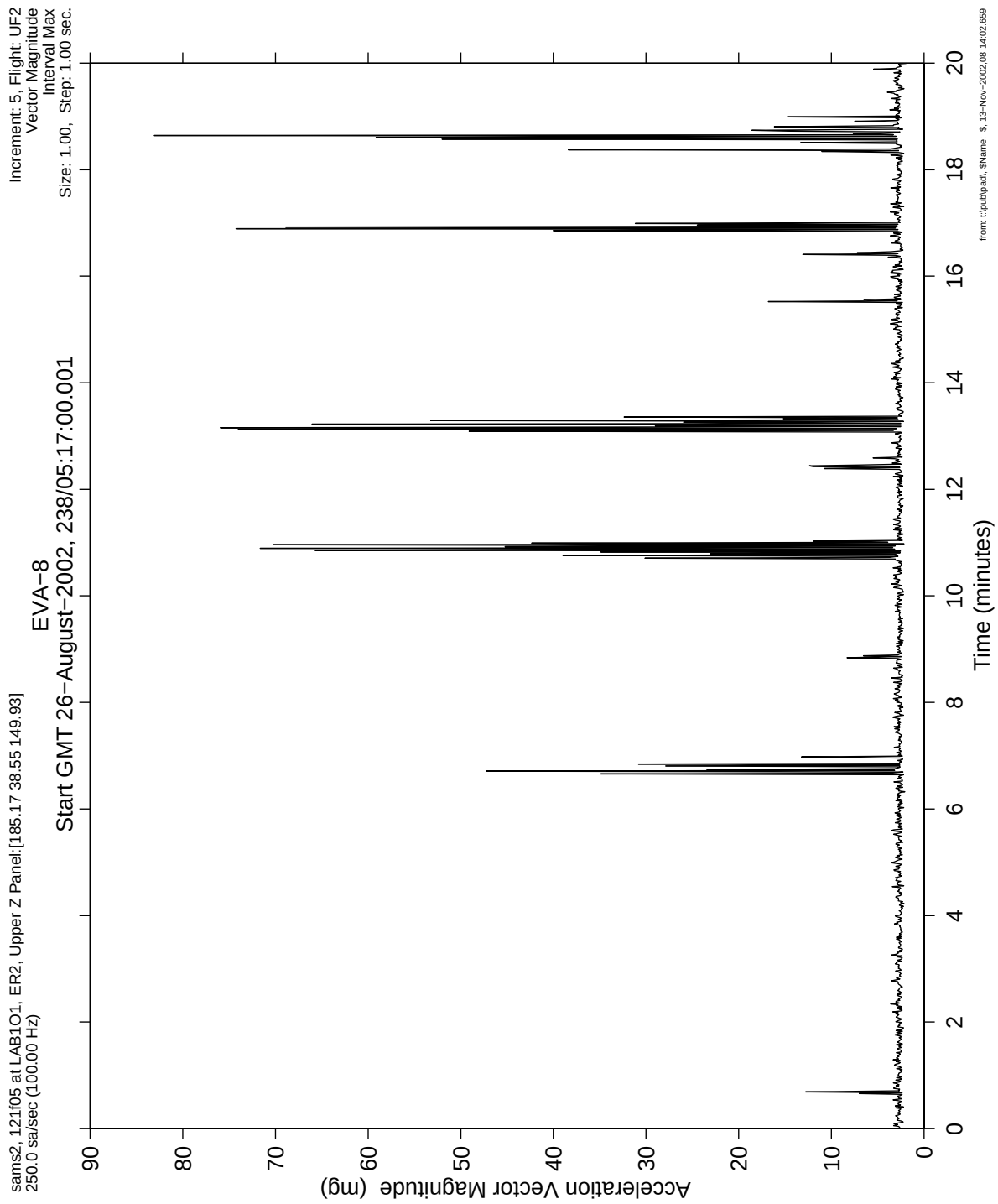

Figure 6-244 Interval Maximum of EVA-8 (121f05)

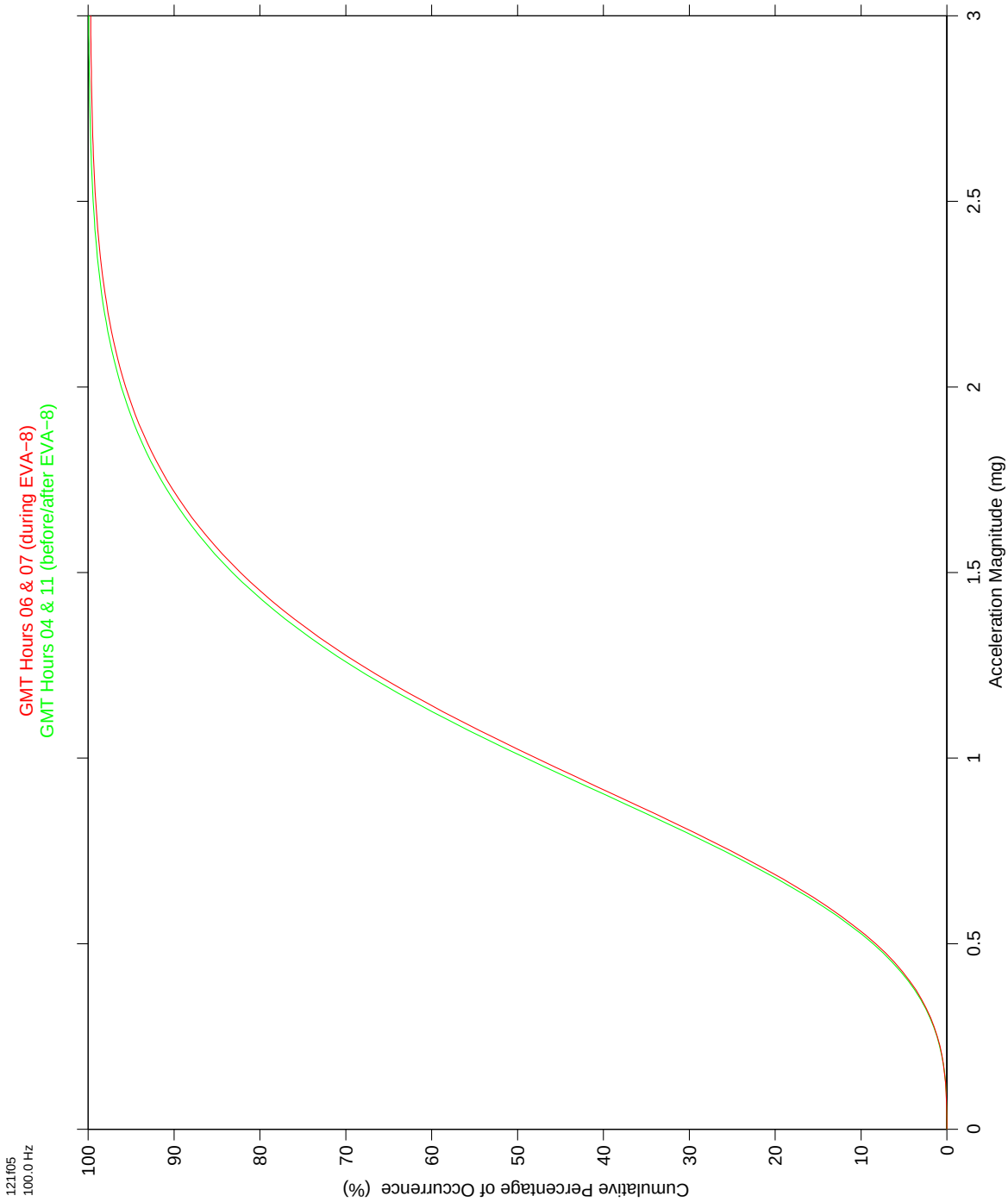

Figure 6-245 Cumulative Occurrence of Magnitudes of EVA-8 (121f05)

7 Principal Component Spectral Analysis

The Principal Component Spectral Analysis (PCSA) histogram is computed from a large number of constituent PSDs. The resultant three-dimensional plot serves to summarize magnitude and frequency variations of significant or persistent spectral contributors and envelops all of the computed spectra over the time frame of interest. The two-dimensional histogram is comprised of frequency-magnitude bins in units of Hz and $\log_{10}(g^2/Hz)$. The third dimension, represented by a color scale, is the percentage of time that a spectral value was counted within a given frequency-magnitude bin.

TABLE 7-1 PCSA PARAMETERS

Data Set #	GMT 2002 Span	SAMS Sensor	Total Hours	PSD Count	Plot
7	16-Jun through 08-Oct (skip 29-Jun, 12-Sep, & 24-Sep)	121f02	1,882.5	827,287	Figure 7-1
		121f03	1,729.1	759,863	Figure 7-2
		121f04	1,617.4	710,758	Figure 7-3
		121f05	1,757.1	772,161	Figure 7-4
8	17-Oct through 24-Nov (skip 01-Nov)	121f02	796.5	350,011	Figure 7-5
		121f03	797.3	350,369	Figure 7-6
		121f04	788.2	346,371	Figure 7-7
		121f05	789.0	346,746	Figure 7-8
SUBSA	23-Jul through 11-Sep[6]	121f08	95.7	10,513	Figure 7-9
PFMI	09-Sep through 21-Nov[7]	121f08	150.1	16,491	Figure 7-10

[6] Only SUBSA days shown with SAMS data in Table 6-25.
[7] Only PFMI days shown with SAMS data in Table 6-27.

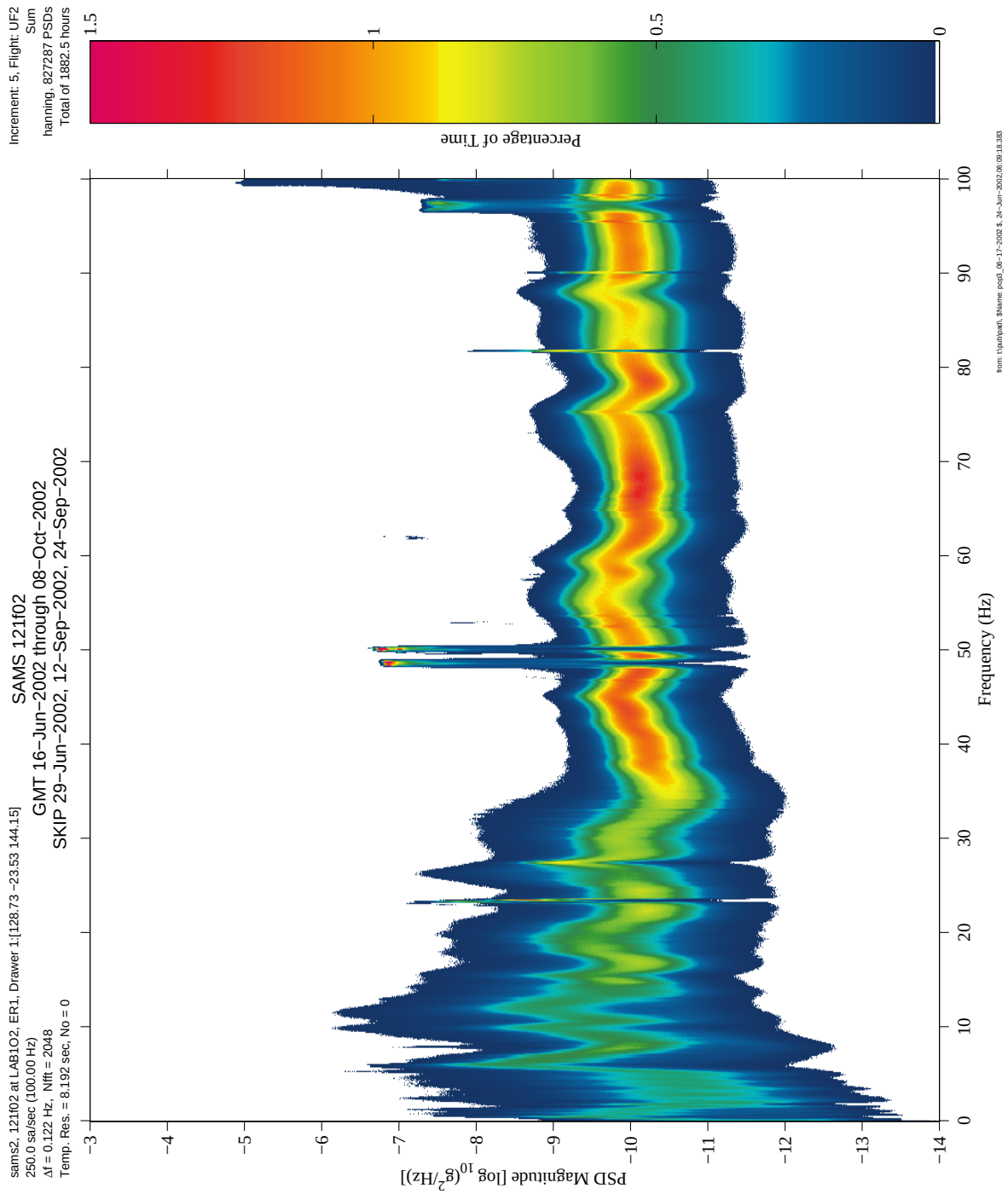

Figure 7-1 PCSA of GMT 16-Jun-2002 through 08-Oct-2002, 100 Hz (121f02)

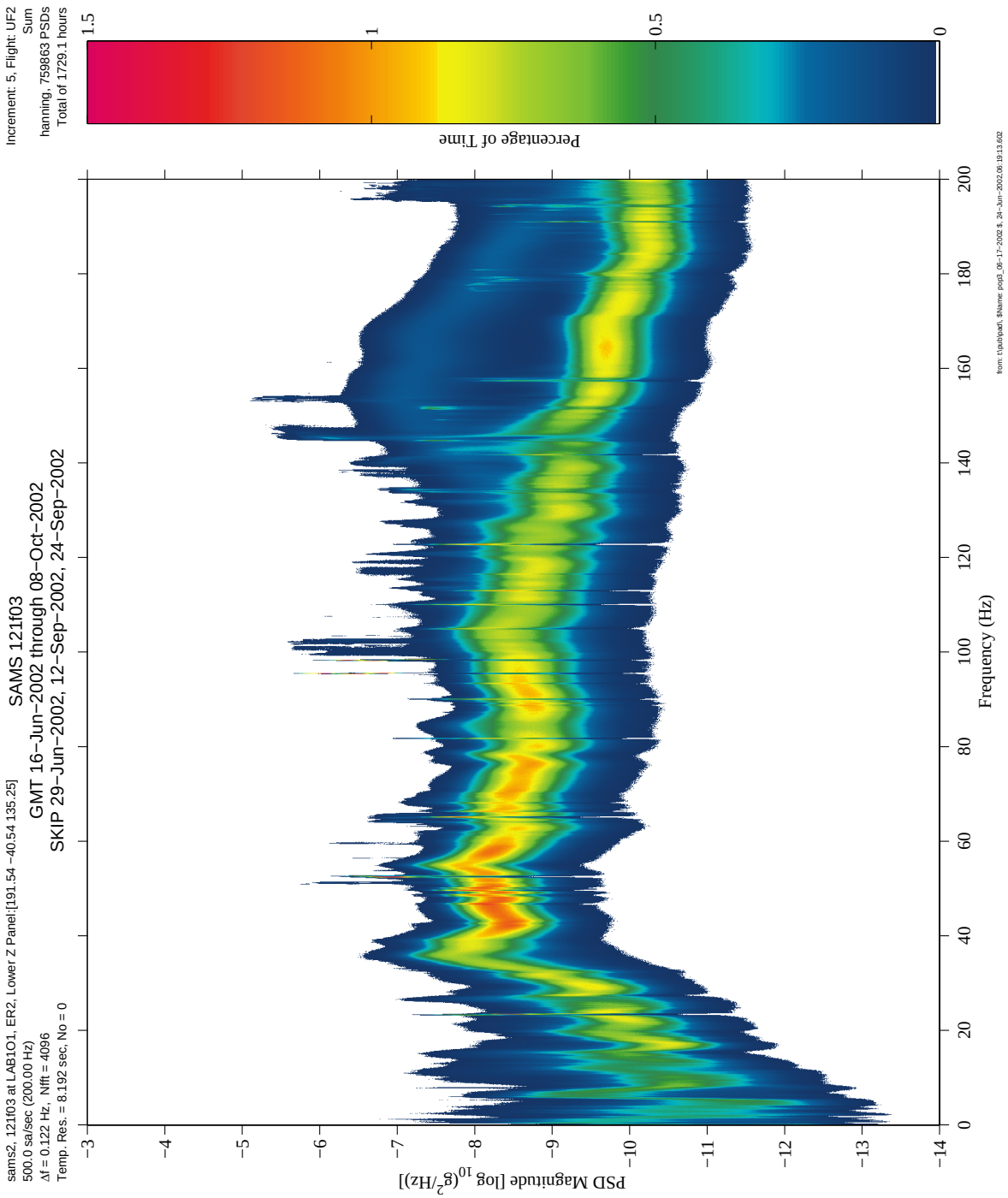

Figure 7-2 PCSA of GMT 16-Jun-2002 through 08-Oct-2002, 200 Hz (121f03)

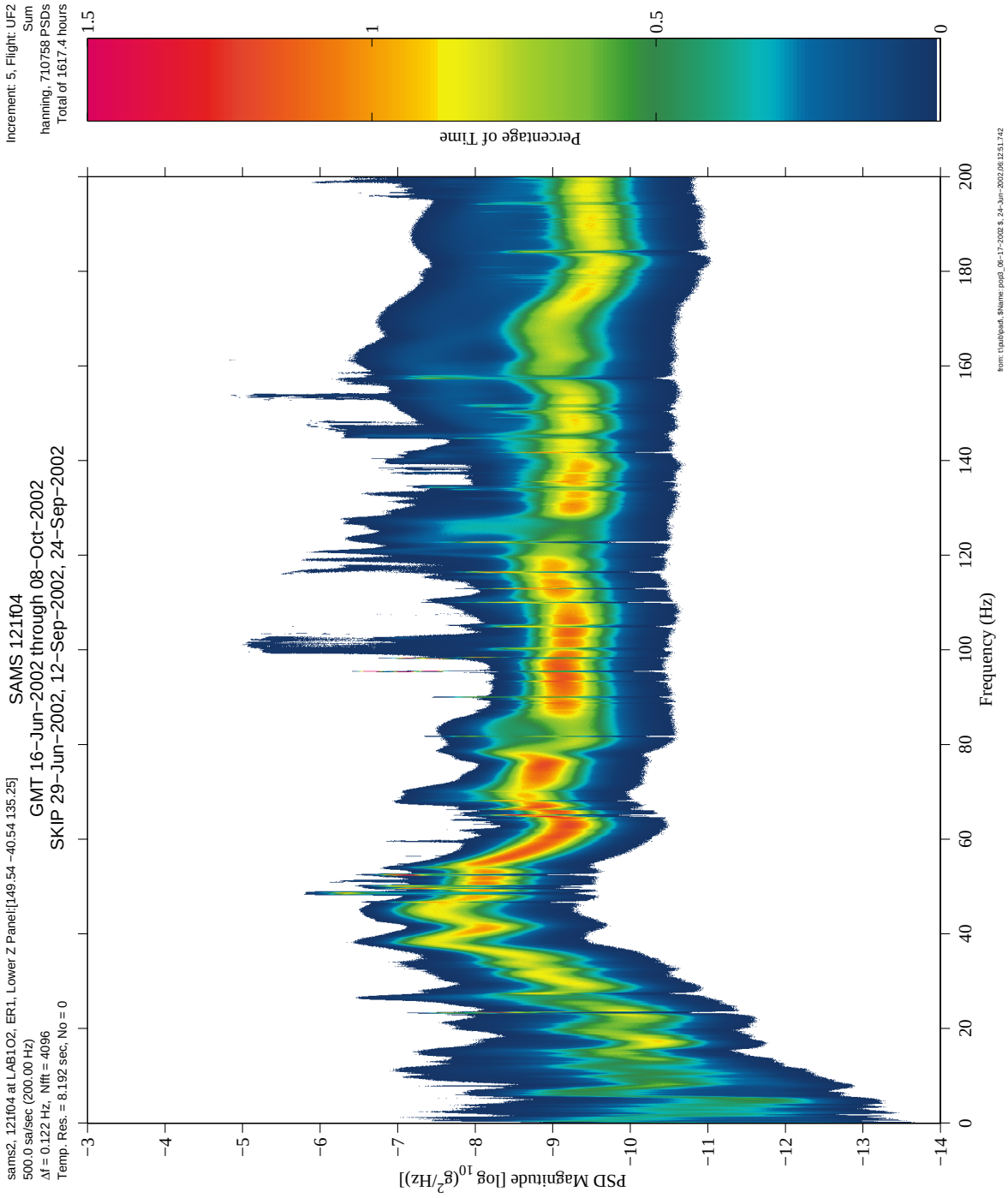

Figure 7-3 PCSA of GMT 16-Jun-2002 through 08-Oct-2002, 200 Hz (121f04)

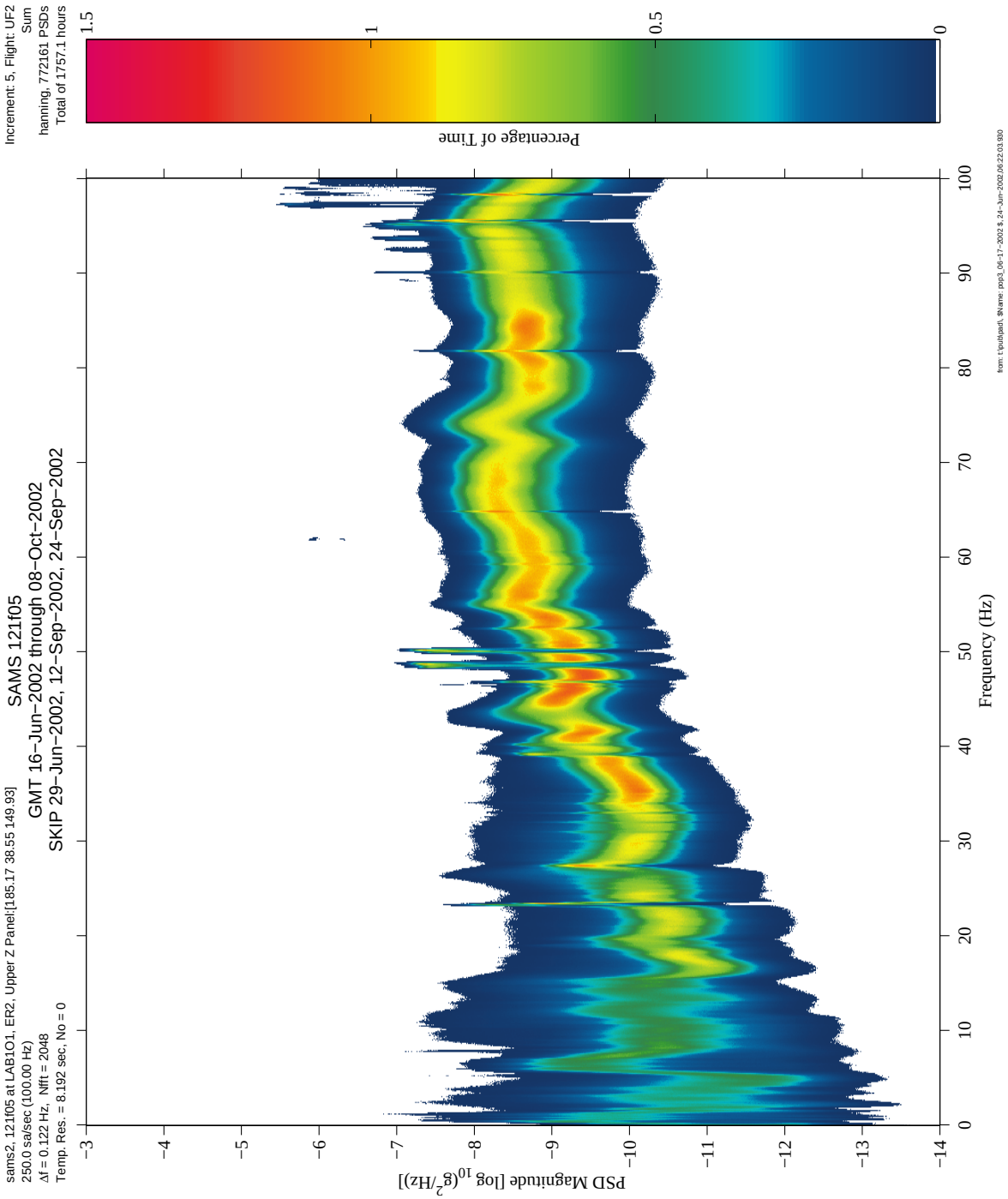

Figure 7-4 PCSA of GMT 16-Jun-2002 through 08-Oct-2002, 100 Hz (121f05)

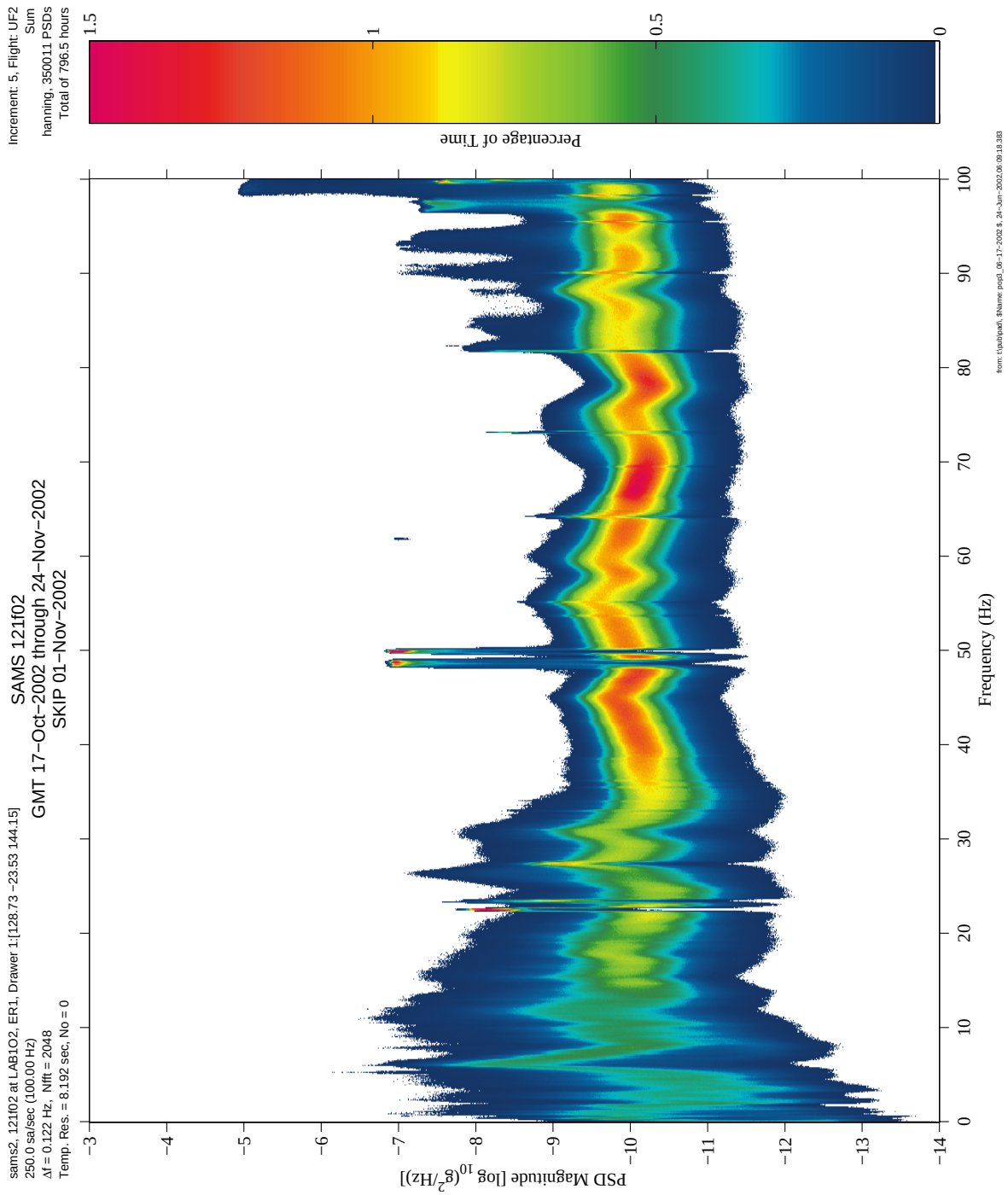

Figure 7-5 PCSA of GMT 17-Oct-2002 through 24-Nov-2002, 100 Hz (121f02)

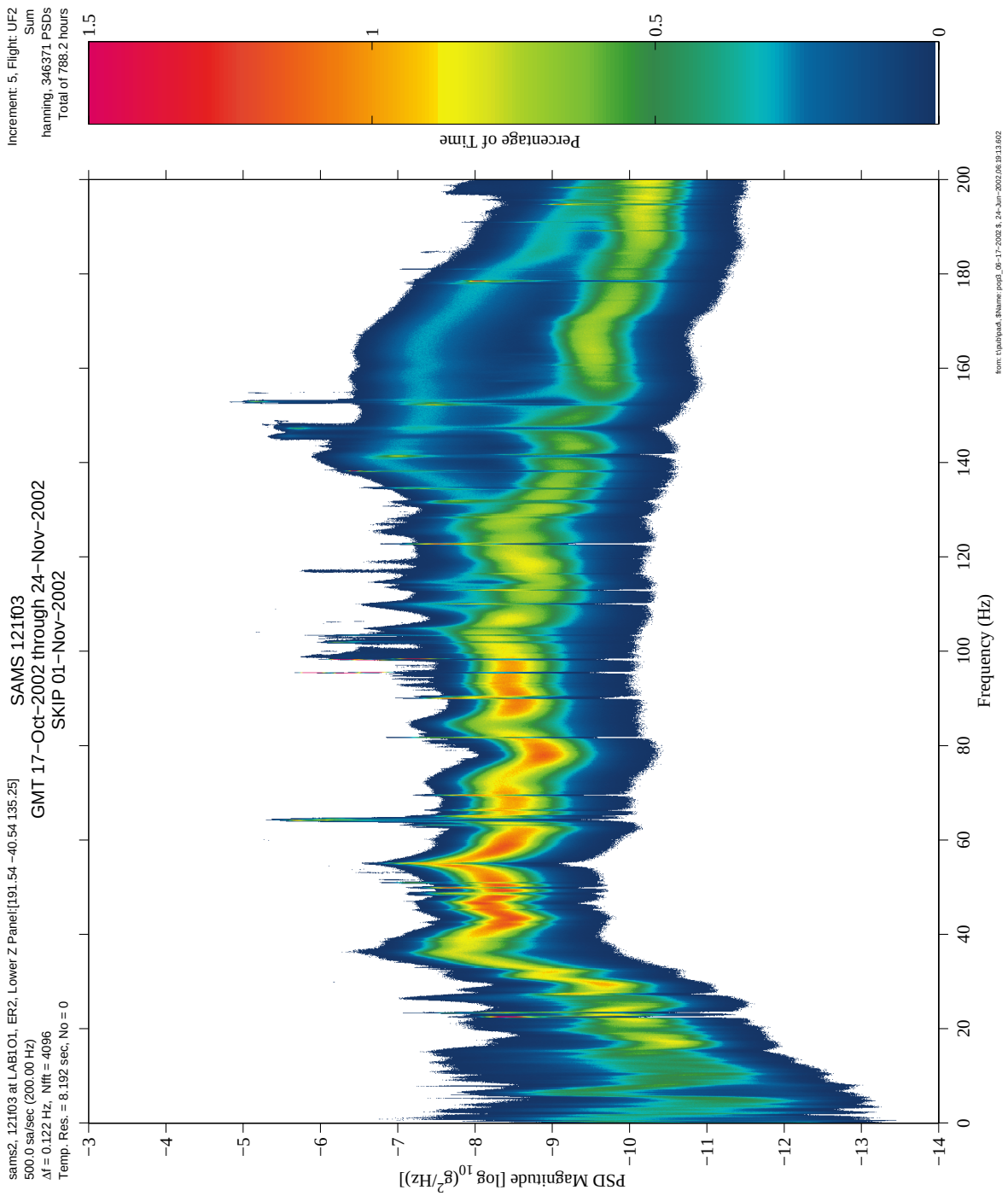

Figure 7-6 PCSA of GMT 17-Oct-2002 through 24-Nov-2002, 200 Hz (121f03)

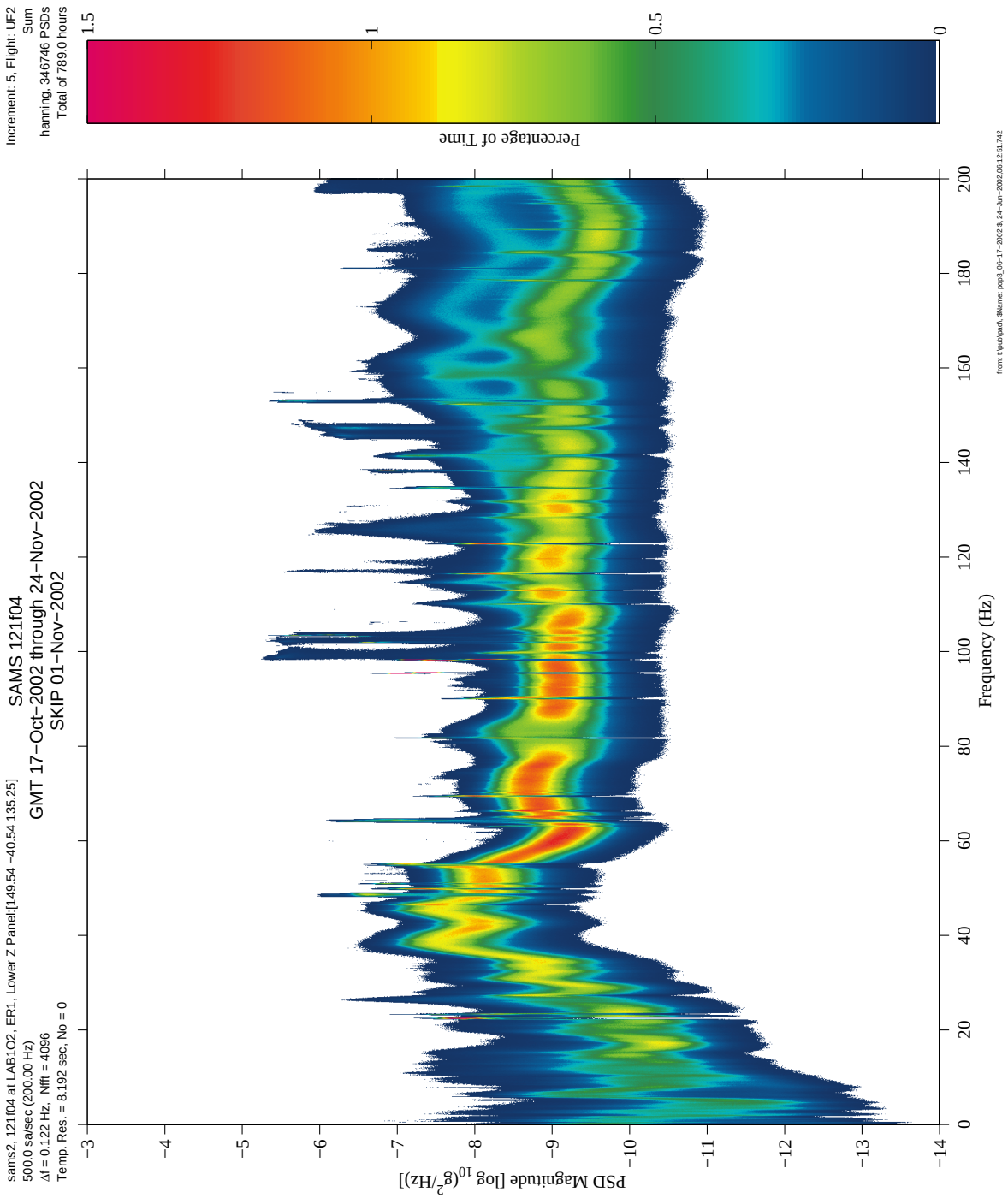

Figure 7-7 PCSA of GMT 17-Oct-2002 through 24-Nov-2002, 200 Hz (121f04)

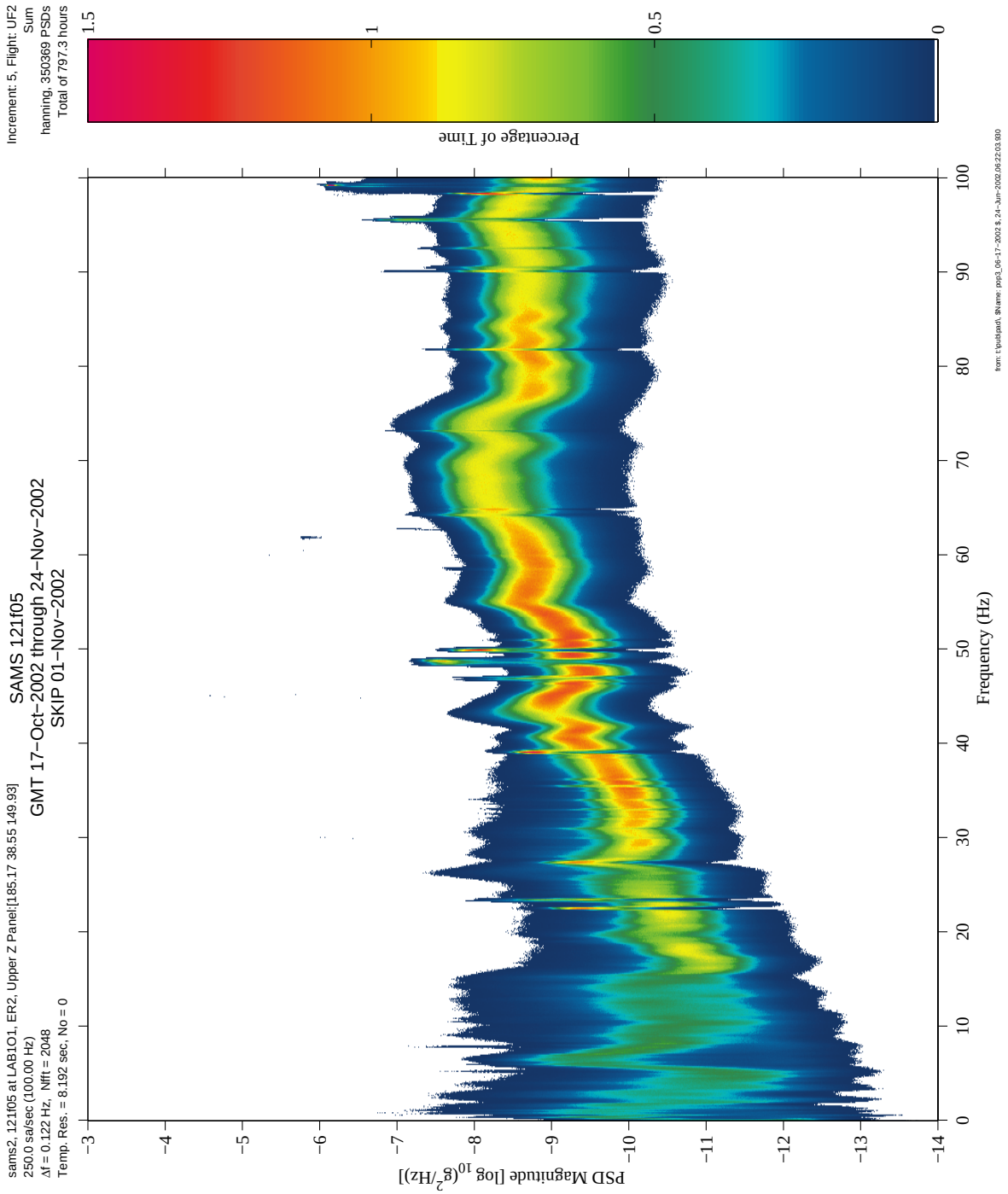

Figure 7-8 PCSA of GMT 17-Oct-2002 through 24-Nov-2002, 100 Hz (121f05)

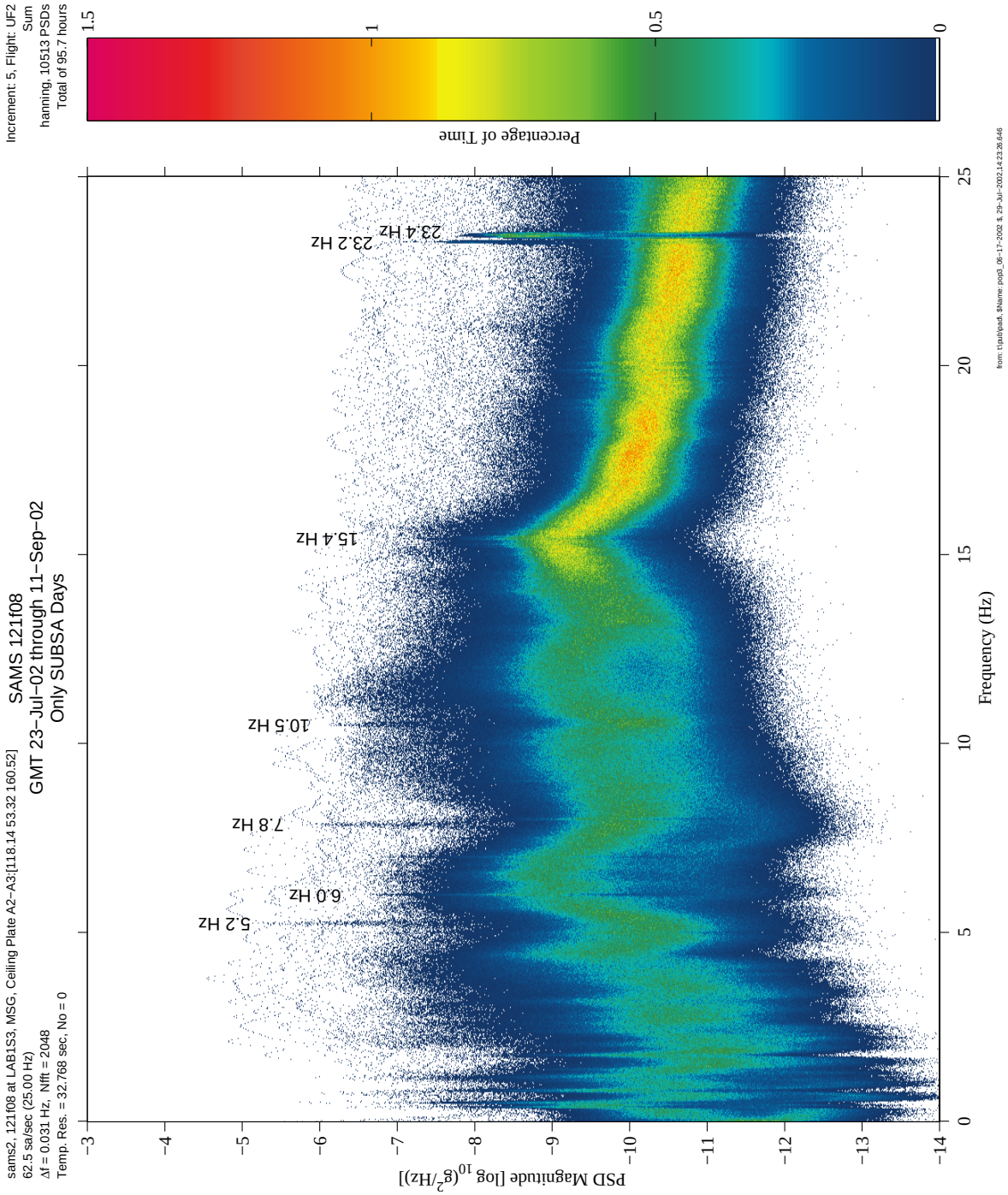

Figure 7-9 PCSA of SUBSA Experiment Days (121f08)

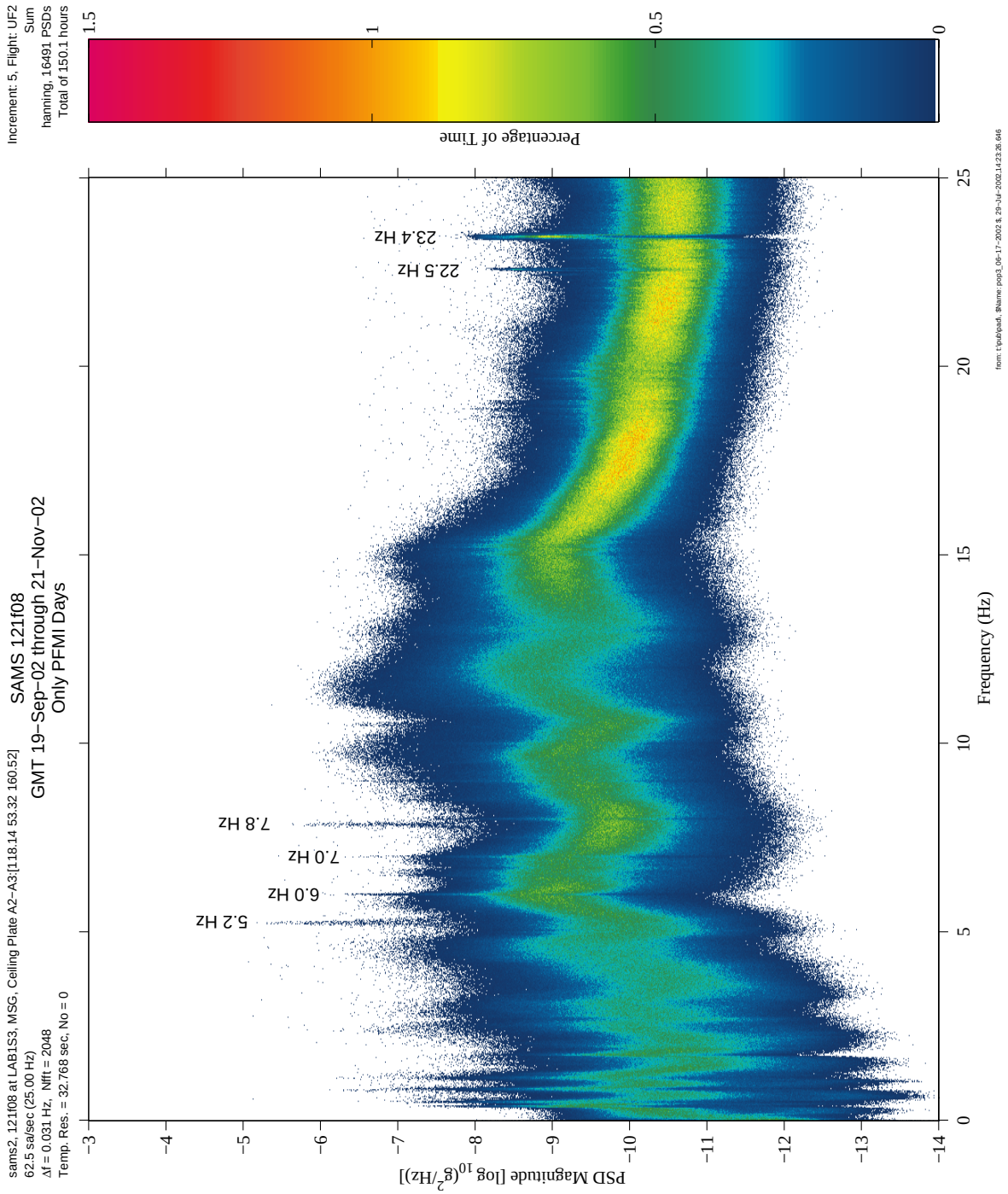

Figure 7-10 PCSA PFMI Experiment Days (121f08)

8 Summary of Increment-4/5 Analysis

8.1 Quasi-steady Environment

This section aims to summarize results from the quasi-steady acceleration analysis for this report. As such, it does not completely characterize the event under consideration, but serves to highlight the key impacts on the quasi-steady regime.

For more detail, see the applicable technical narrative sections of this report. Also, and most importantly, if this report does not include specific analysis for particular event that would aid in correlation with science or other data of interest, then please contact PIMS via email at pimsops@grc.nasa.gov for further assistance.

TABLE 8-1 SUMMARY OF FINDINGS FOR INCREMENT-4/5 QUASI-STEADY ANALYSIS

Source	Effect	GMT	Notes
TEA Attitude, Increment 4	1.09 µg mean magnitude	06-February-2002, 037/23:00	See Table 6-1
TEA Attitude, Increment 5	1.43 µg mean magnitude	10-November-2002, 327/10:30	
TEA Attitude, Increment 6	1.26 µg mean magnitude	12-January-2003, 012/23:00	
XPOP Attitude, Increment 4	2.04 µg mean magnitude	22-February-2002, 053/22:30	See Table 6-1
XPOP Attitude, Increment 5	1.83 µg mean magnitude	19-October-2002, 292/02:00	
XPOP Attitude, Increment 6	1.90 µg mean magnitude	15-December-2002, 349/23:15	
US to Russian Handover	-2.5 µg peak in Y_A axis	04-July-2002, 165/04:00	
Momentum Management	5.8 µg peak in Y_A axis	04-July-2002, 165/04:00	
Progress Dockings/Undockings	20-40 µg in X_A, Z_A axes	Increments 4-5	See Table 6-3
STS Dockings/Undockings	70-90 µg in X_A, Z_A axes	Increments 4-5	See Table 6-3
US Lab Water Dump	-6.4 µg in Z_A axis	12-September-2002, 012/15:30	
DC1 Cabin Depressurization	-4.5 µg peak in X_A axis	16-August-2002, 228/07:20	
Loss of GNC	-8.3 µg peak in Z_A axis	11-February-2002, 042/08:00	
Unidentified 100 Hz Disturbance	-0.5 µg peak in Y_A axis	Increments 4 - 5	
Progress Reboosts	0.66 µg mean in X_A axis	Increments 3 - 5	See Table 6-9

8.2 Vibratory Environment

This section highlights the significant findings for the vibratory acceleration analysis. The column labeled "Effect" in the following table is an attempt to encapsulate the impact of the corresponding "Source" acceleration event on the vibratory regime, and in most cases does not completely characterize the event under consideration. For more detail, the technical narrative sections of this report should be referenced. Also, if this report does not include specific analysis for a particular event that would aid in correlation with science or other data of interest, then please contact PIMS at pimsops@grc.nasa.gov> for further assistance. The quantities referred to in the "Effect" column below are one of the following:

- PEAK, the peak acceleration vector magnitude
- RMS, the acceleration root-mean-square value for the frequency range shown
- 95th, the approximately 95th percentile acceleration vector magnitude

TABLE 8-2 SUMMARY OF FINDINGS FOR INCREMENT INCREMENT-4/5 VIBRATORY ANALYSIS

SOURCE	STATE	EFFECT	FREQUENCY RANGE (HZ)	SENSOR	GMT
Progress Reboost		PEAK: 769 µg	0 - 25	SAMS 121f03	06-Mar-2002, 065/03:37:23 - 06-Mar-2002, 065/03:40:03
GASMAP Sample Pump	OFF	RMS: 24 µg	58.2 - 61.2	SAMS 121f02	26-Jan-2002, 026/16:00:00 - 27-Jan-2002, 027/00:00:00
GASMAP Sample Pump	ON	RMS: 200 µg		SAMS 121f02	
GASMAP Fan	OFF	RMS: 8 µg	57.2 - 57.6	SAMS 121f02	
GASMAP Fan	ON	RMS: 19 µg		SAMS 121f02	
MEPS PCM Insertion		PEAK: 103 mg	0 - 100	SAMS 121f02	18-July-2002, 199/15:12:29
MEPS Sample Run	OFF	RMS: 14 µg	45.85 - 47.39	SAMS 121f02	18-July-2002, 199/08:00:00 - 18-July-2002, 199/22:00:00
	ON	RMS: 24 µg			
	OFF	RMS: 9 µg	52.63 - 53.07		
	ON	RMS: 54 µg			
CEVIS Exercise	ON	RMS: 267 µg RMS: 250 µg RMS: 220 µg RMS: 245 µg	0 - 10	SAMS 121f02 SAMS 121f03 SAMS 121f04 SAMS 121f05	01-Jan-2002, 001/11:17:12 - 01-Jan-2002, 001/11:18:12
CEVIS Exercise	ON	RMS: 63 µg RMS: 46 µg RMS: 43 µg RMS: 47 µg RMS: 16 µg	0 - 10	SAMS 121f02 SAMS 121f03 SAMS 121f04 SAMS 121f05 SAMS 121f06	03-Jan-2002, 001/10:18:30 - 03-Jan-2002, 001/10:19:30
CEVIS Exercise	ON	RMS: 86 µg RMS: 55 µg RMS: 52 µg RMS: 54 µg RMS: 40 µg	0 – 10	SAMS 121f02 SAMS 121f03 SAMS 121f04 SAMS 121f05 SAMS 121f06	03-Jan-2002, 001/10:28:50 - 03-Jan-2002, 001/10:29:50

Table 8-2, continued from previous page

Velo Exercise	OFF	RMS: <50 µg	0 – 5	SAMS 121f02 SAMS 121f03 SAMS 121f04 SAMS 121f05	06-Aug-2002, 218/16:00 - 07-Aug-2002, 219/00:00
Velo Exercise	ON	RMS: >150 µg			
Velo Exercise	ON	RMS: 406 µg RMS: 369 µg RMS: 387 µg	0 – 10	SAMS 121f03 SAMS 121f04 SAMS 121f05	07-Aug-2002, 219/11:12:45 - 07-Aug-2002, 219/11:13:45
RED Exercise	OFF	RMS: 60 µg	0 – 10	SAMS 121f02	02-Sep-2002, 245/08:10 - 40
RED Exercise	squats	RMS: 301 µg	0 – 10	SAMS 121f02	02-Sep-2002, 245/08:58:09
RED Exercise	heel raises	RMS: 691 µg	0 – 10	SAMS 121f02	02-Sep-2002, 245/08:58:26
RED Exercise	deep heel raises	RMS: 336 µg	0 – 10	SAMS 121f02	02-Sep-2002, 245/09:02:42
RED Exercise	deadlifts	RMS: 206 µg	0 – 10	SAMS 121f02	02-Sep-2002, 245/09:10:46
RED Exercise	bench press/bent rows	RMS: 222 µg	0 – 10	SAMS 121f02	02-Sep-2002, 245/09:20:21
RED Exercise	one-leq squats	RMS: 255 µg	0 – 10	SAMS 121f02	02-Sep-2002, 245/09:05:59
RED Exercise	hab soar	PEAK: 9.67 mg	0 – 100	SAMS 121f02	02-Sep-2002, 245/09:33:12
SKV-1 & SKV-2	OFF	RMS: <10 µg	23 – 24	SAMS 121f08	04-Sep-2002
SKV-2	ON	RMS: 30 µg	23 – 24	SAMS 121f08	04-Sep-2002
SKV-1	ON	RMS: 10 µg	23 – 24	SAMS 121f08	23-Sep-2002
CMGs	3 operational	RMS[8]: 48 µg	109.983 -110.017	SAMS 121f03	26-Aug-2002, 238/00:00:00 - 28-Aug-2002, 240/00:00:00
TeSS Impact Test	entry/exit	PEAK: >15 mg	0 – 200	SAMS 121f05	01-Apr-2002, 091/08:11:05 - 01-Apr-2002, 091/08:13:30
EVA-7	NOT During	95th: 1.35 mg	0 – 100	SAMS 121f05	16-Aug-2002, hours 08 & 14
EVA-7	During	95th: 1.43 mg	0 – 100	SAMS 121f05	16-Aug-2002, hours 09 & 10
EVA-8	NOT During	95th: 1.93 mg	0 – 100	SAMS 121f05	16-Aug-2002, hours 04 & 11
EVA-8	During	95th: 1.98 mg	0 – 100	SAMS 121f05	16-Aug-2002, hours 06 & 07

[8] Mean RMS value over the 48-hour span indicated.

9 References

1. Hamacher, H., Fluid Sciences and Materials Science in Space, Springer-Verlag, 1987.

2. International Space Station User's Guide Release 2.0, NASA.

3. Expedition Three Press Kit: Expanding Space Station Scientific Research, Boeing/NASA/United Space Alliance, July 25, 2001

4. The International Space Station Fact Book, NASA, October 2000.

5. International Space Station Coordinate Systems, SSP-30219, Revision F.

6. International Space Station Familiarization, ISS FAM C21109, July 31, 1998

7. International Space Station Flight Attitudes, D-684-10198-06 DCN-002, December 1, 1999.

8. International Space Station Research Plan—Office of Biological and Physical Research, NASA, August 2000.

9. http://spaceflight.nasa.gov/shuttle/archives/STS-110/index.html

10. Expedition Four International Space Station: Science, Assembly and Spacewalks, Boeing/USA/NASA, November 9, 2001

11. Steelman, April, “Flight 6A Microgravity Analysis”, Microgravity AIT, August 1999.

12. Increment-4A and 4B As Flown ISS Attitude Timeline (ATL), ADCO, May 31, 2002

13. Continuing the Human Presence in Space, STS-111, Boeing/USA/NASA, May 16, 2001

14. Increment-5 As Flown ISS Attitude Timeline (ATL), ADCO, December, 2002

15. International Space Station—Expedition 5: Building Scientific Momentum, Boeing/USA/NASA, May 16, 2002

16. On-Orbit Vehicle Configuration Data Book for Mission 6A, Shuttle-ISS NSTS-37324-6A, Rev. 001, NASA, March 01.

17. Microgravity Environment Interpretation Tutorial (MEIT), NASA Glenn Research Center, March 2001.

18. http://spaceresearch.nasa.gov/Research_Projects/ros/arctic.html

19. Expedition Three Overview Fact Sheet, NASA, July 2001.

20. EXPRESS RACKS 1-2 /4-5 Fact Sheet, NASA, February and July 2001.

21. EXPRESS Rack, Flight 6A On-Orbit Configuration, Teledyne Brown Engineering DL 5221003, Nov. 99.

22. NASA Fact Sheets: FS-2002-03-59-MSFC- Release date April 2002

23. NASA Fact Sheets: FS-2002-04-80-MSFC- Release date April 2002

24. NASA Fact Sheets: FS-2002-03-58-MSFC- Release date March 18, 2002

25. http://lsda.jsc.nasa.gov/scripts/cf/hardw.cfm?hardware_id=175

26. Matisak, B.P., Rogers, M.J.B & Alexander J.I.D., "Analysis of the Passive Accelerometer System (PAS) Measurements During USML-1", AIAA 94-0434, December 1994.

27. Software Requirements for Processing Microgravity Acceleration Data from the International Space Station, PIMS-ISS-001, May 2000.

28. Canopus Systems, Inc., OARE Technical Report 149, STS-78 (LMS-1) Final Report, CSI-9604, September 1996.

29. Canopus Systems, Inc., OARE Technical Report 151, STS-94 (MSL-1) Final Report, CSI-9704, August 1997.

30. Hogg, Robert V., "Adaptive Robust Procedures: A Partial Review and Some Suggestions for Future Applications and Theory", Journal of the American Statistical Association, Vol. 69, December 1974.

31. Canopus System, Inc., Microgravity Environment Interpretation Tutorial 2001 Presentation, Section 5, James Fox, March 2001.

32. Microgravity Analysis Integration Team, "Microgravity Control Plan (Revision B)", Report No: SSP-50036 B, the Boeing Company, Houston, TX, NASA Contract No. NAS15-1000 (DRIVE-16), February 1999.

Appendix A. On-line Access to PIMS Acceleration Data Archive

Acceleration data measured by the MAMS and the SAMS on the ISS are available over the Internet via FTP from a NASA GRC file server. The flow chart shown in Figure A - 1 diagrams a procedure that can be used to download data files of interest:

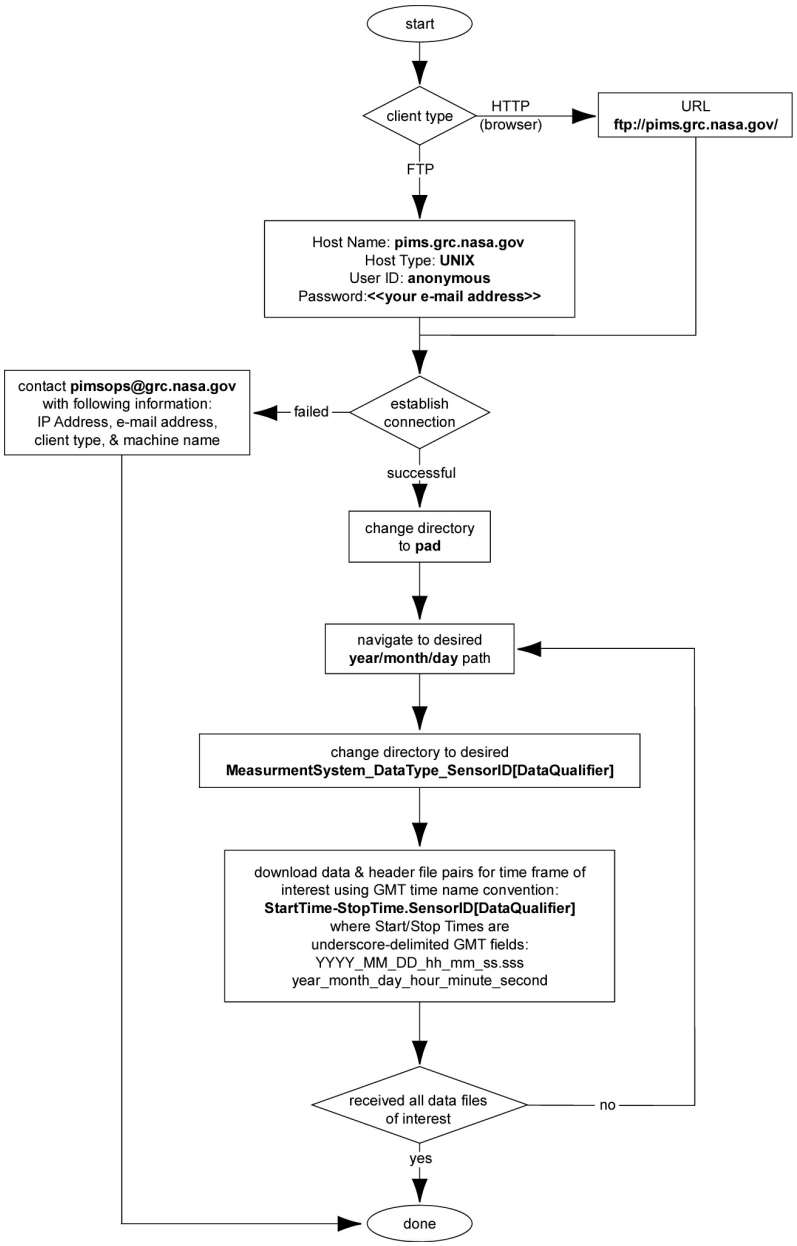

Figure A - 1 On-Line Data Access Flow Chart

A fictitious file listing is shown in Figure A - 2 depicting the PIMS Acceleration Data (PAD) file system hierarchy.

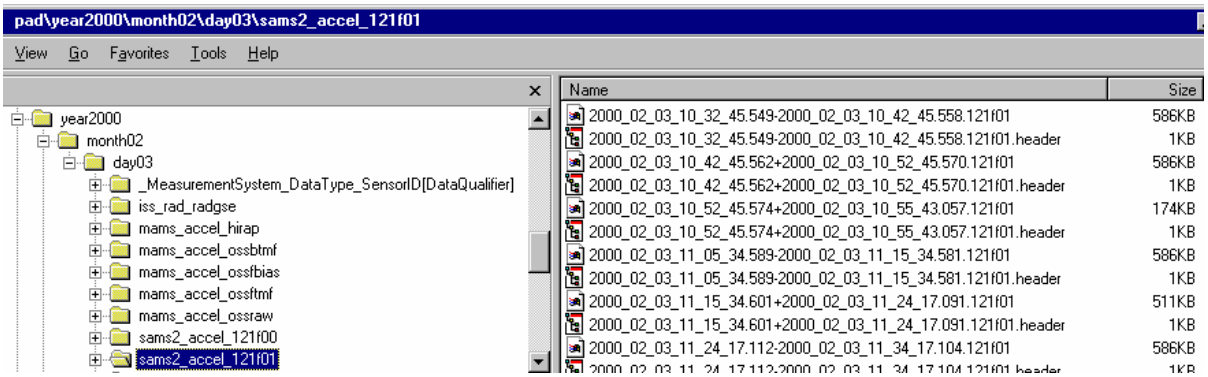

Figure A - 2 Screenshot of Sample PAD File Listing

For the directory highlighted on the left of this sample listing, the measurement system is "sams2" and the sensor identifier is "121f01". On the right, there is a partial listing of the acceleration header and data files available for this sensor collected on the day indicated (day 3). These files are named according to the PIMS-ISS-001 document [27].

If you encounter difficulty in accessing the data using this procedure, then send an electronic mail message to pimsops@grc.nasa.gov. Please describe the nature of the difficulty, and give a description of the hardware and software you are using to access the file server, including the domain name and/or IP address from which you are connecting.

Appendix B. Some Useful Acceleration Data and Microgravity Related URLs

Below is a list of some URLs that the microgravity scientific community might find very useful. They are all microgravity related. NASA does not endorse or cannot be held liable for the information contained on any non-NASA site. The PIMS Project provides this listing only as a service to the microgravity community.

1. For more information on the EXPPCS experiment go to:
   http://microgravity.grc.nasa.gov/6712/PCS.htm

2. For more information on EXPRESS RACK go to:
   http://liftoff.msfc.nasa.gov/Shuttle/msl/science/express.html

3. For more information on ARIS-ICE go to: http://www.scipoc.msfc.nasa.gov

4. For more information on Expedition Three go to:
   http://www1.msfc.nasa.gov/NEWSROOM/background/facts/exp3fact.html

5. For more information on Microgravity Acceleration Measurement go to:
   http://microgravity.grc.nasa.gov/MSD/MSD_htmls/mmap.html

6. For more information on MAMS OSS, MAMS HiRAP and SAMS go to:
   http://pims.grc.nasa.gov

7. For information on MAMS, SAMS data request go to:
   http://pims.grc.nasa.gov/html/RequestDataPlots.html

8. For information on upcoming Microgravity Environment Interpretation Tutorial (MEIT) go to: http://www.grc.nasa.gov/WWW/MMAP/PIMS/MEIT/meitmain.html

9. For information on upcoming Microgravity Meeting Group (MGMG) go to:
   http://www.grc.nasa.gov/WWW/MMAP/PIMS/MGMG/MGMG_main.html

10. For information on SAMS go to:
    http://microgravity.grc.nasa.gov/MSD/MSD_htmls/sams.html

11. For information on MAMS/HiRAP go to:
    http://microgravity.grc.nasa.gov/MSD/MSD_htmls/mams.html

Appendix C. Acronym List and Definition

Acronyms used in this Summary Report are listed below. A more extensive list of NASA ISS-related acronyms can be found through the Internet at:

http://spaceflight.nasa.gov/station/reference/index.html

ACRONYM	DEFINITION
ACS	Attitude Control System
ADCO	Attitude Determination and Control Officer
A/L	Airlock
AOS	Acquisition of Signal
ARED	Advanced Resistive Exercise Device
ARCTIC	Advanced Thermoelectric Refrigerator/Freezer
ARIS	Active Rack Isolation System
ARIS-ICE	ARIS ISS Characterization Experiment
ATL	Attitude Timeline
BCTA	Bias Calibration Table Assembly
CAM	Centrifuge Accommodation Module
CBM	Common Berthing Mechanism
CBOSS	Cellular Biology Operations Support System
CDT	Central Daylight Time
CETA	Crew and Equipment Translation Aid
CEVIS	Cycle Ergometer with Vibration Isolation System
CHeCS	Crew Health Care System
C/L	Crew Lock
CM	Center of Mass
CMG	Control Moment Gyro
CMS	Countermeasures System
CWC	Collapsible Water Container
C&W	Caution and Warning
DC	Direct Current (electrical acronym generalized for mean value)
DC-1	Russian Docking Compartment
ECLSS	Environmental Control and Life Support System
EDT	Eastern Daylight Time
EMU	Extravehicular Mobility Unit
ER 1/2	EXPRESS Rack 1 or 2
ESA	European Space Agency
EVA	Extravehicular Activity
EXPPCS	Experiment of Physics of Colloids in Space
EXPRESS	Expedite the Processing of Experiments to the Space Station
FGB	Functional Cargo Block (Russian translation: Functionalui Germatischeskii Block)
g	nominal gravitational acceleration at Earth's surface (9.81 m/s^2)
GASMAP	Gas Analysis System for Metabolic Analysis of Physiology
GMT	Greenwich Mean Time
GNC	Guidance, Navigation, and Control
GNC MDM	Guidance, Navigation, and Control Computer
GRC	NASA Glenn Research Center

GSE	Ground Support Equipment
HiRAP	High Resolution Accelerometer Package
HOSC	Huntsville Operation Support Center
HRF	Human Research Facility
Hz	Hertz
ICU	Interim Control Unit
iRED	interim Resistive Exercise Device
ISS	International Space Station
ITS	Integrated Truss Structure
JSC	NASA Johnson Space Center
kbps	kilobits per second
KSC	NASA Kennedy Space Center
LAB	U. S. Laboratory Module
LOS	Loss of Signal
LVLH	Local Vertical Local Horizontal
MAMS	Microgravity Acceleration Measurement System
MBS	Mobile Base System
MCOR	Medium-rate Communication Outage Recorder
MCS	Motion Control System
MEIT	Microgravity Environment Interpretation Tutorial
MELFI	Minus Eighty-degree-Celsius Freezer for ISS
MEP	Microgravity Environment Program
MEPS	Microencapsulation Electrostatic Processing System
mg	milli-g, 1 x 10^{-3}g
MGMG	Microgravity Measurement Group
MPEV	Manual Pressure Equalization Valve
MSFC	NASA Marshall Space Flight Center
MSG	Microgravity Science Glovebox
NASA	National Aeronautics and Space Administration
NASDA	National Space Development Agency of Japan
Nm	Newton-Meter
OARE	Orbital Acceleration Research Experiment
ODRC	Operational Data Request Center
ORU	Orbital Replacement Units
OSS	OARE Sensor Subsystem
OSSBTMF	OSS Best Trimmean Filter
OTO	One-Third Octave
PAD	PIMS Acceleration Data
PAO	Public Affairs Office
PCMCIA	Personal Computer Memory Card International Association
PCM	Process Chamber Module
PCSA	Principal Component Spectral Analysis
PFMI	Pore Formation and Mobility During Controlled Directional Solidification in a Microgravity Environment Investigation
PI	Principal Investigator
PIMS	Principal Investigator Microgravity Services
PMA	Pressurized Mating Adapter
PSD	Power Spectral Density
PuFF	Pulmonary Function in Flight
PVA	Photovoltaic Array
P1	Portside Truss Segment 1

QTH	Quasi-steady Three-dimensional Histogram
RAMS	Random Access Mass Spectrometer
RED	Resistive Exercise Device
RHCS	Right-Handed Cartesian System
RMS	Root-Mean-Square
ROS	Russian Orbital Segment
RPM	Revolutions Per Minute
RSS	Root-Sum-Square
SAMS	Space Acceleration Measurement System
SDTO	Station Detailed Test Objective
SE	Sensor Enclosure
SKV	Russian Air Conditioner
SLDs	Subject Load Devices
SM	Service Module
S0	Starboard Truss Segment 0
SSA	Space Station Analysis
STS	Space Transportation System
SUBSA	Solidification Using a Baffle in Sealed Ampoule
S1	Starboard Truss Segment 1
TEA	Torque Equilibrium Attitude
TeSS	Temporary Sleep Station
TMF	Trimmean Filtered
TSC	Telescience Support Center
TVIS	Treadmill Vibration Isolation System
USOS	US Orbital Segment
VELO	Russian Velosiped
VRCS	Vernier Reaction Control System
XPOP	X Principal Axis Perpendicular to the Orbit Plane
XVV	X body axis toward the Velocity Vector
μg	micro-g, 1 x 10^{-6}g
WWW	World Wide Web
XPH	+X-axis parallel to angular momentum vector
YPR	Yaw, Pitch, Roll
ZNN	Z-axis nadir at orbital noon

Appendix D. SAMS and MAMS Data Flow Descriptions

The MAMS hardware contains two acceleration measurement systems called MAMS OSS and MAMS HiRAP, each with a distinct measurement objective. The purpose of the MAMS OSS data is to measure the quasi-steady accelerations on the ISS. MAMS OSS data are obtained at a rate of 10 samples per second and are low-pass filtered with a cutoff frequency of 1 Hz. Each MAMS OSS data packet contains 16 seconds of MAMS OSS acceleration data and is transmitted in real-time at a rate of one data packet every 16 seconds. MAMS has the capability to store 25.6 hours of MAMS OSS data on board. Activated at MAMS power up or via ground command, this on board storage capability allows capturing of critical quasi-steady acceleration events for later downlink. These stored acceleration data can be transmitted to ground at a ground commanded rate between 20 and 200 kbps.

The MAMS HiRAP data are obtained at a fixed rate of 1000 samples per second and low pass filtered with a cutoff frequency of 100 Hz. The purpose of the MAMS HiRAP data is to measure the vibratory and transient accelerations on the ISS. Each MAMS HiRAP data packet contains 192 acceleration readings and is transmitted at a rate of one data packet every 0.192 seconds. MAMS does not have any capability to store MAMS HiRAP data on board.

Like MAMS HiRAP, the SAMS sensor heads are designed to measure the vibratory and transient accelerations on the ISS. Each SAMS sensor can be commanded to measure and downlink acceleration data at one of five sampling rates, with five corresponding cutoff frequencies. Since the SAMS sampling rate can be varied, the number of readings per packet and the number of packets per second varies as a function of the user selected sampling rate. Table D - 1 illustrates the relationship amongst sampling rate, cutoff frequency, acceleration readings per packet, and acceleration data packets per second for the SAMS sensors.

TABLE D - 1 SAMS DATA FLOW RATES

Sampling Rate (samples/sec)	Cutoff Frequency (Hz)	Readings Per Packet	Packets Per Second
62.5	25	31 or 32	2
125	50	62or 63	2
250	100	74 or 51	4
500	200	74 or 28	8
1000	400	74 or 56	14

Telemetry from the ISS is not continuous. A time interval where real time data downlink is available is referred to as an Acquisition of Signal (AOS) interval. Similarly, the lack of real time data downlink availability is referred to as a Loss of Signal (LOS) interval. Both SAMS and MAMS acceleration data must rely on ISS on board storage capabilities to eventually obtain acceleration data collected during LOS intervals. The Medium-rate Communication Outage Recorder (MCOR) provides this ISS on board storage capability. Consequently, real time acceleration data are available on the ground during AOS periods and acceleration data are stored on the MCOR during LOS periods for eventual downlink. Under normal circumstances, both SAMS and MAMS will measure and transmit acceleration data continuously throughout a given increment.

When acceleration data are transmitted to the ground, either real time data downlink or data transmitted from a dump of the MCOR memory, the resultant acceleration data packets are routed through the White Sands Facility, through Johnson Space Center (JSC), through the Marshall Space Flight Center (MSFC), Huntsville Operation Support Center (HOSC), and ultimately to PIMS Ground Support Equipment (GSE) located at the TSC. The PIMS GSE writes each received packet into a database table dedicated to each accelerometer supported by PIMS. Therefore, a separate database table exists for MAMS OSS, MAMS HiRAP, and for each of the five SAMS sensor heads.

The primary function of the database tables is to automatically merge AOS and LOS data packets for each accelerometer. As there exists overlap between the AOS and LOS acceleration data packets received, each sensor's dedicated database table discards any redundant data packets, resulting in a table containing a contiguous set of acceleration data packets.

Data are accessed from the database table to serve two separate purposes. The first purpose involves obtaining the most recent acceleration data from the table to generate real time plots of the acceleration data in a variety of plot formats supported by PIMS [27]. These real time plots are updated during AOS intervals and electronic snapshots of the data are routed to the PIMS ISS web page (http://pims.grc.nasa.gov).

The second purpose involves obtaining the oldest acceleration data from the "bottom" of the table. These acceleration data are used to generate the PIMS acceleration data archives used by the PIMS data analysts to generate the plots described in this report. Since the data are processed from the "bottom" of the table, MCOR dumps will have had time to be downlinked, received, and merged by the database table. PIMS currently waits 24 hours before generating any acceleration data archives. Like the electronic snapshots of the real time acceleration data plots, the acceleration data archives are available for download via the PIMS ISS web page.

Appendix E. Data Analysis Techniques and Processing

E. Data Analysis Techniques and Processing

This section briefly describes some assumptions, considerations, and procedures used to acquire and analyze the acceleration data measurements made by the two accelerometer systems: MAMS and SAMS.

E.1. Acceleration Data Coordinate Conversion

During the life of the Space Station, PIMS will frequently be asked to present acceleration data in a coordinate system other than that of the sensor. The purpose of this section is to provide the mathematical definitions and conventions PIMS will use when performing coordinate transformations.

PIMS maintains a coordinate system database for use in PIMS real-time and offline software that contains the information necessary to describe the location and orientation of various coordinate systems relative to the Space Station Analysis Coordinate System. Each entry for a coordinate system contains the location of the origin in SSA coordinates (x,y,z) and the Euler angles (Y, P, R) describing the orientation in a yaw-pitch-roll sequence of rotations with respect to the SSA frame. A positive rotation follows the right hand rule. So, an observer standing at positive infinity on the axis of rotation, looking towards the origin would see a counterclockwise rotation of the other two axes.

Transformation of acceleration data from the SSA coordinate system to a NEW coordinate system is accomplished by the formulation of a transformation matrix, M.

$$M_A^{NEW} = \begin{bmatrix} \cos P \cdot \cos Y & \cos P \cdot \sin Y & -\sin P \\ \sin R \cdot \sin P \cdot \cos Y - \cos R \cdot \sin Y & \sin R \cdot \sin P \cdot \sin Y + \cos R \cdot \cos Y & \sin R \cdot \cos P \\ \cos R \cdot \sin P \cdot \cos Y + \sin R \cdot \sin Y & \cos R \cdot \sin P \cdot \sin Y - \sin R \cdot \cos Y & \cos R \cdot \cos P \end{bmatrix}^{NEW}$$

Equation E.1-1

$$M_A^{NEW} = \begin{bmatrix} m_{11} & m_{12} & m_{13} \\ m_{21} & m_{22} & m_{23} \\ m_{31} & m_{32} & m_{33} \end{bmatrix}$$

Equation E.1-2

$$\begin{bmatrix} a_x \\ a_y \\ a_z \end{bmatrix}^{NEW} = M_A^{NEW} \cdot \begin{bmatrix} a_x \\ a_y \\ a_z \end{bmatrix}^{A}$$

Equation E.1-3

Transformation of acceleration data from the NEW coordinate system to the SSA coordinate system is accomplished by multiplying the vector by the transpose of matrix M[**]. The transpose of M, M^T, can be calculated by swapping the rows and columns as depicted in Equation E.1-4.

[**] For orthogonal matrices, $M^T = M^{-1}$.

$$M^T = M^A_{NEW} = \begin{bmatrix} m_{11} & m_{21} & m_{31} \\ m_{12} & m_{22} & m_{32} \\ m_{13} & m_{23} & m_{33} \end{bmatrix}$$

Equation E.1-4

$$\begin{bmatrix} a_x \\ a_y \\ a_z \end{bmatrix}^A = M^T \cdot \begin{bmatrix} a_x \\ a_y \\ a_z \end{bmatrix}^{NEW}$$

Equation E.1-5

In general, PIMS will transform data from SENSOR coordinate system to a NEW coordinate system. This is a four step process:

1. **The orientation of the SENSOR coordinate system is found $[YPR]_{SENSOR}$ from the coordinate system database and used to calculate the transformation matrix M,**

$$M^{SENSOR}_A = \begin{bmatrix} \cos P \cdot \cos Y & \cos P \cdot \sin Y & -\sin P \\ \sin R \cdot \sin P \cdot \cos Y - \cos R \cdot \sin Y & \sin R \cdot \sin P \cdot \sin Y + \cos R \cdot \cos Y & \sin R \cdot \cos P \\ \cos R \cdot \sin P \cdot \cos Y + \sin R \cdot \sin Y & \cos R \cdot \sin P \cdot \sin Y - \sin R \cdot \cos Y & \cos R \cdot \cos P \end{bmatrix}^{SENSOR}$$

Equation E.1-6

$$M^{SENSOR}_A = \begin{bmatrix} m_{11} & m_{12} & m_{13} \\ m_{21} & m_{22} & m_{23} \\ m_{31} & m_{32} & m_{33} \end{bmatrix}$$

Equation E.1-7

2. **Since the data is currently in SENSOR coordinates, the transpose of M is calculated.**

$$M^A_{SENSOR} = \begin{bmatrix} m_{11} & m_{21} & m_{31} \\ m_{12} & m_{22} & m_{32} \\ m_{13} & m_{23} & m_{33} \end{bmatrix}$$

Equation E.1-8

$$\begin{bmatrix} a_x \\ a_y \\ a_z \end{bmatrix}^A = M^A_{SENSOR} \cdot \begin{bmatrix} a_x \\ a_y \\ a_z \end{bmatrix}^{SENSOR}$$

Equation E.1-9

3. **The orientation of the NEW coordinate system is found $[YPR]_{NEW}$ from the coordinate system database and used to calculate the transformation matrix N,**

$$N^{NEW}_A = \begin{bmatrix} \cos P \cdot \cos Y & \cos P \cdot \sin Y & -\sin P \\ \sin R \cdot \sin P \cdot \cos Y - \cos R \cdot \sin Y & \sin R \cdot \sin P \cdot \sin Y + \cos R \cdot \cos Y & \sin R \cdot \cos P \\ \cos R \cdot \sin P \cdot \cos Y + \sin R \cdot \sin Y & \cos R \cdot \sin P \cdot \sin Y - \sin R \cdot \cos Y & \cos R \cdot \cos P \end{bmatrix}_{NEW}$$

Equation E.1-10

$$\begin{bmatrix} a_x \\ a_y \\ a_z \end{bmatrix}^{NEW} = N \cdot \begin{bmatrix} a_x \\ a_y \\ a_z \end{bmatrix}^{A}$$

Equation E.1-11

4. **The equivalent transformation matrix T is calculated by substitution of Equation E.1-9 into Equation E.1-11**

$$T_{SENSOR}^{NEW} = N_{A}^{NEW} \cdot M_{SENSOR}^{A}$$

Equation E.1-12

$$\begin{bmatrix} a_x \\ a_y \\ a_z \end{bmatrix}^{NEW} = T_{SENSOR}^{NEW} \cdot \begin{bmatrix} a_x \\ a_y \\ a_z \end{bmatrix}^{SENSOR}$$

Equation E.1-13

E.2. Quasi-steady Regime

MAMS OSS data is collected at 10 samples per second, low pass filtered with a cutoff frequency of 1 Hz and sent to GSE for further processing and storage. PIMS is currently storing the OSS data as raw acceleration files and also trimmean filtered data that are compensated for sensor bias. The trimmean filter algorithm used by the PIMS on the MAMS OSS acceleration data operates on a sliding window of 480 samples, resulting in a data point every 16 seconds. The trimmean filter algorithm is generically described below.

E.2.1. Trimmean Filter

The OSS data is processed with an adaptive trimmean filter (TMF) to provide an estimate of the quasi-steady acceleration signal by rejecting higher magnitude transients such as thruster firings, crew activity, etc. The filtering procedure, depicted in Figure E - 2, sorts the data by magnitude and calculates the deviation from a normal distribution using the Q parameter according to the equation:

$$Q = \frac{\left[Upper(20\%) - Lower(20\%)\right]}{\left[Upper(50\%) - Lower(50\%)\right]}$$

Equation E.2-1

Where the upper and lower percentage is determined from the sorted data set. Q is used in the following equation to calculate α, an adaptively determined amount of data to trim from the tails.

$$\alpha(Q) = \begin{cases} 0.05 & Q <= 1.75 \\ 0.05 + 0.35 * \dfrac{(Q - 1.75)}{0.25} & 1.75 < Q < 2.0 \\ 0.4 & Q >= 2.0 \end{cases}$$

Equation E.2-2

The quasi-steady acceleration level is computed to be the arithmetic mean of the trimmed set. Trimmean filtered data is stored in the PAD archive under "ossbtmf". Further information concerning the trimmean filter can be found in [28-30].

E.2.2. Mapping of Quasi-Steady Data

During the life of the station, PIMS is required to "map" quasi-steady data to locations other than that of MAMS OSS. Mapping is a prediction of what the quasi-steady environment would be at an alternate location, knowing the acceleration levels at MAMS.

E.2.2.1 Background and Assumptions

The methods used by PIMS in offline and real-time algorithms make the assumption that the ISS vehicle can be considered a rigid body in regards to the quasi-steady regime. The three main contributions to the quasi-steady acceleration environment are aerodynamic drag, rotational and gravity gradient effects. Drag effect is the same for any point attached to the vehicle and is considered to act opposite to the direction of flight. Rotational effects are the tangential and radial acceleration contributions due to the rotation of the vehicle. It is assumed that the accelerations in the tangential direction are negligible.

The gravity gradient effect refers to accelerations acting on any point in a rigid body away from the center of mass. An independent particle will tend to gravitate towards the ISS center of mass (CM) if it is in front or behind the CM along the x-axis of LVLH. This is a positive acceleration in the vehicle frame of reference. The particle will also gravitate towards the CM if it is to the left or right of the CM (aligned with the y-axis of LVLH). The gravity gradient will tend to gravitate a particle away from the CM if it is above or below the CM (along the z-axis of LVLH). [26]

E.2.2.2 Mapping Algorithm

The following is a list of required parameters that are necessary to map data to any given location onboard the ISS.

- Location of MAMS sensor in Space Station Analysis (A) Coordinates
- Alternate locations to be mapped to in Space Station Analysis Coordinates
- Location of ISS center of mass in Space Station Analysis Coordinates
- Position of ISS in J2000 coordinate system.
- Quaternion representations for a yaw-pitch-roll sequence describing the orientation of the LVLH coordinate system relative to the Space Station Analysis coordinate system.
- ISS body angular rates about the X_A, Y_A and Z_A-axes.

These are the steps PIMS uses to map MAMS OSS acceleration data from the measurement location (MAMS) to any other location (NEW). All distances are in meters, angles in radians, angular rates in radians/s, radius of the earth, $r_e = 6.3781 \times 10^6$ (meters), and $g_e = 9.81$ m/s^2. Definitions of the various coordinate systems can be found in [5].

1. **Calculate the position vectors of MAMS and NEW relative to the center of mass (CM).**

   The distance from the center of mass to the MAMS location:

$$\vec{r}_{MAMS}^{SSA} = \begin{bmatrix} x \\ y \\ z \end{bmatrix}_{MAMS}^{A} - \begin{bmatrix} x \\ y \\ z \end{bmatrix}_{CM}^{A} = \begin{bmatrix} rx \\ ry \\ rz \end{bmatrix}_{MAMS}^{A}$$

Equation E.2-3

   The distance from the center of mass to the NEW location:

$$\vec{r}_{NEW}^{SSA} = \begin{bmatrix} x \\ y \\ z \end{bmatrix}_{NEW}^{A} - \begin{bmatrix} x \\ y \\ z \end{bmatrix}_{CM}^{A} = \begin{bmatrix} rx \\ ry \\ rz \end{bmatrix}_{NEW}^{A}$$

Equation E.2-4

2. **Calculate transformation matrix from SSA to LVLH coordinate system using transformation matrix.**

$$T_{LVLH}^{A} = \begin{bmatrix} q_0^2 + q_1^2 - q_2^2 - q_3^2 & 2(q_1 \cdot q_2 + q_0 \cdot q_3) & 2(q_1 \cdot q_3 - q_0 \cdot q_2) \\ 2(q_1 \cdot q_2 - q_0 \cdot q_3) & q_0^2 - q_1^2 + q_2^2 - q_3^2 & 2(q_2 \cdot q_3 + q_0 \cdot q_1) \\ 2(q_1 \cdot q_3 + q_0 \cdot q_2) & 2(q_2 \cdot q_3 - q_0 \cdot q_1) & q_0^2 - q_1^2 - q_2^2 + q_3^2 \end{bmatrix} = \begin{bmatrix} m_{11} & m_{12} & m_{13} \\ m_{21} & m_{22} & m_{23} \\ m_{31} & m_{32} & m_{33} \end{bmatrix}$$

Equation E.2-5

   ISS GN&C uses a yaw-pitch-roll sequence from LVLH to SSA coordinates. PIMS uses a yaw-pitch-roll sequence from SSA to LVLH. For this reason, when calculating acceleration transformations, we must use the transpose of the resultant of Equation E.2-5.

$$T_{A}^{LVLH} = \left[T_{LVLH}^{A} \right]^T$$

Equation E.2-6

$$T_{A}^{LVLH} = \begin{bmatrix} m_{11} & m_{21} & m_{31} \\ m_{12} & m_{22} & m_{32} \\ m_{13} & m_{23} & m_{33} \end{bmatrix}$$

Equation E.2-7

3. **Convert position vectors to LVLH coordinate system by matrix multiplication.**
   Position vector of MAMS relative to center of mass in LVLH coordinate system:

$$\vec{r}_{MAMS}^{\,LVLH} = T_A^{LVLH} \cdot \vec{r}_{MAMS}^{\,A} = \begin{bmatrix} rx \\ ry \\ rz \end{bmatrix}_{MAMS}^{LVLH}$$

Equation E.2-8

Position vector of NEW relative to center of mass in LVLH coordinate system:

$$\vec{r}_{NEW}^{\,LVLH} = T_A^{LVLH} \cdot \vec{r}_{NEW}^{\,A} = \begin{bmatrix} rx \\ ry \\ rz \end{bmatrix}_{NEW}^{LVLH}$$

Equation E.2-9

4. Calculate the radius to the vehicle.

$$r_O = \sqrt{r_x^2 + r_y^2 + r_z^2}$$

Equation E.2-10

5. Calculate the gravity gradient components in LVLH coordinates (in micro-g)
Gravity gradient component at MAMS location:

$$gg_{MAMS}^{LVLH} = \left(\frac{g_e \cdot r_e^2}{r_O^2} \right) \begin{bmatrix} rx \\ ry \\ -2 \cdot rz \end{bmatrix}_{MAMS}^{LVLH} \cdot \left(\frac{1x10^6}{g_e} \right)$$

Equation E.2-11

Gravity gradient component at NEW location:

$$gg_{NEW}^{LVLH} = \left(\frac{g_e \cdot r_e^2}{r_O^2} \right) \begin{bmatrix} rx \\ ry \\ -2 \cdot rz \end{bmatrix}_{NEW}^{LVLH} \cdot \left(\frac{1x10^6}{g_e} \right)$$

Equation E.2-12

6. Convert the gravity gradient components to SSA coordinates by matrix multiplication
MAMS gravity gradient component in SSA coordinates:

$$gg_{MAMS}^{A} = T_{LVLH}^{A} \cdot gg_{MAMS}^{LVLH}$$

Equation E.2-13

NEW gravity gradient component in SSA coordinates:

$$gg_{NEW}^{A} = T_{LVLH}^{A} \cdot gg_{NEW}^{LVLH}$$

Equation E.2-14

7. Calculate rotational acceleration matrix

$$A = \begin{bmatrix} -(\omega_y^2 + \omega_z^2) & \omega_x\omega_y & \omega_x\omega_z \\ \omega_x\omega_y & -(\omega_x^2 + \omega_z^2) & \omega_y\omega_z \\ \omega_x\omega_z & \omega_y\omega_z & -(\omega_x^2 + \omega_y^2) \end{bmatrix}$$

Equation E.2-15

8. **Calculate rotational components in SSA coordinates (in micro-g):**
Rotational component at MAMS location:

$$rot^A_{MAMS} = A \cdot \vec{r}^{\,A}_{MAMS} \cdot \left(\frac{1x10^6}{g_e} \right)$$

Equation E.2-16

Rotational component at NEW location:

$$rot^A_{NEW} = A \cdot \vec{r}^{\,A}_{NEW} \cdot \left(\frac{1x10^6}{g_e} \right)$$

Equation E.2-17

9. **Complete acceleration mapping by subtracting MAMS components and adding NEW components:**

$$A^A_{NEW} = A^A_{MAMS} - gg^A_{MAMS} - rot^A_{MAMS} + gg^A_{NEW} + rot^A_{NEW}$$

Equation E.2-18

E.2.3. OSS Bias Measurements

MAMS OSS triaxial sensor bias is measured by a sequence of Bias Calibration Table Assembly (BCTA) rotations. A complete bias measurement for a given axis consists of 50 seconds of data recorded in a normal orientation and 50 seconds of data recorded when the axis has been rotated 180 degrees to its opposite orientation. The 50 seconds of data are processed by the MAMS GSE with TMF algorithm applied to the resulting 500 points. Four measurements are made, corresponding with normal X_{oss} and Y_{oss}, opposite X_{oss} and Y_{oss}, opposite X_{oss} and normal Z_{oss}, and normal X_{oss} opposite Z_{oss}. The outputs for each axis and its opposite are summed and divided by two to obtain the bias value. The value is evaluated in relation to the collection of past bias measurements for a given power cycle and is included in the new mean bias calculation or ignored if determined to be out of range. A disturbance in the microgravity environment is sufficient to cause an up ranging in the OSS sensor, which, in turn, will automatically cause the bias to fail. Failed bias calibrations are not repeated. One of the initial goals during Increment-4/5 operations for MAMS was the characterization of the OSS sensor bias. To accomplish this, bias measurements were initially performed once per hour, but have since been set to one every six hours.

In the past, MAMS predecessor, the Orbital Acceleration Research Experiment (OARE), showed a significant initial transient in the bias measurements that would take one to two days to settle out. This phenomenon was not observed in the MAMS OSS data suggesting that the transient was an effect of launch. However, there is a bias temperature dependency. Ground testing indicates a temperature bias coefficient of 0.05 μg / °C [31]. At power up, the MAMS instrument takes roughly 4-6 hours to reach the nominal operating temperature of 40 °C, at

which point, the bias values can be considered constant. We have not verified the bias coefficient on-orbit. For this reason, PIMS is recommending that users avoid OSS data within the first 6 hours after a MAMS power on event. When MAMS OSS support is requested, this 6-hour "settling" time must be taken into consideration.

E.2.4. Quasi-steady Plot Types

The two types of plots used in the analysis of quasi-steady data are acceleration versus time and the quasi-steady three-dimensional histogram (QTH). Unless otherwise noted, these plot types use trimmean filtered OSS data. Figure E - 1 shows a sample of the ancillary information associated with the quasi-steady plot types described below. Where defined and utilized for a given plot type, the definitions of the optional fields 1-4 are described in a table for that plot type.

E.2.4.1 OSS Trimmean Acceleration versus Time

These are single (X, Y, Z, or vector magnitude) or three axes (X, Y, and Z) plots of acceleration in units of μg versus time. These plots give the best accounting of the quasi-steady acceleration vector as a function of time.

E.2.4.2 Quasi-steady Three-dimensional Histogram (QTH)

This type of analysis results in three orthogonal views of the quasi-steady vector. The time series is analyzed using a two-dimensional histogram method where the percentage of time the acceleration vector falls within a two-dimensional bin is plotted as a color. Areas showing colors toward the red end of the spectrum indicate a higher number of occurrences. Conversely, areas showing colors towards the blue end are indicative of a lower percentage, with no occurrences being shown as white. This plot provides a summary of the quasi-steady vector during the total time period considered. Exact timing of an acceleration event is lost in this type of plot.

TABLE E - 1 ANCILLARY PLOT INFORMATION FOR QTH PLOT TYPE

Ancillary Information Field	Generic Description	Specific Example
Optional Field 1	Timespan	Time Span = 162.8 hours
Optional Field 2		
Optional Field 3	Resolution	Resolution = 0.04 μg
Optional Field 4		

E.3. Vibratory Regime

The frequency response of the accelerometer systems used to collect vibratory data may extend below 0.01 Hz down to DC, but those instruments are not optimized for making quasi-steady or DC measurements. The MAMS OSS instrument is specialized for this purpose. Therefore, unless otherwise noted, it is assumed that the vibratory data have been demeaned for plots and analyses of vibratory data. Access to data availability plots for a given calendar month can be obtained via ftp at,

ftp://pims.grc.nasa.gov/pad/yearXXXX/monthYY/XXXX_YY_padprofile.pdf

where XXXX=the year of interest and YY=the month of interest. For example,

ftp://pims.grc.nasa.gov/pad/year2001/month10/2001_10_padprofile.pdf

provides access to data availability for October, 2001 for the five SAMS SEs and the MAMS sensors. Availability for a given month is listed across the x-axis and cutoff frequencies for the sensor heads are listed at the top. Notice that the figures are color-coded. Each color is associated with a cutoff frequency. The white vertical lines in-between the color bars are the gaps in the acceleration data collected by that specific sensor. This means that data is not available for that time span. These figures should be used as a starting point to determine whether certain sets of data are available before filling out and submitting a data request form at:

http://pims.grc.nasa.gov/html/RequestDataPlots.html.

E.3.1. Demeaned Vibratory Acceleration Data

In the analysis of the vibratory regime, it is understood that a certain amount of bias intrinsic to the measurement process does exist. This bias is manifest as a DC shift of the acceleration measurements away from the true mean value. Similar bias considerations also exist for measurements collected with the intent of analyzing the quasi-steady regime. However, much effort is expended to account for and remove bias from quasi-steady acceleration measurements, whereas in the vibratory regime, the mean value is effectively ignored in the process of demeaning. That is, for vibratory acceleration data, the mean value of the acceleration (on a per-axis basis) is subtracted over the time frame under consideration leaving effectively zero mean acceleration.

E.3.2. Vibratory Plot Types

The two types of plots used in the analysis of quasi-steady data are acceleration versus time and the quasi-steady three-dimensional histogram (QTH). Unless otherwise noted, these plot types use trimmean filtered OSS data. Figure E - 1 shows a sample of the ancillary information associated with the vibratory plot types described below. Where defined and utilized for a given plot type, the definitions of the optional fields 1-4 are described in a table for that plot type.

A plot of acceleration interval statistics in units of g versus time gives some measure of acceleration fluctuations as a function of time. This display type allows relatively long periods to be displayed on a single plot. There are three such interval statistic plots that are employed for this and other reasons as described below: (1) interval average, (2) interval root-mean-square and (3) interval minimum/maximum.

E.3.2.1 Interval Average

Interval average plots show net accelerations, which last for a number of seconds equal to or greater than the interval parameter, used. Short duration, high amplitude accelerations can also

be detected with this type of plot; however, the exact timing and magnitude of specific acceleration events cannot be extracted. This type of display is useful for identifying overall effects of extended thruster firings and other activities that tend to cause the mean acceleration levels to shift. This display type is rarely used for vibratory data.

TABLE E - 2 ANCILLARY PLOT INFORMATION FOR INTERVAL AVERAGE PLOT TYPE

Ancillary Information Field	Generic Description	Specific Example
Optional Field 1		
Optional Field 2		
Optional Field 3	Interval Statistic Plot Type	Interval Average
Optional Field 4	Size: X, Step: Y	Size: 0.25, Step: 0.25 sec.

E.3.2.2 Interval Root-Mean-Square

Interval root-mean-square (RMS) plots show oscillatory content in the acceleration data. For the period of time considered, this quantity gives a measure of the variance of the acceleration signal. This data representation is useful for identifying gross changes in acceleration levels usually caused by the initiation or cessation of activities such as crew exercise or equipment operations.

TABLE E - 3 ANCILLARY PLOT INFORMATION FOR INTERVAL ROOT-MEAN-SQUARE PLOT TYPE

Ancillary Information Field	Generic Description	Specific Example
Optional Field 1		
Optional Field 2		
Optional Field 3	Interval Statistic Plot Type	Interval Root Mean Square
Optional Field 4	Size: X, Step: Y	Size: 0.25, Step: 0.25 sec.

E.3.2.3 Interval Minimum/Maximum

An interval minimum/maximum plot shows the peak-to-peak variations of the acceleration data. For each interval, this plot type shows both the minimum and maximum values, and thereby shows the acceleration data envelope. This type of display is another way to track gross changes in acceleration.

TABLE E - 4 ANCILLARY PLOT INFORMATION FOR INTERVAL MINIMUM/MAXIMUM PLOT TYPE

Ancillary Information Field	Generic Description	Specific Example
Optional Field 1		
Optional Field 2		
Optional Field 3	Interval Statistic Plot Type	Interval Minmax
Optional Field 4	Size: X, Step: Y	Size: 0.25, Step: 0.25 sec.

E.3.2.4 Power Spectral Density

The power spectral density (PSD) is computed from the Fourier transform of an acceleration time series and gives an estimate of the distribution of power with respect to frequency in the acceleration signal. It is expressed in units of g^2/Hz. The method used for computation of the PSD is consistent with Parseval's theorem, which states that the RMS value of a time series signal is equal to the square root of the integral of the PSD across the frequency band represented by the original signal.

TABLE E - 5 ANCILLARY PLOT INFORMATION FOR PSD PLOT TYPE

Ancillary Information Field	Generic Description	Specific Example
Optional Field 1	Frequency Resolution, NFFT	Δf=0.031 Hz, Nfft=8192
Optional Field 2	Overlap %, Number of Overlap Points	P=0.0%, No = 0
Optional Field 3	Window Type, # PSD's Averaged	Hanning, k=3
Optional Field 4	Span	Span = 120.00 secs

E.3.2.5 Power Spectral Density Versus Time (Spectrogram)

Spectrograms provide a road map of how acceleration signals vary with respect to both time and frequency. To produce a spectrogram, PSDs are computed for successive intervals of time. The PSDs are oriented vertically on a page such that frequency increases from bottom to top. PSDs from successive time slices are aligned horizontally across the page such that time increases from left to right. Each time-frequency bin is imaged as a color corresponding to the base 10 logarithm of the PSD magnitude at that time and frequency. Spectrograms are particularly useful for identifying structure and boundaries in time and frequency over relatively long periods of time.

TABLE E - 6 ANCILLARY PLOT INFORMATION FOR SPECTROGRAM PLOT TYPE

Ancillary Information Field	Generic Description	Specific Example
Optional Field 1	Frequency Resolution, NFFT	Δf=0.122 Hz, Nfft=8192
Optional Field 2	Temporal Resolution, Number of Overlap Points	Temp. Res. = 4.096 sec, No = 4096
Optional Field 3	Window Type, # PSD's Considered	Hanning, k=2389
Optional Field 4	Timespan	Span = 180.19 minutes

E.3.2.6 RMS Acceleration Versus Time

This type of plot quantifies the measured acceleration in a fixed frequency band of interest. Nominally, this band extends from above DC to the cutoff frequency, but can be any arbitrary band that is at least as wide as the frequency resolution and wholly contained below the cutoff frequency. These plots are especially useful for tracking a portion of the acceleration spectrum of interest. For example, tracking the RMS level for a narrowband disturbance can isolate activation or deactivation events.

TABLE E - 7 ANCILLARY PLOT INFORMATION FOR RMS ACCELERATION VERSUS TIME PLOT TYPE

Ancillary Information Field	Generic Description	Specific Example
Optional Field 1	Frequency Resolution, Frequency Range	Δf=0.061 Hz, Range: 0-5 Hz
Optional Field 2	Temporal Resolution	Temp. Resolution: 16.384 sec.
Optional Field 3	Window Type, #PSDs	Hanning, k=1
Optional Field 4		

E.3.2.7 RMS Acceleration Versus One-Third Octave Frequency Bands

This type of plot quantifies the spectral content in proportional bandwidth frequency bands for a given time interval of interest (nominally 100 seconds). The (nearly) one-third octave bands are those defined by the ISS microgravity requirements; see Table 4 [32]. The results of this analysis are typically plotted along with a bold stair step curve representing the ISS combined vibratory limits in order to compare the acceleration environment to these prescribed limits. These plots are not particularly useful for identifying the source of a disturbance for a band that exceeds the desired limits.

TABLE E - 8 ANCILLARY PLOT INFORMATION FOR ONE-THIRD OCTAVE BANDS PLOT TYPE

Ancillary Information Field	Generic Description	Specific Example
Optional Field 1	Frequency Resolution, NFFT	Δf=0.010 Hz, Nfft=50568
Optional Field 2	Mode	Mode: 100 sec
Optional Field 3	Window Type, # PSD's Averaged	Hanning, k=1
Optional Field 4	Timespan	Span = 101.00 secs

E.3.2.8 Cumulative RMS Acceleration Versus Frequency

A plot of cumulative RMS acceleration versus frequency quantifies, in cumulative fashion, the contributions of spectral components to the overall measured RMS acceleration level for the time frame of interest. This plot is also derived from the PSD using Parseval's theorem. It quantitatively highlights key spectral regions - steep slopes indicate strong narrowband disturbances that contribute significantly to the acceleration environment, while shallow slopes indicate relatively quiet portions of the spectrum.

TABLE E - 9 ANCILLARY PLOT INFORMATION FOR CUMULATIVE RMS ACCELERATION VERSUS FREQUENCY PLOT TYPE

Ancillary Information Field	Generic Description	Specific Example
Optional Field 1	Frequency Resolution, NFFT	Δf=0.061 Hz, Nfft=8192
Optional Field 2		
Optional Field 3	Window Type, # PSD's Averaged	Hanning, k=2
Optional Field 4	Timespan	Span = 25.00 sec.

E.3.2.9 Principal Component Spectral Analysis (PCSA)

The PCSA histogram is computed from a large number of constituent PSDs. The resultant three-dimensional plot serves to summarize magnitude and frequency variations of significant or persistent spectral contributors and envelops all of the computed spectra over the time frame of interest. The two-dimensional histogram is comprised of frequency bins in units of Hz and PSD magnitude bins in units of $\log_{10}(g^2/Hz)$. The third dimension, represented by a color scale, is the percentage of time that a spectral value was counted within a given frequency-magnitude bin.

TABLE E - 10 ANCILLARY PLOT INFORMATION FOR PCSA PLOT TYPE

Ancillary Information Field	Generic Description	Specific Example
Optional Field 1	Frequency Resolution, NFFT	Δf=0.122 Hz, Nfft=8192
Optional Field 2	Temporal Resolution, Number of Overlap Points	Temp. Res. = 8.192 sec, No = 0
Optional Field 3	Window Type, # PSD's	Hanning, 102694 PSDs
Optional Field 4	Timespan	Total of 233.7 hours

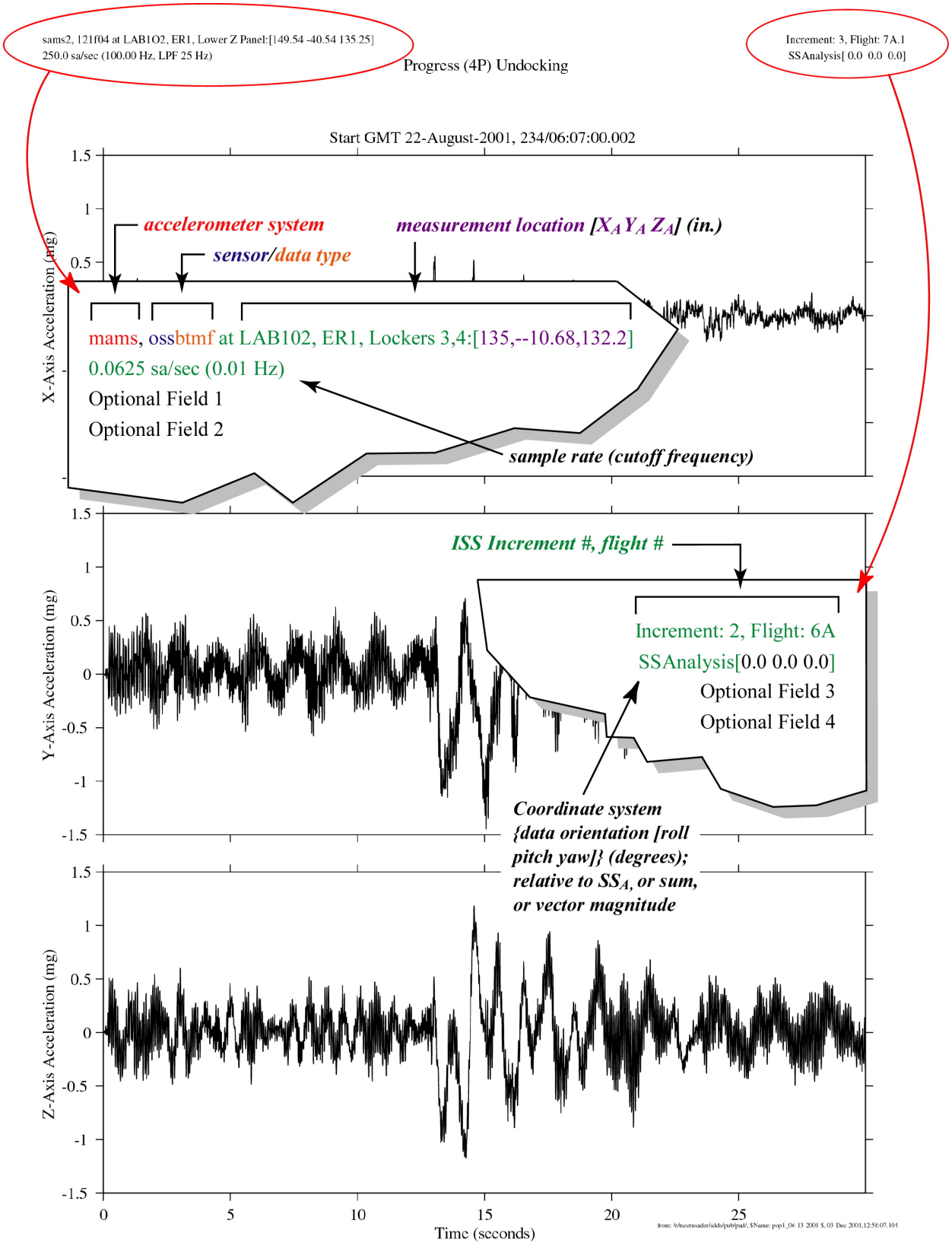

Figure E - 1 Ancillary Plot Information Description

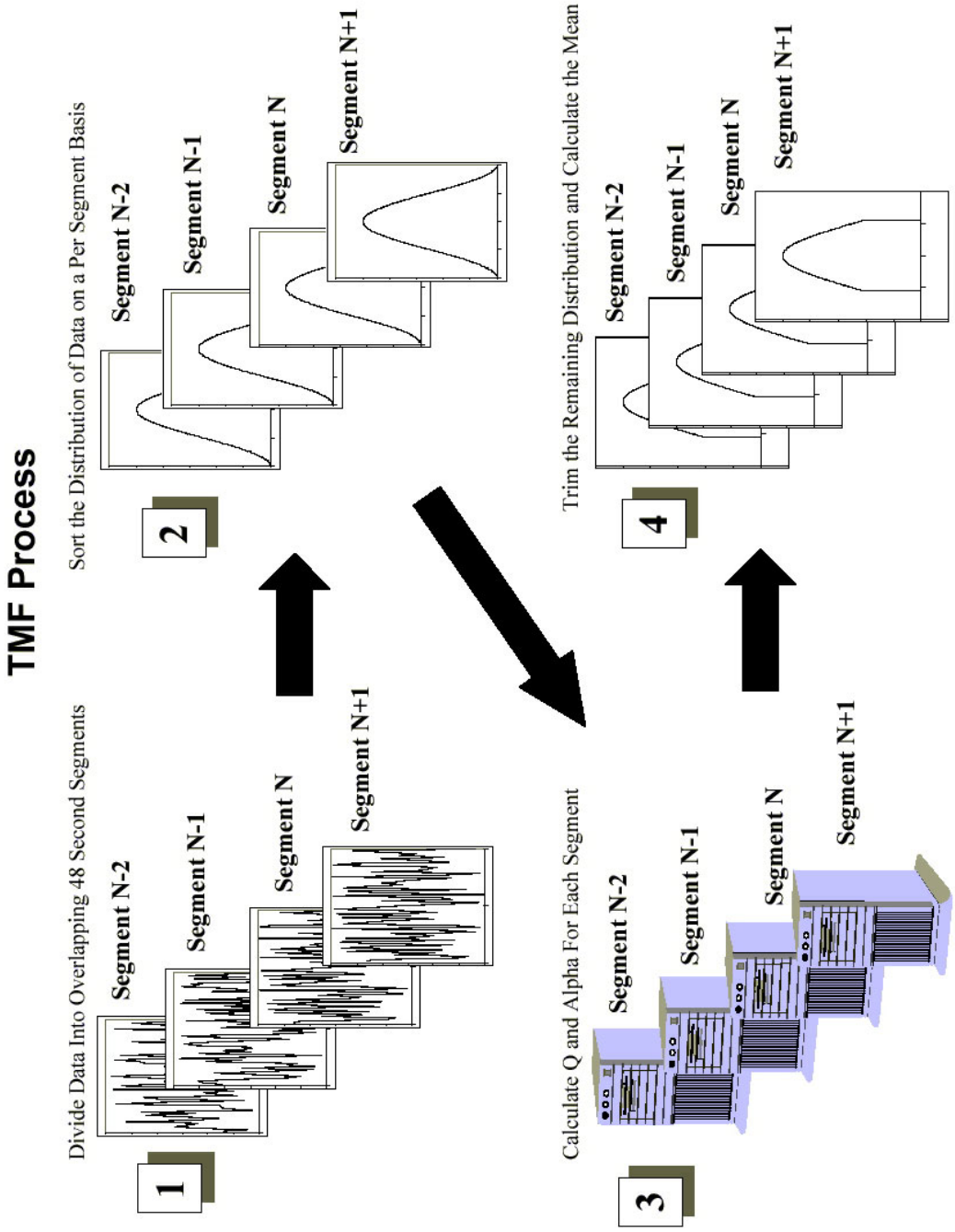

Figure E - 2 Trimmean Filter Process

REPORT DOCUMENTATION PAGE

Form Approved
OMB No. 0704-0188

1. AGENCY USE ONLY (*Leave blank*)	2. REPORT DATE	3. REPORT TYPE AND DATES COVERED
	July 2003	Technical Memorandum

4. TITLE AND SUBTITLE

International Space Station Increment-4/5 Microgravity Environment Summary Report

5. FUNDING NUMBERS

WBS–22–400–35–40–05

6. AUTHOR(S)

Kenol Jules, Kenneth Hrovat, Eric Kelly, Kevin McPherson, and Timothy Reckart

7. PERFORMING ORGANIZATION NAME(S) AND ADDRESS(ES)

National Aeronautics and Space Administration
John H. Glenn Research Center at Lewis Field
Cleveland, Ohio 44135–3191

8. PERFORMING ORGANIZATION REPORT NUMBER

E–13999

9. SPONSORING/MONITORING AGENCY NAME(S) AND ADDRESS(ES)

National Aeronautics and Space Administration
Washington, DC 20546–0001

10. SPONSORING/MONITORING AGENCY REPORT NUMBER

NASA TM—2003-212460

11. SUPPLEMENTARY NOTES

Kenol Jules and Kevin McPherson, NASA Glenn Research Center; Kenneth Hrovat, Eric Kelly, and Timothy Reckart, ZIN Technologies, Inc., Cleveland, Ohio 44142. Responsible person, Timothy Reckart, organization code 6727, 216–433–8147.

12a. DISTRIBUTION/AVAILABILITY STATEMENT

Unclassified - Unlimited
Subject Categories: 18, 20, and 35 Distribution: Nonstandard

Available electronically at http://gltrs.grc.nasa.gov

This publication is available from the NASA Center for AeroSpace Information, 301–621–0390.

12b. DISTRIBUTION CODE

13. ABSTRACT ***(Maximum 200 words)***

This summary report presents the results of some of the processed acceleration data measured aboard the International Space Station during the period of December 2001 to December 2002. Unlike the past two ISS Increment reports, which were increment specific, this summary report covers two increments: Increments 4 and 5, hereafter referred to as Increment-4/5. Two accelerometer systems were used to measure the acceleration levels for the activities that took place during Increment-4/5. Due to time constraint and lack of precise timeline information regarding some payload operations and station activities, not all of the activities were analyzed for this report. The National Aeronautics and Space Administration sponsors the Microgravity Acceleration Measurement System and the Space Acceleration Microgravity System to support microgravity science experiments which require microgravity acceleration measurements. On April 19, 2001, both the Microgravity Acceleration Measurement System and the Space Acceleration Measurement System units were launched on STS-100 from the Kennedy Space Center for installation on the International Space Station. The Microgravity Acceleration Measurement System supports science experiments requiring quasi-steady acceleration measurements, while the Space Acceleration Measurement System unit supports experiments requiring vibratory acceleration measurement. The International Space Station Increment-4/5 reduced gravity environment analysis presented in this report uses acceleration data collected by both sets of accelerometer systems: The Microgravity Acceleration Measurement System, which consists of two sensors: the low-frequency Orbital Acceleration Research Experiment Sensor Subsystem and the higher frequency High Resolution Accelerometer Package. The low frequency sensor measures up to 1 Hz, but is routinely trimmean filtered to yield much lower frequency acceleration data up to 0.01 Hz. This filtered data can be mapped to arbitrary locations for characterizing the quasi-steady environment for payloads and the vehicle. The high frequency sensor is used to characterize the vibratory environment up to 100 Hz at a single measurement location. The Space Acceleration Measurement System, which deploys high frequency sensors, measures vibratory acceleration data in the range of 0.01 to 400 Hz at multiple measurement locations. This summary report presents analysis of some selected quasi-steady and vibratory activities measured by these accelerometers during Increment-4/5 from December 2001 to December 2002.

14. SUBJECT TERMS	15. NUMBER OF PAGES
MAMS; SAMS; NASA; International Space Station; PIMS; Quasi-steady; Vibratory; Microgravity environment; Acceleration measurements	366
	16. PRICE CODE

17. SECURITY CLASSIFICATION OF REPORT	18. SECURITY CLASSIFICATION OF THIS PAGE	19. SECURITY CLASSIFICATION OF ABSTRACT	20. LIMITATION OF ABSTRACT
Unclassified	Unclassified	Unclassified	